13th ICOLD International

BENCHMARK WORKSHOP

ON THE NUMERICAL ANALYSIS OF DAMS, 9th – 11th September 2015

Lausanne, SWITZERLAND

Edited by

Russell Michael Gunn

Marc Balissat

Pedro Manso

Laurent Mouvet

Anton Schleiss

EPFL
ÉCOLE POLYTECHNIQUE
FÉDÉRALE DE LAUSANNE

CIGB
ICOLD

PROCEEDINGS OF THE 13th ICOLD INTERNATIONAL BENCHMARK WORKSHOP ON THE NUMERICAL ANALYSIS OF DAMS

9th to 11th September 2015, Lausanne, SWITZERLAND

Edited by

Russell Michael Gunn
Marc Balissat
Pedro Manso
Laurent Mouvet
Anton Schleiss

Preface

In accordance with the Terms of Reference (ToR) of the International Committee on Large Dams (ICOLD), Technical Committee A (TCA), Committee on Computational Aspects of Analysis and Design of Dams, *"Benchmark Workshops are organised to compare numerical models between one another and/or with reference solutions, including the dissemination and publication of results"*. These benchmarks are typically organised every two years by a member of the TCA in collaboration with his/her National Committee on Dams.

The first benchmark was held in Bergamo, Italy in 1991. The 13th Benchmark Workshop is held in Lausanne, Switzerland. Situated by the Lake of Geneva and surrounded by vineyards, countryside and forests, Lausanne benefits from an enchanting backdrop with spectacular views of the Alps which are the home place of many large dams and hydroelectric power schemes in Switzerland. More information on previous Benchmark Workshops can be found in ICOLD Bulletin 155 http://www.icold-cigb.org/GB/Publications/bulletin.asp.

The main campus of the École Polytechnique Fédérale of Lausanne, the hosting institution for the benchmark, brings together over 11,000 people, students, researchers and staff in the same magical place. With over 350 laboratories and research groups on campus, the EPFL is classed in the top three in Europe and top twenty worldwide in many scientific rankings.

With **1500 hydropower plants** producing **59 percent** of the domestic electricity supply, Switzerland is a hub for Dam Engineering and the Energy Sector. The Swiss Federal Office of Energy (SFOE) requires that Owners verify their schemes including dams for seismic loading. SFOE has published Guidelines allowing such seismic verifications to be performed. By 2015, a vast majority of seismic verifications had already been performed thus representing a milestone in Swiss Dam Engineering. On the basis of this "milestone" achievement (over 15 years of work), the Swiss Committee on Dams was selected by ICOLD, TCA members to host the Benchmark event.

The Benchmark sets a framework for Engineers, Owners and Scientists alike, to perform and share their experiences for predefined and open themes.

The 13th Benchmark comprised of the following themes:

Theme A Seismic safety evaluation of a concrete dam based on guidelines
Formulators: *Russell Michael Gunn & Anton Doytchinov Tzenkov*
Theme B Probability of failure of an embankment dam due to slope instability and overtopping
Formulators: *Adrián Morales-Torres & Ignacio Escuder-Bueno*
Theme C Dam Safety
Moderators: *Guido Mazzà & Massimo Meghella*

Russell Gunn   Marc Balissat   Pedro Manso   Laurent Mouvet   Anton Schleiss

Local Organising Committee

Table of Contents

State Key Laboratory of Hydrology-Water Resources and Hydraulic Engineering, Hohai University, Nanjing 210098, China;

National Engineering Research Centre of Water Resources Efficient Utilization and Engineering Safety, Hohai University, Nanjing 210098, China;

College of Water-conservancy and Hydropower, Hohai University, Nanjing 210098, China.

National Engineering Research Center of Water Resources Efficient Utilization and Engineering Safety, Hohai University, 210098 Nanjing, China

Peter S.J.1, Siviglia A. and Boes R.M.

Laboratory of Hydraulics, Hydrology and Glaciology, ETH Zurich, Hönggerbergring 26, CH-8093 Zürich

Mazzà G.

Conference Organisation

ICOLD Technical Committee A
Computational Aspects of Analysis and Design of Dams

Chairman

Escuder-Bueno, I.	Spain

Vice-Chairman

Mazzà, G.	Italy

Technical Advisory Team

Restelli, F.	Argentina
Lopez, F.	Australia
Zenz, G.	Austria
Curtis, D.	Canada
Chen, S.	China
Marulanda, C.	Colombia
Varpasuo, P.	Finland
Frossard, E.	France
Carrere, A. (Hon. Member)	France
Beetz, U.	Germany
Dakoulas, P.	Greece
Noorzad, A.	Iran
Meghella, M.	Italy
Fanelli, M. (Hon. Member)	Italy
Uchita, Y.	Japan
Tancev, L.	Former Yugoslav Republic of Macedonia
Andersen, R.	Norway
Popovici, A.	Romania
Glagovsky, V.	Russia
Minarik, M.	Slovakia
Hassanzadeh, M.	Sweden
Gunn, R. M.	Switzerland
Özen, O.	Turkey
Matheu, E.	United States

Theme A

Gunn, R. M.	(Leader)
Tzenkov, A, T.	

Theme B

Morales-Torres, A.	(Leader)
Escuder-Bueno, I.	

Theme C

Mazzà, G.	(Leader)

Local Benchmark Organisation

General

Schleiss A. (Director of Laboratory of Hydraulic Constructions and President ICOLD)
Mouvet L. (SwissCOD President)
Gunn, R. M.
Balissat, M.
Manso, P.
Casciana, G. (secretary)

Conference Facilities

Manso, P. (Leader)
Casciana, G.

Sponsoring

Balissat, M. (Leader)
Casciana, G.

Information and Registration

Manso, P. (Leader)
Casciana, G.

Excursions

Balissat, M. (Leader)
Casciana, G.

Wohnlich, A. (Les Toules Dam)
Feuz, B. (Mauvoisin Dam)

Web site http://icold2015bmw.epfl.ch

Manso, P. (Leader)
Bron, C.

Budgets and Financing

Manso, P. (Leader)
Casciana, G.

Proceedings

Gunn, R. M. (Editorial tasks)
Kaelin, C. (Assistant)

Acknowledgements

Sponsors[*]

AF-Consult Switzerland	http://www.afconsult.com/
ALPIQ	http://www.alpiq.com/
ewz, die Energie	https://www.ewz.ch/
Forces Motrices du Grand St Bernard	http://www.dransenergie.ch/
Groupe *e*	http://www.groupe-e.ch/
KWO Grimselstrom	http://www.grimselstrom.ch/
Lombardi	https://www.lombardi.ch/
Pöyry	http://www.poyry.ch/en
Stucky	http://www.stucky.ch/
Swiss Federal Office of Energy	http://www.bfe.admin.ch/

Alphabetical order

Keynote Lecture

The Earthquake Safety of Dams in Switzerland, Past, Present and Future

By

Darbre G. R[1]
Commissioner for Dam Safety

1. Swiss Federal Office of Energy, Supervision of Dams

Location of Dams under Swiss Federal Administrative Supervision
http://www.bfe.admin.ch/themen/00490/00491/00494/index.html?lang=en

Schweizerische Eidgenossenschaft
Confédération suisse
Confederazione Svizzera
Confederaziun svizra

Swiss Federal Office of Energy

The Earthquake Safety of Dams in Switzerland: Past, Present and Future

Georges R. Darbre, Commissioner for dam safety

Past and present activities
Vibration tests & strong-motion network
Focusing on key features at the example of water compressibility
What next in Switzerland

ICOLD 13th International Benchmark on the Numerical Analysis of Dams, Lausanne, 9th-11th September 2015

Past and Present: Regulatory

Up to 1970's	Earthquake safety of dams usually assessed according to international practice of the time (pseudo-static analysis with 10% g ?)
Since 1980's	Earthquake safety of new dam projects systematically assessed based on hazard maps of 1978
2002 / 2003	Publication of Swiss guideline on safety of dams and of supporting technical document on the earthquake safety assessment of dams Earthquake safety evaluation required for all dams in operation within 10 years
On-going	Verification of over 200 earthquake analysis reports by Supervisory authority ★

★ Cf. R. Panduri et al., Seismic safety analysis of dams within the context of the Swiss dam safety concept, 13th ICOLD International Benchmark Workshop, 2015

2

Past and Present: Analytical and Numerical studies

1982-1996	Earthquake response of concrete dams at ETH Zurich (3,6 mio CHF) ★
1989-1996	Earthquake response of embankment dams at ETH Lausanne (1,3 mio CHF) ★
Early 2000's	Comparison of measured and calculated earthquake responses together with the Univ. of Sherbrooke (CA) ★★

★ Main results:

❑ Scientific progress in individual topics (e.g. reservoir modeling and soil-structure interaction)
❑ Confirmation of the complexity of modeling and analyzing the earthquake behavior of dams

★★ Main results:

❑ Calculation models overestimate the actual, measured response of arch dams during earthquakes

3

Past and Present: In-situ tests and recordings

Up to 1980's - 1990's	Seismometer network run by the Swiss seismological service with continuous financial support from the dam owners
1990's:	Installation of a national strong-motion network encompassing a free-field and a dam network, funded by the dam owners (1 mio CHF)
End 1990's	Extensive ambient vibration tests at the arch dam of Mauvoisin together with EMPA - Swiss research institute for Materials Science & Technology
2000's	Extensive forced-vibration tests at the arch dam of Emosson together with the Univ. of Sherbrooke (CA)

4

Objectives of Dam strong-motion network

Dynamic characteristics: resonance frequencies, modes of vibration, energy dissipation.

Dynamic response: linear vs. nonlinear behavior (cracking, joint openings, permanent deformations), 2D vs. 3-D.

Wave propagation.

1 to 2 dam height

Free-field motion: amplitude, strong-motion duration, influence of local geological and soil conditions, attenuation laws and coefficients of wave propagation, seismic hazard.
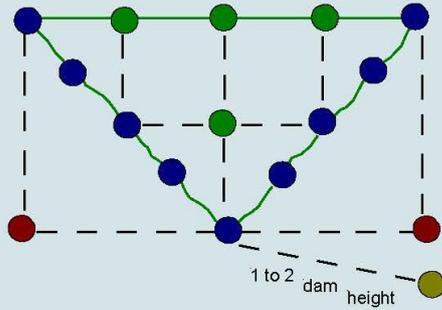
Abutment motion: total effective input motion (canyon effects, kinematic interaction, incoherent excitation)

5

Dam arrays installed
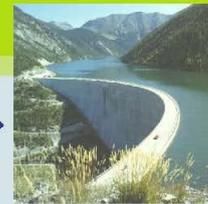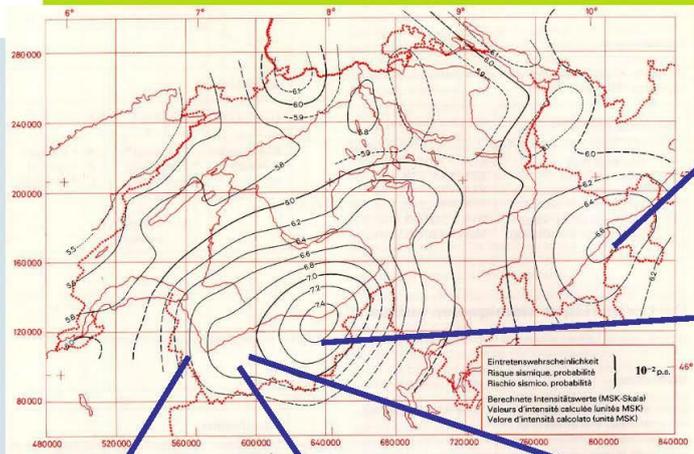
Punt dal Gall
(7 instruments)

Mattmark
(4 instruments)

Emosson
(5 instruments)

Mauvoisin
(12 instruments)

Grande Dixence
(6 instruments)

6

Example of accelerograph array at the dam of Mauvoisin
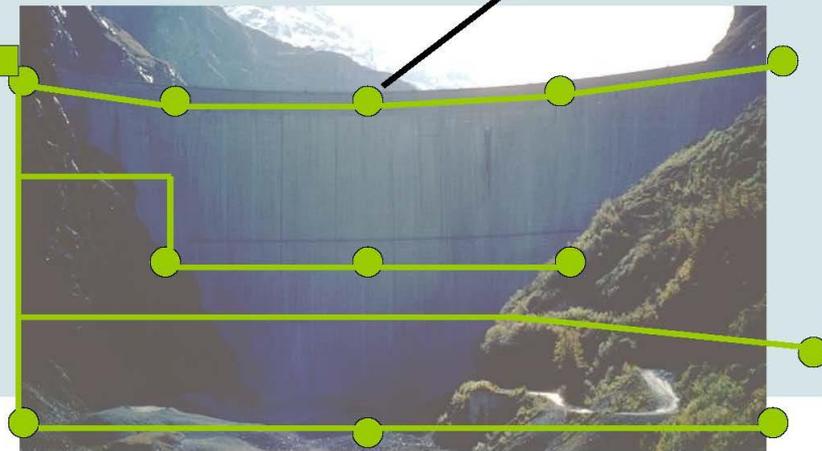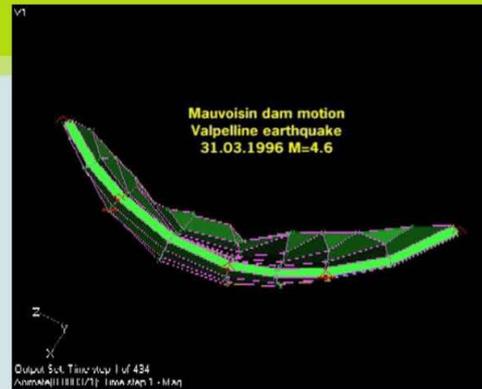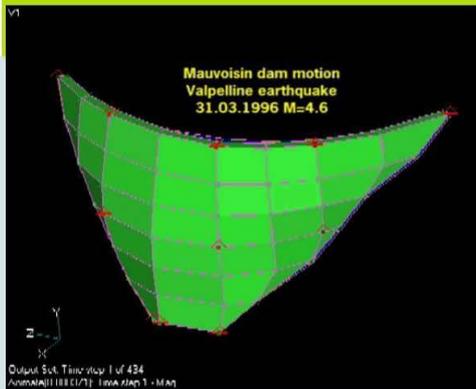
Example of recorded earthquake motions

- Mauvoisin: arch dam, 250 m
- Valpelline quake, 31 March 1996
- M = 4.6
- Distance = 13 km
- Recorded dam motions (amplified ca. 3'000)

Example of recorded earthquake motions

- Mauvoisin: arch dam, 250 m
- Valpelline quake, 31 March 1996
- M = 4.6
- Distance = 13 km
- Recorded dam motions (amplified ca. 3'000)

Valpelline quake: Accelerations at Mauvoisin [cm/s2, s]

Ambient vibration tests at Mauvoisin (together with EMPA)

Discrete (at different water levels) and continuous (6-month period)
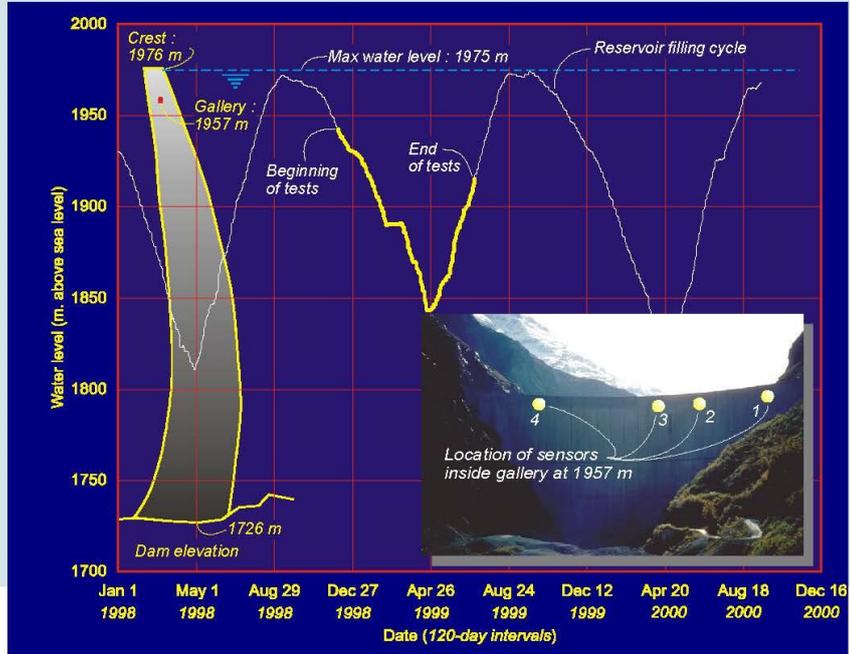
Natural frequency results at the dam of Mauvoisin dam
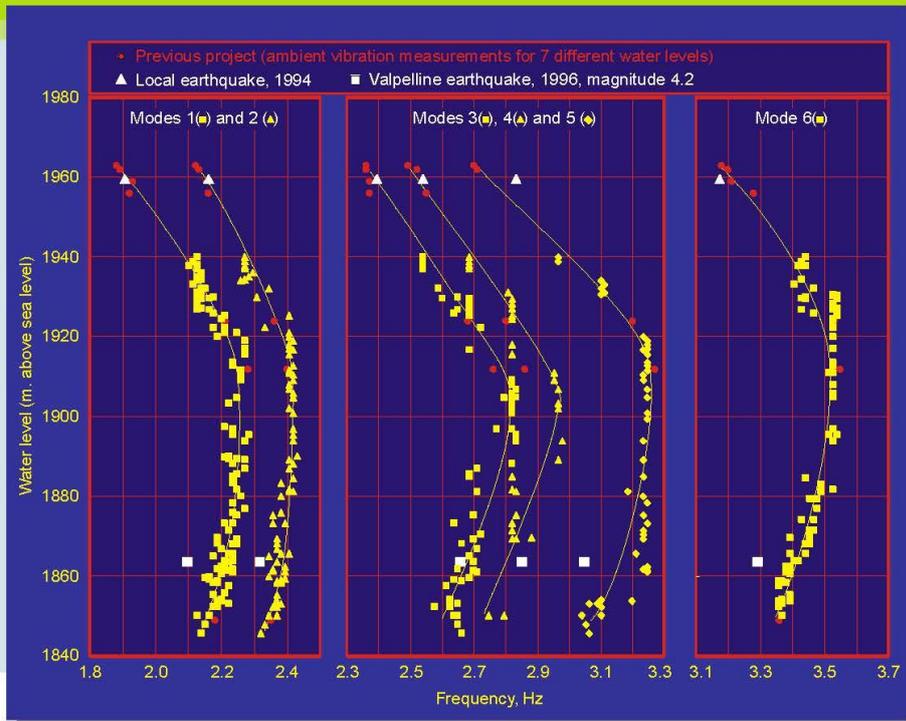
Forced-vibration tests at Emosson dam (different water levels) (together with the Univ. of Sherbrooke)

Sept: Hw = 1924
August: Hw = 1898
July: Hw = 1878
June: Hw = 1878
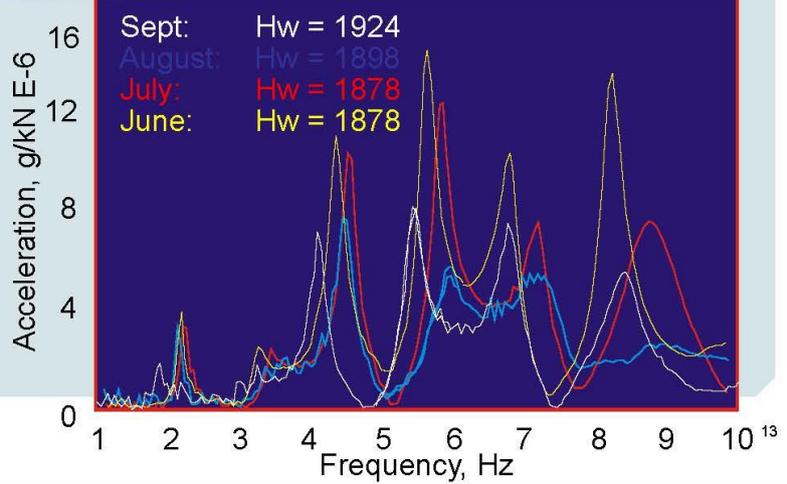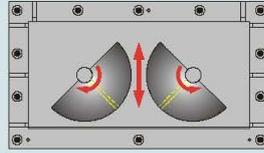
Numerical, model analyses (finite elements): Example Emosson (together with the Univ. of Sherbrooke)

- 3D models for dam-reservoir-foundation
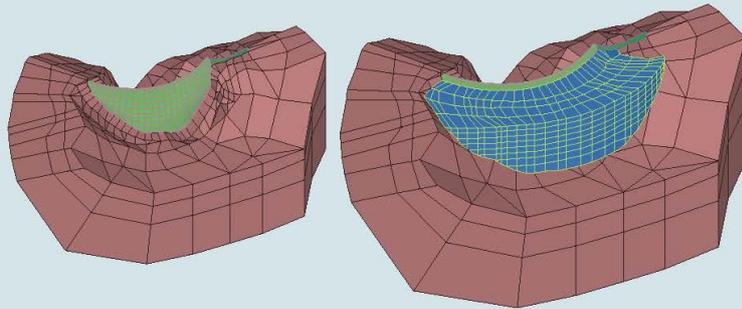
- Programs used

  - EACD-3D-85 : **Massless foundation**

  - EACD-3D-96 : **Energy dissipating foundation**

  - FEMAP & custom conversion programs for pre/post processing

- Models calibrated from ambient & forced vibration tests

- Then used for earthquake analysis

14

Earthquake analysis: Procedure
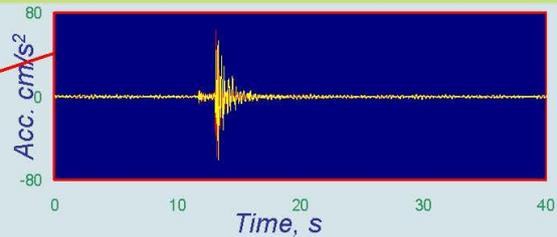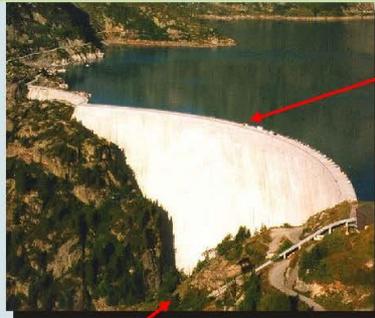
Recorded response – crest level
Computed response
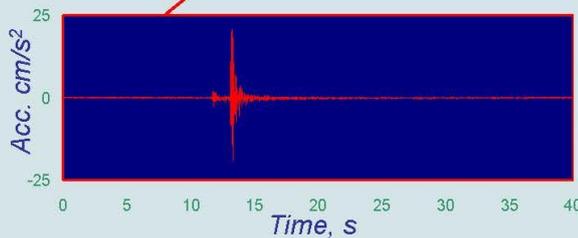
Recorded motion at base of dam
or at free field
Used as input

15

Comparison between calculated and recorded motions at the arch dams of Mauvoisin, Emosson and Punt-dal-Gall

❑ Calibrated numerical models largely overestimate the recorded responses !

❑With massless foundation models: High damping values has to be introduced artificially in dam body to reproduce recorded responses (up to 8 to 15 %)

❑ With energy-dissipating foundation models and dam damping at "reasonable" level : 20% or more foundation damping is required to reproduce recorded responses

❑ These damping values are "numerical values" and not physical ones !
Reasons for high numerical damping needed believed to lie primarily with

  ❑ Assumption of uniform input motion

  ❑ Use of a "localized" input motion rather than a possibly lower "effective" input motion

  ❑ Issue of energy dissipation in foundation (including radiation damping)

16

9

How to move forward

❑ In view of the complexity of the issues and the state of knowledge, R&D and analyses need to focus on the key factors affecting the earthquake response

❑ Example of water compressibility : Numerical modeling is possible ... is it meaningful ? Often (almost) more DOF's to model the reservoir and the foundation than the dam body itself, although it is in the performance of the latter that we are interested in!

   ❑ Proposition: Account only for the most important effects of water compressibility on the dam response

Gravity dam
Infinite reservoir
Bottom wave absorption
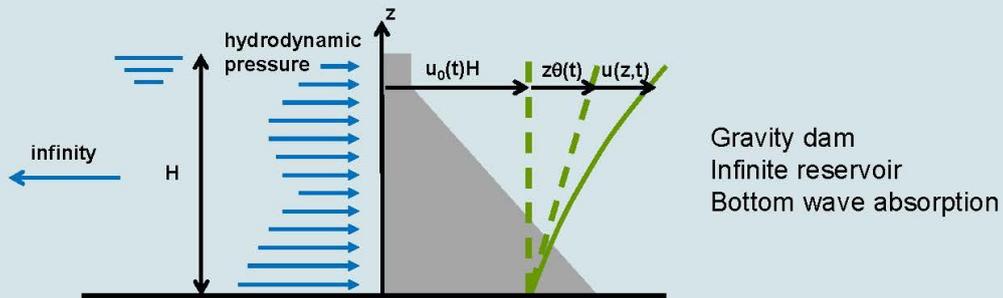
17

Analytical expression in the frequency domain for the base shear (1-mode of deformation)

$$V(\omega) = -B_{01}(\omega)\ddot{Y}_1(\omega) - B_{00}(\omega)\ddot{u}_0(\omega) - B_{0\theta}(\omega)H\ddot{\theta}(\omega)$$

Bottom wave reflection coefficient α

– – – – $\alpha = 1$
– · – · – $\alpha = 0.5$
·········· $\alpha = 0$
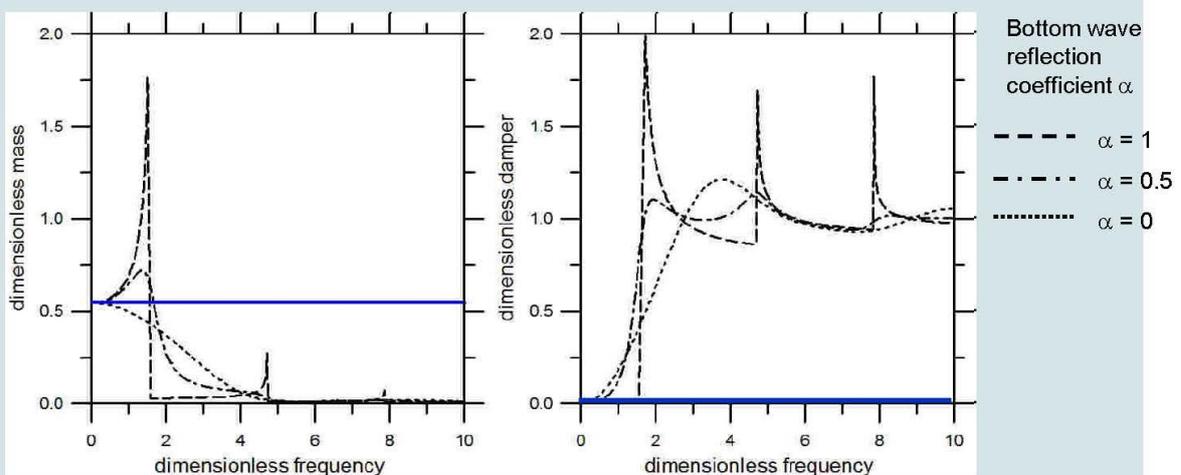
Coefficient B_{00} (base shear due to rigid-body horizontal movement)

———— Incompressible solution (no energy dissipation !)

18

10

Two-parameter model

Two-parameter model solution

Coefficient B_{00}
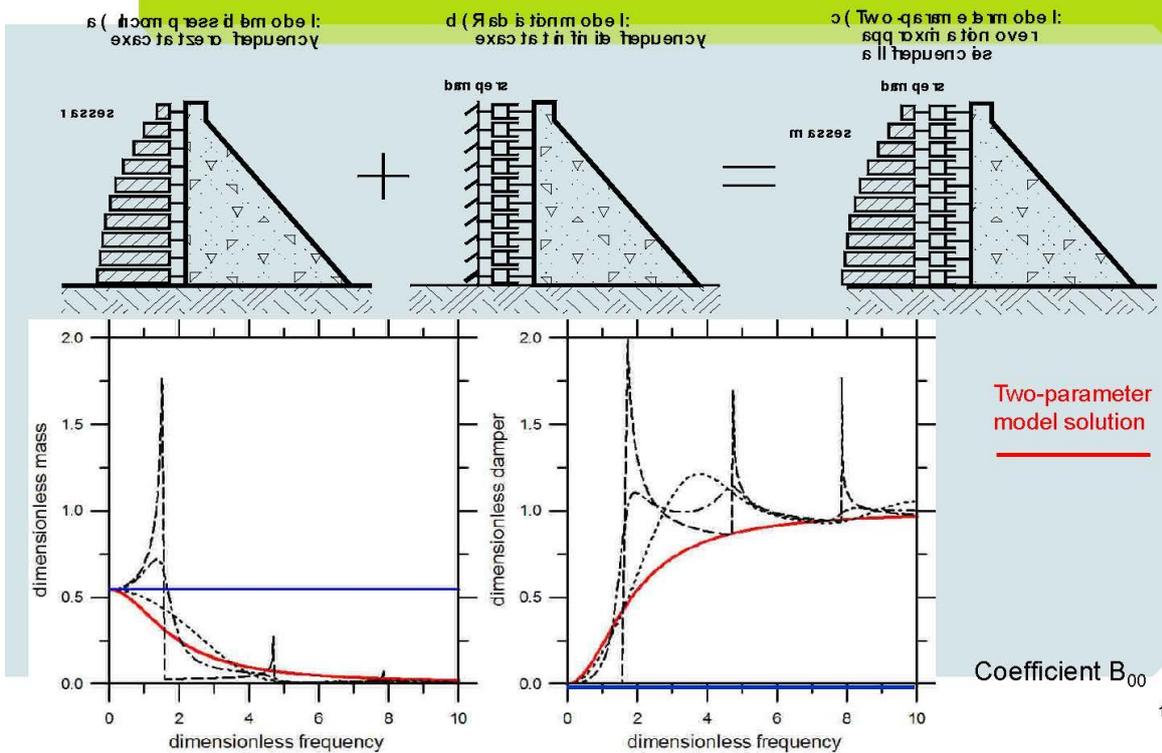
19

Earthquake safety of dams in Switzerland: What next

❑ Regulatory

    ❑ Complete review of all submitted earthquake safety analyses (by 2016)

    ❑ Complete and publish the part of the revised guideline on dam safety which deals with earthquake safety (2015)

    ❑ Assess need for revising seismic hazard to be used in safety assessments (by 2016)

❑ Analytical and numerical studies

    ❑ No specific activities planned.
    Needs include modeling of nonlinear behavior, up to ultimate capacity

❑ In-situ and recordings

    ❑ Decision to be made on renewing or not the strong-motion dam network (by 2016)

20

Theme A:
SEISMIC SAFETY EVALUATIONS OF A CONCRETE DAM BASED ON GUIDELINES

Formulation by:

Russell Michael Gunn[1] & Anton Doytchinov Tzenkov[2]

1. *Swiss Federal Office of Energy, Supervision of Dams (formerly Stucky Ltd)*
2. *Stucky Ltd*

1. *russell.gunn@bfe.admin.ch, 2. atzenkov@stucky.ch*

Schweizerische Eidgenossenschaft
Confédération suisse
Confederazione Svizzera
Confederaziun svizra
Swiss Confederation

Bundesamt für Energie BFE
Office fédéral de l'énergie OFEN
Ufficio federale dell'energia UFE
Swiss Federal Office of Energy SFOE

stucky >
a Gruner company

Luzzone Arch Dam

The information package (available from the authors) for the preparation of contributions for Theme A consists of:
- Finite element mesh data
- Static and seismic load data
- Result forms and other documents to be completed by participants
- Other documents listed in the appendices.

Background

The Swiss Federal Office of Energy (SFOE) is responsible for the monitoring of storage reservoirs and requires that operators evaluate and verify their reservoir schemes including "dams" for seismic loading. SFOE has published Guideline documents ("Directives", [1], [2]) related to these seismic verifications and operators have ensured that the necessary studies are performed accordingly. By April 2013, SFOE had received seismic verifications for 142 of the total of 206 storage schemes and the remaining verifications (mainly for class III structures in accordance with the Swiss Directive nomenclature) shall be performed in due time.

These studies represent an important milestone in Swiss Dam Engineering and have enabled a considerable amount of experience and knowledge to be acquired not only for seismic verifications, but also for the ageing of these structures, remedial measures/rehabilitation works (if required) and a more general contribution to safety evaluations and associated risks.

The proposed benchmark is aimed at the seismic safety evaluation of a Class I concrete arch dam in accordance with Guidelines. The participants of the benchmark may use any guidelines, but in preference from their home countries or international guidelines. Participants are encouraged to make reference to the recently published ICOLD Bulletin B155 on the subject of the "*Use of numerical models in dam engineering*" [3]. The benchmark is not only aimed at comparing analysis results from the different Guidelines (a synthesis report shall be prepared by the formulators), but also the self-evaluation by the participants of the methods applied and their appropriateness to the structure based on "engineering judgement", hence giving the occasion to make recommendations for further studies.

Hence, the proposed benchmark explores the use of numerical tools to satisfy Guidelines specifically related to concrete dams.

Objectives of Theme A

The objective is to perform the seismic verification of a concrete arch dam according to Guidelines. The Swiss Directive [2] has been used as the basis for the problem statement. Participants are encouraged to use <u>any guidelines</u> and judgement necessary to analyse the seismic safety of the structure. Only the concrete dam body shall be addressed noting that the foundation stability (wedge analyses) has already been the subject of a previous benchmark [4]. The phases of the studies are as follows:

1. *Data evaluations (25%)1*: The formulators of the benchmark provide information necessary to perform the studies related to the geometry of the structure, geology, topography, finite element model, material characteristics, boundary conditions, static loading (self-weight, hydrostatic pressure due to reservoir loads and thermal gradients), seismic input (three sets of scalable, three-dimensional stochastically independent inputs); the methodology for seismic evaluation according to the Swiss Directive [2] (storage scheme, dam and foundation classifications, peak acceleration, site spectral response, acceleration-time histories, model verifications, frequency and time-domain analyses, structural, serviceability and stability verifications of the concrete dam, etc.) and the required results (displacements, stresses, strength and stability factors of safety).

   The participants are expected to analyse the data provided and the required results and verifications in light of the Swiss Directive [2] or in light of the

---

1 Percentage values indicate the expected work per phase of the total effort needed to satisfy the benchmark objectives.

national code/international guideline they have chosen to employ. They may introduce additional data, e.g. material parameters, and refine the finite element mesh provided, if required for the purposes of the envisaged dynamic analysis. It is underlined that the current benchmark problem concerns only the concrete dam body verifications and excludes those related to the dam foundation.

2. *Seismic Verifications (25%)*: Static analyses shall be performed considering simplified phased construction (proposal given by formulators) to define self-weight loads, hydrostatic loading and a simplified temperature gradient for the winter and summer conditions taking into consideration the reference contraction joint closure temperatures. The prerequisite condition (in accordance with [2]) for the calibration of the numerical model for thermal and mechanical boundary condition parameters respectively are beyond the scope of this benchmark. Thereafter, seismic analyses are to be performed.

   The Swiss Directive [2] requires that the seismic analysis of a Class I dam should be performed in two main steps. The first step consists in determining and evaluating the dynamic characteristics of the dam-foundation-reservoir system (natural frequencies, natural modes of vibration and participation factors). The second step is performing dynamic analyses in the time domain. These analyses may be linear and/or non-linear; the latter may employ interface models and complex constitutive material laws. The finite element model prepared by the formulators allows for simulating possible non-linear effects due to opening/closing of the contraction joints between the adjacent dam blocks. It is also possible to associate non-linear material models with the concrete and/or rock materials. However, it is up to the participants to refine the basic finite element mesh provided by the formulators, if such non-linear material models require this in order to obtain mesh-independent results.

   As mentioned above, the participants are free to use any national or international guidelines for the seismic evaluation of concrete dams. Nevertheless, they are expected to perform at least the two steps required by [2] for a Class I dam.

3. *Results, evaluations and conclusions (25%)*: The expected results include the structures dynamic characteristics (natural frequencies, natural modes of vibration and participation factors), temporal displacements, principal/Cauchy stresses (vectors and iso-lines), and stability factors of safety at selected points and sections on the upstream and downstream faces of the dam body. The participants can also introduce other evaluation parameters for discussion such as the Flexural Stability Index, Demand Ratios, etc. Finally, the participants may investigate the global stability of a detached rigid block in the top part of the dam.

   High emphasis will be given to the engineering interpretation and analysis of the obtained results in view of the dam's seismic safety.

4. *Proposals for further studies (25%)*: A critical review of the numerical tool and Guideline document employed within the context of the benchmark with proposals and recommendations for further consideration are requested.

   For comparison purposes, or if required by the employed seismic verification code/guidelines, the second step of the seismic verifications, i.e. the dynamic analysis, may be carried out in the frequency domain, if more refined models are deemed necessary to simulate the dam-foundation-reservoir interactions. Finally, hybrid frequency-time domain analyses may also be employed.

Problem Statement

The Luzzone dam is a double-curvature arch dam located in the south-eastern part of Switzerland and has been selected for the benchmark. A photograph of the dam is given in Figure 1.

The problem statement consists of the seismic verification of Luzzone dam only in accordance with Guidelines.
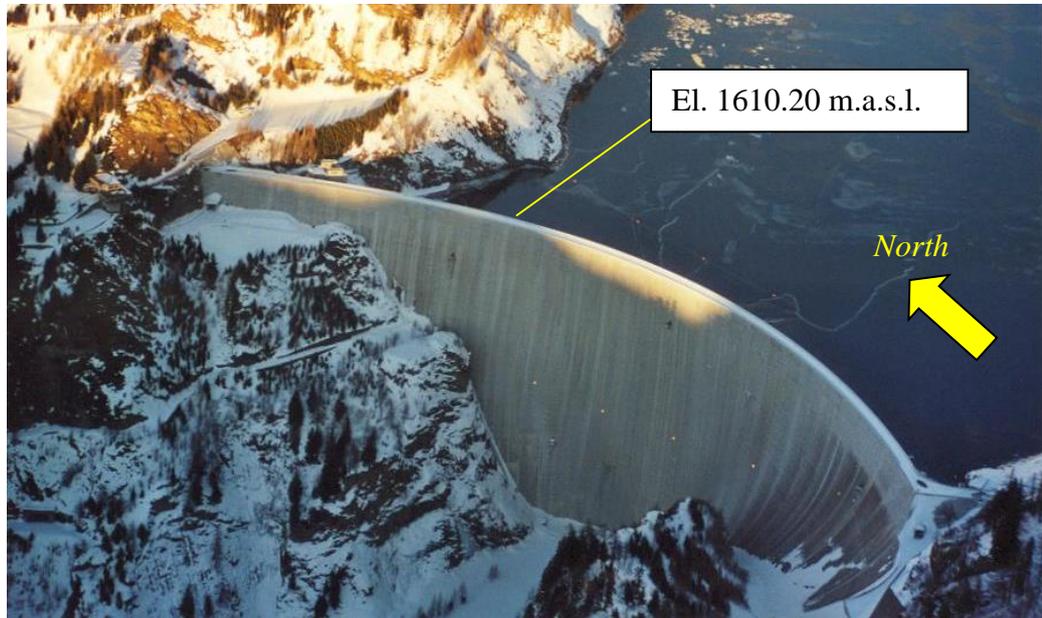
Figure 1 : Luzzone Dam (Switzerland), H = 225 m

The dam was built in the 1960s and heightened in the 1990s. The behaviour of the structure is sound and normal, but presents some interesting aspects for the dam engineering community.

The structure was originally designed as a classic arch dam of parabolic layout until during the construction a family of decompressed joint structures on the left bank opened and provoked an instability which had important consequences on the geometrical definition of the dam and the stability of the abutments. For the upper section of the dam, a geometric rotation was applied. The above figure reveals that the left bank has both an unusual upper elevation abutment and a section closure for the 17 m heightening.

The participants are free to use any national or international guidelines for seismic verification of concrete dams. For those who choose using the Swiss Directives [2], the respective documents are made available in PDF format in French and German languages as indicated in Appendix 1.

According to the Swiss Directives [2], Luzzone dam is a structure of Class 1 whose safety is to be verified for an earthquake of a return period of 10'000 years. The dam is founded on sound rock (diabase); hence its foundation is of Class A.

In general, for a concrete dam of Class 1, the Swiss Directives [2] require the following methodology to be applied:

1. Definition of the seismic excitation:
   - Peak Ground Acceleration (PGA);
   - Response Spectrum of the dam site;
   - Acceleration time histories.
2. Determination of the state of the dam, the geological and geotechnical conditions of its foundation, and the material characteristics of the dam and the foundation.

3. Preparation of a finite element model for seismic verification (geometry, boundary conditions, initial conditions, materials);
4. Analysis of the natural frequencies;
5. Modelling of the operation period loads;
6. Analysis of the dam behaviour during earthquake by means of the direct time-step integration method for three series of three stochastically independent acceleration time histories and linear-elastic materials with viscous damping;
7. Check of the local stability (stresses);
8. Check of the global stability against sliding and overturning;
9. Other verifications (appurtenant structures, abutments, foundation);
10. Conclusions on the seismic safety of the dam;
11. If necessary: design of measures to ensure the seismic safety of the dam.

The participants are expected to perform at least steps (3), (4), (5), (6), (7), (8) and (10), the others are deemed to be **optional**.

Information and data necessary for the participants to perform the seismic verification of Luzzone Dam according to the Swiss Directives or any other chosen Guidelines are supplied in the current document and its appendices, as well as in the input files.

Regarding the seismic input (Point (1) above), the participants are supplied with all the necessary data defined in accordance to the Swiss Directives. However, with exception of the PGA, the participants are free to use a response spectrum and acceleration time histories according to the Guidelines they choose to employ.

Finally, Point (6) may be performed by any other method, as prescribed by Guidelines.

Data Preparation

The participants of the benchmark Theme A are provided with the data listed in Appendix 4. (digital format). The information below gives an overview of the data.

Seismic Excitation

As already mentioned, Luzzone Dam is a structure of Class 1 and its foundation (which consists of sound rock) is of Class A. Therefore, according to [2], the safety of the dam is to be verified for an earthquake of a return period of 10'000 years.

1) Peak Ground Acceleration

The location and the main characteristics of Luzzone Dam are presented in Appendices 2 and 3. As shown in the Seismic Intensity Map of Switzerland, the structure is located in a region for which the estimated intensity of a 10'000-year return period earthquake is 7.7 on the MSK scale. The horizontal component, a_h, of the corresponding Peak Ground Acceleration (PGA) is calculated as follows [2]:

$$\log a_h = 0.26 \cdot I_{MSK} + 0.19 = \ [cm/s^2]$$

Therefore:

$$a_h = 1.56 \ [m/s^2] = 0.16g$$

The Peak Ground Acceleration in the vertical direction is assumed 2/3 of a_h, i.e.

$$a_v = 1.04 \ [m/s^2] = 0.106g$$

2) Response Spectrum of the Dam Site

The site response spectrum defined in [2] is as follows:
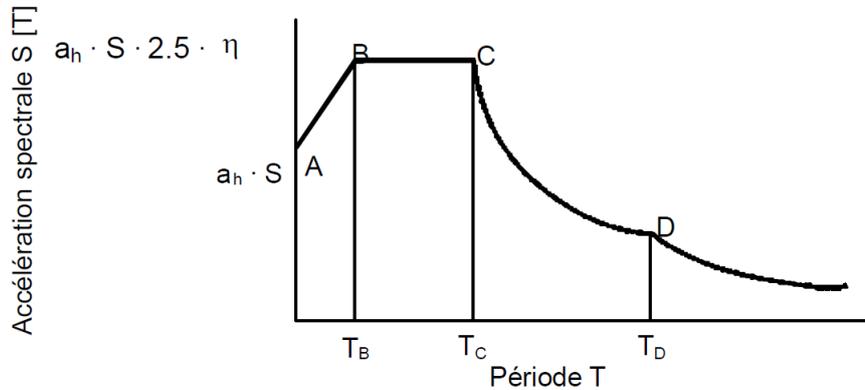
$$S_e(T) = a_h \cdot S \left(1 + \frac{T}{T_B}(2.5\eta - 1)\right) \qquad \text{for } 0 \leq T \leq T_B$$

$$S_e(T) = a_h \cdot S \cdot 2.5\eta \qquad \text{for } T_B \leq T \leq T_C$$

$$S_e(T) = a_h \cdot S \cdot 2.5\eta \cdot \left(\frac{T_C}{T}\right) \qquad \text{for } T_C \leq T \leq T_D$$

$$S_e(T) = a_h \cdot S \cdot 2.5\eta \cdot \left(\frac{T_C \cdot T_D}{T^2}\right) \qquad \text{for } T_D \leq T$$

For foundation of Class A, parameters S, T_B [s], T_C [s] and T_D [s] take the following values:

$$S = 1$$

$$T_B = 0.1 \ s, \qquad T_C = 0.4 \ s, \qquad T_D = 3 \ s$$

Finally, η is calculated from the following formula:

$$\eta = \sqrt{7/(2 + \zeta)}$$

where ζ represents the viscous damping in % of the critical damping. It is suggested to use:

$$\zeta = 5\% \cdot \zeta_{cr}$$

hence:

$$\eta = 1$$

3) Acceleration time histories

Three sets of stochastically independent acceleration time-histories are provided as described in Appendix 4.

The time step is 0.01 second and the total duration is 30.71 seconds giving a total number of 3072 time steps. The peak ground accelerations in the cross valley, vertical and upstream-downstream directions are all equal to 0.1g and Appendices 5, 6 and 7 present the graphs.

The acceleration time histories are compatible to the site spectral response prescribed in the Swiss Guidelines [2] for structures founded on rock and damping equal to 5% of the critical.

The participants are encouraged to define by themselves other acceleration time histories, if the respective Guidelines that they choose to employ provide for a site spectral response and/or damping values that differ from those prescribed in [2].

The scaling factors applied to the acceleration time histories defined in Appendices 5, 6 and 7 are given in the format of *ICOLD_13_BM_Theme_A_Model.fga* data file. Hence, the following peak ground acceleration values shall be applied by all participants:

1. Downstream-upstream (Z - direction):   **+0.160g**
2. Vertically upwards (Y – Direction) :   **+0.106g**
3. Cross-valley direction L - R (X – Direction) **:**   **+0.160g**

The vertical peak ground acceleration is two-thirds (0.6667) of the horizontal components.
If the participants wish to explore the application of the Guidelines that they choose to use in case of strong non-linear behaviour of the structure, they shall scale the acceleration time histories given in Appendix 8 so that the following peak ground accelerations are obtained:

4. Downstream-upstream (Z - direction):   **+0.480g**
5. Vertically upwards (Y – Direction) :   **+0.320g**
6. Cross-valley direction L - R (X – Direction) **:**   **+0.480g**

It is emphasised that multiplying the actual Peak Ground Accelerations defined in accordance to the Swiss Guidelines [2] by a factor of 3.0 is aimed at defining **fictitious loading** conditions whose purpose is triggering the respective Guidelines' provisions (if any) for performing non-linear structural analyses. It is also underlined that this part of the Theme A Problem to be solved by the participants is not mandatory, but only **optional**.

The participants are free to convert the time histories into the frequency domain, but this is not recommended for stability analyses.

Material Characteristics of the Dam and the Foundation

The Swiss Directives [2] prescribe that linear-elastic behaviour is to be associated with the foundation rock and the dam concrete materials. Viscous damping of 5% of the critical can be assumed.

In case no dynamic tests have been carried, [2] specifies that the dynamic characteristics of the materials can be defined from the static ones (obtained by means of tests) by increasing the latter as follows:

- The dynamic modulus of elasticity is obtained from the static one by an increase of 25%:

$$E_d = 1.25 \cdot E_s$$

- Uniaxial dynamic compressive and tensile strength are to be used for the analysis of the local stability (stresses) of the dam, in case linear-elastic analysis is performed and viscous damping is assumed [2]. The uniaxial dynamic strengths can be obtained from the static ones as follows:

  - Uniaxial dynamic compressive strength of concrete:

$$f_{cd} = 1.5 f_c$$

  - Uniaxial dynamic tensile strength of concrete:
    In function of the static tensile strength:

$$f_{td} = 1.5 f_t \leq 4 \, MPa$$

In function of the static compressive strength:

$$f_{td} = 0.1 f_c \leq 4 \, MPa$$

1) Foundation Rock

The dam foundation is composed of homogeneous and massive schist. Neither schistose planes, nor any stratification are present in the foundation rock mass. Its material characteristics are defined as follows:

Table 1 : Rock Foundation Material Properties

Mass Rock Properties	Unit	Value
Static Modulus of Elasticity, E_s	GPa	18.6
Dynamic Modulus of Elasticity, $E_d = 1.25 \cdot E_s$	GPa	23.3
Poisson's Ratio, ν	-	0.20

The foundation is assumed massless.

2) Concrete

The concrete mix of the dam outer zones (upstream and downstream faces, top and base) contains 250 to 280 kg of cement per cubic meter of concrete. The inner zone has 160 to 250 kg of cement.

Concrete quality has continuously been tested during the dam construction, as well as during the dam heightening.
The performed tests reveal that the moduli of elasticity are relatively low: 20 GPa for the old concrete and 18 GPa for the new one.
On the other hand, the compressive strength of the old concrete is 38 MPa (obtained as a mean value) and 32 MPa (also a mean value) for the new concrete used for the dam heightening.
To measure the tensile strength of concrete, flexural strength tests have been carried out. The tests show a flexural strength of 6 MPa for the old concrete and 4.6 MPa for the concrete of the dam heightening. As reported in [5], the uniaxial tensile strength of concrete is between 47% and 62% of its flexural strength. Assuming that for Luzzone dam the ratio between uniaxial tensile strength and flexural strength is 1:2, we obtain:

Uniaxial static tensile strength of the old concrete:

$$f_{t,old} = 3\ MPa$$

Uniaxial static tensile strength of the new concrete:

$$f_{t,new} = 2.3\ MPa$$

Table 2 : Dam Concrete Material Properties

Mass Concrete Properties	Unit	Value	
		Old Concrete	New Concrete
Density, ρ	t/m^3	2.5	2.4
Static Modulus of Elasticity, E_s	GPa	20	18
Dynamic Modulus of Elasticity, $E_d = 1.25 \cdot E_s$	GPa	25	22.5
Poisson's Ratio, ν	-	0.18	0.18
Thermal expansion, α	1/°C	10^{-5}	10^{-5}
Static Compressive Strength, f_c	MPa	38	32
Dynamic Compressive Strength, $f_{cd} = 1.5\ f_c$	MPa	57	48
Static Tensile Strength, f_t	MPa	3	2.3
Dynamic Tensile Strength, $f_{td} = 1.5\ f_t \leq 4\ MPa$	MPa	4	3.5

Geometry and Finite Element Mesh

The arch dam has a crest length of 510 m and a maximum height of 225 m. The thickness of the crown section varies from 4.55 m at the crest to 36 m at the base.

The shape of the dam is defined by parabolic curves in both the horizontal and the vertical directions and features thickening of the arches towards the abutments. The geometric model of the dam and its foundation has been established on the basis of the as-built drawings and the topographic plans of the site.

The domain of the foundation modelled extends from the dam to a distance of approximately two times the dam height. Hence, it is 760 m long, 1200 m wide and 435 m thick below the lowest point of the dam base. The reservoir has been modelled to a distance of 700 m upstream from the crown cantilever in order to enable considering the compressibility of water and the dynamic dam-reservoir interaction.
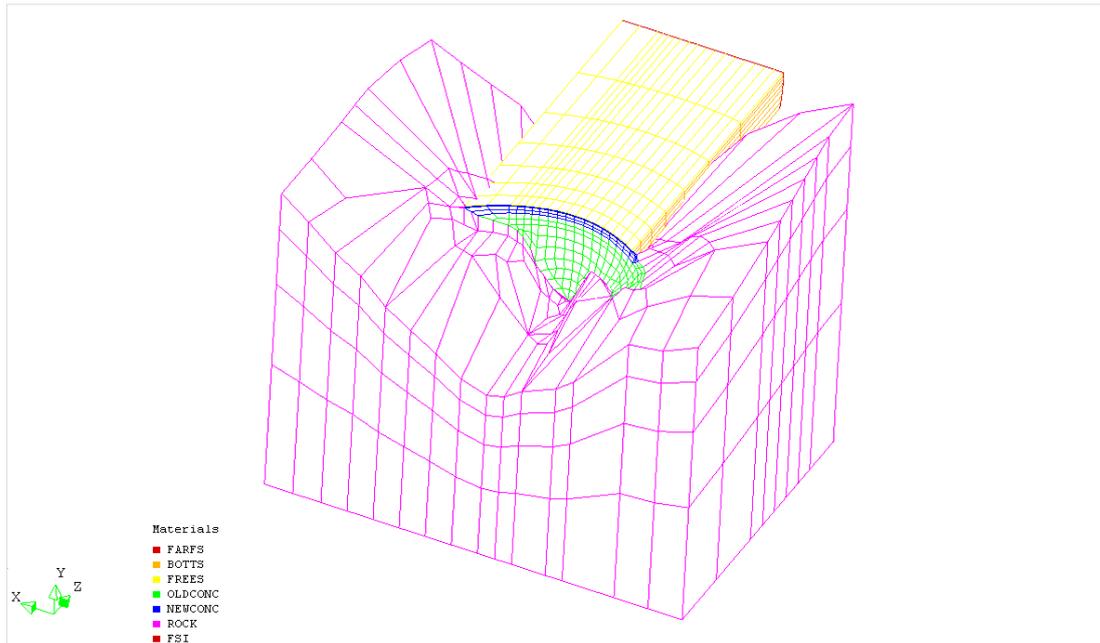
Figure 2 : Dam – Foundation - Reservoir Finite Element Mesh

The finite element mesh has been created by using quadratic elements. The mesh has 3102 elements and 12419 nodes.

The main data is in text (ASCII) format with free formatting and can be found in *ICOLD_13_BM_Theme_A_Model.fga.* The model has been generated using the DIANA software package for which more information can be found on the web (www.tnodiana.com).

The file has been structured in such a way as to facilitate modelling, analyses and evaluation of results. The detailed description of the *ICOLD_13_BM_Theme_A_Model.fga* file is given in Appendix 9.

For result presentation purposes, Appendix 10 provides the participants with three standard cross-sections.
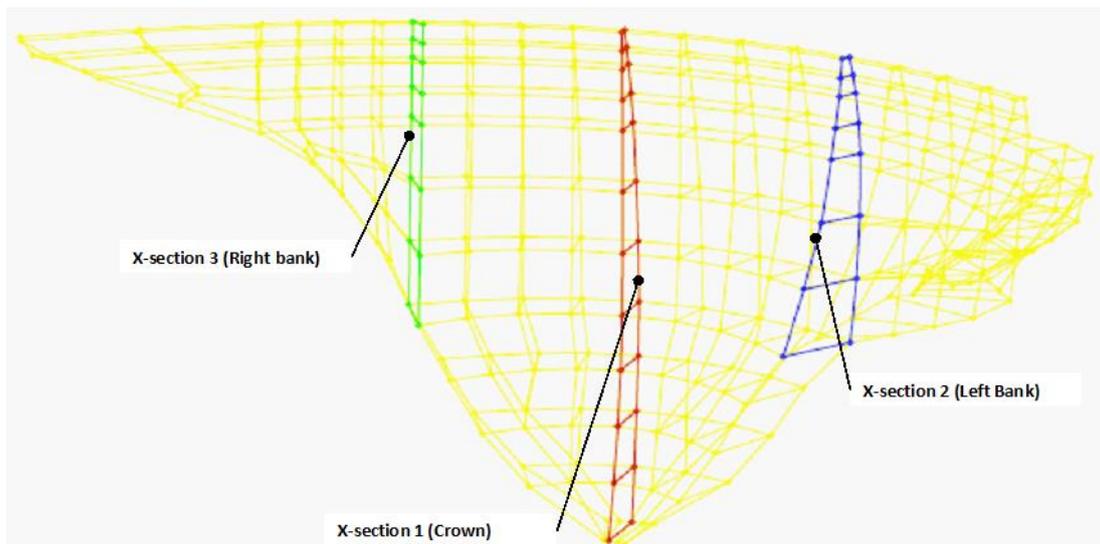
Figure 3 : Cross Sections Location and Definition

Special importance is given to the interface between the dam and the foundation which is named *INFACE*. The labelled geometrical points (*entity name*) are given in Appendix 11 with global

coordinate values (X, Y, Z).

Operation Period Static Loads

The participants have to consider the following static loads:

- Self-weight;
- Hydrostatic pressure for Normal Water Level at El.1606;
- Silt pressure;
- Thermal gradients with respect to the temperature of joint grouting for
  - winter temperature conditions; and
  - summer temperature conditions.

3) Self-weight

The construction of the dam was carried out in four periods (1960, 1961, 1962 and heightening in 1999). The finite element model provided in *ICOLD_13_BM_Theme_A_Model.fga* allows for modelling the construction phases corresponding to these periods, as shown in Figure 4.
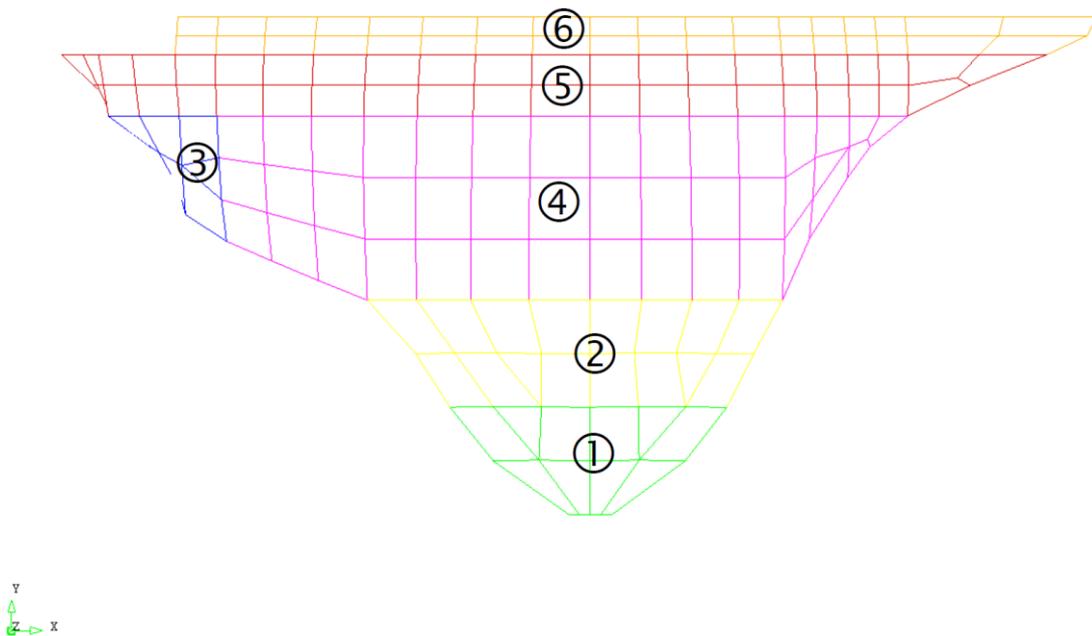
Figure 4 : Modelled Construction Phases

4) Hydrostatic Pressure

The hydrostatic pressure is to be applied on the upstream face of the dam and has to correspond to the Maximum Normal Operating Water Level at El.1606 m a.s.l. It is underlined that the left part of the dam has an unusual upper elevation abutment and a section closure for the 17 m heightening. Therefore, the hydrostatic pressure should be applied only on the dam's upstream face in contact with water, as defined in the finite element model file provided and as shown in Figure 5:
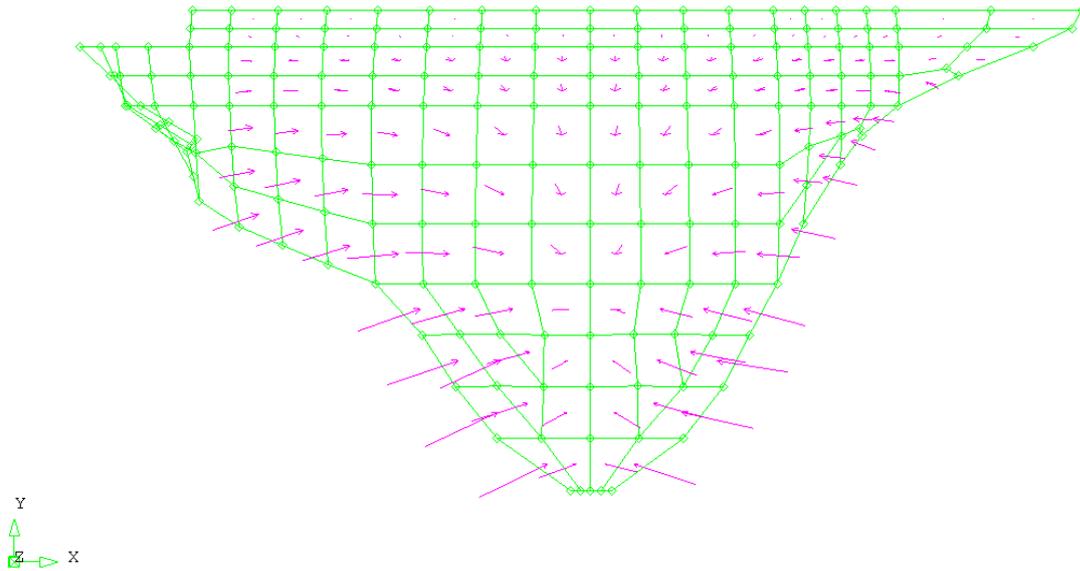
Figure 5 : Hydrostatic Pressure on the Upstream Face for NWL at El.1606

5) Silt Pressure
The silt pressure is to be applied on the wet surface of the upstream face of the dam and has to correspond to a level at El.1440 m a.s.l.
The buoyant density of the silt is estimated to amount to 400 kg per cubic meter.

6) Thermal gradients
The thermal gradients have been determined with respect to the dam body temperature field at the time of grouting of the contraction joints, Figure 6. The load cases considered correspond to an earthquake occurring in wither and an earthquake occurring in summer.
Figure gives the profile of annual variation of the temperature on the upstream and the downstream face of the dam, which take into account the water level variation, as well as the sun exposure.
The calculated thermal gradients within the dam body for the "winter" and "summer" conditions are given in free ASCII text format, as indicated in Appendix 11. It is noted that the thermal gradients are given for each node of each element of the dam-foundation system for the finite element mesh generated by the formulators. If, however, the participants wish to use a different finite element mesh, they will have to calculate themselves the thermal gradients using the information provided in Figure 6 and Figure 7.
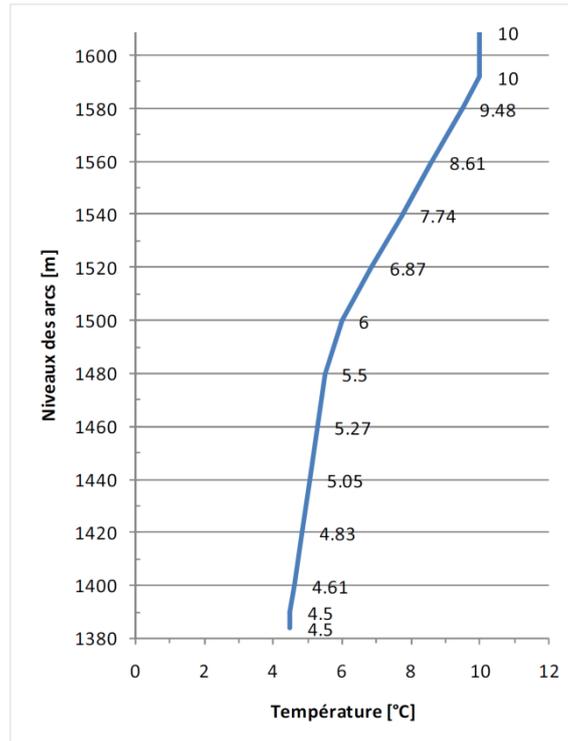
Figure 6 : Temperatures of contraction joint grouting
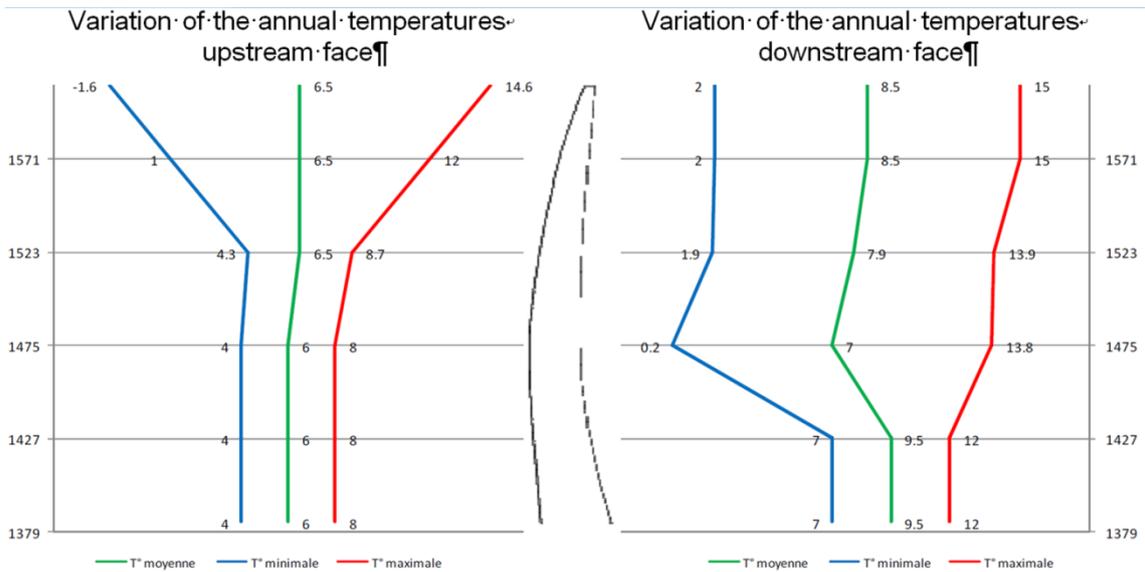
Figure 7 : Profile of variation of the annual temperatures on the upstream face (left) and on the downstream face (right)

Methodology

Modelling
Based on the data provided and as described in the preceding chapter, the participant is asked to model the dam and foundation structure using finite elements and/or any other numerical modelling technique (for example discrete elements). The extent of the foundation has been defined to minimise constraint effects (static and dynamic loading) for different degrees of restraints (translations and rotations).

The structure of the mesh using for example interface elements at the dam's contraction joints shall be the choice of the participant.

It is underlined that the participant is free to modify the mesh by refining it, changing the element types, etc.; however, **the geometry of the problem shall remain unchanged**.

The dam body has been separated into six *construction stages* to allow a reasonable computation of the self-weight loading.

Material Parameters

The material parameters for the mass rock of the foundation and the concrete of the dam are to be defined in accordance with Table 1 and

Table 2, respectively. Uniform properties are assumed for the entire rock foundation for simplicity and the concrete dam shall be treated only as mass concrete (no facing and/or interface concrete).

The influence of softening elements along the upstream dam-rock interface can be defined freely if the participant desires to reduce the effects of stress discontinuities. Such elements are normally defined just in front and/or as part of, the grout curtain (first top layer of foundation elements).

Boundary Conditions
The boundary conditions for the finite element model are defined in accordance with the model data file and selected such as to minimise their influence on the results for static and dynamic loading conditions.

Loading
The static loading (self-weight, full hydrostatic pressure due to Normal Water Level at El. 1606 m a.s.l., Silt Load at El. 1440 m a.s.l. and loading due to summer and winter temperature differences) shall be computed and applied as initial conditions for the dynamic loading. The latter shall be applied in accordance to the method chosen to be employed (direct integration in the time domain, frequency domain analysis, hybrid frequency – time domain analysis, etc.) and shall consider the dam-reservoir interaction. The participant is free to choose the method for modelling the effects due to the dam-reservoir interaction.

Approach to the Analyses
7) Analysis of the Natural Frequencies
The Swiss Directives [2] recommend before all, performing an analysis of the natural frequencies in order to obtain a solid knowledge of the defined numerical model, as well as to enable a preliminary evaluation of the dam dynamic behaviour.
8) Modelling of Load Cases and Load Combinations
The participants are asked to model the load cases and load combinations shown in Table 3.

Table 3: Loads and Load Combinations

Load combinations		Static		Dynamic		
Loads		SU0	SU2	DE2		
Self-weight		1	1	1	1	1
Hydrostatic pressure (El.1606 m a.s.l.)		1	1	1	1	1
Silt pressure		1	1	1	1	1
Temperature gradients	Summer		1	1	1	1
Earthquake	Series 1			1		
	Series 2				1	
	Series 3					1

As indicated above, the participants will have to model three (3) dynamic load combinations to investigate the seismic safety of the dam.

9) Analysis of the Dam Behaviour during Earthquake
The participants shall carry out the numerical calculations on the supplied finite element model of the dam-reservoir-system for the specified load combinations. Based on the results obtained from these analyses, the structural safety shall be evaluated by checking the local and the global stability of the dam.

a) Analysis of the Local Stability
The local stability is checked by comparing the calculated stresses against the strength of the concrete material as defined by the supplied input data and/or in accordance with the employed guidelines. The local stability is guaranteed if the evaluated maximum compressive and tensile stresses do not exceed the corresponding strengths.

b) Analysis of the Global Stability
The global stability concerns the safety against sliding and the safety against overturning of the whole structure or of a part of it. For Luzzone dam, it is proposed to verify the stability of a part of the crown cantilever assuming that during the earthquake the vertical joints on both sides of the block can open, as well as that a horizontal crack can propagate through the whole thickness of the block.
This verification shall consider the self-weight, the hydrostatic pressure, the uplift pressure at the crack (triangular pressure distribution is to be admitted), and the earthquake-induced forces (horizontal and vertical components). It is noted that the thermal loads do not contribute to the stability as the joints are assumed to be open.

10) Conclusion on the Seismic Safety
Based on the results obtained from the analysis of the dam behaviour during earthquake, conclusions on the seismic safety of the structure can be drawn.

Requested Results

Natural Frequencies and Mode Shapes
The participants are required to calculate the first 12 natural frequencies (eigenfrequencies) of the dam-foundation system for the cases of empty and full reservoir.
In addition, it is required to present the first 12 dam mode shapes for the case of full reservoir. In order to evaluate the contribution of the natural modes of vibration for the structure's response in the cross-stream, stream and vertical directions, the participants may present and discuss the participation factors for modes 1-12.
The corresponding results shall be submitted according to the format given in Appendix 12.

Displacements
11) Displacement Time Histories
The participants are asked to present the radial displacement (Z component) time histories at the crest of the central section of the dam (for point with X=0, Y=1609, Z=-29.145) due to the investigated dynamic combinations (the displacements due to self-weight should be set to zero).

12) Displacement Envelopes at Cross Sections
In addition, it is required to present the minimum and the maximum radial displacement envelopes, as well as the static load displacements (without self-weight) for the centrelines of Cross Section 1 (Crown), Cross Section 2 (Left Bank) and Cross Section 3 (Right Bank), see Figure 2. An example for presentation of radial displacements envelopes for an arch dam cross section is given in Figure 8.
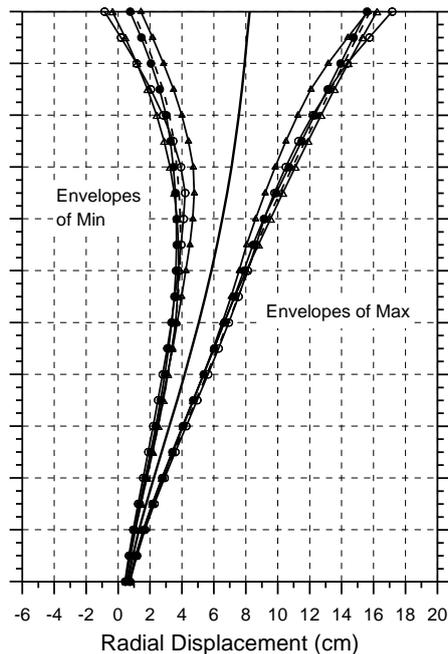
Figure 8: Example Presentation of Radial Displacement Envelopes for a Section of an Arch Dam

Stresses
The following sign convention for stresses shall be used: compressive stresses have a negative value and tensile stresses have a positive value.

13) Stress Envelopes on U/S and D/S Faces
In order to evaluate qualitatively the obtained results, it is asked to present the envelopes of the

computed maximum and the minimum principal stresses for the upstream and for the downstream faces of the dam. The stress envelopes should contain the maxima / the minima obtained from all the investigated dynamic load combinations.

14) Stress Envelopes at Cross Sections

Envelopes of the minimum and maximum hoop and cantilever stresses on the upstream and on the downstream lines of Cross Section 1 (Crown), Cross Section 2 (Left Bank) and Cross Section 3 (Right Bank) are requested to be presented for the investigated dynamic load combinations. The graphs shall also include the results for the corresponding static load combination. An example for the presentation of stress envelopes for an arch dam vertical cross section is given in Figure 9.
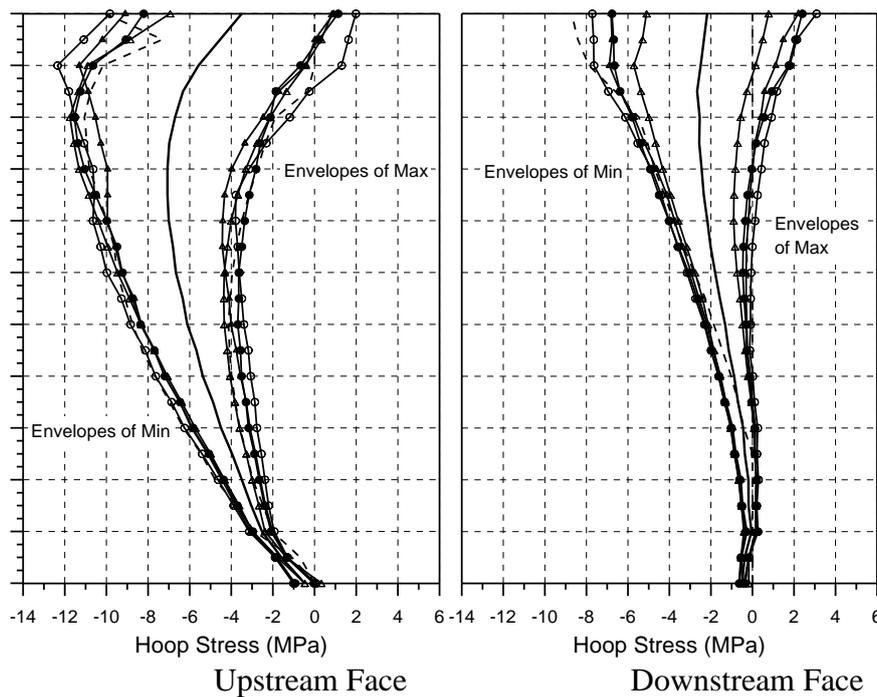
Figure 9 : Example Presentation of Hoop Stress Envelopes for a Section of an Arch Dam

15) Stress Values at Selected Points

The participants are asked to present the maxima and the minima of the computed stresses at selected characteristic points on the dam faces. Ten points have been chosen for each face of the dam (twenty in total) as follows: three at the crest, two in the upper part of the face, two on the left abutment, two on the right abutment and one near the base of the dam. The point coordinates are given in Table 4 and the location of the points is shown in Figure 10.
The results shall be submitted following the table given in Appendix 13.

Table 4: Coordinates of the Points Selected for Stress Analysis

Zone	Upstream Face				Downstream Face			
	Point	X	Y	Z	Point	X	Y	Z
Crest – Left	A	-98.131	1609	-47.793	A'	-96.185	1609	-51.875
Crest – Centre	B	0	1609	-29.145	B'	0	1609	-33.654
Crest – Right	C	84.225	1609	-41.937	C'	79.121	1609	-45.152
Dam Upper Part – Left	D	-52.128	1564.4	-20.648	D'	-47.968	1564.4	-35.948
Dam Upper Part – Right	E	44.469	1564.4	-18.716	E'	40.312	1564.4	-34.193
Abutment Upper – Left	F	-165.7	1545.6	-84.024	F'	-151.19	1551.2	-107.31
Abutment Upper – Right	G	124.13	1554.1	-50.259	G'	116.58	1554.1	-67.933
Abutment Lower – Left	H	-99.273	1481.5	-44.278	H'	-80.397	1481.5	-76.978
Abutment Lower – Right	I	86.112	1481.5	-35.034	I'	72.832	1481.5	-69.382
Dam Lower Part	J	0	1409.1	-4.3636	J'	0	1409.1	-35.262
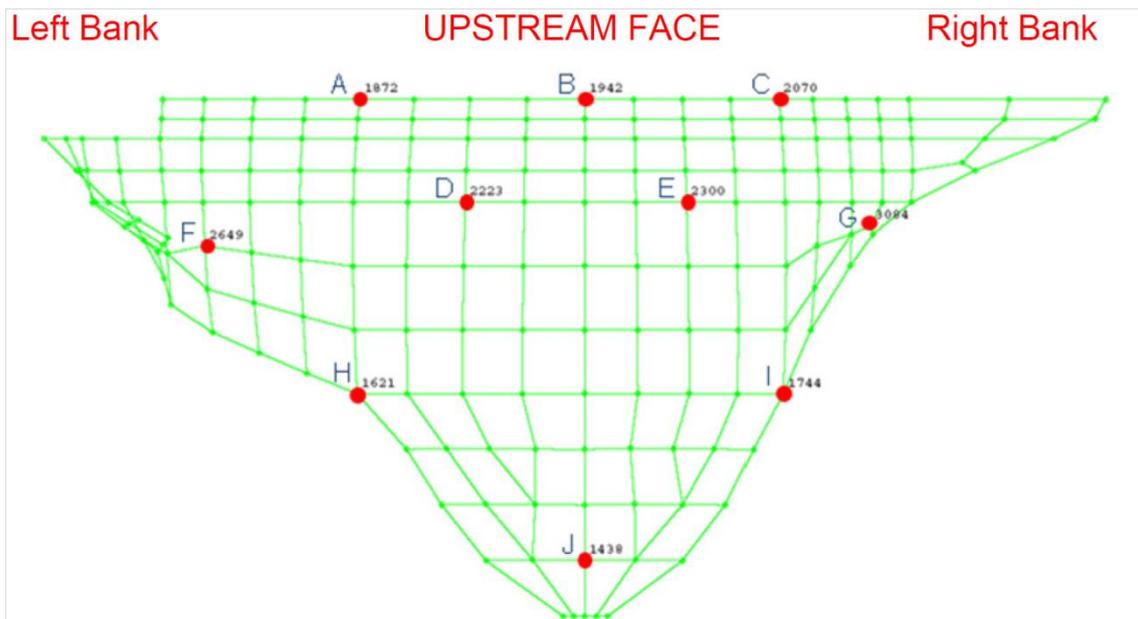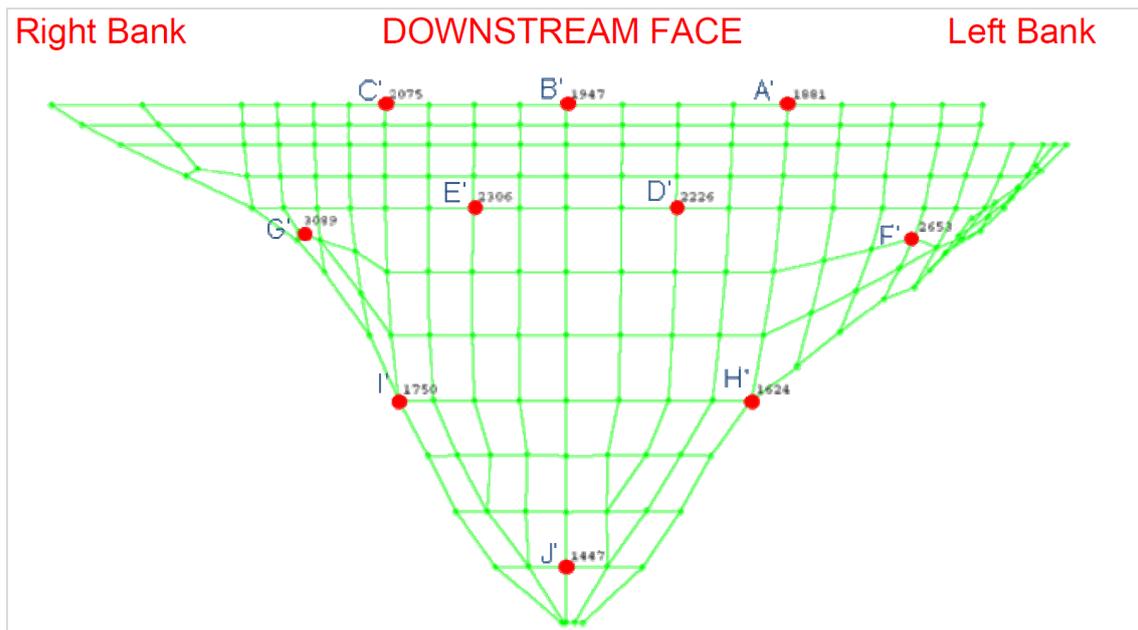
Figure 10 : Identification of the Analysed Zones on the Dam Upstream and Downstream Faces

16) Stress Time Histories
Is it requested to present the time histories of the maximum and minimum principal stresses at Points D, E, D' and E'.

Rocking Block Stability

The results for the factors of safety against sliding and overturning of a so called "rocking block" characterised by opening of the contraction joints and the formation of a horizontal crack that can propagate through the whole thickness of the block as indicated in Figure 11, shall be given according to the table in Appendix 14. The results shall be given for four different levels of the assumed horizontal crack, namely at El. 1600.5 (h = 8.5 m), El.1592 (h = 17 m), El.1578.2 (h = 30.8 m) and El.1564.5 (h = 44.5 m).
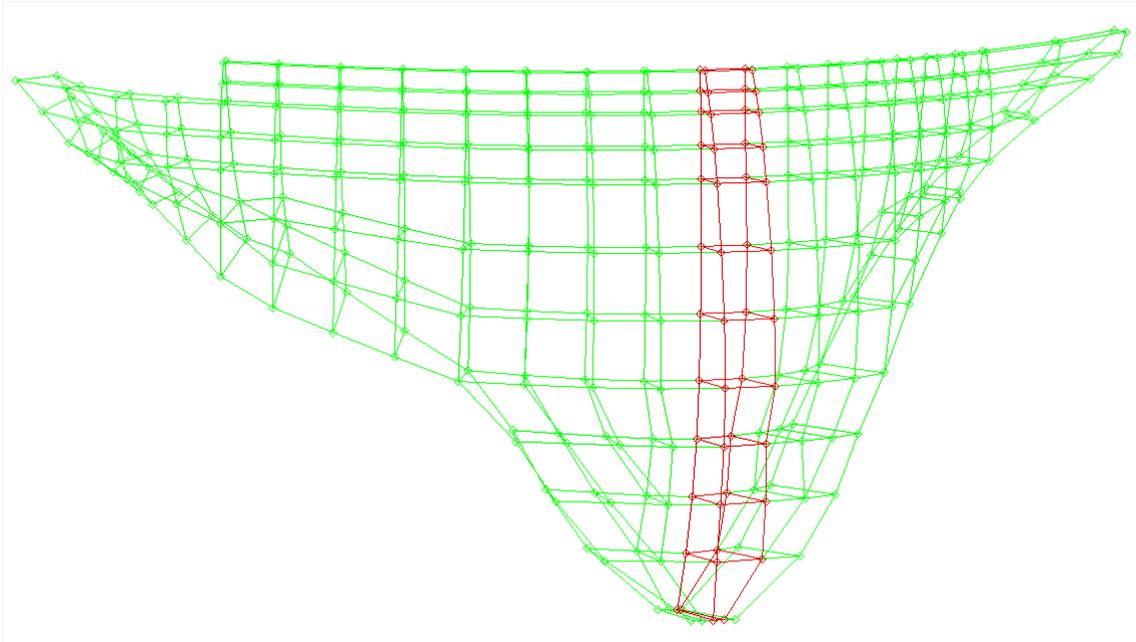
Figure 11 : Dam Cantilever for Rocking Block Stability Investigations

The shear strength at the base of the rocking block shall be assumed as follows:
$$\varphi = 63°, c = 0$$

Evaluation of the Dam Safety

The participants are requested to interpret and analyse the computed displacements, stresses and rocking block stability of the dam and to conclude on the seismic safety of the structure.
It is important that a critical review is made of the software tool and the Guideline used in the studies and hence, the participants are requested to make proposals for further investigations and/or benchmarks.

Time framework

The estimated effort from the participants for the basic studies (without options) ranges from 2 to 3 weeks. The time devoted to solve all seismic analyses (with options – non-linear dynamic analyses, etc.) should not in any case be longer than two months.

References

[1] Sécurité des ouvrages d'accumulation. Directives de l'OFEG, rapports de l'OFEG, série Eaux, version 1.1, novembre 2002.

[2] Sécurité des ouvrages d'accumulation. Documentation de base pour la vérification des ouvrages d'accumulation aux séismes, rapports de l'OFEG, série Eaux, version 1.2, mars 2003.

[3] Guidelines for use of numerical models in dam engineering. ICOLD Bulletin 155, 2013.

[4] Tenth Benchmark Workshop on Numerical Analysis of Dams, September 16-18, 2009 Gennevilliers, Paris, France.

[5] Domone, Peter; Illston, John. Construction Materials: Their Nature and Behaviour, Fourth Edition. 2010.

Acknowledgements

Appendices

(available on request from the organisers)

Appendix 1.   List of Supplied Files of the Swiss Directives (in PDF format)
Appendix 2.   Luzzone Arch Dam Location
Appendix 3.   Luzzone Arch Dam Characteristics
Appendix 4.   List of Supplied Data (ASCII Text Format)
Appendix 5.   Acceleration Time Histories
Appendix 6.   Series 1 Acceleration Time Histories Graphs
Appendix 7.   Series 2 Acceleration Time Histories Graphs
Appendix 8.   Series 3 Acceleration Time Histories Graphs
Appendix 9.   Description of Geometry and Finite Element Model Data Structure and Formatting
Appendix 10.   Luzzone Dam Model - Cross Sections Locations and Definitions
Appendix 11.   Luzzone Dam Model - Interface Point numbering and global coordinates (General Overview)
Appendix 12.   Luzzone Dam - Calculated Factors of Safety of a Rocking Block
Appendix 13.   Luzzone Dam - Calculated Stresses in MPa at Selected Points on the Upstream and Downstream Faces
Appendix 14.   Luzzone Dam - Rocking Block Stability Analysis Results

ICOLD 13th Benchmark Workshop on Numerical Analysis Theme A: Seismic Safety Evaluation of Luzzone Dam

Naji-Mahalleh Nasser[1]

[1]*Tablieh Construction Company, Tehran, Iran*

ABSTRACT: The seismic safety of the 225 m high Luzzone arch dam in Switzerland is evaluated for a Safety Evaluation Earthquake (SEE) with a return period of 10,000 years and estimated intensity of 7.7 on the MSK scale. Fluid-structure interaction analysis is performed to assess linear dynamic stresses. Potential-based compressible fluid elements are utilized to model dam reservoir. Safety evaluation concerns satisfaction of local stability as well as global stability. Local stability control is made by comparing compressive and tensile stresses with the specified uniaxial strengths. Furthermore, alternative tensile strength criteria is set forth and use of concrete biaxial failure envelope to assess local safety factors is discussed. Global stability assures safety against sliding and overturning of a detached block. Due to development of high dynamic arch stresses in crest central part, grouted contraction joints certainly would open and monolithic behavior of dam wall fails and arch stresses are released leading to a few free standing blocks with high tensile cantilever stresses at the base. This leads to development of horizontal cracks on the lifts which are weaker in tensile strength as compared with mass concrete. The detached block must remain stable during and following seismic event. Local stability checks for static load combinations are found satisfactory. Minor damages are expected in seismic events but global stability of investigated block is still acceptable.

E-mail: Naji@Tablieh.com

Introduction

The intention of ICOLD 13th Numerical Benchmark Workshop is to perform the seismic safety evaluation of a Class I concrete arch dam according to Swiss Guidelines. The Luzzone dam that is located in the south-eastern part of Switzerland has been selected for the benchmark. The dam was built in 1960s, heightened by 17 m in 1990s and has a classic parabolic layout. Heightened dam has a crest length of about 510 m and a concrete volume around 1.4×10^6 m^3. The so-called Lombardi's boldness coefficient ($\lambda = S^2/hV$) that gives a measure of dam slenderness is calculated about 12.0 and is well below the limit value ($\lambda_{min} = -0.05h + 25$) of 13.8. In the following, the safety evaluation analysis procedures shall be discussed in broad details.

Load Combinations

Individual load cases are described in the following and consist of staged Self-weight (SW), Hydrostatic Pressure (HSP), Silt Pressure (SP), Thermal gradient (dTS) and mass-proportional seismic (MCE) loads. As thermal gradient, only summer temperature condition is considered. Results are provided for three load combinations designated as SU0 (SW+HSP+SP), SU2 (SW+HSP+SP+dTS) and DE2 (SW+HSP+SP+dTS+MCE). SU stands for Static Usual and DE for Dynamic Extreme load combinations, respectively.

Self-weight

An 11-staged self-weight simulation is carried out (refer to Fig. 8). Indeed, it is assumed that each stage corresponds to one lift of concrete. This fictitious lift is taken equal to the height of one row of finite elements. The concrete of each lift (one stage) is assumed to be placed simultaneously. The element birth option is adequately utilized to resemble addition of finite elements, i.e., concrete lifts to the whole model [1]. At the end of each stage (lift), the dam part located below the lift top elevation is assumed to be totally grouted and behaves monolithically.

Hydrostatic Pressure

It is applied only over wet part of the dam water face assuming reservoir at elevation 1606 corresponding to maximum normal operating condition. Water unit weight is taken 9.81 kN/m^3.

Silt Pressure

The saturated silt load on water face of dam is applied as an equivalent fluid with an effective (buoyant) density of 400 kg/m^3. The silt elevation of reservoir is taken at 1440.

Thermal Gradients

Thermal gradients within dam body for summer condition is submitted by Formulators. The closure temperature is assumed to vary with dam height in range of 4.5~10 ˚C.

Seismic Excitations

Regarding Swiss Guidelines, since the structure is of Class 1 and its foundation is of Class A sound rock (diabase), thus, the dam safety should be verified for an earthquake of a return period of 10,000 years. Regarding dam location, the estimated intensity is taken 7.7 on the MSK scale and corresponding Peak Ground Acceleration (PGA) in horizontal and vertical directions are calculated as a_h=1.56 m/s^2 and a_v=1.04 m/s^2 (a_v=2/3a_h), respectively. Site specific design spectrum (ξ=5%) is defined according to Swiss Guidelines and corresponding compatible acceleration time histories are derived. Three independent series of artificially generated acceleration records (each with three components and PGA around 0.1g) are provided by Formulators. These records are scaled to give rise to the specified PGA values. The scaled horizontal (along stream) component of Series 1 and its response spectrum are shown in Fig. 1.
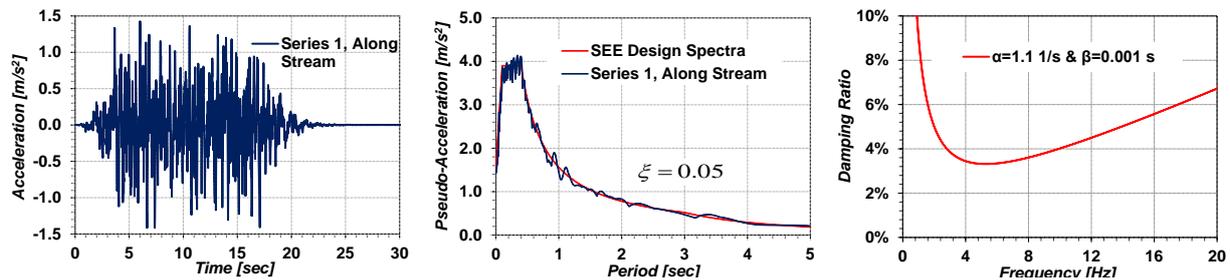
Fig. 1: SEE Design Spectra and Rayleigh Damping Coefficients

Material Properties

Based on Swiss Guidelines, linear elastic material behavior is assumed for rock foundation (massive schist) and concrete. The static modulus of elasticity of rock is assumed E_s=18.6 GPa. Its dynamic modulus of elasticity is taken E_d=1.25E_s and Poisson's ratio v_r=0.2. Considering test results, for old concrete it is obtained E_s=20 GPa and for new E_s=18 GPa. Dynamic modulus of elasticity is assumed E_d=1.25E_s. The Poisson's ratio is taken v_c=0.18 and thermal expansion coefficient α=10^{-5} 1/˚C. Compressive strength of old concrete is obtained f_c=38 and for new f_c=32 MPa. Dynamic compressive strength is taken f_{cd}=1.5f_c. Uniaxial static tensile strength (taken equal to 50% of flexural strength) of old and new concrete are taken f_t=3 and f_t=2.3 MPa, respectively. Uniaxial dynamic tensile strength is taken equal to f_{td}=1.5f_t≤4 MPa.

In Iran, it is a common practice to use a 2/3 power relation proposed by Raphael [2] to assess static (actual) tensile strength of concrete as f_t=0.32$(f_c)^{2/3}$. This relation is obtained from splitting tension test results. Also, in order to find local safety factors a biaxial strength diagram (Fig. 9) given originally by Kupfer-Gerstle [3] and has been improved by Chen is utilized [4].

Finite Element Model

Iso-parametric 20-node elements are incorporated to idealize dam and foundation. Wedge shaped 15-node prism elements utilized by Formulators are transformed to degenerated forms of the general 20-node brick elements with some specific nodes made coincident. The so-called spatial isotropy corrections are imposed on the related interpolation shape functions of the degenerated elements [1]. The direction of global Y and Z-axes are changed as compared with model provided by Formulators (Fig. 2). Now the Y-axis is along river flow pointing towards downstream and coincident with dam reference plane and the Z-axis is pointed upward. As per ICOLD proposals, massless foundation with no radiation damping and wave propagation effects is adopted. Fully restrained boundary conditions are imposed on the boundary surfaces. The stresses are calculated at position of 3×3×3 Gaussian quadrature points and are then assigned directly to nearby nodal points (Fig. 2). Later, averaged nodal stresses are calculated for each element group. The orthogonal stresses in form of arch (hoop) and cantilever are defined in tangential plane to dam surface with arch stresses aligned in horizontal direction.

Potential-based 3D fluid elements are used to idealize the impounded reservoir. It is assumed that the fluid is invicid and irrotational with no heat transfer. Also, fluid displacements are relatively small and no actual fluid flow occurs. To couple structural elements of dam wall with potential-based fluid elements 3D 8-node fluid-structure interface elements are used. Also, the bottom and sides of reservoir are covered with interface elements with all displacement DOF of nodes are set as fixed.

For Luzzone dam the Ω-criteria (water compressibility significance parameter) is found about $\Omega=0.9$. The Ω-criteria is defined as the ratio of fundamental frequency of impounded reservoir to the fundamental frequency of dam alone ($\Omega=\omega_r/\omega_d$). Concerning Swiss Standards, only for $\Omega>1.4$ (US Corps $\Omega>2$) the incompressible fluid assumption in the model is acceptable. Hence, fluid is treated as compressible but with infinitesimally small velocity and density changes. Reservoir level was set at 1609 and water bulk modulus K= 2073.6 MPa.

The energy loss capability of reservoir bottom and sides are ignored. Thus, no wave absorption occurs on these surfaces and in fact they are treated as non-absorptive full reflective boundaries ($\alpha=1$). A significant mitigating effect is expected in dam dynamic response by considering compression wave absorption at reservoir boundaries.

Planar infinite potential interface boundary conditions (radiation type) are imposed at far end of reservoir to resemble zero pressure and velocity at infinity. This allows outwards-going waves to be propagated into the infinite fluid region without reflection [1]. Effect of gravity waves was also neglected by prescribing free surface nodes of reservoir as fixed ($\varphi=0$).
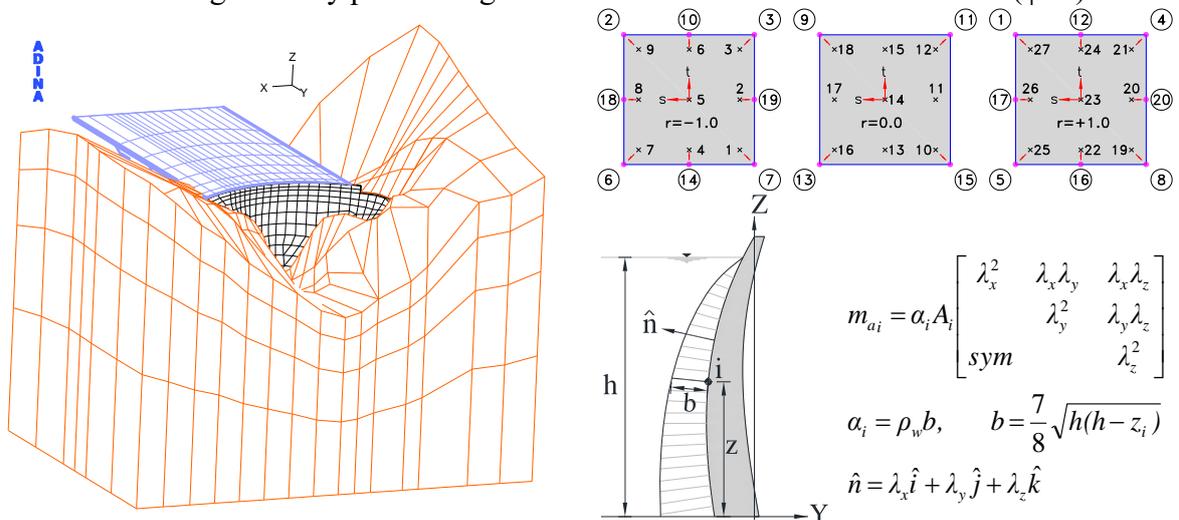
Fig. 2: FE Model, 3×3×3 Gauss Points and Generalized Westergaard Pressure

$$m_{ai} = \alpha_i A_i \begin{bmatrix} \lambda_x^2 & \lambda_x \lambda_y & \lambda_x \lambda_z \\ & \lambda_y^2 & \lambda_y \lambda_z \\ sym & & \lambda_z^2 \end{bmatrix}$$

$$\alpha_i = \rho_w b, \qquad b = \frac{7}{8}\sqrt{h(h-z_i)}$$

$$\hat{n} = \lambda_x \hat{i} + \lambda_y \hat{j} + \lambda_z \hat{k}$$

Analysis Results

Frequencies and Mode Shapes

The eigen value analysis is performed in order to find out a limited number of lower natural frequencies and vibration mode shapes of undamped free vibration of the dam-foundation-reservoir system. In Tab. 1, natural vibration frequencies are listed for empty and full reservoir conditions. For latter, frequencies are given for two separate scenarios. The 1st one corresponds to incompressible fluid which is accomplished by using Generalized Westergaard (GWG) added mass concept (Fig. 2) introduced by Kuo [5]. The 2nd one assumes fluid as a compressible medium and following reservoir discretization performs a Fluid Structure Interaction (FSI) analysis [1]. For GWG case, modes 2 and 4 (both symmetric) have the largest contributions and together excite about 50% of total mass in the along-stream direction (Y). The first 12 vibration mode shapes by FSI analysis and full reservoir condition are illustrated in Fig. 3.

Tab. 1: Eigen Frequencies and Modal Participation Factors

Mode	Empty Reservoir				Full Reservoir				
	Frequency	Effective Mass Percentage [%]			Frequency [GWG]	Effective Mass Percentage [%]			Frequency [FSI]
	f [Hz]	Cross-Stream X	Along-Stream Y	Vertical Z	f [Hz]	Cross-Stream X	Along-Stream Y	Vertical Z	f [Hz]
1	1.945	6.73%	2.44%	0.00%	1.155	7.28%	5.91%	0.30%	1.445
2	2.014	1.21%	25.67%	0.97%	1.194	3.44%	26.96%	0.21%	1.496
3	2.941	0.07%	6.30%	0.43%	1.744	0.18%	7.48%	0.00%	2.092
4	3.600	0.02%	16.16%	5.60%	2.101	0.14%	22.86%	0.77%	2.243
5	3.892	0.05%	0.54%	0.00%	2.310	0.40%	0.43%	0.01%	2.332
6	4.374	36.08%	0.10%	0.49%	2.675	14.16%	0.00%	0.07%	2.757
7	4.495	0.00%	5.69%	66.14%	2.939	0.04%	1.36%	0.08%	3.118
8	4.915	1.68%	1.25%	0.74%	3.206	0.12%	3.79%	0.03%	3.302
9	5.185	26.66%	1.09%	1.06%	3.571	0.06%	7.82%	2.10%	3.379
10	5.611	0.13%	2.91%	1.02%	3.627	0.45%	0.44%	0.34%	3.860
11	6.019	0.37%	2.36%	0.16%	4.082	4.38%	0.52%	0.00%	4.039
12	6.062	0.56%	5.64%	0.04%	4.331	1.93%	0.96%	59.88%	4.239
	Σ	73.56%	70.16%	76.66%	Σ	32.58%	78.53%	63.79%	

MODE 1, F 1.445   MODE 2, F 1.496   MODE 3, F 2.092   MODE 4, F 2.243
MODE 5, F 2.332   MODE 6, F 2.757   MODE 7, F 3.118   MODE 8, F 3.302
MODE 9, F 3.379   MODE 10, F 3.860   MODE 11, F 4.039   MODE 12, F 4.239
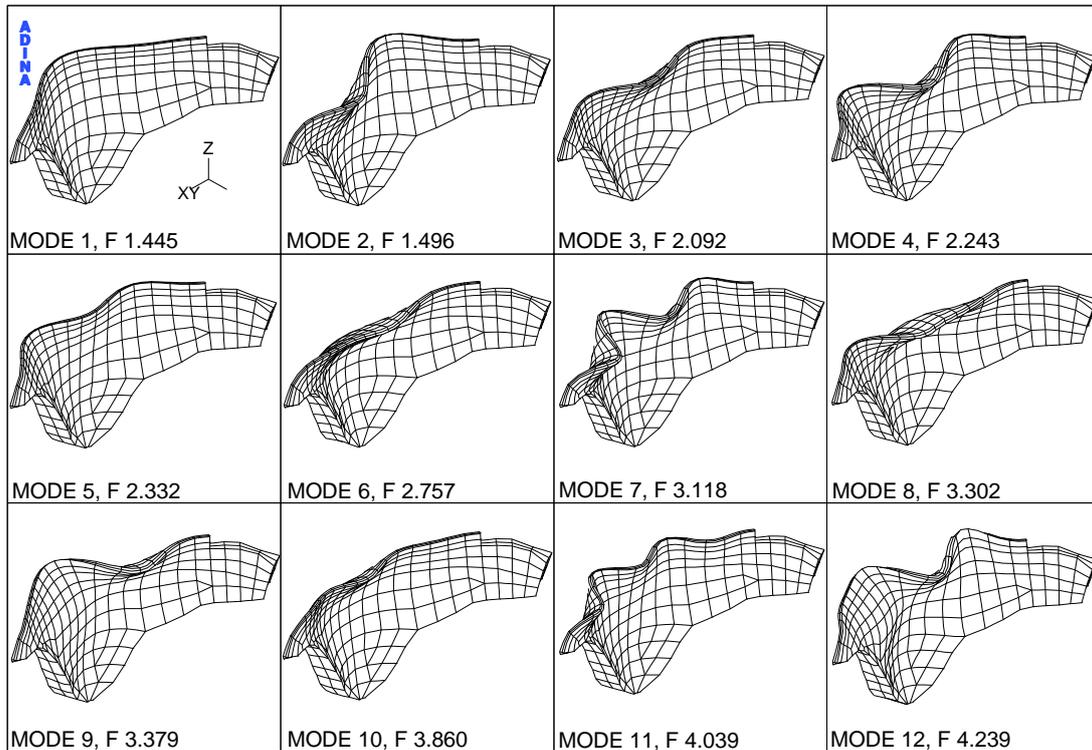
Fig. 3: Mode Shapes and Natural Frequencies (FSI)

Displacement Time History

Time histories of radial displacement (Y-component) for a node located on crest level of dam crown section for all investigated dynamic load combinations (self-weight excluded) are shown in Fig. 4. For SU2 combined static loads, δ_r=11.6 cm is obtained. For DE2 load combination, maximum δ_r=36.7 cm is found for input series 1 and minimum δ_r=-14.6 cm for series 3.
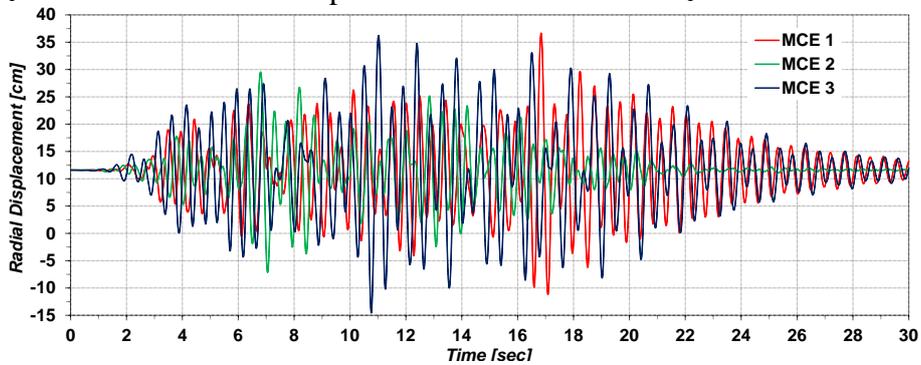
Fig. 4: Radial Displacement Time Histories of Node No. 1942

Displacement Envelopes

Envelope radial displacements (δ_r) for SU2 and DE2 load combinations (self-weight excluded) for centerlines of three radial sections are given in Fig. 5. Section 1 is coincident with dam reference plane (θ=0), section 2 (left) is orientated with respect to it by θ=28° and section 3 (right) by θ=23.8°. Sections 2 and 3 show almost equivalent envelope results of δ_r in the range of -4.9~16.1 cm. Radial displacements (δ_r) towards downstream is assumed positive.
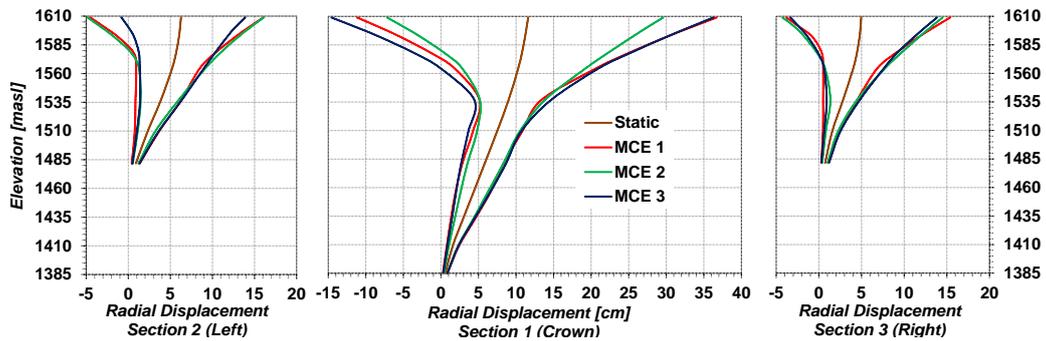
Fig. 5: Envelope Radial Displacements

Stress Envelopes on Water and Air Faces

Envelope of principal stresses S_1 on water face and principal stresses S_3 on air face are made for DE2 load combination (Fig. 6). All seismic inputs (series 1 to 3) are taken into account. On U/S face rather high local tensile stresses of about 16.5 MPa are detected at right bank interface zone. Also, high compressive stresses of -45.5 MPa are seen on opposite face. Certainly, these are stress singularities due to re-entrant corners and thus of less practical importance.
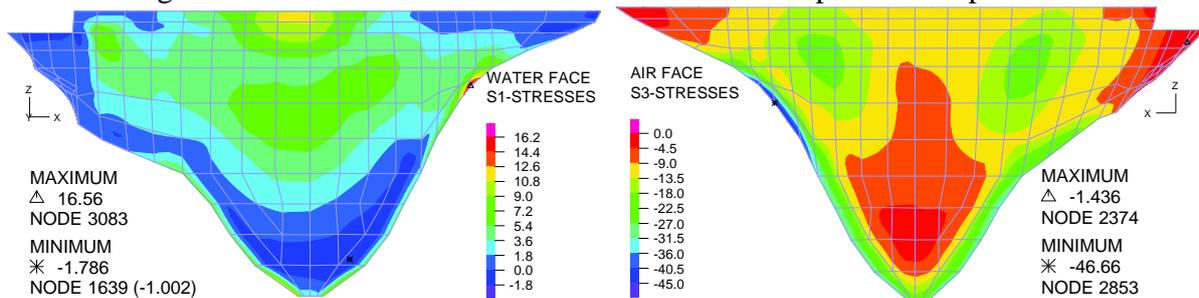
Fig. 6: Water and Air Faces Envelope Stresses (S_1 & S_3)

Stress Envelopes at Cross Sections

Arch (hoop) and cantilever stress results of sections 1 to 3 for SU2 and DE2 load combinations are shown in Fig. 7. Results are given on water and air faces for all seismic input series 1 to 3.
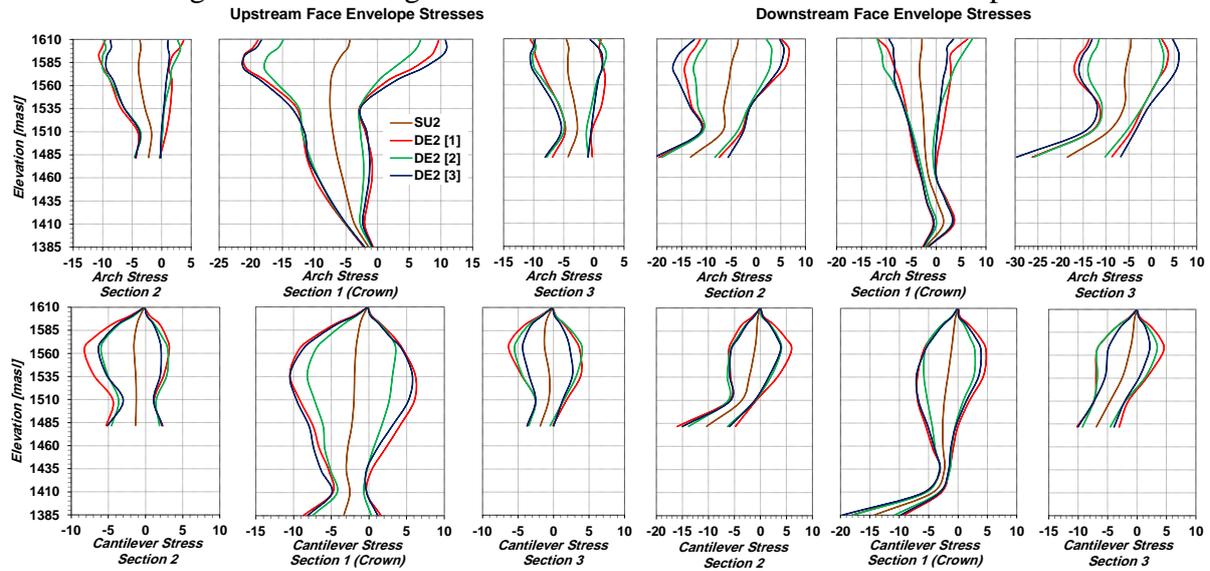
Fig. 7: Envelope Arch and Cantilever Stresses (σ_a & σ_c)

Stress Values at Selected Points

Nodal principal stress results for SU0, SU2 and DE2 at specific points on dam faces (Fig. 8) are summarized in Tab. 2. The highest tensile S_1 of 3.8 MPa was detected at point J' (SU0) and the highest compressive S_3 of -21.3 MPa at point I' (SU2). Tensile stress at J' (SU0) exceeds uniaxial limit f_t=3 MPa. A double check was made using biaxial failure envelope and (σ_a & σ_c) principal stresses (Fig. 9). Factor of safety was obtained 1.32 but it must be at least FS$_{min}$=2.

For DE2, the highest S_1 occurs at point B of 10.7 MPa and the highest S_3 of -33.6 MPa at point I' both due to input series 3. High dynamic tensile arch stresses are seen on upper part of dam that are far above the tensile strength of mass concrete (f_{td}=3.5 MPa). These stresses would release and result to high cantilever stresses. Also, high tensile stresses are seen at point G nearby to rock-concrete interface zone which is mainly due to abrupt change in profile. By modelling of peripheral contact joint it could be shown that the stresses are again unrealistic.

Tab. 2: Stress Results for Load Combinations

| Face | Zone | Node No. | Point | Static Load Combinations | | | | Dynamic Load Combinations DE2 (SW+HSP+SP+dTS+MCE) | | | | | |
| | | | | SU0 (SW+HSP+SP) | | SU2 (SW+HSP+SP+dTS) | | MCE Series 1 | | MCE Series 2 | | MCE Series 3 | |
				S1	S3	S1	S3	S1	S3	S1	S3	S1	S3
Upstream Face	Crest - Left	1872	A	-0.004	-3.155	-0.008	-3.687	3.785	-9.606	2.668	-9.779	1.257	-8.706
	Crest - Centre	1942	B	-0.005	-4.046	-0.011	-4.342	9.733	-18.895	6.835	-14.904	10.720	-18.349
	Crest - Right	2070	C	-0.009	-4.055	-0.014	-4.587	1.390	-10.632	0.898	-10.135	0.477	-9.755
	Dam Upper Part - Left	2223	D	-0.403	-6.086	-0.392	-5.995	3.958	-13.703	4.266	-12.190	4.708	-13.999
	Dam Upper Part - Right	2300	E	-0.405	-6.467	-0.394	-6.438	6.022	-12.137	3.838	-11.527	3.734	-11.664
	Abutment Upper Part - Left	2649	F	0.708	-0.952	0.393	-1.199	1.935	-4.448	1.523	-3.446	2.266	-4.635
	Abutment Upper Part - Right	3084	G	-0.501	-4.087	-0.560	-4.069	8.057	-15.929	7.605	-13.555	9.582	-15.814
	Abutment Lower Part - Left	1621	H	2.649	-3.523	2.091	-3.373	4.976	-7.427	4.318	-7.894	5.531	-7.746
	Abutment Lower Part - Right	1744	I	1.877	-6.096	1.281	-6.153	3.439	-9.979	2.912	-10.861	3.189	-10.341
	Dam Lower Part	1438	J	-1.879	-3.610	-1.972	-3.654	-0.277	-5.130	-0.611	-5.011	-0.252	-5.005
Downstream Face	Crest - Left	1881	A'	-0.001	-3.229	-0.031	-3.595	5.846	-11.421	2.819	-9.941	5.152	-12.737
	Crest - Centre	1947	B'	-0.002	-2.697	-0.030	-2.854	6.327	-11.819	7.274	-11.882	3.545	-9.551
	Crest - Right	2075	C'	-0.018	-4.254	-0.062	-4.531	2.710	-13.924	2.171	-11.585	4.913	-13.109
	Dam Upper Part - Left	2226	D'	-0.022	-3.664	-0.037	-4.433	8.958	-11.930	5.164	-9.355	7.572	-12.297
	Dam Upper Part - Right	2306	E'	-0.021	-3.417	-0.031	-4.178	8.169	-15.457	6.094	-11.033	9.250	-15.104
	Abutment Upper Part - Left	2653	F'	0.019	-3.628	-0.155	-4.502	-0.036	-7.914	-0.015	-7.689	-0.012	-8.075
	Abutment Upper Part - Right	3089	G'	-0.061	-15.013	-0.137	-14.608	0.795	-27.271	1.284	-29.416	1.290	-29.850
	Abutment Lower Part - Left	1624	H'	0.546	-19.494	0.294	-19.471	1.143	-28.855	0.966	-25.792	1.179	-28.733
	Abutment Lower Part - Right	1750	I'	0.527	-20.641	0.370	-21.342	0.973	-30.501	0.916	-29.385	1.016	-33.620
	Dam Lower Part	1447	J'	3.759	-4.216	2.202	-4.856	4.779	-6.652	4.334	-6.296	4.396	-6.656
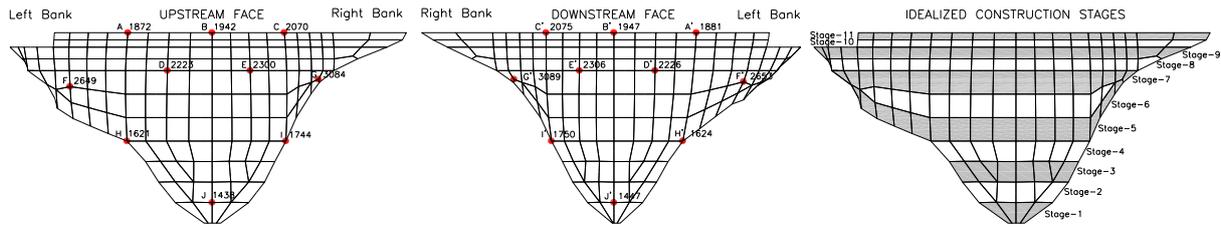
Fig. 8: Stress Points and Self-weight Construction Stages

Stress Time Histories

Time history of principal stresses (S_1 & S_3) for nodal points designated as D, E, D' and E' for DE2 load combinations and each of seismic input series 1 to 3 are given separately in Fig. 9. It is worth to emphasize that direct integration method was employed to solve equilibrium equations at each time step. Rayleigh damping model with coefficients $\alpha=1.1$ s^{-1} and $\beta=0.001$ s was utilized. As depicted in Fig. 1, this leads to a damping ratio of 5.5~6.5% in frequency range of 1.5~15 Hz. For an MCE event, average damping ratio of at least 7% is more reasonable.
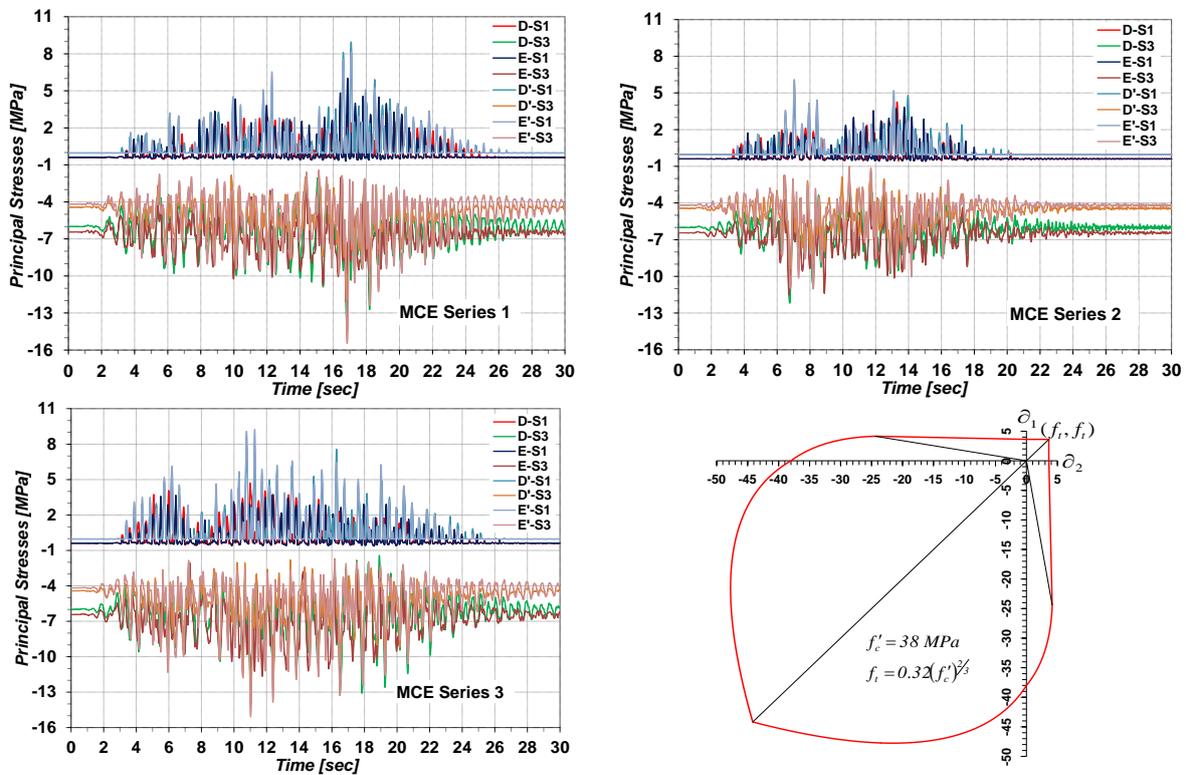
Fig. 9: (S_1 & S_3) Principal Stress Time Histories and Biaxial Failure Envelope

Rocking Block Stability

Linear dynamic analysis results revealed development of high tensile arch stresses in the crest central part of dam. Since, tensile strength of grouted cement in vertical contraction joints is too low, they would open and undergo alternating phases of opening and closing during an earthquake. Within context of a nonlinear analysis and modeling of contraction joints as contact surfaces it could be shown that following joint opening high tensile arch stresses transform to high transitory cantilever stresses leading to formation of horizontal cracks at lower lifts. Crack formation of this type is inevitable as the stresses are much higher than tensile strength of lift joints where for well-prepared lift surfaces (green cutting, etc.) is about 80~90% of intact concrete. Stability control of the detached blocks against sliding and rocking is of main concern.

It is carried out for a central block but with several different heights. Shear strength parameters at base of rocking block are taken c=0 and φ=63˚. Minimum acceptable factors of safety against sliding and overturning are assumed 1.0 and 1.1, respectively. Considering nonlinear analysis results of similar projects a maximum joint opening of about 3 mm is expected. Block instability could be initiated at much lower amount of joint opening.

The results of block stability check considering abovementioned site specific PGA values are submitted in Tab. 3. To assess order of magnitudes, peak values of (absolute) acceleration in Y-component are found at base level of blocks. In 1st block ah=3.32g was calculated and in 4th one ah=1.46g. Reduction factor (2/3) was imposed on calculated in situ acceleration (ah) but resulting factors of safety were quite low and unacceptable.

Tab. 3: Free Standing Block Stability

Acting Forces	Block Height [m]				Equilibrium Diagram
	8.500	17.000	30.815	44.630	
Block Base Elevation [masl]	1600.500	1592.000	1578.185	1564.370	
Block Base Thickness [m]	7.361	10.007	13.356	15.963	
Block Cross Section Area [m^2]	50.448	124.259	285.633	488.154	
Horizontal Seismic Coefficient, C_h	0.159	0.159	0.159	0.159	
Vertical Seismic Coefficient, C_v	0.106	0.106	0.106	0.106	
Self-Weight, PP [kN]	1210.752	2982.216	6855.192	11715.696	
Hydrostatic Force, W [kN]	148.376	961.380	3794.872	8500.644	
Uplift Force, SP [kN]	-198.581	-687.181	-1822.193	-3259.567	
Horizontal Earthquake Force, Q_h [kN]	-192.535	-474.236	-1090.122	-1863.046	
Vertical Earthquake Force, Q_v [kN]	-128.357	-316.157	-726.748	-1242.031	
Factor of Safety against Sliding	Unstable	8.0	3.1	2.1	
Factor of Safety against Overturning	3.2	3.1	3.4	3.8	

Conclusion

Seismic Safety evaluation of Luzzone dam has been made and related analysis results were prepared as per requested by Formulators. Regarding static loads, local safety criteria are fulfilled all over the dam wall except at downstream toe where tensile strength criterion was violated. Dynamic analysis results revealed high tensile arch stresses at upper part of dam that are quite far above the tensile strength of grouted contraction joints. Opening of joints release arch stresses resulting to tensile cantilever stresses that cause formation of horizontal cracks at cantilever base. Stability checks was carried out to find factors of safety against sliding and overturning. This approach is quite conservative since frictional effects of contraction joints on both sides and interlocking of shear keys (if it exists) are ignored. Acceptable results were achieved but only for base acceleration (PGA) values.

Only by modeling of dam vertical contraction joints and/or rock interface zone as contact surfaces and resort to nonlinear analysis these stress uncertainties could be uncovered properly.

Acknowledgements

References

[1] Theory and Modeling Guide Volume I: ADINA, ARD 12-8 (2012). ADINA R&D, Inc.
[2] Raphael J. M. (1984). Tensile Strength of Concrete, ACI Journal, Vol. 81, No. 2.
[3] Kupfer H., Gerstle K. (1973). Behavior of Concrete under Biaxial Stresses, ASCE, Vol. 99
[4] Chen W. F. (1982). Plasticity in Reinforced Concrete, McGraw-Hill, New York.
[5] Kuo J. S.H. (1982). Fluid-Structure Interactions, UCB/EERC-82

Seismic Safety Assessment of the Luzzone Arch Dam

Simon-Nicolas Roth[1] and Martin Roberge[1]

[1]*Hydro-Québec Production, 75 boul. René-Lévesque O., Montréal, Québec, Canada, H2Z 1A4*

ABSTRACT: The seismic safety assessment of Luzzone arch dam (224 m) is achieved considering a combination of thermal, hydrostatic, self-weight and seismic loads. Because these loads have different rates of application as well as time-dependence (creep) the combination needs to take into consideration the deformation modulus (sustained, instantaneous or dynamic modulus) related to a specific load to compute the state of stress and displacement of the structure. This combination is accomplished using a linear combination of the stress / displacement resulting from the analysis carried out for each load associated with its corresponding deformation modulus. The stability of different blocks located in the top center of the dam is verified using three different methods. The first method uses a free body diagram to compute the sliding and overturning safety factors without considering lateral confinement. The second method uses the integration of the stress field obtained from the finite element results and considers the effect of lateral confinement. Finally, the last method uses nonlinear Mohr-Coulomb elements located in the contraction joints as well as is in the base of the four center cantilevers to study the displacement and rotation of these blocks during an earthquake. From the comparison of these approaches, it is concluded that for arch dams, neglecting lateral confinement may result in over conservative factors of safety. The largest displacement computed with the nonlinear model is 91 cm, which is small compared to the block thickness of 7.4 m. This analysis showed that the top blocks neither overturn nor fall.

E-mail: roth.simon-nicolas@hydro.qc.ca, roberge.martin@hydro.qc.ca

Introduction

The object of this work is the seismic verification of Luzzone arch dam, theme A of the 13th ICOLD Benchmark Workshop on Numerical Analysis of Dams [1]. This benchmark case study is modeled with ANSYS 16.0 software and with an in-house post-processing code. The finite element mesh of the structure-foundation-reservoir system is refined compare to the one provided by the formulators for the purpose of capturing nonlinear effects. Static analyses are performed considering phased construction to define self-weight loads, hydrostatic loading and a simplified temperature gradient for the summer conditions taking into consideration the reference contraction joint closure temperatures. The seismic analysis is performed in two main steps. The first step consists in determining and evaluating the dynamic characteristics of the dam-foundation-reservoir system (natural frequencies, natural modes of vibration and modal participation factors). The second step is to perform dynamic analyses in the time domain using three independent spectrum-compatible acceleration time histories. The different load combinations are performed using a linear combination of the stress/displacement resulting from the analysis carried out for each load associated with its corresponding deformation modulus. Because these loads have different rate of application as well as time-dependence (creep) the combination needs to take into consideration the deformation modulus (sustained, instantaneous or dynamic modulus) related to a specific load to compute the state of stress and displacement of the structure. A sliding and overturning seismic stability analysis is done for different blocks located in the top center of the dam. This stability analysis considers a progressive approach: (1) use of a 2D free body diagram to compute the sliding and overturning safety factors without considering the lateral confinement, (2) use of stress field integration obtained from the finite element results with consideration of lateral confinement effects and (3) use of nonlinear Mohr-Coulomb elements located in the contraction joints as well as in the base of the four center cantilevers to estimate the blocks displacements/rotations. Finally, a

discussion about the computed displacements, stresses and rocking block stability of the dam is presented as well as the conclusions about the global safety of the structure.

Model

The mesh is constructed using 105299 nodes and 190888 elements. The reservoir (22263 elements) is meshed with hexahedral acoustic elements. The dam body (44016 elements) and the transition zone between the rock-concrete interface (8904 elements) are composed of trilinear hexahedral enhanced strain elements. The rock foundation (115705 elements) is meshed with constant stress tetrahedral elements. Eight elements are used in the thickness direction of the dam to capture nonlinear effects (lift joint openings and displacements). The finite element mesh is shown in Fig. 1 with its corresponding dimensions.
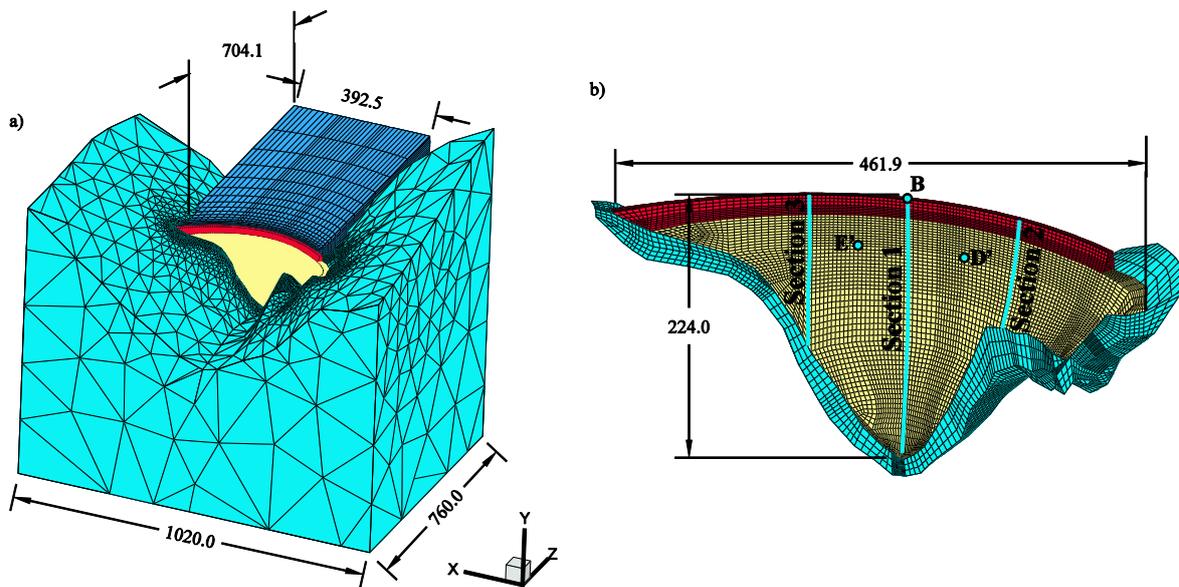
Fig. 1: (a) Three-dimensional view of dam-rock-reservoir system, (b) finite element mesh of the dam body with rock-concrete transition zone (dimensions in meters)

Materials

According to Raphael [2], under sustained static loading conditions, the effects of creep on mass concrete may be important and generally can be considered by determining a sustained modulus of elasticity taken as approximately two-thirds of the tested value of the instantaneous modulus of elasticity. Creep effects also results in substantial losses in thermal-induced force, with decays in force of about 40% in as little time as 24 hours [3]. This reduction in stiffness is due to micro-cracking and thermal creep and causes rapid decays in the restraint forces developed by thermal loads. Thus stresses and displacements caused by self-weight, silt pressure and thermal load should be computed using the sustained modulus of elasticity. For a reservoir with a large drawdown, the hydrostatic load is constantly varying. Therefore creep effects are small and the instantaneous static modulus should be used to compute the displacements caused by hydrostatic loading. Note that this should normally be calibrated with field data, however in the absence of such data, no calibration was performed. Finally, for short duration loading such as earthquakes, the modulus to be considered is the dynamic modulus. In the absence of measured data the dynamic modulus may be estimated by increasing the laboratory value of the instantaneous modulus by 20 to 30 percent. Material properties used in the model are given in Tab. 1.

Tab. 1: Model material parameters

Properties	Value		
	Old concrete	New concrete	Foundation
Density [t/m^3]	2.5	2.4	0.0
Deformation modulus [GPa]	-	-	18.6
Sustained static modulus of elasticity [GPa]	13.3	12.0	-
Instantaneous static modulus of elasticity [GPa]	20.0	18.0	-
Dynamic modulus of elasticity [GPa]	25.0	22.5	23.3
Poisson's ratio	0.18	0.18	0.20
Thermal expansion [1/°C]	10^{-5}	10^{-5}	10^{-5}
Static compressive strength [MPa]	38.0	32.0	-
Dynamic compressive strength [MPa]	57.0	48.0	-
Static tensile strength [MPa]	3.0	2.3	-
Dynamic tensile strength [MPa]	4.0	3.5	-
Friction angle	63°	63°	-

Self-weight load

Construction phase effects are computed using an orthotropic material model in which the modulus in the dam's tangential direction and its related shear modulus are reduced. The dam was built in four stages (1960, 1961, 1962 and heightening in 1999). It was assumed that the cantilever blocks were grouted at the end of the construction in 1962. Thus the stresses are saved after this first phase of construction. Similarly, in the second phase of construction orthotropic properties are applied for the heightened portion of the dam while the part built in the first phase, as it was previously grouted, is considered isotropic and massless. The stresses obtained from this second phase are added to those of the first phase to give the total stress caused by self-weight. These stresses are added during post-processing of the model, thus the displacements caused by self-weight are zero. The maximum compressive principal stress is given for the upstream of the dam is given in Fig. 2. The upstream and downstream maximum and minimum principal stresses in cross section 1 (Fig. 1b) are given in Fig. 3. As expected, the principal stress is zero in this section and the principal compressive stress is maximum at the heel of the dam and decreases gradually to zero with elevation.
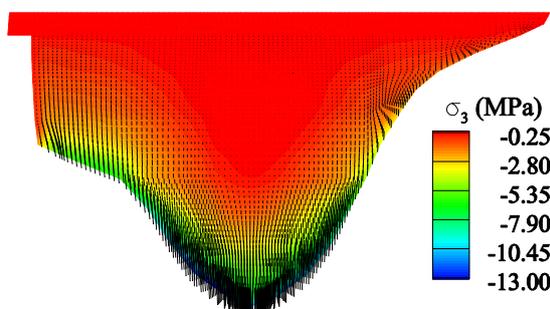
Fig. 2: Upstream maximum stress σ_3
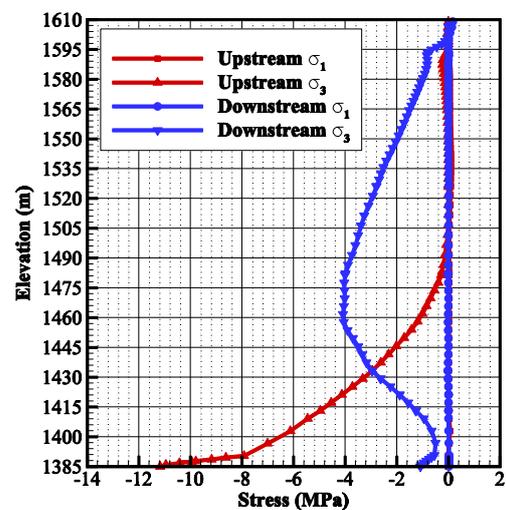
Fig. 3: Principal stress cross section 1

Thermal load

To simplify the temperature distribution computation in the dam body, it was computed using steady state conditions. Normally, the temperature distribution should be computed using transient conditions given the high thermal inertia of dams. Fig. 4 gives the temperature gradient distribution in cross section 1 (corresponding to the difference between the computed temperature and the closure temperature) for summer and winter conditions. The temperatures applied on the dam face boundaries are given in Fig. 5 as well as the grouting temperature as a function of dam elevation. Rock foundation is considered to have adiabatic conditions.
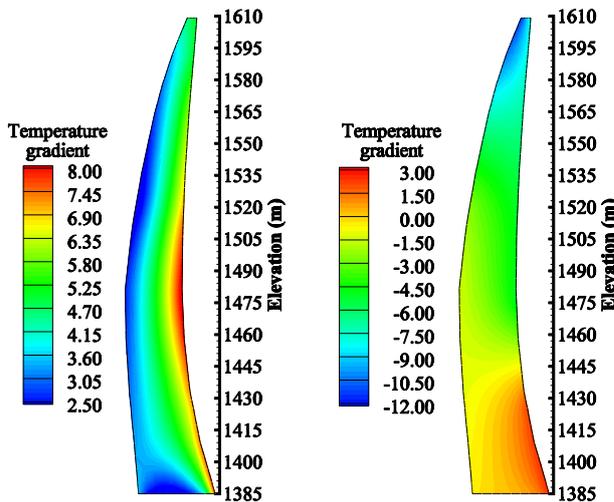
Fig. 4: Summer (left) and winter (right) temperature gradient distribution at cross section 1
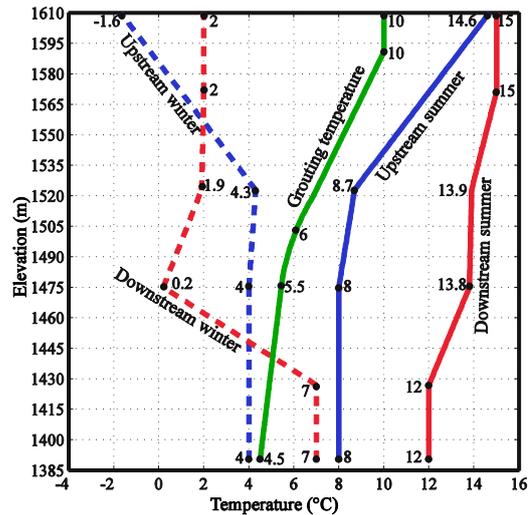
Fig. 5: Temperature applied on the dam face boundaries

Hydrostatic and silt loads

The hydrostatic pressure applied on the upstream face of the dam corresponds to the maximum normal operating water level with elevation 1606 m and has a density of 1000 kg/m³. Silt pressure is added to the hydrostatic pressure on the 55 first meters of upstream face of the dam (corresponding to elevation 1440 m) with a buoyant density to amount 400 kg/m³.

Dam water interaction

Dam water interaction is modeled using acoustic elements. The effects of surface waves (sloshing effects) which are known to be small, are neglected. Therefore the pressure boundary condition at the free surface is zero. The reservoir bottom and the truncated vertical plane at the upstream end are assumed to be rigid. Thus, the ground motion is not applied to the reservoir bottom and no special radiation damping condition due to propagation of pressure waves in the upstream direction is considered. The truncated upstream plane is located at a distance of three times the water depth from the face of the dam. According to studies, this is enough to not affect the hydrodynamic pressure on the dam upstream face.

Dam foundation interaction

A massless foundation model is used where only the flexibility of the foundation rock is considered while its inertia is neglected. In the absence of wave propagation in the rock, the earthquake motions recorded on the ground surface are applied directly at the fixed boundaries of the foundation model.

Transient seismic loads

The safety of the dam is evaluated for an earthquake with a return period of 10 000 years. Three sets of maximum credible earthquake (MCE), stochastically independent, acceleration time-histories were provided. The time step is 0.01 second and the total duration for the three sets is 30.71 seconds giving a total number of 3072 time steps. The acceleration time histories are compatible with structures founded on rock and damping equal to 5%. Scaling factors given in Tab. 2 are applied to the acceleration time histories to obtain the following peak ground acceleration (PGA) values:

- Cross-valley direction   (X - Direction) : +0.160g
- Vertically upwards   (Y - Direction) : +0.106g (2/3 the horizontal components)
- Downstream-upstream   (Z - direction):   +0.160g

Tab. 2: Scaling factors applied on time history data

Direction	MCE1	MCE2	MCE3
X - Cross-valley	1.32	-1.51	1.52
Y - Vertical	-1.14	0.92	-1.01
Z - Downstream	1.72	-1.63	1.38

A baseline correction was applied on each time histories to make sure the final displacement is close to zero.

Load combination method

Earthquakes induce instant dynamic loads on structures that possess initial static loads. Assuming that the structural integrity is not altered, static loads should be kept constant during the whole duration of the earthquake. Therefore, during an earthquake, the dam is simultaneously subjected to static loads and dynamic loads which are associated with different modulus of elasticity. Thus, the approach adopted to properly combine stress and displacements resulting from these loads should be carefully defined. Given the elasticity equation:

$$\nabla \cdot (E \, \nabla \cdot \vec{u}) = \nabla \cdot \sigma_{init} + \vec{f}_{ext} + \vec{f}_{body} \qquad (1)$$

with E the modulus of elasticity, $\vec{u}$ the displacement field, σ_{init} the initial stress tensor and $\vec{f}_{ext}$, $\vec{f}_{body}$ respectively the external and body loads. If σ_{init} is computed with a modulus E_1 and imposed as initial stress on the same problem but using E_2 ($E_1 \neq E_2$), the displacement field computed with E_2 will not be equal to the displacement field computed with E_1. This suggest the combination of stress and displacements during post-processing instead of imposing initial stress in the finite element problem. This proposed approach was used in the present analysis. Hence, given that loads are associated either with sustained, instantaneous or dynamic modulus of elasticity, the stress/displacements resulting from these three analyses are linearly combined during post-processing achieved with an internal computer code.

Results

Static linear-elastic response analysis

Figures 6 and 7 give the maximum principal stress on the upstream and the downstream faces for a summer case at normal water level (NWL) corresponding to 1606 m. At the dam heel, tensile stresses are present, therefore the dam-rock interface must be examined. Because no piezometric data is provided and rock/concrete interface strength is not known, the rock/concrete interface will be assumed closed. Figures 8 and 9 show the minimum principal

stress on the upstream and the downstream faces. The maximum principal compressive stress remains below the compressive strength.
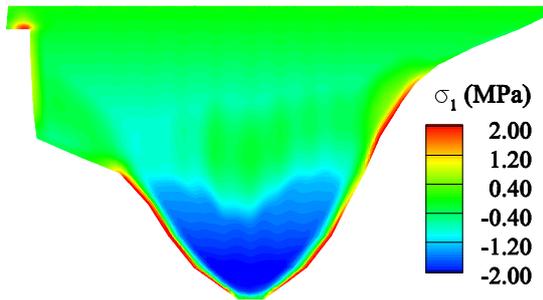
Fig. 6: Upstream maximum stress σ1
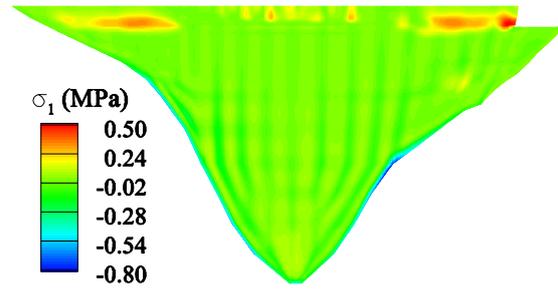
Fig. 7: Downstream maximum stress σ1
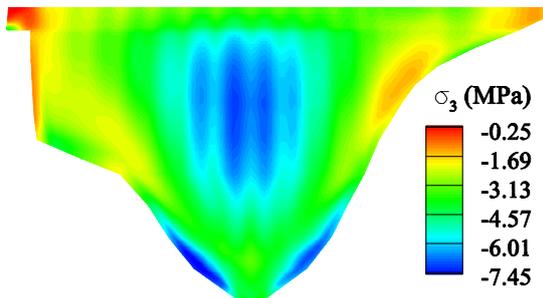
Fig. 8: Upstream minimum stress σ3
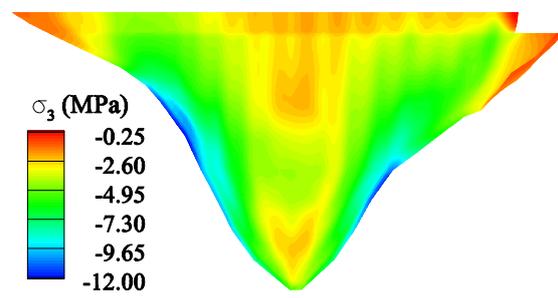
Fig. 9: Downstream minimum stress σ3

Natural frequencies and mode shapes

The first twelve natural frequencies of the dam-foundation-reservoir system for the cases of empty and full reservoir (incompressible and compressible) are given in Tab. 3 with their corresponding effective modal mass percentage. The effective mass computed with the fluid-structure interaction model corresponds to the ratio of the mass excited for a specific mode over the total mass excited for a large number of modes. Approximately 250 modes were required to reach a constant excited cumulative mass fraction. For models considering empty and incompressible reservoir, the sum of the mass excited for the twelve first modes exceeds 70%. When considering water compressibility, the sum of mass excited for vertical and cross-valley directions are below 35%. It is only when considering the first 25 modes that the sum of the effective mass reaches over 70%. Finally, the first natural frequency obtained with empty reservoir is higher than the estimated reservoir natural frequency given by $f_r = 1451/(3.4H)$ [4], therefore water compressibility will be considered for the following time-history analysis. Fig. 10 shows the twelve first mode shapes corresponding to the analysis using water compressibility.
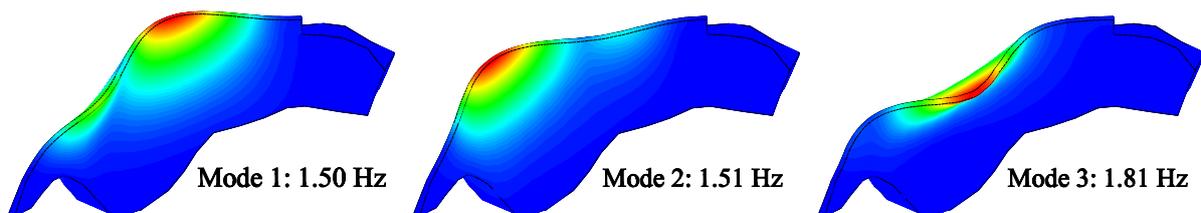
Fig. 10: Mode shapes 1-12
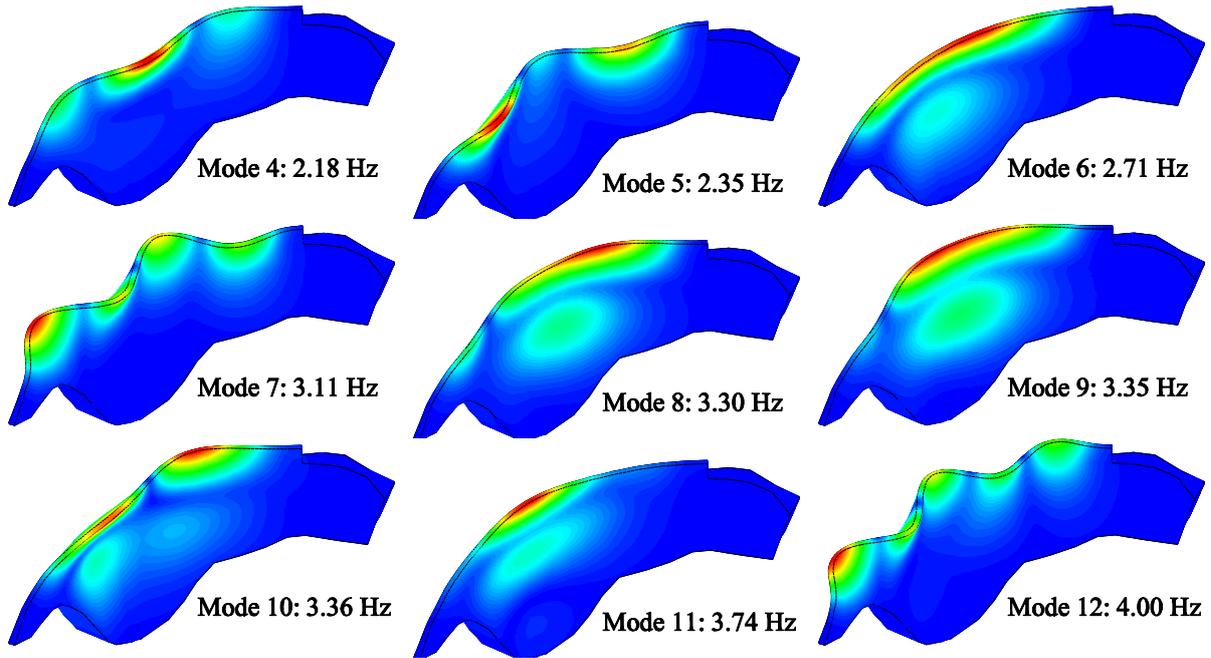
Fig. 10: Mode shapes 1-12 (cont.)

Tab. 3: Natural frequencies

Mode	Empty Reservoir				Full Reservoir Incompressible				Full Reservoir Compressible			
	Freq.	Effective Mass Percent			Freq.	Effective Mass Percent			Freq.	Effective Mass Percent		
	f, Hz	X, %	Y, %	Z, %	f, Hz	X, %	Y, %	Z, %	f, Hz	X, %	Y, %	Z, %
1	1.962	8.78	0.05	0.06	1.518	14.32	0.14	0.40	1.501	13.56	0.26	17.27
2	2.084	0.18	0.93	24.62	1.561	0.20	0.00	39.87	1.514	2.26	0.00	33.48
3	2.964	0.07	0.79	7.88	2.319	0.34	0.44	12.13	1.806	0.00	0.00	0.00
4	3.729	0.09	9.16	14.43	2.843	0.16	2.83	19.83	2.177	0.19	0.6	17.01
5	3.89	0.31	0.38	1.08	3.156	1.34	0.00	0.28	2.348	0.21	0.00	0.67
6	4.367	28.71	0.00	0.20	3.585	19.51	0.00	0.00	2.713	0.00	0.66	6.06
7	4.879	0.10	1.27	2.11	4.049	0.21	0.00	1.39	3.106	2.98	0.00	0.00
8	5.164	1.04	56.17	1.54	4.653	0.00	2.18	4.03	3.296	2.06	1.28	1.86
9	5.739	25.28	1.64	1.43	4.764	0.56	16.61	1.83	3.347	0.00	0.00	0.00
10	5.869	5.84	0.50	2.78	5.010	0.55	0.00	0.20	3.361	12.52	0.17	0.38
11	5.957	0.11	0.03	0.01	5.051	0.83	49.99	6.76	3.735	0.00	0.59	0.00
12	6.176	2.18	1.55	14.63	5.483	34.76	1.02	0.20	3.995	0.31	0.23	1.96
	Σ	72.68	72.48	70.79	Σ	72.77	73.21	86.92	Σ	34.10	3.79	78.69

Damping

Damping is represented by a mass and stiffness proportional damping matrix (Rayleigh damping). A damping of 5% is evaluated from the knowledge of two modes (1 and 30). Mode 30 is the last mode that contributes significantly to the dynamic response. With the selected modes, the coefficient α corresponding to the mass proportional damping coefficient is α =0.757214 for the dam. The coefficient β corresponding to the stiffness proportional coefficient is β=0.002091 for the dam and β=0.010601 for the foundation. Fig. 11 shows the damping as a function of the frequency. The crosses on the graphs are the different modal frequencies, and

the right axis represents the cumulative effective mass. This figure indicates that over 75% of the effective mass has a damping between 4 and 5%.
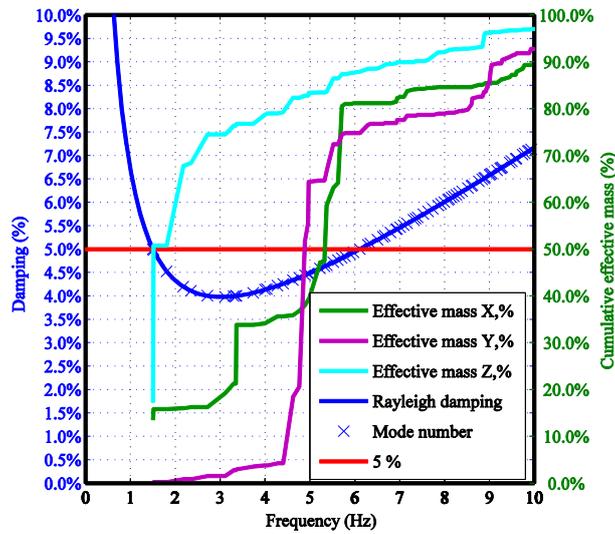
Fig. 11: Rayleigh damping

Combined dynamic-static loads displacements analysis

The relative radial displacement (Z component) time histories at the crest of the central section of the dam (point B, see Fig. 1b) due to the investigated combined static-dynamic loads are shown in Fig. 12.
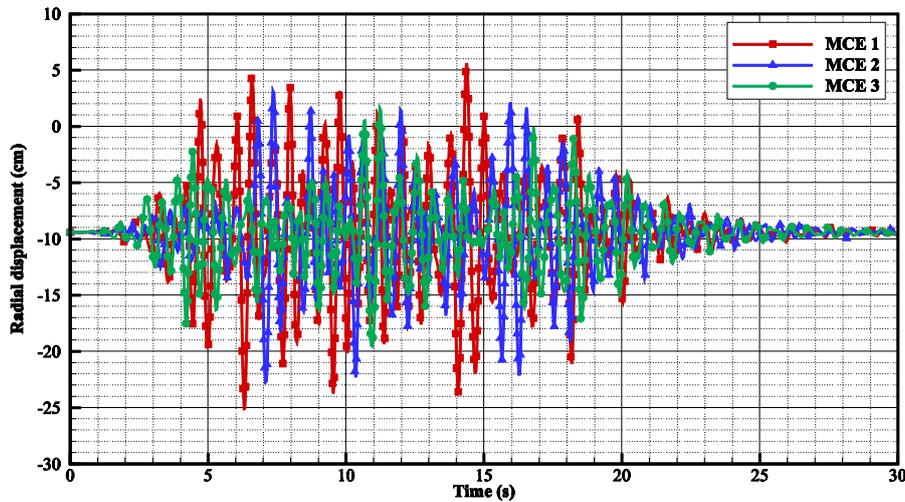
Fig. 12: Displacement time histories point B

The minimum and the maximum radial displacement envelopes, as well as the static load displacements (without self-weight) for cross section 1, cross section 2 and cross section 3 are shown in Figures 13 to 15.
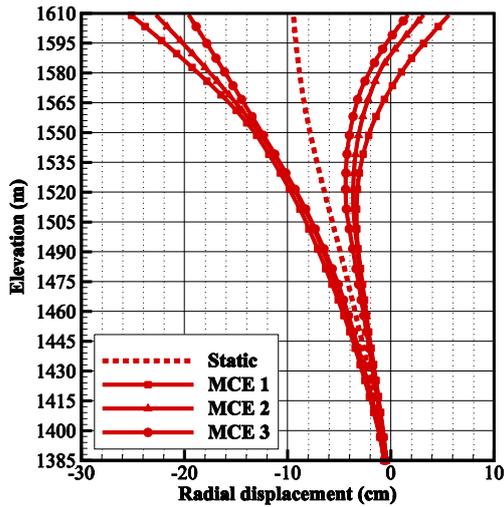
Fig. 13: Displacement envelopes at cross section 1
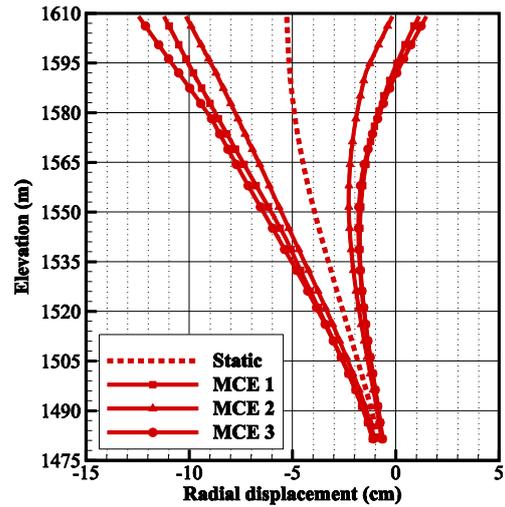
Fig. 14: Displacement envelopes at cross section 2
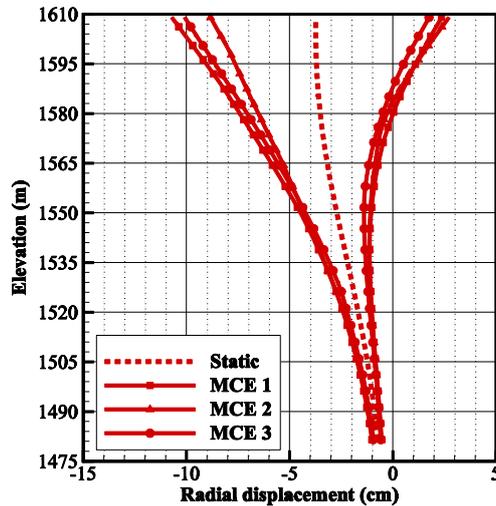
Fig. 15: Displacement envelopes at cross section 3

Combined loads stress analysis

The computed maximum and the minimum principal stresses for the upstream and for the downstream faces of the dam from all the investigated dynamic load combinations are shown in Figures 16 to 19. Principal stresses exceeding the tensile strength appear on the upstream as well as on the downstream face suggesting that cracking should occur. There is also an area at the rock concrete interface on the right bank where a high level of tensile stress is computed. This zone should carefully be examined. The maximum principal compressive stresses remain below the dynamic compressive strength.
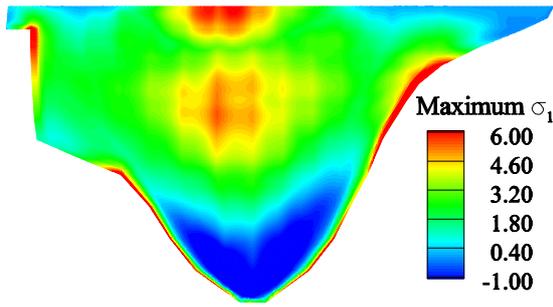
Fig. 16: Upstream maximum stress σ₁
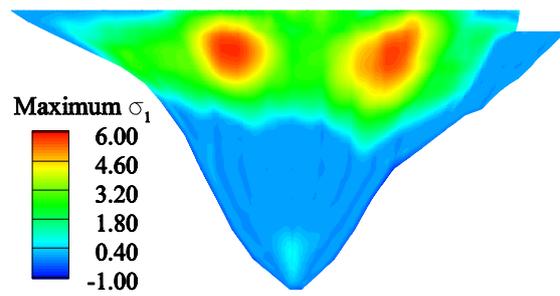
Fig. 17: Downstream maximum stress σ₁
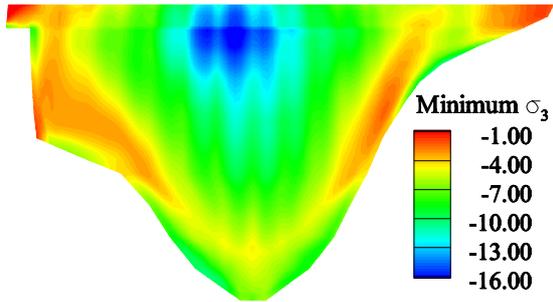
Fig. 18: Upstream minimum stress σ₃
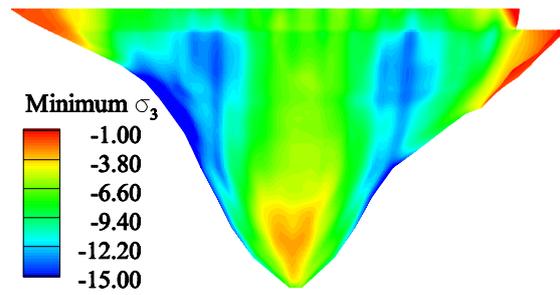
Fig. 19: Downstream minimum stress σ₃

Using a local fixed anisotropic damage model [5] implemented in ANSYS as a USERMAT, the MCE1 acceleration time-histories were used to define the crack pattern. Mesh objectivity requirements are satisfied by introducing a regularization based on the energy equivalence. Because the concrete has a high dynamic tensile strength, the representative volume element characteristic length $l_{rve} = 2EG_F/f_t^2$ is small compared to the size of the structure and the mesh used was not able to fulfill the characteristic length requirements. Therefore, an adjustment was made to the regularization parameter such that it is based on a f_t of 1.25 MPa with a fracture energy of 150 N/m. The level of damage (0: undamaged, 1: completely damaged) corresponding to $\tilde{E} = E(1-d)^2$, (E and $\tilde{E}$ are respectively the undamaged and damaged modulus) is given in Figures 20 and 21. Horizontal cracks develop at the top center of the dam. Upstream and downstream horizontal cracks connect together at level 1560 m. These cracks should be carefully examined during post-seismic analyses as uplift pressure should develop. The large zones of damage (downstream right and left banks) are zones of distributed cracks located only on the surface of the dam.
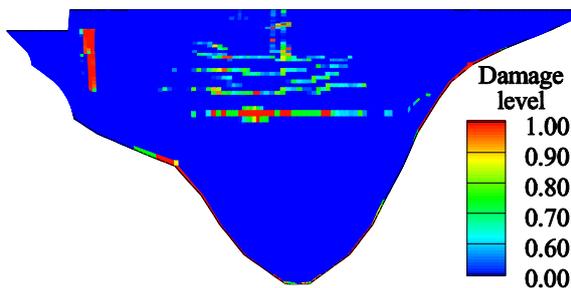
Fig. 20: Upstream damage
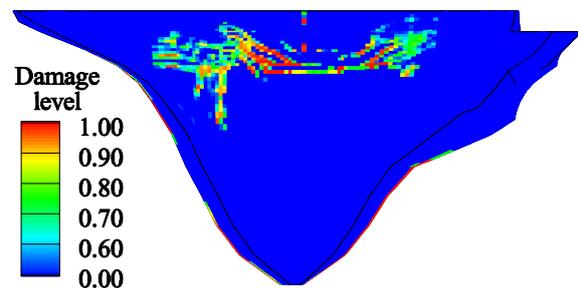
Fig. 21: Downstream damage

Envelopes of the minimum and maximum hoop and cantilever stresses on the upstream and on the downstream lines of cross section 1 to 3 are presented for the investigated dynamic load combinations in Figures 22 to 27. The graphs also include the results for the corresponding static load combination. The time histories of the maximum and minimum principal stresses at points D, E, D' and E' (Fig. 1b) are shown in Figures 28 and 29.
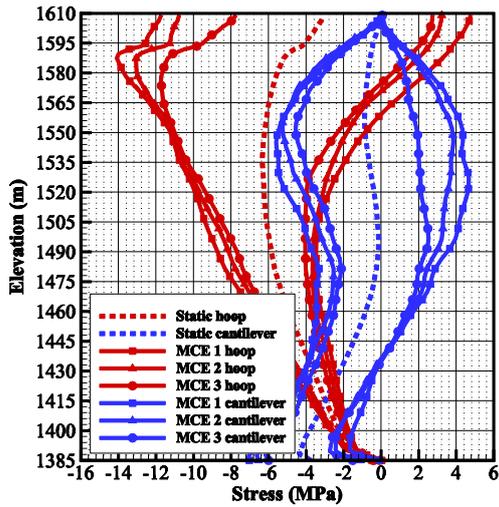
Fig. 22: Stress envelopes upstream cross section 1
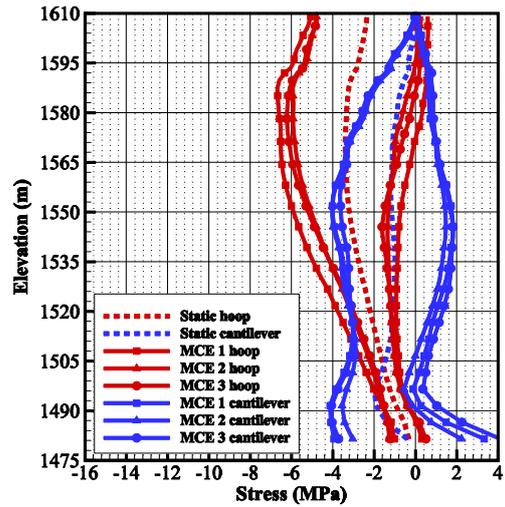
Fig. 23: Stress envelopes upstream cross section 2
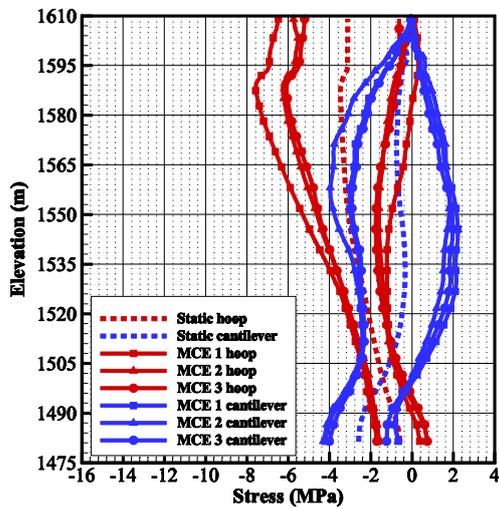
Fig. 24: Stress envelopes upstream cross section 3
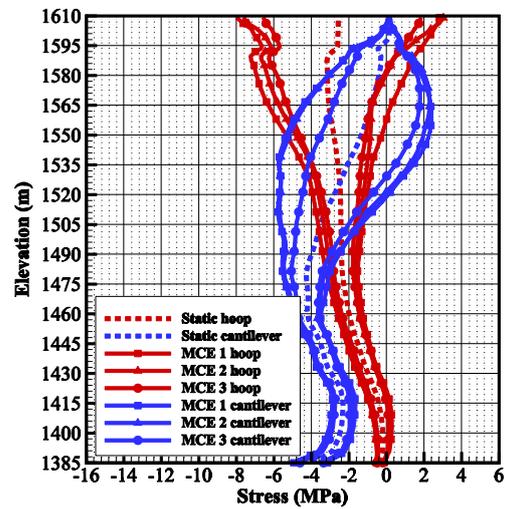
Fig. 25: Stress envelopes downstream cross section 1
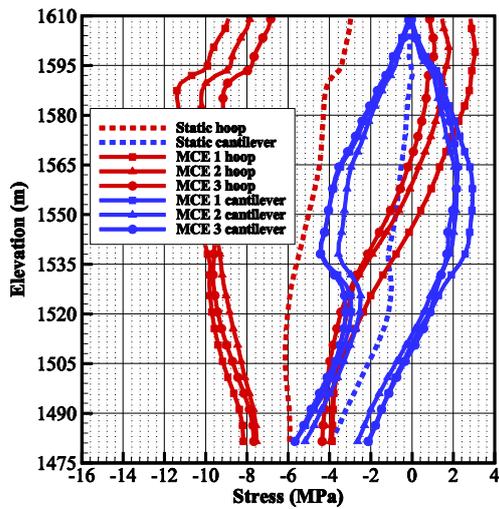
Fig. 26: Stress envelopes downstream cross section 2
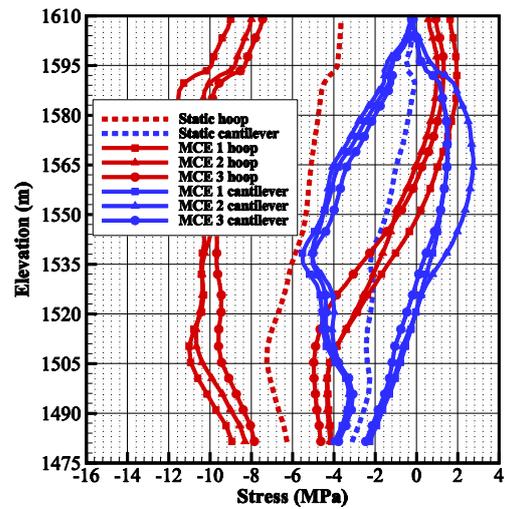
Fig. 27: Stress envelopes downstream cross section 3
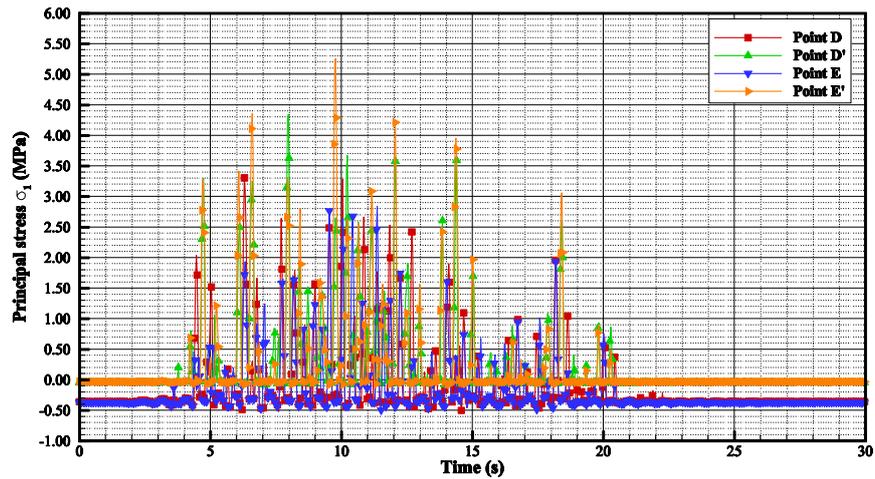
Fig. 28: Minimum stress σ_1 points D, D', E, E'
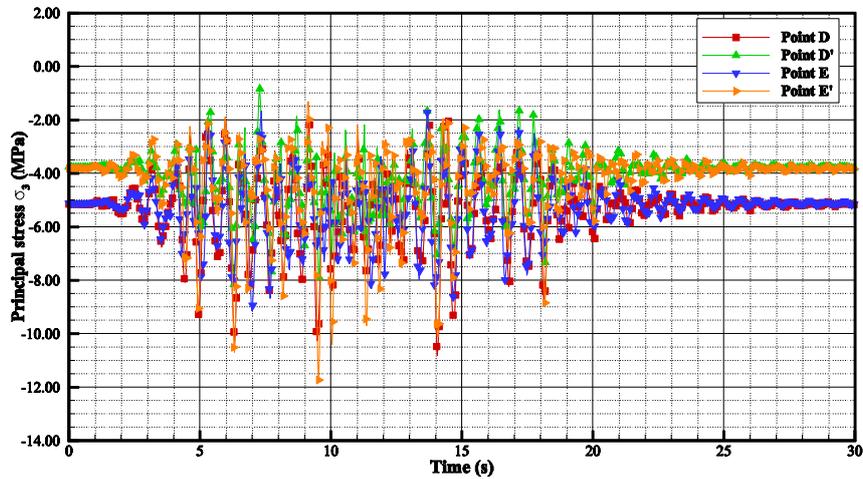
Fig. 29: Minimum stress σ_3 points D, D', E, E'

Block stability analysis

Stability of part of a crown cantilever against sliding and overturning was evaluated on four blocks. For this analysis, the shear keys were neglected. The three load combinations analysed, denoted as MCE1, MCE2 and MCE3, include dam self-weight, hydrostatic pressure for full reservoir, uplift pressure (triangular pressure distribution assumed) and earthquake-induced forces (horizontal and vertical components). The finite element results also include summer thermal condition. Fig. 30 illustrate the four blocks considered for the analysis.
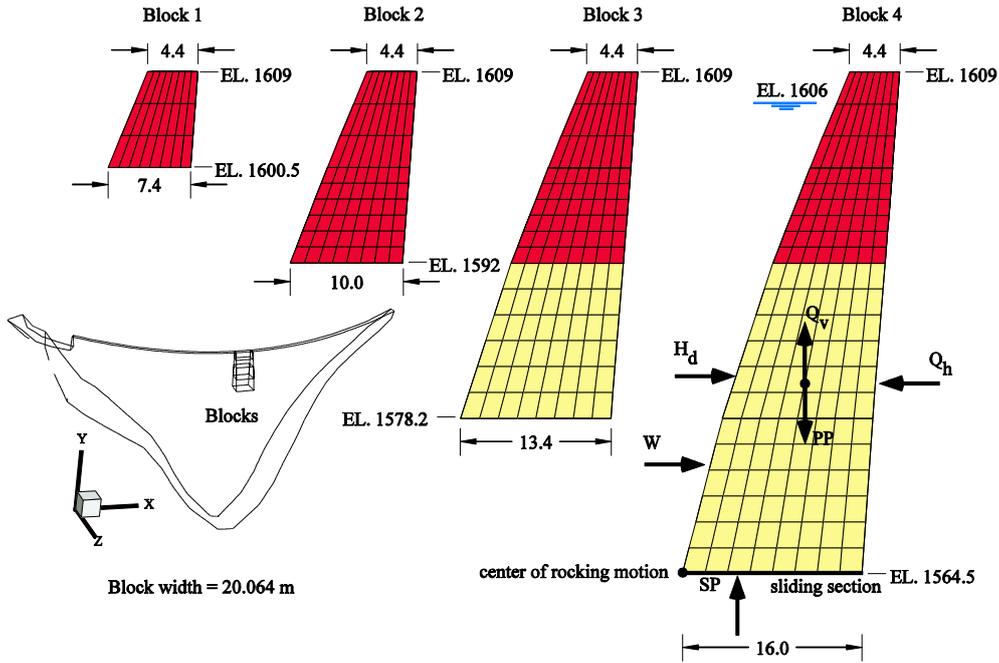
Fig. 30: Concrete blocks considered for rocking-sliding analysis (dimensions in meters)

Method 1: Free body diagram

Stability analysis is carried out considering the block as completely unrestrained on its lateral faces which assumes that the vertical contraction joints remain permanently opened during earthquake, and that a horizontal crack propagates through the whole thickness of the block. Due to the geometrical constraints, the concrete blocks are allowed to move only towards the upstream direction (rocking and sliding motions). Any movement towards downstream is not allowed. This assumption will be confirmed during the nonlinear analysis. 2D rocking-sliding analysis of the four blocks was carried out using the amplified acceleration at the base of each block as the input motion. The time history of the horizontal component of the acceleration at the base of block 1 is plotted in Fig. 31 when the dam is subjected to ground motion MCE1. The acceleration at the base of the block reaches 2.16g which is an amplification of 13.5 times the PGA. The Sliding Safety Factor (SSF) was evaluated by:

$$\text{SSF} = \frac{(\text{PP} + \text{SP} + \text{Q}_v)\tan(\phi)}{\text{W} + \text{H}_d + \text{Q}_h} \tag{2}$$

where PP is the self-weight, SP is the uplift force, Q_v is the vertical component of the earthquake force, W is the hydrostatic force, H_d is the hydrodynamic force and Q_h is the horizontal component of the earthquake force. Sliding initiates when the applied shear force is greater than the static frictional resistance computed along the cracked plane (SSF < 1.0). The hydrostatic force (W), for a unit width, was evaluated considering the vertical ground acceleration on the horizontal component of hydrostatic pressure:

$$\text{W} = \frac{\rho_w H^2}{2}(g + \ddot{a}_v) \tag{3}$$

where ρ_w is the water volumetric density, H is the reservoir depth in contact with the block, g is the gravity acceleration and $\ddot{a}_v$ is the vertical base block acceleration. The hydrodynamic force (H_d) was computed using the Westergaard added mass formulation assuming the water is incompressible and that the upstream face of the block is vertical, thus neglecting the vertical component caused by the curved dam geometry:

$$\mathrm{H}_d = \left(-0.543\left(\rho_w\sqrt{h_r}\left(h_r - h_0\right)^{3/2}\right)\right)\ddot{a}_h \tag{4}$$

where h_r is the total reservoir depth, $h_r - h_0$ is the reservoir depth in contact with the block and $\ddot{a}_h$ is the horizontal block acceleration at the base. The earthquake-induced forces (horizontal and vertical components) were simply evaluated by $\mathrm{Q}_h = \mathrm{PP} \times \ddot{a}_h$ and $\mathrm{Q}_v = \mathrm{PP} \times \ddot{a}_v$. The Overturning Safety Factor (OSF) was evaluated by considering the center of rocking motion at the upstream toe of the block (overturning in the upstream direction):

$$\mathrm{OSF} = \frac{\mathrm{M}_{\mathrm{stab}}}{\mathrm{M}_{\mathrm{overt.}}} = \frac{\mathrm{M}_{\mathrm{PP}} + \mathrm{M}_{\mathrm{W}}}{\mathrm{M}_{\mathrm{SP}} + \mathrm{M}_{\mathrm{H}_d} + \mathrm{M}_{\mathrm{Q}_h} + \mathrm{M}_{\mathrm{Q}_v}} \tag{5}$$

The rotation initiates when OSF < 1.0.
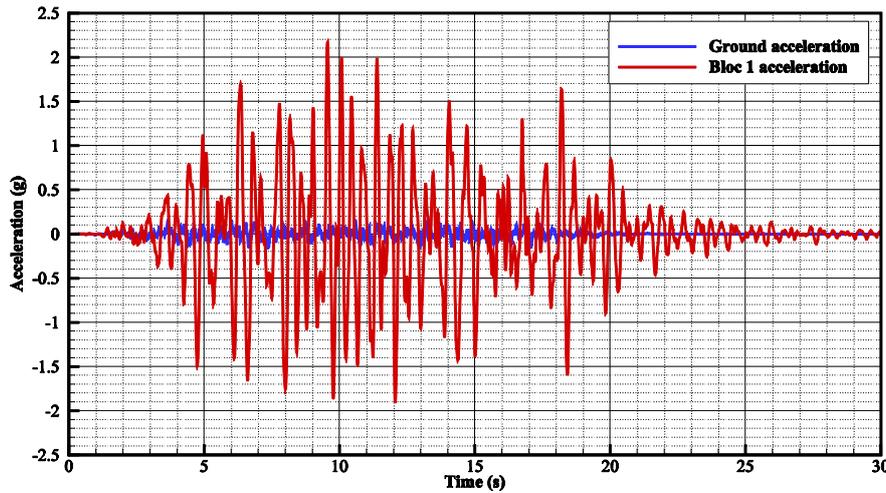
Fig. 31: Horizontal component of acceleration at the base of block 1 subjected to MCE1

Method 2: Finite element results stress integration
To verify if the assumption of permanently opened contraction joints during earthquake is conservative, a second method using stress integration of the finite element results and taking account the lateral confinement is achieved. The forces acting on the block's faces, obtained by stress integration, are show in Fig. 32.
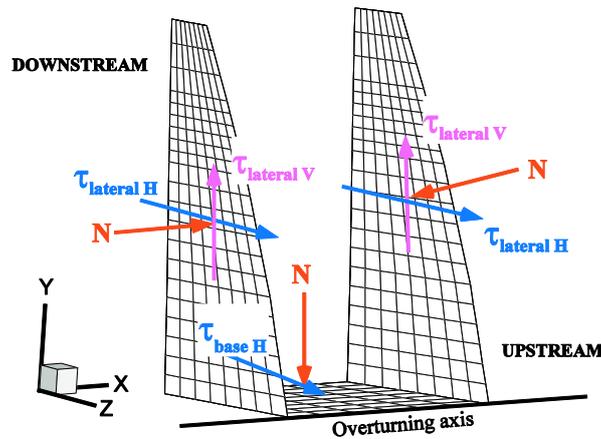
Fig. 32: Stress integration on the block faces

In a first set of analyses (identified as method 2a), the model is linear and assumes that the contraction joints remain closed during the earthquake. In a second set (identified as method

2b), the four central blocks have nonlinear Mohr-Coulomb elements in their contraction joints, leaving them free to open under seismic loads.

Method 3: Nonlinear finite element results block movement analysis
When safety factors are smaller than one, sliding should occur. Small residual sliding displacements do not necessarily indicate that the general safety of the blocks is compromised. Therefore, these displacements should be computed either by a Newmark sliding block analysis or by running a nonlinear finite element model comprising contact elements allowing sliding of blocks. Hence, for the most critical blocks analysed with the previous methods, a nonlinear analysis is used to compute the residual sliding displacements. The four central blocks have their contraction joints as well as their lift joints modeled using nonlinear Mohr-Coulomb elements. Therefore, the blocks are free to slide and rotate during the earthquake. For simplification, load combination with this method is achieved by applying all the loads at once during the analysis and the modulus used corresponds to the dynamic elastic modulus. Because the block inertia is required, self-weight is applied using a gravity load, therefore construction phases are not taken into account. The blocks considered in the analyses are located at the top of the dam, hence self-weight loads computed with this method is similar to those computed when considering construction phases.

Sliding and overturning results
The loads obtained with method 1 are listed in Tab. 4 for the full reservoir conditions for each block height and for the seismic acceleration time-history corresponding to the lowest safety factor.

Tab. 4: Rocking-sliding block stability analysis acting forces

Block Height (m)	8.5	17	30.8	44.6
Corresponding gound motion time-history	MCE1	MCE1	MCE2	MCE1
Acting loads	(kN)	(kN)	(kN)	(kN)
Self-weight, PP	-24 631.9	-60 918.1	-144 265.9	-249 752.8
Hydrostatic force, W	-1 102.0	-12 067.7	-58 629.8	-139 602.9
Uplift force, SP	3 983.8	13 786.2	36 538.0	65 199.8
Hydrodynamic force, H_d	5 672.3	26 539.9	73 519.1	112 259.8
Earthquake force, horizontal component Q_h	43 190.4	77 134.1	128 330 .3	151 496.8
Earthquake force, vertical component Q_v	15 513.8	22 806.3	33 057.9	45 032.0

The minimal safety factors obtained from the rocking-sliding analysis are listed Tab. 5 for a coefficient of friction of 1.96 ($\phi= 63°$). The results obtained with the three methods are compared. For method 1, the minimum SSF for the two smallest block is under 1.0, therefore an upstream sliding motion is expected. Similarly, an upstream rotation of all the blocks is expected. For method 2a, consideration of lateral confinement shows that no sliding should occur. However, the two smallest block are expected to have rotation. Because block 1 has the smallest SSF, only this block is used for nonlinear analysis with free joints (method 2b). This analysis shows that the SSF is between method 1 and method 2a, meaning that the joints open and close during the earthquake. Lateral confinement may therefore be reduced at certain times during the earthquake. The maximum opening computed is 4 mm while the upstream-downstream movement of the joints is 3 mm. With a nonlinear analysis (method 2b), the factors of safety do not necessarily return to pre-seismic values demonstrating that there can be permanent displacement of the blocks. This is shown in Fig. 34, where the sliding and overturning safety factors for block 1 are given as a function of time for earthquake MCE1.

This figure also indicate that safety factors smaller than one occur but only for very short period of time. The computation of displacements is therefore important to assess the safety of the blocks.

Tab. 5: Rocking-sliding block stability analysis results

	Safety factor	Block Height (m)			
		8.5	17	30.8	44.6
Method 1 (free body diagram)	Minimal factor of safety against sliding, SSF	0.21	0.52	1.02	2.21
	Minimal factor of safety against overturning, OSF	0.45	0.53	0.66	0.89
Method 2a (FE - joint closed	Minimal factor of safety against sliding, SSF	1.37	1.68	3.92	7.58
	Minimal factor of safety against overturning, OSF	0.30	0.31	1.28	3.88
Method 2b (FE - Mohr-Coulomb joints	Minimal factor of safety against sliding, SSF	1.25	-	-	-
	Minimal factor of safety against overturning, OSF	0.44	-	-	-
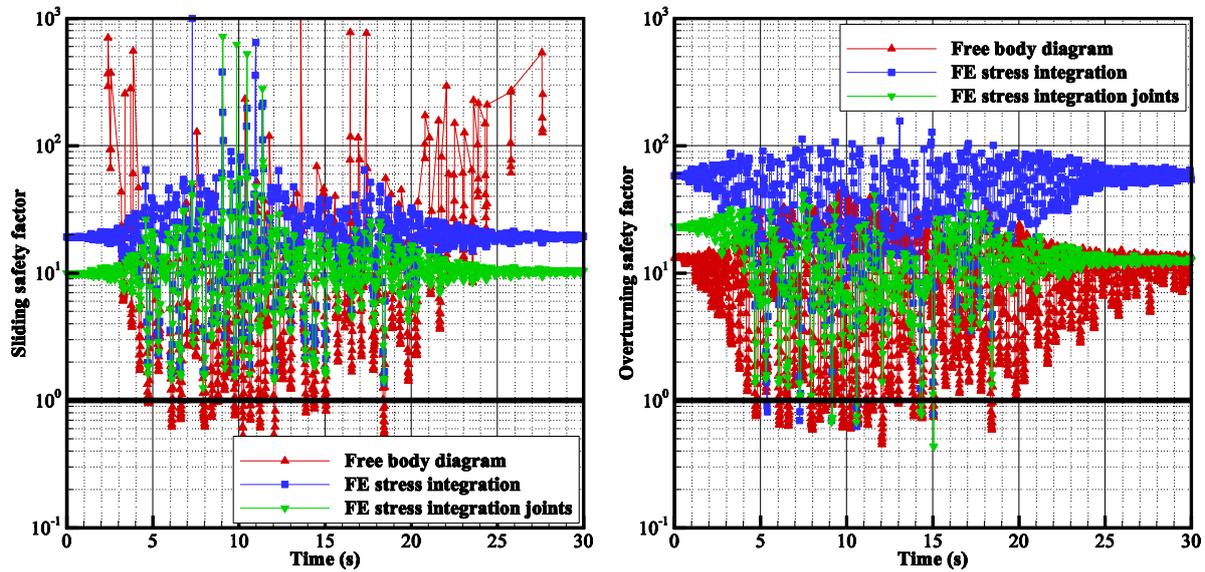
Fig. 33: Sliding and overturning safety factors for block 1, MCE 1

Two methods are compared to estimate the block sliding and opening during the earthquake. The first methods uses a Newmark sliding and overturning block analysis using the computer program RSDAM [6]. The second method uses nonlinear Mohr-Coulomb elements. Tab. 6 gives the maximum lift joint opening ($\Delta_{n,max}$), the final residual lift joint opening ($\Delta_{n,final}$), the maximum upstream displacement ($\Delta_{t,max}$) and the final residual block upstream displacement ($\Delta_{t,final}$) for the three seismic loads analysed. Only the results of the two smallest center blocks (block B and bloc C (previously named block 1)) are given. The results presented using RSDAM consider sliding and overturning separately because when combining both effects, convergence of the solution failed. Computation with RSDAM was only performed on block C. The previous analysis using stress integration showed that the SSF was over one. The sliding occurring during nonlinear analysis appears because when rocking occurs, the block also slides. There are some correlation to make when comparing the results obtained with RSDAM and nonlinear FE. It can be explained by the fact that the smaller displacements amplitudes found by taking into account sliding and overturning separately was compensated by not taking into account the lateral confinement in RSDAM. The earthquake MCE1 is inducing the largest displacements. The sliding and opening computed are of the same order of magnitude with the

exception of the large sliding computed using the nonlinear method for earthquake MCE1. Finally, due to the high friction coefficient used, the water pressure can't push back the blocks to their original position.

Tab. 6: Block displacement and lift joint opening

Method	Signal	Block B				Block C			
		$\Delta_{n,max}$ (cm)	$\Delta_{t,max}$ (cm)	$\Delta_{n,final}$ (cm)	$\Delta_{t,final}$ (cm)	$\Delta_{n,max}$ (cm)	$\Delta_{t,max}$ (cm)	$\Delta_{n,final}$ (cm)	$\Delta_{t,final}$ (cm)
Newmark (RSDAM)	MCE1	N/A	N/A	N/A	N/A	30.90	35.50	0.00	35.50
	MCE2	N/A	N/A	N/A	N/A	29.50	15.60	0.00	15.60
	MCE3	N/A	N/A	N/A	N/A	18.50	3.90	0.00	3.90
Method 3 (Nonlinear FE)	MCE1	27.47	135.14	0.01	129.40	28.82	97.17	0.01	91.01
	MCE2	16.07	12.13	0.01	6.90	12.04	19.56	0.01	16.01
	MCE3	7.58	5.80	0.01	4.80	6.89	5.19	0.01	5.12

Tab. 7 gives the joint opening computed with nonlinear FE for block C. The joint opening computed using this method are larger than those computed using method 2b because block rotation occurs. The final opening is nonzero therefore water flow through the joints could occur.

Tab. 7: Block C contraction joint opening

	Joint left bank		Joint right bank	
	$\Delta_{n,max}$ (cm)	$\Delta_{n,final}$ (cm)	$\Delta_{n,max}$ (cm)	$\Delta_{n,final}$ (cm)
MCE1	17.26	7.29	17.57	8.45
MCE2	9.29	8.55	8.44	5.43
MCE3	1.76	1.15	0.94	0.38

Sliding and rocking movement time-histories at the center of block C are given in Fig. 34 for MCE1. Absolute sliding is always positive showing that because of the dam geometry, the block moves only towards upstream. At some time steps, the upstream and downstream joint openings have a peak showing that the block's base is not in contact with the rest of the dam. The lift joint opening is greater at the upstream edge. Finally, Fig. 35 shows the final position of the four center blocks. The displacement of 91 cm is small compared to the 7.4 m thick blocks, however permanent displacement and possibly water flow through the contraction joints are the main consequences of an earthquake occurring on this dam assuming a detaching block.
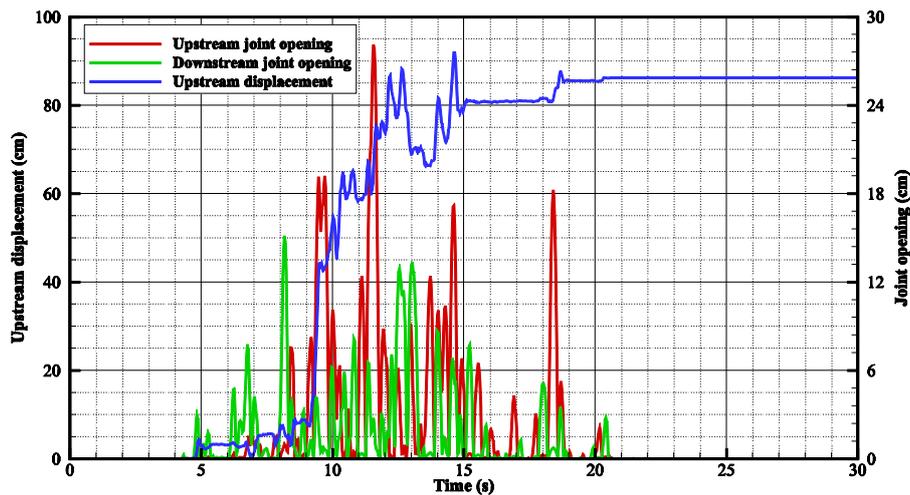
Fig. 34: Time histories of sliding and opening at center of block C
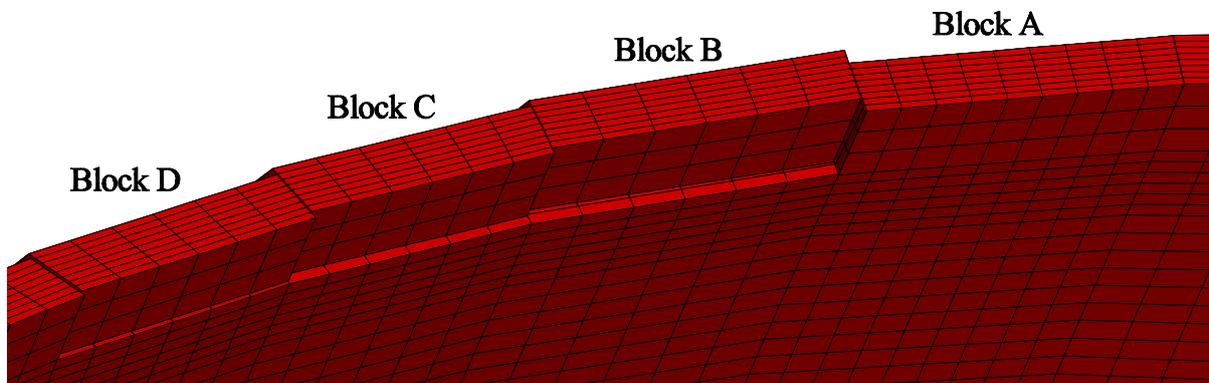
Fig. 35: Final displacements of the four central blocks, MCE 1 (no amplification)

Discussion and conclusion

The seismic safety verification of the Luzzone arch dam was performed considering load combination including thermal, hydrostatic, self-weight and seismic loads. The stresses and displacements caused by these loads were combined during post-processing considering that depending on rate of application as well as time-dependence the elastic modulus is different.

The level of principal tensile stresses found indicates that cracking occurs in the top portion of the dam. Therefore, investigation of a detaching block in the top center of the dam was investigated using three methods. The first method used free body diagram to compute the sliding and overturning safety factors without considering the lateral confinement. It was shown that using this method, all the blocks have a minimum overturning safety factors less than one. The second method using integration of the stress field obtained from the finite element results considered the lateral confinement. This method proved that method 1 was conservative for an arch dam. It was also shown by comparing safety factor time histories that using nonlinear Mohr-Coulomb in the contraction joints gives a more realistic solution, because the contraction joints open and close during the earthquake. The last method using nonlinear Mohr-Coulomb elements located in the contraction joints as well as is in the base of the four center cantilevers was able to determine displacement and rotation of these blocks during an earthquake. This analysis showed that the blocks neither overturn nor fall down. Therefore stability of the blocks

is ensured even if permanent movement as well as water flow through the contraction joints should occur.

To assess the global stability of the dam, questions remain to be completed:

1) The rock-concrete interface was considered monolithic, however high level of stresses were computed in some areas. Thus adequate strength characterization as well as initial piezometric data should be analyzed;

2) A massless foundation was used. It was indicated in [7] that neglecting foundation-rock mass and damping may overestimate the stresses by a factor of 2 to 3. Therefore, this analysis may be conservative;

3) A calibration against data from ambient or forced vibration tests should be performed for a dam of this importance. Stiffness, damping of the dam-water-foundation system as well as natural frequencies and sometimes mode shapes can be calibrated using this type of data;

4) Post seismic analysis should be performed considering seepage of water in the cracks to compute post-cracking behavior.

Acknowledgements

References

[1]   R. M. Gunn and A. D. Tzenkov, "13th Benchmark Workshop on the Numerical Analysis of Dams," ICOLD Committee on Computational Aspects of Analysis and Design of Dams, 2015.

[2]   J. M. Raphael, "The Nature of Mass Concrete in Dams," *Special Publication,* vol. 55, pp. 133-160, 1978.

[3]   F. J. Vecchio, N. Agostino, and B. Angelakos, "Reinforced concrete slabs subjected to thermal loads," *Canadian Journal of Civil Engineering,* vol. 20, pp. 741-753, 1993.

[4]   T. Szczesiak and B. Weber, "Hydrodynamic effects in a reservoir with semicircular cross-section and absorptive bottom," *Soil Dynamics and Earthquake Engineering,* vol. 11, pp. 203-212, 1992.

[5]   S.-N. Roth, P. Léger, and A. Soulaïmani, "A combined XFEM–damage mechanics approach for concrete crack propagation," *Computer Methods in Applied Mechanics and Engineering,* vol. 283, pp. 923-955, 1/1/ 2015.

[6]   M. Leclerc, P. Léger, and R. Tinawi, "RS-DAM user's manual," Ecole Polytechnique de Montréal, Montréal, Canada, 2002.

[7]   A. Chopra, "Earthquake Analysis of Arch Dams: Factors to Be Considered," *Journal of Structural Engineering,* vol. 138, pp. 205-214, 2012.

62

ICOLD 13th International Benchmark Workshop on the Numerical Analysis of Dams
Seismic safety evaluation of a concrete dam based on guidelines

J. Fouqué[1] and E. Robbe[1]

[1]*EDF-CIH, 15 Avenue du Lac du Bourget Savoie Technolac, 73370 Le Bourget du Lac, France*

ABSTRACT: The paper summarizes the main results of the dynamic analysis of Luzzone dam performing in accordance with the Swiss Directives. More precisely, it enables to evaluate and verify the seismic safety of the arch dam checking the global and the local stability of the dam. Thanks to three dynamic load combinations and a FEM with the assumption of massless foundation and water added masses, maximum tensile and compressive stresses have been highlighted. It enables to show that the maximum principal stress of the dam is not necessary checked during ground motion with a simplified model. In fact, the contraction joint between the dam and the foundation is not taking into account that leads to an overtaking of the dynamic tensile strength. Moreover, with this numerical model, the rocking block is not check for an assumed horizontal crack located on the heightened part of the dam.

E-mail: julie.fouque@edf.fr, emmanuel.robbe@edf.fr

Introduction

Because of the global seismic context regulation evolution, concerns are increasing in seismic safety evaluation. Currently, operators have the use of several national or international guidelines to perform seismic verification of their building. That is why the purpose of the 13th ICOLD Benchmark Workshop on the Numerical Analysis of dams (Theme A) is to evaluate and verify the seismic safety of Luzzone dam in order to compare results obtaining by several guidelines.

The analyses have been carried out following the Swiss guidelines and using Code_Aster, a FEM based software developed à EDF [4]. For the record, this code has been currently used in some themes proposed in previous ICOLD Benchmark Workshop [5].

Numerical model

In the Swiss seismic safety evaluation, methods of computation depend on dam class. According to the OSOA criteria, Luzzone dam is a class 1 double curvature arch dam. Therefore, the minimal requirement to evaluate seismic safety is a transient dynamic computation. For the class 1 dam, the Swiss directives prescribe finite elements for the dam and the foundation which is considered massless. The fluid-structure interaction is taken into account by Westergaard added masses. It is now well known that this method leads to an overestimation of the dam response considering that it doesn't take into account radiation damping into the foundation.

Mesh
The finite element mesh used for the computations has been converting into a universal file (*.unv), one of the file format used with Code_Aster thank to NX software. No mesh is needed for the reservoir considering that fluid-structure interaction is represented by added masses with a Westergaard formula: water compressibility is then not considered here which can lead to an

over or under estimation of the dam's response but is considered good enough in a first approximation.
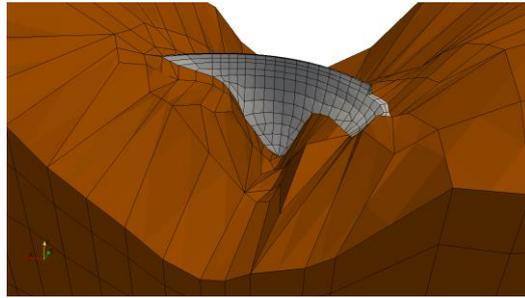
Fig. 1 : Dam-Foundation Finite Element Model

Material properties and constitutive laws
In accordance with the Swiss directives, modeling assumptions are the following ones:
- The dam is linear elastic material with 5% viscous damping;
- The foundation is elastic and massless (the massless foundation modeling prevents wave reflexion phenomena near boundaries but does not take into account radiative damping);
- The reservoir is represented with Westergaard added masses.

The material properties used for the computations are the ones provided by the formulators in section 4.2 [6]. It has to be said that here, the dynamic properties of the concrete have been taken into account, even for the static computation which is not correct and may lead to a certain error in the displacements and stresses computed.

Westergaard added mass approach
The added masses representation of dam water interaction during earthquake ground motion was introduced by Westergaard [1] in 1933. It enables to represent inertial fluid structure interaction during earthquake by approaching the hydrodynamic forces resulting from seismic loadings. For this approach developed for an infinite reservoir, a vertical upstream face and a rigid dam, added masses are applied in the normal direction of the upstream face. The Westergaard distribution (1) applied at each node is proportional to a surface density of mass which depends on:
- ρ_w : Water density
- H : Water depth
- z_0 : Reservoir level
- z : Level of the point on the dam upstream face

$$f(z) = \frac{7}{8} \times \rho_w \times \sqrt{H \times (z_0 - z)} \ (1)$$

Modal analysis

The first natural frequencies computed with a modal analysis on Code_Aster are shown in Tab. 1, for an empty and full reservoir, and the modal shape in Tab. 2. As expected, the added masses decrease the natural frequencies of the dam. In Tab. 1, an important point can be notice: whatever the reservoir configuration, the first two eigenfrequencies are very close. Moreover, it is interesting to observe that eigenfrequencies 1, 2, 3, 4, 8 and 9 contribute strongly to the u/d

direction participation factor whereas in side-to-side direction, it is the eigenfrequencies 2 and 6. In addition, if we compare eigenfrequencies for the empty and full reservoir, it is possible to note that the first two eigenfrequencies are reversed.

Finally, a link between participation factors and modal shape can be made. In fact, when the participation factor in the upstream/downstream direction is important, the modal shape of the eigenfrequency is symmetrical. It is the case for the eigenfrequencies 1, 3, 4, 8 and 9.

For information, dynamic computations have been performed with a modal base going up to 30Hz.

Tab. 1 : First eigenfrequencies

Mode	Empty Reservoir				Full Reservoir			
	f, Hz	X, %	Y, %	Z, %	f, Hz	X, %	Y, %	Z, %
1	2,01	6,91	0,02	0,18	1,26	2,02	0,31	17,51
2	2,10	0,24	0,78	20,51	1,29	7,23	0,00	9,68
3	3,02	0,04	0,57	5,95	1,97	0,18	0,05	7,97
4	3,78	0,03	7,74	12,52	2,29	0,08	1,08	21,33
5	3,98	0,21	0,18	0,60	2,61	0,46	0,00	0,12
6	4,47	25,00	0,00	0,13	2,89	13,67	0,05	0,01
7	5,01	0,07	2,22	1,87	3,35	0,01	0,00	1,54
8	5,21	0,98	47,29	1,12	3,47	0,03	0,92	6,08
9	5,83	24,08	1,33	0,81	3,87	0,01	3,23	5,77
10	5,96	3,61	0,42	2,28	4,13	0,84	0,08	0,01
11	6,16	0,10	0,01	0,05	4,40	4,70	0,02	0,18
12	6,31	1,03	1,05	11,99	4,82	0,83	0,51	2,13

Tab. 2 : Modal Shapes

Mode 1 – 1.26 Hz   Mode 2 – 1.29 Hz   Mode 3 – 1.97 Hz   Mode 4 – 2.29 Hz

Mode 5 – 2.61Hz   Mode 6 – 2.89 Hz   Mode 7 – 3.35 Hz   Mode 8 – 3.47 Hz

Mode 9 – 3.87 Hz   Mode 10 – 4.13 Hz   Mode 11 – 4.40 Hz   Mode 12 – 4.82 Hz
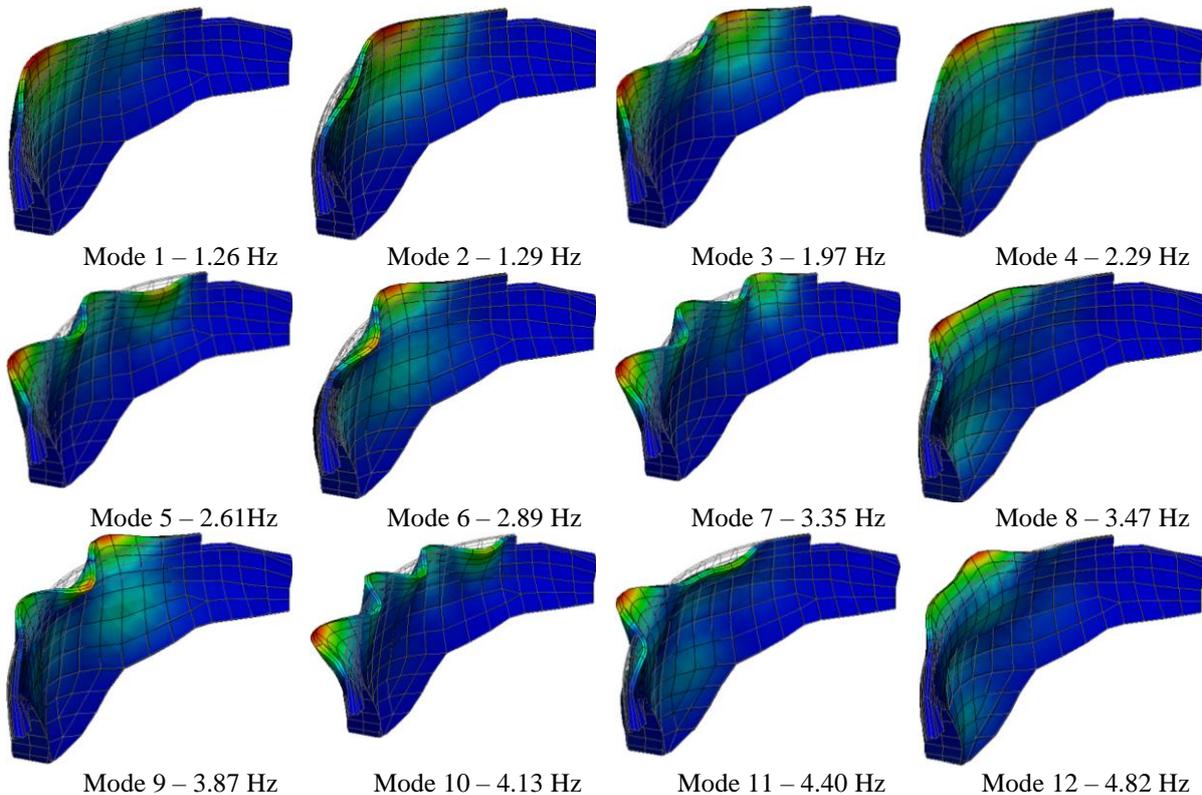
Dam behaviour static analysis

Under statics loads, the maximum radial displacement reaches 7.22 cm at the top of the central cantilever (Fig. 2) due to hydrostatic load, silt pressure and thermal effect (summer).
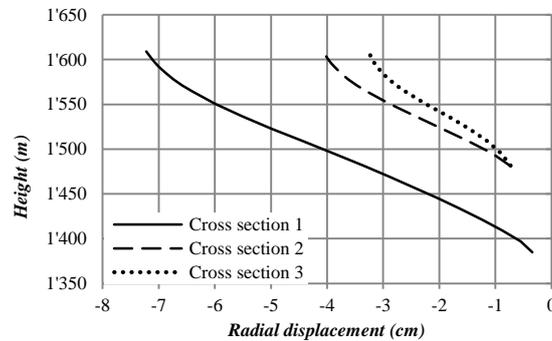
Fig. 2 : Radial static displacement Envelopes

The maximum static principal stresses in tensile is located in the lower portion of the upstream face, more precisely at the contact between dam and the foundation. The tension reaches 5.77 MPa after the impounding and 6.05 MPa when the silt pressure is applied. After the thermal loading (summer), the tensile strength decreased and yields 3.04 MPa (as shown in Fig. 3).
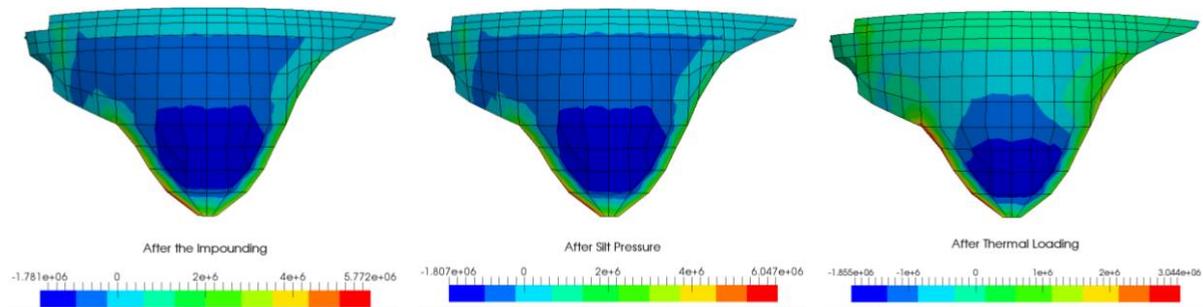
Fig. 3 : Maximal Principal Stress Envelopes on upstream face

The minimum static principal stress (compression) is located in the lower portion of the downstream face at the rock abutment level. The value computed after the impounding is 10.82 MPa, whereas the one computed after the thermal loading reaches 12.21 MPa.
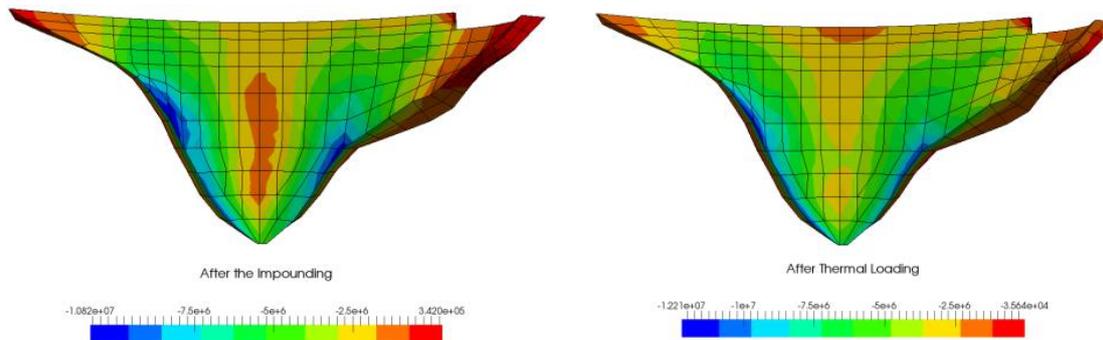
Fig. 4 : Minimal Principal Stress Envelopes on Downstream face

Dam behaviour analysis during Earthquake

Displacements

During ground motion, the maximum radial displacements are obtained at the top of the central cantilever to the downstream for the first earthquake with 8.78 cm (Fig. 5). The second earthquake triggers a maximal displacement of 7.47 cm to the upstream ant the third earthquake 7.40 cm to the downstream.
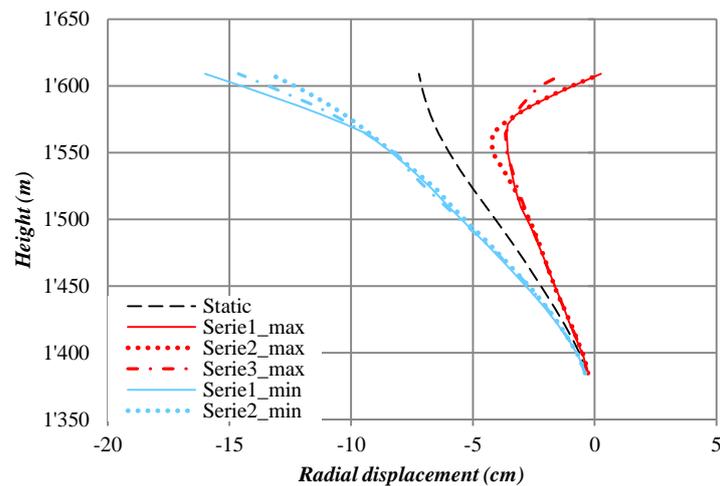
Fig. 5 : Radial displacement Envelopes for the X-section 1

Local stability

Local stability is evaluated by checking principal stresses obtained during ground motion. In fact, in accordance with the Swiss guidelines [2], if the dynamic tensile strength of the concrete is lower than 4 MPa and the dynamic compressive strength is lower than 57 MPa, local stability of the dam is checking. In Fig. 3 and Fig. 7, it is possible to notice that the maximum and minimum principal stresses obtained from all the investigated dynamic load combinations reached respectively 4.63 MPa (tensile) and 13.78 MPa (compressive).

The important values of tensile strength are located near to breaking slopes. In fact, the maximum principal stresses is located in one point on the upstream face (as shown in Fig. 7), but it seems to result for the mesh shape and a wrong interpolation of the stress in this point. So, the maximal tensile strength is rather located in the lower part of the left abutment of the upstream face (on the breaking slope). As seen previously in the static analysis, the important tensile strength is strongly linked to the static load combinations (impounding). It might be useful in the future to evaluate the tensile stress in this point in winter condition with the earthquake.

This important tensile stress could lead to the opening of a joint at the contact between the dam and the foundation. That could be done using a non-linear analysis.

The minimum principal stresses are located in the lower part of the downstream face as shown in Fig. 6.
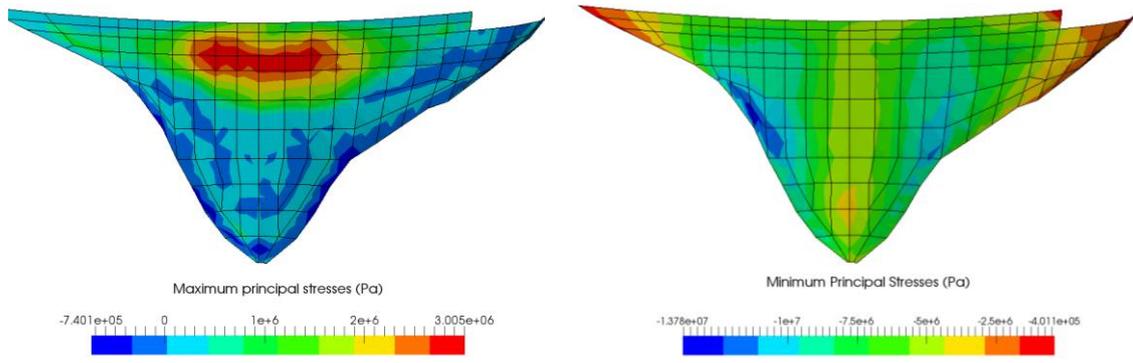
Fig. 6 : Principal stress Envelopes on downstream face
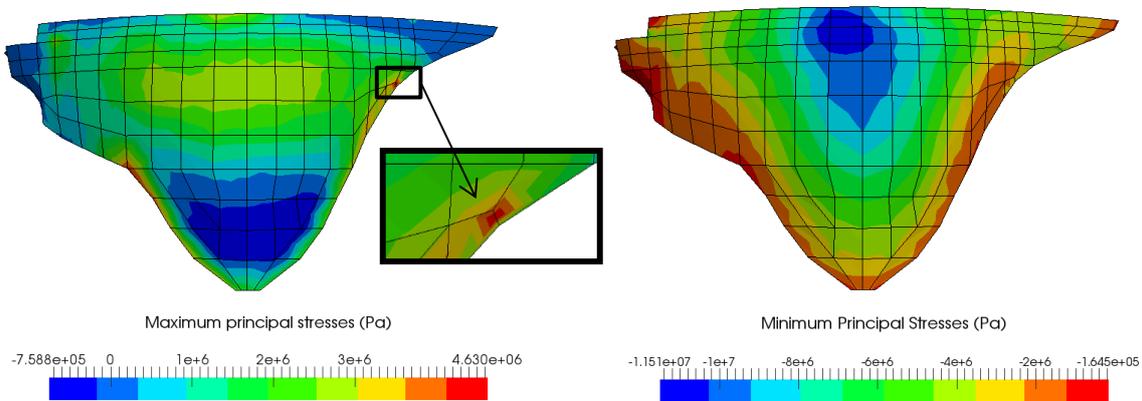
Fig. 7 : Principal stress Envelopes on upstream face

Global stability

A safety factor related to the sliding of the dam corresponds to the ratio between the normal and the tangential forces. It has been calculated at different levels during dynamic computation. It has been evaluated with a 63 ° friction angle, 0 MPa cohesion and a triangular distribution for the computation of the uplift force.

$$F_S(t) = \frac{(F_{N\_STATIC} + F_{N\_DYNAMIC}(t)) \times \tan \varphi + c \times S}{F_{T\_STATIC} + F_{T\_DYNAMIC}(t)}$$

With F_{N_STATIC}, $F_{N\_DYNAMIC}$: Static and dynamic normal forces

F_{T_STATIC}, $F_{T\_DYNAMIC}$: Static and dynamic tangential forces

φ : Friction angle

c : cohesion

S : surface

Here, the safety factor has been evaluated at each instant of the earthquake. Then, the minimum value during the whole 3 earthquake case has been extracted.

It is interesting to observe that under static load (Tab. 3), the safety factor is higher than 1.5, so according to the Swiss directives [3] there is no risk of sliding for the four different levels of the assumed horizontal crack. However, during earthquake, values obtained for the elevation 1600.5 and 1592 are lower than 1.1. It is important to note that the safety factor does not take into account the lateral friction and the hoop effects more important in the upper part of the dam for the static component. So in these conditions, and in accordance with the Swiss prescriptions [3], there might be a risk of sliding during the earthquake if the assumed horizontal crack is located at 1600.5 m or 1592 m. A non-linear analysis with joint element might be useful in order to evaluate more precisely this matter.

Tab. 3 : Safety factor against sliding

	Static Safety Factor	Dynamic Safety factor
El. 1600.5 (H = 8.5 m)	11.77	0
El. 1592 (H = 17 m)	4.37	0.4
El. 1578.2 (H = 30.8 m)	2.49	1.42
El. 1564.5 (H = 44.5 m)	1.9	1.22

Conclusion

The dynamic analysis of Luzzone dam has been performed according to the Swiss Directives and the basic requests of the Formulators. A 3D finite element model with the assumption of a massless foundation and water added masses with a Westergaard repartition has been used for the computations.

The analysis of the dam under static loads highlights important tensile stresses on the lower part of the upstream face, especially after the impounding. Due to the important tensile stresses, during ground motion, the seismic safety of the dam is not checked since the maximum principal stress overtakes the dynamic tensile strength. However, it can be notice that these important tensile stresses could lead to the opening of a joint at the contact between the dam and the foundation that is why for future numerical model, it would be interesting to take into account the contraction joint.

Considering this simplified numerical model, the global stability of the dam is not checked for an assumed horizontal crack located in the heightening part of the dam. But, it can be notice that the computed safety factor does not take into account the lateral friction and the hoop effects more important in the upper part of the dam.

To conclude, with a simplified finite element model, the seismic safety of the Luzzone dam is partially checked. For future studies, it could be also interesting to evaluate the effect of radiative damping in the foundation and also compressibility of the water on the results of the seismic safety analysis of the dam.

References

[1] Westergaard, H.M (1933). Water pressure on dam during earthquakes. transactions American Society of Civil engineers, Vol 98.

[2] Sécurité des ouvrages d'accumulation. Documentation de base pour la vérification des ouvrages d'accumulation aux séismes, rapports de l'OFEG, série Eaux, version 1.2, mars 2003.

[3] Sécurité des ouvrages d'accumulation. Documentation de base relative à la sécurité structurale, rapports de l'OFEG, série Eaux, Août 2002.

[4] www.code_aster.org

[5] A. Diallo and E. Robbe, "12th International Benchmark Workshop on Numerical Analysis of Dams, Fluid Structure Interaction Arch Dam – Reservoir at Seismic Loading".

[6] Dr. Russell Michael Gunn and Dr. Anton Doytchinov Tzenkov (2015).13th Benchmark Workshop on the Numerical Analysis of Dams, Seismic Safety Evaluation of a Concrete Dam Based on Guidelines.

Seismic Safety Evaluation of a Concrete Dam Based on Guidelines Theme A – 13th Benchmark Workshop on the Numerical Analysis of Dams

Goldgruber M.[1], Shahriari S. [1] and Zenz G.[1]

[1]*Institute of Hydraulic Engineering & Water Resources Management, Stremayrgasse 10/2, A-8010 Graz, Austria*

ABSTRACT: The 13th Benchmark Workshop on the Numerical Analysis of Dams is held in the city of Lausanne. Every two years different topics are formulated to investigate and evaluate. The focus of this year's theme A topic is to perform a seismic verification of the Luzzone arch dam based on guidelines. Upon the evaluation of different stresses and displacements the local and global stability should be judged. The safety factors are calculated by using the limit equilibrium method and applying the guideline from the U.S. Army Corps of Engineers. Based on this method the integrity of the structure cannot be ensured, because three dimensional effects are not taken into account in the right way. The radial orientation of the block/contraction joints or shear keys, for instance, are neglected. Therefore, as conclusion, it is recommended to perform additional nonlinear analyses of the structure to evaluate the safety of the dam properly.

E-mail: markus.goldgruber@tugraz.at

Introduction

For the International Commission on Large Dams (ICOLD) the "Committee on Computational Aspects of Analysis and Design of Dams" is the general Organizer of Benchmark Workshops. The 13th Benchmark Workshop is held in the city of Lausanne from 9th – 11th of September 2015. Since 1991, eleven benchmark workshops have been organized for different numerical problems in the field of concrete and fill dams under static and dynamic loading conditions. The results of these benchmark workshops are made available to the dam engineering community on the internet and in proceedings (http://www.icold-cigb.org).

In this benchmark workshop, in Lausanne 2015, the focus of theme A [1] is to perform a seismic verification of an arch dam based on guidelines. The structure under consideration is the Luzzone dam. It is a double-curvature arch dam located in the south eastern part of Switzerland in the Kanton Tessin. It was built in the 1960s and later heightened by 17.0 meters in the 1990s. The Swiss directives categorized it as a "Class 1" dam whose safety has to be evaluated for an earthquake with a return period of 10000 years, which is the main subject of this benchmark. Among others, which are in general claimed for a "Class1" dam, the formulators requested following points at least to be performed:

- Preparation of a finite element model for seismic verification (geometry, boundary conditions, initial conditions, materials);
- Analysis of the natural frequencies;
- Modelling of the operation period loads;
- Analysis of the dam behavior during earthquake by means of the direct time-step integration method for three stochastically independent acceleration-time histories and linear-elastic materials with viscous damping;
- Check of the local stability (stresses);
- Check of the global stability against sliding and overturning;
- Conclusions on the seismic safety of the dam;

Therefore, the formulators provided a complete mesh and material properties of all parts (dam, foundation and reservoir), three different and independent acceleration-time histories for all three directions (x, y and z), etc.

Furthermore, it should be mentioned that the same structure has already been investigated in a previous benchmark regarding the safety of the abutment at the left bank. The same problem has been investigated by Goldgruber in 2011 [2].

Numerical Model

The program which is used for the simulations is Abaqus/Cae; therefore, the finite element model/mesh provided by the formulators [1] was converted from DIANA. The geometry and mesh topology are kept the same. Quadratic element formulation with reduced integration is used for all parts (dam, foundation and reservoir). Due to the fact that in Abaqus/Cae the z-direction must be vertical to define hydrostatic loading in the simulations the model is rotated to fit this condition. Hence, the x-axis stays the same, the y-axis is now in stream direction and the z-axis is vertical. The three acceleration-time histories defined by the formulators are transformed to be consistent with the coordinate system from the original model. Fig. 1 shows the model in Abaqus/Cae with the new coordinate system.
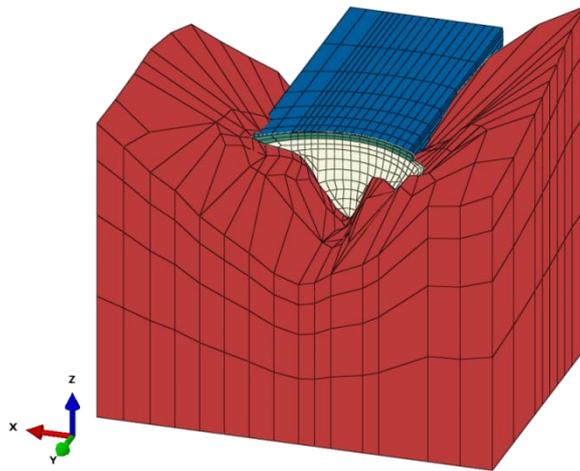
Fig. 1: Finite element model in Abaqus/Cae with the new coordinate system

Material properties

The material properties for all parts are defined as prescribed by the formulators in [1] and summarized in Tab. 1. For the initial summer temperature distribution in the dam structure specific heat capacity and thermal conductivity are needed. They were not provided and therefore typical values are chosen. Furthermore, all parts are homogenous and isotropic and nonlinearities of the material or contacts are not taken into account.

Tab. 1: Material properties of all parts

Dam		
	Old Concrete	**New Concrete**
Density	2.5 t/m³	2.4 t/m³
Static Modulus of Elasticity	20 GPa	18 GPa
Dynamic Modulus of Elasticity $E_d = 1.25 E_s$	25 GPa	22.5 GPa
Poisson's Ratio	0.18	0.18
Thermal Expansion	10^{-5} 1/°C	10^{-5} 1/°C
Specific Heat Capacity	880 J/kg°K	880 J/kg°K

Thermal Conductivity	2.222W/m°K	2.222W/m°K
Static Compressive Strength f_c	38 MPa	32 MPa
Dynamic Compressive Strength $f_{cd} = 1.5f_c$	57 MPa	48 MPa
Static Tensile Strength f_t	3 MPa	2.3 MPa
Dynamic Tensile Strength $f_{td} = 1.5f_t \leq 4\ MPa$	4 MPa	3.5 MPa
Foundation		
	Rock Mass	
Static Modulus of Elasticity	18.6 GPa	
Dynamic Modulus of Elasticity $E_d = 1.25Es$	23.3 Gpa	
Poisson's Ratio	0.20	
Reservoir		
	Water	
Density	1.0 t/m³	
Bulk Modulus Kw	2073.6 MPa	

Boundary conditions of the foundation and dam

For static loading the boundaries of the foundation are locked normal to their surfaces. In the dynamic case these boundary conditions are replaced by the acceleration-time histories.
The dam and foundation are completely tied; hence opening and/or relative displacement is not possible between these parts. The same coupling is used between the dam and the reservoir.

Reservoir modelling

The reservoir for the seismic simulations is modelled as acoustic fluid. Such fluids or elements describe the sound wave/pressure distribution over time in acoustic media like gases or water. Commonly used in sound simulations, such elements also allow for simulating fluid-structure interaction problems if the following assumptions are valid:

- the fluid is compressible (density changes due to pressure variations),
- the fluid is inviscid (no viscous dissipation),
- the fluid is irrotational,
- there is no mean flow of the fluid (only small translations and small velocity $v \ll$)
- no body forces

These elements are governed by the following equation:

$$\frac{\partial^2 \boldsymbol{p}}{\partial t^2} - \frac{K_w}{\rho_w} \nabla^2 \cdot \boldsymbol{p} = 0 \tag{1}$$

Where K_w and ρ_w are the bulk modulus and the density of water, respectively.
Following additional boundary conditions are specified for the reservoir:

- The upper boundary of the reservoir is set to be a free surface with $p = 0$.
- The back-end boundary is defined to be non-reflecting. In this case no pressure waves will be reflected back to the dam structure.

- The side boundaries are modelled as partly absorbing boundaries. Therefore, impedance values c are defined to match a wave reflection coefficient of $\alpha = 0.5$ (50% reflection). The impedance c in terms of the reflection α and material properties of the water is

$$c = \frac{1 + \alpha}{1 - \alpha} \sqrt{\rho_w K_w} = \frac{1 + 0.5}{1 - 0.5} \sqrt{0.001 \cdot 2073.6} = 4.32 \qquad (2)$$

Loading

According to the formulators 5 different loadings should be applied to the model, dead weight, hydrostatic water load (1606 m a.s.l.), silt pressure, summer temperature and seismic acceleration. For the case of seismic loading three different acceleration-time histories are provided and are asked to be simulated. Tab. 2 shows the load combination which have to be evaluated by the participants.

Tab. 2: Load combination to be evaluated

Load combinations		Static		Dynamic		
		SU0	SU2	DE2		
Dead weight		x	x	x	x	x
Hydrostatic water load		x	x	x	x	x
Silt pressure		x	x	x	x	x
Summer temperature			x	x	x	x
Earthquake	Series 1			x		
	Series 2				x	
	Series 3					x

Dead weight loading
The stresses in the structure due to dead weight loading are computed in 6 steps which correspond to the construction stages from bottom to the top, see [1]. In case of civil engineering structures, where the gravity is mostly the essential loading, the displacements during construction are compensated and the structures are built according to the design drawings. This fact leads to the problem in the simulations that the gravity loading is acting on the structure and therefore a displacement is computed. As long as these displacements are small and the systems behavior is linear they can be ignored and subtracted from subsequent steps and only the stresses are considered and added to further results. Nevertheless, Abaqus/Cae offers the possibility of a simulation step which iterates to find a solution which is in equilibrium with the applied loading and zero displacement. This procedure is used for dead weight loading in these simulations and the specified tolerance for this iterative procedure is set to 10^{-7}, which is the ratio between the maximum absolute displacement and the characteristic element length.

Hydrostatic water load
The applied hydrostatic pressure corresponds to the maximum operating water level of the dam at 1606 m a.s.l. (Note: Crest is at 1609 m a.s.l.). No water pressure from the downstream side is accounted for.

Silt pressure
As the hydrostatic load, the silt load is also only acting on the upstream face of the arch dam. The elevation of the silt is defined by the formulators to be at 1440 m a.s.l., with a buoyant density of 400 kg/m³. Hence, by assuming a hydrostatic behavior of the silt the maximum pressure at the upstream heel is 216 kPa.

Summer temperature
The temperature gradients on the upstream and downstream face and the grouting temperature were provided by the formulators [1]. The temperature when the grout is injected and the blocks stay fully in contact is set to be the initial temperature. This means that any change relative to the grouting temperature will lead to compressive or tensile stresses in the structure.
The simulations are split up into two parts:

- Steady state temperature distribution calculation in the dam body due to the applied annual summer temperatures from Fig. 4-6 in [1] on the upstream and downstream side.
- Standard temperature loading simulation which computes strains and stresses due to expansion of the structure. The temperature distribution from the preceding steady state simulation is imported and the initial temperature is defined to be the grouting temperature.

Earthquake
The formulators provided three different acceleration-time history records for all three directions. All records should be simulated, evaluated and compared. The maximum accelerations in the three directions according to coordinate system in the Abaqus/Cae model are as follows:

- x-direction (cross valley): 0.160g
- y-direction (upstream-downstream): 0.160g
- z-direction (vertical): 0.106g

For the damping of the structure Rayleigh damping is used with mass- and stiffness proportional factors of $\alpha = 0.6$ and $\beta = 0.001$. These values have been directly taken from the provided files by the formulators.

Results

Due to the restricted number of pages not all of the requested results by the formulators are shown in hear. However, following simulations have been carried out and evaluated:

- Analysis of the first 12 natural frequencies (full and empty reservoir) and mode shapes (only full reservoir).
- Displacement-time history at one node at the crest (x=0, z=1609, y=29.145)
- Displacement envelopes at three cross sections (left bank, right bank and middle section)
- Maximum and minimum principle stress envelopes on the up- and downstream face
- Stress envelopes at three cross sections (left bank, right bank and middle section) on the up- and downstream face
- Maximum and minimum principle stress values at 10 points on the up- and downstream face, respectively, for all load combinations and each loading alone.

- Maximum and minimum principle stress-time history at two nodes on the up- and downstream face, respectively.
- Rocking block stability of one dam cantilever for 4 different block heights and a friction angle of 63° and zero cohesion.
- Evaluation of the dam safety regarding local and global stability according to a preferred guideline.

It should be mentioned that superimposing results of different stresses and displacement is only valid if the direction stays the same, e.g. hoop stresses, vertical stresses, etc. Therefore, superimposing principle stresses isn't allowed, because their directions change in each step according to the loading. Because of this fact and the problem that changing material parameters between steps in Abaqus/Cae isn't possible, the results of principle stresses of the requested 10 points up- and downstream, respectively, have been evaluated for dynamic material properties for all simulation steps, including the static ones for the loading combination DE2 from Tab. 2. This is also the case for the evaluated principle stress time histories. These results are only provided to the formulators and not depicted in this paper.

Natural frequencies and mode shapes
Tab. 3 shows the natural frequencies and effective mass for the first 12 modes of the empty and full reservoir case (acoustics and added mass approach). For the empty case, 12 modes are covering already around 70% in each direction, whereas the full reservoir reaches much less percentage. This is attributable to coupled reservoir (acoustic fluid) and dam system, where the mass of the water is implicitly affecting the total excited mass.

Tab. 3: Natural frequencies and effective mass percentage of the empty and full reservoir

Mode	Empty Reservoir				Full Reservoir (Acoustic)			
	Natural Freq.	Effective Mass Percentage			Natural Freq.	Effective Mass Percentage		
	f [Hz]	X [%]	Y [%]	Z [%]	f [Hz]	X [%]	Y [%]	Z [%]
1	1.99	8.20	0.16	0.03	1.51	0.43	13.66	0.44
2	2.09	0.22	24.27	0.91	1.53	4.52	0.63	0.00
3	3.00	0.04	7.20	0.70	2.10	0.00	0.05	0.02
4	3.76	0.03	14.36	9.09	2.26	0.00	0.93	0.19
5	3.94	0.24	0.91	0.31	2.39	0.01	1.90	0.04
6	4.43	30.11	0.18	0.00	2.80	0.00	0.97	0.40
7	4.95	0.12	2.06	1.56	3.15	0.48	0.00	0.06
8	5.18	1.27	1.38	55.69	3.34	0.51	3.05	1.24
9	5.76	29.41	1.57	2.26	3.42	4.09	1.16	0.27
10	5.91	2.02	2.04	0.37	3.92	0.02	0.71	0.90
11	6.06	0.29	0.03	0.03	4.06	0.82	0.59	0.07
12	6.27	1.11	14.22	1.31	4.25	0.52	0.22	0.13
Σ		**73.05**	**68.40**	**72.26**		**11.41**	**23.87**	**3.74**

Mode	Full Reservoir (Added Mass)							
	Natural Freq.	Effective Mass Percentage						
	f [Hz]	X [%]	Y [%]	Z [%]				
1	1.18	8.20	0.16	0.03				
…	…	…	…	…				
12	4.40	5.314	0.034	0.139				
Σ		**20.53**	**66.52**	**2.617**				

For comparison reasons the sum for considering 50 modes for the full reservoir case with acoustic elements will result in almost the same percentages as the empty case.

The frequency evaluation has additionally been performed with the added mass approach according to Westergaard [6]. Similar to the full reservoir case with acoustic elements this model also yields much less effective mass in z-direction (vertical) and x-direction (cross valley), because the added mass matrix is modified (consistent mass matrix) in a way that only normal forces are acting on the dam's upstream face and shear forces (parallel to the face) are neglected. This effect is automatically taken into account by using acoustic elements. However, they are yielding much less effective mass sums for the 12th mode in y-direction than the added mass approach.

Fig. 2 depicts the first 3 mode shapes of the full reservoir case. Modes 4 to 12 are only provided to the formulators.
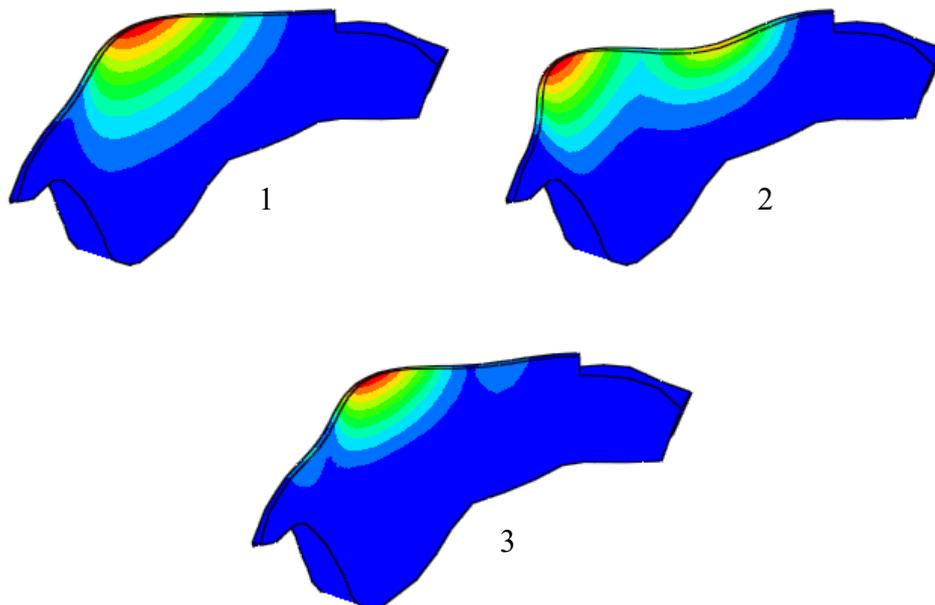
Fig. 2: First 3 natural mode shapes for full reservoir conditions

Displacement time histories

Fig. 3 shows the radial displacement-time histories for all load cases combined and all three seismic records of one node at the crest (x=0, z=1609, y=29.145).
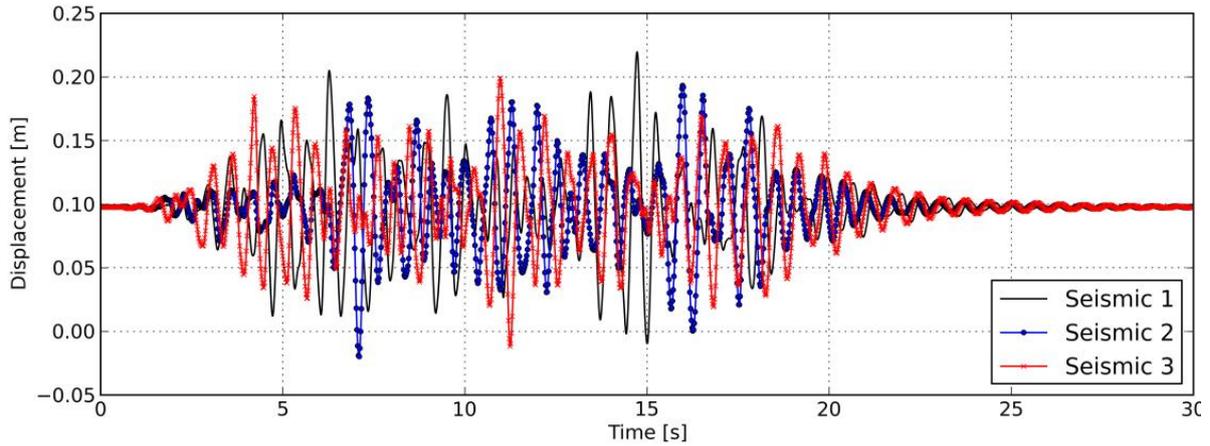
Fig. 3: Displacement-time histories at the crest in middle section of the dam at (x=0, z=1609, y=29.145)

Displacement envelopes at cross sections

Fig. 4 shows the displacement envelope in the middle section for all load cases combined and the three different seismic records in the middle section of the dam.
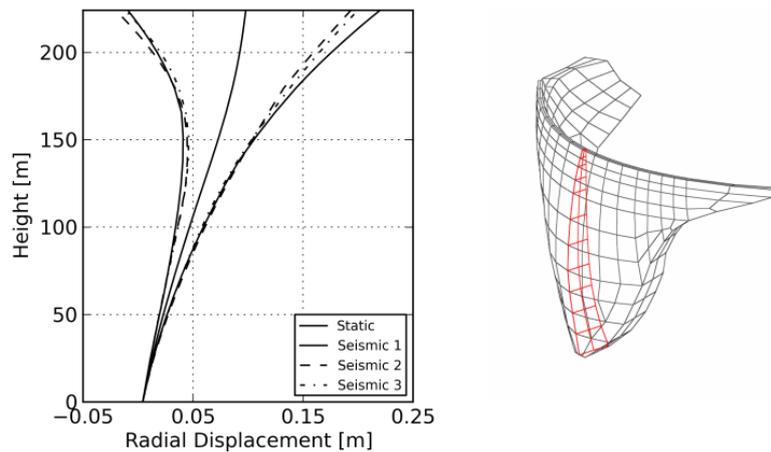
Fig. 4: Displacement envelope in the middle section of the dam

Principle stress envelopes on U/S and D/S faces

Fig. 5 shows the maximum principle stress (tensile stresses) envelopes on the up- and downstream face for all load cases combined and the three different seismic records. The legend is scaled so that grey areas are the ones which exceed the dynamic tensile strength of the old concrete of 4.0 MPa.
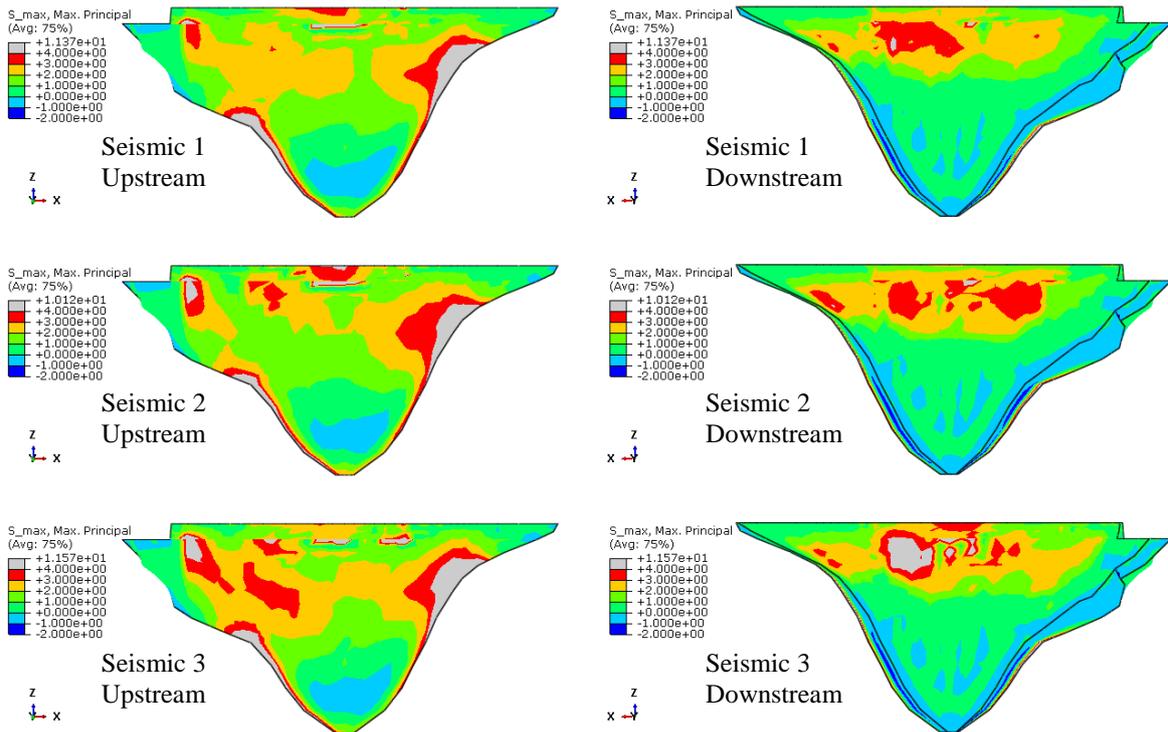
Fig. 5: Maximum principle stress envelope on the up- and downstream face

Fig. 6 shows the minimum principle stress envelope on the up- and downstream face for all load cases combined and the three different seismic records. The legend is scaled to a maximum compressive stress value of -25.0 MPa and hence should indicate that these stresses are rather small compared to the maximum dynamic compressive strength of the old and new concrete of -57.0 MPa and -48.0 MPa, respectively.
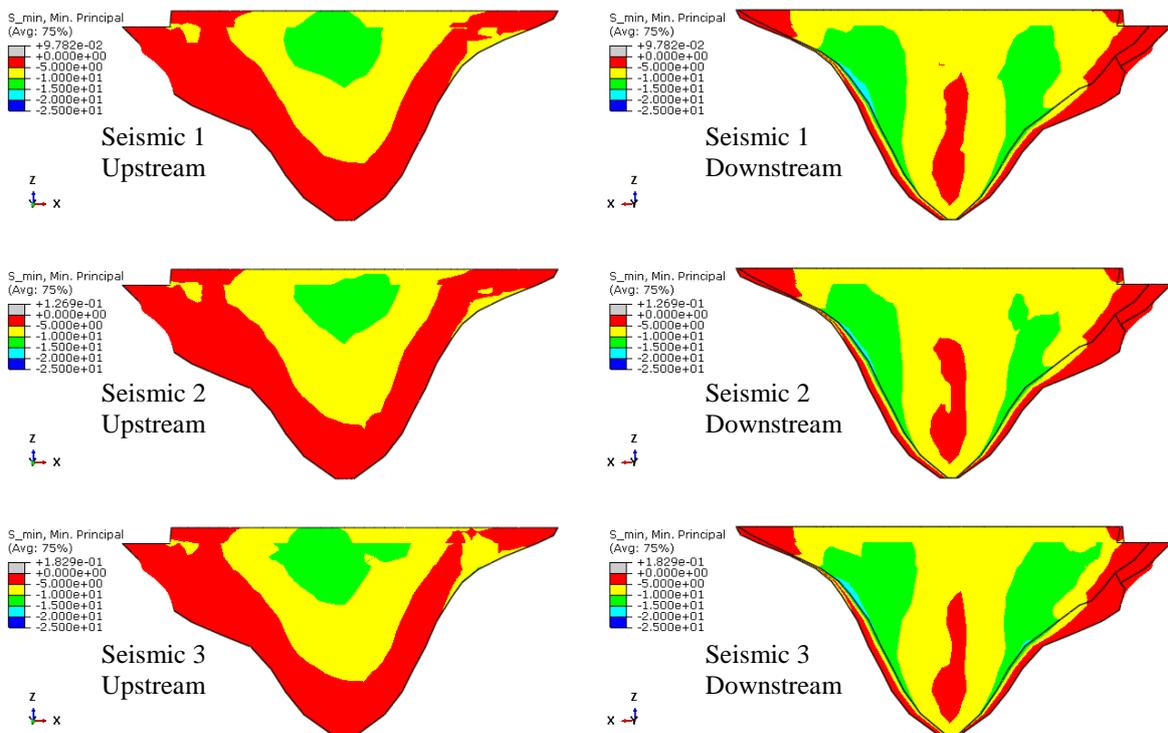
Fig. 6: Minimum principle stress envelopes on the up- and downstream face

Hoop stress envelopes in the middle section of the dam

Fig. 7 shows the hoop stress envelope in the middle section for all load cases combined and the three different seismic records in the middle section of the dam on the up- and downstream side. The gap in the stress distribution is attributable to the change of the material properties of the old- and new concrete.
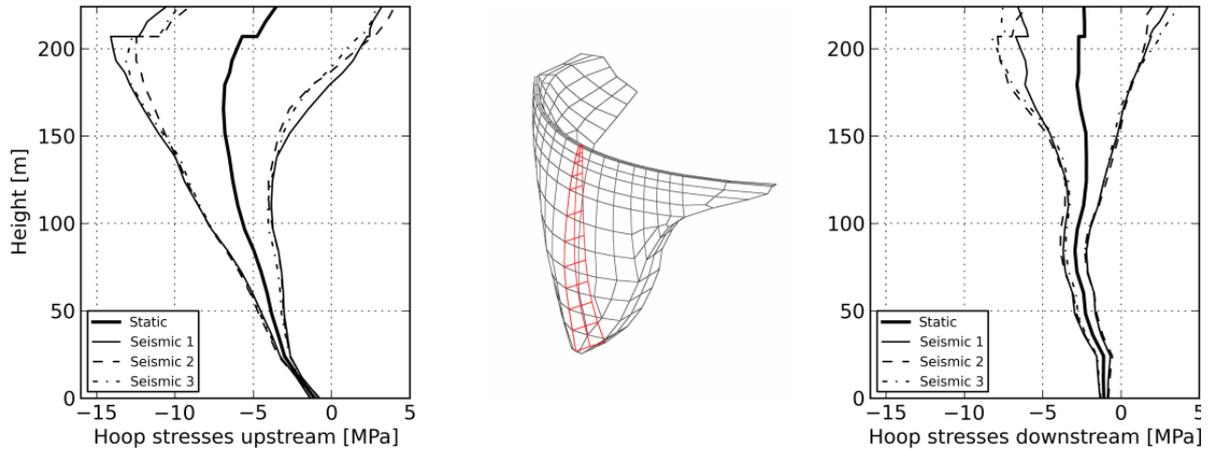
Fig. 7: Hoop stress envelope in the middle section of the dam

Vertical stress envelopes in the middle section of the dam

Fig. 8 shows the vertical stress envelope in the middle section for all load cases combined and the three different seismic records in the middle section of the dam on the up- and downstream side. The gap in the hoop stress distribution in Fig. 7 also exists here but much smaller due to the lower stress level and hence is not visible in the diagrams.
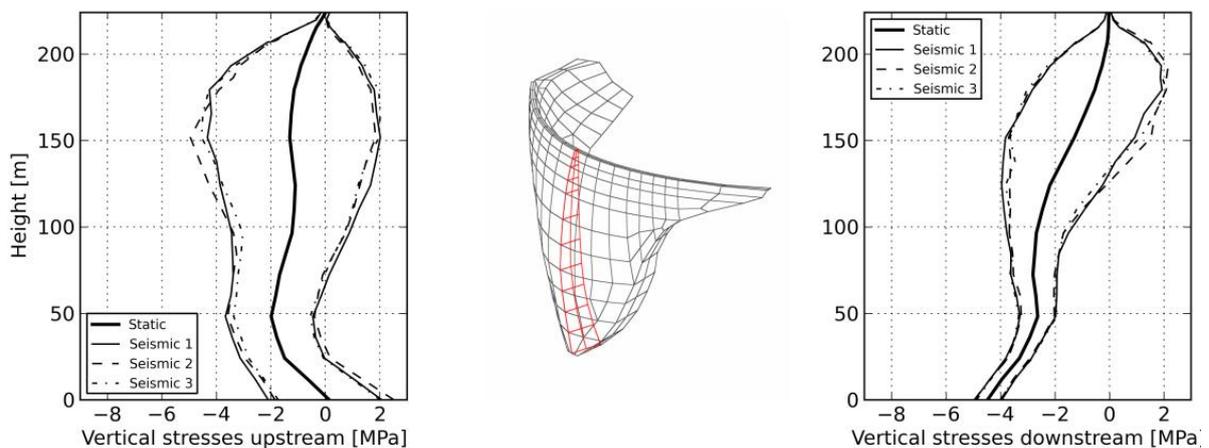
Fig. 8: Vertical stress envelope in the middle section of the dam

Local stability evaluation

The local stability evaluation is done based on the guideline "Arch Dam Design" by the U.S. Army Corps of Engineers [3].

The local stability is fulfilled if the stresses, compressive or tensile, don't exceed the allowed corresponding strength of the material. The analyzed dam and the applied load combination correspond to extreme loading conditions according to the guideline. Therefore, stress safety factors, which must not be exceeded, are summarized in Tab. 4.

Tab. 4: Safety factors according to U.S. Army Corps of Engineers Guideline and corresponding maximum compressive and tensile strength

	SF	Old Concrete	New Concrete
Dynamic Compressive Strength	1.5	38 MPa	32 MPa
Dynamic Tensile Strength	1.0	4 MPa	3.5 MPa

A comparison of the allowed compressive stresses with the simulation results from Fig. 6 reveals that the allowed stresses are exceeded nowhere in the structure. On the other hand, the tensile stresses in Fig. 5 (grey areas) show that they are even three times higher in some areas, especially near the abutment on the upstream side. However, the guideline says that for such loading conditions nonlinear, inelastic behavior will be allowed while maintaining the structural integrity of the dam as long as uncontrolled release of water is prevented. Taking under consideration that arch dams are constructed in vertical monoliths with vertical contraction joints these tensile stresses will lead to openings and therefore a possible stress release in the other regions. Nevertheless, water penetration and seepage in the abutment due to opening because of these stresses might influence the stability significantly, hence nonlinear analysis and further investigation regarding base and block opening is recommended and might be an interesting topic for upcoming benchmark workshops in the future. The conclusion is that the local safety of the Luzzone arch dam is not given for this load combination, based on linear finite element analysis.

Global stability evaluation (Rocking block stability)
As there is now special treatment in the arch dam guideline by the U.S. Army Corps of Engineers for fully cracked surfaces in the structure from the up- to the downstream side in specific heights, but only for sliding at the base of the arch dam, the guideline for "Gravity Dam Design" U.S. Army Corps of Engineers [4] is used for the safety evaluation. The safety factors against sliding and overturning for extreme loading conditions at horizontally cracked concrete blocks are summarized in Tab. 5.

Tab. 5: Safety factors against sliding and overturning according to U.S. Army Corps of Engineers Guideline for Gravity Dam Design [4]

	SF
Minimum Sliding Factor of Safety	1.3 (1.1 for base sliding of arch dams)
Resultant location at the base for fulfilling the overturning stability	Must be within the base

The global sliding stability in simple limit equilibrium methods is fulfilled if the resistant forces (friction angle = 63°, cohesion = 0.0) are larger than the acting forces on the rigid body (block in this case). Fig. 9 shows a sketch of the system for the applied method and the forces acting on the cracked block.
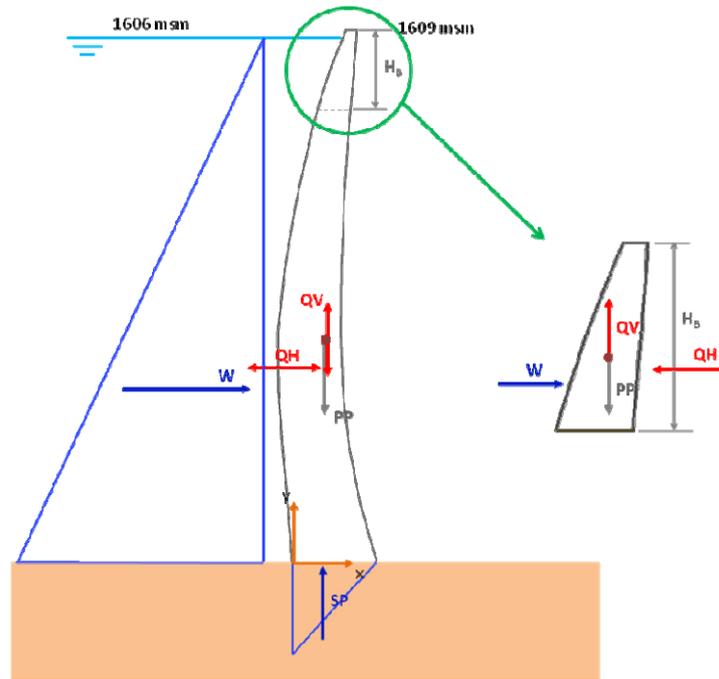
Fig. 9: Sketch and applied forces on the cracked block of the arch dam by [1]

The hydrodynamic water force (not in the sketch) is calculated by using the added mass approach according to Westergaard [6] and is acting on the upstream side of the dam.

The maximum accelerations acting on the block are listed in Tab. 6. These accelerations represent the maximum values out of acceleration-time histories at the specified block heights and are only present for a very low time span of only a few hundredths of seconds. The acceleration at the block with a height of 8.5 meters, for instance, is amplified by a factor of 10 from 0.16g to 1.6g.

Tab. 6: Maximum accelerations at the specified crack heights H_S of the blocks by the formulators

Block Height H_S [m]	8.5	17.0	30.8	44.6
Maximum Horizontal Acceleration [g]	1.6	1.2	0.91	0.85
Maximum Vertical Acceleration [g]	0.56	0.56	0.52	0.48

Tab. 7: Forces on the concrete block for the accelerations listed in Tab. 6

Acting Force	Block Height H_S, m			
	8.5	17	30.8	44.6
Self-Weight, PP [kN]	24632.9	60920.1	144256.1	249743.0
Hydrostatic Force, W [kN]	148.4	961.4	3790.8	8488.4
Uplift Force, SP [kN]	4141.0	14407.0	38548.7	69420.6
Earthquake Force, horizontal component, Qh [kN]	40176.0	74520.0	133815.5	216393.0
Hydrodynamic Force (Westergaard), horizontal [kN]	6098.4	29635.2	88613.8	185343.0
Earthquake Force, vertical component Qv [kN]	14061.6	34776.0	76466.0	122198.4

The sliding safety is calculated for different inertia force directions with the accelerations from Tab. 6. The hydrodynamic force is assumed to be always acting in the same direction as the horizontal inertia force (worst case).

The results of the sliding safety calculation are summarized in Tab. 7 and immediately indicate that the block is not safe for several combinations of the inertia force directions. However, keeping in mind that in reality the block/contraction joints are radially oriented with shear keys in-between, one will conclude that the downstream failure mechanism (sliding to the front side) isn't possible. Nevertheless, sliding to the upstream side (inertia acting upstream) will also exceed a safety factor of 1.3 clearly if the vertical inertia force points upwards. So, it can be concluded that sliding failure of these blocks is highly influenced by the vertical acceleration direction.

According to the guideline, the overturning stability for a concrete block is given if the resultant vertical force is within the base for extreme loading conditions. The resultant location r along the base is calculate by

$$r = \frac{\sum M}{\sum V} \tag{3}$$

For this calculation again different directions of the inertia forces are applied. All mass forces are acting in the volume centroid of the specific block partitions. The calculated factors of safety for overturning to the downstream side are also far beyond the stipulated safety for the case of inertia forces acting downstream. Therefore, the direction of the horizontal inertia forces influences the overturning safety the most. Infinite safety factors to the downstream side in Tab. 8 indicated that overturning to the upstream will be triggered.

Tab. 8: safety factor against sliding and overturning for the acceleration listed in Tab. 6

Factor of Safety against Sliding				
Inertia horizontal-downstream, vertical-up	0.3	0.2	0.2	0.2
Inertia horizontal-downstream, vertical-down	1.4	1.3	1.2	1.0
Inertia horizontal-upstream, vertical-down	1.6	1.9	2.5	2.7
Inertia horizontal-upstream, vertical-up	0.3	0.3	0.4	0.5
Factor of Safety against Overturning to the Downstream Side				
Inertia horizontal-downstream, vertical-up	0.2	0.1	0.1	0.1
Inertia horizontal-downstream, vertical-down	0.8	0.6	0.5	0.4
Inertia horizontal-upstream, vertical-down	∞ (upstream below 1.0!)	∞ (upstream below 1.0!)	∞ (upstream below 1.0!)	∞ (upstream below 1.0!)
Inertia horizontal-upstream, vertical-up	∞ (upstream below 1.0!)	∞ (upstream below 1.0!)	∞ (upstream below 1.0!)	∞ (upstream below 1.0!)

The conclusion is that both, the sliding and overturning stability, aren't fulfilled for most of the cases of the direction of the inertia forces. But it should be kept in mind that the maximum accelerations are occurring for only very small time instant as already mentioned; therefore, judging the safety of such a block with a limit equilibrium method with these high values is not suitable. As for the local stability, nonlinear or linear analysis with proper boundary conditions is also required here to evaluate and ensure the sliding stability.

Conclusion

The local stability of the structure regarding tensile stresses isn't fulfilled in large areas on the upstream face of the dam. On the other hand, compressive stresses are exceeded nowhere. High tensile stresses primarily occur near the base on the left and right bank, which is attributable to the tied interface between dam and foundation. This fact leads to stress concentrations in these areas. Based on linear finite element analysis the Luzzone arch dam wouldn't be safe, because of the wrong model. However, in reality the base will open and different stress distributions will develop. To model this behavior properly nonlinear analysis and further investigation regarding base and block opening is recommended

Using a limit equilibrium method to calculate the global safety is not suitable, because the real behavior of the structure isn't modelled in the right way. Effects of radially oriented blocks and shear keys are not taken into account with such a method. Hence, safety factors are exceeded for almost all cases of the block failure mechanism, regardless of sliding or overturning. Here also, nonlinear or linear analysis with proper boundary conditions is also required to judge the stability in the right way.

It can be concluded that the local and global stability should be evaluated by performing nonlinear analysis on the Luzzone arch dam. This might be an interesting topic for upcoming benchmark workshops in the future.

References

[1] Gunn R. M., Doytchinov Tzenkov A. (2015). Seismic Safety Evaluation of a Concrete Dam Based on Guidelines, 13th Benchmark Workshop on the Numerical Analysis of Dams – Theme A Formulation. St-Légier-la-Chiésaz, Switzerland.

[2] Goldgruber M. (2011). Numerische Untersuchung der Felskeilstabilität im Fundament einer Bodenstaumauer bei Erdbebenbelastung. Masterarbeit, Graz University of Technology, Institute of Hydraulic Engineering and Water Resources Management, Graz, Austria.

[3] U.S. Army Corps of Engineers (1994). Arch Dam Design. Department of the Army U.S. Army Corps of Engineers, Washington, DC 20314-1000, US.

[4] U.S. Army Corps of Engineers (1995). Gravity Dam Design. Department of the Army, U.S. Army Corps of Engineers. Washington, DC 20314-1000, US.

[5] Dassault Systemes (2013). Abaqus 6.13-EF Documentation. Dassault Systemes.

[6] Westergaard H. M. (1933). Water Pressure on Dams during Earthquakes. Transactions, ASCE, Vol. 98, 418-472.

Seismic Safety Assessment of Luzzone Dam
Finite element Modelling

Faggiani G.[1] and Masarati P.[1]

[1] *Ricerca sul Sistema Energetico - RSE SpA, via R. Rubattino 54, 20134 Milano, ITALY*

ABSTRACT: The seismic assessment of Luzzone Dam, a large double-curvature concrete arch dam located in Switzerland, proposed as Theme A of the 13th ICOLD Benchmark Workshop on the Numerical Analysis of Dams, has been performed. Dynamic simulations have been carried out using the RSE in-house FEM code CANT-SD, specifically designed for dynamic linear and non-linear analyses of dam-reservoir systems and provided with acoustic compressible elements to model fluid-structure interaction. The seismic verification has been performed according to the Swiss Directive by subjecting the dam-reservoir system to three acceleration time histories compatible with the site spectral response, evaluating the resulting stresses on the basis of the properties of the dam concrete and calculating the factors of safety against sliding and overturning of the upper part of the crown cantilever. Additional analyses have been carried out and the results have been evaluated according to the Italian standards. Based on the results of the performed seismic assessment, some in-depth analyses, able to simulate the non-linear effects due to the opening and sliding of vertical contraction joints, have been performed to better represent the actual behaviour of the structure and conclude on its seismic safety.

E-mail: giorgia.faggiani@rse-web.it

Introduction

Theme A of the 13th ICOLD Benchmark Workshop on the Numerical Analysis of Dams [1] is aimed at performing the seismic verification in accordance with Guidelines of Luzzone Dam, a large double-curvature concrete arch dam located in Switzerland: the Swiss Directive [2] has been used as basis for the problem statement. The study has been carried out using the RSE in-house FEM code CANT-SD [3], specifically designed for linear and non-linear dynamic (seismic) analyses of dam-reservoir systems. This code is currently used at RSE for the safety assessment of concrete dams, and it was adopted to deal with some themes proposed in previous ICOLD Benchmark Workshops, as referred in [4]. Regarding the main simulation options required for the present theme, CANT-SD models the fluid by means of acoustic elements, considers friction no-tension structural elements and solves the transient dynamic coupled problem using an implicit direct time integration method.

Seismic safety assessment of dams has nowadays become a major topic, as focused in [1] with regard to the Swiss situation. The topic is of considerable concern in Italy too: operators have been required to perform the seismic evaluations according to the recently updated standards [5][6] which, inter alia, involve seismic loadings stronger than the previously considered ones [7]. The modelling of arch dams subjected to such strong earthquakes must properly consider both dam-reservoir interaction and non-linear opening and sliding of contraction joints.

The seismic verification of Luzzone Dam has been performed according to the Swiss Directive [2]; some additional analyses have been carried out and then evaluated according to the Italian standards [5].

Geometrical and physical model

The FEM parabolic mesh of the dam-foundation-reservoir is reported in Fig. 1: it is the same provided by the formulators of the Theme, except for a layer of interface elements between the dam and the foundation. Vertical joints, about 40 m spaced, have been modelled in the upper 40 m of the dam as interface elements for some in-depth analyses only. The interface elements have a friction no-tension elastic-plastic constitutive model. Normal contact stress can be either

compressive, in closed state, or zero, in open state (no-tension model). In closed state, the constitutive law reproduces the Coulomb friction behaviour: the friction angle is assumed equal to 45° and 37° for dam-foundation and vertical interfaces respectively.
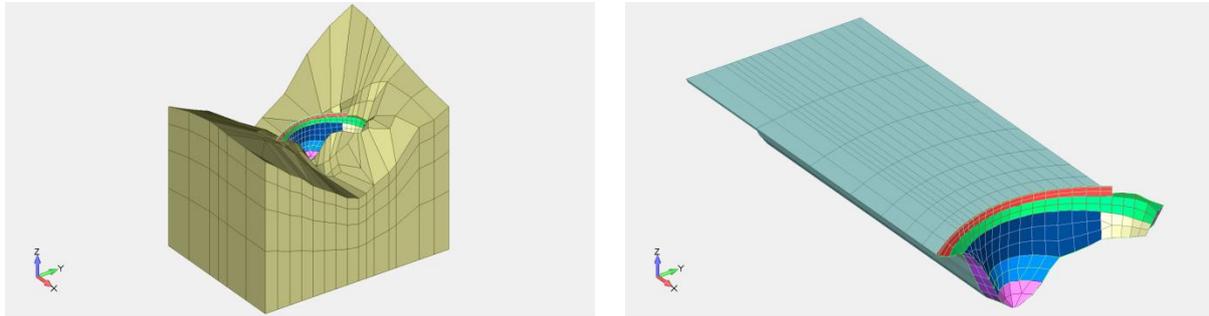
Fig. 1: FEM model

Physical-mechanical parameters of dam concrete and foundation rock, assumed to behave linear-elastically, are provided in [1] and reported in Tab. 1. The fluid has density and sound velocity equal to 1000 kg/m^3 and 1440 m/s respectively.

Tab. 1: Material properties

Parameter	Rock mass	Old Concrete	New Concrete
Static Modulus of elasticity [MPa]	18600	20000	18000
Dynamic Modulus of elasticity [MPa]	23300	25000	22500
Poisson's ratio [-]	0.20	0.18	0.18
Density [kg/m^3]	0	2500	2400
Static Compressive Strength [MPa]	-	38	32
Dynamic Compressive Strength [MPa]	-	57	48
Static Tensile Strength [MPa]	-	3	2.3
Dynamic Tensile Strength [MPa]	-	4	3.5

Damping matrix is expressed as linear combination of mass and stiffness matrices according to Rayleigh formulation. The structural damping ratio from the combination coefficients provided in [1] results equal to 5% at 2 Hz and 14 Hz.

The dynamic fluid-structure interaction is modelled in CANT-SD following the classic coupled mechanical-acoustic approach [8], already outlined in [4]. This approach allows taking into account both the water compressibility and the damping effects on the boundary of the reservoir. The water compressibility may have great influence on the dynamic response of a dam: the higher the natural frequencies of the empty dam compared to the natural frequencies of the reservoir, the greater the importance of water compressibility. A simplified parameter often used to predict the significance of water compressibility is the ratio between the fundamental frequencies of the dam and the reservoir: the threshold value 0.7 is suggested in [2]. As this ratio can be estimated about 1.0 for Luzzone Dam, compressible fluid is considered. The damping effects on the reservoir boundaries are due to the partial absorption of hydrodynamic pressure waves. The damping coefficient q is conveniently expressed in terms of the wave reflection coefficient α by (1), where C is the velocity of sound in the fluid:

$$q = \frac{1}{C} \frac{(1-\alpha)}{(1+\alpha)} \tag{1}$$

In the case of Luzzone Dam α is assumed equal to 0.6, as suggested in [1].

Loadings

The numerical analyses simulate the effects of the following actions:

1. 1. self-weight, considering the construction phases specified in [1]
2. 2. hydrostatic pressure for Normal Water Level at 1606 m a.s.l.
3. 3. silt pressure (density equal to 400 kg/m^3) at 1440 m a.s.l.
4. 4. summer thermal gradient supplied in [1]
5. 5. seismic loading

The seismic excitation, applied to the bottom and sides of the foundation, is provided in terms of three sets of acceleration time histories (TH1, TH2, TH3) compatible with the site spectral response, with peak ground acceleration (PGA) of 0.160 g in the horizontal directions and 0.106 g in the vertical direction [1]. Fig. 2 reports, as an example, the acceleration time history 3 (TH3) in the three coordinate directions X (upstream), Y (cross-stream) and Z (vertical).
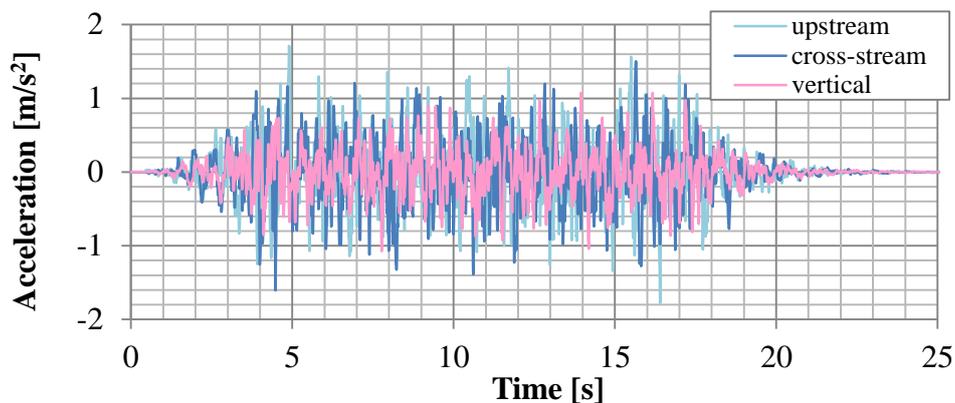
Fig. 2: Acceleration time history 3 (TH3)

The transient dynamic coupled problem has been solved using an implicit direct time integration method (HHT) [9]; an integration step of 0.005 s was chosen, in order to well represent frequencies up to 10 Hz.

Results

The following sections present the results of modal analyses and of time history analyses performed to estimate dam behaviour during earthquake in terms of local and global stability. Due to the size limits required for the paper, only some representative results can be shown.

Modal analysis
The modal analysis provides the natural frequencies and the effective mass participation ratios (for each coordinate direction) of the dam-foundation system both for full and empty reservoir. Tab. 2 shows the results of the analysis for the first 12 modes (required in [1]), and for the 30th mode: referring to the full reservoir, a good modelling of the dynamic dam behaviour requires at least 30 modes of vibration, as 12 modes are not enough to involve a significant effective mass in the cross-stream and vertical directions.

Tab. 2: Natural frequencies (f) and cumulative effective mass (x, y, z)

Mode	Full reservoir				Empty reservoir			
	f [Hz]	x [%]	y [%]	z [%]	f [Hz]	x [%]	y [%]	z [%]
1	1.52	48	1	0	2.00	0	8	0
2	1.54	48	14	0	2.10	24	8	1
3	2.10	53	14	0	3.02	31	8	2
4	2.27	65	14	1	3.78	46	8	11
5	2.40	65	14	1	3.97	47	9	11
6	2.80	71	14	1	4.46	47	38	11
7	3.18	71	17	1	5.01	49	38	14
8	3.35	73	18	3	5.20	50	39	69
9	3.44	73	31	3	5.81	51	68	71
10	3.92	74	31	3	5.96	54	71	71
11	4.12	75	31	3	6.15	54	71	71
12	4.26	75	32	4	6.31	68	72	72
…								
30	6.45	84	76	71	11.5	87	84	92

Time history analysis: stresses and displacements during earthquake

The transient dynamic analyses supply displacements and stresses in the dam-reservoir system. Fig. 3 reports the displacements of the dam, represented by the time histories at the centre of the dam crest, expressed in centimetres and positive if directed downstream. A downstream displacement of about 10 cm occurs under static loadings. The effect of the earthquake is an oscillation of the same order of magnitude as upstream as downstream. The three seismic signals cause quite similar displacements.
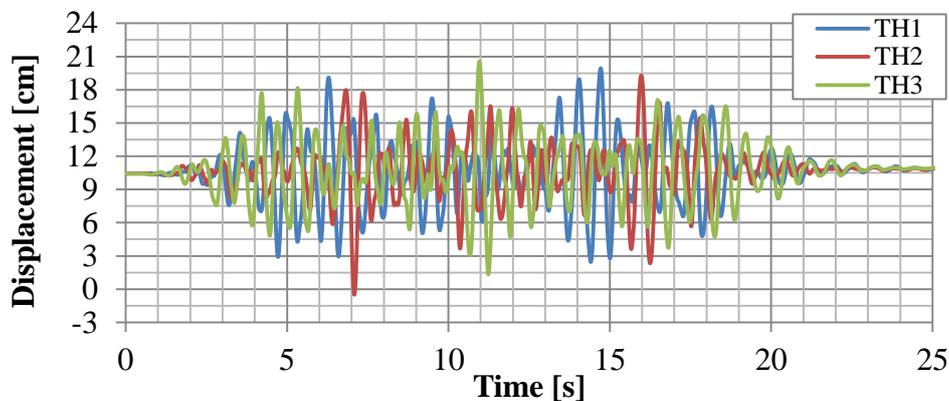
Fig. 3: Radial displacement time histories at the crest of the central section of the dam

The stress state resulting from the application of the three acceleration time histories (expressed in mega pascal, positive if tensile) can be summarized in diagrams showing the vertical and hoop stress envelopes on the upstream and downstream faces of the dam main section (Fig. 4). The general trend of stresses is about the same for the three different acceleration time histories. Due to the seismic loading, vertical stresses vary (in respect to the static ones) about 1÷2 MPa upstream and about 0.5÷1.5 MPa downstream respectively. Vertical stresses are slightly tensile in the upper half of the dam up to 1 MPa both upstream (between 1475÷1585 m a.s.l.) and downstream (between 1525÷1595 m a.s.l.). Compressive vertical stress reaches at most 4.5 MPa. The effect of the seismic loading on hoop stresses is greater in the upper part of the dam, involving a stress variation of about 5÷6 MPa upstream and 3÷4 MPa downstream at

about 1585 m a.s.l. These stresses are generally compressive both upstream and downstream (with maximum value of about 12 MPa) except for the upper 20÷30 m, where tensile stresses reach 1.5÷2 MPa: it follows that vertical joints, actually existing in Luzzone Dam, could open in the upper central part of the dam during an earthquake of the simulated intensity.
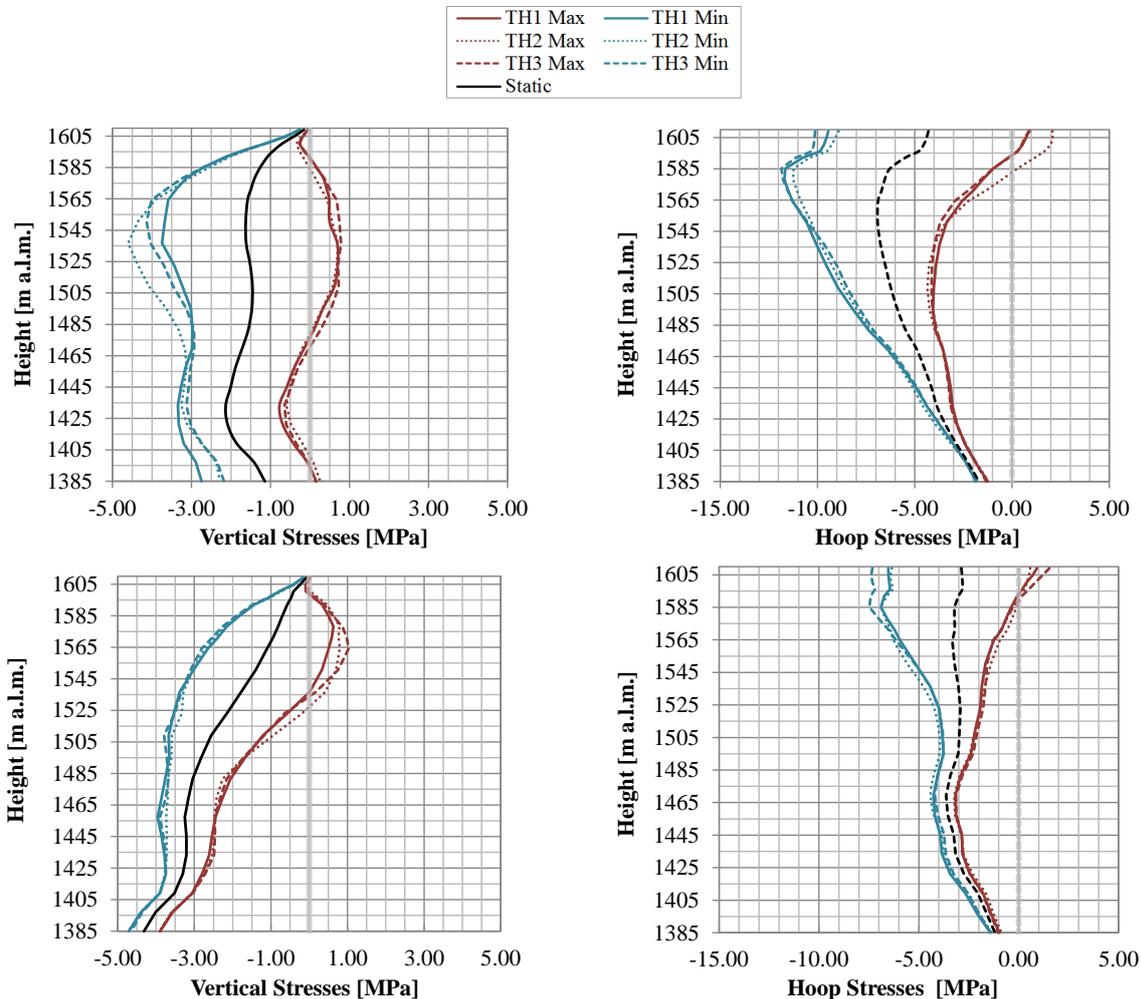
Fig. 4: Vertical (left) and hoop (right) stresses on the upstream (up) surface and downstream (down) surface

Rocking block stability analysis

The upstream sliding and overturning stability of the upper part of the crown cantilever has been tested, considering the four rocking blocks proposed in [1]: both static and seismic forces have been applied as static loads. The factor of safety against sliding (sliding F.S.) is defined as the ratio between the horizontal resisting (at the base of the block) and driving forces, while the factor of safety against overturning (overturning F.S.) is defined as the ratio between the resisting and the driving moments around the upstream toe of the block. The seismic forces acting on the block, i.e. the concrete inertial load and the hydrodynamic pressure, have been deduced from the results of the seismic analyses of the whole dam. Each finite element of the block has been loaded by horizontal and vertical body forces, spatially uniform within the element and calculated as the average of the time-enveloped nodal accelerations. Each upstream finite element face of the block has been loaded by pressure linearly varying with height: the values of pressure at bottom and top levels of the face are calculated as the average of the time-enveloped nodal hydrodynamic pressures. Tab. 3 sums up the calculated factors of safety of the

four blocks for each of the three acceleration time histories: all these factors are less than one, except the sliding factors of the highest block.

Tab. 3: Calculated Factors of Safety (F.S.) against sliding and overturning of rocking blocks for the four different levels of the horizontal crack

	TH1				TH2				TH3			
	Block Height [m]				Block Height [m]				Block Height [m]			
	8.5	17	30.8	44.6	8.5	17	30.8	44.6	8.5	17	30.8	44.6
Sliding F.S.	0.33	0.36	0.70	1.27	0.22	0.23	0.47	0.97	0.24	0.27	0.59	1.22
Overturning F.S.	0.56	0.53	0.61	0.69	0.47	0.44	0.51	0.59	0.50	0.48	0.56	0.66

Seismic safety assessment according to guidelines

Principal stress envelope contour plots allow the evaluation of the local stability of the dam by comparing the calculated stresses with the strength of the concrete (Tab. 1). Fig. 5 and Fig. 6 report the minimum and the maximum principal stresses respectively, for acceleration time history 3 (TH3): although the seismic response of the dam has turned out to be quite independent from the specific signal, the stress state resulting from the acceleration time history 3 is a little bit more severe than the others, hence the seismic safety assessment is discussed referring to this case.
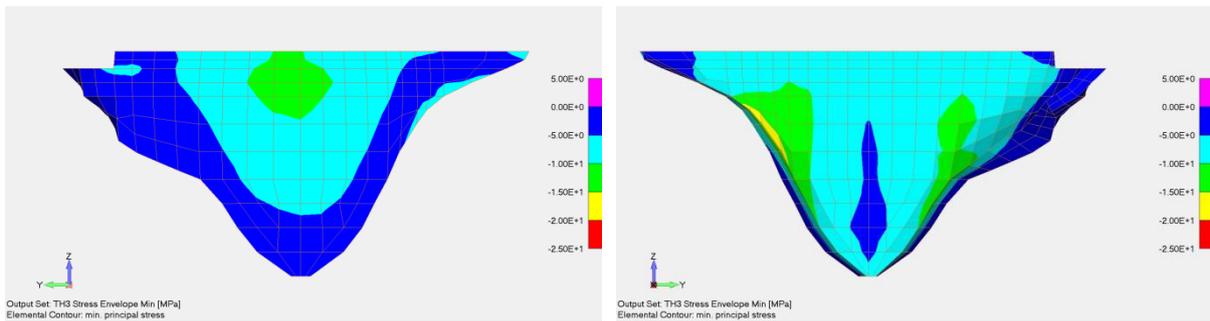
Fig. 5: Time history 3 - Minimum principal stress, upstream (left) and downstream (right) view
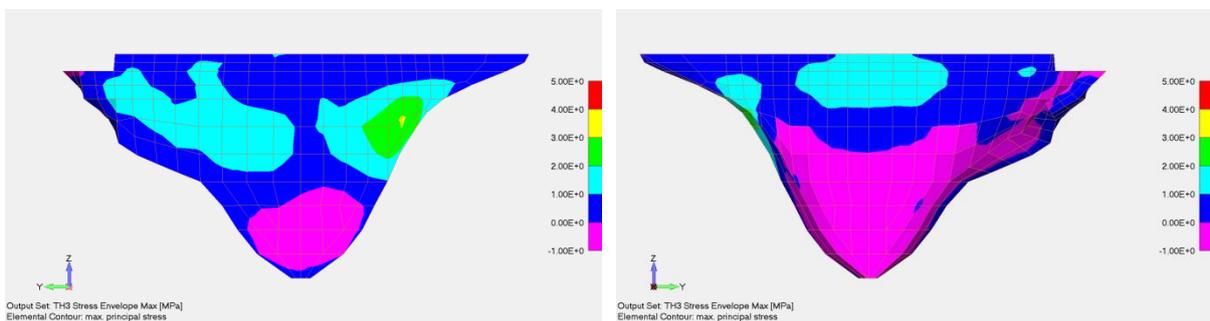
Fig. 6: Time history 3 - Maximum principal stress, upstream (left) and downstream (right) view

Compressive stress is largely lower than the dynamic compressive strength of both the old (57 MPa) and the new (48 MPa) concrete: maximum values (less than 20 MPa) occur downstream near the abutments. The upstream face of the dam shows a widespread tensile state (except for the lower 90 m): the stresses are higher near the left and chiefly near the right bank,

where stress slightly exceeds 3 MPa. On the downstream face only the upper 100 m of the dam show tensile stresses, not significantly higher than 1 MPa. It follows that tensile stresses never exceed the dynamic tensile strength of old (4 MPa) and new (3.5 MPa) concrete.

In addition to the stress evaluation, Theme A proposes to verify the global seismic stability against sliding and overturning of four concrete blocks in the upper part of the crown cantilever, assuming open vertical joints and fully propagated horizontal crack at the base of each block. The outcomes of the stability assessment, reported in Tab. 4, are positive only for the sliding safety of the highest block. However, the overall hypotheses of the performed stability check seem indeed very conservative: no vertical tensile strength of concrete (horizontal crack through the whole thickness), simultaneous application of the most demanding seismic forces (horizontal acceleration, vertical acceleration and hydrodynamic pressure from the envelopes), static application of seismic loading.

A more realistic way to check the stability of the upper part of the dam may consist in explicitly modelling the vertical joints in the overall finite element simulation, as their opening may trigger the cantilever structural scheme. Tensile stresses resulting from such an analysis allow the evaluation of the dam safety both for open and closed vertical joints. Referring to acceleration time history 3, Fig. 7 reports the maximum principal stress for the analysis with vertical joints (shown in Fig. 8 along with their maximum opening). Although the upper part of the joints (mostly the one in the main section) withstands evident openings, the value and the trend of maximum principal stress, vertically oriented near the interfaces, result almost unchanged: therefore the stability of the dam is confirmed, also in the upper part.

In case vertical strength of the horizontal lift line surfaces were supposed much lower than concrete tensile strength, they could also be modelled by means of interface elements to investigate the structural effects of horizontal cracks propagated through the whole thickness of the dam.
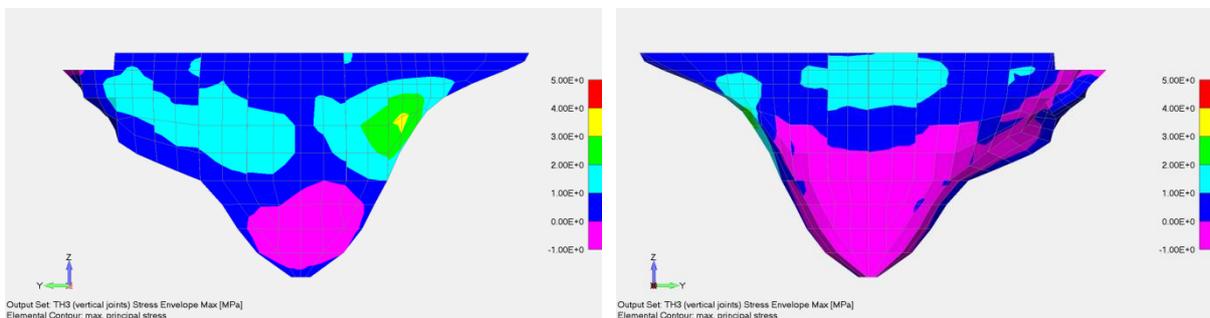
Fig. 7: Time history 3 (mesh with vertical joints) - Maximum principal stress, upstream (left) and downstream (right) view
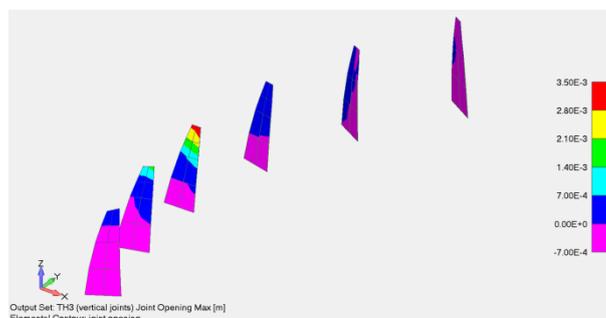
Fig. 8: Time history 3 (mesh with vertical joints) - Maximum joint opening

Some additional analyses (without modelling the vertical joints) have been carried out applying the seismic components according to the scheme of the Italian guidelines [5]. This scheme requires that, for each set of acceleration time histories, three loading combinations have to be considered: for each combination two of the three components are multiplied by 0.3, while the third one (main component) survives unchanged. Fig. 9 and Fig. 10 report the maximum principal stress for the two considered combinations of seismic loading (referring to the acceleration time history 3), which respectively assume the upstream and the cross-stream component as the main one. In evaluating the results, characteristic static tensile strength (0.7 times the mean static strength [6], i.e. 2.1 MPa and 1.6 MPa for old and new concrete) must be used. In case the calculated stresses exceed the static characteristic strength values, the safety assessment could be further developed (making also use of international recommendations such as [10][11]), considering that the Italian guidelines, for very severe earthquakes, require to avoid uncontrolled release of water as well as serious damage of the dam possibly leading to its collapse. In the analysed loading combinations tensile stresses always fulfil the reference tensile strengths, so no other check or analysis is needed.
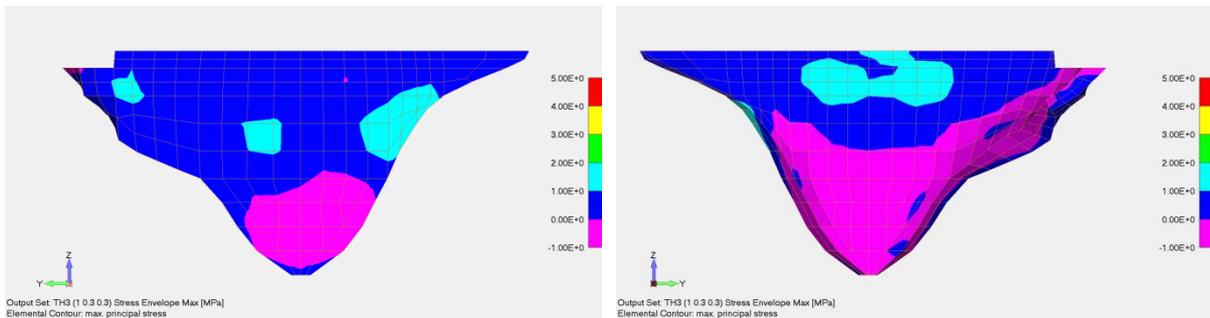
Fig. 9: Time history 3 (combination 1, 0.3, 0.3) - Maximum principal stress, upstream (left) and downstream (right) view
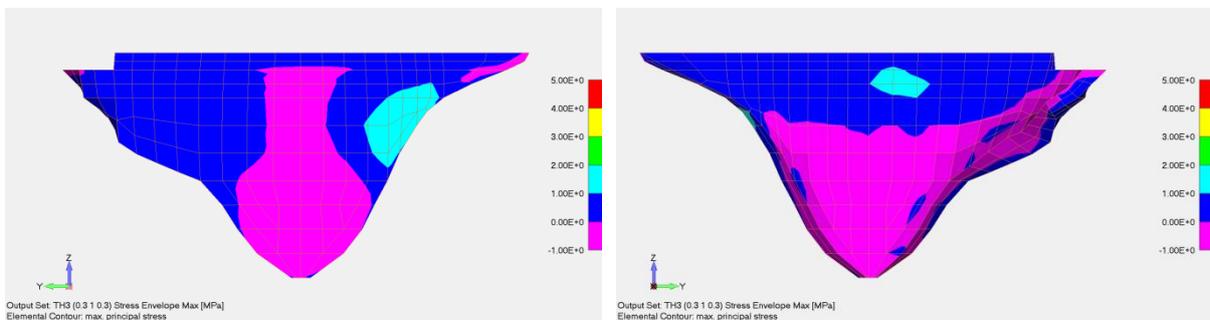
Fig. 10: Time history 3 (combination 0.3, 1, 0.3) - Maximum principal stress, upstream (left) and downstream (right) view

Conclusion

Theme A of the 13th ICOLD Benchmark Workshop on Numerical Analysis of Dams, dealing with the seismic assessment of Luzzone Dam, has been approached with CANT-SD, an RSE in-house FEM code suitable for structural analysis of dam-reservoir systems: the code, supplied with acoustic compressible elements and friction no-tension structural interfaces, solves the transient dynamic coupled problem using an implicit direct time integration method. The problem concerns a very large double-curvature concrete arch dam under an earthquake of moderate intensity (if compared with those of some Italian and Swiss seismic regions). The analyses with three site spectrum compatible acceleration time histories have provided stresses and displacements in the dam body, assumed monolithic and made of linear-elastic concrete.

Compressive and tensile stresses fulfil the check of both Swiss and Italian guidelines, despite their different approaches and evaluation criteria; displacements look coherent with the size of the dam and its structural scheme. The outcomes of the global stability assessment against sliding and overturning of four blocks in the upper part of the crown cantilever are positive only for the sliding safety of the highest block. Nevertheless, as the overall hypotheses of the check are very conservative (no vertical tensile strength of concrete, simultaneous and static application of the most demanding seismic forces), the stability of the upper part of the dam has been best evaluated by modelling vertical joints in an additional dynamic time history finite element simulation, obtaining very reassuring results.

Acknowledgements

References

[1] Gunn R.M., Tzenkov A.D. (2015). Theme A formulation. Seismic Safety Evaluation of a Concrete Dam Based on Guidelines. 13th ICOLD Benchmark Workshop on the Numerical Analysis of Dams, Lausanne, Switzerland.

[2] Sécurité des ouvrages d'accumulation (2003). Documentation de base pour la vérification des ouvrages d'accumulation aux séismes, rapports de l'OFEG, série Eaux, version 1.2.

[3] Masarati P., Meghella M. (2000). The FEM computer code CANT-SD for non-linear static and dynamic analysis of dams. Enel.Hydro PIS n. 6045, Milano, Italy.

[4] Faggiani G., Masarati P. (2013). Finite element modelling of seismic fluid-structure interaction for a large arch dam. 12th ICOLD Benchmark Workshop on Numerical Analysis of Dams, Graz, Austria.

[5] Decreto Ministeriale 26/06/2014. Norme tecniche per la progettazione e la costruzione degli sbarramenti di ritenuta (dighe e traverse). Gazzetta Ufficiale 08/07/2014 n. 156.

[6] Decreto Ministeriale, 14/01/2008.Consiglio Superiore dei LL.PP. Norme Tecniche per le Costruzioni. Gazzetta Ufficiale 04/02/2008 n. 29 - Suppl. Ordinario n. 30

[7] Decreto Ministeriale 24/03/1982. Norme tecniche per la progettazione e la costruzione delle dighe di sbarramento. Gazzetta Ufficiale 04/08/1982 n. 212.

[8] Zienkiewicz O. C. (1977). The Finite Element Method, 3rd Edition, McGraw-Hill.

[9] Hilber H.M., Hughes T.J.R., Taylor R.L. (1977). Improved numerical dissipation for time integration algorithms in structural dynamics. Earthquake Engineering and Structural Dynamics, Vol. 5, pp. 283-292.

[10] US Army Corps of Engineers – USACE (2007). Earthquake design and evaluation of concrete hydraulic structures. EM 1110-2-6053.

[11] US Army Corps of Engineers – USACE (2003). Engineering and Design - Time-History Dynamic Analysis of Concrete Hydraulic Structures. EM 1110-2-6051.

Theme A Seismic Safety Evaluation of a Concrete Dam Based on Guidelines
Contribution by Tractebel Engineering (Coyne et Bellier)

C. Tsai[1], X. Molin[2], C. Noret[3]

[1] Intern, [2] Project Engineer, [3] Technical Director (Dam safety)

ABSTRACT: The problem statement of Theme A of the 2015 ICOLD's 13th numerical Benchmark Workshop aims to compare different guidelines to evaluate the safety of a concrete arch dam under seismic loads. In this contribution, the analysis of the dam's behaviour was performed according to the French recommendations. Static loads combination and determination of the modal shapes were performed with finite element software COBEF and the dynamic interaction between fluid and structure with the boundary finite element software MISS3D. The dam behaviour is verified by the analysis of the stress fields. The evaluation of the overturning of a block towards upstream direction is estimated from block energy analysis. It was concluded that the compressive stresses are below the concrete strength and the overturning stability does not represent a risk to the dam safety.

Email: xavier.molin@gdfsuez.com

Introduction

This paper describes the study conducted by Tractebel Engineering, acting under the commercial trade name Coyne et Bellier, in reply to the 13th Numerical Benchmark Workshop of the International Commission on Large Dams (ICOLD) [1]. The aim of this Benchmark's Theme A is to compare different guidelines on seismic safety evaluation of concrete arch dams. The case study is based on the Luzzone dam, a double curvature arch dam located in Switzerland. The dam body was initially built in the 1960s and heightened of 17 m in the 1990s. The height of the final structure is 224 m.

In this report, the safety of the dam was evaluated according to French guidelines [2].

Static loads including ungrouted dead weight, hydrostatic and silt pressure, and 3 sets of acceleration time histories (PGA = 0.16 g) were considered. Static loads combination and the determination of the modal shapes were performed with the finite element software COBEF and the dynamic interaction between fluid and structure with the boundary finite element software MISS3D. In this last, the analysis was carried in frequency domain, and therefore under the hypothesis of linear behaviour. The results were then post-treated back into time domain and the final response of the dam is calculated with the linear combination of each modal shape.

Dam behaviour was verified by the analysis of the stress fields. The evaluation of the overturning of a block towards upstream direction was estimated from a block energy analysis, assuming the opening of the contraction joints and the formation of a horizontal downstream crack.
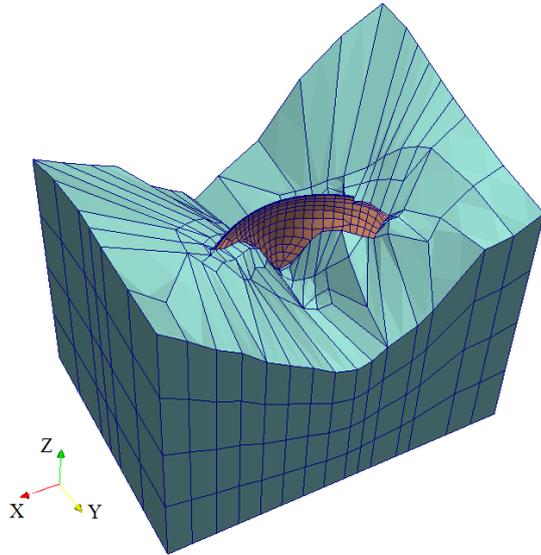
Fig. 1: Finite element model
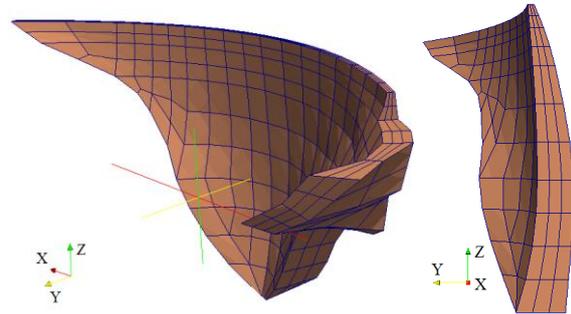
Fig. 2: Dam mesh and cross section of key cantilever

Finite element model (FEM) and boundary element model (BEM)

The geometry of the dam and the foundation provided by the Formulators of the problem were imported to COBEF, a 3D finite element software designed by Coyne et Bellier which includes specific and powerful pre and post-processing tools dedicated to arch dam analysis. The finite element mesh was refined by considering 3 elements in the dam thickness. All the degrees of freedom at the foundation boundary were blocked. A linear behaviour is finally assumed for this case study. Thus, the vertical construction joints were not modelled and no joints were introduced at the contact between the dam and its foundation.

The interaction between the fluid in the reservoir and the dam under dynamic loads was simulated with MISS3D [3], a frequency-based boundary element model code developed by Ecole Centrale de Paris. It is a powerful tool for semi-infinite medium analysis and it is currently applied in nuclear engineering projects, in order to evaluate complex structure-foundation interaction.
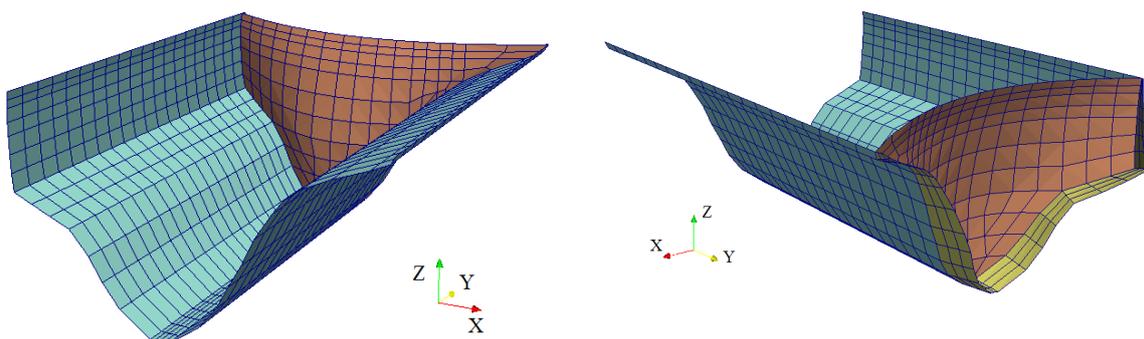
Fig. 3: Boundary element model (interface between dam - fluid - foundation)

Material properties

All the material properties were adopted as proposed by the Formulators, except for the damping. Following the French recommendations, a ratio between 5% and 7% is commonly applied to analyse the dynamic behaviour of concrete structures. Damping values up till 10%

96

is accepted for very high distortions. This value is nevertheless still considered conservative compared to feedback results on dams that had suffered earthquakes: back analyses show that a high damping ratio is needed (15 to 20%) to reproduce observed dam behaviour with linear models. The damping ratio was thus set to 10% for the analysis.

	New concrete	Old concrete	Rock
Density (kg/m^3)	2400	2500	-
Young modulus static (GPa)	18	20	18.6
Young modulus dynamic (GPa)	22.5	25	23.3
Poisson's ratio	0.18	0.18	0.2
Damping	10%	10%	10%

Tab. 1 : Material properties

The static strength of the concrete is adopted as proposed by the Formulator. According to French guidelines, the dynamic strength can be determined empirically as follow:

- Compressive strength: $f_{cd} = 1.25 \, f_{cs}$
- Tensile strength: $f_{td} = \min(1.5 \, f_{ts}, 0.1 \, f_{cd}, 4MPa)$

Therefore, the concrete compressive and tensile strength considered are presented in Tab. 2:

	Old concrete	New concrete
f_{cs} (MPa)	38	32
f_{cd} (MPa)	47.5	40
f_{ts} (MPa)	3.0	2.3
f_{td} (MPa)	4.0	3.45

Tab. 2: Static and dynamic concrete compressive and tensile strength

The behaviour of the water in the reservoir is described through acoustic properties (shearing is neglected). The following parameters were considered:

- Water wave celerity = 1500 m/s
- Damping = 5%

Seismic action

In this section, a brief comparison between the seismic risk level and seismic response spectra suggested by the French recommendations and the one provided by the Formulators is presented.
In French guidelines, the peak ground acceleration (PGA) to be considered is firstly evaluated according to the class and the location of the dam. There are 3 classes depending on the dam height and the reservoir volume. French territories have been divided into 5 seismic risk zones (see Fig. 4). Then if a specific site study is performed and a lower PGA is estimated, French recommendations state that it is only acceptable to adopt one level below the risk determined by the zoning scale.
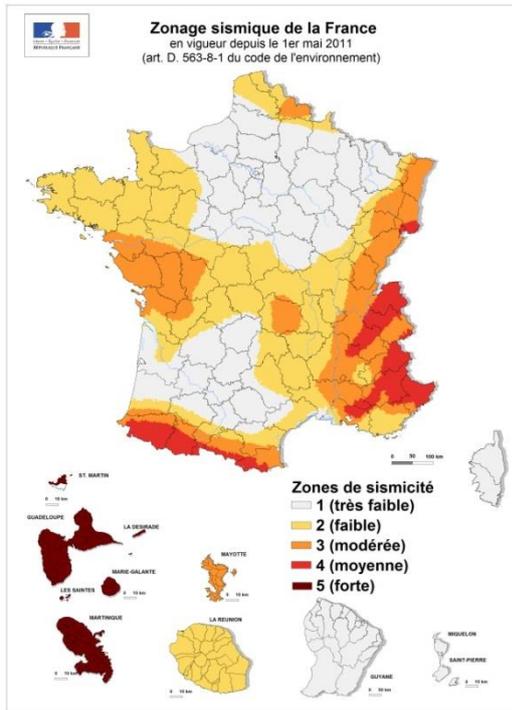
Fig. 4: French seismic hazard zoning map
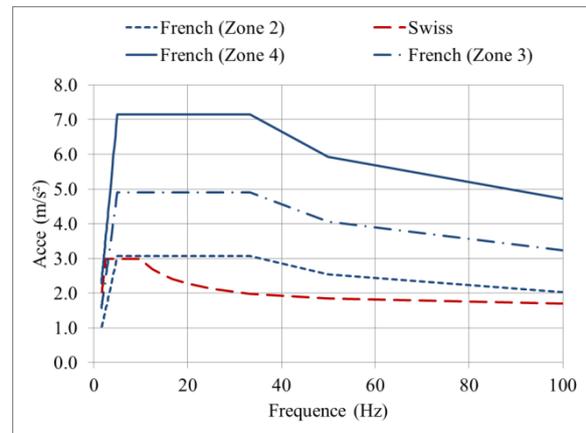
Fig. 5: Response spectrum of the dam site for French and Swiss Guidelines (damping = 10%)

Dams higher than 20 m are belonging to Class A. We extrapolated the seismic hazard level for Luzzone dam from the zoning map of French territories. In the Alpes region, the risk level varies between moderate and medium (zones 3 and 4, respectively). Thus, the horizontal PGA would be estimated between 2.4 and 3.5 m/s².

In case of specific site study is performed and a lower PGA is determined, the risk correspondent to a zone 2 (1.5 m/s²) or 3 can be considered.

The seismic response spectra suggested by the French recommendations and provided by the Formulators are compared in Fig. 5. The spectrum provided in the benchmark corresponds to the risk of the zone 2 in French guidelines (low risk).

For this case study, the seismic excitation and acceleration time histories were adopted as proposed by the Formulator (PGA = 0.16g = 1.56 m/s² for horizontal action and PGA = 0.106 g =1.04 m/s² for vertical action), for comparison purposes.

Despite the differences between guidelines, the essential is to maintain coherence between initial hypotheses and consequent interpretation. When one adopts severe loads, it is possible to assume a more moderate security factor, and vice versa. In French guidelines, the minimal security factor for dynamic combinations is equal to 1.

Finally, the combination of the seismic accelerations in the three directions with their maximal values is considered to be extremely conservative, since the PGA is previously chosen as an exceptional load.

For arch dams the most significant seismic action is in the upstream-downstream direction. Therefore, the vertical and bank to bank actions were neglected.

Dynamic Analysis

The dynamic behaviour of the dam was obtained via modal analysis. Two situations are considered: empty and full reservoir.

Each analysis was performed using the modal decomposition, which provides an orthotropic basis of vectors. The dam's response $\underline{U}$ is obtained with the linear combination of the eigenmodes $\underline{\phi}_j$:

$$\underline{U}(t) = \sum_j \alpha_j(t) \cdot \underline{\phi}_j \tag{1}$$

The problem is thus reduced to the determination of the coordinates $\alpha_j(t)$ for all selected vibration modes.

Empty reservoir

The analysis of the dam behaviour in this situation was performed with the FEM software COBEF, which calculates the eigenfrequencies and the associated eigenmodes.

Expressed in the base of eigenmodes, the degrees of freedom α_j shall satisfy the classical equation, given here in frequency domain:

$$\left(\omega_j^2 + 2i\xi_j\omega\omega_j - \omega^2\right) \cdot \hat{\alpha}_j(\omega) = \frac{\hat{p}_j(\omega)}{m_j} \tag{2}$$

For each eigenfrequency ω_j, damping ratio ξ_j and Fourier transform of the seismic acceleration $\hat{p}_j(\omega)$. This relation can be written with the transfer function $\hat{H}_j(\omega)$:

$$\hat{\alpha}_j(\omega) = \hat{H}_j(\omega) \cdot \hat{p}_j(\omega) \tag{3}$$

Full reservoir

In the case of full reservoir, the dam-reservoir interaction was conducted with MISS3D. The study field is split in three domains (dam, reservoir and foundation). We focused only on the dam and reservoir domains and their interface.

The resolution is made through the continuity between the elastic behaviour of the dam and the acoustic behaviour of the fluid.

For this analysis, the following stages were followed:

- The resolution of the "*local problems*", which consists to determine the behaviour of each domain in the interfaces. Only the displacement issued from the combination of first eigenmodes were considered, decreasing thus the number of degrees of freedom. *In fine*, the impedance matrix projected on the base of eigenmodes was determined for each domain:

    - The dam behaviour is evaluated in COBEF (eigenfrequencies and modal shapes).
    - The foundation behaviour is included in the modal shapes determined by COBEF.
    - The fluid behaviour at its boundaries is solved by MISS3D as a semi-infinite acoustic domain using the Green's function.

- The resolution of the "*global problem*" through the continuity of displacements and efforts, assuming the interaction of each domain. The transfer function $\hat{H}_j(\omega)$ is determined for each frequency step in the calculation range (Fig. 13).

The analysis is made over the frequency domain and then post treated back into the time domain with the Fourier Transform.

Dynamic dam response is afterwards added to the static one. French guidelines do not require thermal gradient verifications for dynamic analyses and therefore those were not investigated in this study.

Static Loads

Self-weight

The self-weight load was analysed considering the construction phases of arch dams: each cantilever is raised separately and, at the end of the construction, the joints are grouted to ensure the hyperstatic nature of the structure.

For this reason, the most significant stresses due to self-weight are developed for each independent cantilever (called ungrouted dead weight).

In order to simulate this process in COBEF, the self-weight was first calculated with the geometry of the old dam (g = 9.81 m/s²), considering the properties of an orthotropic material in which the hoop stresses are relaxed and set to zero and the stress field is gradually redistributed (see result in Fig. 6 below).

After this first loading, the following construction phase was calculated to simulate the heightening of the dam.

Hydrostatic pressure

The reservoir level is set at 1606 m a.s.l (3 m from the crest), with a triangular pressure distribution in depth.

Silt pressure

Silt pressure was applied with triangular distribution up to level 1440 m a.s.l (55 m from the foot), with density of 400 kg/m³.

Static behaviour

The results of the static loads combination are presented in Appendix A1 and A2.
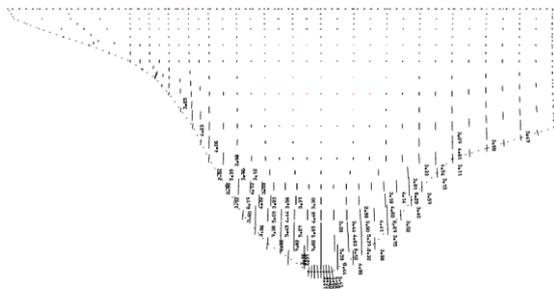
Fig. 6: Vertical stresses on the upstream face of the dam from the ungrouted self-weight
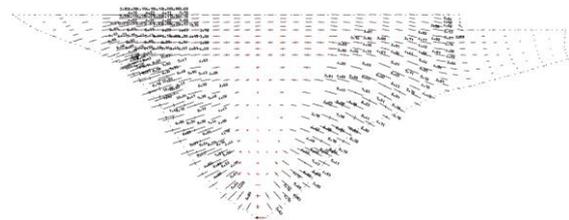
Fig. 7: Stresses on the downstream face of the dam under hydrostatic pressure
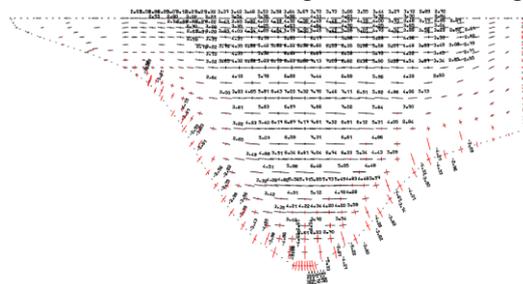
Fig. 8: Stresses on the upstream face of the dam under hydrostatic pressure
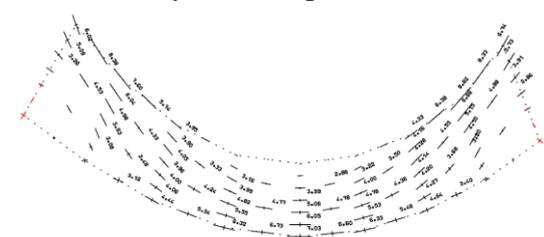
Fig. 9: Stresses on arch in level 1481.5 m a.s.l (96.5 m from the foot) under hydrostatic load

The advantage of the overall view of the stress fields compared to the isovalues curves is the possibility to interpret the general behaviour of an arch dam by the visualization of the stresses trajectories. It also permits to judge the reliability of the numerical results, indicating, for example, if an unusual high stress is caused by a particular boundary condition of the finite element model.

The principal stresses are distributed alongside to the dam faces as shown in Fig. 7 and Fig. 8. Also, the results highlight the notion of active arches in an arch dam (Fig. 9). At this level, the mean stress is around 3.5 MPa in compression at the crown cantilever and around 8.5 MPa closed to the abutments. These values remain far from concrete strength.

Analysis of the Natural Frequencies

The lower the percentage of modal mass of the neglected modes, the more accurate modal analysis results will be. Usually, it is considered that a satisfactory approximation of the global behaviour can be obtained with 90% of the total mass.

Empty reservoir

The 25 first natural frequencies of the dam with an empty reservoir are presented in Tab. 3. They represent about 85% of the modal mass, which is acceptable. The mode shapes are presented in Fig. 10. Modes 2, 4 and 12 (frequencies 2.10 Hz, 3.80 Hz and 6.37 Hz respectively) present the most significant effective mass percentage in the upstream-downstream direction.

The calculated eigenfrequencies of the dam (empty reservoir) are almost all in the maximum amplification range of the response spectra deduced from the 3 accelerograms, between 3 and 20 Hz (see Fig. 11). Nonlinearities and fluid-structure interaction should however decrease the eigenfrequencies of the vibration modes and move some of them out of the spectrum peak range.

Full reservoir

The same base of modal shapes is used for the full reservoir case. MISS3D determines the new transfer function $\widehat{H}_j(\omega)$ taking into account the fluid-structure interaction. It's not possible to identify quickly the eigenfrequencies of the vibration modes with this method. This method is illustrated in Fig. 12 (calculus of the transfer function in case of empty reservoir by MISS3D, in which the peaks for each mode correspond to the eigenfrequencies obtained by COBEF) and Fig. 13 (situation of full reservoir).

Nevertheless, it is possible to extrapolate from Fig. 13 that the transfer function peaks are situated at lower frequencies: the first important frequency peak for this situation corresponds to mode 2 and is around a 1.5 Hz. As the full reservoir situation simulates a system with additional masses, it is fair to assume a shift towards lower eigenfrequencies compared to the empty reservoir situation.
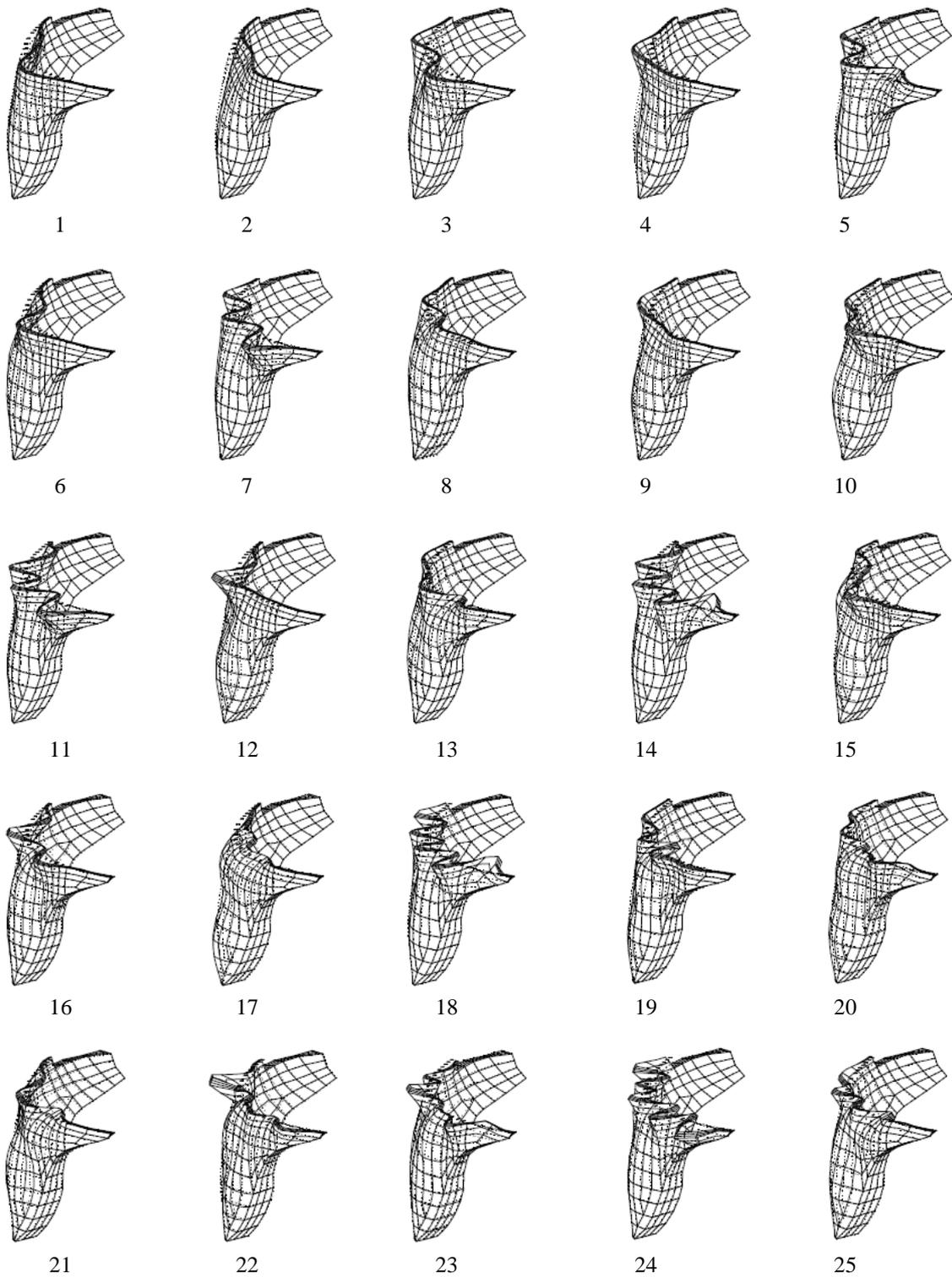
Fig. 10: 25 first modal shapes (empty reservoir, calculated by COBEF)

Mode	Empty Reservoir			
	Eigenfrequency	Effective Mass Percentage		
	f (Hz)	X (%)	Y (%)	Z (%)
1	2.02	7.8	0.3	0
2	2.10	0.3	23.4	0.9
3	3.04	0	6.7	0.6
4	3.80	0	14.5	8.8
5	4.00	0.3	0.7	0.2
6	4.50	28.7	0.2	0
7	5.04	0.1	2	2.2
8	5.26	1.1	1.1	54.5
9	5.87	28	0.9	1.3
10	6.01	4	2.3	0.6
11	6.19	0.1	0	0
12	6.37	1	14.1	1.5
13	6.99	0.1	1	1.1
14	7.41	0.1	0.7	0
15	7.70	0.1	0.2	0.7
16	7.91	3.1	0.3	0
17	8.48	0	3.8	0.8
18	8.64	0.2	0.7	0.6
19	8.94	0	1	4.5
20	9.15	0	1.4	0.9
21	9.62	1.3	1	4
22	9.63	0.5	7.6	0
23	9.75	3.2	0.4	2.2
24	9.99	0.1	0.3	0.8
25	10.39	0.1	0	0
Σ		**80.5**	**84.5**	**86.3**

Tab. 3: Natural frequencies for empty reservoir
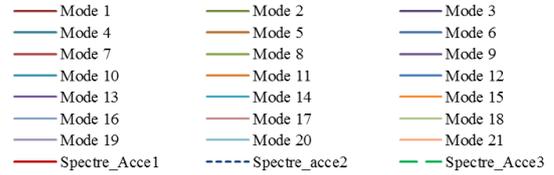
Upstream-downstream direction
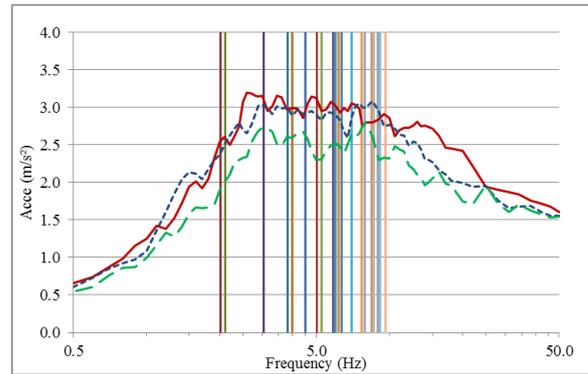
Fig. 11: Response spectrum for seismic loading in direction Y (empty reservoir)
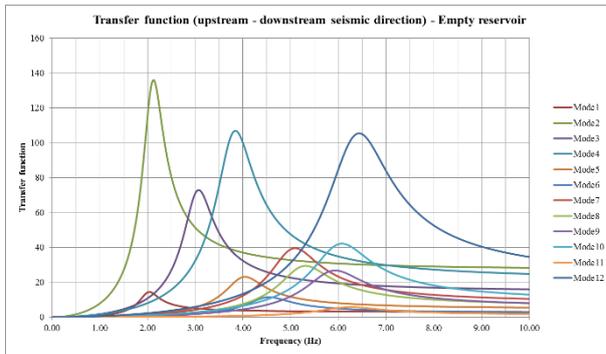
Fig. 12: Transfer function $\widehat{H}_j(\omega)$ in upstream-downstream direction for empty reservoir (solution of equation 2 obtained by, which correspond to COBEF results)
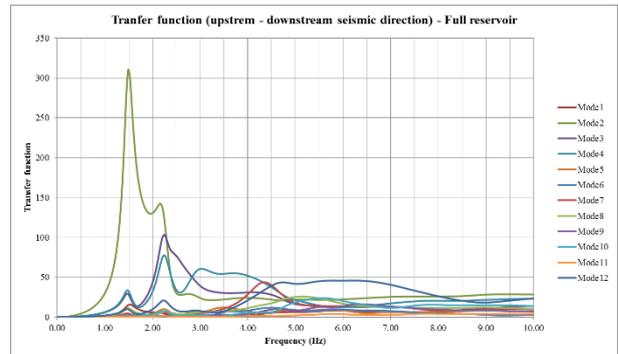
Fig. 13: Modification of transfer function $\widehat{H}_j(\omega)$ in upstream-downstream direction including the fluid-structure interaction (determined by MISS 3D in the same displacements base - vibration modes of empty reservoir)

Amplification by the dam

The amplification of the seismic load can be quantified by the maximal accelerations calculated along the crown cantilever. We obtained a maximal upstream-downstream acceleration of 17.7 m/s² at crest for full reservoir situation (Fig. 14), which indicates an amplification factor higher than 10. This value is significant, but the amplification mainly concerns the top third of the dam.
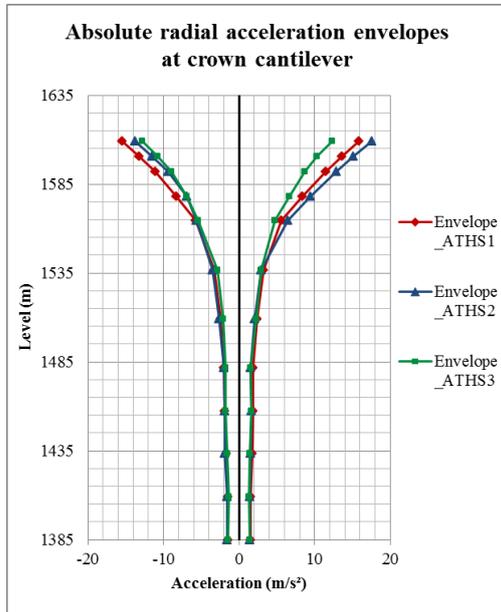
Fig. 14: Absolute upstream-downstream acceleration envelope for crown cantilever (full reservoir)
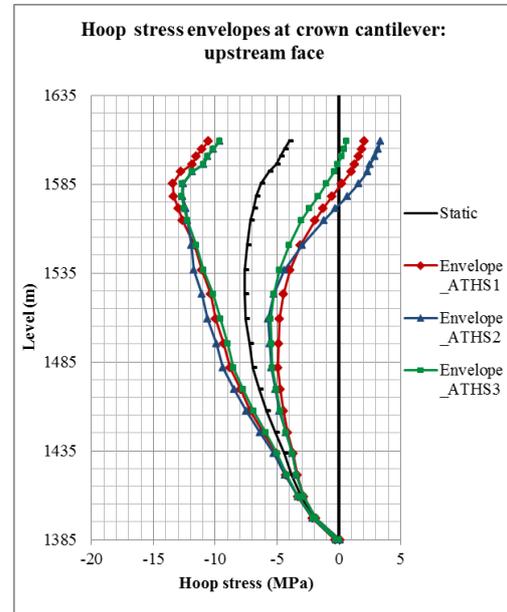
Fig. 15: Hoop stress envelopes on upstream face

Dam behaviour during an earthquake

When the seismic action is oriented towards downstream, the arch dam is mainly under compression and the construction joints are closed. Therefore, the calculated stresses are representative of the reality as the cantilevers operate jointly.

On the other hand, when the dam is moving towards upstream, the tensile hoop stresses are relaxed by the opening of the construction joints. In this case, since the dam was modelled as a monolithic structure, the calculated horizontal tensile stresses do not correspond to the real behaviour of the dam. Furthermore, while the opening of the joints neutralizes the horizontal stresses, it increases the vertical tensile stresses on the downstream face.

The finite element model is thus efficient to analyse the maximum compressive stresses reached during the earthquake, while tensile stresses and resulting potential local instabilities are analysed with a specific post-processing presented in section 11.

Hoop stress envelopes

The hoop stresses envelopes for the crown cantilever on the upstream and downstream faces are presented in Fig. 15 and Fig. 16.

Stress field at maximal crest displacement

In order to analyse the general behaviour of the dam, the stress fields were calculated when the central cantilever's crest reached its maximum upstream and downstream positions.

The displacement time history at this point is shown in Fig. 17.
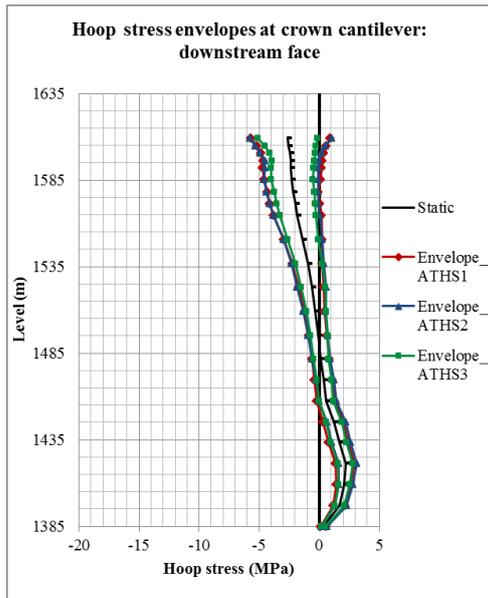
Fig. 16: Hoop stress envelopes on downstream face
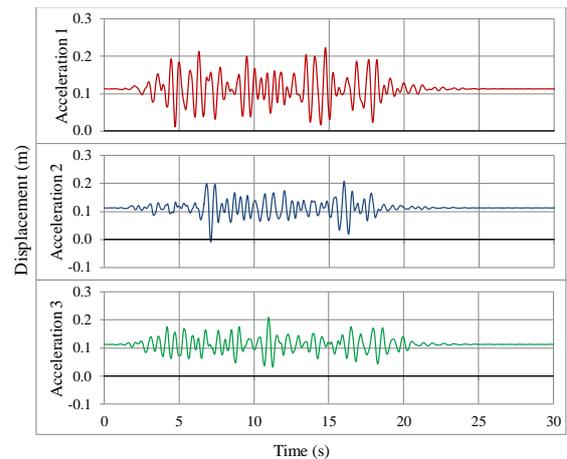
Fig. 17: Upstream-downstream displacement time history at crest crown section

The maximal compressive hoop stress in the crown cantilever is twice higher than in static conditions, but remains below 15 MPa.

Direction	Instant		
	ATHS 1	ATHS 2	ATHS 3
Upstream	4.72 s	7.10 s	11.25 s
Downstream	14.74 s	15.99 s	10.98 s

Tab. 4: Moments of maximum and minimum upstream-downstream displacement

The principal stresses on each dam face are presented in Appendix A3 and A4. Graphical results allow the visualization of the direction of principal stresses, the areas of stress concentration and the possible failure mechanisms.

Some of the results (static + dynamic loads) for the first set of acceleration time history (ATHS1) are displayed in the following Figures.
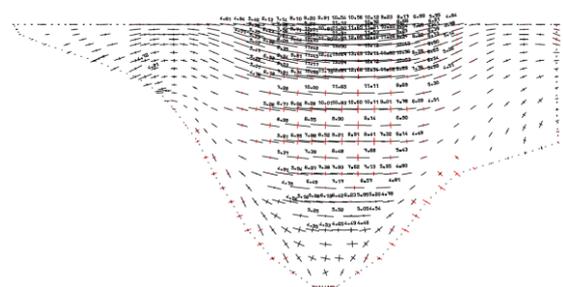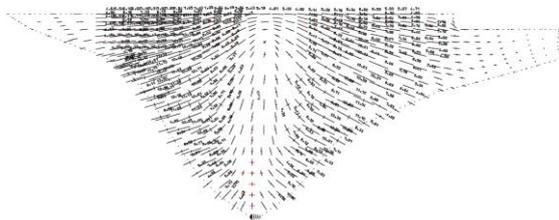
Fig. 18: Stress field on downstream face of the dam at maximum downstream displacement

Fig. 19: Stress field on upstream face of the dam at maximum downstream displacement

When maximum crest displacement towards downstream is reached (see Fig. 18 and Fig. 19), tensile vertical stresses can be noticed on the upstream face. This suggests a potential formation of a horizontal crack through the dam thickness. Nevertheless, this event should not question the global safety of the dam, since the structure works mainly in arch compression.

Overturning Stability

When crest displacement is maximal towards upstream (Fig. 20 and Fig. 21), there are vertical tensile stresses on the downstream face and an opening of the joints (represented by the horizontal tensile stresses) in the upper part of the upstream face. In this event, horizontal cracks can appear on the downstream face of the dam, enabling the upper vertical block to overturn towards upstream.
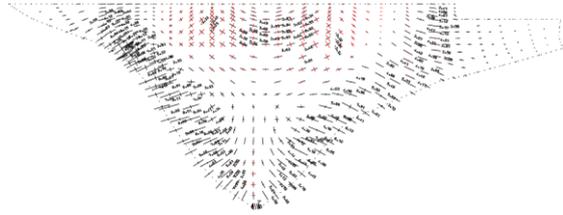
Fig. 20: Stress field on downstream face of the dam at maximum upstream displacement   Fig. 21: Stress field on upstream face of the dam at maximum upstream displacement
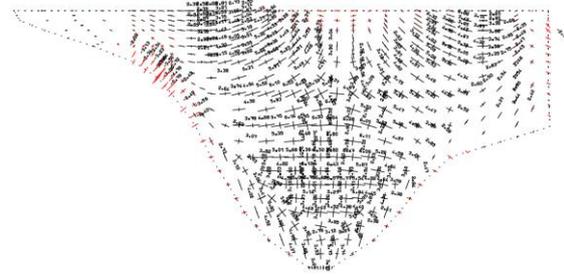
The "Kinebloc" method [4], developed by Coyne et Bellier, allows studying the risk of overturning for a vertical arch dam block towards upstream through energy analysis.
It is assumed that the tensile stresses are high enough to create a crack on the downstream face. This is a very conservative assumption as the energy dissipation of crack initialization is neglected.
The following further assumptions are considered:

- The crack is supposed horizontal.
- The block is rigid and rotates around a narrow yield surface with the maximum speed of its gravity centre.
- The yield surface can be estimated by the area needed to support vertical loads with stresses corresponding to the concrete strength. The movement of the pivot point P is considered insignificant.
- The dissipation of energy by the opening of the crack and the elastoplastic deformation are neglected.

The rotation of the block represents the transformation of the initial kinetic energy into the potential energy for the raising of the block's gravity centre (which is needed to turn) and the work of the hydrostatic pressure. Therefore, the equilibrium is formulated as follow:

$$E_{kinetic} = E_{potential} + F_{hydrostatic} \cdot \Delta l \qquad (4)$$

$$\frac{1}{2}\left(m_{block} + m_{westergaard}\right)v_g^2 = m_{block}\, g\, \Delta z_g + \frac{\rho g h^2}{2}\Delta l \qquad (5)$$

Where Δz_g is the vertical displacement of the center of gravity of the block, m_{block} and $m_{westergaard}$ are the overturning block and the Westergaard attached water mass (in kg/m), v_g and Δl are the velocity and the horizontal displacement of the center of gravity.
Knowing the block elevation Δz_g (by equation 5), the downstream vertical opening of the crack ε and the overturning angle $\Delta \theta$ can then be calculated geometrically.
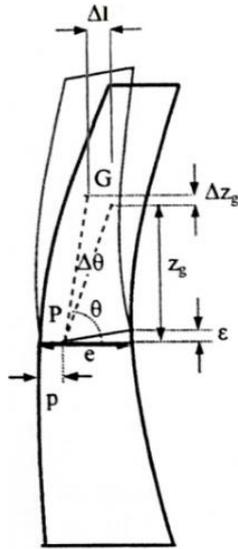
Fig. 22: Kinebloc method diagram
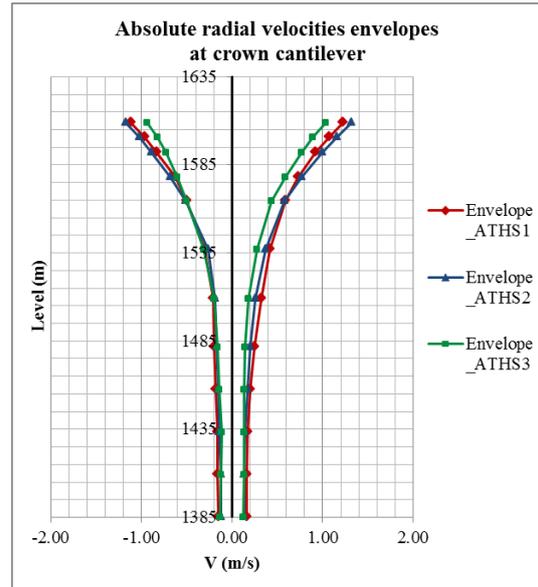
Fig. 23: Absolute radial velocity for crown cantilever (full reservoir)

Kinetic energy is highest when the velocity of the gravity centre is maximal. The envelopes of the absolute radial velocities were calculated at the crown cantilever (Fig. 23).

The verification is usually conducted for the minimal operating level, when overturning risk is maximal (no stabilizing hydrostatic pressure). In this study, in lack of information, we considered the full reservoir.

Elevation (m)	h (m)	v_g (m/s)	θ (°)	ΔZ_g (mm)	ε (mm)	$\Delta\theta$ (°)	v_{limit} (m/s)
1600.5	8.5	-1.09	40.3	62.8	100.2	0.78	-10.1
1592.0	17	-1.01	47.9	52.7	78.6	0.45	-10.8
1578.2	30.8	-0.89	54.3	37.4	53.7	0.23	-11.8
1564.4	44.6	-0.78	58.6	26.4	37.4	0.14	-12.5

Tab. 5: Crack opening and overturning angle for different block heights

The stresses field analysis at crown cantilever (Fig. 15) show that hoop stresses remain in compression below el. 1575. It means that the assumption of a horizontal crack is not valid for the lower part. In the upper section, where tensile stresses appear, potential blocks remain stable.

Moreover, the required velocities to overturn the block towards upstream are extremely high compared to the calculated ones (Fig. 23).

Conclusion

There are two main factors that must be analysed in the verification of an arch dam: the dam resistance itself and the stability of its abutments, since the structure transfers the efforts to them. The aim of this benchmark was focused on the first aspect. Thus, this paper assumes that the abutments are stable.

This study concluded that the local and global behaviours of the dam are verified under the static and dynamic loads. Some remarks on the assumptions and methodology applied are discussed below.

The analyses were conducted according to French guidelines. As the recommendations concerning the seismic acceleration combinations to be taken into account are not clear, we followed the most common practice applied to arch dam projects, which is to consider only the upstream-downstream accelerations, neglecting the bank to bank and vertical accelerations.

For the choice of the PGA, the new French seismic hazard zoning map is more unfavorable compared with the Swiss evaluation. On the other hand, French guidelines require a minimal safety factor of 1 for dynamic combinations.

Through the presented results, we observed that the compressive stresses are far below the concrete strength both in static and dynamic combinations. Also, the tensions are very local and the overturning stability does not represent a risk to the dam's safety.

Finally, we concluded that the dam resists well to the seismic loads. It behaves better when the reservoir is full, since the water pressure implies an initial compression state, reducing the opening of joints and cracks, without reaching the limit compressive strength.

References

[1] Committee on Computational Aspects of Analysis and Design of Dams, *Theme: Seismic Safety Evaluation of a Concrete Dam Based on Guidelines*, 13th ICOLD Benchmark Workshop on Numerical Analysis of Dams (2015)

[2] Groupe de Travail Barrages et Séismes, *Risque sismique et sécurité des ouvrages hydrauliques* – 2014

[3] MISS3D, *Miss 6.4: Manuel Utilisateur: Version 2.3* – 2004

[4] http://www.mssmat.ecp.fr/home/moyens/moyens_techniques_logiciels/miss

[5] Tardieu B., Bertrand J. *Calculation of arch dams subjected to earthquakes.* Antiseismic design of arch dams, Symposium on Earthquakes and Dams, Beijing, 1987.

Appendix A – Stress fields

Stresses fields are presented on different views (tensions represented in red):

- A1 – Stresses fields on the dam under ungrouted dead weight load:
  - Upstream face (cylindrical projection)

- A2 – Stresses fields on the dam under hydrostatic pressure load:

  - Downstream and upstream faces (cylindrical projection)

  - Arch in $Z = 1481.50$ m (96.50 m from the dam foot)

- A3 – Stresses fields on the dam under static + dynamic loads (acceleration time history 1) - maximum downstream displacement:

  - Downstream and upstream faces (cylindrical projection)

- A4 – Stresses fields on the dam under static + dynamic loads (acceleration time history 1) - maximum upstream displacement:

  - Downstream and upstream faces (cylindrical projection)

Appendix B - Additional requested results for the benchmark

For additional comparison of the requested results for the benchmark, the following parameters were calculated:

- Radial displacement: in this study, these parameters were simplified as the upstream-downstream displacement.
- Hoop stresses: it was considered as the projection of the stresses on the horizontal plane.
- Vertical stresses.
- Principal stresses.

Displacement envelopes at cross section

Three sections were selected at the problem statement: at crown, left bank and right bank. The results are presented in Fig. B2 and the displacements in crest are summarized in Tab. B1.
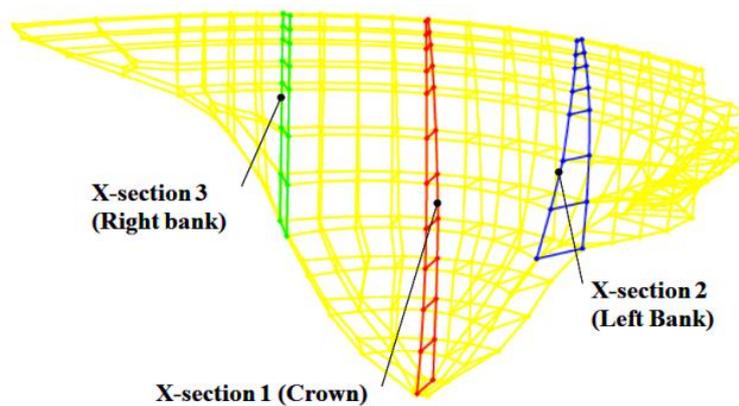
Fig. B1: Selected sections

	Static (cm)	Static + Dynamic	
		Min (cm)	Max (cm)
Crown	11.3	-2.3	24.3
Left bank	6.6	1.8	10.9
Right bank	5.1	1.9	8.4

Tab. B1: Upstream-downstream displacement at crest of cross sections
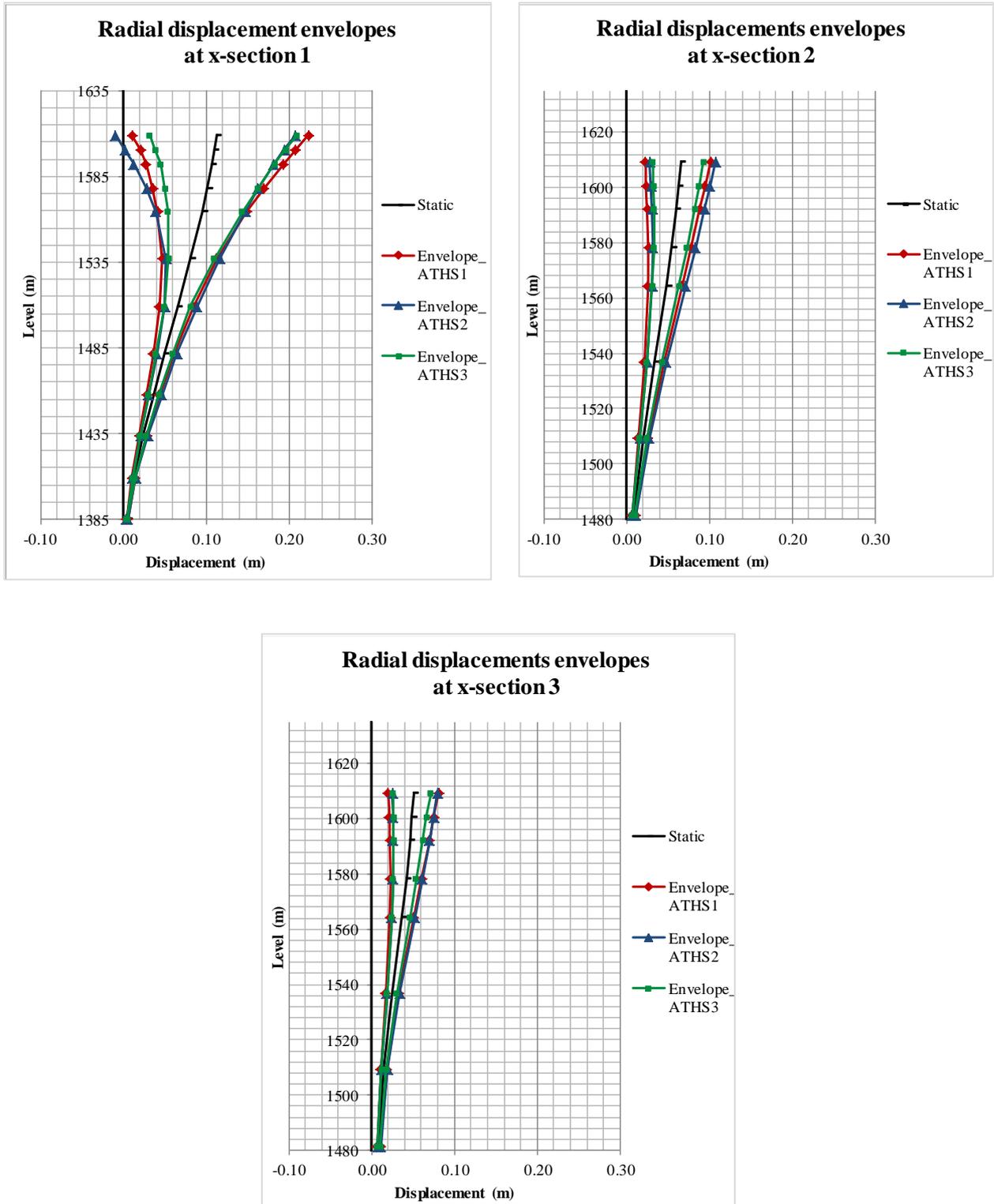
Fig. B2: Radial displacement envelopes for crown section, left bank ant right bank.

Stress envelopes at cross section

The hoop and vertical stress envelopes were calculated on the upstream and downstream of the chosen sections (positive for tensile stress). The results are presented in Fig. B3 and Fig. B4 and the stresses in crest are summarized in Tab. B2 and Tab. B3.

	Static + Dynamic	
	Min (MPa)	Max (MPa)
Crown-Upstream	-14.7	4.3
Crown-Downstream	-6.8	3.2
Left bank-Upstream	-6.6	2.9
Left bank-Downstream	-11.1	3.1
Right bank-Upstream	-6.3	2.2
Right bank-Downstream	-13.3	3.0

Tab. B2: Hoop stresses at crest of cross sections

	Static + Dynamic	
	Min (MPa)	Max (MPa)
Crown-Upstream	-5.1	2.2
Crown-Downstream	-4.1	1.4
Left bank-Upstream	-3.3	3.1
Left bank-Downstream	-4.4	1.4
Right bank-Upstream	-3.1	0.6
Right bank-Downstream	-3.2	0.4

Tab. B3: Hoop stresses at crest of cross sections
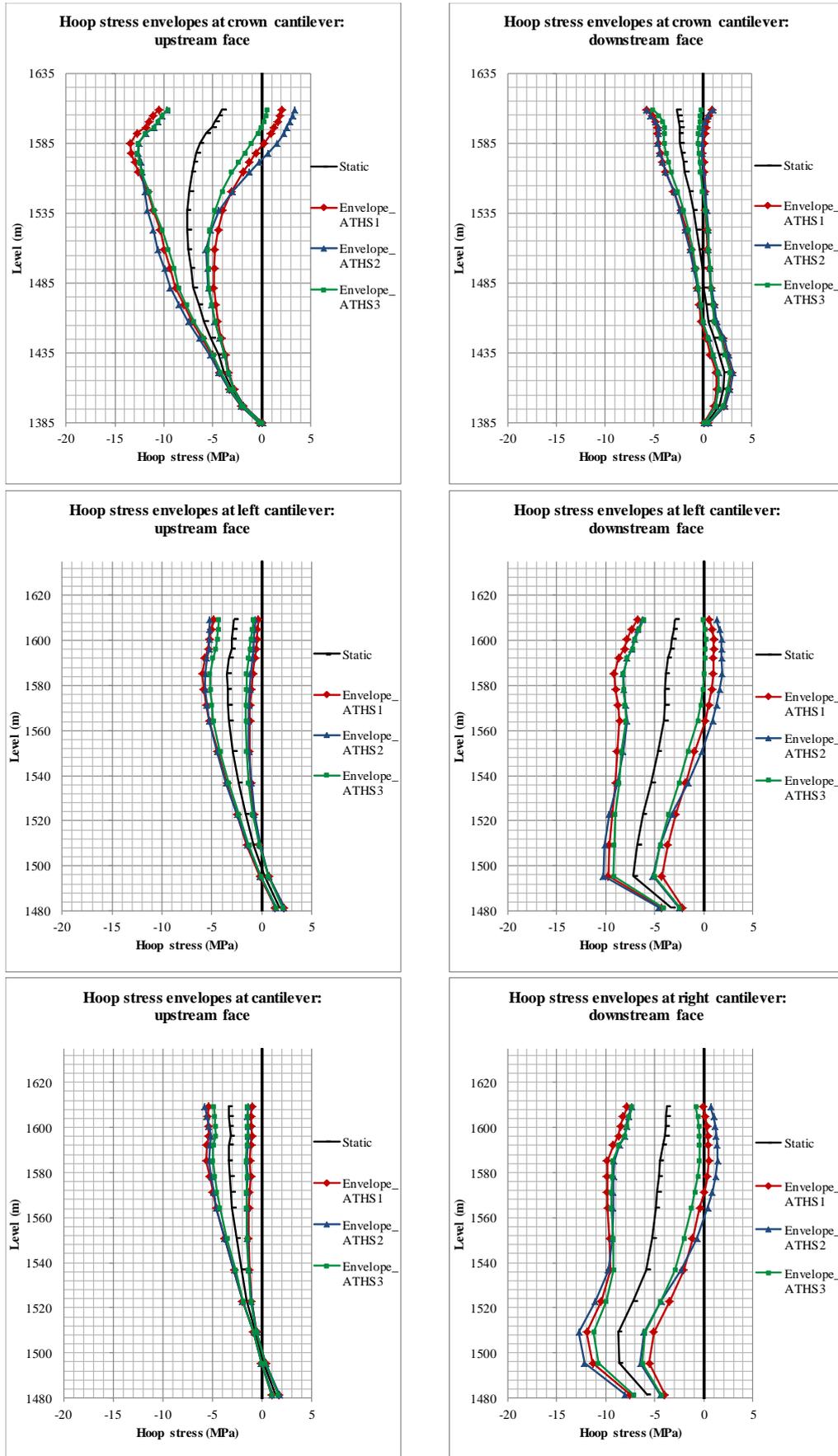
Fig. B3: Hoop stress envelopes in upstream and downstream faces of selected sections
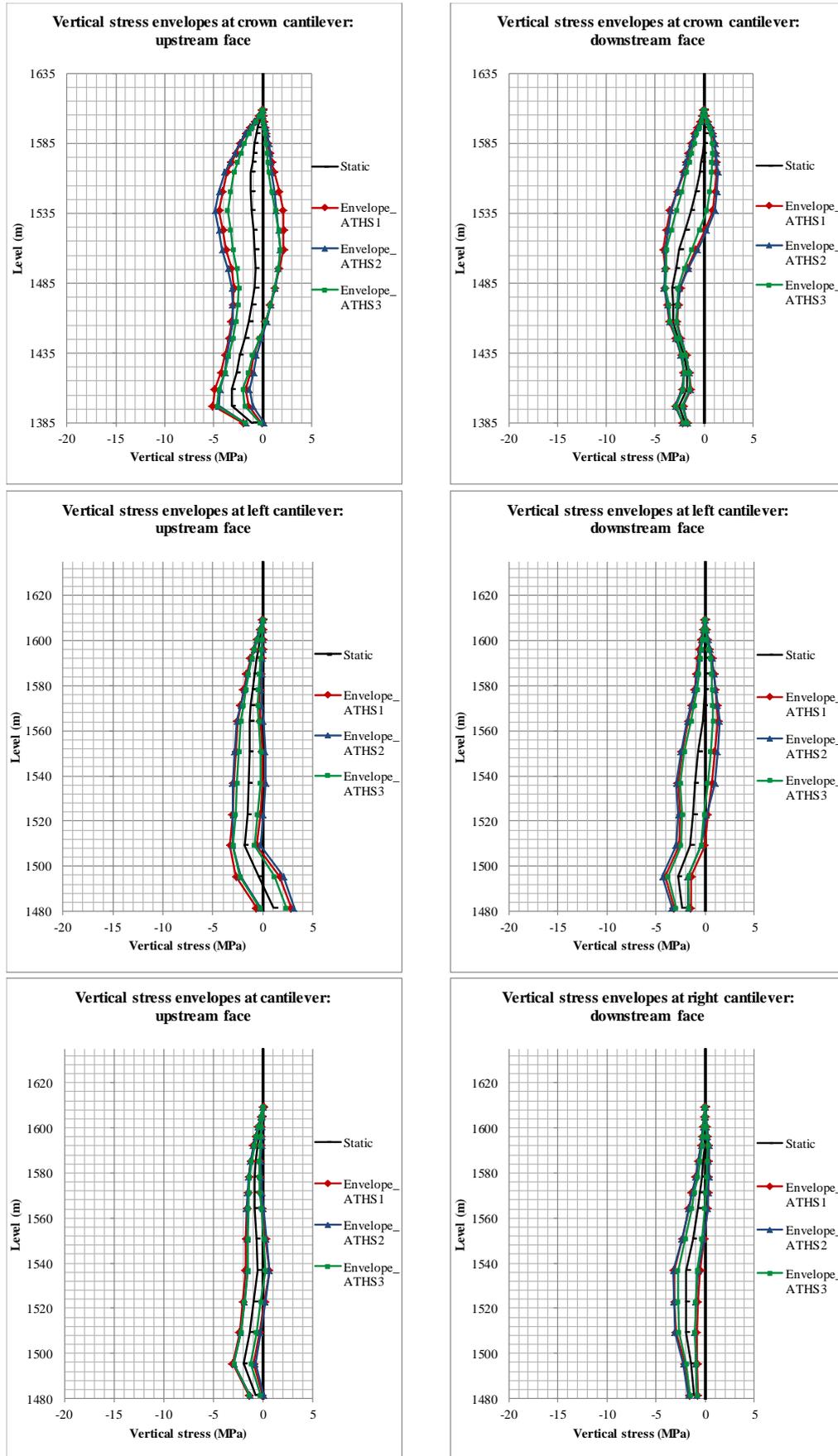
Fig. B4: Vertical stress envelopes in upstream and downstream faces of selected sections

Stress envelopes at selected points

The maximum and minimum stresses were calculated for 10 points in the upstream and downstream face each (Fig. B5). The results are presented in Tab. B4:

| Face | Zone | Point | Elementary Load Cases | | | | | | Static Load Combinations | | Dynamic Load Combinations DE2 (SW+HSP+SP+dTS+MCE) | | | | | |
| | | | Self-Weight (SW) | | Hydrostatic Pressure (HSP) | | Silt Pressure (SP) | | SU0 (SW+HSP+SP) | | MCE Series 1 | | MCE Series 2 | | MCE Series 3 | |
			S1	S3	S1	S3	S1	S3	S1	S3	S1	S3	S1	S3	S1	S3
Upstream Face	Crest - Left	A	-0.09	-0.01	-2.72	0.02	-0.001	0.000	-2.78	0.01	-4.82	0.24	-5.24	0.24	-4.33	0.15
	Crest - Centre	B	-0.32	-0.02	-3.73	-0.02	0.002	0.000	-4.04	-0.02	-10.54	2.12	-9.68	3.40	-9.62	0.75
	Crest - Right	C	-0.10	-0.01	-3.32	0.01	0.000	0.000	-3.41	0.00	-5.43	0.10	-5.81	0.13	-4.90	0.07
	Dam Upper Part - Left	D	-0.08	0.03	-5.90	-0.99	0.001	0.000	-5.84	-1.04	-9.77	1.23	-9.68	0.96	-9.36	0.72
	Dam Upper Part - Right	E	0.09	-0.04	-5.69	-0.92	0.001	0.000	-5.66	-0.89	-8.49	0.86	-9.04	0.68	-7.98	0.57
	Abutment Upper Part - Left	F	-0.82	-0.04	1.39	0.39	-0.003	0.000	-0.38	0.35	-1.00	2.10	-1.16	2.05	-0.92	1.79
	Abutment Upper Part - Right	G	-0.02	-1.46	2.64	-0.69	-0.003	0.001	1.33	-0.84	-2.83	5.08	-3.62	4.94	-2.72	4.29
	Abutment Lower Part - Left	H	-3.76	-0.71	5.73	2.07	-0.003	0.001	2.74	1.40	-0.89	4.42	-0.59	4.72	-0.65	3.89
	Abutment Lower Part - Right	I	-3.11	-0.70	3.56	1.54	-0.003	0.002	-1.07	0.90	-1.54	2.83	-1.47	2.90	-1.48	2.77
	Dam Lower Part	J	0.01	-5.67	2.61	-1.76	-0.158	-0.131	-3.30	-1.88	-4.88	0.00	-4.38	0.00	-4.47	0.00
Downstream Face	Crest - Left	A'	-0.15	0.01	-2.79	-0.03	-0.001	0.000	-2.94	-0.03	-6.83	0.81	-6.27	1.48	-6.22	0.27
	Crest - Centre	B'	-0.21	0.01	-2.47	0.01	0.003	0.000	-2.68	-0.02	-5.57	0.86	-5.80	0.78	-4.98	0.08
	Crest - Right	C'	-0.12	0.01	-3.68	-0.01	-0.001	0.000	-3.79	-0.02	-7.87	0.19	-7.39	0.80	-7.33	0.05
	Dam Upper Part - Left	D'	-1.46	0.02	-2.86	0.90	0.002	0.000	-2.96	-0.54	-5.96	2.66	-5.45	3.11	-5.27	1.72
	Dam Upper Part - Right	E'	-1.45	0.00	-3.01	0.68	-0.002	0.000	-3.11	-0.75	-8.01	3.14	-7.08	3.79	-7.18	1.93
	Abutment Upper Part - Left	F'	0.08	-0.11	-3.65	0.16	-0.003	0.000	-3.58	-0.06	-5.26	0.17	-5.54	0.15	-4.82	0.15
	Abutment Upper Part - Right	G'	-0.84	0.06	-8.07	-1.20	-0.004	0.001	-8.21	-1.84	-12.27	0.14	-12.46	0.14	-11.09	0.13
	Abutment Lower Part - Left	H'	-0.51	0.36	-6.93	-1.47	-0.013	0.003	-7.10	-1.53	-9.41	0.00	-9.92	0.00	-8.88	0.00
	Abutment Lower Part - Right	I'	0.39	0.00	-7.01	-1.11	-0.020	0.002	-6.86	-0.94	-8.88	0.00	-9.51	0.00	-8.47	0.00
	Dam Lower Part	J'	-0.02	-0.66	2.03	-1.42	0.063	-0.001	2.08	-2.00	-2.48	2.64	-2.49	2.80	-2.42	2.54

Tab. B4: Static and dynamic loads combinations at selected points (principal stresses)
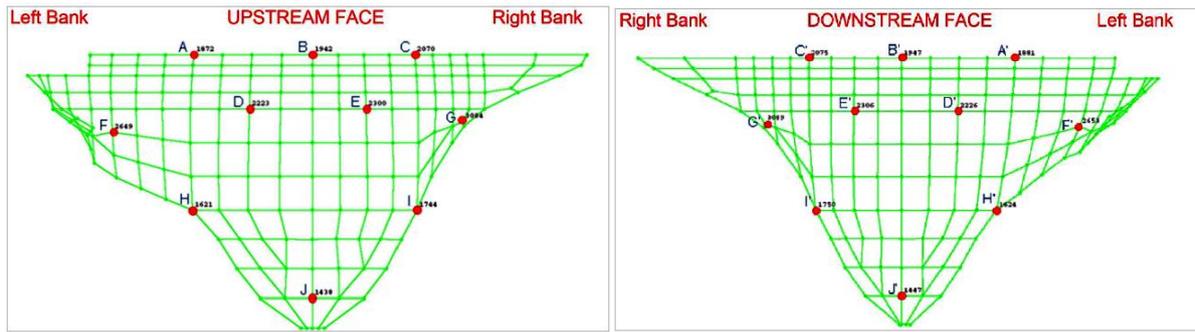
Fig. B5: Selected points for stress analysis

Stress time history

The principal stresses time histories were calculated for 2 points of the dam upper part of each face (points D, E, D' and E').

On each face of the dam, one of the principal stresses is perpendicular to the dam surface. This stress is equal to zero on the downstream surface and varies slightly around the hydrostatic pressure on the upstream face. As this stress has little interest for the dam behaviour analysis, we have studied the variation of the other two principal stresses directed in the dam surface: σ_{min} for the maximum compression and σ_{max} for the maximum tension.

The stresses responses are shown at Figures B6 to B9.
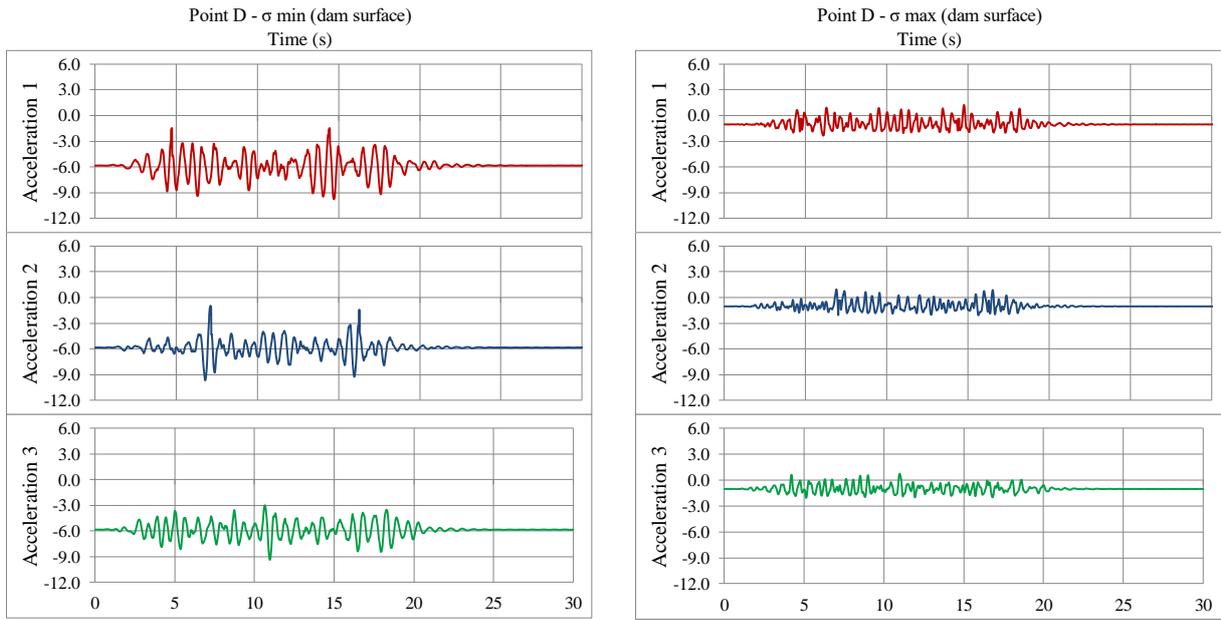
Fig. B6: Maximal and minimal stresses time history at point D (dam upper part – left bank at upstream face) (MPa)
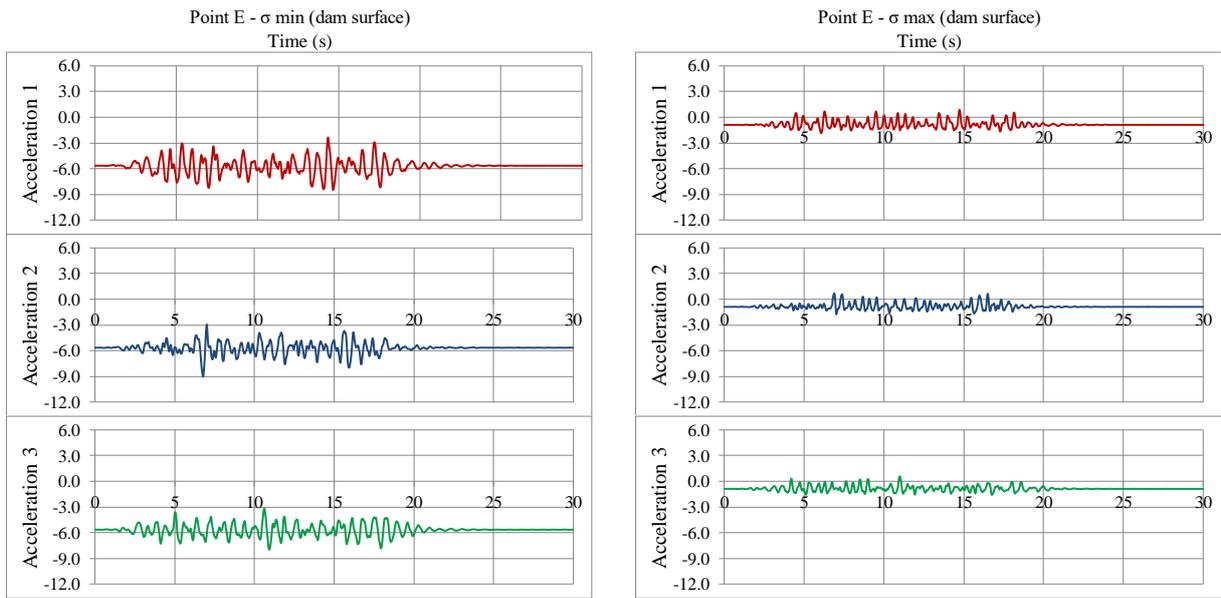
Fig. B7: Maximal and minimal stresses time history at point E (dam upper part – right bank at upstream face) (MPa)
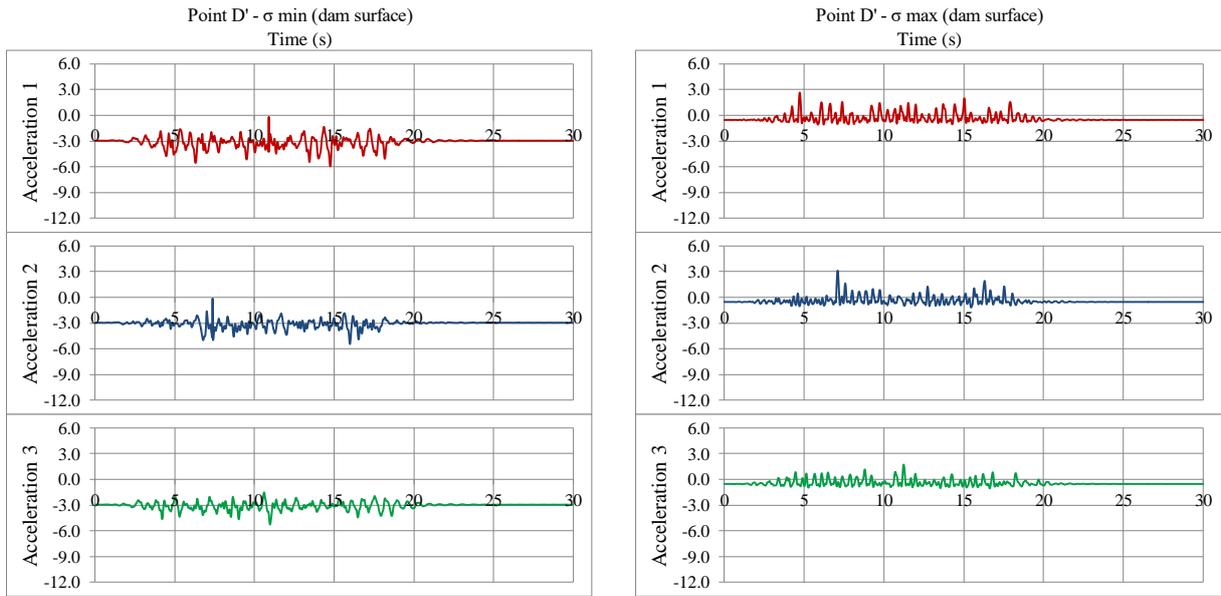
Fig. B8: Maximal and minimal stresses time history at point D' (dam upper part – left bank at downstream face) (MPa)
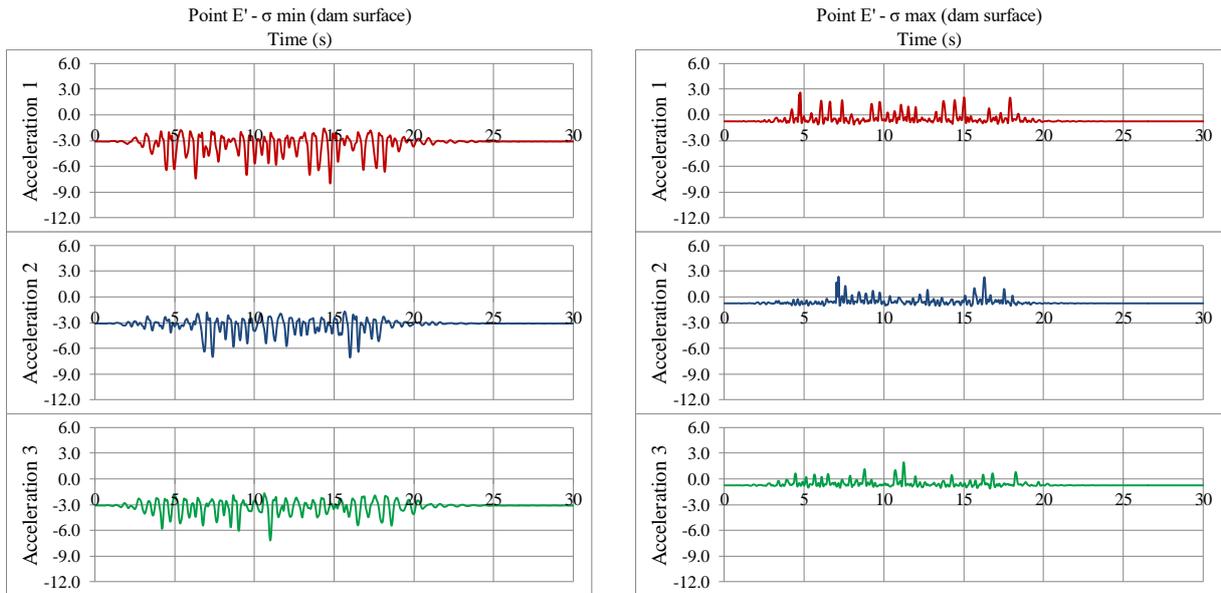
Fig. B9: Maximal and minimal stresses time history at point E' (dam upper part – right bank at downstream face) (MPa)

Theme A: Seismic Safety Evaluation of a Concrete Dam Based on Guidelines

Preisig, M.[1] and Commend, S.[1]

[1]*Geomod Consulting Engineers, Epinettes 32, CH-1007 Lausanne, Switzerland*

ABSTRACT: A concrete arch dam was analyzed according to the directive published by the Swiss Federal Office of Energy. The investigated Luzzone dam is with a height of 225 meters the 3rd tallest in Switzerland. The dynamic analyses yield tensile stresses that exceed the dynamic strength of 4 MPa. Stability against sliding and overturning of individual blocks is satisfied. A nonlinear analysis with discontinuities introduced between individual blocks indicates that the seismic stability of the dam seems to be sufficient.

E-mail: mpreisig@geomod.ch

Introduction

The selection of appropriate model parameters, mesh discretizations, algorithms as well as the validation of finite element models represents a considerable challenge and can lead to a large spread in the results obtained by different groups of analysts. This paper documents the modeling choices and the main results obtained for the specified object, with the goal of being compared with the analyses of other contributors.

The finite element software ZSoil 14.10 [2] was used for all FE analyses.

Analysis of provided input data

Material parameters

The material parameters were taken as proposed by the organizers, with the exception of the Rayleigh damping coefficients. According to [1] the damping ratio should not exceed 5%. The parameters suggested by the organizers ($\alpha=0.6$, $\beta=0.01$) lead to a damping ratio of 8% in the range of the longest eigenperiods and much larger for shorter periods, as can be seen in Fig. 1. The parameters have thus been slightly reduced in order to obtain 5% for the longest eigenperiods ($\alpha = 0.47$, $\beta = 0.005$).
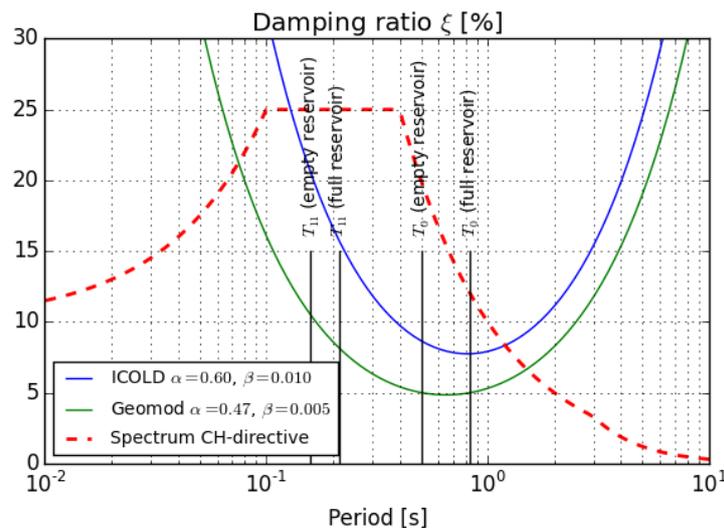
Fig. 1: Damping ratios for selected Rayleigh damping parameters. The first and the twelfth eigenperiods for the empty and the full reservoir are also shown.

Seismic input

Three earthquakes were applied to the model by applying separate accelerograms in all three directions on all boundary nodes. From the boundaries the seismic input travels through the rock foundation to the arch dam and is thereby modified. In Fig. 2 the response spectra are shown for all input motions and for 5 nodes on the rock-dam interface. The requirement in [1] is met in the long period range, while in the range of the plateau the input spectra reach in some cases only about 90% of the spectrum given by the guidelines. The motions at the rock-dam interface are amplified and therefore meet the requirement in general. The small period range below 0.1 s is of minor interest, since the relevant eigenperiods of the dam are all within the plateau.
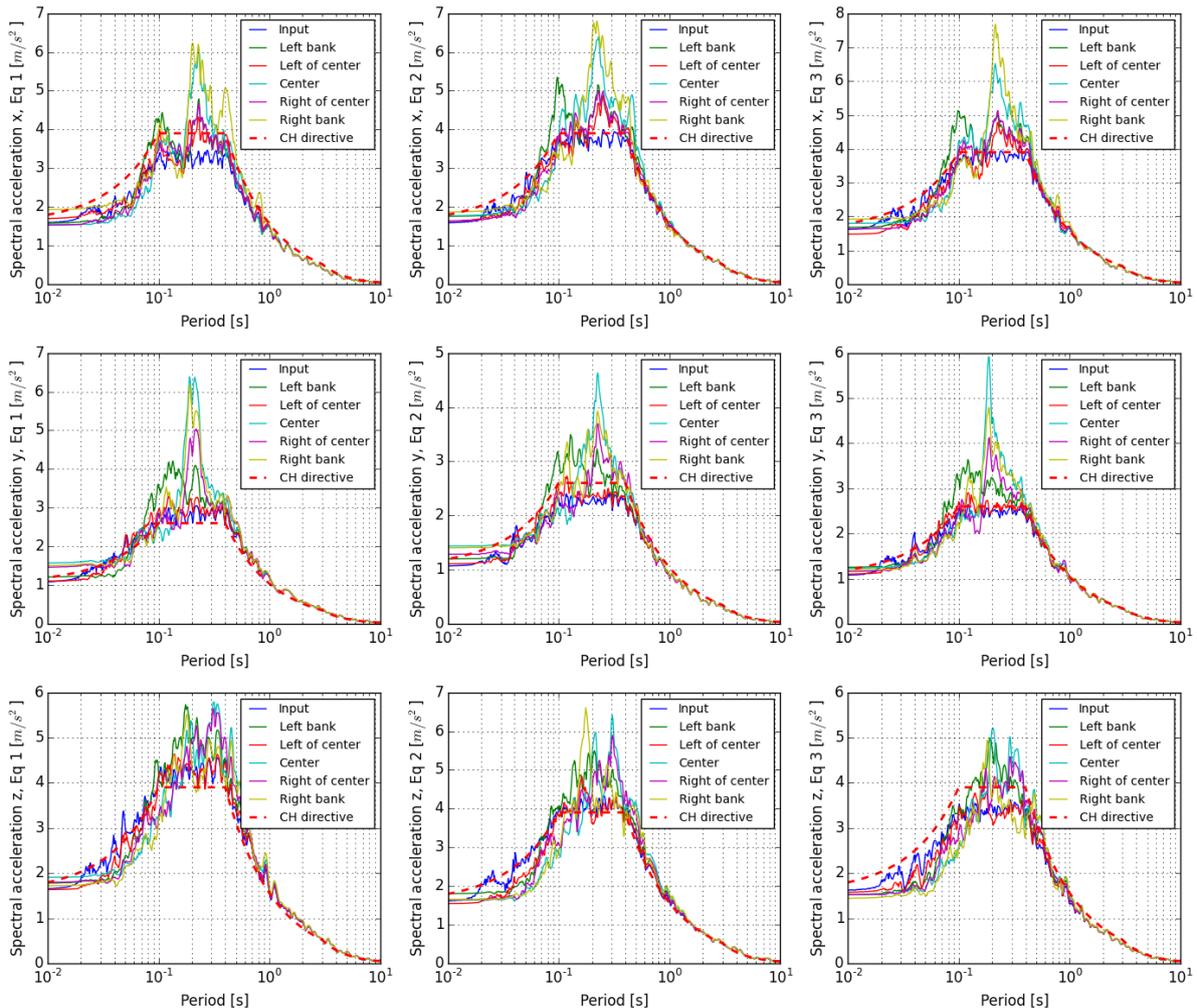
Fig. 2: Response spectra of the input motions and at 5 nodes on the rock-dam interface in all 3 directions for the 3 earthquakes. The requirement of the Swiss directive [1] is also shown.

Geometry of finite element mesh

The model of the arch dam is based on the model provided by the symposium organizers. As far as the mesh is concerned, the authors might have used a slightly different approach, were they required to build the model from scratch:

- If information about the foundation depth was available, the authors would have used it to represent the geometry of the dam as realistically as possible. Since in the provided mesh the dam geometry did not extend under the ground surface,

introduction of interface elements between the rock-concrete interface was not possible. Unrealistically high tensile stresses at the interface are thus unavoidable.

- A potential stair-profile of the foundation on the flanks would be easy to reproduce using brick elements. In that case the mesh of the dam could be considerably simplified by having a grid aligned with horizontal and vertical lines throughout the dam. Interface elements could be introduced at all construction joints. Approximating the surrounding ground surface with right-angled steps is acceptable, as results are extracted only from the dam itself.
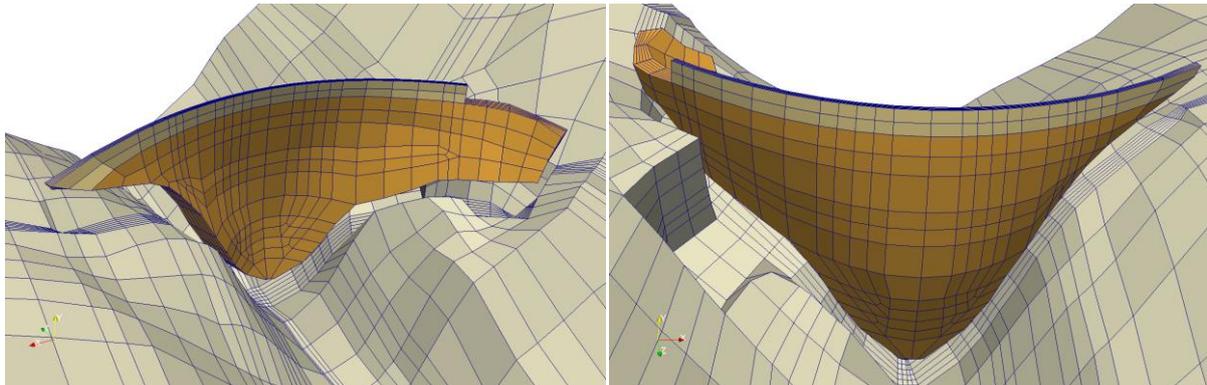
Fig. 3: Finite element mesh (linear hexahedrons) used in the analyses. A gap is introduced to show that the mesh at the rock-concrete interface is fully consistent.

Discretization of finite element mesh

The provided mesh was adapted along the rock-concrete interface in order to remove hanging nodes and to make it fully consistent. Furthermore linear hexahedral elements were used instead of quadratic elements. In order to still obtain a sufficiently fine resolution of stresses, the original model was refined to include 6 elements across the dam thickness.

The mesh size (or distance between 2 nodes) is required to be sufficiently fine to be able to resolve the shortest wavelength of interest (λ_{min}):

$$\Delta h \leq \frac{\lambda_{min}}{10} = \frac{v_s}{10 \times f_{max}} \tag{1}$$

where v_s is the shear wave velocity and f_{max} is the highest frequency of interest for the analysis. Since the rock density was chosen to be zero, all wavelengths in the rock are infinite and the above criterion was automatically satisfied. For the concrete, the shear wave velocity was determinant ($v_s = 1840$ m/s for the old concrete). For an f_{max} of 15 Hz Equation (1) required a mesh size smaller than 12 m.

With nodal spacings of up to 28 m the minimum wave length is sampled at only 4 to 5 nodes. In order to validate the mesh used in the analyses a second mesh with a minimum nodal spacing of 14 m in vertical direction was analyzed. Differences amounted to about 1% for maximum displacements and 4 to 5% as far as maximal stress values were concerned. The first 12 eigenfrequencies differ by maximum 1.5%. For the purpose of this study the use of the coarse mesh was acceptable.

Dynamic interaction with reservoir

The mass of water interacting with the concrete dam was modeled according to the Westergaard approach. The mass was, however, only applied in z-direction, thus neglecting the cross-valley component for the elements on the flanks.

Seismic verifications

The following seismic verifications were performed according to the Directives issued by the Swiss Federal Office of Energy [1]:

- Eigenvalue analysis in order to determine the dynamic properties of the (linearized) structure-ground system.
- Linear dynamic analysis in time domain.
- Nonlinear dynamic analysis in time domain (for one accelerogram only)
- Verification of rocking-block stability using a spreadsheet calculation.

The results of the verifications as requested by the organizers are presented in the Appendix.

Analysis of the results

The static analysis (SU2, Tab. 2) yielded maximum tensile stresses of the order of 1.4 MPa in the area of the abutments on the upstream face. The stresses in that area are likely to be overestimated due to the assumption of perfect bonding between rock and concrete. Maximum tensile stresses of about 1.2 MPa occur on the downstream side of the crest. All tensile stresses remain below the static tensile strength of both old and new concrete (3.0 MPa and 2.3 MPa).

The linear analyses of the three earthquakes yielded tensile stresses of the order of 8 MPa on the upstream side of the dam crest and slightly smaller on the downhill side (Fig. 4).
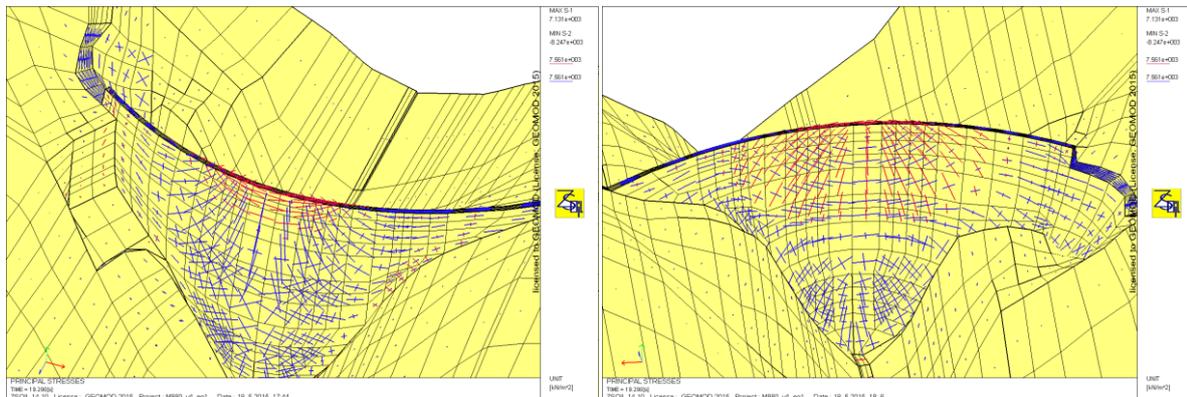
Fig. 4: Maximum tensile stresses (in red) for earthquake 1 at 9.3 s.

Since these tensile stresses exceed the tensile strength of concrete, further investigations were needed. To this end construction joints were introduced at three vertical sections where the maximum tensile stresses occur. On these construction joints interfaces with 55° friction angle, zero dilatancy and zero cohesion were introduced.

The nonlinear study on the model with interfaces on selected construction joints was conducted for one accelerogram (Eq1, no additional scaling by 3 to trigger nonlinear behaviour as suggested in the problem description). The deformed mesh at the end of shaking is shown in Fig. 5. The analysis resulted in a maximum relative displacement between two adjacent blocks of 20 cm. Compared to the width of the crest of about 3 m this displacement should not cause major 2nd order effects, such as additional overturning moments or stress concentrations.
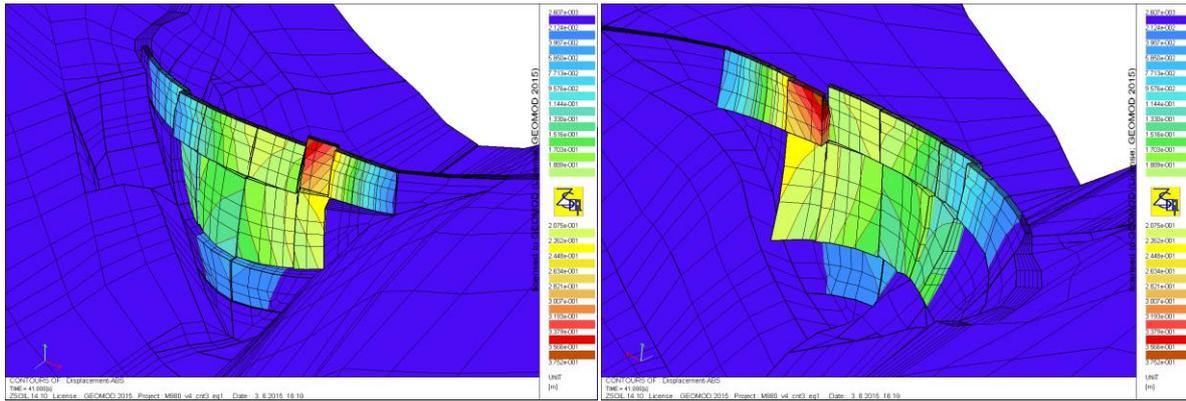
Fig. 5: Deformed mesh at the end of shaking (displacements scaled by 80, nonlinear analysis).

The analysis of maximum tensile stresses (Fig. 6) shows tensile stresses exceeding 4 MPa in individual elements in contact with the rock foundation, where no interface elements have been introduced. Maximum compressive stresses (not shown) are of the order of 12 MPa.
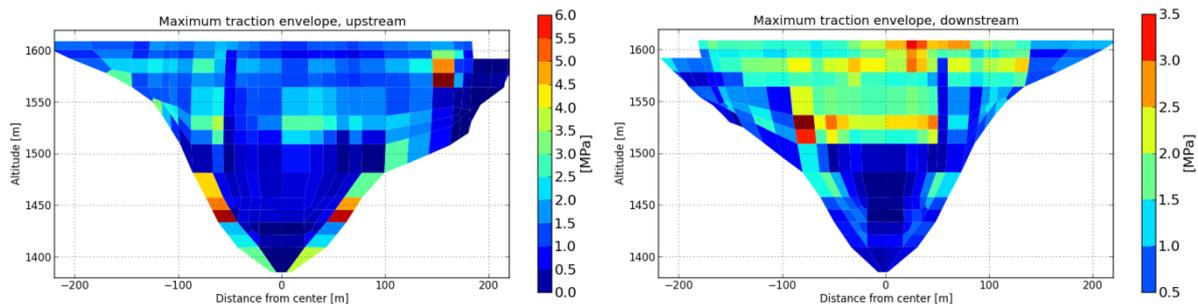
Fig. 6: Maximum traction envelopes for the nonlinear analysis.

The stability analysis (Tab. 3) yielded safety factors of sliding and overturning below 1.0 for all blocks. The condition of block stability is therefore not satisfied.

Proposal for further studies

The analysis using interface elements along construction joints produced very useful results. However, the provided mesh did not allow easy introduction of joints along the entire height of the dam. The introduction of interface elements on the real rock-concrete interface (below ground level) might be useful in order to reduce unrealistic tensile stresses. With this in mind, an improved mesh should include at least the major vertical joints, some horizontal fracture planes as well as the below ground geometry of the foundation.

Conclusion

Linear seismic analyses of a concrete arch dam have been performed according to the problem description and the data provided by the conference organizers. Tensile stresses of up to 8 MPa exceed the dynamic tensile strength of the concrete. An additional nonlinear analysis, performed on a model with discontinuities introduced between selected construction blocks, yielded displacements and stresses that should not lead to a collapse of the structure. Sliding and overturning of individual blocks might, however, happen. If the amount of sliding or rotation is likely to lead to a gap opening in the dam and thus to an uncontrolled release of water has to be investigated more closely.

References

[1] Sécurité des ouvrages d'accumulation. Documentation de base pour la vérification des ouvrages d'accumulation aux séismes, rapports de l'OFEN, série Eaux, version 1.2, mars 2003.

[2] ZSOIL.PC 2014, User manual. Zace Services Ltd. (www.zsoil.com), Lausanne, Switzerland. 2014.

Appendix

Natural frequencies and mode shapes

Tab. 1: Natural frequencies and effective masses.

Mode	Empty Reservoir				Full Reservoir			
	Eigenfrequency	Effective Mass Percentage			Eigenfrequency	Effective Mass Percentage		
	f, Hz	X, %	Y, %	Z, %	f, Hz	X, %	Y, %	Z, %
1	2.0	7.4	0.0	0.1	1.2	0.1	0.1	61.6
2	2.1	0.2	0.7	22.7	1.3	2.2	0.1	5.8
3	3.0	0.1	0.4	6.0	2.0	0.1	0.2	19.6
4	3.8	0.1	6.8	14.7	2.2	0.0	0.9	52.8
5	3.9	0.6	0.2	1.0	2.6	0.5	0.0	0.2
6	4.4	24.2	0.0	0.2	2.9	3.1	0.0	0.0
7	5.0	0.1	0.3	1.3	3.3	0.1	0.0	3.7
8	5.4	1.9	49.8	0.4	3.5	0.0	0.2	26.0
9	5.9	28.6	2.3	0.6	4.0	0.0	1.3	12.1
10	6.0	5.1	0.8	1.8	4.0	0.0	0.1	1.6
11	6.1	0.5	0.0	0.1	4.5	0.9	0.0	0.1
12	6.3	0.6	3.1	14.9	4.7	0.0	0.3	10.6
	Σ	69.2	64.4	63.7	Σ	6.9	3.3	194.2
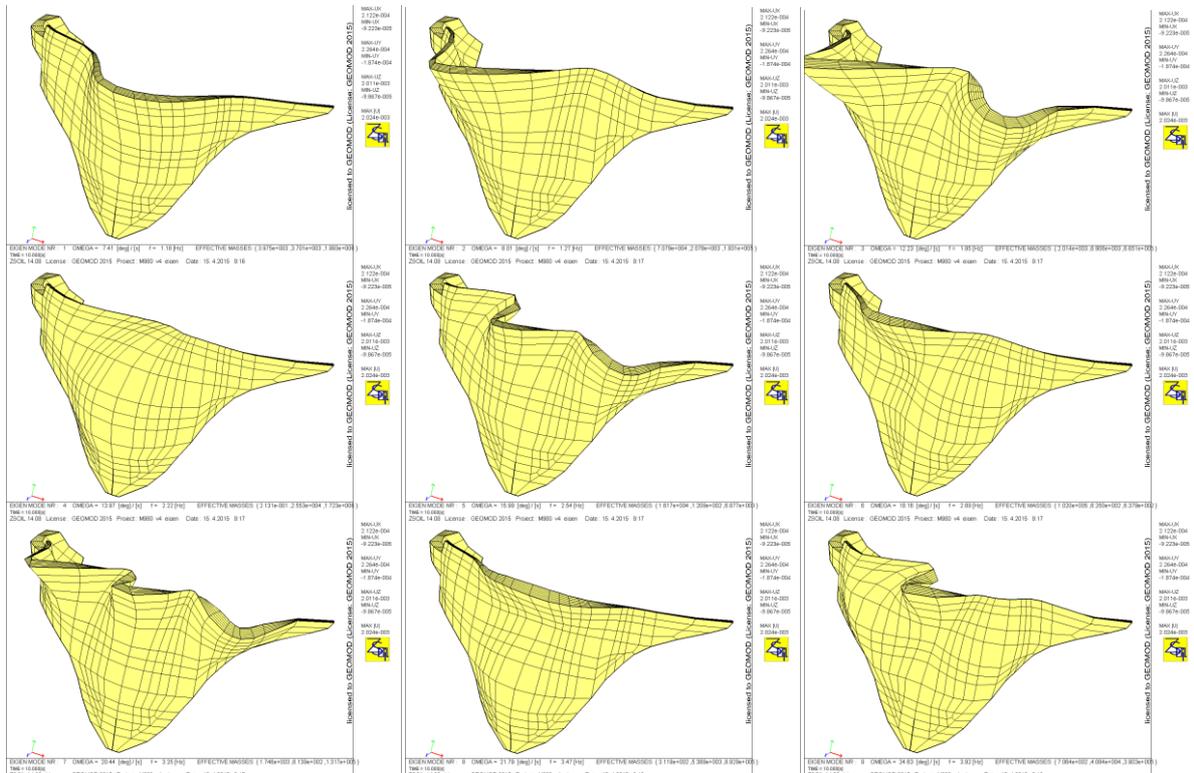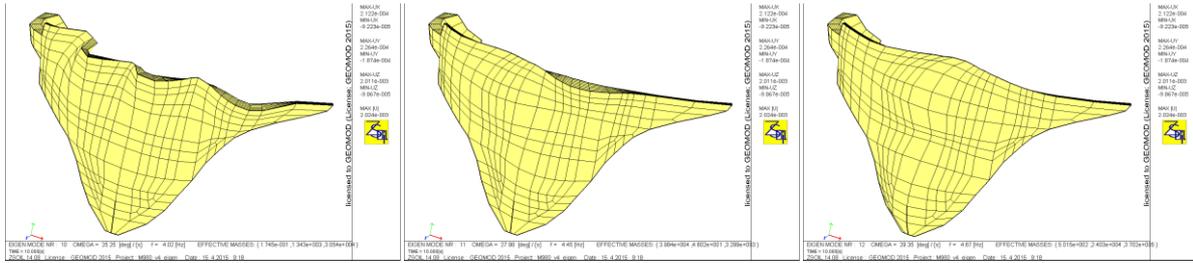
Fig. 7: Eigenmodes 1 to 12.

Displacements

Displacement Time Histories
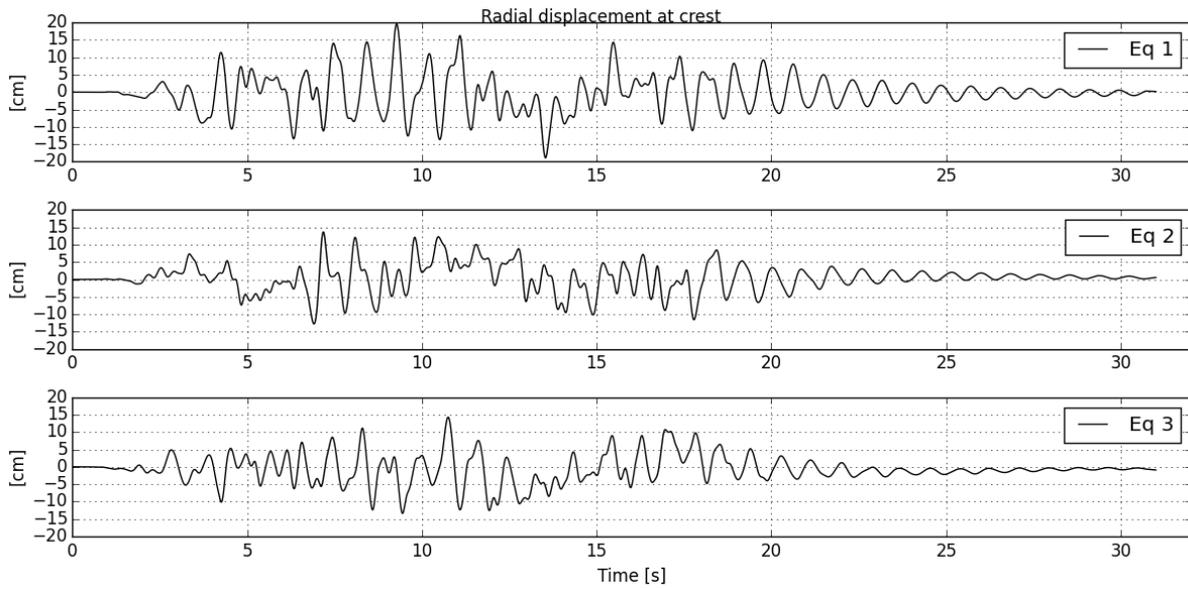
Fig. 8: Radial displacement time histories at dam crest.

Displacement Envelopes at Cross Sections
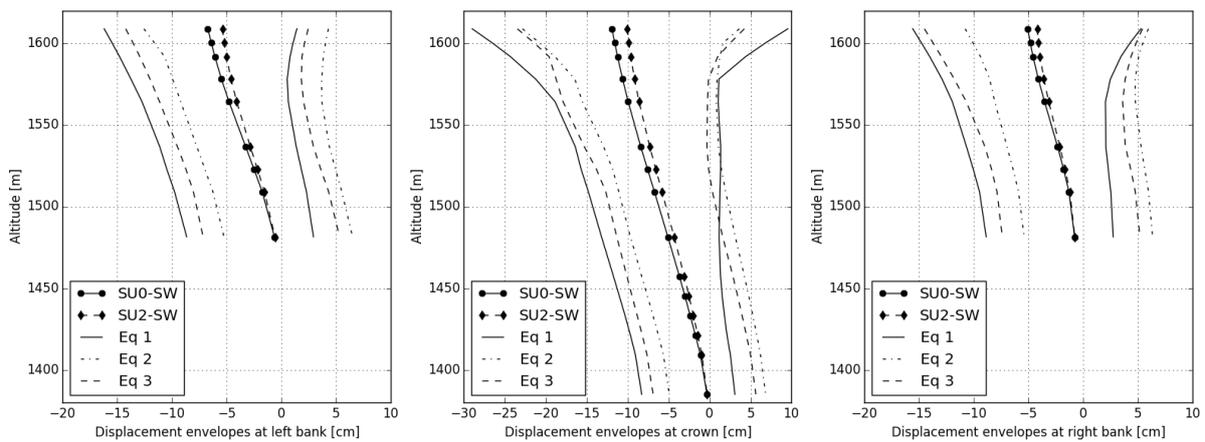
Fig. 9: Displacement envelopes in 3 cross sections.

Stresses

Stress envelopes on U/S and D/S faces
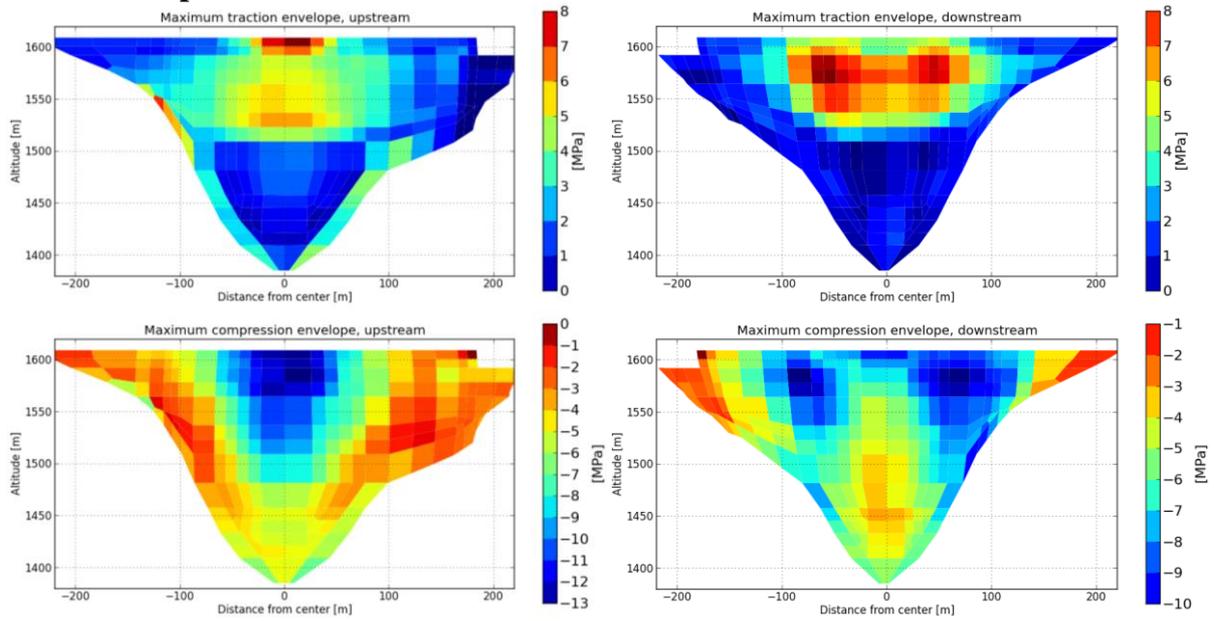
Fig. 10: Stress envelopes for all earthquakes on upstream and downstream faces.

Stress envelopes at cross sections
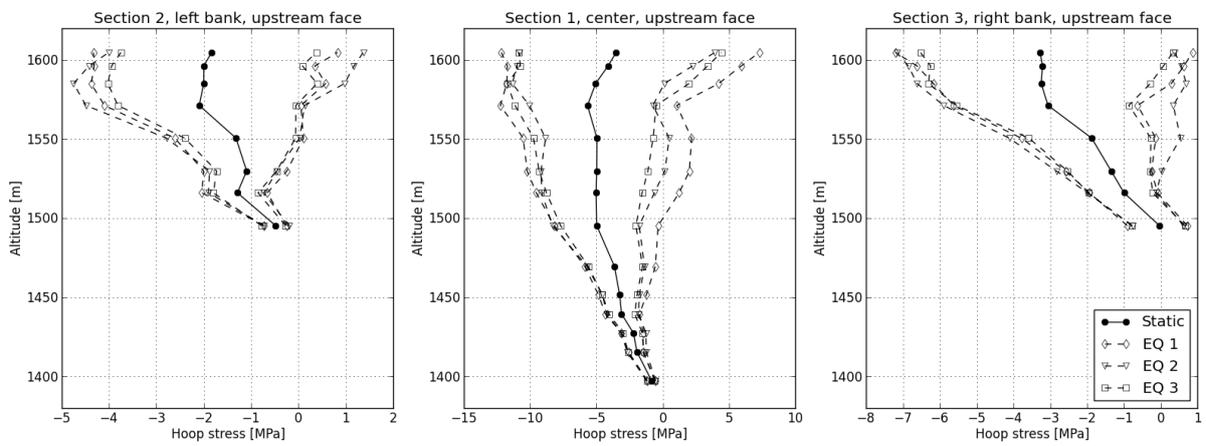
Fig. 11: Hoop stress envelopes on upstream face.
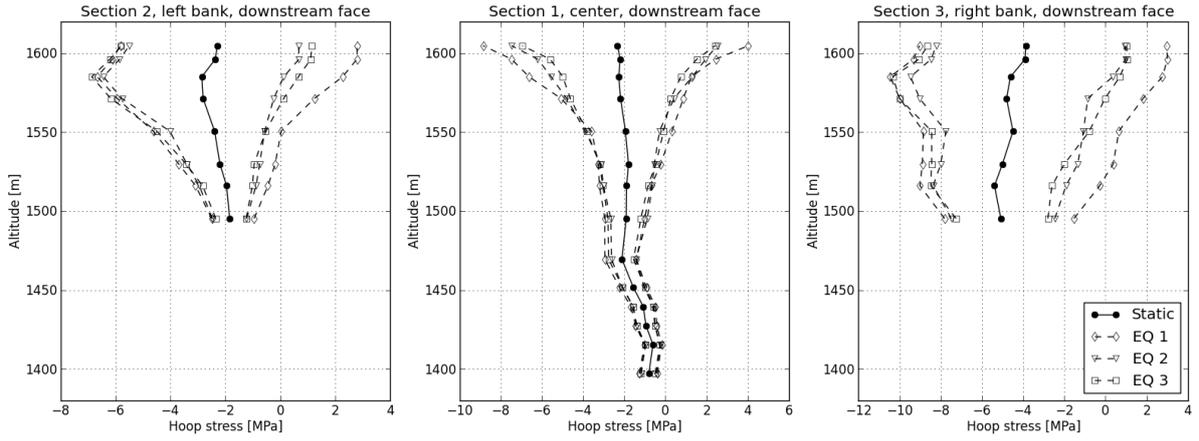
Fig. 12: Hoop stress envelopes on downstream face.
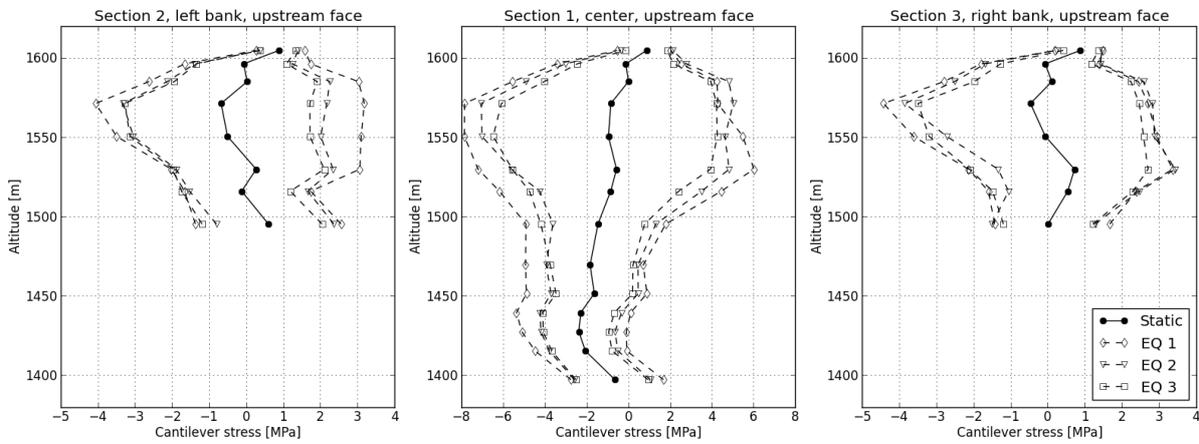
Fig. 13: Cantilever stress envelopes on upstream face.
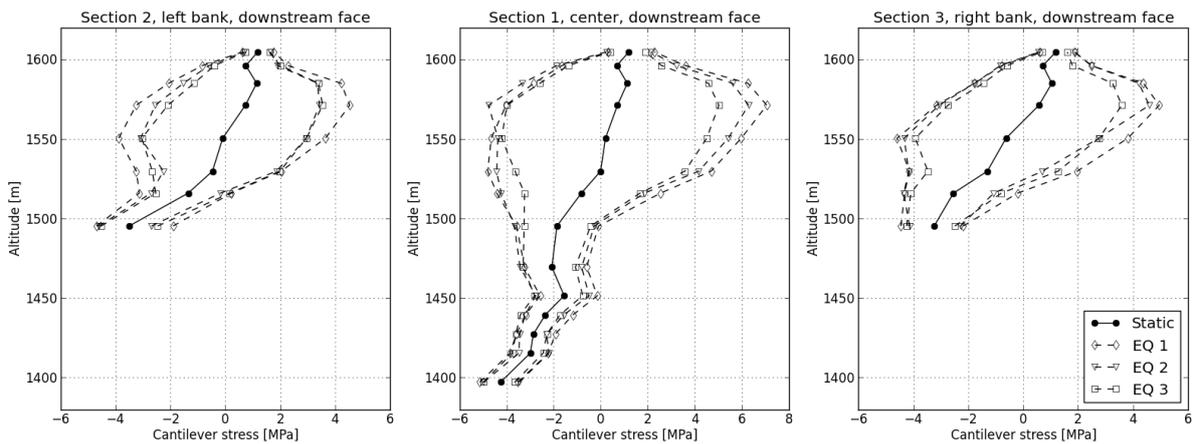
Fig. 14: Cantilever stress envelopes on downstream face.

Stress Values at Selected Points

Tab. 2: Stress values at selected points.

Face	Zone	Point	Self-Weight (SW)		Hydrostatic Pressure (HSP)		Silt Pressure (SP)		Summer T°C Gradient (dTS)		SU0 (SW+HSP+SP)		SU2 (SW+HSP+SP +dTS)		MCE Series 1		MCE Series 2		MCE Series 3	
			S1	S3	S1	S3	S1	S3	S1	S3	S1	S3	S1	S3	S1	S3	S1	S3	S1	S3
Upstream Face	Crest - Left	A	0.96	-0.03	0.91	-2.46	0.91	-2.46	0.93	-2.30	0.91	-2.46	0.93	-2.30	1.79	-4.83	1.58	-4.61	1.82	-4.20
	Crest - Centre	B	0.81	-0.14	0.62	-4.32	0.62	-4.32	0.64	-3.67	0.62	-4.32	0.64	-3.67	7.85	-12.50	4.68	-11.16	4.84	-12.04
	Crest - Right	C	0.92	-0.08	0.90	-3.07	0.90	-3.07	0.91	-2.96	0.90	-3.07	0.91	-2.96	1.70	-5.68	1.69	-5.76	1.44	-5.45
	Dam Upper Part - Left	D	0.76	-0.20	-0.79	-4.79	-0.79	-4.79	-0.77	-4.26	-0.79	-4.79	-0.77	-4.26	4.00	-7.77	3.63	-6.73	4.17	-6.95
	Dam Upper Part - Right	E	0.49	-0.08	-0.72	-4.87	-0.72	-4.87	-0.70	-4.36	-0.72	-4.87	-0.70	-4.36	4.60	-8.48	3.95	-7.62	3.09	-8.40
	Abutment Upper Part - Left	F	-0.02	-1.42	-0.19	-1.12	-0.19	-1.12	-0.27	-1.53	-0.19	-1.12	-0.27	-1.53	0.90	-2.63	0.70	-2.38	0.82	-2.44
	Abutment Upper Part - Right	G	-0.07	-1.80	1.25	-0.88	1.25	-0.89	1.39	-1.61	1.25	-0.89	1.39	-1.61	4.60	-3.83	4.97	-2.89	4.32	-3.65
	Abutment Lower Part - Left	H	-0.36	-4.02	1.35	-0.25	1.34	-0.25	1.35	-0.60	1.34	-0.25	1.35	-0.60	3.65	-1.31	3.49	-0.98	2.93	-1.13
	Abutment Lower Part - Right	I	0.23	-3.13	1.24	-0.23	1.24	-0.23	1.02	-0.45	1.24	-0.23	1.02	-0.45	3.51	-1.46	2.78	-1.61	2.68	-0.99
	Dam Lower Part	J	0.16	-4.05	-1.04	-1.96	-1.06	-2.10	-1.51	-1.99	-1.06	-2.10	-1.51	-1.99	0.68	-3.80	0.11	-3.32	-0.17	-3.28
Downstream Face	Crest - Left	A'	1.02	-0.21	1.21	-2.75	1.21	-2.75	1.20	-2.86	1.21	-2.75	1.20	-2.86	3.72	-7.41	1.87	-7.12	2.14	-7.64
	Crest - Centre	B'	0.85	-0.18	1.05	-2.61	1.05	-2.61	1.02	-2.39	1.05	-2.61	1.02	-2.39	4.45	-9.20	3.37	-7.92	2.64	-7.00
	Crest - Right	C'	0.95	-0.19	1.20	-3.88	1.20	-3.88	1.19	-3.84	1.20	-3.88	1.19	-3.84	3.27	-8.74	2.21	-7.95	2.11	-8.18
	Dam Upper Part - Left	D'	0.02	-0.13	0.78	-2.24	0.78	-2.24	0.32	-2.84	0.78	-2.24	0.32	-2.84	8.05	-7.44	6.13	-7.66	5.33	-7.23
	Dam Upper Part - Right	E'	0.07	0.04	0.43	-2.36	0.43	-2.36	0.14	-2.92	0.43	-2.36	0.14	-2.92	7.29	-8.36	6.16	-7.68	5.48	-7.99
	Abutment Upper Part - Left	F'	1.39	-0.09	-0.02	-1.32	-0.02	-1.32	-0.36	-1.61	-0.02	-1.32	-0.36	-1.61	0.06	-2.94	0.04	-2.87	-0.01	-2.80
	Abutment Upper Part - Right	G'	1.34	0.15	-1.07	-3.06	-1.07	-3.06	-1.51	-3.56	-1.07	-3.06	-1.51	-3.56	1.24	-6.09	1.12	-5.86	0.72	-5.90
	Abutment Lower Part - Left	H'	1.02	-0.27	-1.57	-4.47	-1.57	-4.48	-2.53	-4.98	-1.57	-4.48	-2.53	-4.98	-0.65	-6.90	-1.37	-6.99	-1.36	-6.65
	Abutment Lower Part - Right	I'	0.99	-0.32	-1.41	-4.89	-1.42	-4.89	-2.63	-5.44	-1.42	-4.89	-2.63	-5.44	-0.84	-8.09	-1.20	-7.52	-1.54	-7.34
	Dam Lower Part	J'	-0.10	-1.02	1.25	-2.99	1.25	-3.02	-0.45	-3.70	1.25	-3.02	-0.45	-3.70	-0.16	-4.59	-0.23	-4.28	-0.22	-4.46

Stress Time Histories
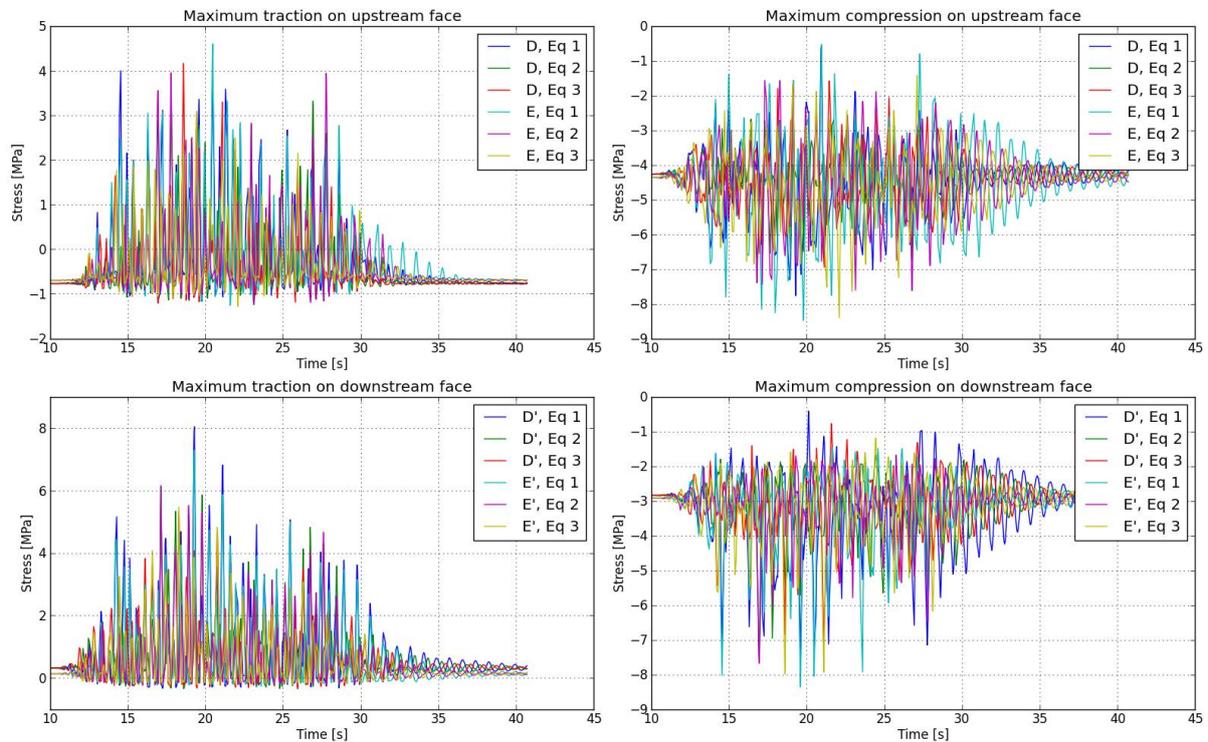
Fig. 15: Time histories of principal stresses on selected points on up- and downstream faces.

Stability analysis

Tab. 3: Results of the stability analyses of the 4 blocks.

Acting Force	Block Height, m			
	8.5	17	30.8	44.6
Self-Weight, PP [kN]	25'105	62'099	147'055	254'577
Hydrostatic Force, W [kN]	3'312	21'462	84'626	189'496
Uplift Force, SP [kN]	4'006	13'811	36'602	65'472
Earthquake Force, horizontal component, Qh [kN]	84'714	179'930	255'920	442'844
Earthquake Force, vertical component, Qv [kN]	18'977	42'270	80'542	126'521
Factor of Safety against Sliding	0.05	0.07	0.34	0.48
Factor of Safety against Overturning	0.26	0.30	0.50	0.55

Seismic Safety Evaluation of Luzzone Dam
Use of a 3DFEM State Formulation in Pressures and Displacements

Oliveira S.[1], Alegre A.[2], Silvestre A. [1], Espada M. [1] and Câmara R.[1]

[1]*Laboratório Nacional de Engenharia Civil, Concrete Dams Dep., Av. Brasil 101, 1700-066 Lisboa, Portugal*
[2]*Instituto Superior de Engenharia de Lisboa, Civil Eng. Dep., R. Cons. Emídio Navarro 1, 1959-007 Lisboa*

E-mail: soliveira@lnec.pt

ABSTRACT: In this paper is presented a study on the seismic safety evaluation of Luzzone dam. The results were obtained using a MATLAB 3DFEM program, DySSA7.0, developed in Concrete Dams Department of LNEC (Portugal), for the dynamic analysis of dam-reservoir-foundation systems. The program is based on a coupled model, of pressures (fluid) and displacements (solid). The time-do-main response for applied seismic accelerograms (a time-series for each direction is applied at the foundation: three sets of seismic accelerograms are considered, with a peak acceleration of 0.16g) is computed using a state formulation and a modal approach for the diagonalization of the differential equations system. Complex or non-stationary modes arise as eigenvectors of the state matrix of the dam-reservoir-foundation system. The foundation is computed as a substructure, elastic and massless. The principal stresses and displacements for the main load combinations (including static and seismic loads) are presented, as well as the hoop and cantilever stresses envelopes at the central cantilever (at the upstream and downstream faces). The safety factors for concrete local failure are evaluated for the dam body and the safety against sliding and overturning is studied on four blocks arising at the top of the central cantilever.

Introduction

In this paper a seismic safety evaluation study of Luzzone dam (Fig.1) is presented. It was used a 3DFE code developed at LNEC. The water-structure dynamic interaction is simulated using a coupled model based on pressures and displacements [1]. A state formulation [2] and a modal approach were used (Fig.2). The foundation is computed as a substructure, elastic and massless.

3DFE model

The 3DFE model was developed in MATLAB, using 20 node finite elements for the dam-reservoir-foundation system, based on a coupled state formulation for the solid and fluid domains. The developed model allows the user to carry out both static and dynamic analysis, computing modal characteristics, displacements and stress histories.

Reservoir
$c_p = 1440$ m/s

Old Concrete
$E = 20$ GPa $\nu = 0.18$
$\gamma = 25$ kN/m^3
$f_c = 38$ MPa; $f_t = 3$ MPa

New Concrete (crest)
$E = 18$ GPa $\nu = 0.18$
$\gamma = 24$ kN/m^3
$f_c = 32$ MPa; $f_t = 2.3$ MPa

Foundation
$E = 18.6$ GPa $\nu = 0.20$

Rayleigh Damping:
$\alpha = 0.66$ $\beta = 0.0038$

$E_{din} = 1.25$ E $f_{cdin} = 1.5 \times f_c$ $f_{tdin} = 1.5 \times f_t$

Modal superposition: $N_{mod} = 2 \times 80$

Fig. 1: Luzzone dam (225 m high) and 3DFEM discretization (20 node cubic isoparametric elements of 2nd degree) used in DySSA7.0: MATLAB program developed at LNEC.

Equation for pressure waves propagation for the fluid

$$\nabla^2 \mathbf{p} - \frac{1}{c_p^2} = 0 \qquad \Omega_f$$

c_p Velocity of pressure waves propagation in water

Navier equation for the solid

$$\underline{L}^T \left(\mathbf{D}(\underline{L}\underline{u}) \right) + \underline{f} = \underline{0}$$

Total d.o.f.

$$N = N_u + N_p$$

Classical approach in displacements

$$\underline{m}\,\ddot{\underline{u}} + \underline{c}\,\dot{\underline{u}} + \underline{k}\,\underline{u} = \underline{f}$$

Approach using displacements and pressures

$$\underline{M}\,\ddot{\underline{q}} + \underline{C}\,\dot{\underline{q}} + \underline{K}\,\underline{q} = \underline{F}_{SF} \qquad , \qquad \underline{q} = \begin{bmatrix} \underline{u} \\ \underline{p} \end{bmatrix} \; (N \times 1)$$

$$\underbrace{\begin{bmatrix} \underline{m} & \underline{0} \\ m_w \underline{Q}^T & \underline{S} \end{bmatrix}}_{\underline{M} \; (2N \times 2N)} \begin{bmatrix} \ddot{\underline{u}} \\ \ddot{\underline{p}} \end{bmatrix} + \underbrace{\begin{bmatrix} \underline{c} & \underline{0} \\ \underline{0} & \underline{c}_R \end{bmatrix}}_{\underline{C} \; (2N \times 2N)} \begin{bmatrix} \dot{\underline{u}} \\ \dot{\underline{p}} \end{bmatrix} + \underbrace{\begin{bmatrix} \underline{k} & -\underline{Q} \\ \underline{0} & \underline{H} \end{bmatrix}}_{\underline{K} \; (2N \times 2N)} \begin{bmatrix} \underline{u} \\ \underline{p} \end{bmatrix} = \begin{bmatrix} \underline{F}_S \\ \underline{F}_F \end{bmatrix}$$

Interation matrix

Usually

$$\underline{F}_F = \underline{0}$$

[Zienkiewicz, Taylor & Zhu 2005]

This second order equation could be converted on a system of two first order equations considering velocity as a new variable $\underline{v} = \dot{\underline{q}}$. This corresponds to a **state formulation** based on displacements and pressures, and at the correspondent velocities and pressure derivatives. So, we can write

$$\underline{M}\,\ddot{\underline{q}} + \underline{C}\,\dot{\underline{q}} + \underline{K}\,\underline{q} = \underline{F}_{SF} \quad \Leftrightarrow \quad \begin{cases} \underline{M}\,\dot{\underline{v}} + \underline{C}\,\dot{\underline{q}} + \underline{K}\,\underline{q} = \underline{F}_{SF} \\ \dot{\underline{q}} = \underline{v} \end{cases} \quad \Leftrightarrow \quad \begin{cases} \underline{M}\,\dot{\underline{v}} + \underline{C}\,\dot{\underline{q}} + \underline{K}\,\underline{q} = \underline{F}_{SF} \\ \underline{M}^T \dot{\underline{q}} - \underline{M}^T \underline{v} = \underline{0} \end{cases}$$

Or, using two state matrices, we have a system of 2N differential equations of first order

$$\underbrace{\begin{bmatrix} \underline{C} & \underline{M} \\ \underline{M}^T & \underline{0} \end{bmatrix}}_{\substack{A \\ (2N \times 2N)}} \begin{bmatrix} \dot{\underline{q}} \\ \dot{\underline{v}} \end{bmatrix} + \underbrace{\begin{bmatrix} \underline{K} & \underline{0} \\ \underline{0} & -\underline{M}^T \end{bmatrix}}_{\substack{B \\ (2N \times 2N)}} \begin{bmatrix} \underline{q} \\ \underline{v} \end{bmatrix} = \underbrace{\begin{bmatrix} \underline{F}_{SF} \\ \underline{0} \end{bmatrix}}_{\substack{F \\ (2N \times 1)}}$$

That is, finally

$$\underline{A}\,\dot{\underline{x}} + \underline{B}\,\underline{x} = \underline{F} \qquad , \text{ being} \qquad \underline{x} = \underline{x}(t) = \begin{bmatrix} \underline{q} \\ \underline{v} \end{bmatrix} = \begin{bmatrix} \underline{u} \\ \underline{p} \\ \dot{\underline{u}} \\ \dot{\underline{p}} \end{bmatrix}$$

The solution of this system of first order differential equations is easly obtained using modal coordinates in order to obtain a diagonalized form

$$\underline{A}\,\dot{\underline{x}} + \underline{B}\,\underline{x} = \underline{F}$$

The diagonalization of this system is obtained by solving the correspondente eigenproblem:

$$\left[\underline{B} + \lambda\,\underline{A} \right] \underline{\phi} = \underline{0}$$

[eigVec, eigVal] = eig(B, −A)

The correspondent matrices of eigenvalues $\underline{\lambda}$ (diagonal) and eigenvectores $\underline{\phi}$ are complex.
(Note: In this case we have allways complex values for $\underline{\lambda}$ and $\underline{\phi}$, even if the Rayleigh hypothesis damping is used !)

Then, using the known transformation for modal coordinates $\underline{z}$ (complex values)

$$\underline{x} = \underline{\phi}\,\underline{z}$$

We can write

$$\underline{A}\,\underline{\phi}\,\dot{\underline{z}} + \underline{B}\,\underline{\phi}\,\underline{z} = \underline{F} \qquad \text{and} \qquad \underbrace{\overline{\underline{\phi}}^T \underline{A}\,\underline{\phi}}_{\mathcal{A}} \dot{\underline{z}} + \underbrace{\overline{\underline{\phi}}^T \underline{B}\,\underline{\phi}}_{\mathcal{B}} \underline{z} = \underbrace{\overline{\underline{\phi}}^T \underline{F}}_{\tilde{F}}$$

Obtaining, then, the required diagonal system

$$\mathcal{A}\,\dot{\underline{z}} + \mathcal{B}\,\underline{z} = \tilde{F} \quad \underset{\times\,\mathcal{A}^{-1}}{\Leftrightarrow} \quad \dot{\underline{z}} - \underbrace{\underline{\lambda}}_{-\mathcal{A}^{-1}\mathcal{B}} \underline{z} = \underbrace{\mathcal{A}^{-1}\tilde{F}}_{\tilde{F}} \qquad , \; \tilde{F} = \mathcal{A}^{-1}\tilde{F} = \mathcal{A}^{-1}\overline{\underline{\phi}}^T F$$

Wich corresponds to a system of 2N independent ordinary diferencial equations of first order:

$$\dot{z}_n - \lambda_n\,z_n = F_n \quad , \; n = 1 \text{ to } 2 \times N$$

Recursive formula for time integration

$$z_n(t_{i+1}) = e^{\lambda_n \Delta t}\,z_n(t_i) + \frac{1}{\lambda_n}\left(e^{\lambda_n \Delta t} - 1 \right) F_n(t_i) \qquad , \; n = 1 \text{ to } 2 \times N$$

and finally

$$\underline{x} = \underline{\phi}\,\underline{z} \qquad \text{Note: a reduced number of modes } (N_{mod} \ll N) \text{ can be used}$$

Fig. 2: Formulation used in DySSA7.0. Water-structure interaction is simulated using a coupled formulation in displacements and pressures and a modal state approach.

Numerical Results

Static Response

The maximum principal stresses for the combination SW+HSP+SP (Fig.3) are of about 10.6 MPa for compression and 4.2 MPa for tension. The maximum displacement is 134.2 mm at the top of the central cantilever. For the combination SW+HSP+SP+ΔTsummer the maximum compression is 11.3 MPa and the maximum tension is 2.8 MPa (Fig.4).

The computed principal stresses (maximum, S1, and minimum, S3) for the main static load combinations are presented at table 1. By comparing the presented results it can be noted that the summer thermal gradient causes a state of stress mainly of compression. Thus the obtained results for the static load combination SU2 demonstrate that the tension values tend to decrease, while the compression values increase.
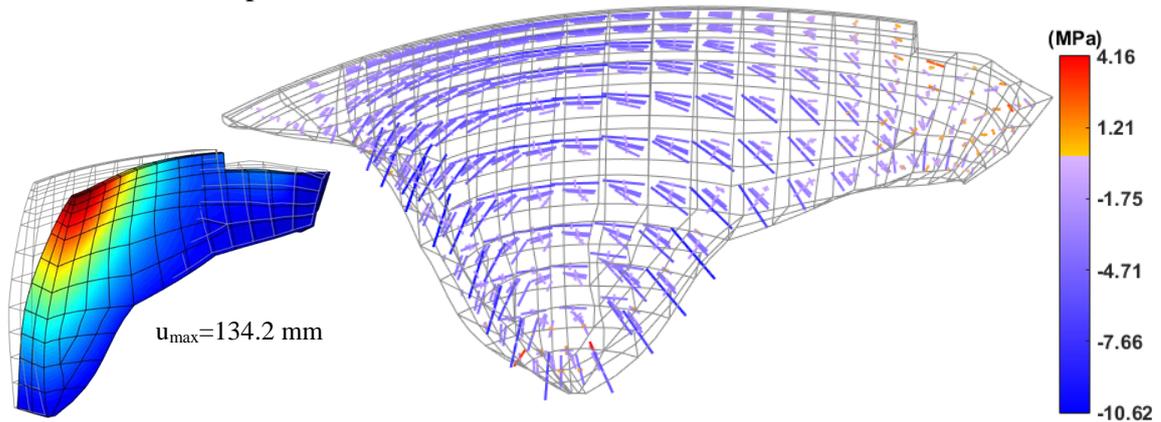
Fig. 3: SU0 (SW+HSP+SP) – Displacements and stresses.
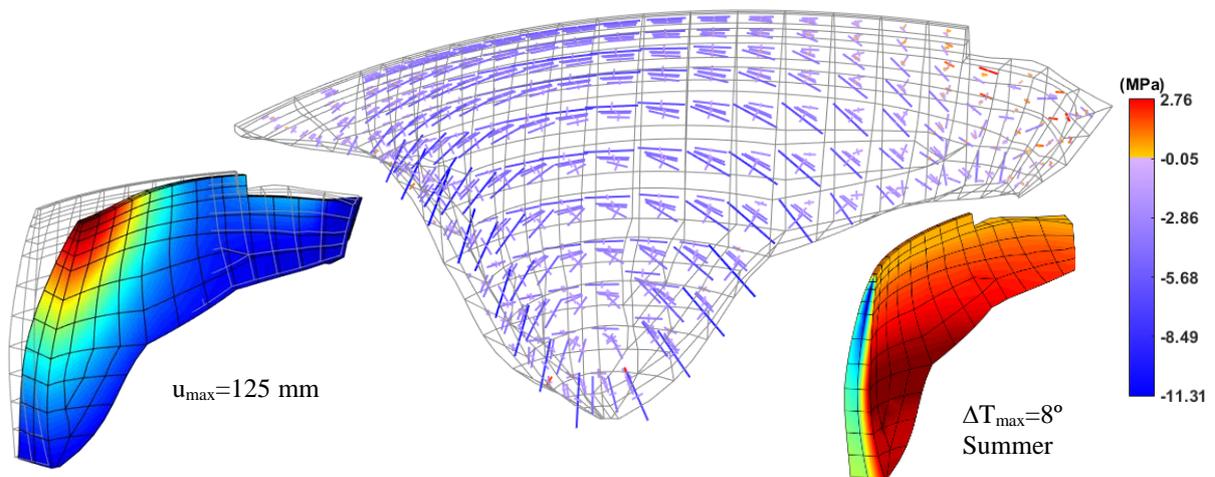
Fig. 4: SU2 (SW+HSP+SP+ΔT$_{summer}$) – Displacements, stresses and thermal gradient.

Dynamic Response

Mode shapes and natural frequencies for full reservoir (and empty) are presented in Fig.5. As usual the 1st vibration mode is symmetric and the 2nd is anti-symmetric. In Fig.6 is presented the dam seismic response for the load combination SW+HSP+SP+ΔT$_{summer}$+MCE1(0.16g). Envelopes of displacements and stresses, and principal stresses at the two main time steps are presented (upstream and downstream positions). The maximum compression hoop stress, ~17.5 MPa, occurs at the crown cantilever (downstream face), at the elevation 1580 m. The maximum tension cantilever stress, ~4.5 MPa, occurs at the crown cantilever, near the insertion.

Tab. 1: Static load combinations. Max. and min. principal stresses (MPa) at selected points

	Point	SW		HSP		SP		ΔTs		SU0 (SW+HSP+SP)		SU2 (SW+HSP+SP+ΔTs)	
		S1	S3	S1	S3	S1	S3	S1	S3	S1	S3	S1	S3
UPSTREAM FACE	A	0.647	-0.032	-0.006	-3.053	0.00090	-0.00005	-0.010	-0.390	-0.008	-2.414	-0.019	-2.803
	B	-0.002	-1.062	-0.021	-4.684	0.00243	-0.00002	-0.015	-0.339	-0.025	-5.743	-0.040	-6.082
	C	0.146	-0.027	-0.006	-3.891	0.00023	-0.00026	-0.015	-0.644	-0.011	-3.745	-0.026	-4.390
	D	0.412	-0.276	-0.470	-6.401	0.00138	-0.00016	0.027	-0.369	-0.473	-6.011	-0.446	-6.026
	E	0.125	-0.396	-0.467	-6.316	0.00180	-0.00048	0.025	-0.478	-0.471	-6.280	-0.445	-6.358
	F	-0.007	-1.903	0.704	-0.792	0.00000	-0.00130	-0.167	-0.723	-0.324	-1.736	-0.501	-2.415
	G	0.695	-2.174	2.986	-0.800	0.00171	-0.00265	0.023	-0.610	0.818	-0.472	0.596	-0.701
	H	-0.604	-6.440	8.578	0.908	0.00451	-0.00258	0.078	-0.739	2.684	-0.506	2.355	-0.616
	I	0.641	-4.341	5.441	-0.391	0.00430	-0.00246	0.110	-0.897	2.131	-0.690	1.586	-0.856
	J	-0.011	-3.000	3.050	-3.358	-0.11669	-0.17238	0.120	-0.370	-0.072	-3.542	-0.426	-3.437
DOWNSTREAM FACE	A	0.484	-0.046	0.019	-3.097	0.00042	-0.00004	-0.041	-0.129	0.003	-2.638	-0.042	-2.761
	B	-0.002	-0.951	0.013	-3.138	0.00405	-0.00002	-0.028	-0.123	-0.012	-4.084	-0.046	-4.207
	C	0.032	-0.070	0.021	-4.249	0.00001	-0.00045	-0.033	-0.388	-0.006	-4.259	-0.055	-4.646
	D	0.030	-1.510	0.749	-3.113	0.00280	-0.00188	-0.032	-1.002	-0.012	-3.644	-0.045	-4.554
	E	0.035	-1.049	0.528	-3.372	0.00208	-0.00228	-0.016	-0.988	-0.007	-3.628	-0.023	-4.555
	F	0.800	0.071	0.834	-4.549	0.00114	-0.00239	0.484	-0.817	1.093	-3.784	0.755	-4.338
	G	1.485	-1.097	-0.072	-9.435	0.00071	-0.00442	0.088	-1.582	-0.032	-8.682	0.056	-9.402
	H	1.138	-1.127	-0.914	-11.713	0.00247	-0.01949	-0.134	-1.890	-0.776	-11.353	-1.145	-12.246
	I	1.422	-0.891	-0.192	-9.993	0.00062	-0.02555	-0.170	-1.930	-0.087	-9.393	-0.354	-10.780
	J	-0.041	-1.513	1.795	-1.550	0.05867	-0.00151	-0.068	-2.344	1.251	-2.942	-0.145	-3.907
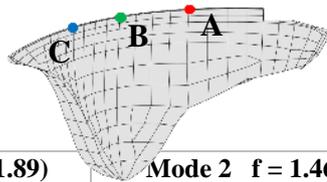
For each mode, the waves representing the oscillatory movement at points A, B and C show that the computed vibration modes are non-stationary (as is measured in some large arch dams [2])
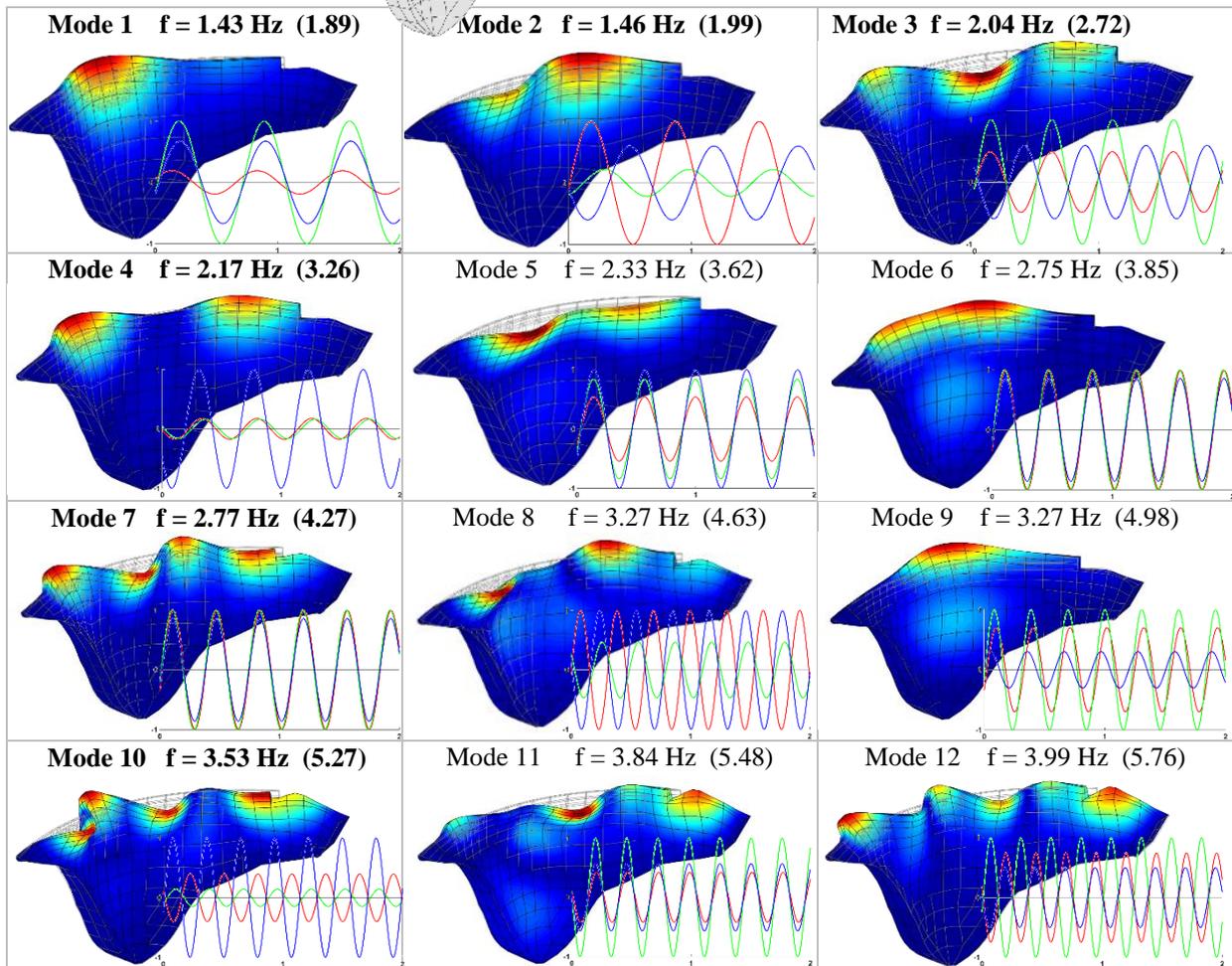
Fig. 5: Mode shapes and natural frequencies for reservoir (and natural freq. for empty)

DE2: SU2 + MCE (Series1. λ=1)
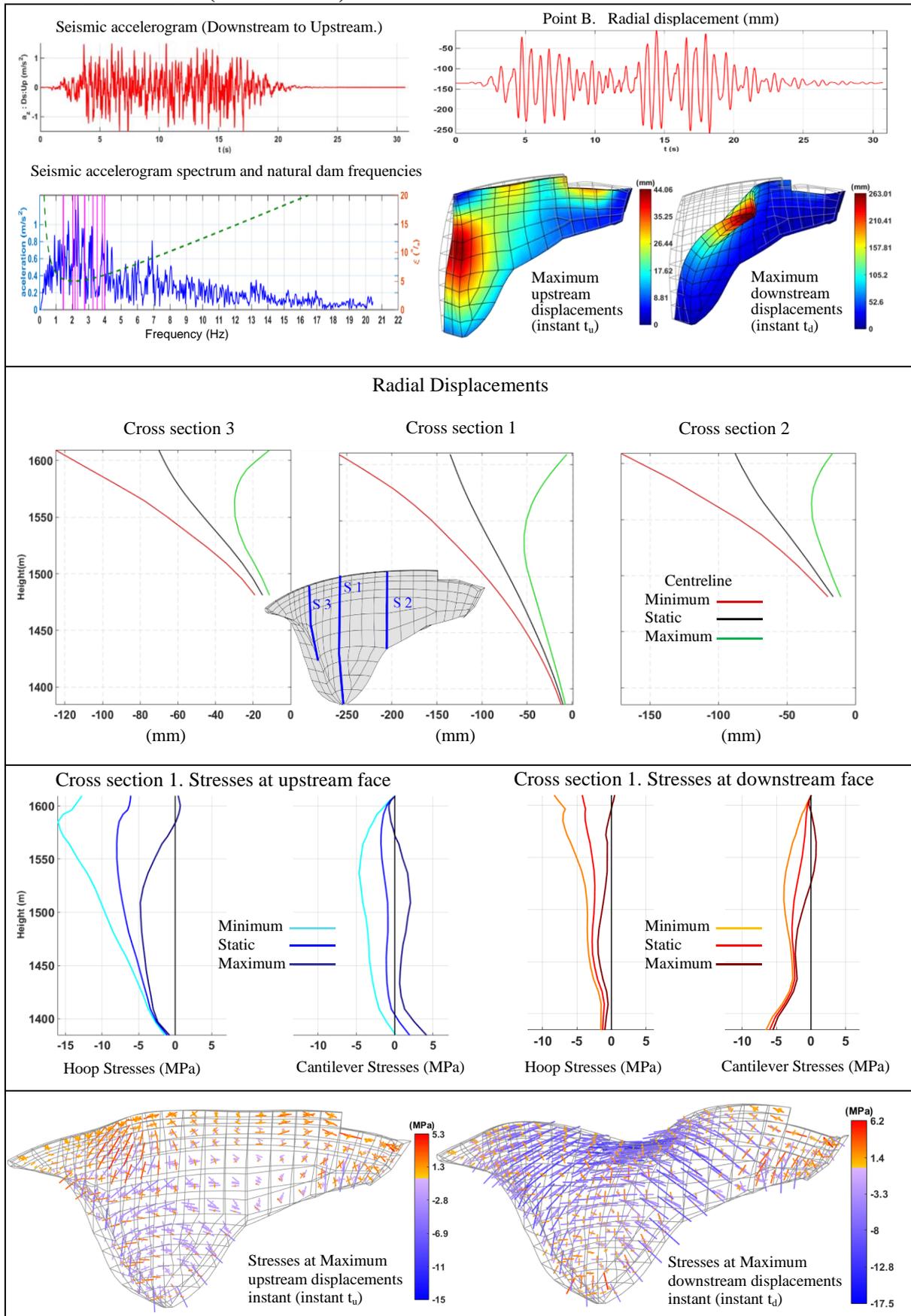
Fig. 6: Seismic response for the load combination SU2+MCE1 considering accelerograms of series1. Envelopes of displacements and stresses, and principal stresses at instants t_u and t_d.

DE2: SU2 + MCE (Series 2. λ=1)
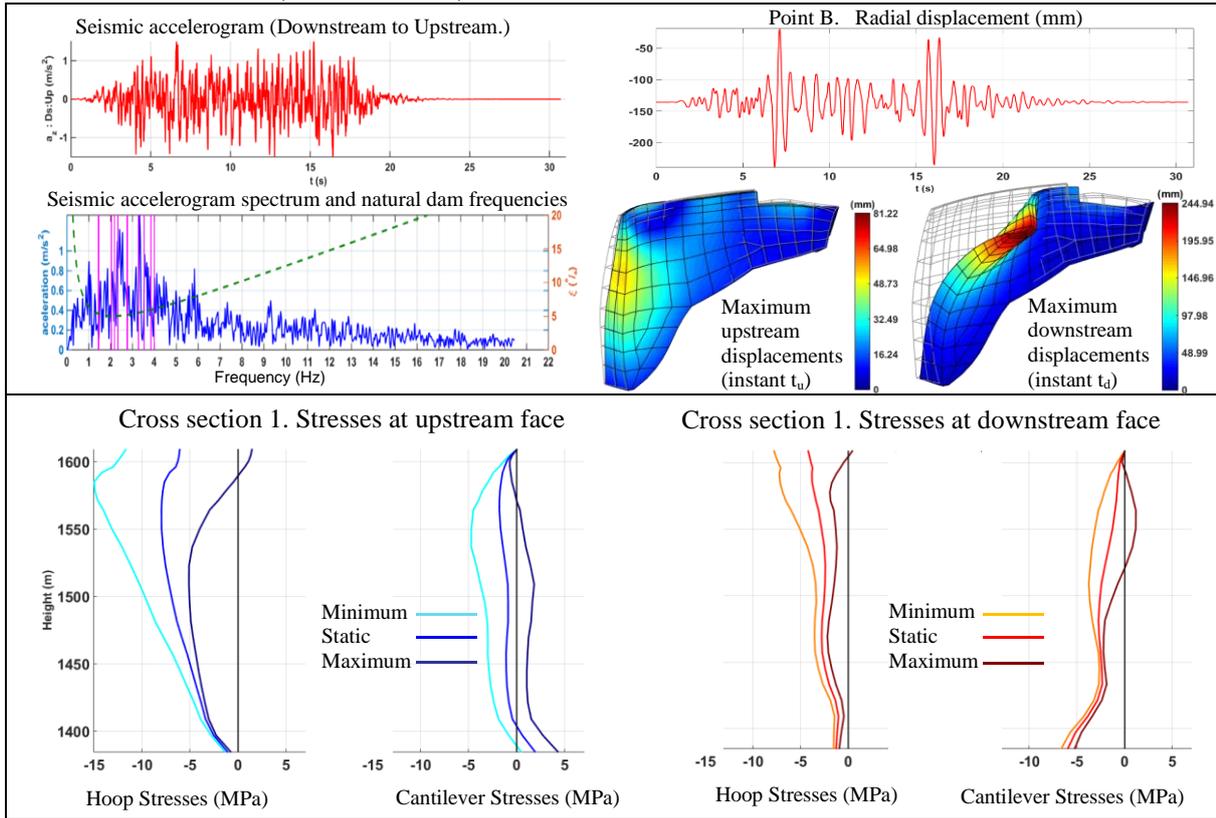
DE2: SU2 + MCE (Series 3. λ=1)
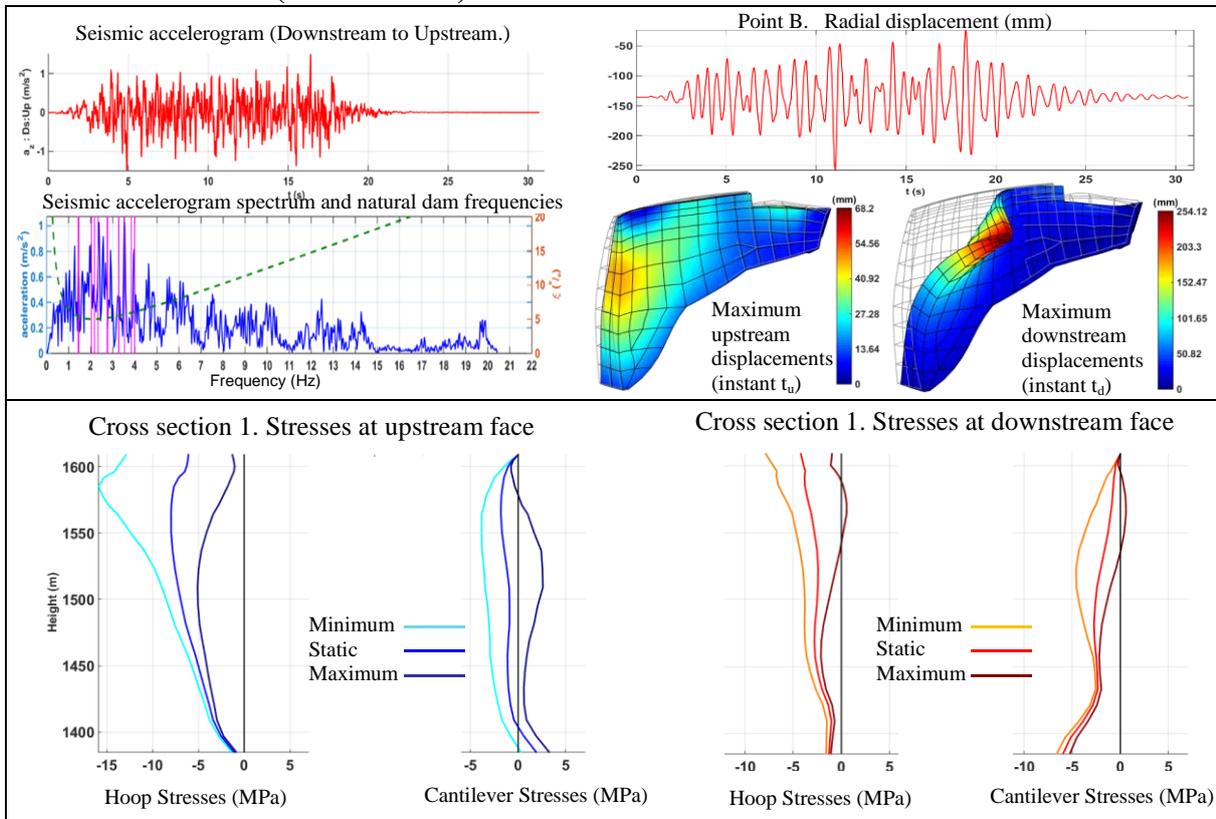
Fig. 7: Seismic response for the load combination SU2+MCE2 (a) and SU2+MCE3 (b) considering accelerograms of series 2 and 3. Envelopes of displacements and stresses, and principal stresses at the two main time steps.

Tab. 2: Dynamic combinations. Max. and min. principal stresses(MPa) at selected points

Face	Point	SU2+MCE1 Series 1		SU2+MCE2 Series 2		SU2+MCE3 Series 3	
		S1	S3	S1	S3	S1	S3
UPSTREAM FACE	A	1.470	-7.613	1.070	-5.670	0.883	-6.618
	B	0.806	-12.822	1.699	-11.705	0.461	-12.863
	C	0.021	-6.847	0.007	-6.874	0.016	-7.496
	D	1.699	-11.351	1.695	-10.976	1.345	-10.706
	E	0.946	-11.411	0.382	-9.380	1.387	-10.155
	F	1.014	-5.037	1.023	-5.021	2.074	-4.346
	G	6.526	-7.500	6.195	-6.173	6.600	-5.664
	H	6.564	-3.015	7.527	-2.643	5.343	-2.632
	I	4.354	-2.118	4.197	-1.998	4.034	-2.764
	J	1.586	-3.841	1.532	-3.952	0.894	-3.838
DOWNSTREAM FACE	A	0.779	-6.623	0.802	-6.575	0.361	-5.347
	B	0.941	-8.201	0.726	-7.813	0.186	-7.832
	C	0.134	-9.578	0.467	-8.844	0.023	-8.952
	D	1.891	-7.457	1.279	-7.631	1.919	-8.433
	E	1.845	-10.748	3.068	-9.928	1.215	-10.160
	F	3.040	-8.408	2.641	-7.430	2.659	-8.154
	G	0.243	-15.067	0.186	-13.567	0.175	-14.316
	H	-0.741	-16.381	-0.860	-17.138	-0.833	-15.856
	I	-0.215	-15.231	-0.234	-13.596	-0.201	-13.095
	J	-0.120	-4.366	-0.128	-4.342	-0.129	-4.363

Seismic Safety

Concerning the seismic safety evaluation, the presented results concern the load combination using MCE1-Series 1, knowing that, for this dam, this is the most severe seismic accelerogram (all three time-histories were analyzed).

Safety in order to material local failure (Seismic accelerogram: series 1)

For the analysis of the local stability, a rupture index (I_R) that indicates the "distance to failure", was calculated for each point of the dam body, using the Mohr-Coulomb and Rankine criteria. This index varies between 0 and 100% (failure). In Fig. 8 the computed values of this failure index are presented: the green colors represent the areas with acceptable values according the Portuguese guidelines (less than 40%) and the orange/red represent the areas with no acceptable values (states of stress that do not meet the Portuguese guidelines requirements).

a) $\lambda = 1$, $a_{peak} = 0.16g$ (1.57 m/s^2)
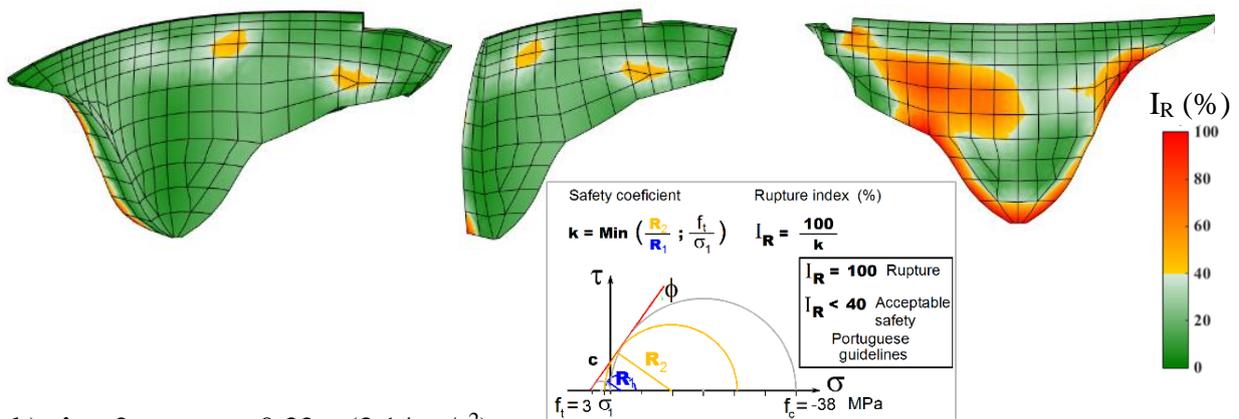
b) $\lambda = 2$, $a_{peak} = 0.32g$ (3.14 m/s^2)
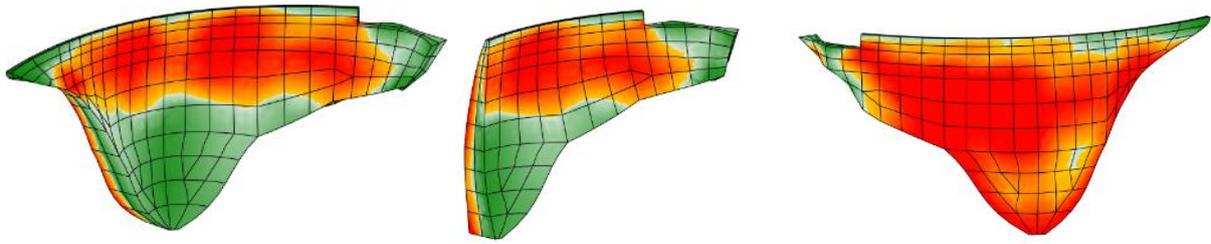
Fig. 8: Local failure safety. Representation of the rupture index (I_R)

Global Stability (Seismic accelerogram: series 1)

The global stability is verified on four dam blocks of the crown cantilever. The sliding and overturning are calculated in the time-domain by comparing the resistant and acting radial forces and the stabilizing and overturning moment for each time-step. In table 3 are presented the safety factors calculated when the maximum block acceleration (to upstream) occurs. The minimum safety factors are obtained for block 1. In addition the safety factors are computed along the earthquake duration as shown in Fig.9 (time-domain analysis) and are generally greater than 1.2 both for sliding and overturning (as required by Portuguese guidelines).

Tab. 3: Rocking block stability analysis results

Acting Force [kN]	Rocking Block. SU2 + MCE Series 1			
	Block 1. H=8.5 m	Block 2. H=17 m	Block 3. H=30.8 m	Block 4. H=44.6 m
SW	25178.86	62474.34	148287.85	256379.74
Wh	7772.64	31344.77	104105.03	220300.77
Wv	3242.70	12387.01	35858.46	66330.16
Hdyn.h (t)	10813.83	32511.92	67910.36	92992.66
Hdyn.v (t)	4507.69	12982.21	24578.41	31260.46
SP	6533.66	17868.06	43643.72	76086.25
Qh (t)	37307.29	81682.41	154410.08	210887.83
Qv (t)	4505.705	8791.18	13152.52	13478.96
S.F. Sliding	$SF_{t.amax} = 1.41$ $SF_{min} = 1.38$	$SF_{t.amax} = 3.01$ $SF_{min} = 2.96$	$SF_{t.amax} = 20.5$ $SF_{min} = 15.0$	$SF_{t.amax} = 30.0$ $SF_{min} = 20.0$
S.F. Overturning	$SF_{t.amax} = 0.96$ $SF_{min} = 0.87$	$SF_{t.amax} = 0.996$ $SF_{min} = 0.89$	$SF_{t.amax} = 1.13$ $SF_{min} = 1.09$	$SF_{t.amax} = 1.19$ $SF_{min} = 1.09$
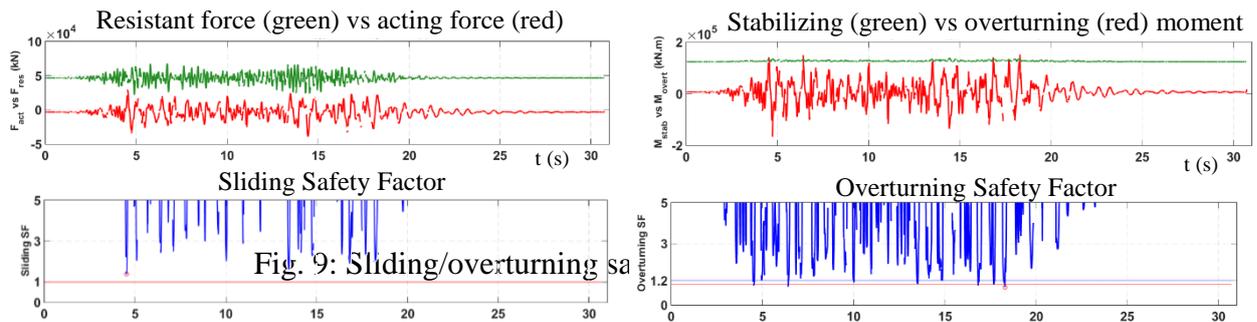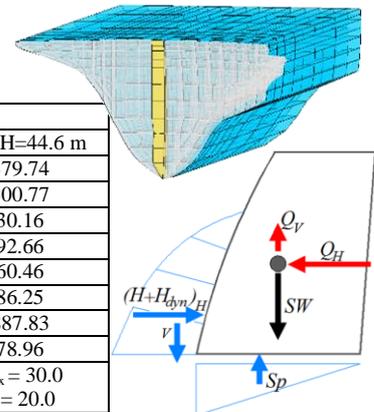
Fig. 9: Sliding/overturning safety factors

Conclusion

For the peak ground acceleration of 0.16g the local safety to concrete failure is verified: the computed values of the failure index are generally less than 40% (it is acceptable that in some localized areas near the dam surfaces the values of this index are greater than 40%). For a peak acceleration of 0.32g (magnification factor λ=2) the local safety is not verified in a significant volume of the dam body (values of the failure index greater than 40% are attained not only near the dam surfaces but also inside the dam body).

Regarding the safety of blocks against sliding and overturning, it can be observed that the global safety is verified for the peak acceleration of 0.16g. The calculated safety factors during the earthquake are generally greater than 1.2, as required by Portuguese guidelines. Values less than 1.2 only occur during very short time intervals (in some cases it occurs only during 0.01s).

Analyzing the presented results, it can be concluded that the seismic safety is verified.

References

[1] Zienkiewicz O.C., Taylor R.L. and Zhu.J.Z. (2005). The Finite Element Method: Its Basis and Fundamentals: Sixth ed., Elsevier Butterworth-Heinemann.
[2] Oliveira,S., Espada, M. and Câmara,R. (2012) Long term dynamic monitoring of arch dams. The case of Cabril dam, Portugal, Lisboa: 15 WCEE, 2012.

Seismic safety evaluation of an arch dam with Akantu FE code developed at EPFL

M. Corrado[1], G. Anciaux[1], D. Scantamburlo[1], S. Laffely[1], M. Chambart[2], T. Menouillard[2] and J.-F. Molinari[1]

[1]*LSMS, EPFL, CH-1025 Lausanne, Switzerland*
[2]*Stucky SA, Rue du Lac 33, CH-1020 Renens, Switzerland*

ABSTRACT: This paper explains the application of an open source Finite Element code Akantu developed at EPFL-LSMS for the evaluation of seismic safety of an arch for the "12th ICOLD International Benchmark on Numerical Analysis of Dams". The benchmark was a good opportunity for developing efficient collaboration between a university lab and an engineering consulting company. Therefore, the development of the code focused on the different goals of the numerical analysis of an arch dam. Specific load of hydrodynamic pressure for such an analysis should have been implemented. The strategy for the seismic evaluation follows the SFOE (Swiss Federal Office of Energy) guidelines.

E-mail: jean-francois.molinari@epfl.ch

Introduction

This document explains the study performed at LSMS-EPFL for the "12th ICOLD International Benchmark Workshop on Numerical Analysis of Dams". This work was done in collaboration between a lab at university and an engineering consulting company: LSMS-EPFL and Stucky SA. The development of a free opensource Finite Element [2] software named Akantu [3, 4] (http://lsms.epfl.ch/akantu) provided the opportunity for both parts to take advantage of such a collaboration.

As an engineering company, Stucky brings its expertise of seismic evaluation of arch dams. The SFOE asked all the dams operator to lead a seismic safety evaluation of their dams before March 2013. Stucky took a large part of it, being mandated to lead the evaluation for about 40 of the 206 dams and dykes in Switzerland. The finite elements modelings, when required, were done with either Diana or Zsoil. Difficulties were encountered when new features or development were required, having no access to the source code.

Therefore, a collaboration with an university laboratory is a good opportunity for an engineering company to reconsider its practices, confront them with the latest developments and imagine new possibilities. Furthermore, it gave Stucky access to a very efficient opensource finite-element software. This is also a good opportunity for the university lab to find applications for their research.

For this benchmark, the SFOE guidelines were applied for seismic evaluation. It aimed at making feasible that kind of modeling, having all the necessary and specific tools ready for the future.

This bridge demonstrated the possibility to apply research work at a university level. The paper presents the modeling strategy and hypothesis, the results and finally the concluding remarks.

Model

Geometry

The geometry of the Luzzone dam, built in 1963, is briefly presented in Fig. 1. It deals with an arch dam, whose height hits 225 m and its length 600 m. It makes it a class A dam according to the SFOE guidelines. The figure also presents the three vertical sections where the results are to be extracted.
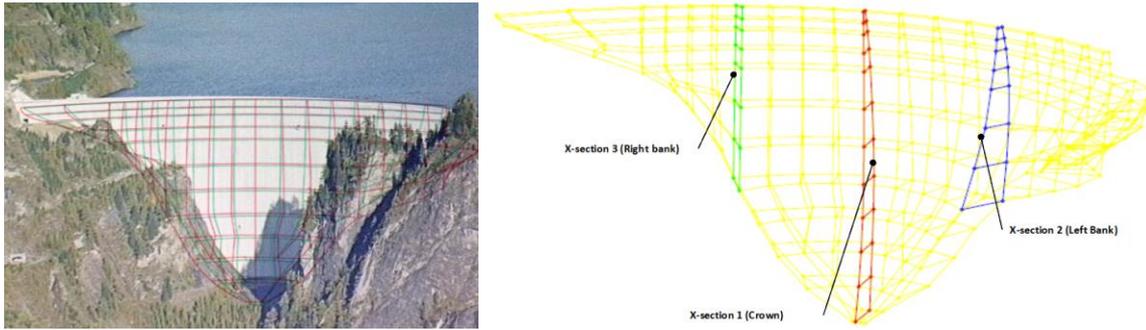
Fig. 1: Cross sections locations and definitions.

Materials

The materials model used in the presented analysis are linear elastic for the foundation and the concrete. At first the linear elastic models are sufficient in order to check whether the stresses reach the strength of the concrete, before nonlinear materials models could be used.

Tab. 1: Material properties of old and new concrete.

Properties	Values
Density	2.5 and 2.4 t/m^3
Static Young's modulus	20 and 18 GPa
Dynamic Young's modulus	25 and 22.5 GPa
Poisson ratio	0.18
Coefficient of thermal expansion	10^{-5}/°C
Static compressive strength	38 and 32 MPa
Dynamic compressive strength	57 and 48 MPa
Static tensile strength	3 and 2.3 MPa
Dynamic tensile strength	4 and 3.5 MPa

Loadings

As static loads remain the self-weight and the hydrostatic and the silt pressure. They are all computed through their densities. Construction stages are taken into account in the self-weight loading effect. Hydrostatic and silt pressures are only modeled by an surface force on the upstream face of the dam.

The acceleration of the ground is the main dynamic load for the case of an Earthquake acting on a dam. Then, the hydrodynamic pressure of the water on the upstream face of the dam must be taken into account, where different models are available. That dynamic effect modeling was the subject of the previous Benchmark on numerical analysis of dams in 2013 [7]. Chambart et al. [6] chose to model this action with added masses coming from Westergaard theory [5]. This modeling is recommended by the SFOE guidelines. As demonstrated in [7], the Westergaard theory, in comparison with other explicit fluid structure interaction techniques, leads to slightly overestimate the water dynamic effect. On a safety evaluation point of view, the Westergaard theory remains on the safe side. In this current paper, this theory is used again to model the hydrodynamic pressure of the reservoir on the upstream face of the dam. Finally, the damping is taken into account with the Rayleigh coefficients chosen from the knowledge of the eigenmodes and the participating masses. No dynamic effect is taken into account for the silt pressure. Discussions exist about considering it or not. If the silt and dense and compact, we can assume that in case of an earthquake, they act on the dam as an additional dynamic force. Otherwise, the silt is most likely going to dilute in the water under the effect of the moving

water, creating no extra forces. In this case, given the height of silt level compared to the water level, together with the silt density, our modeling choice is reasonable.

Thermal loading is also considered. The presented results are the displacements and stresses computed for summer. The summer temperature field is obtained after a thermal transient analysis. It is assumed that the upstream and downstream temperature fields follow a sinusoidal variation between the 2 fields on the upstream and downstream faces of the dam during a year. The transient analysis is carried over 3 years in order to have a stabilized temperature field at the center of the dam. As the temperature for each node was given in this benchmark, it was not required to compute the temperature field. However it has been computed with Akantu, as such a tool is already available.

Results

Eigenmodes

In order to estimate the dynamic behavior of a structure, the first step consists in determining the eigenfrequencies, the eigenmodes and the participating masses of the structure. Tab. 2 presents the results of the first 12 modes for empty and full reservoir. The difference lies in the hydrodynamic pressure modeled as added masses acting normally to the upstream face of the dam for the full reservoir. Fig. 2, respectively Fig. 3, presents the first eigenmodes for the empty reservoir, respectively full reservoir.

Tab. 2: Eigenmodes analysis.

Mode	Empty Reservoir				Full Reservoir			
	Eigenfrequency	Effective Mass Percentage			Eigenfrequency	Effective Mass Percentage		
	f, Hz	X, %	Y, %	Z, %	f, Hz	X, %	Y, %	Z, %
1	1.988	8.16	0.03	0.19	1.179	0.28	0.18	24.05
2	2.087	0.27	0.92	23.88	1.258	3.33	0.10	3.19
3	3.003	0.05	0.69	7.09	1.902	0.16	0.29	8.41
4	3.763	0.05	8.98	14.37	2.235	0.00	0.94	20.66
5	3.944	0.26	0.28	0.86	2.519	0.53	0.00	0.10
6	4.439	28.88	0.01	0.15	2.859	7.17	0.02	0.00
7	4.959	0.09	1.86	2.10	3.224	0.08	0.00	1.52
8	5.184	1.18	55.13	1.44	3.410	0.01	0.14	8.61
9	5.800	26.65	1.61	0.85	3.806	0.09	1.71	5.88
10	5.923	5.36	0.52	2.83	3.976	0.01	0.01	0.03
11	6.071	0.10	0.03	0.01	4.298	36.75	0.23	0.07
12	6.266	1.25	1.18	13.89	4.422	21.00	0.76	0.41
	Σ	72.32	71.24	67.68	Σ	69.41	4.39	72.92
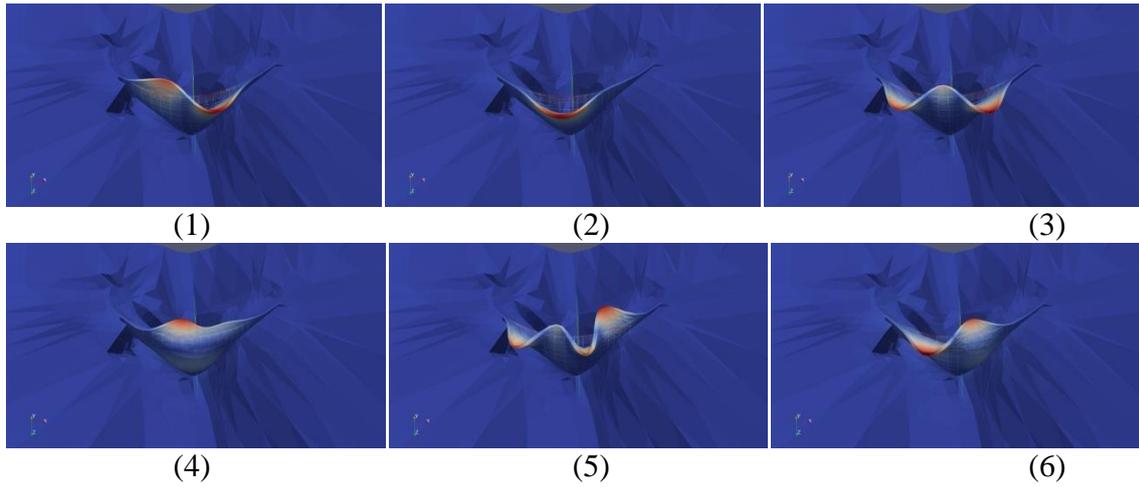
Fig. 2: Eigenmodes for empty reservoir.
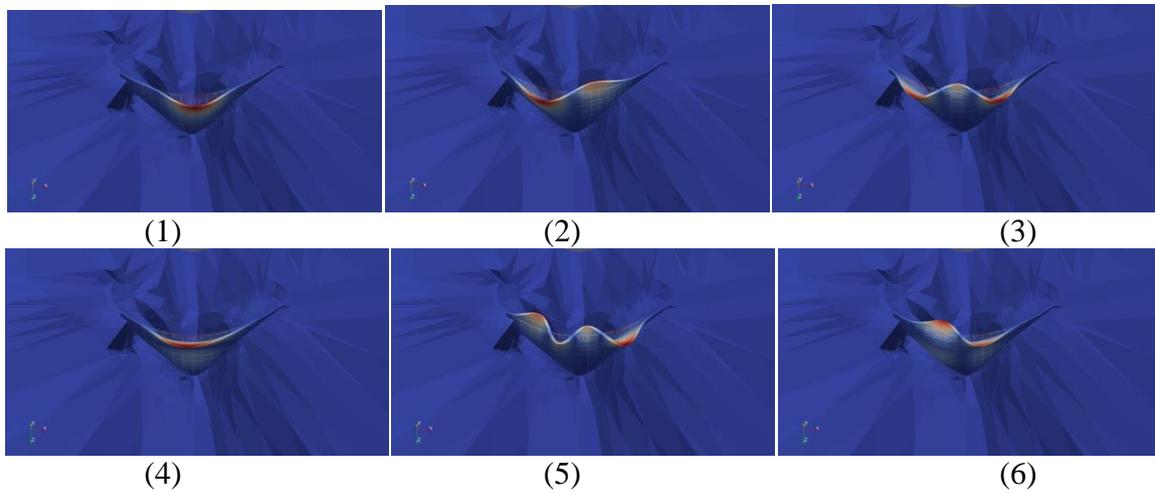
Fig. 3: Eigenmodes for full reservoir with Westergaard hydrodynamic pressure.

Displacements

Fig. 4 presents the time evolution of the radial displacement at the crest of the central section of the dam. The figure shown presents the result for one ground acceleration, but the analysis has been carried out with the 3 acceleration time histories provided. The maximum displacement obtained is around 9 cm, which is in the order of magnitude expected.

Figures 5 and 6 present the maximum, minimum and static radial and vertical displacements at two different sections (middle and side). The characteristic profile for summer case can be recognized. The maximum displacement obtained at the middle is about 17.5 cm on the radial direction and 2.8 cm on the vertical direction. These results are consistent with other similar cases studied.
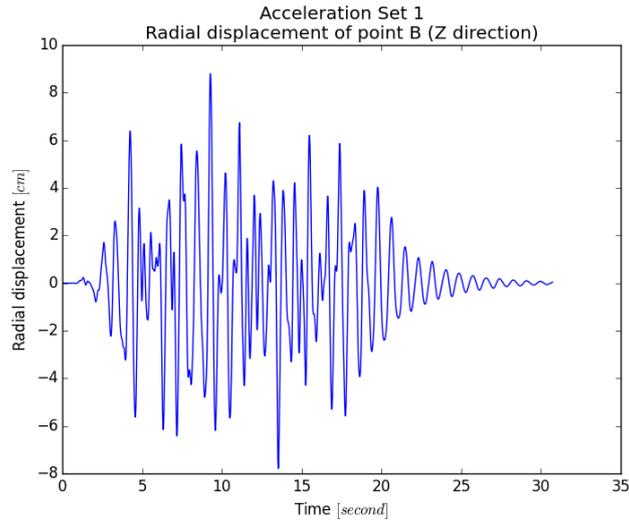
Fig. 4: Radial displacement of top crest point of the arch dam during Earthquake 1.
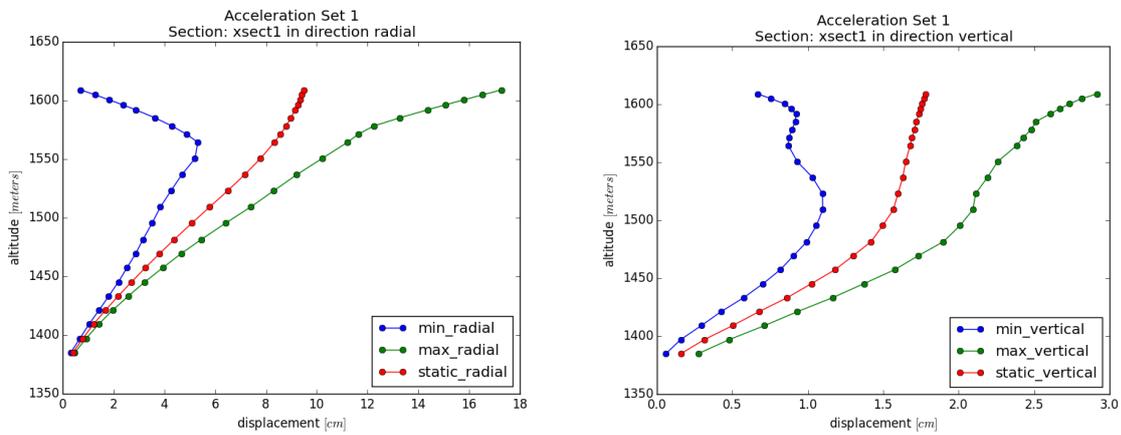
Fig. 5: Radial and vertical displacement envelopes at the mid section for Earthquake 1.
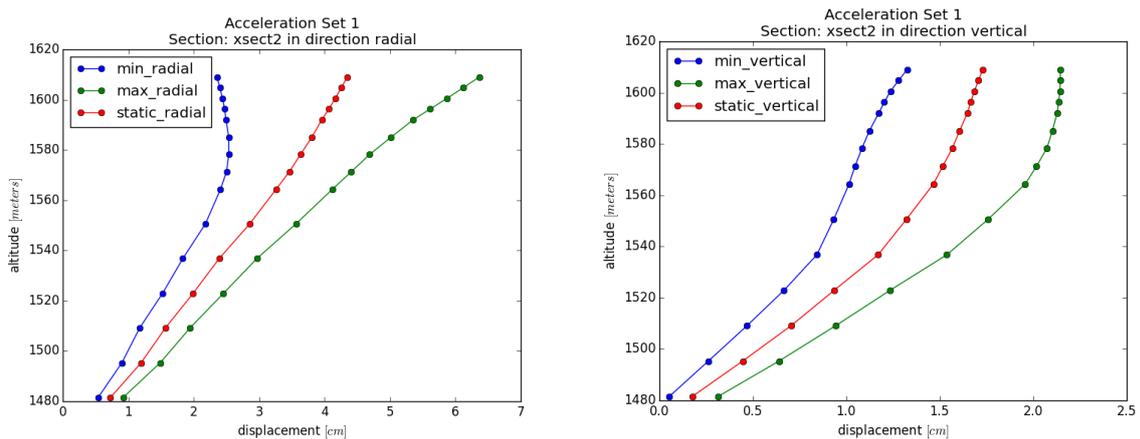
Fig. 6: Radial and vertical displacement envelopes at the side section for Earthquake 1.

Stresses

Fig. 7 and 8 present isovalues envelops maps of the principal stresses for the upstream and downstream faces. As usual, the maximum tensile forces are encountered near the crest and on the side. The values on the crest stay lower than 3 MPa, which mean that they remain within the safe limit given by the SFOE guidelines. The dynamic tensile strength is 3.5-4 MPa.

One should not pay too much attention to the values on the side, because tensile forces there mean that the dam apply a tensile force to the ground, which is, in reality not possible because there is no rigid interaction between the dam and the ground. To avoid this, the solution would be to create in interface between the soil and the concrete that is rigid in compression and free (or almost free in tension). Numerical solutions, such as cohesive elements exist, and are implemented in Akantu [8, 9].

In compression, the maximum stress obtained is 11.7 MPa, so once again in the safe limits given by SFOE. The dynamic compressive strength is 48-57 MPa.
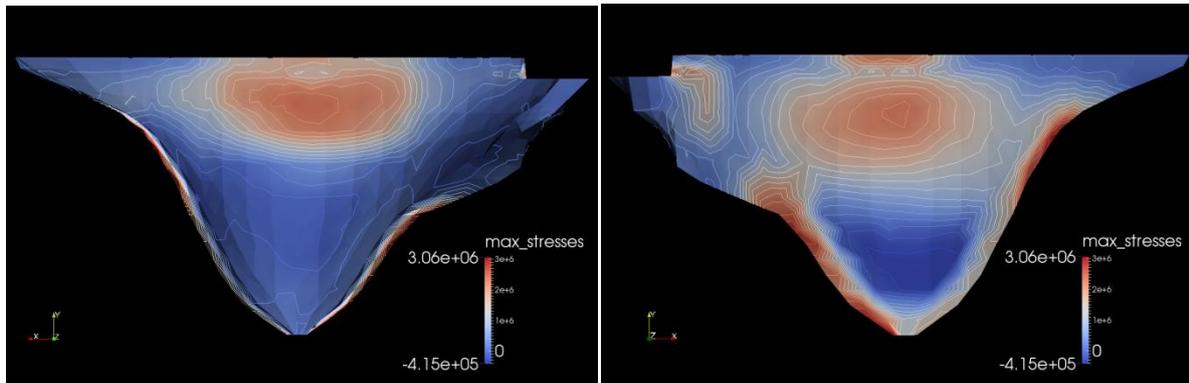
Fig. 7: Max principal stress on the upstream and downstream face of the dam for Earthquake 1.
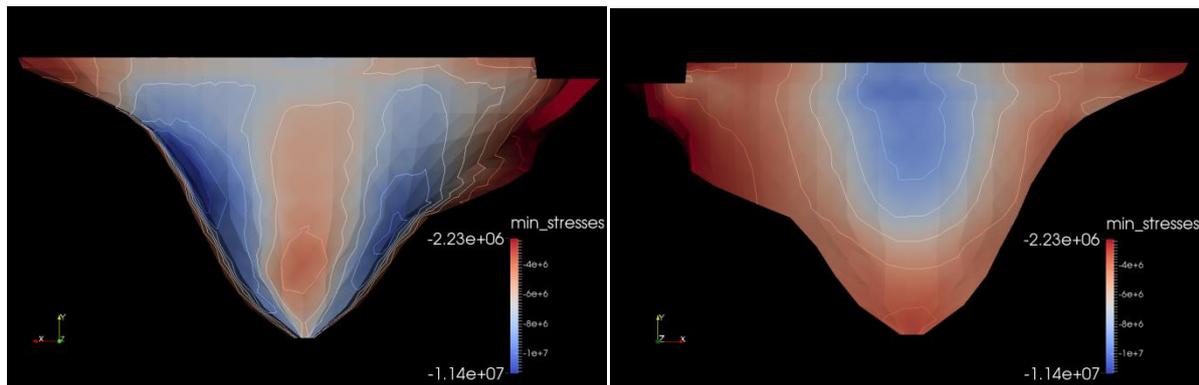
Fig. 8: Min principal stress on the upstream and downstream face of the dam for Earthquake 1.

The following figures (9, 10 and 11) present different stresses at different section. One of the interests of this benchmark is to compare these results with the ones obtained by the other researchers in order to validate the modeling and hypothesis.
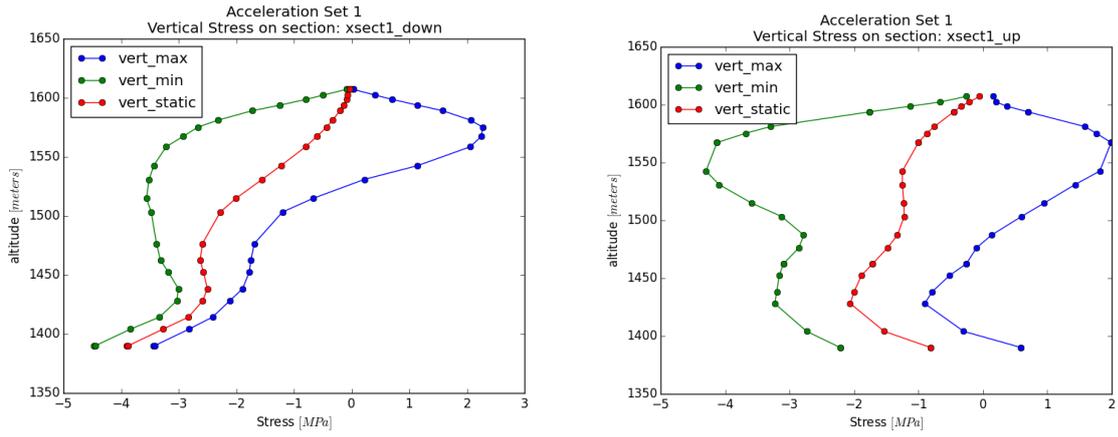
Fig. 9: Vertical stress envelopes on the downstream and upstream side of the mid section for Earthquake 1.
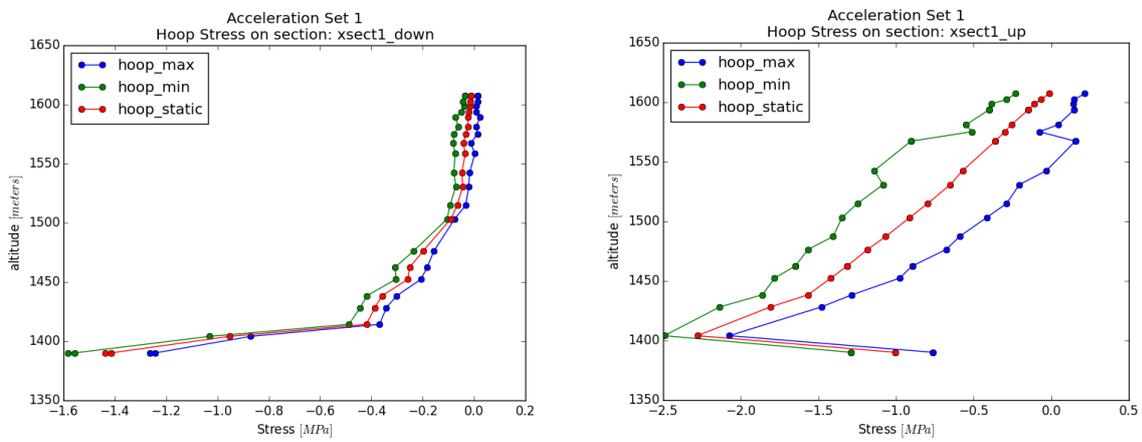
Fig. 10: Hoop stress envelopes on the downstream and upstream side of the mid section for Earthquake 1.
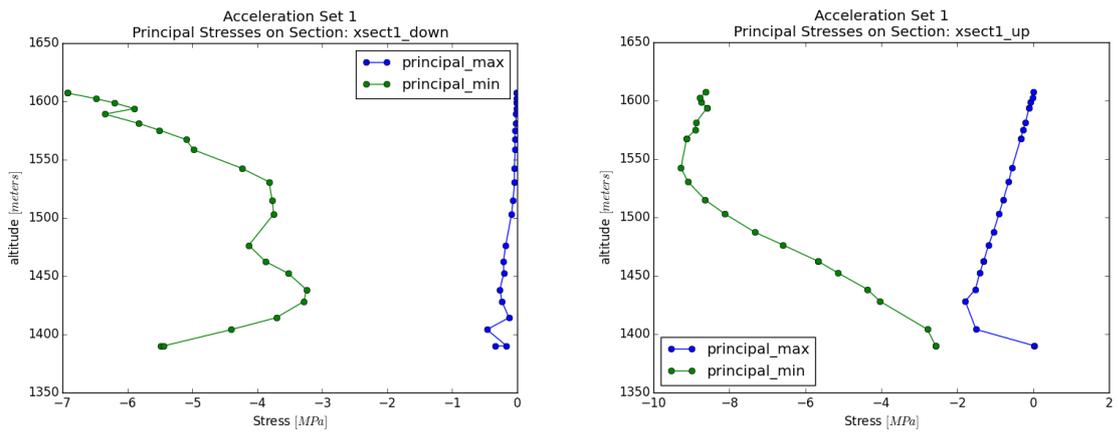
Fig. 11: Principal stress envelopes on the downstream and upstream side of the mid-section for Earthquake 1.

Conclusion

The safety of the considered arch dam is ensured according to the SFOE guidelines since no significant damage of the concrete can lead to an uncontrolled flow of water through the dam, and no instability of block is relevant.

This study was a good opportunity to develop and adapt a FE code from the university to the application field of civil engineering. The different challenges were the application of special loadings required for this analysis (construction by stages, thermal transient analysis) and the routines needed to extract the results (max /min over time and space). The Westergaard approach has been specially implemented for this kind of computation. In terms of future developments, the authors plan to assess the soil-structure interaction and the modeling of the construction joints with cohesive elements.

References

[1] Sécurité des ouvrages d'accumulation – Documentation de base pour la vérification des ouvrages d'accumulation aux séismes, rapports de l'OFEG, série Eaux, version 1.2, mars 2003

[2] Zienkiewicz O.C., Taylor R.L. (2000). The Finite Element Method, Fifth edition, Vol. 1: The Basis, Butterworth-Heinemann, Oxford.

[3] Wolff C., Richart N. and Molinari J.-F. (2015) A non-local continuum damage approach to model dynamic crack branching, in International Journal For Numerical Methods In Engineering, vol. 101, num. 12, p. 933-949.

[4] Richart N. and Molinari J.-F. (2015) Implementation of a parallel finite-element library: test case on a non-local continuum damage model, in Finite Elements in Analysis & Design, vol. 100, p. 41-46.

[5] Westergaard, Harold Malcolm. "Water pressures on dams during earthquakes." Trans. ASCE 98 (1933): 418-432.

[6] M. Chambart, T. Menouillard, N. Richart, J.-F. Molinari, and R.M. Gunn. Dynamic analysis of an arch dam with fluid-structure interaction. 12th Int. Workshop on Numerical Analysis of Dams, ICOLD BENCHMARK, Graz (Austria), 2013.

[7] Final Proceedings of the "12th ICOLD International Benchmark Workshop on Numerical Analysis of Dams", ICOLD BENCHMARK, Graz (Austria), 2013

[8] On the influence of transgranular and intergranular failure mechanisms during dynamic loading of silicon nitride, (2014) S.M. Taheri Mousavi, B. Hosseinkhani, Ch. Vieillard, M. Chambart, P. Kok, J.F. Molinari, Acta Materialia 67, pp. 239-251

[9] Dynamic crack propagation in a heterogeneous ceramic microstructure, insights from a cohesive model, (2015) S.M. Taheri Mousavi, N. Richart, C. Wolff, J.F. Molinari, Acta Materialia, 88, 136-146

Earthquake assessment of Luzzone dam using DIANA

Kikstra, W.P.[1], Manie, J.[1] and Schreppers, G.M.A.[1]

[1]*TNO DIANA BV, Delftechpark 19a, Delft, The Netherlands*

ABSTRACT: After a phased buildup of the dam, eigenvalue analysis is used to characterize the eigenfrequencies of the dam-foundation system, with and without fluid reservoir. Response Spectrum Analysis is used to assess the envelopes of displacement and stress amplitudes. Then transient dynamic analysis is performed using either Newmark time integration for an incompressible reservoir or modal superposition in time domain using a Hybrid Frequency Time Domain Analysis for compressibility effects in the reservoir.

E-mail: info@tnodiana.com

Finite Element model description

As the formulators of Theme A for the 13th Benchmark Workshop on the Numerical Analysis of Dams [1] conveniently provided a finite element model for DIANA [2], this model was adapted as is. It comprises quadratic isoparametric solid hexahedron and wedge elements for foundation and dam body. Having only two solids elements over the thickness of the dam body is a limited number, because the quadratic displacement interpolation gives a linear strain field. The reservoir is modelled with quadratic acoustic finite elements, i.e. the D.O.F. of these elements are dynamic fluid pressures. It could be noted that for the wave equation of motion in the fluid reservoir, linear elements would have been sufficient. Nevertheless, we have chosen to use the given model as is. Boundary elements will allow for surface waves, far field Sommerfeld radiation and bottom absorption for the computations with a compressible reservoir. The fluid-structure interaction between dam body and fluid reservoir is modelled with fluid-structure interface elements, which have displacement D.O.F. on the dam side and dynamic pressure D.O.F. on the reservoir side. Note that there is no modelling of interaction between reservoir and foundation other than the bottom absorption in the computations with a compressible reservoir, i.e. the reservoir mesh and foundation mesh are not connected. Note that the coordinate system is: Y vertical direction, X cross valley direction and Z the upstream direction.
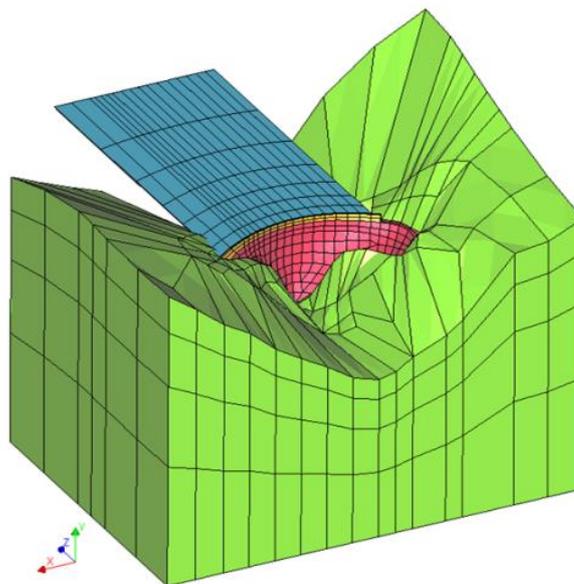
Fig. 1: Finite element model

Eigenfrequencies of Luzzone dam

Eigenfrequency analysis can be performed on different parts of the dam, reservoir and foundation system. The benchmarks required eigenfrequencies for empty and full reservoir. Stresses in a construction may change the eigenfrequencies $f=\omega/2\pi$. A phased construction of the dam followed by the hydrostatic load of the silt and reservoir water and a temperature gradient provides the stress needed for the geometric stress stiffness matrix K_G.

$$(K + K_G)\varphi = \omega^2(M + M_{reservoir})\varphi \qquad (1)$$

The stiffness matrix K is constructed using the dynamic modulus of elasticity for the dam and foundation rock. As modal mass participation serves for selection of the number of eigenmodes φ to take into account for response spectrum analysis or other modal reduction techniques, empty reservoir was interpreted as omitting the added reservoir mass $M_{reservoir}$. However, the contribution of the hydrostatic water load in the geometric stress stiffness matrix K_G was kept. As incompressible fluid is taken for the eigenvalue computations, the boundary conditions for the reservoir are zero dynamic pressures at the free surface and the far field, and a fully reflective reservoir bottom.

Tab. 1: First twelve eigenfrequencies for dry (left) and wet (right) dam

Mode	Empty Reservoir				Full Reservoir			
	Eigenfrequency	Effective Mass Percentage			Eigenfrequency	Effective Mass Percentage		
	f, Hz	X, %	Y, %	Z, %	f, Hz	X, %	Y, %	Z, %
1	1.94E+00	6.77E+00	3.37E-03	2.31E+00	1.48E+00	1.34E+00	3.07E-03	7.03E+01
2	2.01E+00	1.16E+00	9.66E-01	2.57E+01	1.51E+00	1.37E+01	1.41E-01	2.38E+01
3	2.93E+00	7.54E-02	4.35E-01	6.36E+00	2.30E+00	3.80E-01	1.60E-01	2.09E+01
4	3.60E+00	1.91E-02	5.56E+00	1.62E+01	2.72E+00	8.87E-02	1.04E+00	4.18E+01
5	3.88E+00	5.07E-02	3.81E-03	5.50E-01	3.15E+00	8.56E-01	2.92E-02	3.66E-01
6	4.37E+00	3.60E+01	4.77E-01	9.91E-02	3.59E+00	2.04E+01	3.11E-02	6.32E-03
7	4.49E+00	4.42E-04	6.62E+01	5.67E+00	4.06E+00	3.88E-01	1.63E+00	4.23E+00
8	4.91E+00	1.65E+00	7.56E-01	1.24E+00	4.33E+00	1.29E+00	5.06E+01	4.58E+00
9	5.18E+00	2.68E+01	1.07E+00	1.11E+00	4.53E+00	3.97E-03	2.16E+01	2.35E+00
10	5.61E+00	1.37E-01	1.04E+00	2.90E+00	4.81E+00	7.01E+00	7.42E-02	1.52E+01
11	6.01E+00	3.95E-01	1.50E-01	2.09E+00	4.98E+00	3.69E+01	9.95E-01	4.53E-01
12	6.05E+00	5.28E-01	5.04E-02	5.93E+00	5.07E+00	3.91E+00	5.55E-03	1.33E-01
Σ		7.36E+01	7.67E+01	7.02E+01	Σ	8.63E+01	7.63E+01	1.84E+02

Taking into account the first 12 modes yields an effective mass of 70% in the upstream downstream direction Z. The 3.12E9 kg mass of the dam amounts to 100% effective mass as the foundation is modelled massless. The total added mass of the reservoir is 3.47E9 kg, so more than the mass of the concrete dam. Compared to the 3.44E10 kg of water in the modelled reservoir, the added mass of the reservoir on the dam is roughly 10%. Therefore, the modelled length from upstream face of the dam to the far-field face of the reservoir is more than adequate to capture the added mass effect. The first twelve modes yield an effective mass of 184% of the mass of the concrete dam in upstream downstream direction. This is roughly 2.5 times the effective mass of the dam body for the same twelve modes.

Fig. 2: Mode shapes of first 12 eigenmodes for dry (left) and wet (right) dam

For the first six modes, the mode shape changes slightly due to the added mass of the reservoir. Mode shape 7 and mode shape 8 seem to be interchanged, as are mode shapes 9 and 10. Computation of phased construction of the dam followed by 50 dry and 50 wet (incompressible reservoir) eigenfrequencies and eigenmodes took 40 wall clock seconds on a computer with two Intel Xeon E5-2667 v2 processors and 384 GB of memory.

Response Spectrum Analysis of Luzzone dam

As the first twelve empty reservoir modes show effective mass contributions less than 80% in all three excitation directions, more modes were computed. 50 empty reservoir modes give an effective mass contribution of more than 95% in all three excitation directions, therefore we take 50 modes for the modal superposition using the Square Root of Summed Squares rule. Superposition of the three earthquake load components (X, Y, Z-direction) is also done using the SRSS rule. The response spectrum of the dam site, given by the formulators, is like the horizontal Eurocode 8 EN 1998-1 elastic response spectrum for region type1 with custom parameters S, T_B, T_C and T_D. Note that Eurocode 8 EN 1998-1 gives a different elastic response spectrum for the vertical direction. We followed the formulators, using the given response spectrum, also for the vertical direction with $a_v = 2/3 \, a_h$. The Response Spectrum Analysis uses the added mass approach for the contribution of the reservoir, i.e. incompressible fluid.
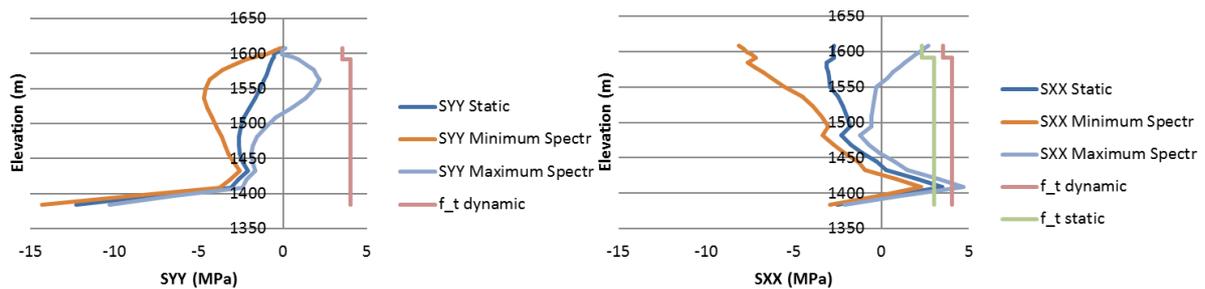
Fig. 3: Vertical stress SYY and hoop stress SXX in cross section 1 downstream face

Striking are the tensile hoop stresses between altitudes 1390 and 1450 m. The static tensile strength f_t =2.3 MPa is already exceeded by the static hoop stress just above the altitude of 1400 m. Also worth mentioning, is the upstream–downstream amplitude of the crest of the dam at point B: 0.106 m. This is less than the static downstream motion of the same point B .114 m due to the combination of hydrostatic pressure, silt pressure and summer temperature conditions. Radial displacement, vertical stress, hoop stress and principal stress results for all required cross sections can be found in Figs. 6 to 13 along with the transient dynamic and HFTD analysis results. Computation of phased construction of the dam followed by response spectrum analysis for 50 modes with incompressible reservoir took 39 wall clock seconds.

Time history analysis of Luzzone dam

Assessment of the earthquake signal series
The provided three earthquake signal series were first checked against the given horizontal and vertical elastic spectra by computing the spectral accelerations S_a for 25 different single degree of freedom (SDOF) oscillators with eigenfrequencies ranging from 1 Hz to 25 Hz. The oscillators all have a fixed mass m=1 kg, hence a spring stiffness $k_i = (2\pi f_i)^2$ and damping coefficient $c_i = 2\xi\sqrt{k_i m}$ with $\xi = 0.05$ (5% of the critical damping).
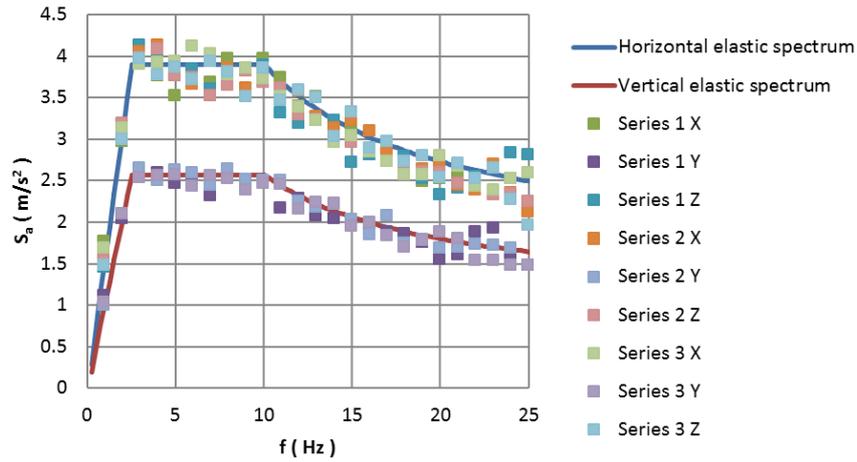
Fig. 4. Elastic response spectra and spectral accelerations for earthquake signals

Indeed, the provided three earthquake acceleration signals match closely the provided elastic response spectra of the dam site. Clearly, the three earthquake acceleration signals are artificial signals and match the requirements in section 3.2.3.1.2 of Eurocode 8 EN 1998-1.

Transient dynamic analysis with incompressible reservoir
The construction of Luzzone dam is simulated using phased static analysis. Under deadweight load, consecutively the foundation and the six construction parts of the dam are made active in the phased analysis. Any deformations from the building sequence with deadweight load are reset to zero. When the dam foundation system is complete, hydrostatic water load, silt load and summer condition temperatures are applied to get a realistic initial stress state. Then the reservoir is activated to provide the added fluid mass and material properties are switched from static elastic moduli to dynamic elastic moduli. Newmark time integration was used to follow through the acceleration signals. The time step size for the Newmark algorithm Δt=0.01 s is the same as the sampling time of the earthquake acceleration signals, such that no peak information will be missed and interpolation is avoided. Of interest are the provided Rayleigh damping parameters. The combination of a=1.1 and b=0.001 gives less than 5% of the critical damping in a frequency range from 2 Hz to 14 Hz. The first wet eigenfrequency, however, is found at 1.48 Hz, which has a damping ratio of 6.4%. As the second wet eigenfrequency at 1.51 Hz is very close to the first, its damping ratio is 6.3%.
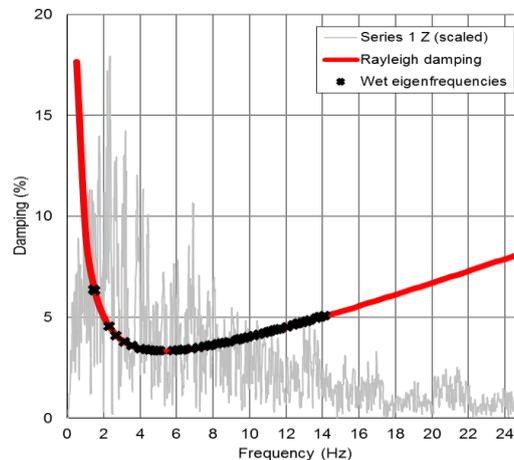
Fig. 5: Rayleigh damping values at first 50 eigenfrequencies and scaled discrete Fourier transformation of series 1 upstream-downstream acceleration signal

In Fig. 5 the Discrete Fourier Transformation of the series 1 upstream-downstream acceleration signal (scaled with a factor 300) was plotted to show that a considerable part of the signal is in the heavily damped frequency range below 2 Hz. The combination of the signal content below 2 Hz, the two eigenfrequencies close to 1.5 Hz and the heavy mass related damping below 2 Hz may lead to an under-prediction of the response; nevertheless, we will compute with the Rayleigh damping parameters as proposed by the formulators. The computation time for phased construction sequence followed by Newmark time integration with an incompressible reservoir for 3071 steps was 4880 seconds.

Hybrid Frequency Time Domain analysis with compressible reservoir

For high dams like Luzzone dam the compressibility of the reservoir water may lead to an upward shift of the equivalent inertial force of the reservoir on the face of the dam. This can lead to higher stresses in the dam. On the other hand, far-field radiation and bottom absorption may reduce the stresses in the dam due to energy absorption in the reservoir. All of the mentioned effects lead to frequency dependent behaviour and cannot be solved directly in time domain. Hybrid Frequency Time Domain analysis uses modal reduction and Discrete Fourier Transformation to switch from time domain to frequency domain and back. For its details, the reader is referred to [3] and [4]. Like for the Response Spectrum Analysis, we take the first 50 modes into account. In order to prove that HFTD gives reasonable results for this reduction to 50 modes, we first ran it with incompressible reservoir. The crest displacement for HFTD follows almost exactly the crest displacement found by means of Newmark time integration (see Fig. 06). To perform HFTD with frequency dependency, the reservoir boundary conditions of zero dynamic pressure at water surface and far-field boundary were replaced by appropriate boundary surface elements to represent bottom absorption, far-field Sommerfeld radiation and free surface waves. Computation of phased construction of the dam followed by HFTD analysis with incompressible reservoir took 4362 wall clock seconds, with compressible reservoir it took 8480 wall clock seconds. That the computation with compressible reservoir takes even longer than transient analysis with Newmark integration for an incompressible reservoir is due to the re-computation of the fluid structure interaction matrices for every frequency in the discrete Fourier transformation of the earthquake signal.

Displacement results
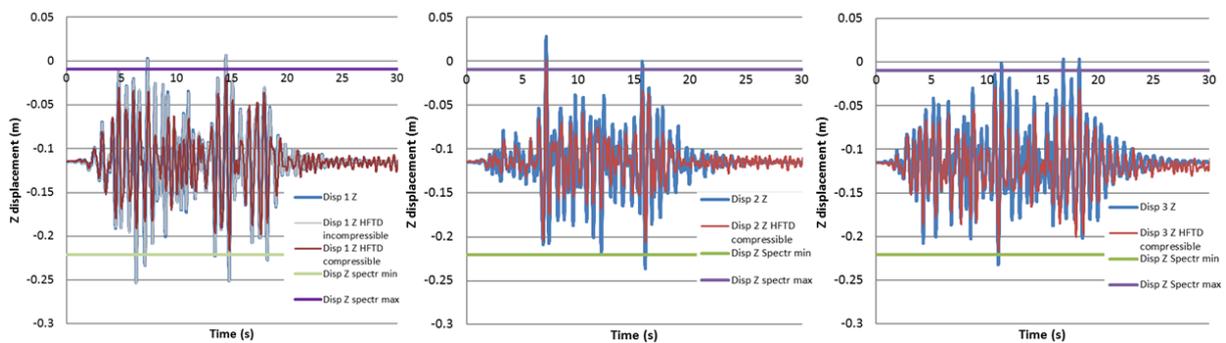
Fig. 6: Crest upstream – downstream displacement series 1(left), 2(middle) and 3 (right)

The combined effect of compressible reservoir, bottom absorption, far field radiation and free surface waves shows a damping effect on the earthquake response of Luzzone dam. Newmark time integration results and HFTD results with incompressible reservoir for the crest upstream

downstream movement during the earthquake are virtually equal. Comparing HFTD compressible displacement results to the Newmark incompressible results, the onset of the earthquake is followed equally. The peak displacements of the HFTD compressible computation appear to be in phase with the Newmark incompressible results but with lower amplitudes during the peaks of the earthquake. After the earthquake has passed, the incompressible response is damped, while the compressible response keeps vibrating with a frequency close to first and second eigenfrequency and an amplitude up to 0.01 m. Comparison of the series 1 time transient signals against the response spectrum prediction of the crest amplitude around its static displacement, shows that only 8 peaks of the Newmark incompressible results show a bigger amplitude than the indication from response spectrum analysis. For series 2 and 3 this is even less (Fig. 6).
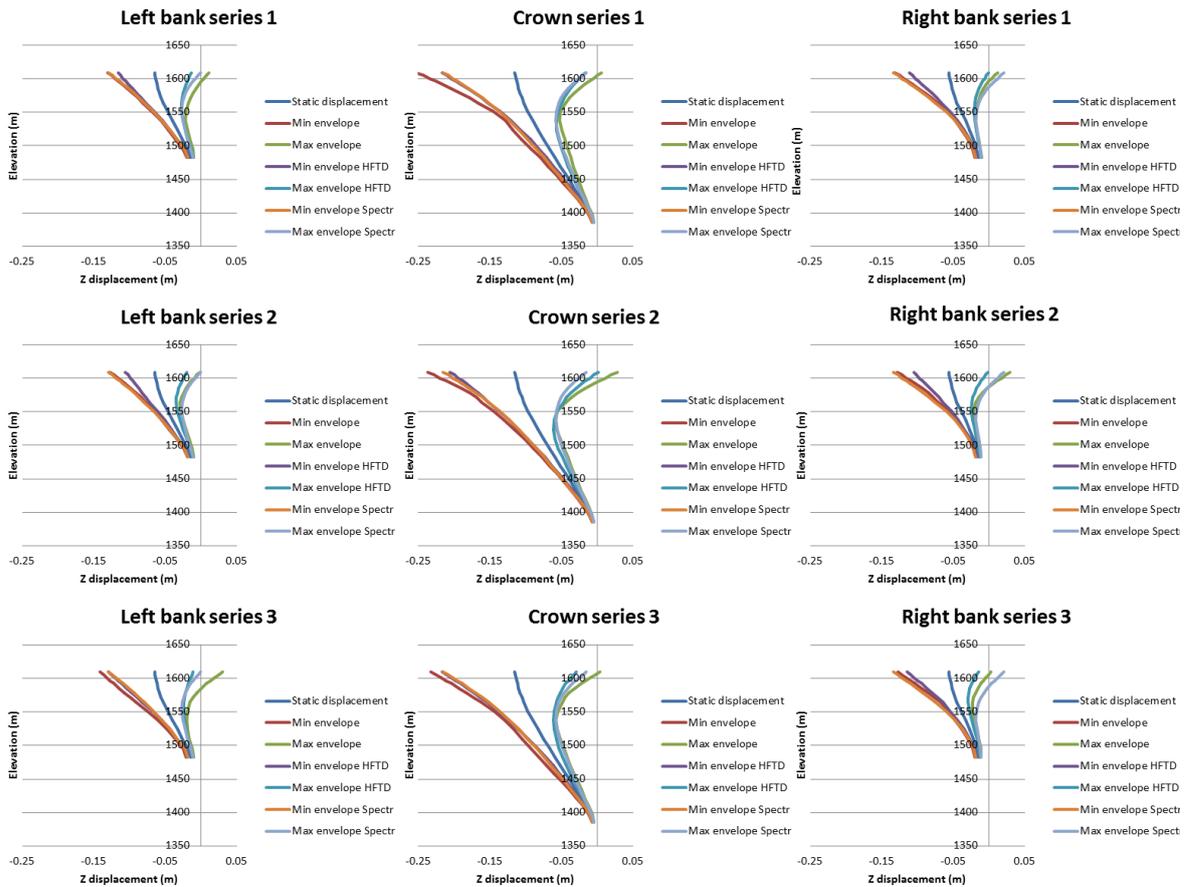
Fig. 7: Envelopes of cross section upstream downstream displacements

The envelopes of upstream downstream displacements (Fig. 7), show the time history envelopes found from HFTD analysis with compressible reservoir which are always within the envelope found with Newmark time integration with incompressible reservoir. This is due to the damping effects of bottom absorption, far field radiation and different dynamic pressure distribution on the upstream face of the dam. The envelopes given by Response Spectrum Analysis generally show the same shape as those found with time transient analysis. However, as already shown from the crest node B displacement, is does not form the biggest envelope. e.g. for series 2 the crown (cross section 1) upstream displacements are not only exceeded by the Newmark time integration results but also by the results from HFTD analysis with compressible reservoir.

Stress results
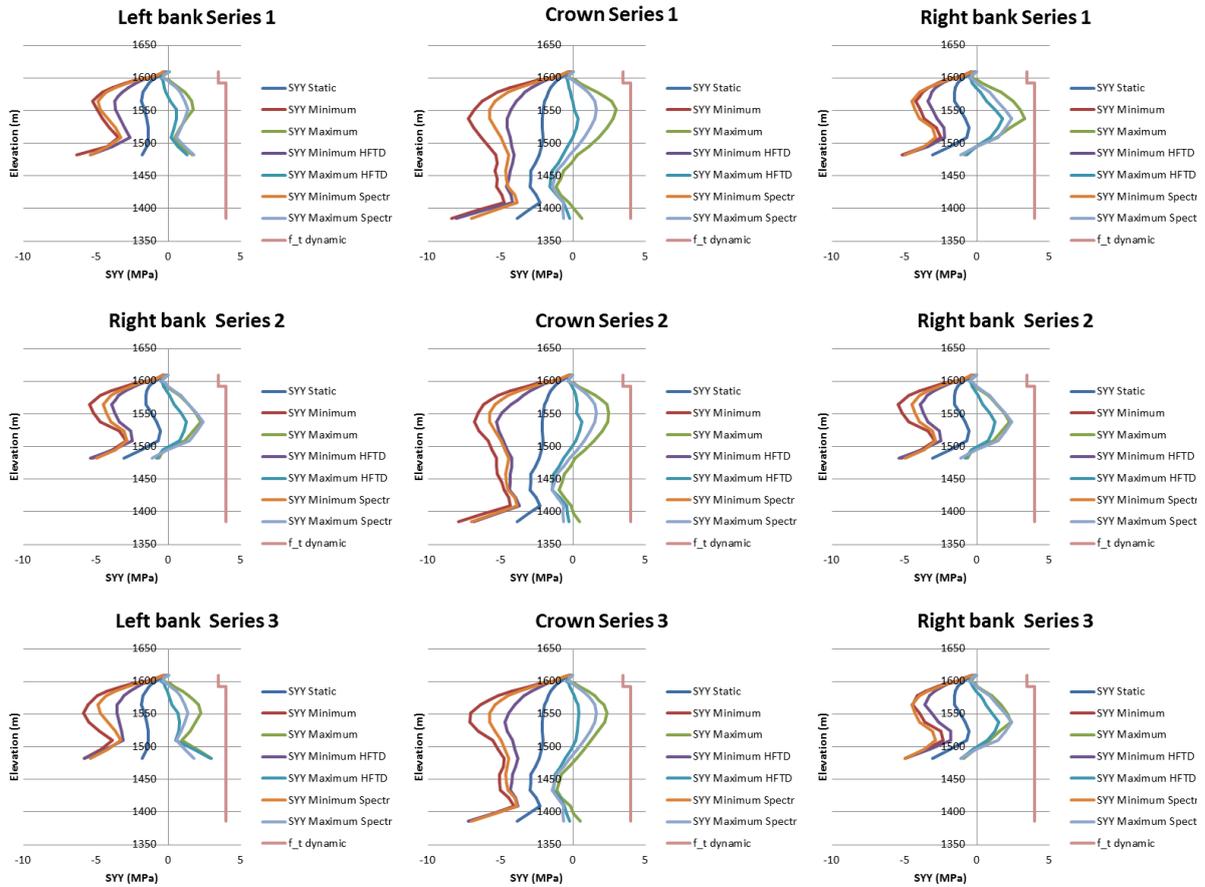
Fig. 8: Upstream face vertical stresses
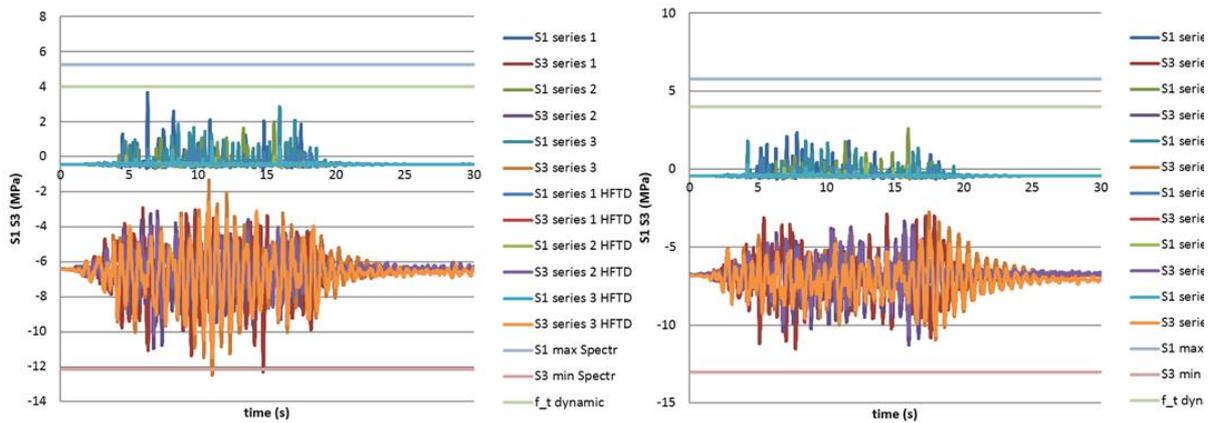
Fig. 9: Highest and lowest principal stress upstream face point D (left) and E (right)

For assessment of local stability, the dynamic tensile strength of the concrete (old and new concrete values for the cross section pictures, old concrete for the time history diagrams of up- and downstream points D and E) are plotted along with the vertical, horizontal and principal stress results (Figs. 8 to 13). It must be noted that the depicted cross valley stress SXX is really the hoop stress for the crown section (cross section1), but the cross valley stress SXX of course deviates from the hoop stress in the left and right bank cross sections (cross section 2 and 3).
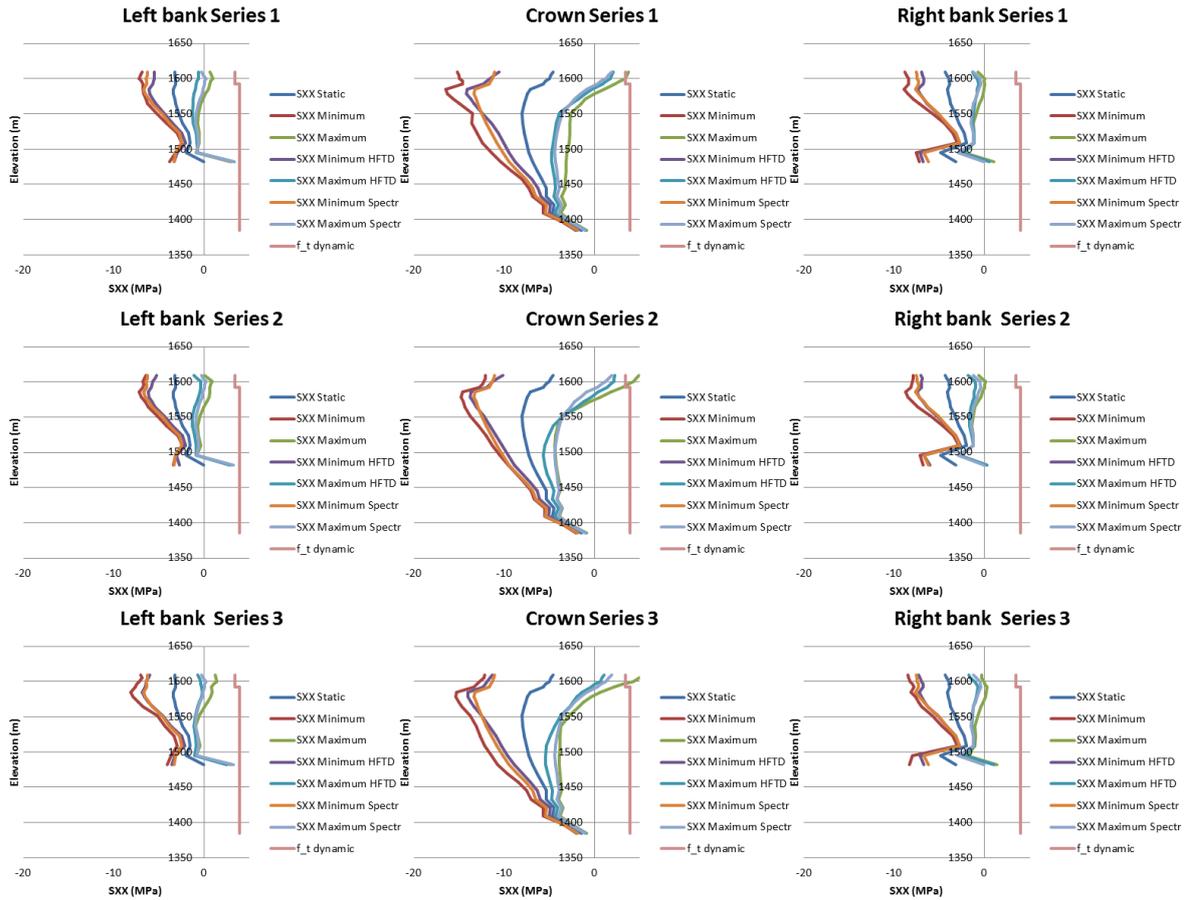
Fig. 10: Upstream face cross valley stresses
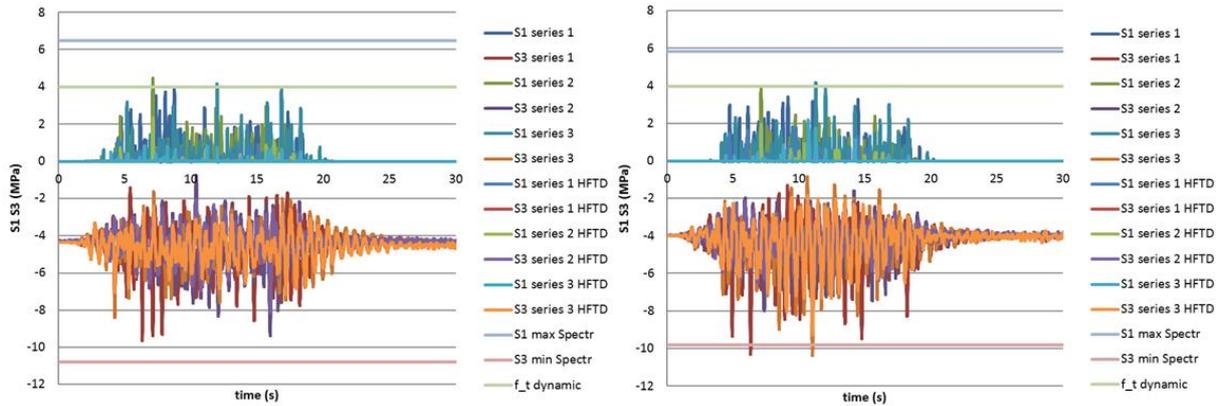
Fig. 11: Highest and lowest principal stress downstream face point D (left) and E (right)

At the crest of the dam the maximum envelope of cross valley stresses found with Newmark time integration and incompressible reservoir are higher than the dynamic tensile strength of the concrete, both on upstream and downstream face. On the downstream face of the dam, around 1410 m. altitude, all three methods (Newmark time integration, HFTD analysis and Response Spectrum Analysis) give cross valley stresses higher than the dynamic tensile strength. On the same spot, the static cross valley stresses are already higher than the static tensile strength.
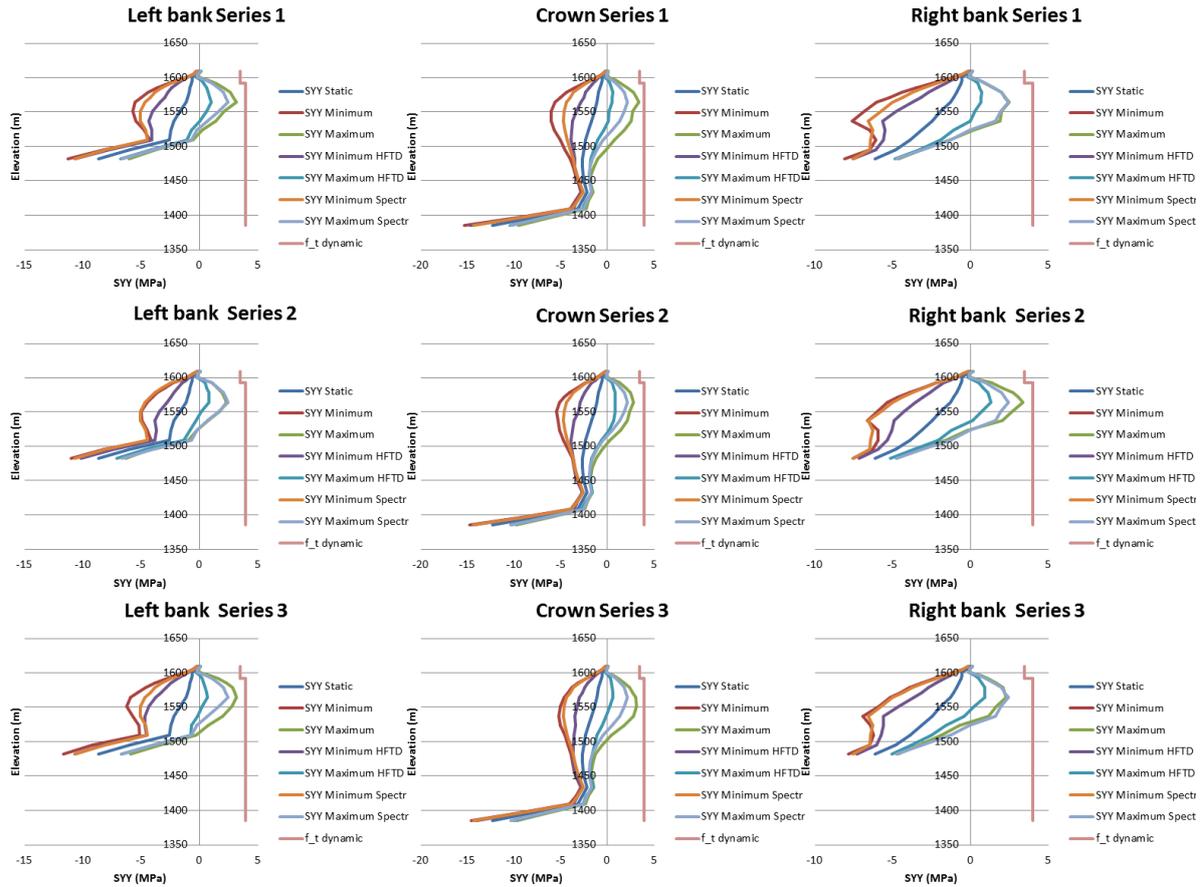
Fig. 12: Downstream face vertical stresses

Like the displacement envelopes, the envelopes of stress at the three cross sections also show the same shape - regardless whether they were computed using Newmark time integration with incompressible reservoir, HFTD analysis with compressible reservoir or Response Spectrum Analysis with incompressible reservoir. Envelopes of vertical and cross valley stress from HFTD analysis with compressible reservoir are always within the envelopes from Newmark time integration. The envelopes of horizontal and vertical stress found from Response Spectrum Analysis are within those from Newmark time integration.

From the time response diagrams of points D and E at downstream face (Fig. 11) computed with incompressible reservoir, the curves for S1 may seem strange at first sight, as they seem only to give amplitudes above the static solution and not below. The static S1 and S2 are closer together than their amplitudes during dynamic analysis. Therefore, they can interchange during the dynamic analysis. This interchanging of principal stresses S1 and S2 leads to the S1 vs. time diagram of Figs 9 and 11. We see peaks of S1 higher than the dynamic tensile strength in point E on both upstream and downstream face. The Response Spectrum Analysis principal stress results are computed taking the following considerations: *"For principal strains or stresses of individual modes the amplitudes of the major compressive principal stress S3 may yield a larger amplitude than the major tensile principal stress S1. Note that during the modal superposition and load superposition signs of the results are lost due to the superposition rules. Therefore, the superposed results, are rearranged such that S1H≥ S2H≥ S3H≥ S1L≥ S2L ≥ S3L Furthermore, for combination with a static solution, only the extreme dynamic amplitudes S1H = -S3L are used to form the widest result envelopes around static results S1, S2 and S3 for principal stresses."* Where the vertical and cross valley stress Response Spectrum Analysis

results compare well to the results from transient dynamic analysis, the principal stresses envelopes are over-predicted.
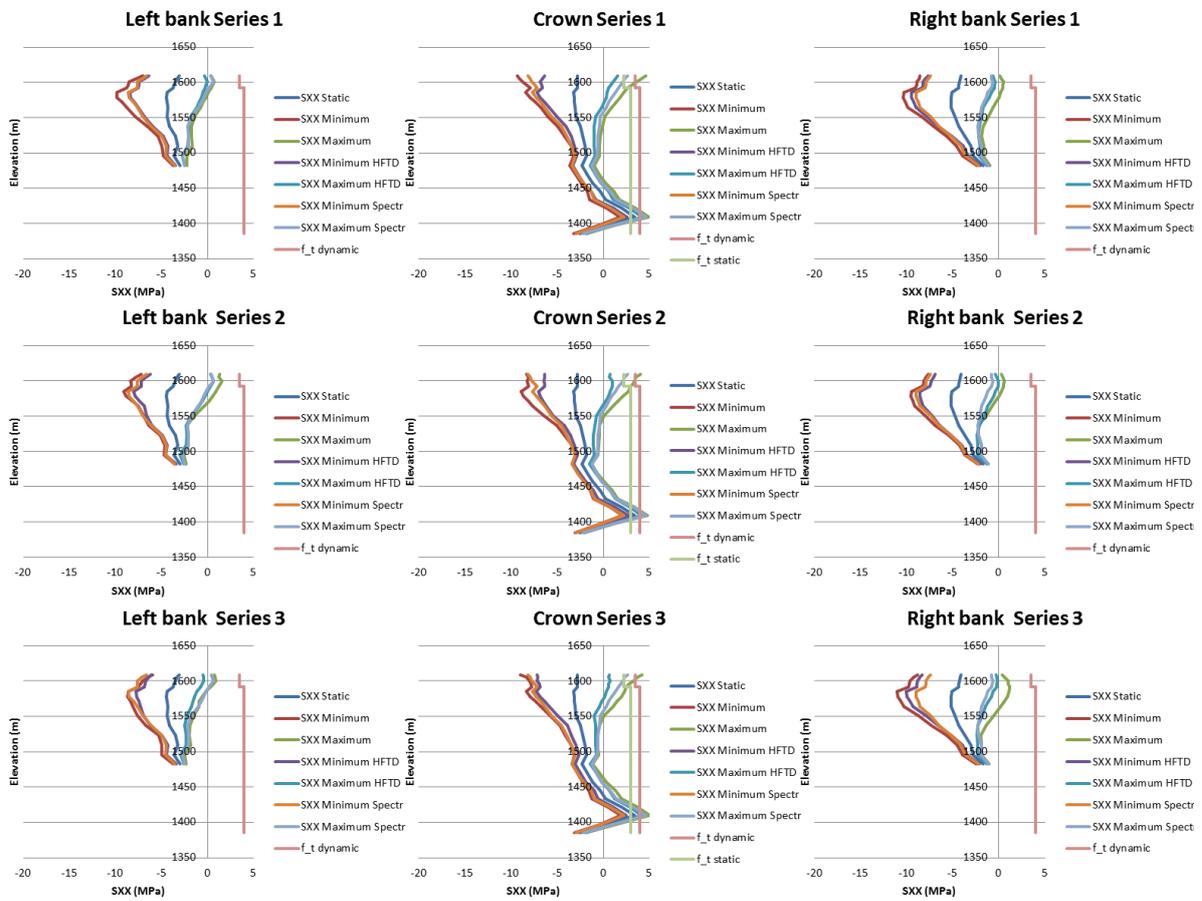
Fig. 13: Downstream face cross valley stresses
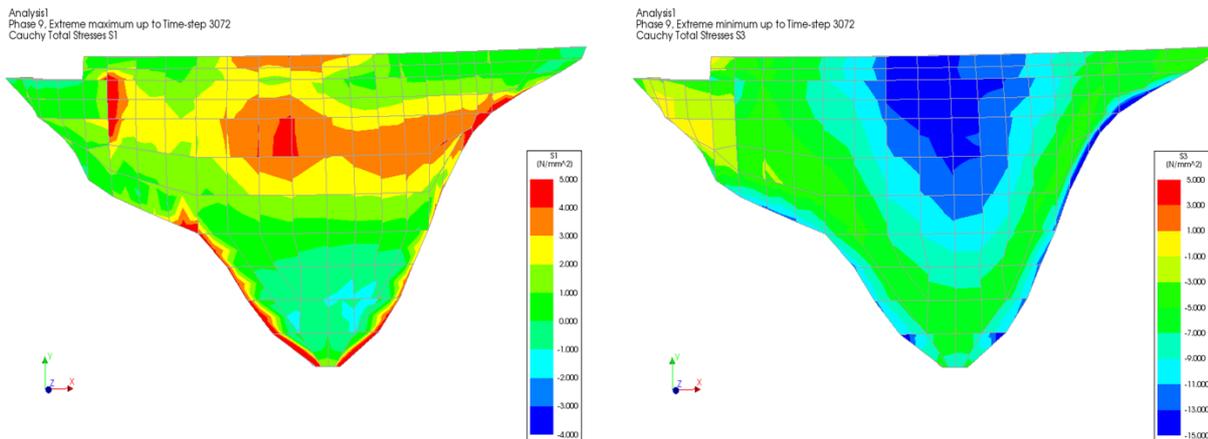
Fig. 14: Maximum and minimum upstream principal stress envelope series 1
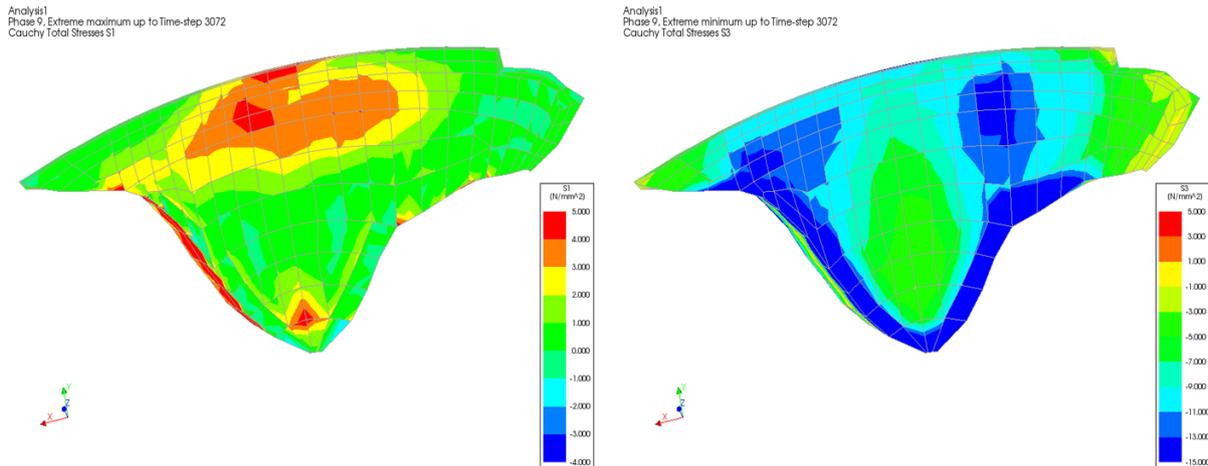
Fig. 15: Maximum and minimum downstream principal stress envelope series 1

Conclusions

After performing eigenfrequency analysis, three different computational approaches, Newmark time integration with incompressible reservoir, Hybrid Frequency-Time Domain analysis with compressible reservoir and Response Spectrum Analysis with incompressible reservoir, were performed on the same finite element model using finite element software package DIANA. Within reasonable computation times (less than 2.5 hours for the most elaborate analysis with compressible reservoir and therefore frequency dependent behaviour) the local stability of Luzzone dam has been assessed. As local failure due to violation of the tensile strength is predicted for the case with incompressible reservoir and already the static solution for phased construction of the dam followed by hydrostatic load, silt load and summer temperature conditions has shown inadmissible tensile stresses on the crown downstream cross section at elevations between 1390 and 1430 m., the next computation should include a crack model to analyse redistribution of stresses due to cracking.

References

[1] R.M. Gunn & A.D. Tzenkov (2015) 13th benchmark Workshop on the Numerical analysis of Dams, Theme A formulation, Seismic Safety Evaluation of a Concrete Dam Based on Guidelines. Lausanne, Switzerland.

[2] J. Manie (2014). DIANA User's Manual - Release 9.6. Delft, The Netherlands.

[3] F. Sirumbal (2013) Numerical modelling of dam-reservoir interaction seismic response using the Hybrid Frequency-Time Domain (HFTD) method. Master thesis, Faculty of Civil Engineering and Geosciences, Delft University of Technology, Delft, The Netherlands.

[4] W. Kikstra, F. Sirumbal and G. Schreppers HFTD (2013) Analysis of an arched dam at seismic loading. Proceedings of the 12th Benchmark Workshop on the Numerical Analysis of Dams. Graz, Austria.

Theme A:
SEISMIC SAFETY EVALUATIONS OF A CONCRETE DAM BASED ON GUIDELINES

Synthesis Report by:

Dr. Russell Michael Gunn[1] & Dr. Anton Doytchinov Tzenkov[2]

1. Swiss Federal Office of Energy, Supervision of Dams (formerly Stucky Ltd)
2. Stucky Ltd

Schweizerische Eidgenossenschaft
Confédération suisse
Confederazione Svizzera
Confederaziun svizra
Swiss Confederation

Bundesamt für Energie BFE
Office fédéral de l'énergie OFEN
Ufficio federale dell'energia UFE
Swiss Federal Office of Energy SFOE

stucky >
a Gruner company

Luzzone Arch Dam

Contributors, Programs and Approaches

Theme A Benchmark related to the *Seismic Safety Evaluation of a Concrete Dam Based on Guidelines* (refer to the figures below) attracted a total of **seventeen *Call for Paper*** inscriptions and finally, **ten *contributions*** from eight countries (Austria, Canada, France, Holland, Iran, Italy, Portugal and Switzerland). Compared to previous benchmarks (1991-2015), the number of contributions is high demonstrating the continued importance of numerical analyses, seismic loading and the application of directives and/or standards to Dam Engineering.

The figures below provide a graphical picture of these data.

	A	B	A	B	A1	A2	B1	B2	A1	A2	A1	A2	B1	B2	A	B	C	A	B	C	A	B	C	A	B	C	A	B	C	A	B	C	D	A	B	C	D	A	B	C
	1991		1993		1995				1997		1999				2001			2003			2005			2007			2009			2011				2013				2015		
	IT		IT		FR				ES		US				AT			RO			CN			RU			FR			ES				AT				CH		
	1		2		3				4		5				6			7			8			9			10			11				12				13		
Contributions	17	3	9	1	10	7	8	4	10	7	5	3	3	3	2	1	9	6	7	6	1	1	1	7	3	6	5	4	3	9	1	8	10	11	1	8	8	10	3	17
Totals		20		10				29		17				14			12			19			3			16			12				28				28			30

N° ▼ Country ▼ Date ▼ Theme ▼
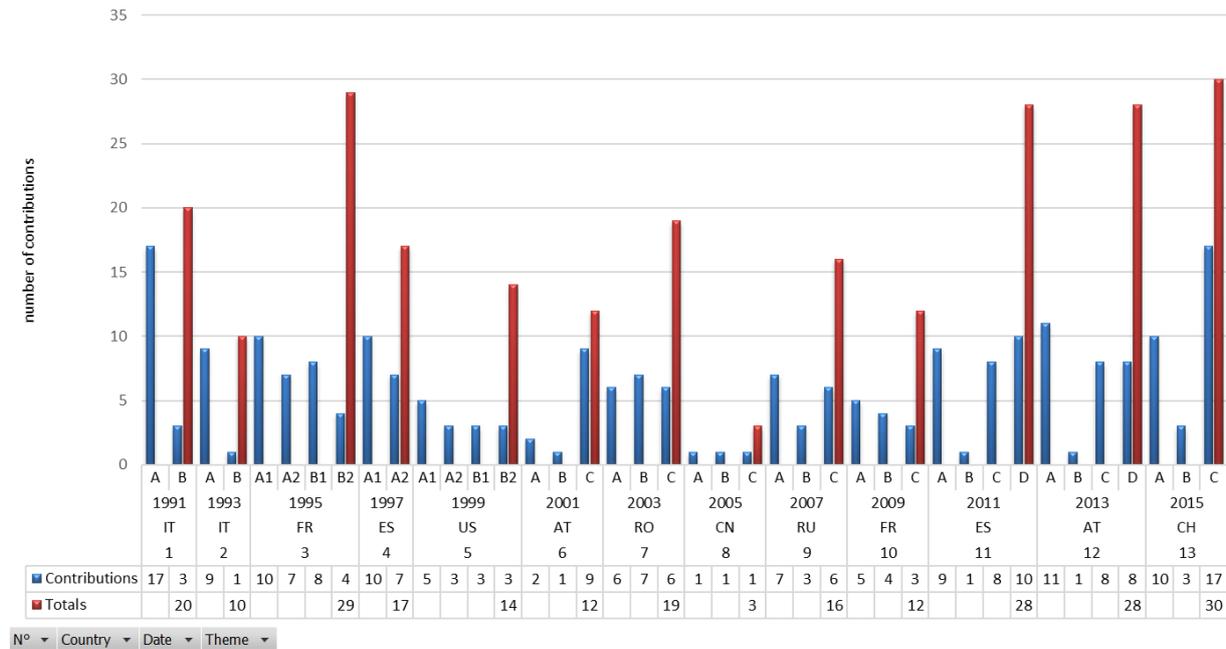
Figure 1 ICOLD Technical Committee A, Benchmark Contributors Status 1991-2015 per Theme, Date, and Country.

The list of benchmark themes denoted by uppercase letters in Figure 1 can be found in reference [7] and on the ICOLD web site [6], [8]. The Swiss Directives can also be found in reference [5] . Figure 3 shows that seismic studies have largely dominated the benchmark themes over the past 25 years and that safety and durability such as AAR/ASR are now becoming an important issue for existing (ageing) structures.

Table 1 List of Participants, FE Code, Fluid-Interaction Method Applied, Spatial Mesh and Directive Applied is given below. It is noted that **sign conventions** for Cartesian coordinate systems and stresses (for example, the French assume Engineering stresses/strains whereby traction is negative and tension is positive which is the contrary to many other Anglo-Saxon software packages for which the opposite applies) have been normalised throughout for the comparison of results.

In addition to the results requested in the Benchmark formulation statement, many contributors provided further results based on non-linear seismic analyses using "smeared crack" constitutive models and/or discrete interface finite elements. The use of advanced techniques was indeed one of the goals of the benchmark and the reason why the seismic loading was amplified. Some of the most important results and conclusions are provided in this chapter and a complete description of all performed Theme A studies is given in the individual papers presented in the proceedings [7].
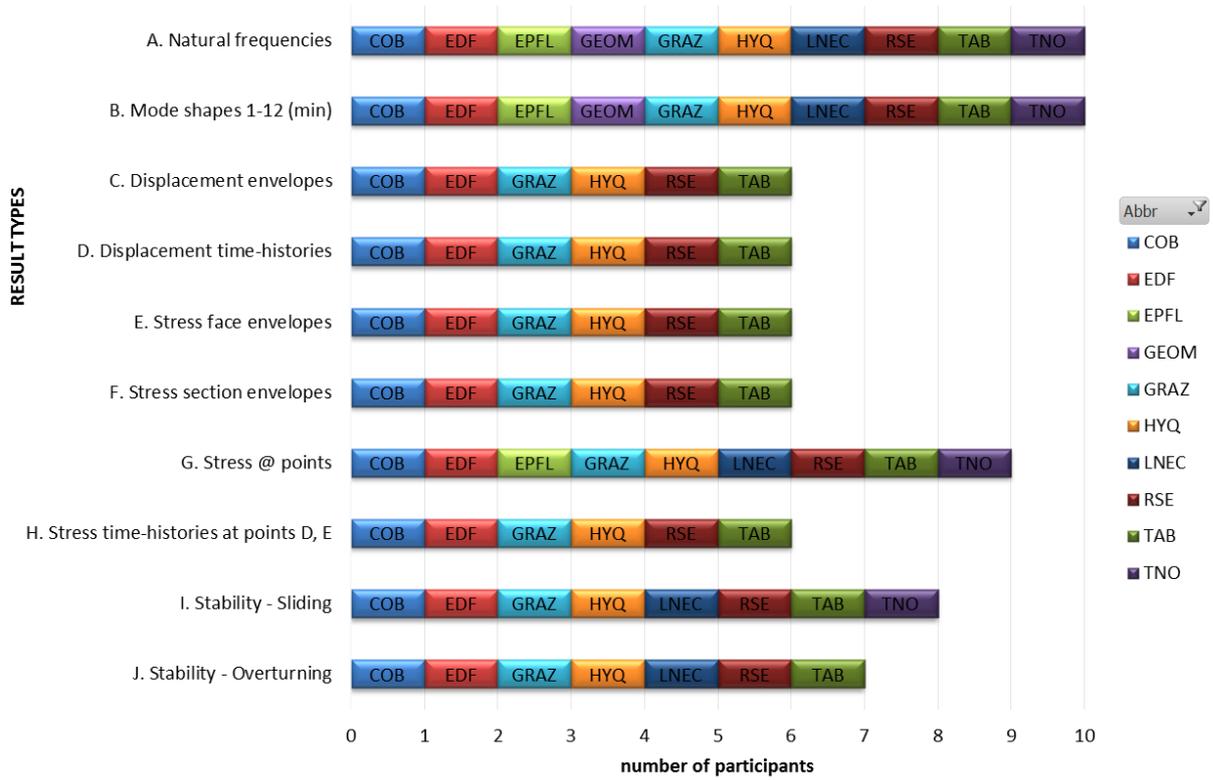
Figure 2 Theme A Results (letters A to J) per the number of participants (abbreviations given in papers)
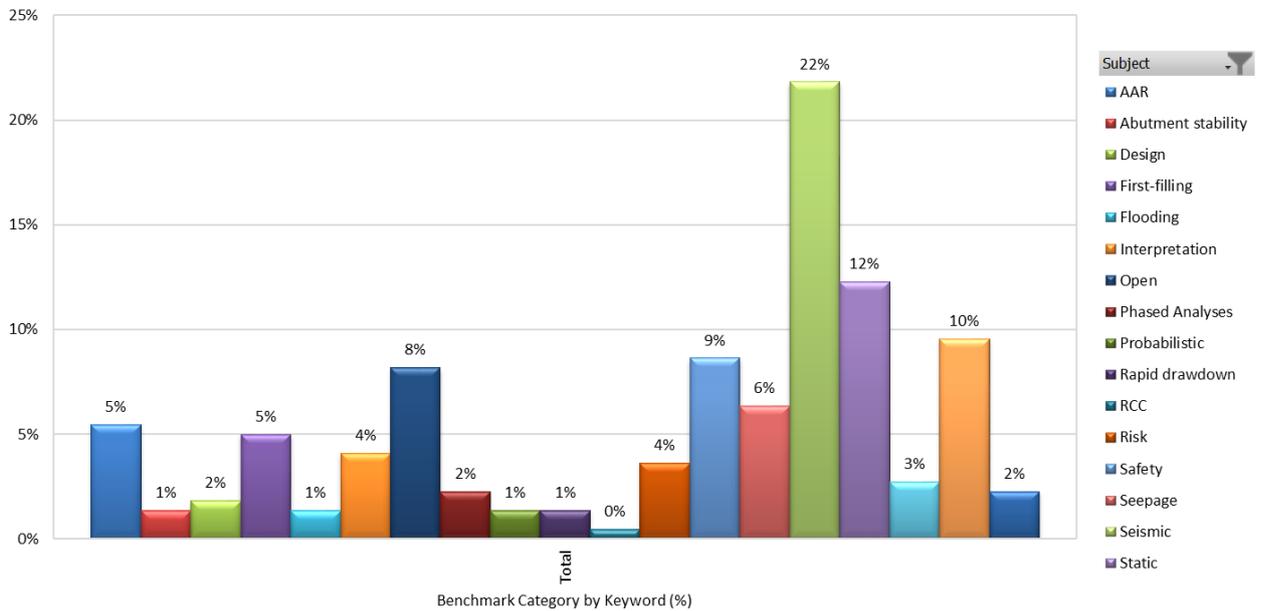
Figure 3 Total Number of Contributions between 1991-2015 per Keyword

Abbr	Theme A Contributors	FE Program	Method	Mesh	Directive
RSE	G. Faggiani and P. Masarati (Ricerca sul Sistema Energetico - RSE SpA, Italy)	CANT-SD	Compressible Fluid	Benchmark Data	CH/Italian
GRAZ	M. Goldgruber, S. Shahriari S.and G. Zenz (Institute of Hydraulic Engineering & Water Resources Management, Graz Technical University, Austria)	ABAQUS	Compressible Fluid	Benchmark Data	USACE
TAB	N. Naji-Mahalleh (Tablieh Construction Company, Iran)	ADINA	Compressible Fluid	Benchmark Data	CH/Hybrid
GEOM	S. Commend, M. Preisig (Geomod Consulting Engineers, Switzerland)	ZOIL	Westergaard, U/S direction only	Benchmark Data	CH
LNEC	Oliveira S., Alegre A., Silvestre A., Espada M. & Câmara R (Laboratório Nacional de Engenharia Civil/Instituto Superior de Engenharia de Lisboa, Concrete Dams Department, Portugal)	DYSAA	Incompresible Fluid	Benchmark Data	Hybrid
TNO	W.P. Kikstra, J. Manie and G.J. Schreppers (TNO Diana BV, Holland)	DIANA	Compressible Fluid	Benchmark Data	Hybrid
HYQ	Roth, S.-N and M. Roberge (Hydro-Québec Production, Canada)	ANSYS	Incompresible Fluid	Mesh finer than Benchmark Data	CH
EDF	E. Robbe, J. Foqué (EDF-CIH)	CODE_ASTER	Incompresible Fluid	Benchmark Data	F
EPFL	M. Corrado, G. Anciaux, D. Scantamburlo, S. Laffely, M. Chambart, T. Menouillard and J.-F. Molinari (EPFL-LSMS, Switzerland)	AKANTU	Incompresible Fluid	Benchmark Data	CH
COB	C. Tsai, X. Molin, C. Noret (TRACTEBEL, France)	COBEF_MISS3D	Incompresible Fluid	Benchmark Data	F
REF	**R. M. Gunn and A. Tzenkov (Swiss Federal Office of Energy / Stucky Ltd, Switzerland)**	**DIANA**	**Compresible Fluid**	**Benchmark Data**	**CH**

Table 1 List of Participants, FE Code, Fluid-Interaction Method Applied, Spatial Mesh and Directive Applied

Comparison of Results

The quantity of data received from the contributors for such a benchmark is obviously considerable. The formulators of the Theme A were aware of this issue and have tried to focus on the essential results needed to achieve the benchmark objectives.

The comparison of results presented below is based on raw data as supplied by the contributors. It seems meaningless to perform statistical studies and the accent has been placed on graphical comparisons which remain both qualitative and quantitative in themselves.

When making the comparison and evaluation of results, the formulators have tried to be as objective as possible noting that a **unique and perfect solution** is **not** feasible. Moreover, it should be pointed out that the formulated benchmark, although based on a real dam in operation, is fictitious and therefore, the conclusions of the contributors related to safety, which are quite variable in nature, bear no relevance to the actual structure itself. However, the numerical methods employed may be relevant to the use of certain Guidelines highlighting the need for further developments and/or limitations in their application.

The categorisation of dams by height, volume, thickness, etc. should not defer from the fact that each dam body and the appurtenant structures annexed to the dam are quite unique and as stated many times in the past, the Dam Engineers *judgement* based on his experience and technical skills shall be a determining fact.

Natural Frequencies [A] and Mode Shapes [B]
The contributors were required to present the first 12 natural frequencies/modes (eigen-properties) of the dam-foundation system for the cases of **empty and full reservoir**. This requirement was meant only for the comparison of eigenvalues/modes and not as a restriction to the number of modes to be considered in the complete seismic solution. Standards, Directives or Guidelines, typically stipulate that 80% of the participating mass defines the number of modes to be considered in the analyses (modal superposition methods) or at least all modes of the solid body less than 33 Hz. Most contributors applied direct time-integration methods and this restriction does not affect the results but should be borne in mind for the comparison of certain results. The results are given below in tabular and graphical formats.

Contribution	Code	Directive	X	Y	Z	Mode ϕ	f_e (Hz)	E_{Xe} (%)	E_{Ye} (%)	E_{Ze} (%)	f_f (Hz)	E_{Xf} (%)	E_{Yf} (%)	E_{Zf} (%)	Fluid
RSE	CANT-SD	CH/I	Y-	Z+	X-	1	2.00	0.03%	0.20%	8.12%	1.52	0.13%	47.57%	1.46%	CP
RSE	CANT-SD	CH/I	Y-	Z+	X-	2	2.10	0.90%	24.06%	0.27%	1.54	0.09%	0.44%	12.51%	CP
RSE	CANT-SD	CH/I	Y-	Z+	X-	3	3.02	0.68%	7.03%	0.05%	2.10	0.14%	4.55%	0.02%	CP
RSE	CANT-SD	CH/I	Y-	Z+	X-	4	3.78	9.16%	14.57%	0.04%	2.27	0.39%	12.38%	0.18%	CP
RSE	CANT-SD	CH/I	Y-	Z+	X-	5	3.97	0.22%	0.70%	0.26%	2.40	0.00%	0.36%	0.16%	CP
RSE	CANT-SD	CH/I	Y-	Z+	X-	6	4.46	0.00%	0.17%	29.32%	2.80	0.61%	5.67%	0.05%	CP
RSE	CANT-SD	CH/I	Y-	Z+	X-	7	5.01	2.66%	2.19%	0.08%	3.18	0.12%	0.01%	2.68%	CP
RSE	CANT-SD	CH/I	Y-	Z+	X-	8	5.20	55.43%	1.29%	1.06%	3.35	1.25%	1.87%	0.87%	CP
RSE	CANT-SD	CH/I	Y-	Z+	X-	9	5.81	1.51%	1.17%	28.72%	3.44	0.08%	0.15%	12.88%	CP
RSE	CANT-SD	CH/I	Y-	Z+	X-	10	5.96	0.41%	2.31%	3.13%	3.92	0.54%	0.55%	0.11%	CP
RSE	CANT-SD	CH/I	Y-	Z+	X-	11	6.15	0.01%	0.05%	0.14%	4.12	0.12%	1.22%	0.53%	CP
RSE	CANT-SD	CH/I	Y-	Z+	X-	12	6.31	1.32%	14.14%	1.22%	4.26	0.09%	0.00%	0.24%	CP
RSE		**CH/I**				**Total**		**72.32%**	**67.88%**	**72.41%**		**31.69%**	**3.57%**	**74.77%**	**CP**
GRAZ	ABAQUS	USACE	X+	Z+	Y-	1	1.99	8.20%	0.16%	0.03%	1.51	0.43%	13.66%	0.44%	CP
GRAZ	ABAQUS	USACE	X+	Z+	Y-	2	2.09	0.22%	24.27%	0.91%	1.53	4.52%	0.63%	0.00%	CP
GRAZ	ABAQUS	USACE	X+	Z+	Y-	3	3.00	0.04%	7.20%	0.70%	2.10	0.00%	0.05%	0.02%	CP
GRAZ	ABAQUS	USACE	X+	Z+	Y-	4	3.76	0.03%	14.36%	9.09%	2.26	0.00%	0.93%	0.19%	CP
GRAZ	ABAQUS	USACE	X+	Z+	Y-	5	3.94	0.24%	0.91%	0.31%	2.39	0.01%	1.90%	0.04%	CP
GRAZ	ABAQUS	USACE	X+	Z+	Y-	6	4.43	30.11%	0.18%	0.00%	2.80	0.00%	0.97%	0.40%	CP
GRAZ	ABAQUS	USACE	X+	Z+	Y-	7	4.95	0.12%	2.06%	1.56%	3.15	0.48%	0.00%	0.06%	CP
GRAZ	ABAQUS	USACE	X+	Z+	Y-	8	5.18	1.27%	1.38%	55.69%	3.34	0.51%	3.05%	1.24%	CP
GRAZ	ABAQUS	USACE	X+	Z+	Y-	9	5.76	29.41%	1.57%	2.26%	3.42	4.09%	1.16%	0.27%	CP
GRAZ	ABAQUS	USACE	X+	Z+	Y-	10	5.91	2.02%	2.04%	0.37%	3.92	0.02%	0.71%	0.90%	CP
GRAZ	ABAQUS	USACE	X+	Z+	Y-	11	6.06	0.29%	0.03%	0.03%	4.06	0.82%	0.59%	0.07%	CP
GRAZ	ABAQUS	USACE	X+	Z+	Y-	12	6.27	1.11%	14.22%	1.31%	4.25	0.52%	0.22%	0.13%	CP
GRAZ		**USACE**				**Total**		**73.05%**	**68.40%**	**72.26%**		**11.41%**	**23.87%**	**3.74%**	**CP**
TAB	ADINA	CH/Hybrid	X+	Z+	Y-	1	1.95	6.73%	0.00%	2.44%	1.15	7.28%	0.30%	5.91%	CP
TAB	ADINA	CH/Hybrid	X+	Z+	Y-	2	2.01	1.21%	0.97%	25.67%	1.19	3.44%	0.21%	26.96%	CP
TAB	ADINA	CH/Hybrid	X+	Z+	Y-	3	2.94	0.07%	0.43%	6.30%	1.74	0.18%	0.00%	7.48%	CP
TAB	ADINA	CH/Hybrid	X+	Z+	Y-	4	3.60	0.02%	5.60%	16.16%	2.10	0.14%	0.77%	22.86%	CP
TAB	ADINA	CH/Hybrid	X+	Z+	Y-	5	3.89	0.05%	0.00%	0.54%	2.31	0.40%	0.01%	0.43%	CP
TAB	ADINA	CH/Hybrid	X+	Z+	Y-	6	4.37	36.08%	0.49%	0.10%	2.68	14.16%	0.07%	0.00%	CP
TAB	ADINA	CH/Hybrid	X+	Z+	Y-	7	4.49	0.00%	66.14%	5.69%	2.94	0.04%	0.08%	1.36%	CP
TAB	ADINA	CH/Hybrid	X+	Z+	Y-	8	4.92	1.68%	0.74%	1.25%	3.21	0.12%	0.03%	3.79%	CP
TAB	ADINA	CH/Hybrid	X+	Z+	Y-	9	5.19	26.66%	1.06%	1.09%	3.57	0.06%	2.10%	7.82%	CP
TAB	ADINA	CH/Hybrid	X+	Z+	Y-	10	5.61	0.13%	1.02%	2.91%	3.63	0.45%	0.34%	0.44%	CP
TAB	ADINA	CH/Hybrid	X+	Z+	Y-	11	6.02	0.37%	0.16%	2.36%	4.08	4.38%	0.00%	0.52%	CP
TAB	ADINA	CH/Hybrid	X+	Z+	Y-	12	6.06	0.56%	0.04%	5.64%	4.33	1.93%	59.88%	0.96%	CP
TAB		**CH/Hybrid**				**Total**		**73.56%**	**76.66%**	**70.16%**		**32.58%**	**63.79%**	**78.53%**	**CP**
GEOM	ZSOIL	CH	X+	Y+	Z+	1	2.00	7.36%	0.04%	0.08%	1.18	0.12%	0.12%	61.57%	ICZ
GEOM	ZSOIL	CH	X+	Y+	Z+	2	2.09	0.18%	0.69%	22.73%	1.28	2.17%	0.06%	5.83%	ICZ
GEOM	ZSOIL	CH	X+	Y+	Z+	3	3.03	0.05%	0.45%	5.98%	1.95	0.06%	0.21%	19.63%	ICZ
GEOM	ZSOIL	CH	X+	Y+	Z+	4	3.76	0.10%	6.75%	14.69%	2.24	0.00%	0.85%	52.82%	ICZ
GEOM	ZSOIL	CH	X+	Y+	Z+	5	3.94	0.55%	0.20%	0.97%	2.55	0.48%	0.00%	0.22%	ICZ
GEOM	ZSOIL	CH	X+	Y+	Z+	6	4.44	24.16%	0.00%	0.18%	2.91	3.06%	0.02%	0.02%	ICZ
GEOM	ZSOIL	CH	X+	Y+	Z+	7	4.99	0.10%	0.25%	1.34%	3.26	0.05%	0.02%	3.70%	ICZ
GEOM	ZSOIL	CH	X+	Y+	Z+	8	5.42	1.91%	49.85%	0.41%	3.51	0.01%	0.24%	26.01%	ICZ
GEOM	ZSOIL	CH	X+	Y+	Z+	9	5.86	28.56%	2.27%	0.56%	3.95	0.02%	1.33%	12.13%	ICZ
GEOM	ZSOIL	CH	X+	Y+	Z+	10	5.96	5.09%	0.78%	1.78%	4.03	0.00%	0.10%	1.61%	ICZ
GEOM	ZSOIL	CH	X+	Y+	Z+	11	6.10	0.53%	0.01%	0.10%	4.49	0.95%	0.00%	0.10%	ICZ
GEOM	ZSOIL	CH	X+	Y+	Z+	12	6.32	0.57%	3.08%	14.88%	4.74	0.00%	0.31%	10.59%	ICZ
GEOM		**CH**				**Total**		**69.17%**	**64.37%**	**63.70%**		**6.92%**	**3.25%**	**194.20%**	**ICZ**

Table 2 Natural Frequencies, effective participating masses, fluid-structure methods (X+ Left-Right Banks, Y+ Vertical, Z+ Downstream-Upstream, CP = Compressible Fluid, ICP =Incompressible Fluid Normal to Surface, ICN = Incompressible Fluid U/S->D/S)

Contribution	Code	Reference(s) Directive	X	Y	Z	Mode ϕ	Empty Reservoir Eigenvalue f_e (Hz)	E_{Xer}(%)	E_{Yer}(%)	E_{Zer}(%)	Full Reservoir Eigenvalue f_f (Hz)	E_{Xfr}(%)	E_{Yfr}(%)	E_{Zfr}(%)	Fluid
LNEC	DYSAA	Hybrid	X+	Z+	Y-	1	1.99	8.20%	0.16%	0.03%	1.51	0.43%	13.66%	0.44%	ICN
LNEC	DYSAA	Hybrid	X+	Z+	Y-	2	2.09	0.22%	24.27%	0.91%	1.53	4.52%	0.63%	0.00%	ICN
LNEC	DYSAA	Hybrid	X+	Z+	Y-	3	3.00	0.04%	7.20%	0.70%	2.10	0.00%	0.05%	0.02%	ICN
LNEC	DYSAA	Hybrid	X+	Z+	Y-	4	3.76	0.03%	14.36%	9.09%	2.26	0.00%	0.93%	0.19%	ICN
LNEC	DYSAA	Hybrid	X+	Z+	Y-	5	3.94	0.24%	0.91%	0.31%	2.39	0.01%	1.90%	0.04%	ICN
LNEC	DYSAA	Hybrid	X+	Z+	Y-	6	4.43	30.11%	0.18%	0.00%	2.80	0.00%	0.97%	0.40%	ICN
LNEC	DYSAA	Hybrid	X+	Z+	Y-	7	4.95	0.12%	2.06%	1.56%	3.15	0.48%	0.00%	0.06%	ICN
LNEC	DYSAA	Hybrid	X+	Z+	Y-	8	5.18	1.27%	1.38%	55.69%	3.34	0.51%	3.05%	1.24%	ICN
LNEC	DYSAA	Hybrid	X+	Z+	Y-	9	5.76	29.41%	1.57%	2.26%	3.42	4.09%	1.16%	0.27%	ICN
LNEC	DYSAA	Hybrid	X+	Z+	Y-	10	5.91	2.02%	2.04%	0.37%	3.92	0.02%	0.71%	0.90%	ICN
LNEC	DYSAA	Hybrid	X+	Z+	Y-	11	6.06	0.29%	0.03%	0.03%	4.06	0.82%	0.59%	0.07%	ICN
LNEC	DYSAA	Hybrid	X+	Z+	Y-	12	6.27	1.11%	14.22%	1.31%	4.25	0.52%	0.22%	0.13%	ICN
LNEC		**Hybrid**				**Total**		**73.05%**	**68.40%**	**72.26%**		**11.41%**	**23.87%**	**3.74%**	**ICN**
TNO	DIANA	Hybrid	X+	Y+	Z+	1	1.94	6.77%	0.00%	2.31%	1.48	1.34%	0.00%	70.30%	CP
TNO	DIANA	Hybrid	X+	Y+	Z+	2	2.01	1.16%	0.97%	25.75%	1.51	13.74%	0.14%	23.80%	CP
TNO	DIANA	Hybrid	X+	Y+	Z+	3	2.93	0.08%	0.43%	6.36%	2.30	0.38%	0.16%	20.90%	CP
TNO	DIANA	Hybrid	X+	Y+	Z+	4	3.60	0.02%	5.56%	16.15%	2.72	0.09%	1.04%	41.80%	CP
TNO	DIANA	Hybrid	X+	Y+	Z+	5	3.88	0.05%	0.00%	0.55%	3.15	0.86%	0.03%	0.37%	CP
TNO	DIANA	Hybrid	X+	Y+	Z+	6	4.37	35.98%	0.48%	0.10%	3.59	20.45%	0.03%	0.01%	CP
TNO	DIANA	Hybrid	X+	Y+	Z+	7	4.49	0.00%	66.15%	5.67%	4.06	0.39%	1.63%	4.23%	CP
TNO	DIANA	Hybrid	X+	Y+	Z+	8	4.91	1.65%	0.76%	1.24%	4.33	1.29%	50.60%	4.58%	CP
TNO	DIANA	Hybrid	X+	Y+	Z+	9	5.18	26.80%	1.07%	1.11%	4.53	0.00%	21.61%	2.35%	CP
TNO	DIANA	Hybrid	X+	Y+	Z+	10	5.61	0.14%	1.04%	2.90%	4.81	7.01%	0.07%	15.18%	CP
TNO	DIANA	Hybrid	X+	Y+	Z+	11	6.01	0.39%	0.15%	2.09%	4.98	36.87%	0.99%	0.45%	CP
TNO	DIANA	Hybrid	X+	Y+	Z+	12	6.05	0.53%	0.05%	5.93%	5.07	3.91%	0.01%	0.13%	CP
TNO		**Hybrid**				**Total**		**73.58%**	**76.66%**	**70.17%**		**86.32%**	**76.31%**	**184.09%**	**CP**
HYQ	ANSYS	CH	X+	Y+	Z+	1	1.96	8.78%	0.05%	0.06%	1.50	13.56%	0.26%	17.27%	ICN
HYQ	ANSYS	CH	X+	Y+	Z+	2	2.08	0.18%	0.93%	24.62%	1.51	2.26%	0.00%	33.48%	ICN
HYQ	ANSYS	CH	X+	Y+	Z+	3	2.96	0.07%	0.79%	7.88%	1.81	0.00%	0.00%	0.00%	ICN
HYQ	ANSYS	CH	X+	Y+	Z+	4	3.73	0.09%	9.16%	14.43%	2.18	0.19%	0.61%	17.01%	ICN
HYQ	ANSYS	CH	X+	Y+	Z+	5	3.89	0.31%	0.38%	1.08%	2.35	0.21%	0.00%	0.67%	ICN
HYQ	ANSYS	CH	X+	Y+	Z+	6	4.37	28.71%	0.00%	0.20%	2.71	0.00%	0.66%	6.06%	ICN
HYQ	ANSYS	CH	X+	Y+	Z+	7	4.88	0.10%	1.27%	2.11%	3.11	2.98%	0.00%	0.00%	ICN
HYQ	ANSYS	CH	X+	Y+	Z+	8	5.16	1.04%	56.17%	1.54%	3.30	2.06%	1.28%	1.86%	ICN
HYQ	ANSYS	CH	X+	Y+	Z+	9	5.74	25.28%	1.64%	1.43%	3.35	0.00%	0.00%	0.00%	ICN
HYQ	ANSYS	CH	X+	Y+	Z+	10	5.87	5.84%	0.50%	2.78%	3.36	12.52%	0.17%	0.38%	ICN
HYQ	ANSYS	CH	X+	Y+	Z+	11	5.96	0.11%	0.03%	0.01%	3.74	0.00%	0.59%	0.00%	ICN
HYQ	ANSYS	CH	X+	Y+	Z+	12	6.18	2.18%	1.55%	14.63%	4.00	0.31%	0.23%	1.96%	ICN
HYQ		**CH**				**Total**		**72.68%**	**72.48%**	**70.79%**		**34.10%**	**3.79%**	**78.69%**	**ICN**
EDF	CODE_ASTER	F	X+	Y+	Z+	1	2.01	6.91%	0.02%	0.18%	1.26	2.02%	0.31%	17.51%	ICN
EDF	CODE_ASTER	F	X+	Y+	Z+	2	2.10	0.24%	0.78%	20.51%	1.29	7.23%	0.00%	9.68%	ICN
EDF	CODE_ASTER	F	X+	Y+	Z+	3	3.02	0.04%	0.57%	5.95%	1.97	0.18%	0.05%	7.97%	ICN
EDF	CODE_ASTER	F	X+	Y+	Z+	4	3.78	0.03%	7.74%	12.52%	2.29	0.08%	1.08%	21.33%	ICN
EDF	CODE_ASTER	F	X+	Y+	Z+	5	3.98	0.21%	0.18%	0.60%	2.61	0.46%	0.00%	0.12%	ICN
EDF	CODE_ASTER	F	X+	Y+	Z+	6	4.47	25.00%	0.00%	0.13%	2.89	13.67%	0.05%	0.01%	ICN
EDF	CODE_ASTER	F	X+	Y+	Z+	7	5.01	0.07%	2.22%	1.87%	3.35	0.01%	0.00%	1.54%	ICN
EDF	CODE_ASTER	F	X+	Y+	Z+	8	5.21	0.98%	47.29%	1.12%	3.47	0.03%	0.92%	6.08%	ICN
EDF	CODE_ASTER	F	X+	Y+	Z+	9	5.83	24.08%	1.33%	0.81%	3.87	0.01%	3.23%	5.77%	ICN
EDF	CODE_ASTER	F	X+	Y+	Z+	10	5.96	3.61%	0.42%	2.28%	4.13	0.84%	0.08%	0.01%	ICN
EDF	CODE_ASTER	F	X+	Y+	Z+	11	6.16	0.10%	0.01%	0.05%	4.40	4.70%	0.02%	0.18%	ICN
EDF	CODE_ASTER	F	X+	Y+	Z+	12	6.31	1.03%	1.05%	11.99%	4.82	0.83%	0.51%	2.13%	ICN
EDF		**F**				**Total**		**62.31%**	**61.62%**	**58.02%**		**30.06%**	**6.25%**	**72.33%**	**ICN**
EPFL	AKANTU	CH	X+	Y+	Z+	1	1.99	8.16%	0.03%	0.19%	1.18	0.28%	0.18%	24.05%	ICN
EPFL	AKANTU	CH	X+	Y+	Z+	2	2.09	0.27%	0.92%	23.88%	1.26	3.33%	0.10%	3.19%	ICN
EPFL	AKANTU	CH	X+	Y+	Z+	3	3.00	0.05%	0.69%	7.09%	1.90	0.16%	0.29%	8.41%	ICN
EPFL	AKANTU	CH	X+	Y+	Z+	4	3.76	0.05%	8.98%	14.37%	2.24	0.00%	0.94%	20.66%	ICN
EPFL	AKANTU	CH	X+	Y+	Z+	5	3.94	0.26%	0.28%	0.86%	2.52	0.53%	0.00%	0.10%	ICN
EPFL	AKANTU	CH	X+	Y+	Z+	6	4.44	28.88%	0.01%	0.15%	2.86	7.17%	0.02%	0.00%	ICN
EPFL	AKANTU	CH	X+	Y+	Z+	7	4.96	0.09%	1.86%	2.10%	3.22	0.08%	0.00%	1.52%	ICN
EPFL	AKANTU	CH	X+	Y+	Z+	8	5.18	1.18%	55.13%	1.44%	3.41	0.01%	0.14%	8.61%	ICN
EPFL	AKANTU	CH	X+	Y+	Z+	9	5.80	26.65%	1.61%	0.85%	3.81	0.09%	1.71%	5.88%	ICN
EPFL	AKANTU	CH	X+	Y+	Z+	10	5.92	5.36%	0.52%	2.83%	3.98	0.01%	0.01%	0.03%	ICN
EPFL	AKANTU	CH	X+	Y+	Z+	11	6.07	0.10%	0.03%	0.01%	4.30	36.75%	0.23%	0.07%	ICN
EPFL	AKANTU	CH	X+	Y+	Z+	12	6.27	1.25%	1.18%	13.89%	4.42	21.00%	0.76%	0.41%	ICN
EPFL						**Total**		**72.30%**	**71.24%**	**67.66%**		**69.41%**	**4.38%**	**72.93%**	**ICN**
COB	COBEF_MISS3D	F	X+	Z+	Y-	1	2.02	7.80%	0.00%	0.30%					ICN
COB	COBEF_MISS3D	F	X+	Z+	Y-	2	2.10	0.30%	0.90%	23.40%					ICN
COB	COBEF_MISS3D	F	X+	Z+	Y-	3	3.04	0.00%	0.60%	6.70%					ICN
COB	COBEF_MISS3D	F	X+	Z+	Y-	4	3.80	0.00%	8.80%	14.50%					ICN
COB	COBEF_MISS3D	F	X+	Z+	Y-	5	4.00	0.30%	0.20%	0.70%					ICN
COB	COBEF_MISS3D	F	X+	Z+	Y-	6	4.50	28.70%	0.00%	0.20%					ICN
COB	COBEF_MISS3D	F	X+	Z+	Y-	7	5.04	0.10%	2.20%	2.00%					ICN
COB	COBEF_MISS3D	F	X+	Z+	Y-	8	5.26	1.10%	54.50%	1.10%					ICN
COB	COBEF_MISS3D	F	X+	Z+	Y-	9	5.87	28.00%	1.30%	0.90%					ICN
COB	COBEF_MISS3D	F	X+	Z+	Y-	10	6.01	4.00%	0.60%	2.30%					ICN
COB	COBEF_MISS3D	F	X+	Z+	Y-	11	6.19	0.10%	0.00%	0.00%					ICN
COB	COBEF_MISS3D	F	X+	Z+	Y-	12	6.37	1.00%	1.50%	14.10%					ICN
COB						**Total**		**71.40%**	**70.60%**	**66.20%**		**0.00%**	**0.00%**	**0.00%**	**ICN**

Table 3 Natural Frequencies, effective participating masses, fluid-structure methods (continued)
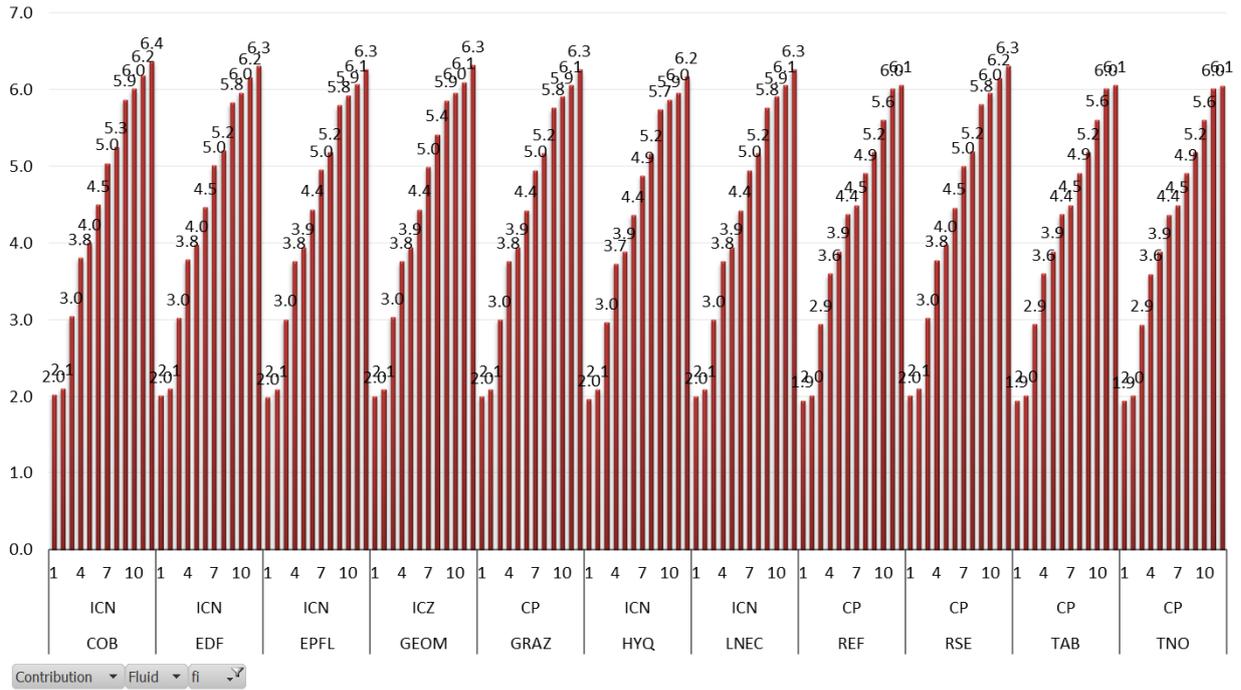
Figure 4 Natural Frequencies (Hz) – Empty Reservoir
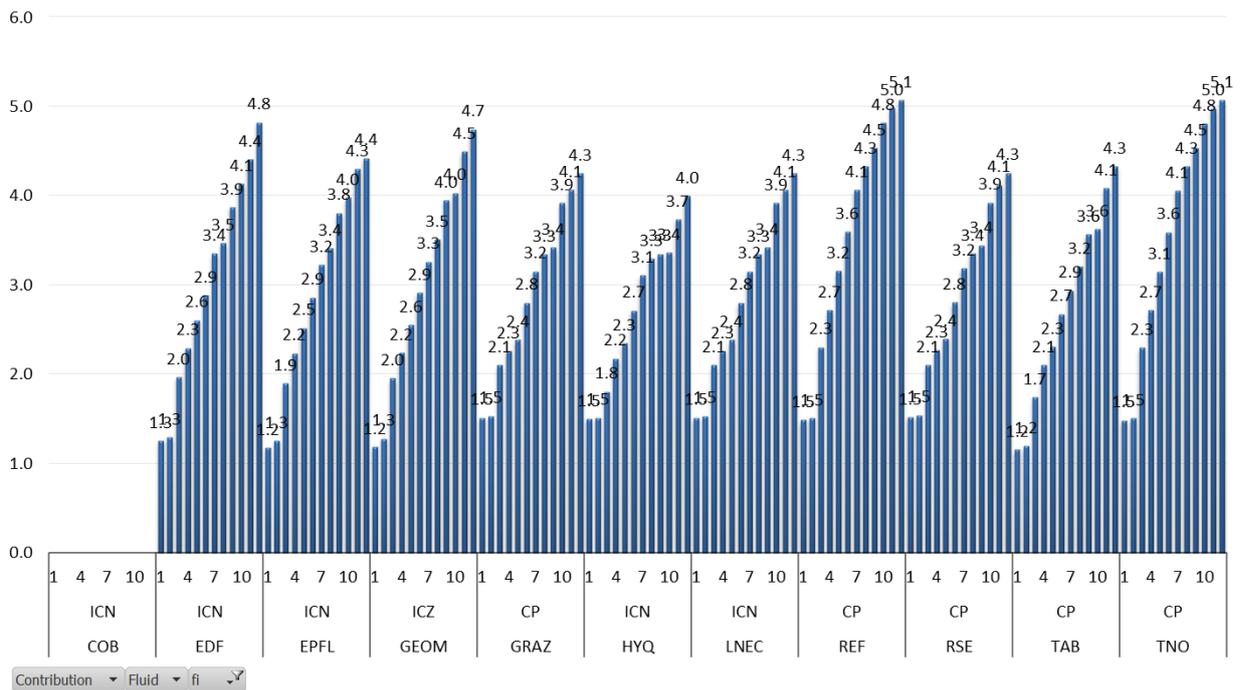
Figure 5 Natural Frequencies (Hz) – Full Reservoir

In general, an excellent agreement between the eigenvalues is observed for the empty reservoir case. The full reservoir condition leads to a slight dispersion between eigenvalues.

Table 2 shows that modes 2, 6, and 7/8 remain dominate in the X, Y and Z directions respectively. The transfer functions produced by some contributors (refer to the papers individually) also substantiates these findings indicating the importance of higher order modes and their contributions in relation to the response spectra provided in the problem statement and

guidelines/Standards and the directional movement.
The reference solution mode shapes are also presented in Figure 6.
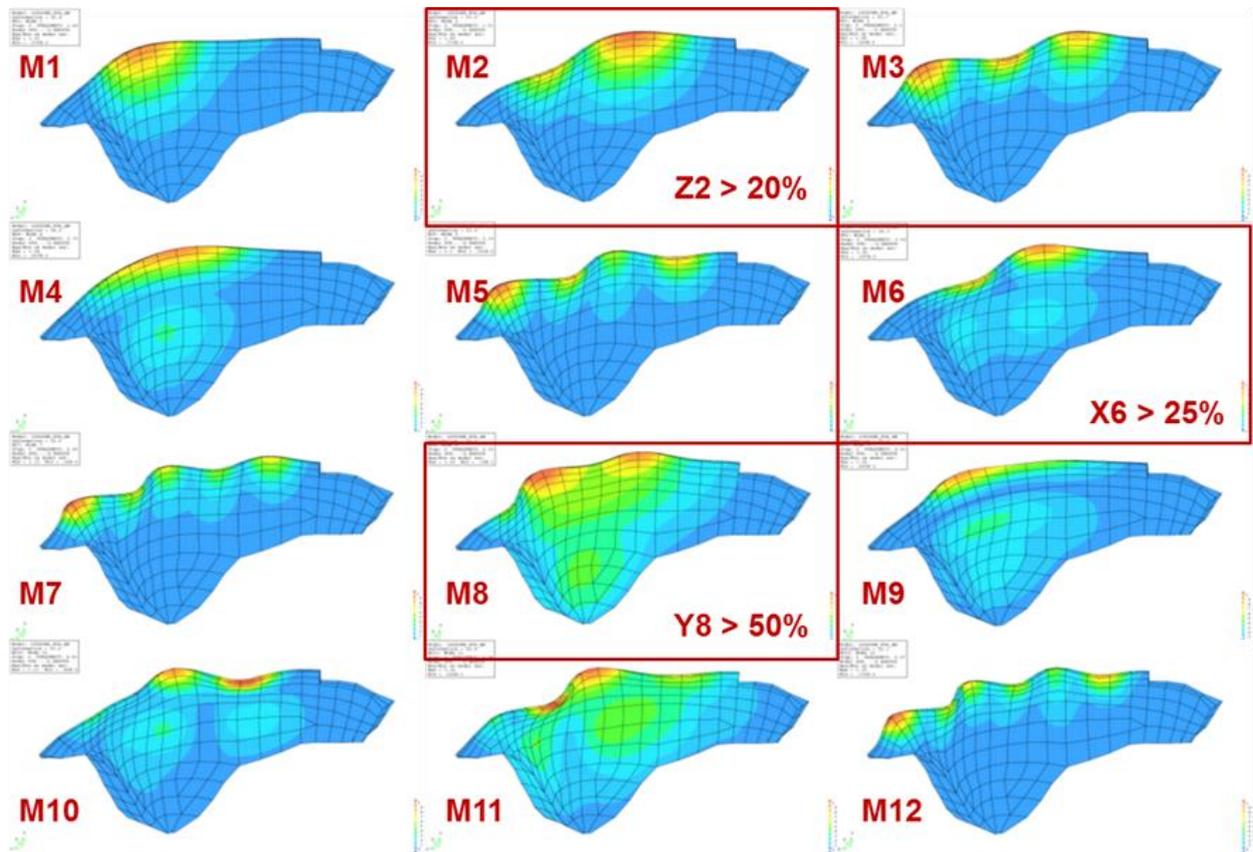
Figure 6 Reference Solution Mode Shapes with the maximum effective participating masses

Displacements

1) Displacement Time Histories [D]

The contributors were asked to present the radial displacement (Z component) time histories at the crown crest section of the dam (for point with X=0, Y=1609, Z=-29.145) for the investigated dynamic combinations (the displacements due to self-weight should be set to zero). The figure below presents the results for those contributors (six) who performed the exercise.
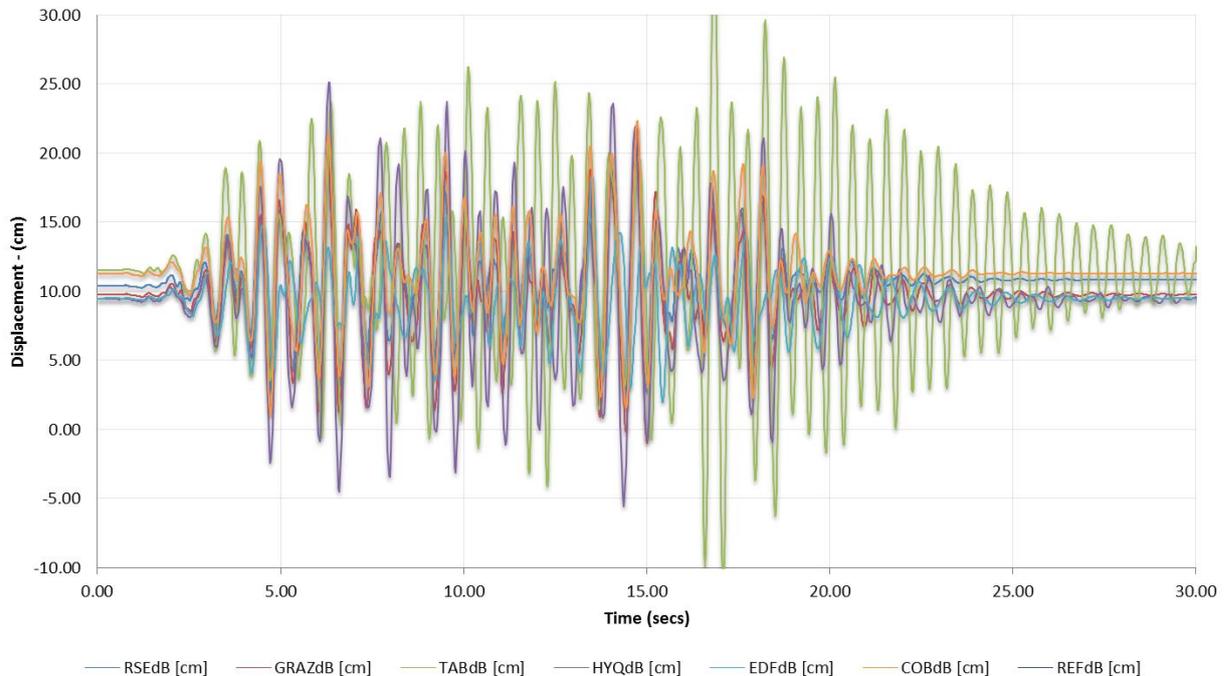
Figure 7 Radial displacement time-histories (seismic load case MCE 1) Point B (crown-crest section)

With the exception of two results, the pics and troughs for the remaining contributors occur at the same time and with similar magnitudes. The amplification factor of the base acceleration at the crest is approximately 10 which may be considered rather high for this structure without taking into consideration any foundation-structure interaction (massless foundation applied in benchmark studies).

2) Displacement Envelopes at Cross Sections [C]

The contributors were asked to produce the minimum and the maximum radial displacement envelopes, as well as the static load displacements (without self-weight) for the centrelines of Cross Section 1 (Crown), Cross Section 2 (Left Bank) and Cross Section 3 (Right Bank). The comparison between the results is given below.

For the static load cases, the correspondence between the results is excellent. Dynamic results are however less obvious to evaluate and present a greater dispersion in the upper 50 m height of the dam. The difference between the maximum and minimum responses for the crown section alone, eliminating the contributor TAB, indicate almost a 30% discrepancy for the crown-crest section. The same affirmation can be made for the results presented in Figure 7. Possible explanations for the difference might be attributed to the FE type used by COB for the reservoir, dynamic boundary conditions or the degree of mesh refinement (e.g. HYQ).

More about contributor specific analysis techniques and evaluations is presented below.
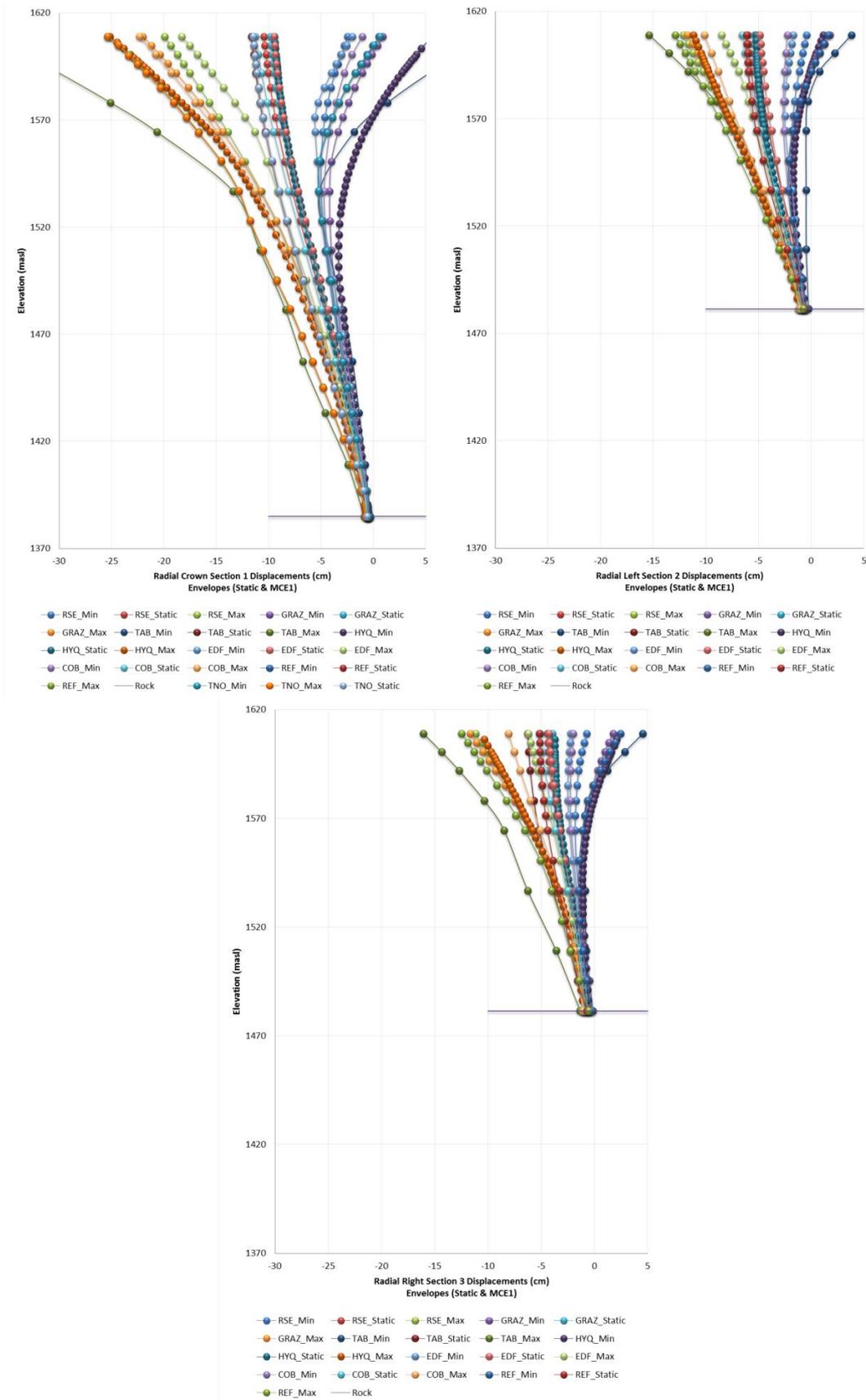
Figure 8 Radial Displacement Envelopes (Static + MCE 1) for Sections 1 (Crown), 2 (Left) and 3 (Right)

Stresses

The following sign convention for stresses shall be used: compressive stresses have a negative value and tensile stresses have a positive value.

3) Stress Envelopes on U/S and D/S Faces [E]

In order to evaluate qualitatively the obtained results, it was asked to present the envelopes of the computed maximum and the minimum principal stresses for the upstream and for the downstream faces of the dam. The stress envelopes should contain the maxima / the minima obtained from all the investigated dynamic load combinations.

Due to the large variation of received principal stress envelope data and the fact that many contributors performed a variety of linear and non-linear seismic analyses, only the results for the reference solution (equal to TNO results) are provided below. It is recommended that for a qualitative comparison, the results below are compared with those given in the papers and for a quantitative evaluation, the reader refers to the comparison of the hoop and vertical stresses per contributor as given in the next chapter.
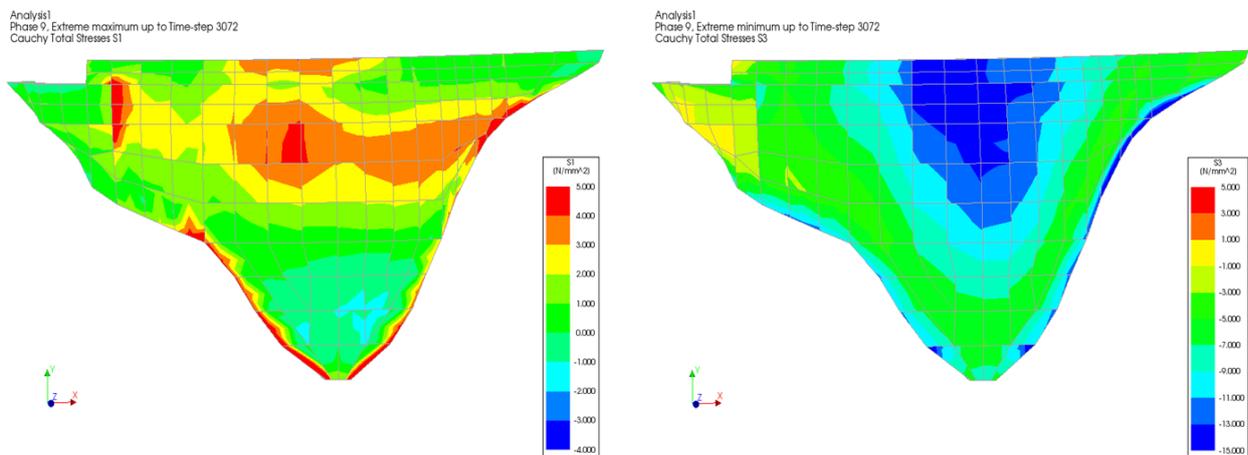
Figure 9 Maximum (Left) and minimum (Right) upstream principal stress (MPa) envelopes for MCE 1
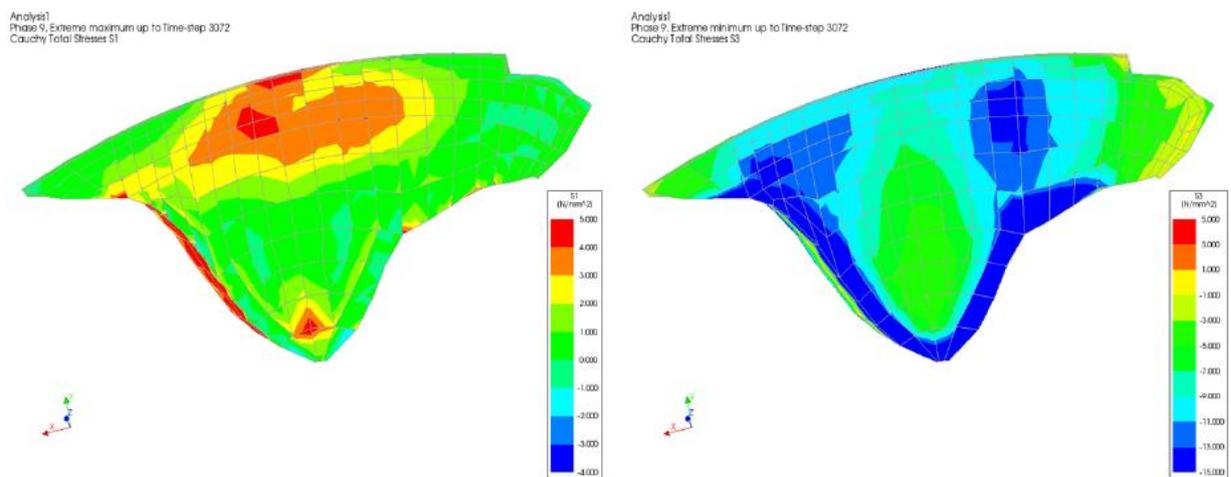
Figure 10 Maximum (Left) and minimum (Right) downstream principal stress (MPa) envelopes for MCE 1

4) Stress Envelopes at Cross Sections [F]

Envelopes of the minimum and maximum hoop and cantilever (vertical) stresses on the upstream and on the downstream lines of Cross Section 1 (Crown), Cross Section 2 (Left Bank) and Cross Section 3 (Right Bank) were requested. The comparison of results is given below.
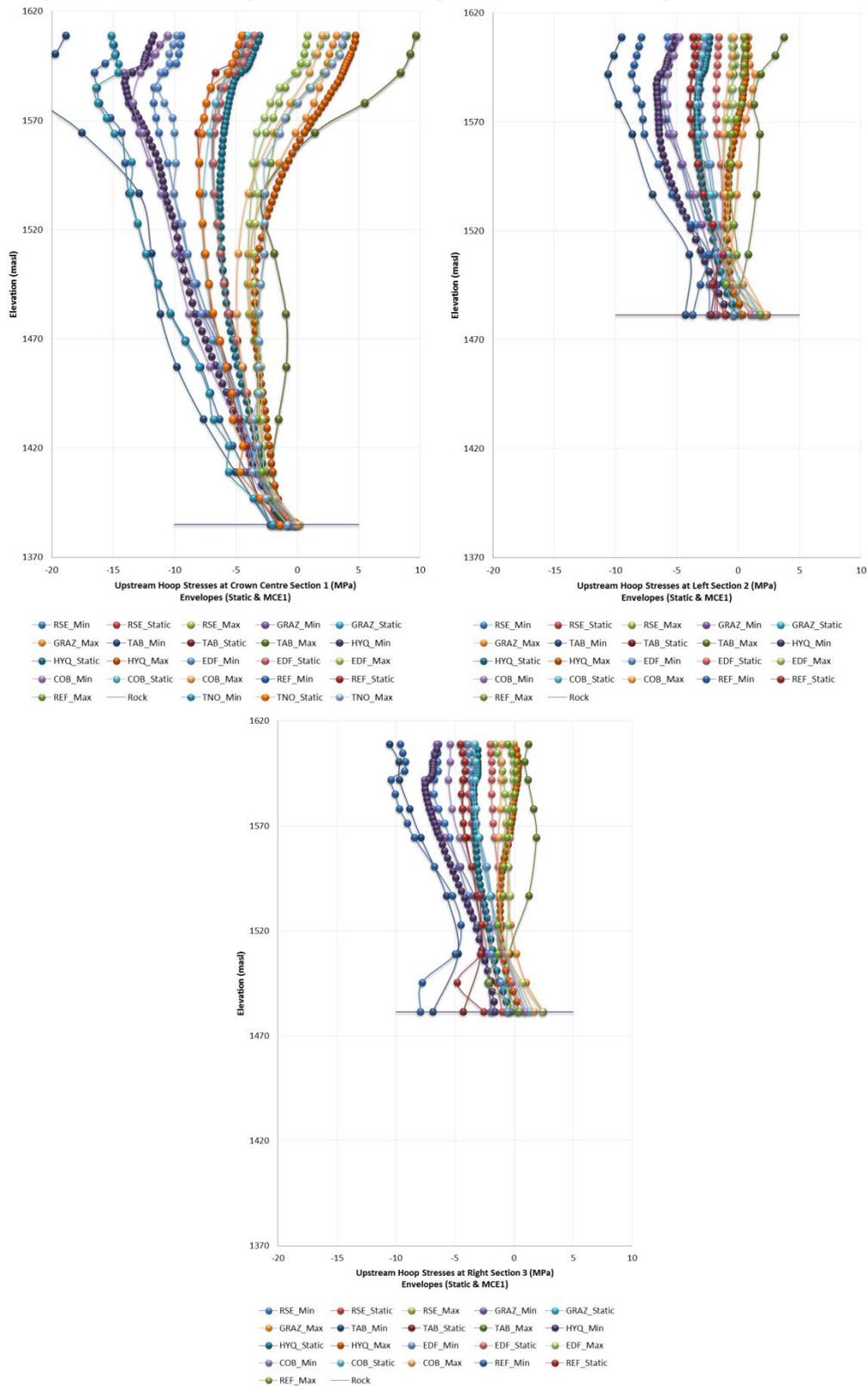
Figure 11 Upstream Hoop Stresses (MPa) (Static + MCE 1) for Sections 1 (Crown), 2 (Left) and 3 (Right)
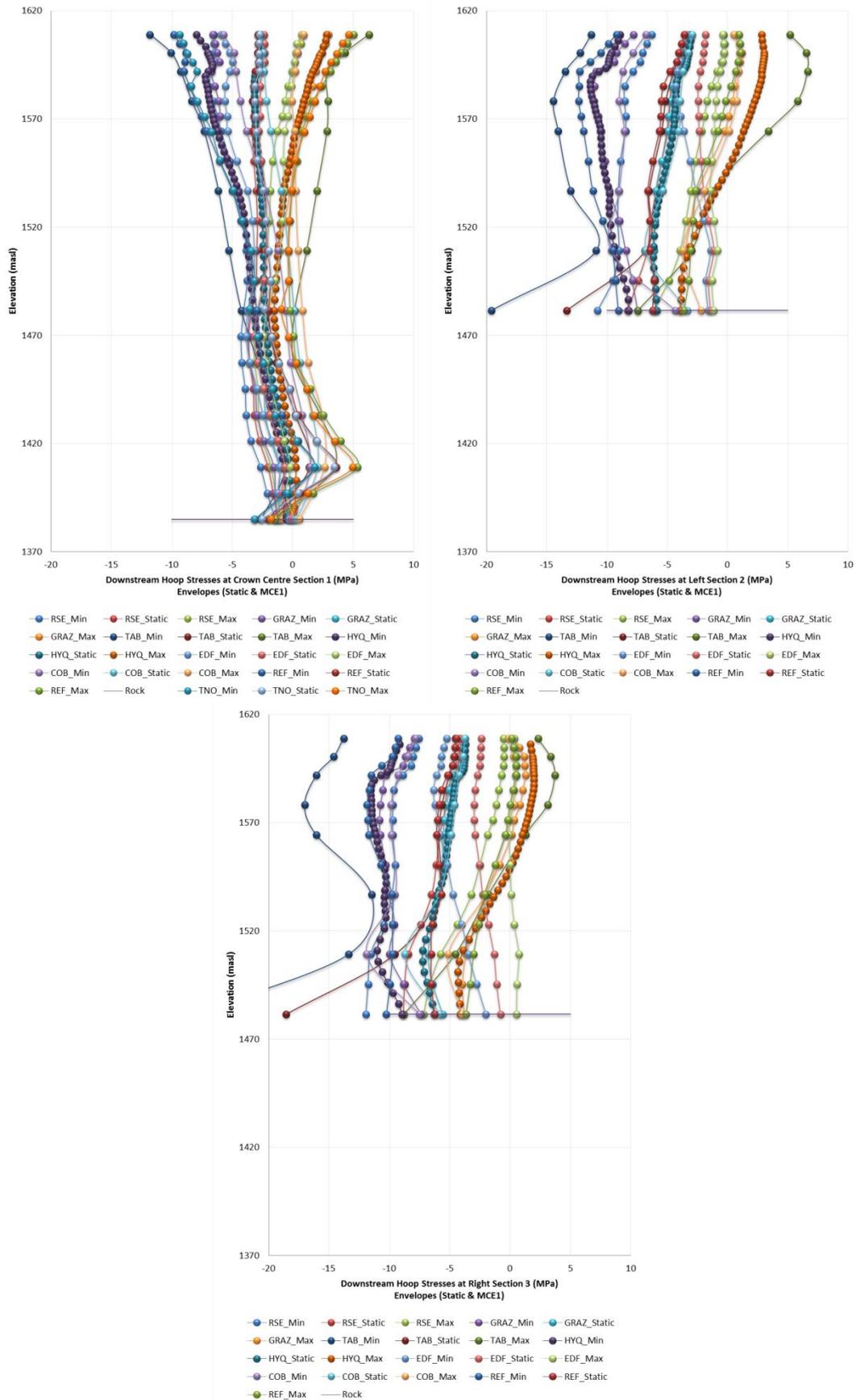
Figure 12 Downstream Hoop Stresses (Static + MCE 1) for Sections 1 (Crown), 2 (Left) and 3 (Right)
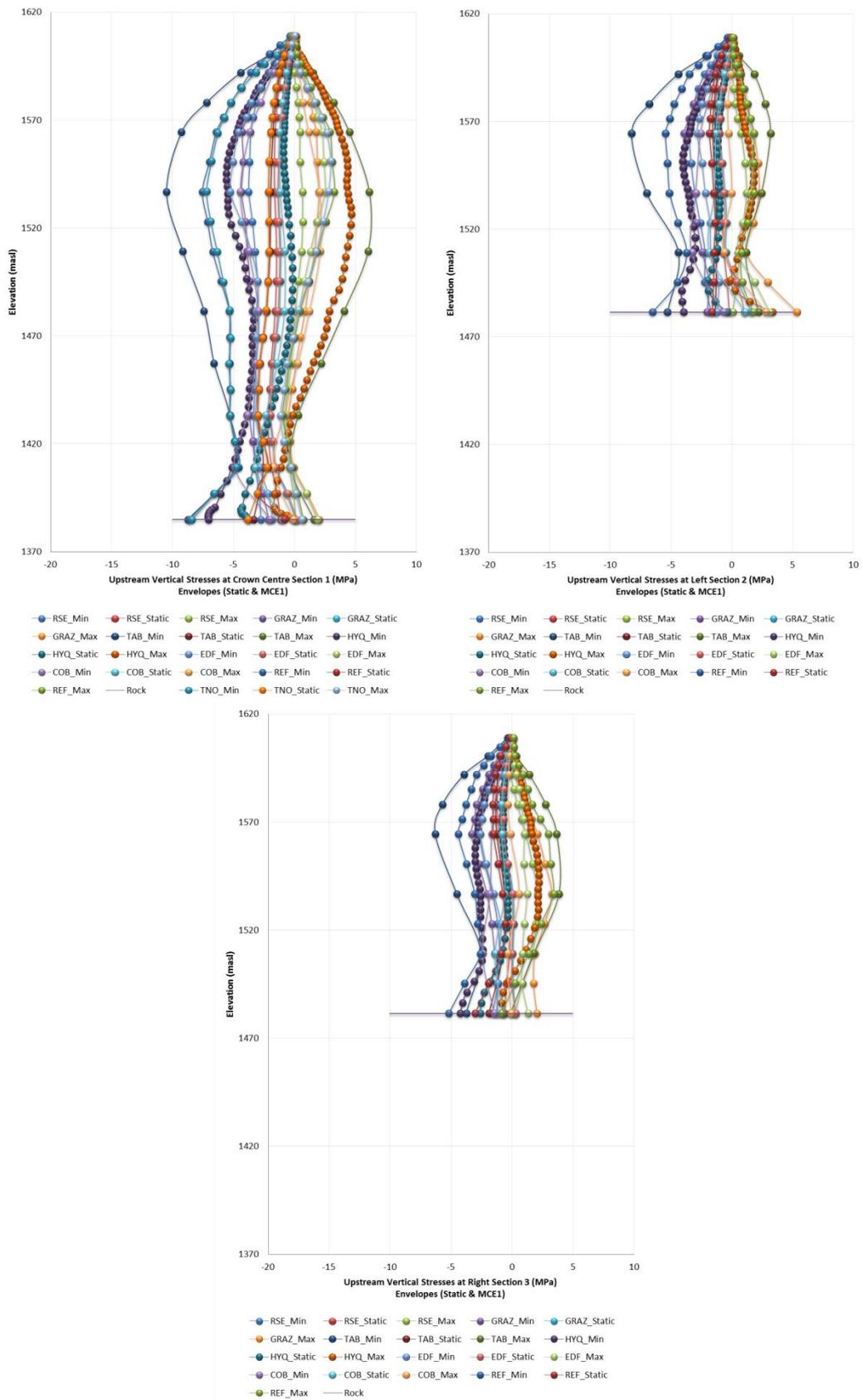
Figure 13 Upstream Vertical Stresses (MPa) (Static + MCE 1) for Sections 1 (Crown), 2 (Left) and 3 (Right)
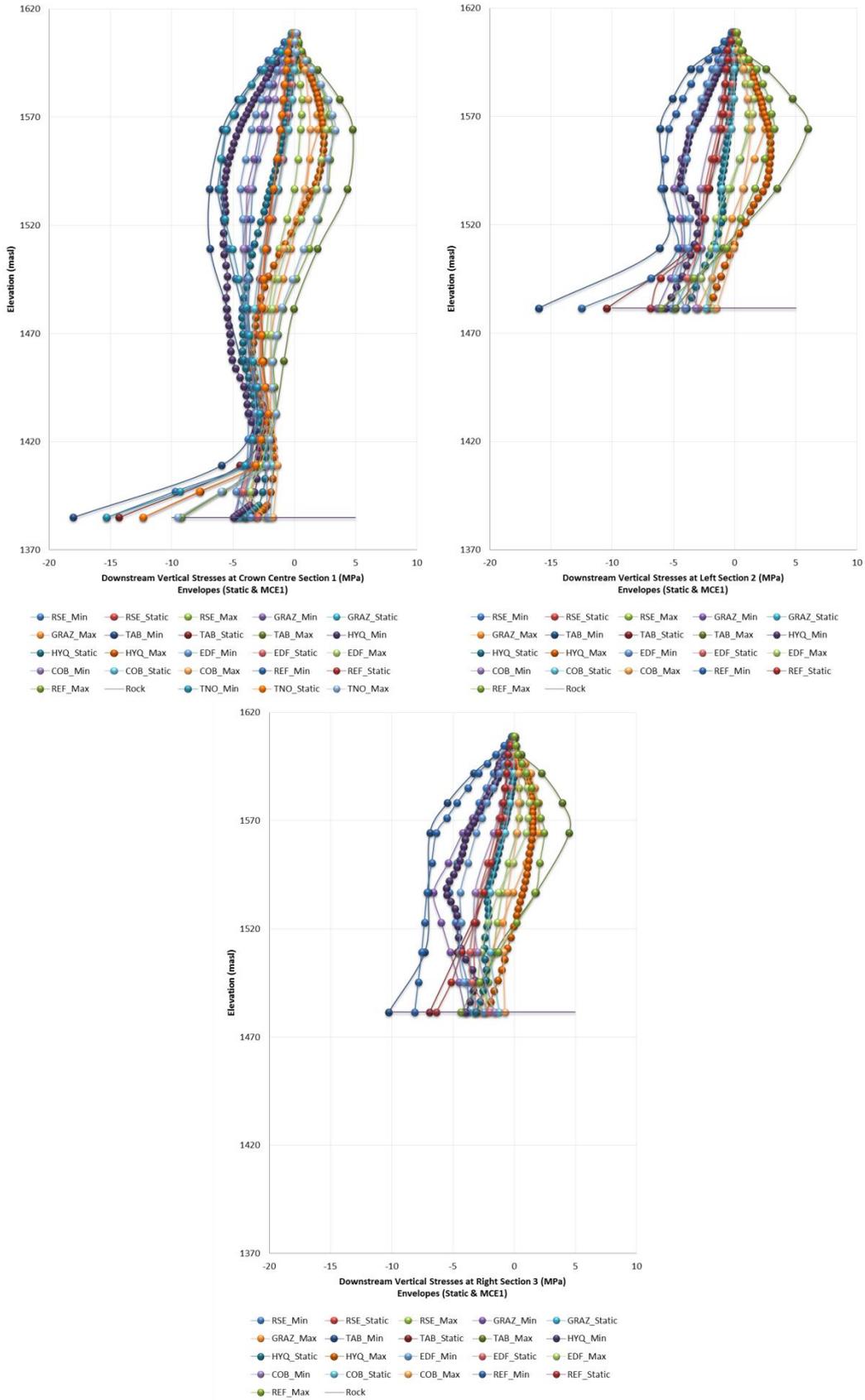
Figure 14 Downstream Vertical Stresses (MPa) (Static + MCE 1) for Sections 1 (Crown), 2 (Left) and 3 (Right)

5) Stress Values at Selected Points [G]

The participants were asked to present the maxima and the minima of the computed stresses at selected characteristic points on the dam faces. Ten points were chosen to capture the critical numerical issues related to such structures (singularities, foundation-dam contact, etc.) and other points to allow an undistorted comparison of the results which are represented below.

Figure 15 Static Principal Stresses – Upstream/Downstream Points A, A' to C, C' (MPa)

Figure 16 Static Principal Stresses – Upstream/Downstream Points D, D' to G, G' (MPa)

	H	I	J	H	I	J	H	I	J	H	I	J	H	I	J	H	I	J	H	I	J	H	I	J	H	I	J	H	I	J	H	I	J
		COB			EDF			EPFL			GEOM			GRAZ			HYQ			LNEC			REF			RSE			TAB			TNO	
SU0_S1	1.4	0.9	-1.	3.4	2.6	-0.	0.7	0.2	-0.	1.3	1.2	-1.	3.5	2.8	-1.	3.1	2.1	-2.	2.7	2.1	-0.	2.7	1.8	-1.	0.0	-0.	-1.	2.6	1.9	-1.	3.8	2.6	-1.
SU0_S3	2.7	-1.	-3.	-0.	-0.	-3.	-1.	-1.	-2.	-0.	-0.	-2.	-0.	-0.	-3.	-1.	-3.	-3.	-0.	-0.	-3.	-4.	-7.	-4.	-1.	-1.	-2.	-3.	-6.	-3.	-3.	-6.	-4.
SU2_S1				2.9	1.6	-1.	0.6	-0.	-1.	1.4	1.0	-1.	3.0	1.7	-1.	2.7	1.5	-2.	2.4	1.6	-0.	2.2	1.1	-1.	0.1	-0.	-1.	2.1	1.3	-2.	3.0	1.8	-1.
SU2_S3				-0.	-0.	-3.	-1.	-1.	-2.	-0.	-0.	-2.	-1.	-3.	-3.	-0.	-0.	-3.	-4.	-7.	-4.	-1.	-1.	-2.	-3.	-6.	-3.	-3.	-6.	-4.			

Contribution ▼ Point ↗

	H'	I'	J'	H'	I'	J'	H'	I'	J'	H'	I'	J'	H'	I'	J'	H'	I'	J'	H'	I'	J'	H'	I'	J'	H'	I'	J'	H'	I'	J'	H'	I'	J'
		COB			EDF			EPFL			GEOM			GRAZ			HYQ			LNEC			REF			RSE			TAB			TNO	
SU0_S1	-1.	-0.	-2.	-0.	-0.	1.5	-0.	-0.	0.8	-1.	-1.	1.2	-0.	0.1	1.3	-1.	-0.	1.7	-0.	-0.	1.3	0.7	1.2	5.5	-0.	-0.	0.0	0.5	0.5	3.8	0.6	1.3	5.2
SU0_S3	-7.	-6.	2.1	-10	-8.	-2.	-8.	-7.	-3.	-4.	-4.	-3.	-11	-9.	-2.	-11	-10	-1.	-11	-9.	-2.	-24	-25	-2.	-9.	-8.	-2.	-19	-20	-4.	-24	-23	-3.
SU2_S1				-0.	-0.	0.1	-0.	-0.	-0.	-2.	-2.	-0.	-0.	0.0	0.1	-1.	-0.	0.0	-1.	-0.	-0.	0.5	1.1	3.7	-0.	-0.	-0.	0.3	0.4	2.2	0.3	1.3	3.5
SU2_S3				-11	-10	-3.	-8.	-7.	-3.	-5.	-5.	-3.	-11	-10	-3.	-11	-10	-2.	-12	-10	-3.	-24	-26	-3.	-9.	-9.	-3.	-19	-21	-4.	-24	-24	-3.

Contribution ▼ Point ↗

Figure 17 Static Principal Stresses – Upstream/Downstream Points H, H' to J, J' (MPa)

	D	E	F	G	D	E	F	G	D	E	F	G	D	E	F	G	D	E	F	G	D	E	F	G	D	E	F	G	D	E	F	G	D	E	F	G	D	E	F	G	D	E	F	G
		CO	B			ED	F			EP	FL			GE	OM			GR	AZ			HY	Q			LN	EC			RE	F			RS	E			TA	B			TN	O	
MCE1_S1	1.	0.	2.	5.	2.	2.	1.	3.	1.	1.	0.	1.	4.	4.	0.	4.	2.	2.	1.	7.	3.	2.	3.	7.	1.	0.	1.	6.	4.	3.	3.	5.	1.	1.	1.	1.	4.	6.	1.	8.	3.	2.	2.	5.
MCE1_S3	-9	-8	-1	-2	-8	-7	-1	-2	-5	-5	-1	-1	-7	-8	-2	-3	-1	-9	-3	-5	-1	-9	-3	-6	-1	-1	-5	-7	-1	-1	-5	-9	-9	-9	-2	-6	-1	-1	-4	-1	-1	-1	-5	-9
MCE2_S1	1.	0.	2.	4.	1.	2.	1.	3.	1.	1.	0.	1.	3.	4.	0.	5.	2.	2.	2.	6.	2.	3.	3.	5.	1.	0.	1.	6.	2.	2.	3.	4.	0.	1.	0.	1.	4.	3.	1.	7.	2.	2.	3.	4.
MCE2_S3	-9	-9	-1	-3	-7	-8	-1	-2	-5	-5	-1	-1	-6	-7	-2	-2	-9	-1	-3	-4	-9	-9	-2	-4	-1	-9	-5	-6	-1	-1	-4	-9	-8	-9	-2	-6	-1	-1	-3	-1	-1	-1	-4	-9
MCE3_S3	-9	-8	-0	-2	-7	-8	-1	-2	-5	-5	-1	-1	-6	-8	-2	-3	-1	-9	-3	-6	-1	-8	-2	-5	-1	-1	-4	-5	-1	-1	-5	-8	-9	-8	-2	-6	-1	-1	-4	-1	-1	-1	-5	-9
MCE3_S1	0.	0.	1.	4.	1.	1.	1.	3.	1.	1.	1.	2.	4.	3.	0.	4.	1.	1.	1.	7.	2.	1.	3.	7.	1.	1.	2.	6.	3.	2.	3.	5.	0.	0.	1.	1.	4.	3.	2.	9.	2.	1.	2.	5.

Contribution ▾ Point ⟋

	A'	B'	C'	A'	B'	C'	A'	B'	C'	A'	B'	C'	A'	B'	C'	A'	B'	C'	A'	B'	C'	A'	B'	C'	A'	B'	C'	A'	B'	C'	A'	B'	C'
		COB			EDF			EPFL			GEOM			GRAZ			HYQ			LNEC			REF			RSE			TAB			TNO	
MCE1_S1	0.8	0.9	0.2	0.1	0.8	0.1	0.2	0.6	0.2	3.7	4.5	3.3	0.9	3.1	0.7	3.2	3.1	1.9	0.8	0.9	0.1	1.3	5.1	0.4	0.4	1.1	0.3	5.8	6.3	2.7	0.8	4.7	0.4
MCE1_S3	-6.	-5.	-7.	-5.	-5.	-6.	-2.	-2.	-3.	-7.	-9.	-8.	-7.	-6.	-8.	-9.	-8.	-9.	-6.	-8.	-9.	-9.	-9.	-9.	-6.	-6.	-7.	-11	-11	-13	-8.	-9.	-9.
MCE2_S1	1.5	0.8	0.8	0.1	1.0	0.1	0.1	0.9	0.2	1.9	3.4	2.2	1.7	2.1	0.5	1.7	3.3	0.9	0.8	0.7	0.5	2.3	4.3	0.7	0.6	0.6	0.2	2.8	7.3	2.2	1.6	4.1	0.6
MCE2_S3	-6.	-5.	-7.	-5.	-6.	-6.	-2.	-2.	-3.	-7.	-7.	-7.	-7.	-6.	-7.	-8.	-7.	-8.	-6.	-7.	-8.	-8.	-8.	-8.	-6.	-6.	-6.	-9.	-11	-11	-8.	-8.	-8.
MCE3_S3	-6.	-5.	-7.	-6.	-6.	-6.	-2.	-2.	-3.	-7.	-7.	-8.	-7.	-7.	-8.	-7.	-6.	-7.	-5.	-7.	-9.	-8.	-9.	-9.	-6.	-7.	-7.	-12	-9.	-13	-7.	-9.	-9.
MCE3_S1	0.3	0.1	0.0	0.2	1.7	0.1	0.1	1.6	0.1	2.1	2.6	2.1	1.0	3.8	0.9	1.2	2.0	1.2	0.4	0.2	0.0	0.8	5.5	0.6	0.2	1.5	0.2	5.2	3.5	4.9	0.9	4.3	0.6

Contribution ▾ Point ⟋

Figure 18 Dynamic Principal Stresses – Upstream/Downstream Points A, A' – C, C' (MPa)

Figure 19 Dynamic Principal Stresses – Upstream/Downstream Points D, D' to G, G' (MPa)

|	H	I	J	H	I	J	H	I	J	H	I	J	H	I	J	H	I	J	H	I	J	H	I	J	H	I	J	H	I	J	H	I	J
		COB			EDF			EPFL			GEOM			GRAZ			HYQ			LNEC			REF			RSE			TAB			TNO	
MCE1_S1	4.4	2.8	0.0	4.1	2.9	-0.	1.7	0.9	-0.	3.6	3.5	0.7	8.0	4.5	-0.	6.1	4.1	-1.	6.6	4.4	1.6	6.7	3.4	0.0	0.6	0.8	-0.	5.0	3.4	-0.	4.9	3.1	0.0
MCE1_S3	-0.	-1.	-4.	-0.	-1.	-3.	-1.	-1.	-2.	-1.	-1.	-3.	-2.	-2.	-3.	-4.	-4.	-5.	-3.	-2.	-3.	-9.	-13	-5.	-3.	-2.	-3.	-7.	-10	-5.	-8.	-10	-5.
MCE2_S1	4.7	2.9	0.0	4.4	3.0	-0.	1.9	0.7	-0.	3.5	2.8	0.1	6.4	4.4	0.1	5.0	4.4	-1.	7.5	4.2	1.5	7.0	3.4	0.1	0.5	0.8	-0.	4.3	2.9	-0.	4.7	3.4	0.1
MCE2_S3	-0.	-1.	-4.	-0.	-1.	-3.	-1.	-1.	-2.	-1.	-1.	-3.	-1.	-2.	-3.	-3.	-4.	-5.	-2.	-2.	-4.	-8.	-12	-5.	-2.	-2.	-3.	-7.	-10	-5.	-7.	-11	-5.
MCE3_S3	-0.	-1.	-4.	-0.	-1.	-3.	-1.	-1.	-2.	-1.	-1.	-3.	-3.	-2.	-3.	-4.	-4.	-4.	-2.	-2.	-3.	-8.	-14	-5.	-2.	-2.	-3.	-7.	-10	-5.	-7.	-11	-5.
MCE3_S1	3.9	2.8	0.0	3.9	3.2	-0.	2.0	0.8	-0.	2.9	2.7	-0.	7.4	4.4	-0.	6.9	3.7	-1.	5.3	4.0	0.9	7.4	3.9	0.1	0.6	1.0	-0.	5.5	3.2	-0.	5.1	3.2	0.1

Contribution ▾ Point ↗

	H'	I'	J'	H'	I'	J'	H'	I'	J'	H'	I'	J'	H'	I'	J'	H'	I'	J'	H'	I'	J'	H'	I'	J'	H'	I'	J'	H'	I'	J'	H'	I'	J'
		COB			EDF			EPFL			GEOM			GRAZ			HYQ			LNEC			REF			RSE			TAB			TNO	
MCE1_S1	0.0	0.0	2.6	-0.	-0.	0.1	-0.	-0.	0.1	-0.	-0.	-0.	-0.	0.0	0.2	-0.	-0.	0.6	-0.	-0.	-0.	4.9	2.7	5.5	-0.	0.0	-0.	1.1	1.0	4.8	1.0	2.2	5.0
MCE1_S3	-9.	-8.	-2.	-8.	-9.	-4.	-8.	-7.	-3.	-6.	-8.	-4.	-15	-14	-4.	-16	-15	-3.	-16	-15	-4.	-37	-39	-4.	-13	-12	-4.	-28	-30	-6.	-34	-34	-4.
MCE2_S1	0.0	0.0	2.8	-0.	-0.	0.1	-0.	-0.	0.1	-1.	-1.	-0.	-0.	0.0	0.2	-0.	-0.	0.5	-0.	-0.	-0.	4.8	2.6	5.4	-0.	0.1	-0.	1.0	0.9	4.3	0.8	2.2	4.9
MCE2_S3	-9.	-9.	-2.	-8.	-9.	-4.	-8.	-7.	-3.	-7.	-7.	-4.	-15	-14	-4.	-15	-14	-3.	-17	-13	-4.	-35	-37	-4.	-13	-12	-4.	-25	-29	-6.	-31	-32	-4.
MCE3_S3	-8.	-8.	-2.	-8.	-8.	-4.	-8.	-7.	-3.	-6.	-7.	-4.	-16	-13	-4.	-15	-13	-3.	-15	-13	-4.	-37	-38	-4.	-12	-12	-4.	-28	-33	-6.	-34	-33	-4.
MCE3_S1	0.0	0.0	2.5	-0.	-0.	0.1	-0.	-0.	-0.	-1.	-1.	-0.	-0.	0.0	0.2	-0.	-0.	0.4	-0.	-0.	-0.	5.1	2.6	5.6	-0.	0.0	-0.	1.2	1.0	4.4	1.0	2.2	5.1

Contribution ▾ Point ↗

Figure 20 Dynamic Principal Stresses – Upstream/Downstream Points H, H' – J, J' (MPa)

6) Stress Time Histories [H]

Is was also requested to present the time histories of the maximum and minimum principal stresses at Points D, E, D' and E'. The comparison between results is given below. It is noted that COB results start from a different static stress values, hence the negative stress shift in time-histories.
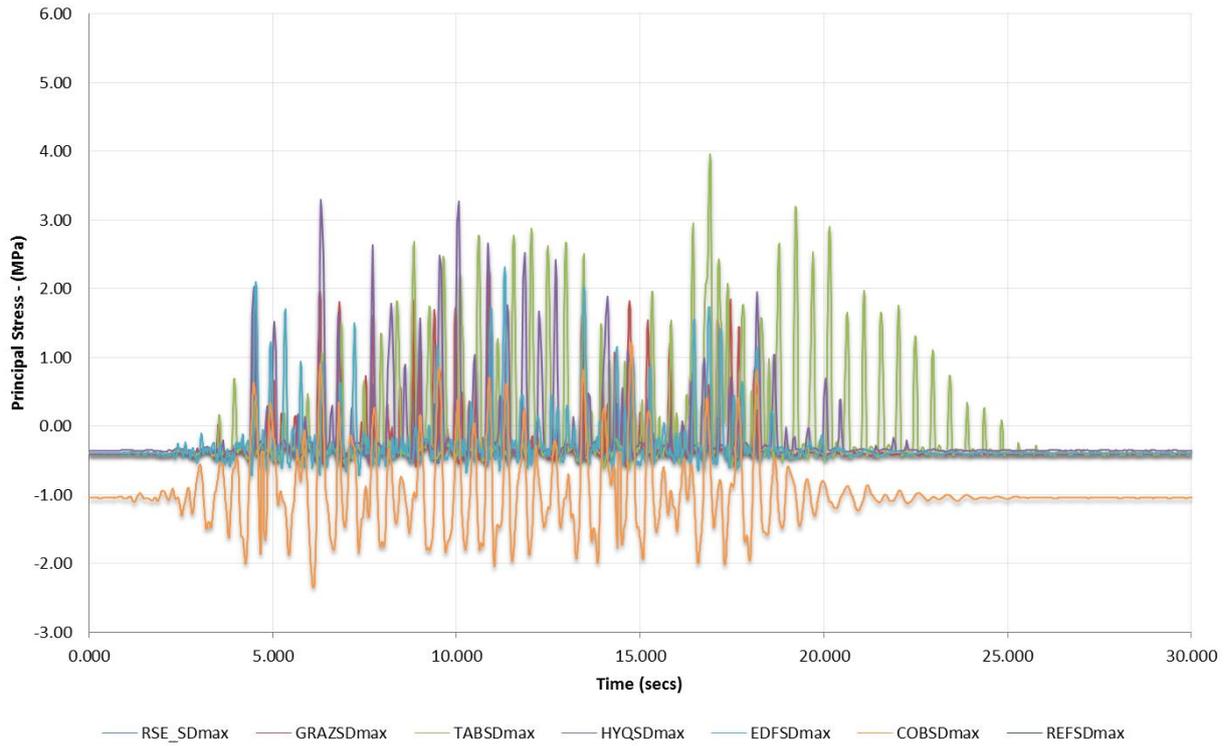
Figure 21 Maximum Principal Stress Time-History (MCE 1) for Point D
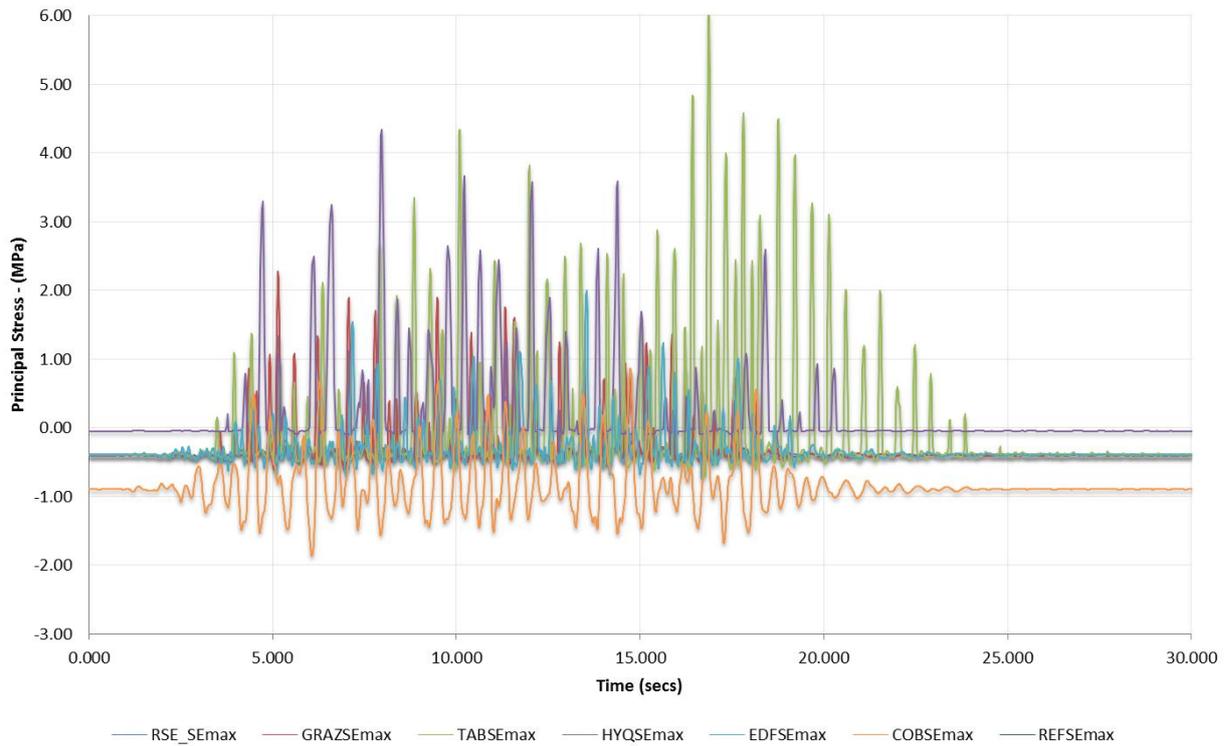
Figure 22 Maximum Principal Stress Time-History (MCE 1) for Point E
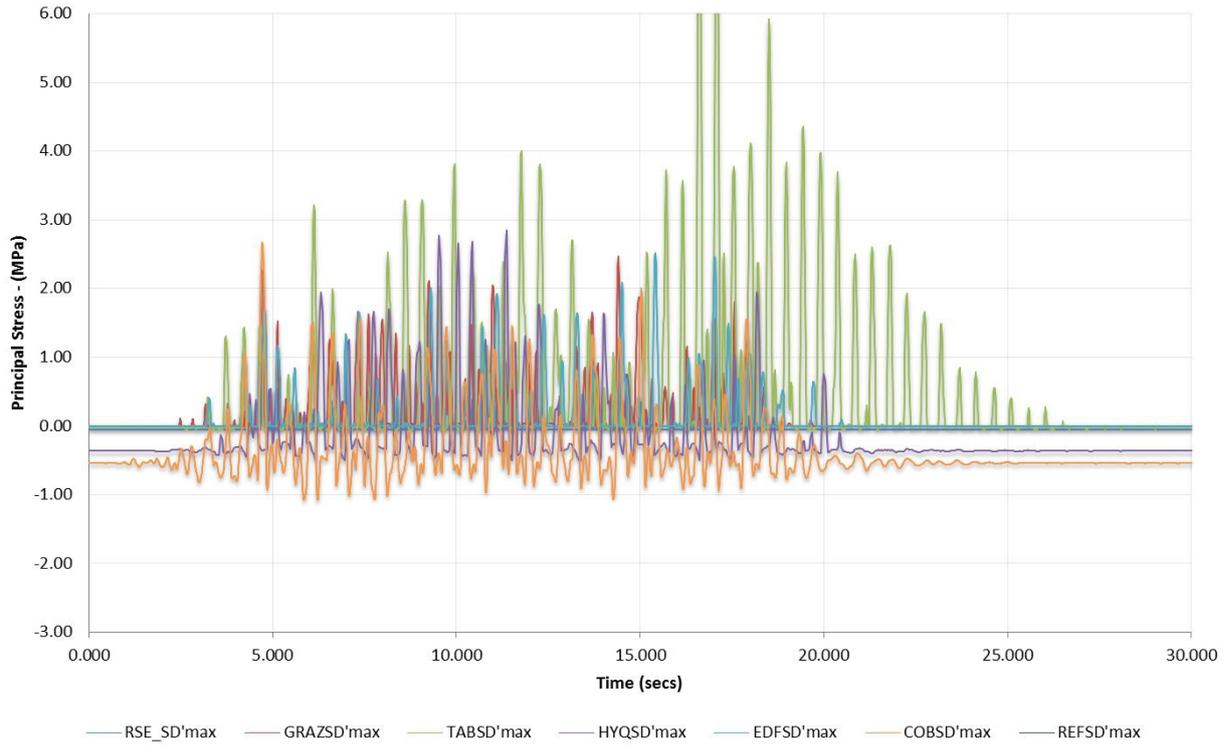
Figure 23 Maximum Principal Stress Time-History (MCE 1) for Point D'
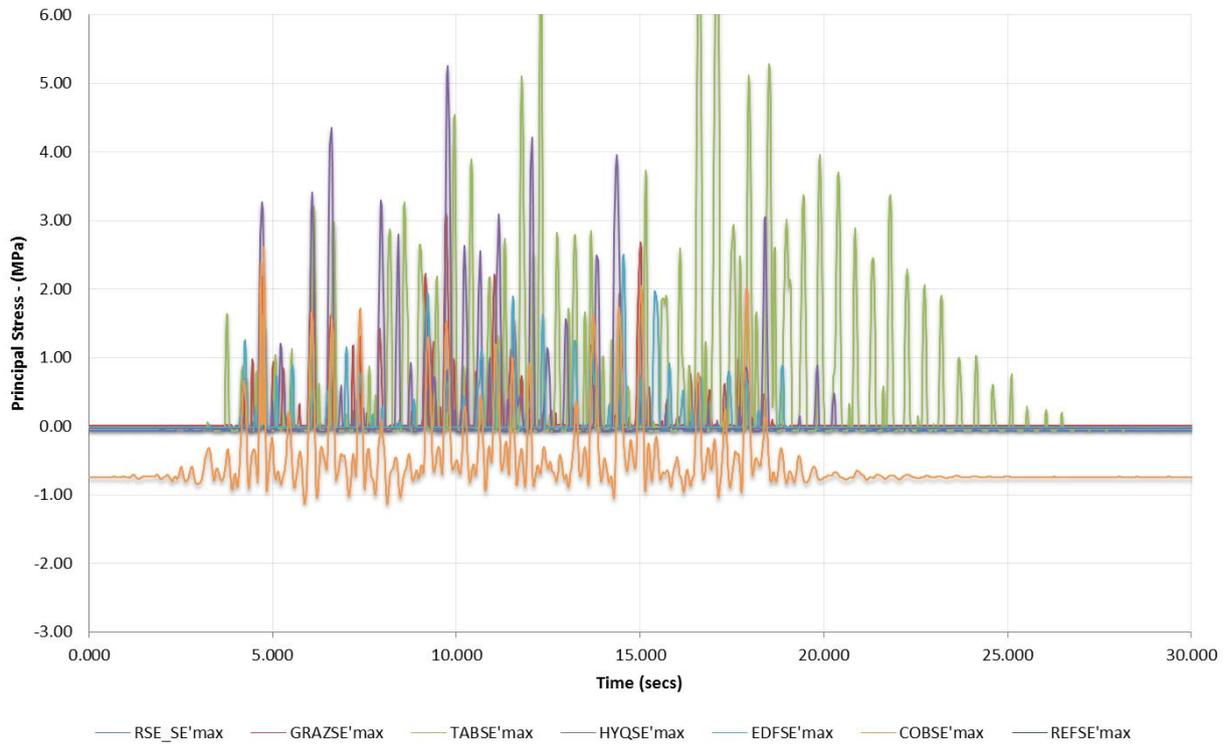
Figure 24 Maximum Principal Stress Time-History (MCE 1) for Point E'
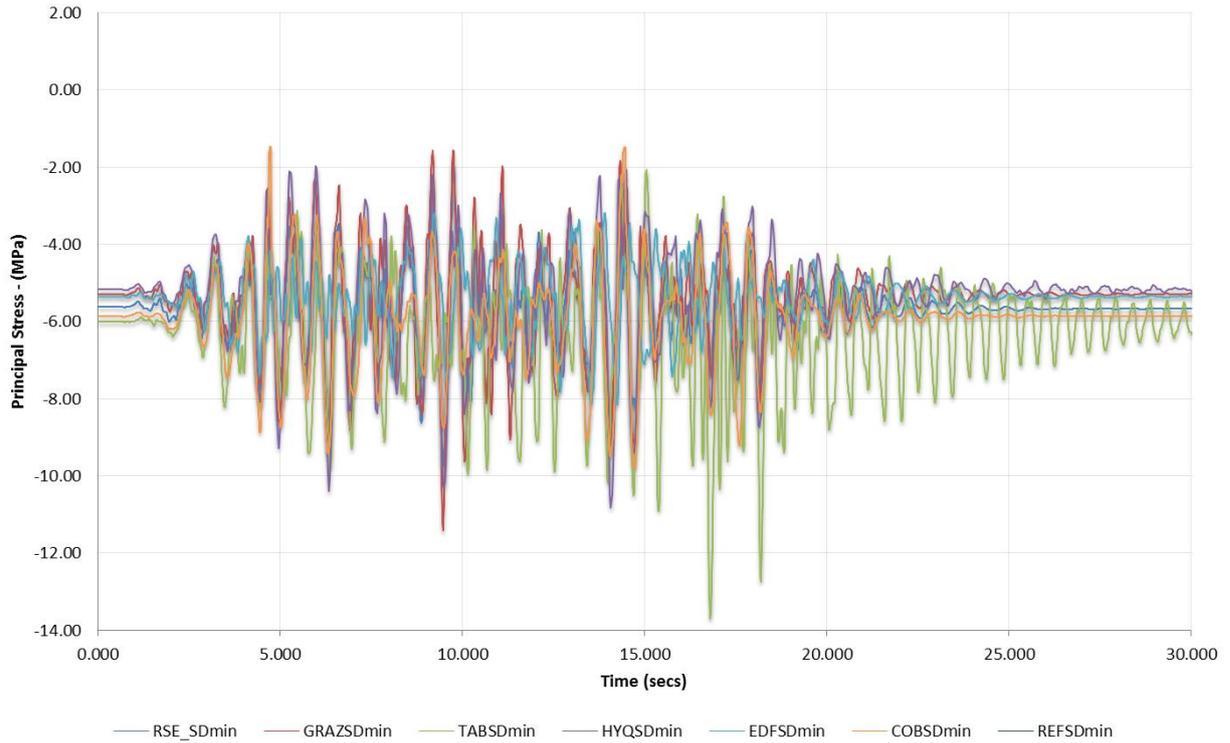
Figure 25 Minimum Principal Stress Time-History (MCE 1) for Point D
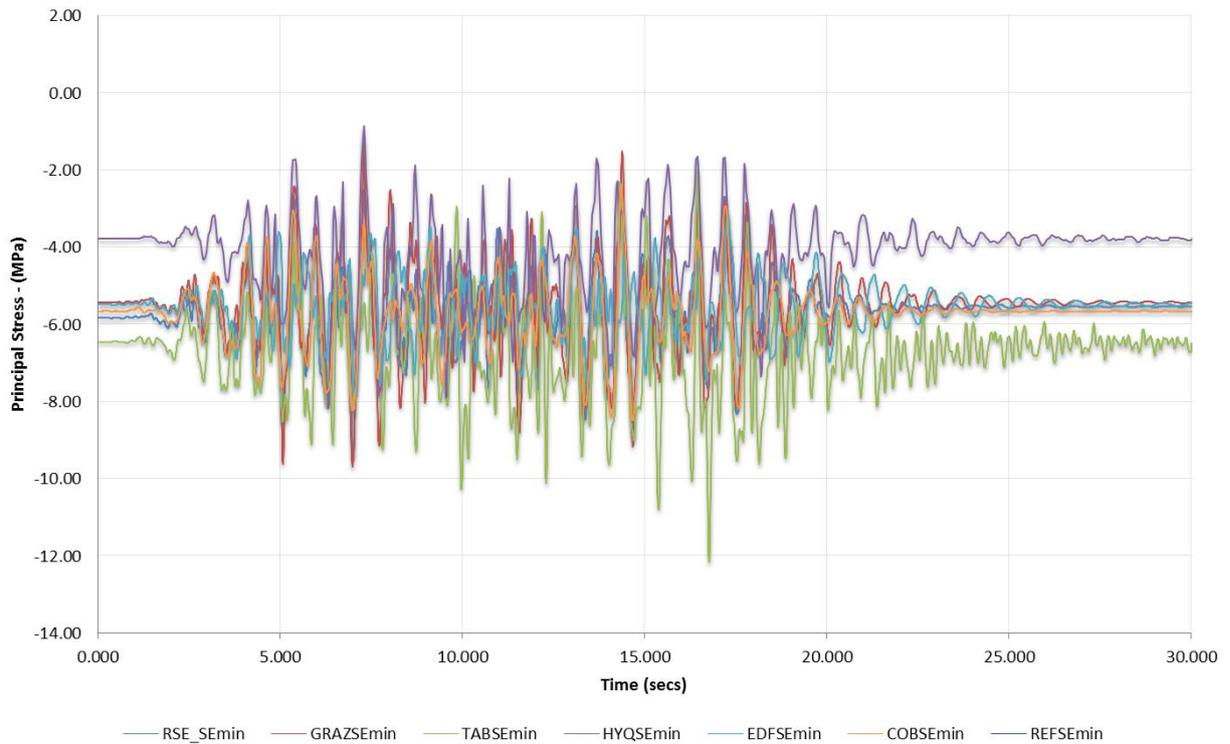
Figure 26 Minimum Principal Stress Time-History (MCE 1) for Point E
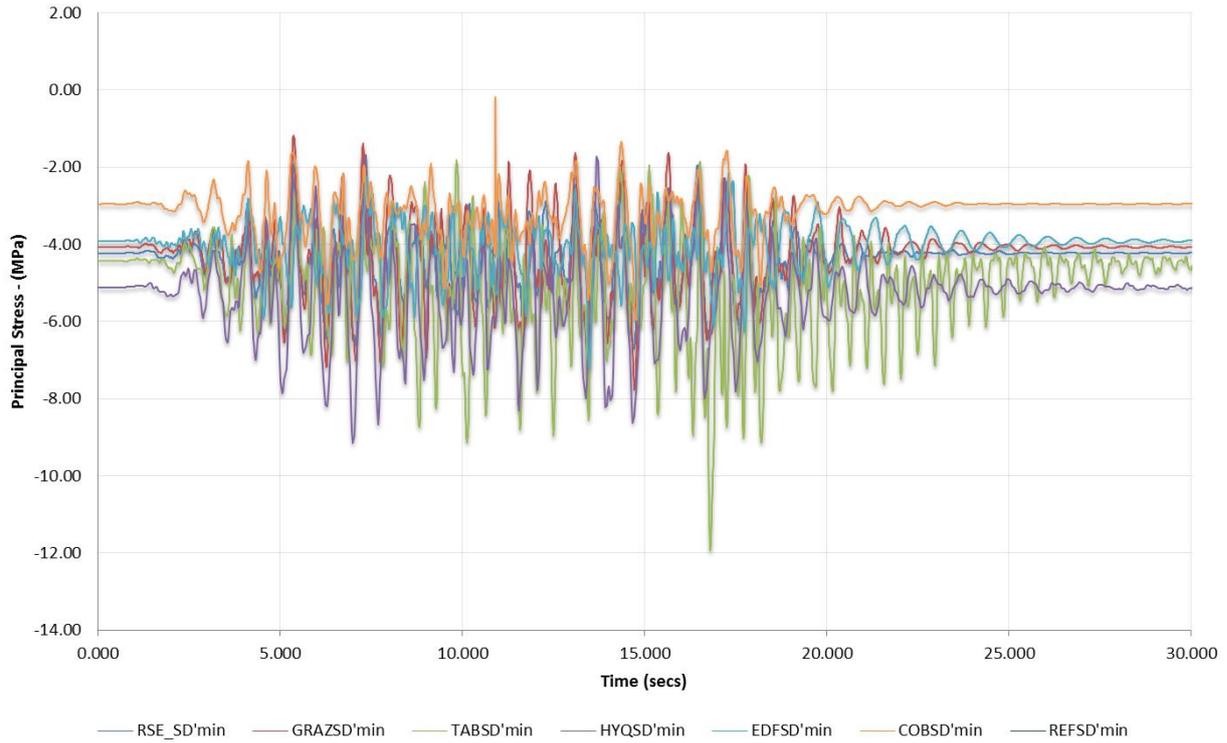
Figure 27 Minimum Principal Stress Time-History (MCE 1) for Point D'
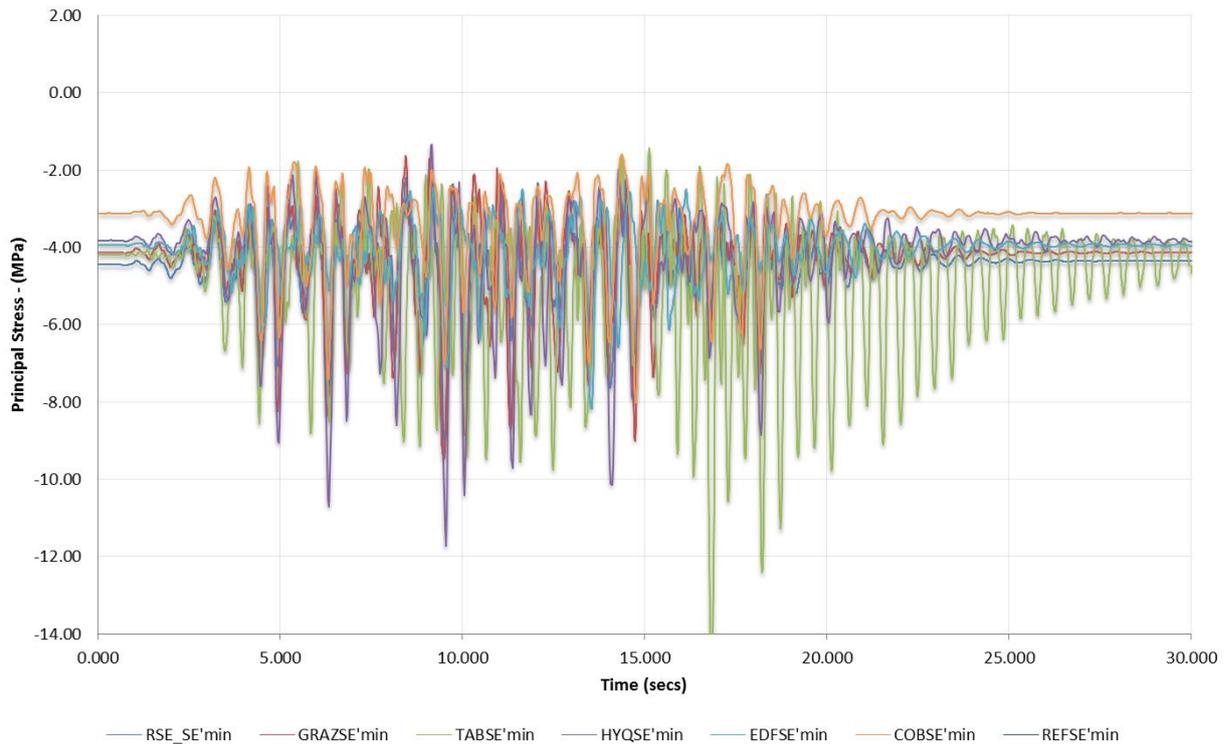
Figure 28 Minimum Principal Stress Time-History (MCE 1) for Point E'

The comparison of stress envelopes and time-histories indicates a certain consistency in that TAB results are quite different from all other contributors and hence to be reviewed with caution and HYQ results are based on a very fine unstructured mesh which produces stresses that are in some cases 50% higher than the reference solution.

Rocking Block Stability [I] and [J]

The results for the factors of safety against sliding and overturning of a so called "rocking block" characterised by opening of the contraction joints and the formation of a horizontal crack that can propagate through the whole thickness of the block were requested. The results were to be given for four different levels of the assumed horizontal crack, namely at El. 1600.5 (h = 8.5 m), El.1592 (h = 17 m), El.1578.2 (h = 30.8 m) and El.1564.5 (h = 44.5 m). The comparison of results for the factors of safety for overturning and sliding are given below in accordance with the analytical method adopted by the contributors (energy, free body, LFEM and NLFEM).
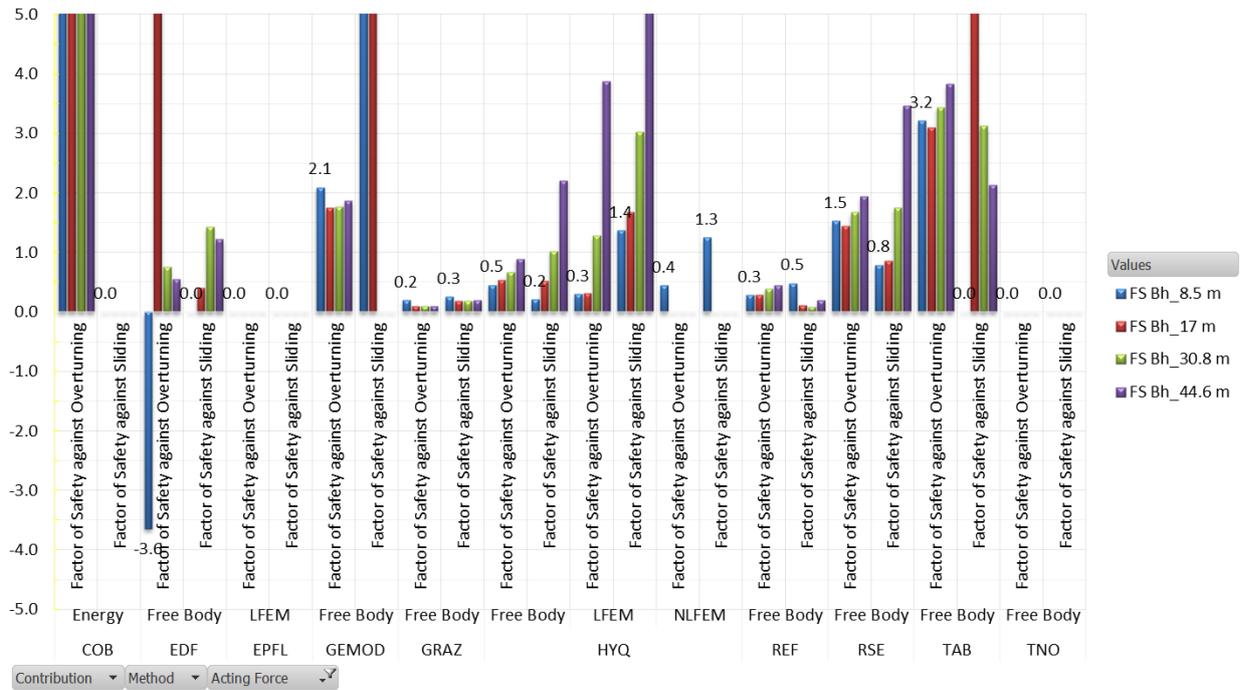
Figure 29 Factors of Safety against Sliding and Overturning for four heights of sections.

Up until this point in the comparison and evaluation of results (eigenvalues, displacements and stresses), the overall picture of the dam behaviour during a seismic event has been consistent taking into account previous comments (mesh density, FE types, fluid-structure interaction methods applied and the associated boundary conditions, etc.). The variation in block sliding and overturning results, firstly for the free body case (linear assumptions), demonstrates clearly the staggering variability in results (factors of 3 and more). Bearing in mind that the main performance criterion for a dam subjected to an extreme event such as an earthquake, is to have **no uncontrolled release of the reservoir volume**, the obtained results become of quite some concern from a safety point of view not to mention possible strengthening of the structure. **What is interesting is, why?** To answer this question, further information was requested from the contributors as described in the next chapter.

Evaluation of the Dam Safety

The participants were requested to interpret and analyse the computed displacements, stresses and rocking block stability of the dam and to conclude on the seismic safety of the structure.

It was important that a critical review be made of the software tool and the Guideline used in the studies and hence, the contributors were requested to make proposals for further investigations and/or benchmarks.

With the above goals in mind and following the review of the contributions by the formulators of the Theme A benchmark, a set of *three questions* were formulated per contributor expressly based on the contents of their studies which were then presented/discussed during the benchmark event itself. In addition, for a better comprehension of possible differences between the results, the methods/strategies adopted by the contributors and deviations from the benchmark formulation, **comments** were made per contribution.

The formulators "questions" and "comments" and the contributors "responses" are provided below.

Ref.	Benchmark Questions	Benchmark Answers (for BM PowerPoint presentations)	Benchmark Comments (for information/review only)
RSE	Q1. - What is the theoretical background/logic of using seismic load/material factors in Italian Guidelines? Q2. - As a rule, should block stability (sliding & overturning/rocking) factors of safety be determined only with time to avoid over-conservative safety evaluations ?	A1. - The approach of Italian Guidelines (as well as Eurocodes) to assess structural reliability is based on the semi-probabilistic limit state method: **factors are applied both to loadings and material strength parameters**. A2. -Assuming the simultaneous application of the most demanding seismic forces is surely a conservative hypothesis, but not crucial in evaluating block stability. The modelling of arch dams subjected to strong earthquakes must properly consider the **non-linear behaviour of dams**, at least the opening and sliding of contraction joints.	C1. - Wave reflection coefficient (α) equal to 0.6. C2. - 30 modes used to achieve 80% effective mass participation. C3. - Average time-enveloped nodal accelerations applied to FE block. C4. - Seismic safety based on TH3 only (severe case). C5. - Non-linear joint analyses needed to assess the safety of the structure. C6. - Future BM -> Nonlinear sliding-rocking block stability.
GRAZ	Q1. - How does water compressibility effect block stability and which method is more conservative, incompressible or compressible? Q2. - Are displacement results (rather than forces) more suitable to determine the performance criteria or *service states* of the structure during seismic actions ?	A1. - The key parameter for the significance of the compressibility is the ratio between the natural frequency of the reservoir to the natural frequency of the dam. Fok and Chopra (1987). Depends on the geometry (natural frequency). **Consideration of a compressible reservoir for modelling dam-reservoir interaction is recommended for most problems**, because the constitutive behaviour of water is modelled more accurately. A2. - Depends on the intensity. If nonlinearities are surely triggered because the strength is exceeded, forces are not suitable in these areas. In nonlinear analyses displacements should rather be used.	C1. - Attention - Z+ vertically upwards (for pressures). C2. - Wave reflection coefficient (α) equal to 0.5. C3. - 50 modes computed to general enough effective participating mass. C4. - USACE Arch Dam 1994 used which advocates different safety concepts (Demand-capacity ratios) to EM 1110-2-6051 *Time History Dynamic Analysis of Concrete Hydraulic Structures,* 2003. C5. - Note - Contraction joint surfaces for double curvature arch dams for a given block are in actual fact *helical* and not planar in the radial direction. This will influence greatly the stability results. C6. - Future BM -> Nonlinear sliding-rocking block stability.

Ref.	Benchmark Questions	Benchmark Answers (for BM PowerPoint presentations)	Benchmark Comments (for information/review only)
GEOM TAB	Q1. - How is the biaxial failure criterion applied to seismic loading with time? (number of strength points inside/outside of the envelope) Q2. - What is the relevance of applying a *reduction factor* to block accelerations?	A1. - Time history of principal stresses (s1 & s2) with input series 1 (worst case) are prepared for nodes D, E, D' and E' and are placed on biaxial dynamic failure envelope. As an old tradition, at any point on dam faces only 3~5 stress peaks are allowed to be outside of failure envelope but little substantiation exists for it. Presently, **Demand-Capacity Ratio** (DCR) is adopted for assessment of local damages. A2. - Vertical contraction joints would undergo opening/closing phases during an earthquake. Only by **nonlinear analysis**, it could be shown that following joint opening high tensile arch stresses transform to high transitory cantilever stresses leading to formation of horizontal cracks on lifts. With in situ calculated (absolute) accelerations (ah = 1.5g ~ 3.3g) and imposition of reduction factor (2/3), the resulting factors of safety were quite low and unacceptable. Thus, block stability check is made considering site specific base PGA values (ah = 0.16g) This approach is quite conservative since **frictional effects of contraction joints and interlocking of shear keys** on both sides of block are ignored **making imposition of reduction factor quite reasonable**.	C1. - Rayleigh damping coefficients α= 1.1 and β =0.001 C2. - Full reflective reservoir boundaries α= 1. C3. - 12 modes considered for both compressible and incompressible fluid cases. C4. - Future BM -> Nonlinear analyses with treatment of interface joints (dam/foundation) are needed.
GEOM	Q1. - What is the importance to the studies of applying only horizontal upstream-downstream hydrodynamic forces on the dam upstream surface? Q2. - What approach (methodology) should be adopted in capturing "*major vertical/interface joints*" in terms of width, breadth and depth?	A1. - We used Westergaard in z-direction. Applying added mass perpendicular to all faces: Generates inertial forces in 'weak direction' of dam; Stronger shear at flanks Stronger bending at centre? **Westergaard in z-direction is probably not conservative**. A2. - Based on reality (shear joints at foundation, construction joints). What joints to model? With what spacing? -> **parametric studies…**	C1. - Contraction joints modelled in seismic nonlinear analyses. C2. - Modified Rayleigh Damping values to capture main structural eigenvalues (α = 0.47 and β = 0.005, ξ = 5%) C3. - Interface elements applied at 3 sections of max. tensile stress (ϕ = 55 °). C4. - Permanent post-seismic relative displacement of 20 cm computed. C5. - FE Mesh modified compared to the BM formulation.
LNEC	Q1. - What is the Rupture Index I_R and how is the "acceptance level" defined? Q2. - How does the use of the Modal Superposition method compare to Direct Time Integration?	A1. - I_R = LRC is 100 divided by the minimum of resistance over applied stress. The Portuguese guidelines require LRC < 40 for acceptable safety and LRC = 100 indicates rupture. A2. - No reply given.	C1. - Modified Rayleigh Damping values to capture main structural eigenvalues (α = 0.66 and β = 0.0038, ξ = 5%) C2. - Incompressible fluid formulation for reservoir. C3. - Stability factors of safety presented with time showing only brief exceedance values. C4. - Portuguese Standards applied in Safety Evaluation. C5. - Results based on the Modal Superposition method.

Ref.	Benchmark Questions	Benchmark Answers (for BM PowerPoint presentations)	Benchmark Comments (for information/review only)
TNO	Q1. - Comparing incompressible with compressible (HTFD) fluid stress results, it would appear that fluid compressibility reduces stresses in the lower sections of arch dams but perhaps not the top sections - discuss ? Q2. - What type of "crack model" is best suited to the problem ?	A1. - We only looked to effect of compressible fluid in combination with other frequency dependent conditions. The stress differences between Newmark/HFTD **show largest reduction in the upper half of the dam**. A2. - Crack modelling for this application: Foundation-dam interaction: discrete crack model with interface elements. Concrete cracking: smeared crack model Joint-modelling: discrete crack model with interface elements. Considerations for model choice: Interface elements: fluid pressure development in opening (up-lift). Smeared crack models: stress-softening, crack energy, multi-directional options, energy absorption in cyclic loadings.	C1. - Wave reflection coefficient (α) equal to 1.0 - Fully reflective reservoir bottom. C2. - Eigenvalues are based on an incompressible fluid and the added mass of the reservoir is approx. 10%. C3. - 50 modes considered to capture > 95% of the effective mass contributions. C4. - DIANA does not compute hoop stresses (parallel to the arch) in global coordinates.
HYQ	Q1. - How important is block geometry and shear keys to the stability/movement of blocks - discuss ? Q2. - What is the importance of a compressible fluid on the results (especially block stability) - discuss?	A1. - No reply given. A2. - The compressible results using the rigid boundary condition are on the safe side; Crest acceleration is amplified and stress envelope is wider.	C1. - FEM modified to capture non-linear effects. C2. - Incompressible fluid, modal superposition with specific modulus values depending on the loading condition applied along with compressible fluid. C3. - Progressive Stability Approach adopted with and without lateral confinement. C4. - Sufficient effective mass participation ensured when 25+ modes employed. C5. - Modified Rayleigh Damping values to capture main structural eigenvalues (α = 0.757214 and β = 0.002091, ξ = 5%) C6. Fixed anisotropic damage model used with fracture energy, same mesh and hence a reduced tensile strength f_t = 1.25 MPa. C7. - It is demonstrated that block movement towards the upstream is the only possible mechanism due to the block geometry/shape.
EDF	Q1. - How does the Swiss Directive for seismic verifications compare to the French counterpart - discuss ? Q2. - What is the importance of Rocking Block Stability - discuss?	A1. - **Swiss Directives**: Order of 7th December 1998, Dam class, SF 1.1, Dynamic compressive strength 1.5 fcs, dynamic tensile strength 1.5 fts less than 4 MPa, 0.1 fcd less than 4 MPa. **French Directives**: Guidelines of the profession: Dam class / Seismic zone, Type of dam (arch, gravity, …) FS: 1.0 fcd = 1.25 fcs; ftdmin(1.5 fts; 0.1 fcd; 4 MPa). A2. - Proposal: Evaluate - Radiative damping in the foundation with a FULL FEM -> The current mesh need to be refined. Water compressibility. Non linear analysis (Numerical model with contraction joint): Opening of the contracting joint. Evaluate the global stability.	C1. - FEM with incompressible fluid, massless foundation. C2. - Triangular distribution of uplift pressures across cracked section.

Ref.	Benchmark Questions	Benchmark Answers (for BM PowerPoint presentations)	Benchmark Comments (for information/review only)
EPFL	Q1. - What are the actual analysis and pre/post-processing capabilities of AKANTU and how is the development from possible multiple-users/developers managed? Q2. - Does the use of the Westergaard approach over or under estimate the safety of potential sliding & rocking blocks?	A1. - No reply given. A2. - No reply given.	C1. - Development of Free Open Source code called AKANTU C2 - Future benchmark solutions could include joint/interface elements along with soil-structure interaction.
COB	Q1. - What are the numerical and practical advantages and disadvantages of using Boundary Finite Elements for dam-fluid-foundation interaction ? Q2. - How do the vertical and cross-valley motions affect the seismic rocking response of blocks - discuss?	A1. - No reply given. A2. - No reply given.	C1. - Only overturning (or Rocking Block) stability was verified possibly because this is the only requirement for French codes. C2. - FE mesh refined with 3 elements in the thickness. C3. - Material properties as per Formulation (CH) except damping (French - 5% - 7% - 10% -> applied). C4. Seismic input reviewed as per French Guidelines leading to higher PGAs unless site specific studies performed giving 1 zone lower thus equivalent to CH values (approx.). Only the upstream-downstream motion is considered, other directions are neglected. C5. - French Standards do not require thermal gradients to be applied in dynamic analyses. C6. - Block stability (overturning) normally performed for minimum reservoir level, but full reservoir taken. C7. - Block stability based on energy release are evaluated on the basis of a limiting velocity which is compared to the actual value. The blocks remain stable.
REF	Reference Solution C1. - Thermal properties (specific heat and conductivity missing) C2. - 12 eigenvalues were requested for plotting and not as the number for computational purposes which depends on the Guideline used or current analysis practices.	Reference Solution C1. - Thermal properties (specific heat and conductivity missing) C2. - 12 eigenvalues were requested for plotting and not as the number for computational purposes which depends on the Guideline used or current analysis practices.	Reference Solution C1. - Thermal properties (specific heat and conductivity missing) C2. - 12 eigenvalues were requested for plotting and not as the number for computational purposes which depends on the Guideline used or current analysis practices.

Table 4 Evaluation of Results – Questions, Answers and Reviewers Comments

Conclusions and Recommendations for Future Benchmarks

The objective of the benchmark was to perform the seismic evaluation of a concrete arch dam in Switzerland according to guidelines. For the Swiss Dam community this had a particular relevance because a campaign of seismic verifications in accordance with National guidelines for over 200 large dams in Switzerland has recently been undertaken taking over ten years to achieve. This placed numerical tools and methods within the context of Guideline and/or Standard requirements allowing the dam community to establish whether or not:

- Today's numerical tools have the **capabilities** to satisfy guideline/standard requirements and whether or not the numerical capabilities of these tools **go beyond** these requirements and beyond the practical identification of input parameters for example, in the case of compressible fluid-structure interaction and the identification in the field of input parameters and the calibration of the numerical model.
- Certain numerical methods are **appropriate** to satisfy the guideline requirements for example, the use of simplified linear elastic static and dynamic methods for structures that clearly have inherent discontinuities such as contraction joints.
- The numerical tools and guidelines are **compatible** in terms of methods, results, post-processing techniques, the need for plausibility checking and the general engineering evaluation/interpretation of results. The interaction between the dam and software development communities is important. The latter must clearly have general purpose products that are attractive to a broad based range of clients and the former, tools that not only perform the analyses, simple and complex alike, but have the post-processing capabilities to enable a coherent evaluation of the results. A good example of this is how some contributors used biaxial stress vector failure criteria to evaluate scalar required concrete strengths which ultimately serves the purpose of producing a concrete mix design.
- The **qualitative** and **quantitative** precision of the tools to predict the real behaviour of the structure (dam, foundation, and appurtenant works) subjected to complex loading/restraint conditions can be achieved.

The number and quality of contributions received and the participation in the two-day benchmark themes and one-day excursions to Les Toules and Mauvoisin dams was very encouraging and certainly, in terms of numbers, in the upper ranks compared to previous benchmarks that have taken place over nearly twenty-five years. It should also be borne in mind that the preparation time for benchmark solutions is generally in the order of a few weeks to a maximum of one month not including the actual participation in the benchmark conference itself. For the contributors this means a "one-off" task from start to finish of a problem that is not linked to a project and must in general be budgeted under research and development or as is now more often the case, the contributors "free-time". This observation must also be taken into account in the formulation of future benchmarks.

For the most part, the contributor's solutions were based on the use of finite element techniques although one solution included a mix of finite and boundary elements. As was hoped, some contributors went beyond the formulators result requirements and adopted new meshes and methods to solve the problem. A good example of this is the contribution from the Canadian team from Hydro-Québec who implemented a pragmatic step-by-step approach to the displacement, stress and block stability problems using a combination of linear elastic, non-linear smeared and discrete crack/interface modelling techniques which proved ultimately to be indispensable in the understanding/solution of the problem. Other contributors such as the Italian team from RSE, used their National directive and/or guideline simplified methods to arrive more or less to the same conclusions as Hydro-Québec and certainly in terms of block stability. This combination of "pure" numerical and "mixed" numerical-guideline approaches was exactly the response that the formulators were hoping to achieve.

Comparing the methods employed and the use of numerical tools with those of just ten years ago, it is clear that the hardware and software capabilities have made important steps to such a point that even if the **physical parameters** [9] have not been measured in-situ/laboratory and the numerical models are not fully calibrated, this perceptively "minor" inconvenience shall more than likely not prevent todays engineers and scientists from presenting all kinds of fluid-soil-structure interaction, constitutive models, meshing techniques (structured, non-structured, point-to-point particle, etc.) on macro, meso or micro scale levels, the handling of complex loading conditions, etc. Shall the controlling factors in the future be related to Guidelines/Standards, "dam expert" opinions (engineering judgement) or a mixture of these?

More specifically, the eigen-problem solutions have in general produced very consistent results especially for the empty reservoir case. The fully reservoir eigenvalues also showed a good correlation. The major observation for the full reservoir condition in terms of guidelines/standards was the requirement to take into consideration a number of eigenmodes that corresponds to a total of 80% or more of the effective mass participating in the solution. The addition of the reservoir loads led to percentage values greater than 100% and hence, the interpretation of results with guidelines had to be based on the empty reservoir. This issue is certainly one for the software developers to address in the future.

The comparison of displacements and stresses for static loads was very good providing a sound starting condition for seismic verifications. However, even for this condition and certainly when the seismic event is added to the static results, it is interesting to note that for some contributors, the post-processing treatment of stresses (principal, hoop and vertical) along the interface between the concrete and rock and at points of singularity (points D, E) still poses a problem. This explains to a large extent the "bumps" in stress plots for lower elevations (approx. 1400 m.a.sl.) and excessive "fictitious" stresses at the base, in particular the downstream concrete-rock interface whereby the average of "usual" vertical stress is -3 MPa and the average of the "unusual" vertical stress is -15 MPa! A similar observation was made for stress points D, E and D' E'. Alternatively, the addition of discrete elements at the concrete-rock interface or the treatment of singularities with softening techniques would improve this stress pictures.

Another important issue to mention is the direction of stresses. Very few contributors concerned themselves about the direction of principal stress vectors and/or the effects of tensile hoop stresses on contraction joints. This is where well defined guidelines and standards play a crucial role for the dam analyst because a regulated limit of say 2 to 4 MPa in any direction or the exceedance of this value with time such as defined in Demand-Capacity Ratio [9] can be the turning point between the use of a linear or non-linear model.

Having performed the displacement-stress analyses for static and seismic conditions, the seismic verification of arch dams often finally results in the checking of **sliding and rocking stability of upper elevation blocks** of the structure. In other words, both the local (stress) and global (displacement) stability conditions must be satisfied and their interaction of stresses and displacements investigated (partially or fully cracked sections). This verification is a direct result of guideline specifications which are more concerned that **no uncontrolled release of water occurs downstream**. The quantity and extent of dam break/water release is normally part of the overall safety concept for the structure (lowering of the reservoir elevation for example).

Generally, all contributors recognised that for a double-curvature arch dam by virtue of its geometric shape (horizontal and vertical directions and block geometries), the physical mechanism of block movement could only occur in the upstream direction. The stress results would normally delimit the height of the block to be considered in stability analyses (extent of base cracking across the entire upstream-downstream section), but for the benchmark, four block heights were imposed, the critical block obviously being the shortest (H = 8.5 m). The variability in factors of safety for sliding and rocking was considerable.

The team from Hydro-Québec clearly demonstrated that free-body calculations imposed **severe**

stability requirements that could more than likely not be met and certainly in the case of the seismic verification of existing structures that were designed for much smaller seismic loading conditions (constant pseudo-static loads applied over the entire height of the dam). Recourse had to be made to non-linear analyses taking into consideration stress redistributions, damaged sections and the contact between sliding planes (vertical and horizontal sections). The complete set of results produced a much clearer picture of the dam behaviour during a seismic event. As well as stability factors, the **displacements/openings** in the radial and tangential direction of single and multiple blocks can be predicted over the complete duration of the earthquake and the final "at rest" position of the block post-earthquake evaluated. In fact, the **temporal behaviour of a block during a seismic event leads to quite a different assessment of the structure** when compare to the methods currently prescribed in most guidelines.

To compensate for these types of complex analyses in directives, applying load reduction factors whilst maintaining linear assumptions, is an important observation/conclusion of benchmark theme A and also a possible indicator for future events.

References

[1] Sécurité des ouvrages d'accumulation. Directives de l'OFEG, rapports de l'OFEG, série Eaux, version 1.1, novembre 2002.

[2] Sécurité des ouvrages d'accumulation. Documentation de base pour la vérification des ouvrages d'accumulation aux séismes, rapports de l'OFEG, série Eaux, version 1.2, mars 2003.

[3] Guidelines for use of numerical models in dam engineering. ICOLD Bulletin 155, 2013.

[4] Tenth Benchmark Workshop on Numerical Analysis of Dams, September 16-18, 2009 Gennevilliers, Paris, France.

[5] SFOE Web site: http://www.bfe.admin.ch/themen/00490/00491/00494/index.html?lang=en

[6] ICOLD Web site: http://www.icold-cigb.org/

[7] 13th Benchmark Workshop on the Numerical Analysis of Dams, September 9th to 11th, 2015 – EPFL, Lausanne, Switzerland, web site: http://icold2015bmw.epfl.ch/

[8] SwissCOD Swiss Committee On Dams http://www.swissdams.ch/index.php/en/

[9] US Army Corp of Engineers, Engineering Manual, EM 1110-2-6051 Time History Dynamic Analysis of Concrete Hydraulic Structures, version 2003.

[10] Domone, Peter; Illston, John. Construction Materials: Their Nature and Behaviour, Fourth Edition. 2010.

Theme B:

PROBABILITY OF FAILURE OF AN EMBANKMENT DAM DUE TO SLOPE INSTABILITY AND OVERTOPPING

Formulation by:

Adrián Morales-Torres & Ignacio Escuder-Bueno

Universitat Politècnica de València and iPresas, Spain

Email: adrian.morales@ipresas.com, iescuder@hma.upv.es
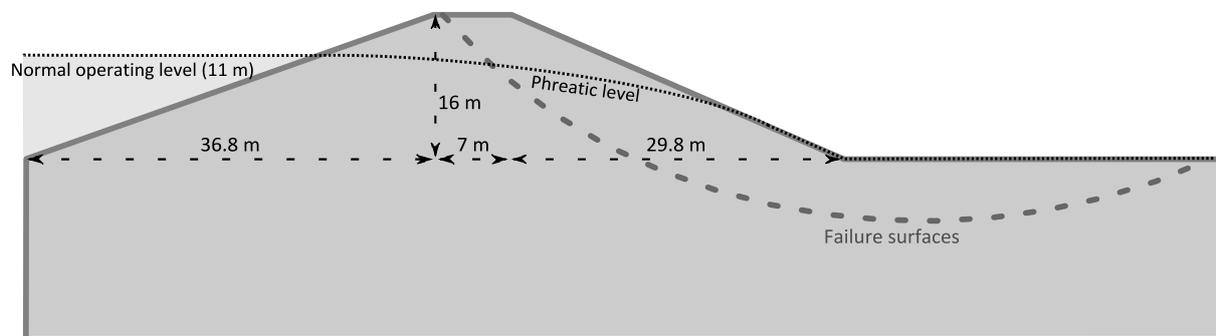
Embankment Dam

The information package (available from the authors) for the preparation of contributions for Theme B consists of:

- The present description: *THEME B.pdf*
- File with flood routing data: *THEME B - Flood routing data.xls*

Introduction

Dam engineers can no longer ignore the techniques of performing risk assessments, which are more and more required to sanction appropriate funds for major rehabilitations.

The analyses can range from very rigorous, complex, and costly analyses to pragmatic evaluations using semi-empirical methods, all of them dealing one way or another with typically large uncertainties to inform decisions.

Since 2011, ICOLD Committee A is contributing to address the issue from a computational perspective, but also providing enough context to understand and pay due attention to a set of decisions that are typically made in risk analyses but also in standard design techniques (frequency of events, factors of safety, breaching parameters, etc.).

The present theme follows the tradition initiated in Valencia 2011, where the aim was analyzing the probability of failure of a concrete dam due to sliding failure mode, and Graz 2013, where the purpose was comparing the estimation of consequences due to dam failure, to focus this time on the probability of failure of embankment dams due to slope instability and overtopping.

In this case study, inspired in a real Spanish dam but with non-real resistant and hydrological data, the main focus consists in calculating fragility curves for slope instability and overtopping and use them to calculate annualized failure probability, accounting for both natural and epistemic uncertainty.

Previous concepts

Concept of uncertainty

When failures of complex structures are analyzed, evaluation of uncertainty should play an important role in the analysis of the behavior of a constructed facility. In general, two sources of uncertainty should be considered:

- **Natural uncertainty or randomness:** Produced by the inherent variability in the natural processes. An example of this kind of uncertainty is the variability of the loads that the structure has to withstand, for instance, the variability in the earthquakes intensity that can occur. Another example is the resistance's variability of the terrain where the structure is settled. This type of uncertainty, sometimes also called aleatoric uncertainty, cannot be reduced, though it can be estimated.

- **Epistemic uncertainty:** Resulting from not having enough knowledge or information about the analyzed system. This lack of information can be produced by deficiency of data or because the structure's behavior is not correctly represented. The more knowledge is available about a structure, the more this type of uncertainty can be reduced. On the other hand, it is usually very difficult to estimate or quantify this uncertainty. An example of this type of uncertainty can also be found in the resistance of the terrain. The information about the foundations may be limited so the parameters used to characterize its resistance are estimated from probing and exploration. With more resources, the terrain can be better characterized and the epistemic uncertainty is reduced, although the natural variability of the terrain may still be very significant.

The distinction between natural and epistemic uncertainty takes added importance for a quantitative risk analysis in complex structures. In this context, natural uncertainty is usually related to the occurrence of events that can produce the structural failure and the

randomness of the structure's resistant behavior for the load produced by the events. In contrast, epistemic uncertainty is mainly focused on the lack of knowledge of the failure mechanisms, the structure's resistance parameters and the consequences produced by the failure.

Fragility curves and uncertainty

When risk is analyzed quantitatively for dam safety, three main concepts are usually combined: probability of loads, dam response for these loads and failure consequences. Fragility curves address the second term, since they represent a relationship between failure probability and the magnitude of the loads that produce the failure. Fragility curves are useful in risk analysis of complex structures, since they facilitate the evaluation of the structural response for different load values.

In general, a single fragility curve is used when only natural uncertainty is considered to analyze the system response. For each loading state, this curve represents the probability of structural failure produced by the natural randomness in the structure and the terrain. In Figure 1, the standard deviation of this single curve is represented with βR. In this exercise, this curve is called reference fragility curve.

In order to characterize the epistemic uncertainty, a probabilistic distribution can be defined for the mean of the reference fragility curve. The standard deviation of this probability distribution is represented with βU. Variations in the fragility curve average produce a family of fragility curves that characterize both uncertainties, as shown in Figure 1. In this figure, the mean of the distribution for both uncertainties is assumed to be the same.
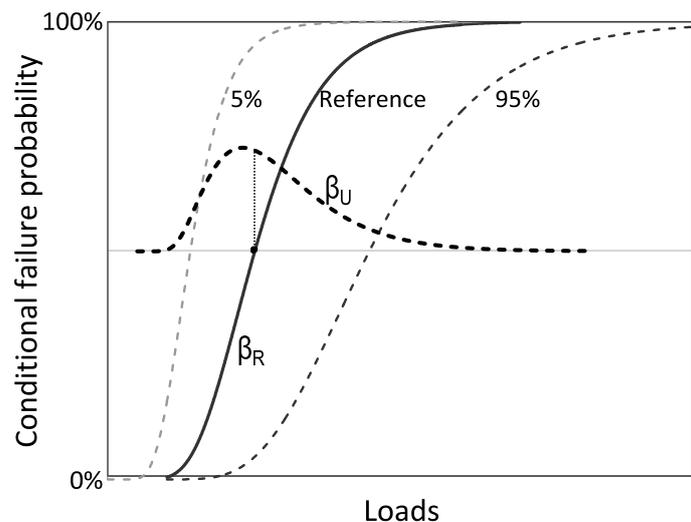
Figure 1: Example of family of fragility curves.

In general, for a defined loading state, a complex structure can fail due to different failure modes, controlled by failure mechanisms. Commonly, fragility curves are defined for each failure mechanism separately and later combined within the framework of risk calculation by means of different techniques (i.e. common cause adjustment).

From fragility curves to failure probability

In order to calculate failure probability results in annualized terms (which is the current state of practice in dam engineering), fragility curves should be combined with the probability of the loads that may produce the failure, which are usually characterized by their annual exceeding probability (in this exercise, such load/driver of the failure is the water pool level).

Exceedance probability curves are usually discretized in several intervals in order to obtain a representative value (usually the average) and an occurrence probability value for each interval subsequently used to compute the total failure probability. The failure probability for each interval is computed multiplying the occurrence probability of each interval by the conditional failure probability of the interval's representative value. This conditional failure probability value is calculated directly from the fragility curve. Adding the failure probability of all the intervals examined yields the total failure probability of the structure. The higher the number of intervals, the more accurate the results will be.

When a family of fragility curves is used in the risk model to define the system response, a risk profile is calculated to characterize the dam situation instead of a single risk result, as shown in Figure 2. This profile allows to characterize the effect of epistemic uncertainty in the failure probability results and to compare them with risk reduction measures. A steep failure probability profile shows the importance of the epistemic uncertainty in the results.
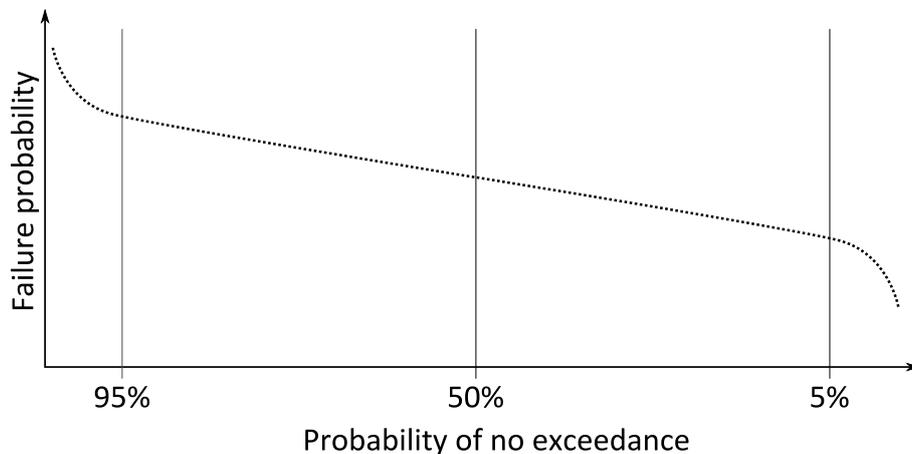
Figure 2: Example of failure probability profile computed with a family of fragility curves.

Data

The embankment to be analyzed is a homogeneous earth fill dam. Its upstream slope is 23.5 degrees and its downstream slope is 28 degrees, being the total height 16 meters. The normal operating level in the dam is 11 meters. This geometry is shown in Figure 3. The specific weight of the material in the dam is 19 KN/m³.

This dam has a non-gated spillway whose crest level is 11 meters and a bottom outlet with one conduit and two gates.

In recent years, this embankment has had small instability problems in the downstream slope, so a quantitative risk analysis is performed to estimate annual failure probability. Two failure modes are analyzed in this embankment: overtopping and dam instability. In both failure modes, water pool level is supposed to be the driving force of failure.
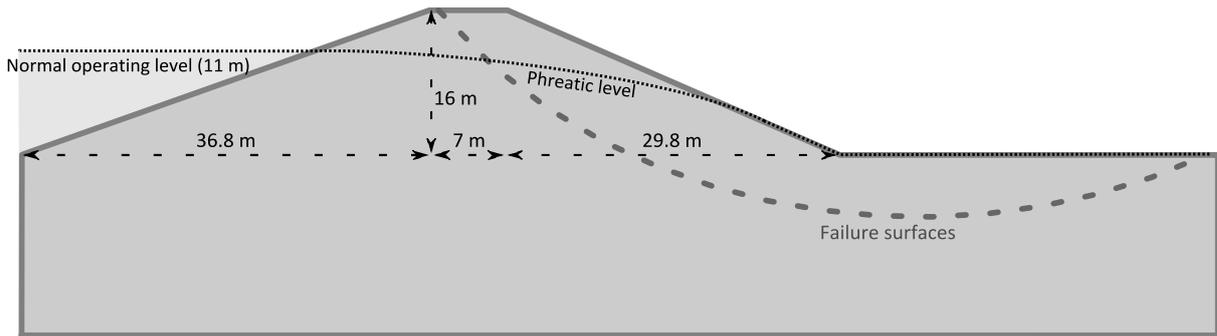
Figure 3: Embankment Geometry.

As explained in Phase 3, a spreadsheet is provided with the data required to analyze flood routing in the reservoir. The name of this file is *THEME B - Flood routing data.xlsx* (*this file is also attached to the benchmark PDF file*).

Phases

The problem to solve is divided in four different phases:

Phase 1: Analysis of the information for the instability failure mode.

- Elaboration of a slope instability limit model for the downstream slope of the embankment. This instability model should quickly check dam stability in order to allow many stability computations in the following steps. This model can be able to check different failure surfaces.
- This model must consider the effect of water pressure in the dam instability. Water pressure can be optionally considered in a very simplified manner: the top flow line inside the embankment varies linearly from the water pool level in the upstream face to a fixed point in the downstream face located at 3.3 meters above the downstream toe, as shown in Figure 3.
- Define random variables in this model. Two random variables are recommended following a Mohr-Coulomb type of failure criteria: friction angle and cohesion, although other random variables can be introduced. Probabilistic distribution for natural and epistemic uncertainties should be defined separately.
- To evaluate the natural uncertainty, the recommended distribution for the friction angle is a truncated normal distribution with average 25º, standard deviation 2º, maximum 30º and minimum 20º. The proposed distribution for the cohesion is a lognormal distribution with average 10 kPa and standard deviation 3 kPa. These distributions have been estimated from available information and tests about dam materials.
- Other random variables can be introduced with their probability distribution.
- Written evaluation of how epistemic uncertainty could be introduced and how it may modify the estimated results. Which are the main epistemic uncertainty sources in this instability analysis?

Phase 2: Calculation of reference fragility curves.

- First, the reference fragility curve for the slope instability should be computed using the natural uncertainty distributions. A large number (N) of groups of values of random variables should be sampled within the natural uncertainty distributions for friction angle and cohesion following the Monte Carlo method.

- In order to compute this fragility curve, the recommended range of analyzed pool levels comprises from 11 to 20 meters over the embankment base. This range of pool levels should be discretized to define the fragility curve.
- For each discretized water level, stability is checked for each sampled group of random variables. Failure probability of each water level is estimated dividing the number of failure cases by the total number of cases analyzed (N).
- Third, the reference fragility curve for the overtopping failure mode should be represented in the same way that Figure 1. This fragility curve is directly calculated with a log-normal distribution with mean 17 m and standard deviation 0.2 m.
- Finally, the reference fragility curves of both failure modes should be combined in order to compute a single reference fragility curve that represents the structural behavior of this embankment for different pool levels. Which technique is followed to combine these curves? Which will be the predominant failure mode in each range of water pool levels?

Phase 3: Computation of water pool level probabilities.

The objective of this phase is calculating a relation between water pool levels and annual exceedance probability (AEP). This curve should be estimated evaluating flood routing in the reservoir for different flood events and bottom outlet availability situations. The following data is provided to compute this curve:

- The return period of the floods to be analyzed range from 10 to 10,000 years. They are included in file *THEME B - Flood routing data.xlsx* (*sheet: Floods*).
- Previous pool level in the reservoir: 11 meters.
- Bottom outlet operation rules: This outlet is opened at maximum capacity when the pool level in the reservoir is above 11 meters.
- Bottom outlet reliability: 85%.
- Discharge curves for spillway is included in the file *THEME B - Flood routing data.xlsx* (*sheet: Discharge curves*).
- Capacity curves for bottom outlet is included in the file *THEME B - Flood routing data.xlsx* (*sheet: Discharge curves*).
- Pool level – reservoir capacity curve is included in the file *THEME B - Flood routing data.xlsx* (*sheet: Pool level - volume curve*).

Phase 4: Computing failure probability and sensitivity analysis.

In this phase, the results of Phase 2 and Phase 3 should be combined to calculate failure probability. The next steps should be followed:

- Combine the curve computed in the previous phase with the reference fragility curve to calculate the reference failure probability. Please, describe how the curve that represents water pool levels vs. AEP is discretized for this computation.
- Sensitivity analysis over some of the main parameters and assumptions made in the previous phases. Which are the most important issues to be consider in detail when this procedure is applied?

Phase 5: Assessing epistemic uncertainty (Optional).

- First, epistemic uncertainty should be defined with a probability distribution for the mean of each random variable. The mean of the friction angle follows a truncated normal distribution with average 25°, standard deviation 1°, maximum 30° and minimum 20° while the mean of the cohesion follows a lognormal distribution with average 10 kPa and standard deviation 0.5 kPa.

- Second, a family of fragility curves should be computed for the instability failure mode. M (a large number) different groups of values for random variables are sampled from these epistemic uncertainty distributions using the Monte Carlo method.
- For each selected group of random variables, a new probability distribution should be defined for the natural uncertainty, using as "new mean" these selected values and keeping the same standard deviations and probability distributions defined for the natural uncertainty.
- Afterwards, for each group of random variables, a fragility curve is computed with the stability model and the new probability distribution defined for natural uncertainty. Therefore, the differences between the fragility curves are the mean values of the probability distributions used to compute them. Therefore, a family of M fragility curves is computed. This family of fragility curves will then capture both the epistemic and natural uncertainty of the structure.
- Explain the statistical characteristics of the family of fragility curves computed. What does a wide family of curves mean? What do step curves mean?
- Third, the family of fragility curves for the overtopping failure mode should be represented. In order to define this family, the mean of overtopping the fragility curves varies according to a log-normal distribution with mean 17 m and standard deviation 0.25 m.
- Fourth, the family of fragility curves of both failure modes should be combined in order to compute a single family of fragility curves, as made in Phase 2.
- Finally, combine the curve computed in phase 3 with the family of fragility curves to calculate the profile of failure probability. Provide statistical characteristics of this profile. Explain your main conclusions about these results.

Time framework

The estimated effort for the participants ranges from 1 to 2 weeks per phase. The time devoted to solve the five phases should not in any case be longer than two months.

References:

[1] L. Altarejos-García, F. Silva-Tulla, I. Escuder-Bueno, A. Morales-Torres, Practical risk assessment for embankments, dams, and slopes. Risk and Reliability in Geotechnical Engineering, CRC Press, 2015, Ch. 11, pp. 437–470.
[2] EPRI, Methodology for Developing Seismic Fragilities, Electric Power Research Institute, 1994.
[3] SPANCOLD, Risk analysis applied to management of dam safety – Technical Guide 8 (Vol. 1), Spanish National Committee on Large Dams, 2012.

Probability of Failure of an Embankment Dam Due to Slope Instability and Overtopping:
First Order Second Moment Method for Assessment of Uncertainty

Andreev S.H.[1], Zhelyazkov A.Z.[1]

[1]*Risk Engineering Ltd. Sofia, Bulgaria*

ABSTRACT: The current paper presents the analysis of the probability of failure of an embankment dam for slope instability and overtopping triggered by flooding-a benchmark project by the ICOLD. Natural and epistemic uncertainty is introduced with probability distributions of soil properties and different analysis assumptions. Sensitivity analysis has been conducted to assess the influence of the assumed soil property distributions and to verify specific prerequisites for the validity of the applied assessment methods. Probability distributions of the results are evaluated using the Monte Carlo method and the First Order Second Moment (FOSM) method. Families of fragility curves for both failure modes are constructed and combined using the Uni-modal limits theorem.
Overall conclusions are made for the obtained results along with recommendations for the reduction in their uncertainty.

E-mail: Stoyan.Andreev@RiskEng.bg , Aleksandar.Zhelyazkov@RiskEng.bg

Input data for the case study

This case study is performed as part of the 13th ICOLD Benchmark workshop, Theme B [9].

Embankment geometry
The embankment to be analysed is a homogeneous earth fill dam with crest length 263.5 m. Its height is 16 meters, the upstream slope is 23.5 degrees and the downstream slope is 28 degrees (Fig. 3). The normal operating water level in the dam is 11 meters. This dam has a non-gated spillway whose crest level is 16 meters and a bottom outlet with one conduit and two gates. The bottom outlet reliability is 85%. Pore-water pressure (PWP) is considered in a very simplified manner: the top flow line inside the embankment varies linearly from the water pool level in the upstream face to a fixed point in the downstream face located at 3.3 meters above the downstream toe [9].

Soil properties and evaluation of natural uncertainty
To evaluate the natural uncertainty, the recommended distribution for the effective stress friction angle ϕ' is a truncated normal distribution with mean 25º, standard deviation 2º, maximum 30º and minimum 20º. The proposed distribution for the effective stress cohesion c' is a lognormal distribution with mean 10 kPa and standard deviation 3 kPa [9].

Calculation of reference fragility curves

Two failure modes are considered for the embankment – sliding instability of the downstream slope and overtopping [9].

Numerical model for sliding failure mode
The dam model for sliding failure mode is created and analysed using the computer code SLOPE/W 2012 [6]. Pore-water pressure is calculated from the proposed pool water levels for

11 to 20 m with an increment of 1 m. For pool levels above the embankment crest the water table shapes are calculated for the expected overflow velocities using standard hydraulic equations [3], see Fig. 1.
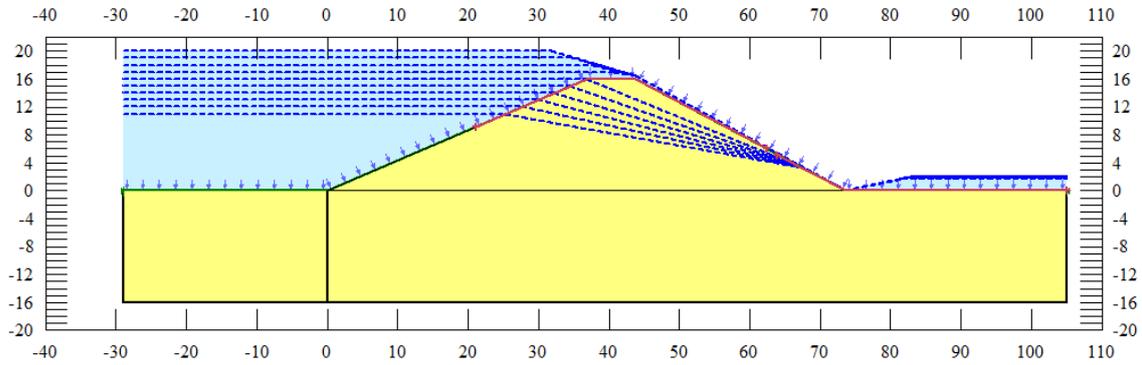

Fig. 1: SLOPE/W embankment model with water tables for different water levels

The limit equilibrium procedure of Morgenstern and Price is used for the sliding stability calculations of the embankment. The M-P solution satisfies all the static equilibrium equations and gives plausible results compared to other more sophisticated methods like the finite element method [4], [6]. In the calculations of pore-water pressures a phreatic surface correction was included to account for the non-vertical equipotential lines [6].

Properties of saturated and unsaturated soil
Since it is only partially saturated, the soil above the water table has higher shear strength and lower unit weight than the soil below the water table. Starting from saturated unit weight $\gamma_r=19$ kN/m^3 and assuming specific gravity $G_s=2.7$ for sandy/silty clay the void ratio is $e=0.81$. An average saturation degree of 60% is assumed for the soil above the water table, giving unit weight $\gamma_n=17.4$ kN/m^3. The shear strength s for saturated soil is calculated for Mohr-Coulomb material model, as illustrated in Equation (1) with effective stress parameters (σ'_n is the effective normal stress on the shear plane).

$$s = c' + \sigma'_n . \tan \phi' \tag{1}$$

The above expression is conservative for lower pool levels where a significant part of the critical slip surfaces cut across unsaturated soil. The increased shear strength due to soil suction is calculated in SLOPE/W with Equation (2) proposed by Vanapalli et al. [6].

$$s = c' + (\sigma'_n - u_a) . \tan \phi' + (u_a - u_w) . \left[\left(\frac{\theta_w - \theta_r}{\theta_s - \theta_r} \right) . \tan \phi' \right] \tag{2}$$

In Equation (2) u_a is the pore-air pressure, u_w is the pore-water pressure, θ_w is the volumetric water content, θ_s is the saturated volumetric water content and θ_r is the residual volumetric water content. The volumetric water content of $\theta_s=0.44$ m^3/m^3 is a result of the suggested void ratio and it is assumed that $\theta_r=0.044$ m^3/m^3. The relation between matric suction and volumetric water content used in the analyses is estimated from sample function in SLOPE/W for silty clay [6].

Monte Carlo sampling and conditional probability of sliding failure
As proposed in the benchmark theme description [9], Monte Carlo (MC) sampling was used to calculate the *CPF* for sliding by sampling large group of values from the assumed natural soil

property distributions. For each of the prescribed pool levels from 11 to 20 m 5000 deterministic analyses (trials) were performed giving approximately 90% confidence in the obtained results. The conditional failure probability (*CPF*) is assumed to be the ratio between the Monte Carlo trials giving factor of safety *FoS*<1 and the total number of trials. It has been observed that with the increase of Monte Carlo trials the probability distribution of the *FoS* approximates a log-normal distribution [4], [5].

Reference fragility curves for sliding and overtopping
The analyses gave discrete distribution for sliding *CPF* (Fig. 2, solid dots). However, it is more convenient to fit them to continuous probability distributions, using the Maximum Likelihood Estimation method [2]. The conditional probability of failure is usually approximated with log-normal probability distribution [5].

The approximation (fitting) of the reference fragility curve for sliding failure with log-normal distribution is shown with a dashed line on Fig. 2. It is obvious that the log-normal is not a very good fit and underestimates the CPFs for low and high pool water levels. After some trials for fitting with different continuous distributions, the Gumbel Type I (minimum) [1] was eventually chosen as best suited (Fig. 3 with solid line). It has mode $\mu_{R,S}$=15.9 and scaling parameter $\beta_{R,S}$=0.6. (median capacity $L_{m,S}$=15.3 m, covariance *COV*=0.143).

The reference fragility curve for overtopping is given in [9] as log-normal CDF with mean capacity 17 m and standard deviation 0.2 m. The corresponding fragility curve parameters are $L_{m,O}$=17.00 m; logarithmic deviation $\beta_{R,O}$=0.012; *COV*=0.012, see Fig. 2 (dash dotted line).
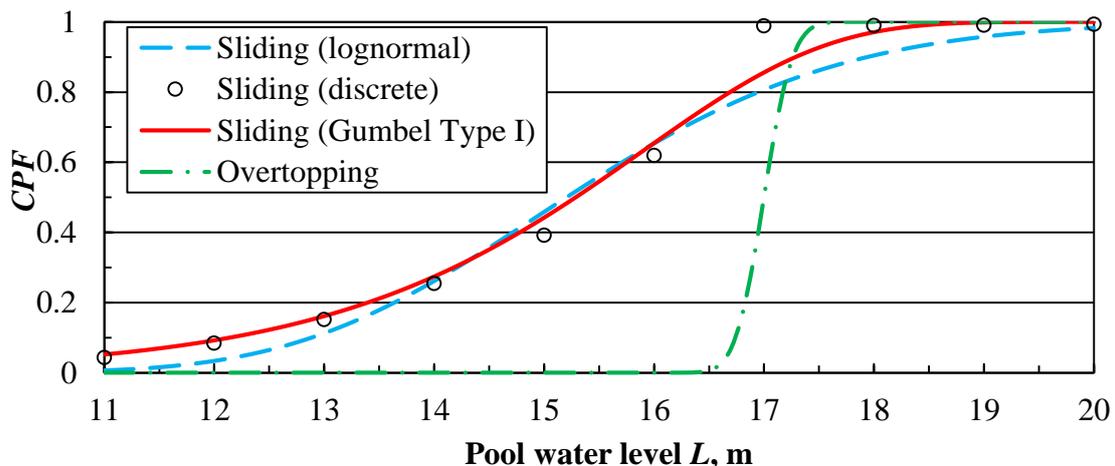
Fig. 2: Reference (median) fragility curves for sliding and overtopping failure modes

Combination of reference fragility curves and common cause adjustment
In order to calculate the overall conditional probability of failure a combination of the reference fragility curves is needed. A common cause adjustment should be made assuming that the failure modes are not mutually exclusive [8], [10]. The Theorem of uni-modal limits [8], [10] states that for *k* positively correlated failure modes, with conditional branch failure probabilities P_i, the system branch failure probability, P_f, lies between the following upper and lower limits:

$$\max[P_i] \leq P_f \leq 1 - \prod_{i=1}^{k}(1-P_i) \tag{4}$$

Fig. 3 presents three adjusted combinations of the reference (median) fragility curves using the upper and lower limits from Equation (4) and their average. The average value is recommended by SPANCOLD [10] for the case when the degree of correlation between the failure modes is

unknown. Obviously, for pool water levels below 16 m, overtopping is improbable, so the combined fragility is equal to the sliding fragility. The difference is pronounced for a small interval (around L=17 m), which corresponds to very low annual probabilities of exceedance of the pool water level.
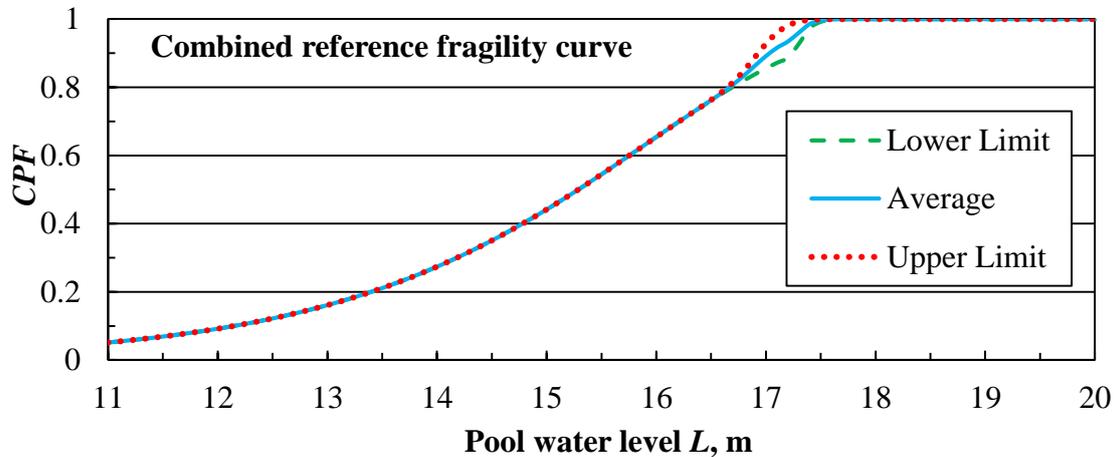
Fig. 3: Combined reference fragility curves for sliding and overtopping failure modes

Evaluation of epistemic uncertainty

Sources of epistemic uncertainty
The authors of [9] recommend the evaluation of epistemic uncertainty with probability distributions for the mean values of the soil properties. The mean effective stress friction angle – ϕ_m' has a truncated normal distribution with 25º mean, 1º standard deviation, 30º maximum and 20º minimum. The mean effective stress cohesion – c_m' has a lognormal distribution with 10 kPa mean, and 0.5 kPa standard deviation. In addition to this other sources of model uncertainties are evaluated:

- Use of increased unsaturated shear strength above water table.
- Use of different volumetric water content functions.
- Use of lower unit weight above water table.
- Use of phreatic surface correction.

An important source of epistemic uncertainty in this analysis is the seepage process through the embankment during heavy rains and pool water levels increase. Steady-state conditions with the water tables in Fig. 1 are conservative assumptions, but since there is limited information, the back calculations of the hydraulic properties of the soil for transient analyses are hard to perform and will carry a lot of additional epistemic uncertainties.

Conditional probabilities of failure
To evaluate the epistemic uncertainty for sliding failure the First Order Second Moment (FOSM) method, also known as the Taylor series method [4], [7], was used, see Equation (5).

$$\sigma_P = \sqrt{\left(\frac{\Delta P_1}{2}\right)^2 + \left(\frac{\Delta P_2}{2}\right)^2 + \ldots + \left(\frac{\Delta P_n}{2}\right)^2}, \text{ where } \Delta P_i = P_i^+ - P_i^- \tag{5}$$

In the above equations P_i^+ and P_i^- denote the conditional probabilities of failure, calculated by using Monte Carlo analysis, when varying the mean of the *i-th* variable with ±1 standard deviations, while the means of the other random variables are kept at their expected values. Equation (5) is a simplified form [7] of the general FOSM. It is valid for cases when the sensitivity analysis doesn't show strong non-linear change of the response parameter with the increase of the number of standard variations of the input. Fig. 4 shows the calculated CFPs for *L*=13 m and *L*=16 m when varying the mean values of the effective friction angle and cohesion with up to ±2 epistemic standard deviations (approximately 95% confidence interval). For the analysed embankment the change of the CPFs was close to linear trend, so the FOSM was preferred to the costly MC. The distribution of water levels, giving the same *CPF* for different confidence levels (epistemic uncertainty) is fitted to a log-normal distribution with 15.3 m median and 1.03 m standard deviation ($\beta_{U,S}$=0.067, *COV*=0.067).
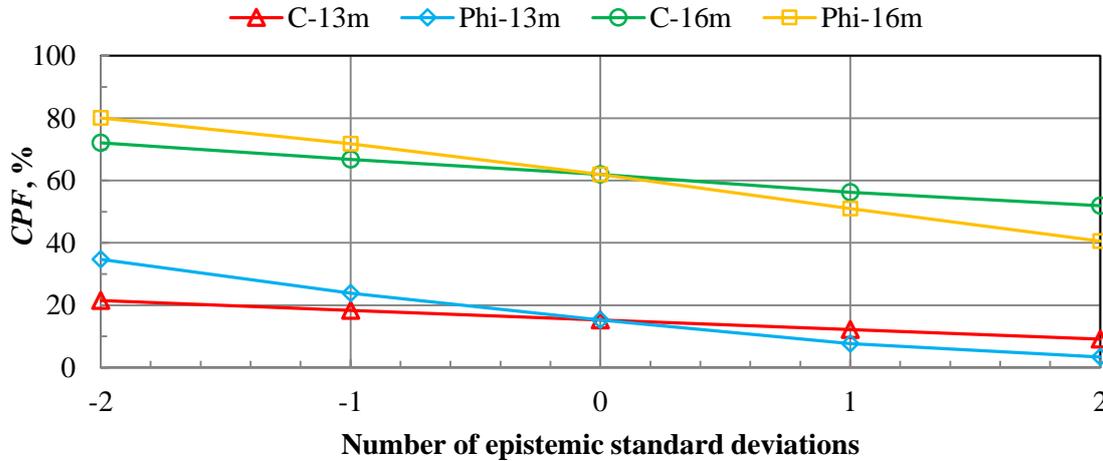
Fig. 4: CPFs for varying mean soil properties up to ±2 epistemic standard deviations

Families of fragility curves for sliding and overtopping failure

The family of fragility curves for sliding failure is approximated with Gumbel Type I (minima) continuous probability distribution – the discrete 5% and 95% CPFs are fitted using the MLE method, as shown in Fig. 5. All curves in the family have a scaling parameter (aleatory) $\beta_{R,S}$=0.6 and modes $\mu_{Q,S}$ calculated with Equation (6) for confidence levels *Q*:

$$\mu_{Q,S}=L_{m,S}.\exp\left[-\beta_{U,S}.\Phi^{-1}(Q)\right] + 0.36651/\beta_{R,S} \tag{6}$$

In the above equation $\Phi^{-1}(Q)$ is the inverse of the standard normal CDF of *Q*.

The family of fragility curves for overtopping (Fig. 6) is defined with a mean value of 17 m and a standard deviation of 0.25 m ($\beta_{U,O}$=0.015) [9].

Combined family of fragility curves

The combination is done according to the recommendation given by SPANCOLD [10], to use the average of the upper and lower boundaries in Equation (4). In [10] it is not explicitly stated how to combine families of fragility curves. In the current paper Equation (4) was applied for each subjective probability (confidence level): 5% curve for sliding with 5% curve for overtopping, 50% curve for sliding with 50% curve for overtopping, etc. (Fig. 7).
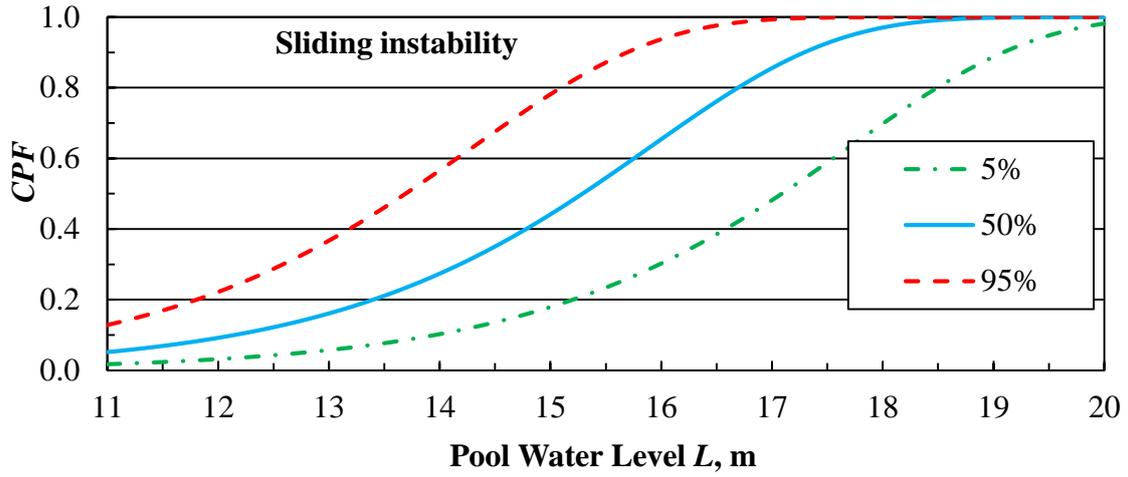
Fig. 5: Family of fragility curves for sliding failure mode
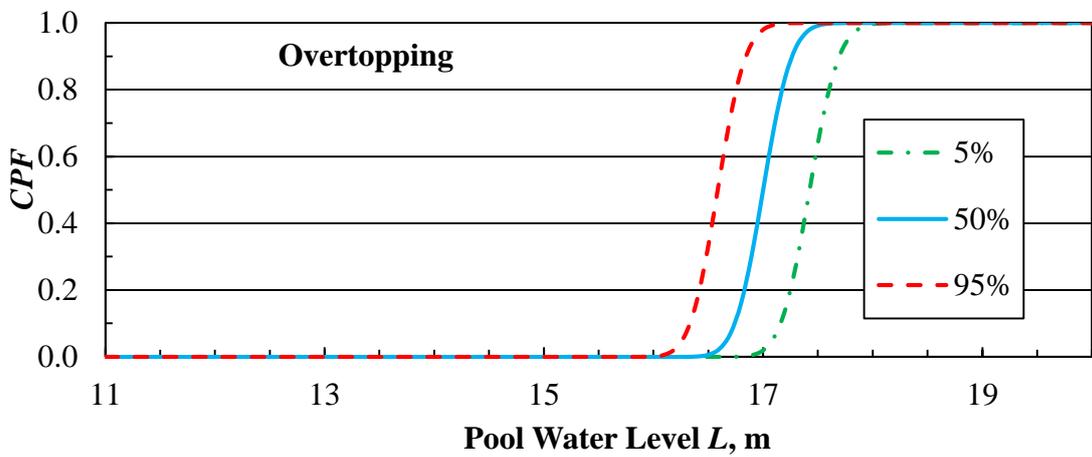
Fig. 6: Family of fragility curves for overtopping failure mode
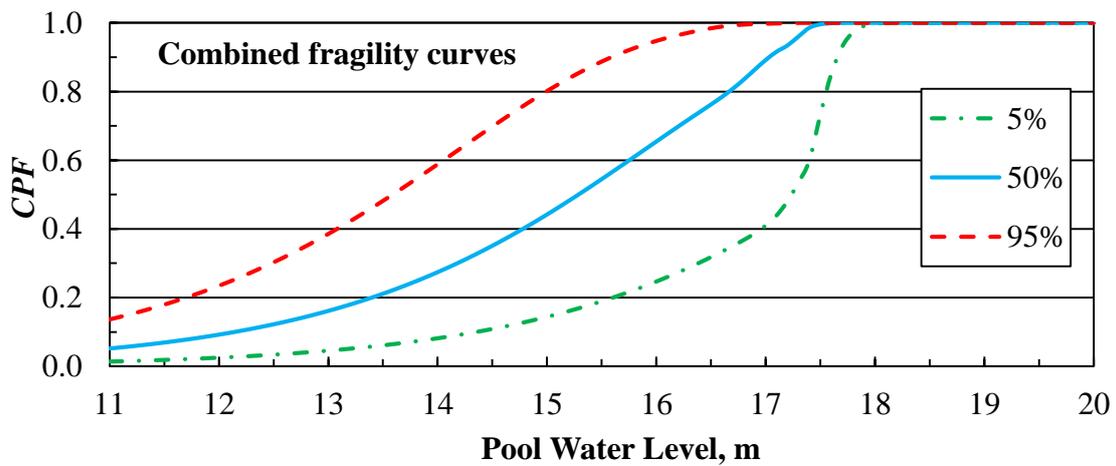
Fig. 7: Family of combined fragility curves

Flooding hazard

As part of the input information, [9] gives flood rooting data for return periods from 10 to 10 000 years and discharge capacities for the bottom outlet and the spillway, and the pool water levels as a function of the pool water volume. Since the bottom outlet has a reliability of 0.85<1.0, two scenarios should be considered by an event tree with two branches: one for functioning outlet and one for failure of the outlet [10]. In this case study, the bottom outlet has a much smaller discharge capacity than the spillway – up to 2 orders of magnitude (OM). The maximum pool levels for the two scenarios differ less than 0.3%, so the Annual failure probabilities are calculated only for the case of a working bottom outlet. The hazard curve for maximum pool water levels is calculated and plotted in Fig. 7 (extrapolated for Annual exceedance frequencies lower than 1E-04).
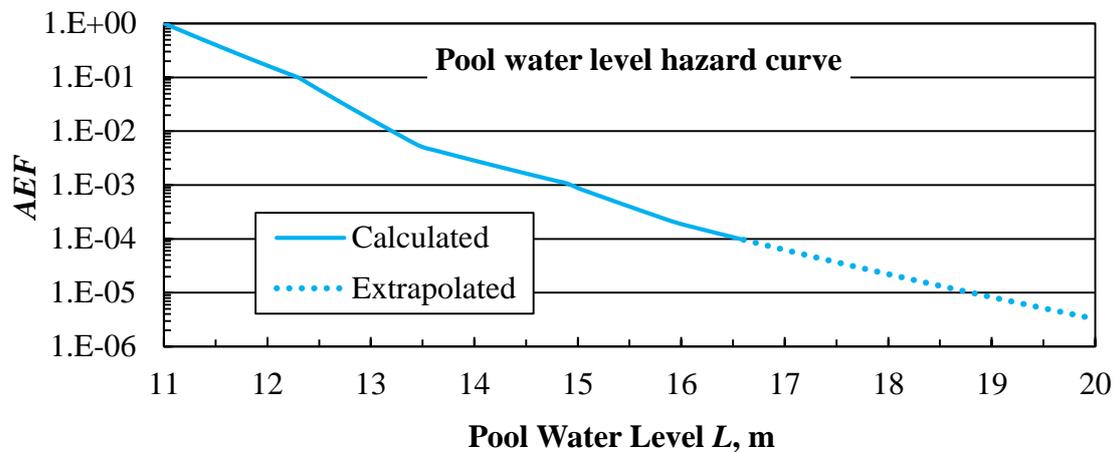
Fig. 8: Hazard curve for maximum pool water levels

Annual failure probability

The annual failure probability P_f is calculated by integrating the CPF, denoted as $P_{f/L}$ and the hazard curve $H(L)$ using Equation (9) [5].

$$P_f = -\int_{11}^{20} P_{f|L} \cdot \frac{dH}{dL} \cdot dL \tag{9}$$

A numerical solution with discretization interval ΔL=0.1 m was implemented for the calculation of the AFP integral. The annual failure probability profile is provided in Fig. 9, representing the AFP for confidence levels from 0.3% to 99.7%. The AFP fits precisely to a log-normal distribution (see also [5]): median AFP=0.08 and logarithmic standard deviation β=0.566, giving COV=0.615. It should be noted that for all subjective probabilities, only the water levels below 13 m contribute significantly to the AFP.
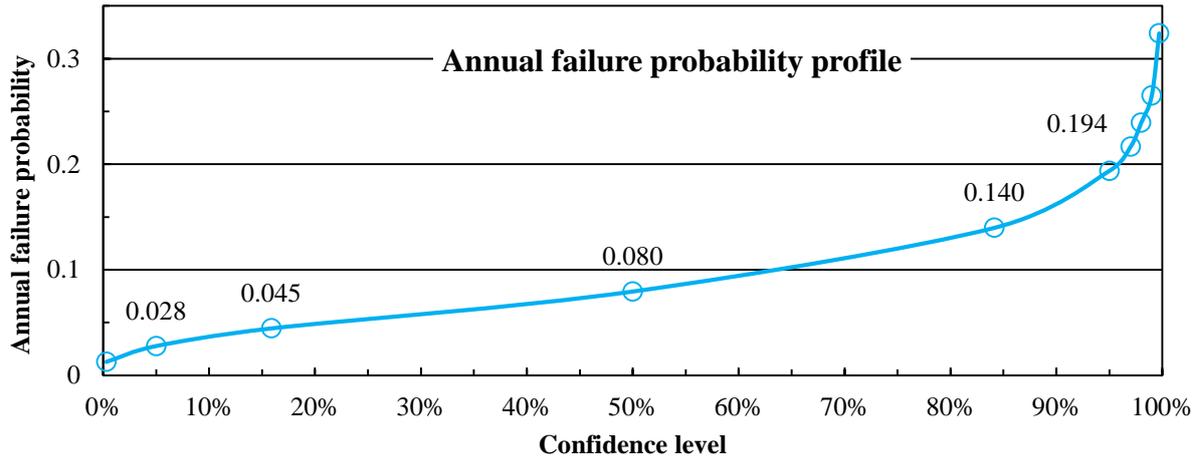
Fig. 9: Annual failure probability profile

Sensitivity analysis

Sensitivity analysis was performed to get an insight on the influence of varying mean values of the soil properties and other analysis assumptions: different probability distribution types for the sliding fragility curve, upper and lower limit combination (Equation (4)) phreatic correction, increase of shear strength due to matrix suction and lower unit weight above water table, and different volumetric water content functions. The results are presented in Fig. 10.
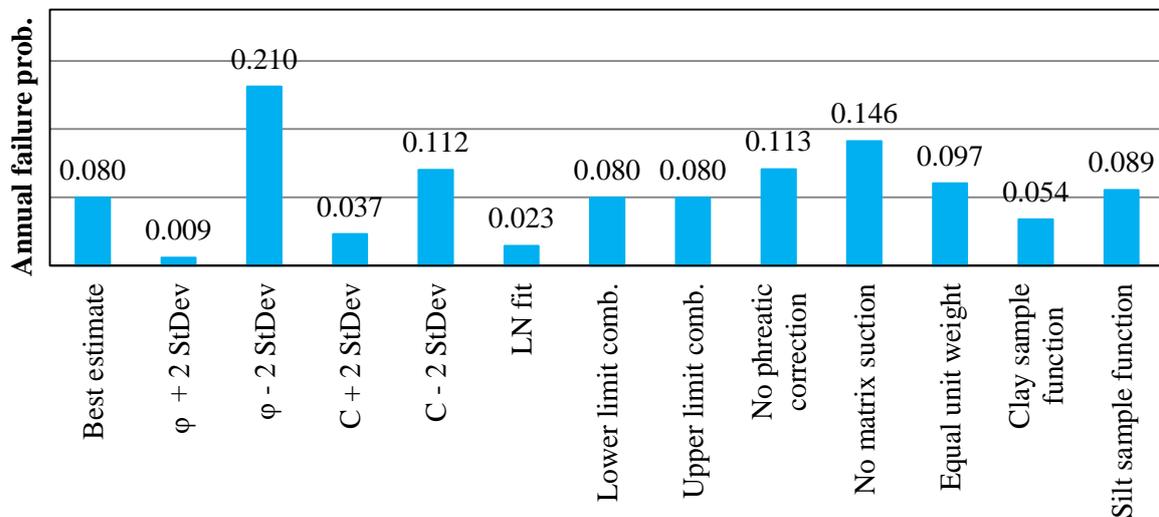
Fig. 10: Median AFP for different mean soil properties and analysis assumptions

The variation of the mean effective friction angle has the most significant effect on the median *AFP*, followed by the use of unsaturated shear strength. On the other hand, the chosen method for the combination of fragility curves (upper/lower boundary or average) has an insignificant influence on the median *AFP*. The log-normal fitting of sliding fragility has also a strong tendency for underestimating the overall failure probability due to its underestimation of the low pool level CPFs. All four effects, given above, are consequence of the low pool water levels significant for the *AFP*.

Conclusions

The paper presents the results of a case study on probability of failure of an embankment dam for sliding instability and overtopping.

The calculated median *AFP* for the embankment is 0.08, much larger than the recommended acceptable value for loss of 1 life which is 0.001 [10]. The covariance of the AFP (*COV*=0.615) reflects well the large epistemic uncertainty (both from soil properties and model assumptions) for the low pool water levels, significant for the *AFP*. This is a hint that the overall probability analysis procedure could be improved. The epistemic standard deviation of the soil properties may be reduced with extensive testing. Introducing more precise steady-state seepage analysis, regarding the actual soil properties, will give a better estimation of PWP, thus reducing the uncertainty associated with the use of phreatic correction and unsaturated shear strength.

Acknowledgement

References

[1] Ang A.H., Tang W.H. (2007). Probability Concepts in Engineering. Emphasis on Applications in Civil & Environmental Engineering, 2nd edition, John Wiley & Sons inc.

[2] Baker J.W. (2011) Fitting Fragility Functions to Structural Analysis Data Using Maximum Likelihood Estimation. http://web.stanford.edu/~bakerjw/fragility.html.

[3] Chow V.T. (1959).Open channel hydraulics, McGraw Hill, New York

[4] Duncan J.M., Wright S.G. (2005), Soil strength and slope stability, John Wiley and Sons inc., Hoboken NJ, USA.

[5] EPRI (1994). Methodology for Developing Seismic Fragilities, Electric Power Research Institute.

[6] GEO-SLOPE (2014). Stability modelling with SLOPE/W: An engineering methodology, September 2014 edition, GEO-SLOPE International Ltd., Calgary AL, Canada.

[7] Grifiths D.V., Fenton G.A., Tveten D.E. (2002). Probabilistics in Geotechnics: How difficult does it need to be?, Proceedings of the International conference on Probabilistics in Geotechnics. Technical and economic risk estimation, Graz Austria

[8] Hill P., Bowles D., Jordan P., Nathan R. (2003). Estimating overall risk of dam failure: practical considerations in combining failure probabilities, ANCOLD 2003 Risk Workshop, Australian National Committee on Large Dams.

[9] Morales-Tores A., Escuder-Bueno I. (2015). Theme B: Probability of failure of an embankment dam due to slope instability and overtopping, 13th ICOLD Benchmark Workshop on Numerical Analysis of Dams, Lausanne, Switzerland.

[10] SPANCOLD (2012). Risk analysis applied to management of dam safety – Technical Guide 8 (Vol. 1), Spanish National Committee on Large Dams.

Theme B: System approach to probability of failure of an embankment dam

Westberg Wilde, M.[1] and Vazquez Borragan, A. [1]

[1]ÅF Industry AB, Frösundaleden 2A, 169 99 Stockholm, Sweden

ABSTRACT: A system approach was applied to estimate the probability of failure of an embankment dam, with input variables defined according to theme B of the ICOLD Benchmark. Reference fragility curve of the most critical slip surface was combined with the reference fragility curve of overtopping. The resulting reference fragility curve of failure was combined with the annual exceedance probability and an estimate of the probability of failure for floods of return period >10 years was estimated. For two different water levels (12 and 16) m a series system analysis of the five most critical slip surfaces was applied to investigate the effect on the failure probability. To identify slope instability a limit equilibrium model was created with Slope/W and the built-in probabilistic algorithm utilizing a Monte Carlo scheme.

E-mail: marie.westberg.wilde@afconsult.com, alejandro.vazquez@afconsult.com

Introduction

The present work is prepared as part of the benchmark workshop on Numerical analysis of Dams. The scope of Theme B is to estimate probability of failure of an embankment dam due to slope instability and overtopping. Probability-based assessments of dams are becoming increasingly used, both in quantitative risk analysis and in decision making.

Design decisions are made under a great deal of uncertainty as uncertainties are involved in every step of planning, design, execution and management of a dam. Models to describe structural behavior are only just that, models of the real world. Load effects as well as resistances are representations of our (best) understanding and knowledge. In a deterministic process uncertainties are not included and instead conservative assumptions are made and a safety factor is considered to give sufficient safety. As pointed out already by Höeg and Murarka in 1974 [1] use of conventional safety factors can be deceptive and may lead the engineer into false sense of safety. Another important point to be made is that the definition of the safety factor is ambiguous which means that the safety factor may vary depending on how it is defined. In a probabilistic context both aleatory and epistemic uncertainties are involved and due to definition it is unambiguous [2].

The dam to be analyzed is a fairly simple homogeneous dam. Its upstream slope inclination 23,5° and its downstream slope inclination 28°, with total height 16 m being the normal operating level 11 m. This geometry is shown in Fig. 1. The specific weight of material is 19 kN/m³. This dam has a non-gated spillway with crest at 11 m and bottom outlet with one conduit and two gates. Crest length 263,5 m. Two failure modes are analyzed: slope stability and overtopping. In both failure modes the water pool level is considered the driving force of failure.

Phase 1: Analysis of the information for the instability failure mode

To identify slope instability a limit equilibrium model was created with the software Slope/W. The model for phase 1 showed 400 failure surfaces with a critical safety factor of 1.04 (See Fig. 1). Some of the characteristics of the methodology are included in Tab. 1.

The effect of pore water pressure was considered by drawing a piezometric line in Slope/W from the water pool level upstream to the exit point at 3.3 meters over downstream face. It was

also applied an automatic correction of the piezometric line. The same procedure was applied for higher pool levels in the following phases.
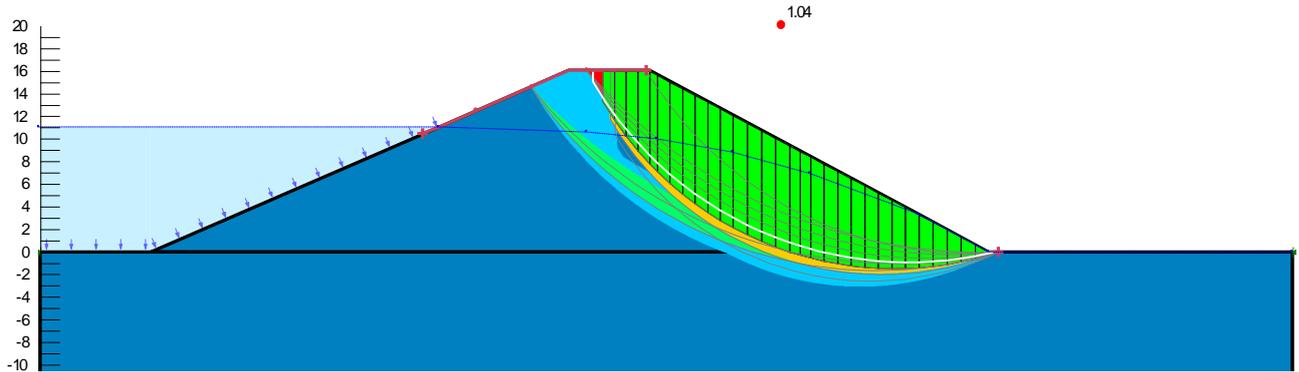
Fig. 1 Slope instability limit model

Tab. 1 Characteristics of slope instability limit model

Limit equilibrium method	Soil failure mode	Pore-water pressure	Search slips method	Tension cracks	Failure surface
Morgenstern-Price	Mohr-Coulomb	Manual piezometeric line with automatic correction	Entry at crest and exit at toe	At base of slip surface when slope was > 60°	Circular slip

Random variables

For this theme two random variables are given: cohesion and friction angle. The given information was that these have been estimated from available information and tests. Cohesion has a lognormal distribution with mean value 10 kPa and standard deviation 3 kPa.

ϕ has a normal distribution with mean value 25° and standard deviation 2°. It is truncated at minimum 20° and maximum 30°. These density functions shown in Fig. 2 were inserted in Slope/W. Note that an offset value of -10 for cohesion and 25 for friction angle was applied respectively in each function. This is due to specific values set for the material properties in the program [3]. Introduction of further random variables is optional and has not been utilized.
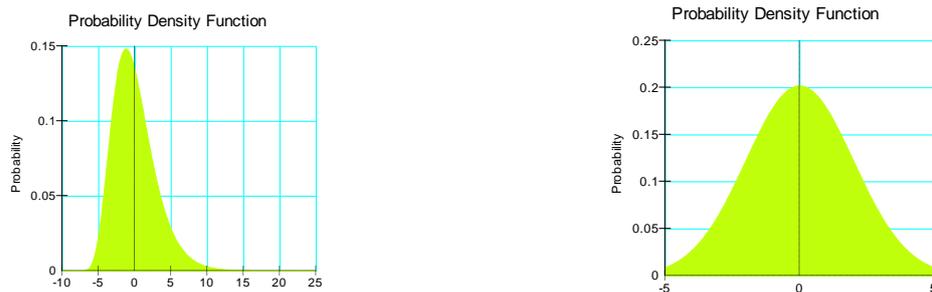
Fig. 2 Cohesion log normal distribution (left) and friction angle normal distribution (right)

Introduction and evaluation of epistemic uncertainty

Epistemic uncertainty is related to lack of information, either due to insufficient understanding of e.g. behaviour or to insufficient data. The main epistemic uncertainties in the slope instability model assuming Mohr-Coulomb failure; are: the pore water pressure; and the effective strength parameters, as shown in Equation (1).

$$S_m = \frac{\beta}{F_s}\{c' + (\sigma_n - u_w)\tan\varphi'\} \qquad (1)$$

However, this is not true if unsaturated conditions were applied [4]. In such case, the shear mobilized force for unsaturated soils considers two more epistemic uncertainties shown in Equation (2); the matric suction and φ^b.

$$S_m = \frac{\beta}{F_s}\{c' + (\sigma_n - u_a)\tan\varphi' + (u_a - u_w)\tan\varphi^b\} \qquad (2)$$

Where, S_m is the shear force mobilized on the base of the slice; β is the length along the base of a slice; F_s is the overall factor of safety; c' is the effective cohesion; σ_n is the normal stress acting on the base of a slice; φ' is the effective angle of internal friction; u_a is the pore-air pressure at the base of a slice; $u_a - u_w$ is the matric suction and φ^b is the angle defining the rate of increase of strength due to an increase in the suction. As a result of that, other failure surfaces would be achieved; perhaps more realistic surfaces [5]. Therefore, the assumption of saturated soils might have underestimated the stability of the embankment [4] and [5].

Other random variables could have been introduced in the probabilistic model, such as: the unit weight, earthquake acceleration, point loads (e.g., ice load), spatial variability, etc… However, due to lack of data and time limitation it was not possible to include all of these analyses. Furthermore, if other failure modes were considered such as: undrained failure, hardening soil, HS-Small, hyperbolic, etc… other epistemic uncertainties could be discussed. For instance, if a hardening soil model was assumed with Finite element software, then, the Young modulus or the Poisson's ratio would be some of the main epistemic uncertainties in the instability model.

It has been shown in several publications [5] and [10] there is often a negative correlation between c and ϕ. This negative correlation means that for high ϕ the cohesion is often low and vice versa. The effect needs to be input to the probabilistic analysis, but since no such information was available this was not possible. The effect of this correlation is likely that the very high and very low values of shear strength are slightly "smoother"; for very low ϕ, c is likely to be higher and for very high ϕ, c is likely to be lower. Hence the lowest and highest capacity achieved without consideration of correlation may not be reached. The probability of failure will be affected, but it is not possible to know the effect in advance.

Due to geological processes and man-made influence there are fluctuations of properties within soil layers. Random fields can be used to describe this spatial variability. This has been described by e.g. [6] and [7]. No spatial variability was considered in this case.

For long structures, e.g. a dike or a long earth dam, there is also correlation between failure in different points along the structure. This has not been considered in this example.

Phase 2: Calculation of reference fragility curves

Reference fragility curves for slope instability
In Slope/W the built-in probabilistic algorithm utilizing a Monte Carlo scheme is used to compute a probability distribution of the resulting safety factor.

In general, each simulation in a Monte Carlo simulation would result in input data for the statistical parameters and "all" possible slip surfaces would be analysed. Failure of any one slip surface implies failure of the structure (series system). The probability of failure would then be estimated as

$$p_f = \frac{Number\ of\ simulations\ resulting\ in\ failure\ in\ any\ slip\ surface}{total\ number\ of\ simulations}$$

For a series system it is also possible to estimate the global failure probability by calculating probability of failure of all possible failure modes and combining them. When the correlation

between all failure modes is known, the global probability of failure may be estimated, either by integration or by different types of reliability bounds [8] and [9].

For a series system the simple bounds are given by Equation (3);

$$\max_{i=1}^{n} P(E_i) \leq P_f \leq 1 - \prod_{i=1}^{n} \left(1 - P(E_i)\right) \tag{3}$$

where the minimum failure probability is the result of full correlation between failure modes and given by the maximum probability of event E_i. The maximum probability of failure is the result of no correlation.

In the model it was considered the failure probability of each slip surface separately. However, a certain combination of input parameters may result in failure of several slip surfaces, but this analysis was not performed. The correlation between different failure surfaces is not known and hence it is not possible to calculate the complete failure probability of the series system.

To take advantage of the simple slope analysis provided by Slope/W the choice was therefore to estimate the failure probability in three ways:

1. Failure probability of the most critical slip surface[1] (similar to series systems analysis assuming full correlation), calculated according to the first part of Equation (3).
2. Series systems analysis of the five most critical slip[1] surfaces, assuming zero correlation, calculated according to the last part of Equation (3).
3. Series systems analysis of the five most critical slip surfaces by the integration of the bivariate normal distribution Φ_2 according to Equation (4), assuming correlation of ρ in every step; See e.g. [8].

$$\beta_{sys} = -\Phi^{-1}\left(P_f\right) \approx -\Phi^{-1}\left(1 - \Phi_2\left(\beta_1, \beta_2; \rho\right)\right) \tag{4}$$

1. Most critical surface was identified by analysis of different slip surfaces for the mean values of cohesion and friction angle

Points 2 and 3 were only applied to water levels of 12 and 16 m to investigate the effect on the failure probability.

Each Monte Carlo simulation was based on 2000 trials. The water levels were varied in the range between 11-20 m and the probability of failure was estimated for each 0.5 m and for each 0.25 m in the range between 16-18 m. The resulting fragility curve of the most critical failure surface is shown in Fig. 3. Note that the jump from 17.25-17.5 m in the probability of failure is due to the fact that the piezometric line drawn was slightly above the boundaries of the dam. Therefore, Slope/W included the water above surface as a load in the limit equilibrium analysis.
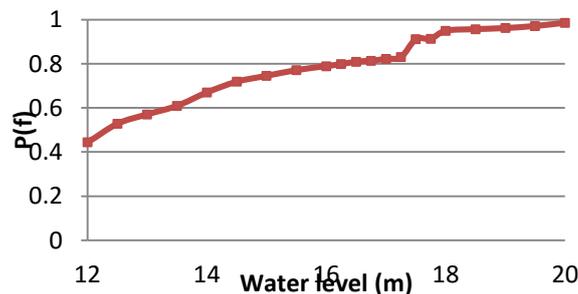
Fig. 3 Reference fragility curve for the most critical failure surface

The systems analysis gave the following results in Tab. 2. Italic letters are for the full and no-correlation cases resulting from a simple series system analysis of point 2 above, the others from the analysis in point 3. As can be clearly seen, it is of major importance to know the correlation between the different slip surfaces when a system analysis is performed.

Tab. 2 Systems analysis

ρ	12 m β	pf	16m β	pf
1		0,44		0,79
0,98	0,11	0,46	-0,83	0,80
0,9	-0,09	0,53	-1,05	0,85
0,75	-0,33	0,63	-1,33	0,91
0,5	-0,64	0,74	-1,77	0,96
0,001	-1,28	0,90	-2,89	1,00
0		0,91		1,00

For a cohesive-frictional soil the correlation between different slip surfaces is believed to be high [10]. The main reason for this assumption is that sensitivities of cohesion and friction angle are likely to be similar for the different failure surfaces and thus the correlation coefficient is expected to be high. Hence it is the belief of the authors that the system approach with critical slip surface is sufficient to give an estimate of the failure probability, although it should be noted that our approach may underestimate the failure probability.

Reference fragility curves for overtopping
In the assignment the reference fragility curve for overtopping was to be represented by a log-normal distribution with mean 17 m and standard deviation 0.2 m. In physical terms this means that the dam will fail for a water level of 17 m, but with a variability. The reference fragility curve is shown in Fig. 4.
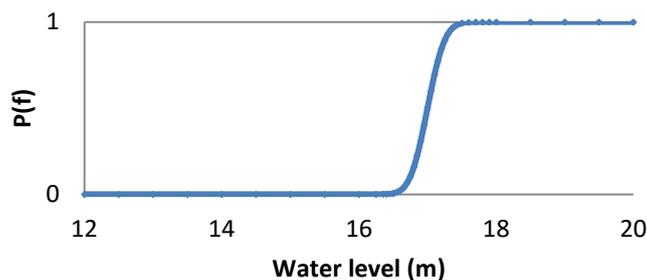
Fig. 4 Reference fragility curve for overtopping

Reference fragility curves for slope stability and overtopping
Next the fragility curves for slope stability and overtopping should be combined. These may be considered as a series system; failure occurs if either the slope fails or if the dam overtops.
The correlation between slope stability and overtopping is not known, and both upper and lower bounds according to Equation (3) were calculated.
Slope stability is the predominant failure mode up to approximately 17.2 m, then the overtopping failure mode is predominant.
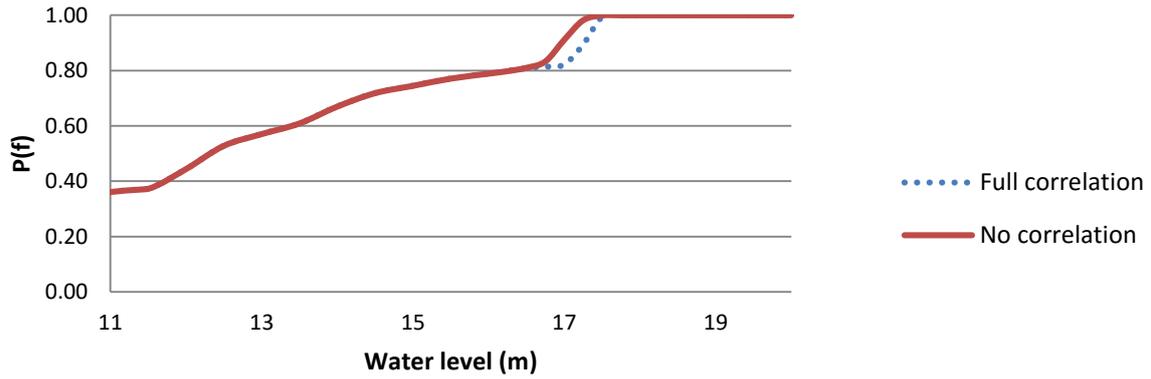
Fig. 5 Reference fragility curve for slope stability and overtopping combined

Phase 3: Calculation of water pool level probabilities

Information was provided regarding the previous pool level (11 m), discharge curves for bottom outlet and overflow spillway, return periods of floods and pool level-reservoir capacity. A reservoir model, taking account for inflow, outflow and volume in time steps was used to analyse the annual exceedance probability for different water levels. In Fig. 6 output for the 10 year return period flood (inflow, outflow and water level) is shown.
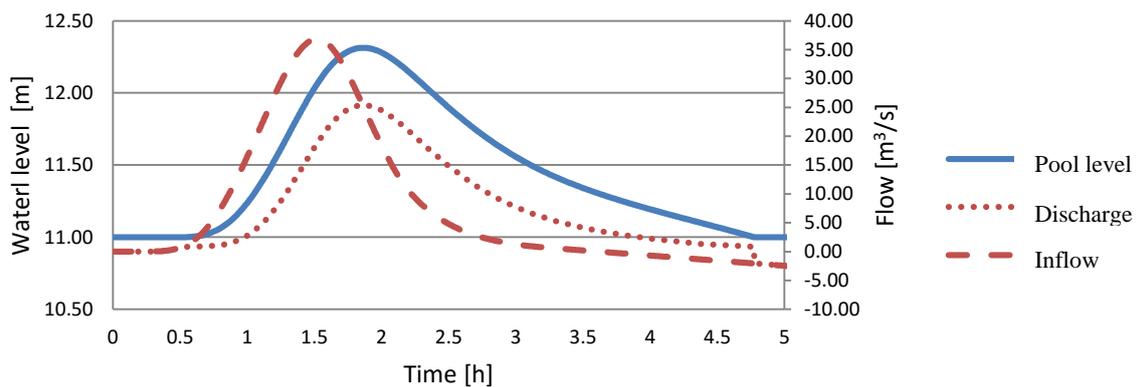
Fig. 6 Pool level-Inflow-discharge curves for T=10 years

The resulting water levels for different return periods are shown in Fig. 7. The availability of the bottom outlet has only a small effect on the end result, about 2-4 cm. The AEP (annual exceedance probability) should also be combined with the probability of having available bottom outlet or having unavailable bottom outlet. It is also important to note that the floods analysed is for 10-10 000 years, and that 1-9 year floods were not analysed. For this reason, the AEP-curve is shown only for the upper part of the cumulative distribution function.
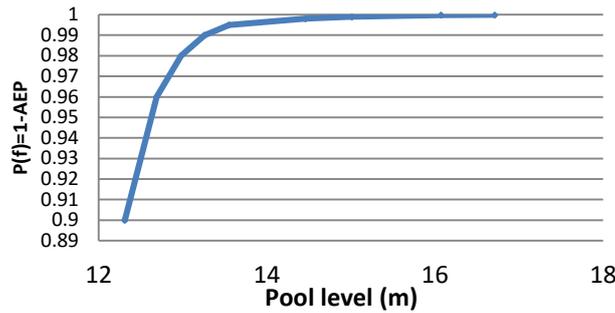
Fig. 7 AEP of pool level for the case with bottom outlet in function

Phase 4: Computing failure probability and sensitivity analysis

Combined curves for AEP and reference fragility
To combine the curves shown in Fig. 5 and Fig. 7 the best way would be to identify the type of cumulative distribution function best describing the fragility curve and the AEP and integrating these. Another, less exact, way was applied here.
From the law of total probability in Equation (5) we have

$$P(B) = \sum_{i=1}^{n} P(A_i) \cdot P(B|A_i) \tag{5}$$

Applying this to the present problem we have in Equation (6) that

$$P_f = \sum_{i=1}^{n} P(wl_i) \cdot P(fail|wl_i) \tag{6}$$

As the probability of having exactly wl_i is per definition zero, the probability of each water level was estimated from the frequency curve with Equation (7) as

$$P(wl_i) = F(wl_i - \Delta w) - F(wl_i + \Delta w) \tag{7}$$

The probability of failure for each water level as well as the total probability of failure for flood events is shown in Tab. 3. Due to the insignificant difference in water level with bottom outlet in function/malfunction the below values are taken assuming bottom outlet in function.

Tab. 3 Reference failure probability results

wl	P(wl)	wl	$P_{failmin}$	wl	$P_{failmax}$	wl	$P_{fmin\ combined}$	$P_{fmin\ combined}$
12,31-12,69	0,06	12,5	0,528		0,528		0,032	0,032
12,69-12,98	0,02	12,85	0,558		0,558		0,011	0,011
13,26-12,98	0,01	13,15	0,582		0,582		0,006	0,006
13,55-13,26	0,005	13,4	0,601		0,601		0,003	0,003
13,55-14,46	0,003	14	0,670		0,670		0,002	0,002
14,46-15,01	0,001	14,75	0,732		0,732		0,001	0,001
15,01-16,07	0,0008	15,5	0,771		0,771		0,001	0,001
16,07-16,71	0,0001	16,5	0,809		0,810		0,0001	0,0001
				Total P_f			0,055	0,055

Sensitivity analysis of main parameters
The next step suggested was to perform a sensitivity analysis. This has not been performed, but instead a discussion of sensitivities is given.
The first important point to be made is that the present analysis was done simply by analysing the critical slip surface. As discussed in [10] slope stability problems of cohesive-frictional soils

like this case need to be treated as a system of potential slip surfaces in order to obtain a better estimate of the true critical slip surface based on a maximum probability of failure.

The overtopping probability of failure will be largely affected by the chosen distribution and its mean value and standard deviation. If the standard deviation is increased or the mean value is decreased, the failure probability for overtopping would be quite different from that estimated here.

Slope stability has the largest effect on failure probability. This is due to the fact that the uncertainty of the strength parameters and pore-water pressure is present in any cross section even when there is no water in the reservoir. Nevertheless, input of different slope stability parameters in the same model; such as; cohesion, friction angles, unit weight, spatial variability, point loads, seismicity, slip surface limits, cross correlation c-φ, and piezometric lines would have a significant impact on the results. Furthermore, the given parameters computed very low safety factors (SF≤1) which implied obviously high probability of failure.

Changes to the estimates of discharge, inflow hydrograph and reservoir capacity would also change the end result. The effect of the bottom outlet to function or not to function is not very important, as it only affects the water level to a limited extent. Even though the dam seems to resist some overtopping, and the probability of very high water levels is very small overtopping may be affected by natural uncertainty; such as: waves from strong winds; and trees or debris blocking the spillway.

Conclusion

The analysis presented here was based on a probabilistic analysis of the most critical failure surface. The estimated probability of failure for the critical slip surface is approximately 0,055 for floods exceeding return period of 10-years. However, correlation between different slip surfaces is probably low hence the above probability of failure will underestimate the "real" probability of failure. Despite of that, slope stability was found to affect the annual probability of failure more than overtopping up to a water level of approximately 17.2 m. The results for each failure mode showed sensitivity to different uncertainties discussed above. Therefore, the concluding remark is that with the conditions analysed the slope stability was more sensitive to epistemic uncertainties than overtopping. Although, further analyses (phase 5) to characterize the effect of epistemic uncertainty need to be accomplished for a comparison with risk reduction measures.

References

[1] Höeg, K., & Murarka, R. P. (1974). Probabilistic analysis and design of a retaining wall. *Journal of the Geotechnical Engineering Division*, *100*(3), 349-366.

[2] Robert E. Melchers. (1999). *Structural reliability analysis and prediction*. John Wiley & Son Ltd.

[3] El-Ramly, H., Morgenstern, N.R. and Cruden, D.M. (2002). Probabilistic Slope Stability Analysis for Practice, *Canadian Geotechnical Journal, Vol. 39, No. 3, pp. 665-683.*

[4] Fredlund, D. G., & Rahardjo, H. (1993). Soil mechanics for unsaturated soils. *John Wiley & Sons*

[5] Geo-Slope, International Ltd Manual, GeoStudio User's. (2012) "Geo-Slope" Calgary, Alberta, Canada T2P 2Y5.

[6] E.H. Vanmarcke. Random fields: analysis and synthesis. The M.I.T., 3rd edition, 1983.

[7] G.B. Baecher and J.T. Christian. Reliability and statistics in geotechnical engineering. *John Wiley & Sons Inc, 2003.*

[8] Hohenbinchler & Rackwiths (1982), First-order concepts in system reliability. *Structural Safety. 1:177-188.*

[9] Efstratidos, N, Ghiocel. C & Singhal. S. (2005) *Engineering Design Reliability handbook. ISBN 0-8493-1180-2.*

[10] Javankhoshdel, S., & Bathurst, R. J. (2014). Simplified probabilistic slope stability design charts for cohesive and cohesive-frictional (c-ϕ) soils. *Canadian Geotechnical Journal, 51(9), 1033-1045.*

Probability of Failure of an Embankment Dam Due to Slope Instability and Overtopping

Mouyeaux A.[1,2], Carvajal C.[1], Peyras L.[1], Bressolette P.[2,3], Breul P.[2,3], Bacconnet C.[2,3]

[1]*IRSTEA – Institut national de Recherche en Sciences et Technologies pour l'Environnement et l'Agriculture, 3275 Route de Cézanne, CS 40061, 13182 Aix en Provence Cedex 5, France*
[2] *Clermont Université, Université Blaise Pascal, Institut Pascal, BP 10448, F-63000 Clermont-Ferrand, France.*
[3]*CNRS, UMR 6602, Institut Pascal, F-63171 Aubière, France.*

ABSTRACT: Two mechanical models of different complexity – one using Limit Equilibrium Method (Geostudio software) and the other Finite Element Method (code Cast3M) – are developed to assess the probability of failure due to slope instability considering cohesion and friction angle as random variables. Two hydraulic conditions (steady-state and transient) are also tested for both mechanical models.

Fragility curves for sliding failure mode but also overtopping failure mode are then computed and combined using the Common Cause Adjustment. In order to compute the global failure probability of the dam, the resulting fragility curve representing the structural behaviour is finally combined with water pool level probabilities. The latter are calculated considering available floods data and the hydraulic behaviour of the dam-reservoir system.

This paper aims to compare several cases based on different methods and assumptions to show their potential influence on the final failure probability. In this simple geometry case, the probability of failure is not affected by the mechanical model. On the other hand, the assumptions made on hydraulic conditions have a great influence on the risk of failure.

The authors finally highlight that the developed finite element model is able to use random fields instead of random variables.

E-mail: anthony.mouyeaux@irstea.fr

Introduction

Embankment dams represent majority of dams in the world and are more concerned by failures than others types of dams [1]. These hydraulic works may induce high technological risks. The safety of such structures has so to be evaluated in the best accurate way. Risk assessments techniques provide adapted tools to take uncertainties on loads and dams resistance into account in the dams safety evaluation.

In France, regulations impose since a decade the realization of risk assessment studies for all large dams.

In this purpose, IRSTEA has launched some researches on the subject including a thesis on the analysis of earth dam reliability. This one aims to answer some of the questions raised by this benchmark.

The epistemic uncertainty assessment (phase 5) is not treated in this paper.

Analysis of instability failure mode (Phase 1)

Description of the slope instability models
Dam stability is evaluated through two different mechanical models:

1. The first one is made on the commercially available code Geostudio and uses a traditional Limit Equilibrium Method (LEM) of Morgenstern&Price. The failure surface is assumed to be circular and stability is checked on multiple preset circles.
2. The second is a Finite Element (FE) model developed on the user-free code Cast3M. The factor of safety is obtained through the shear strength reduction method [2]. This method

consists in reducing the parameters c and φ of the elasto-plastic Mohr-Coulomb failure criterion until failure occurs.

In our model, failure is assumed to appear in case of non-convergence of the solution. It is accompanied with an important increase of nodal displacements from which the factor of safety is calculated. Our model, under development, is able to assess a factor of safety (FoS) but not yet if it is lower than 1.

Both models take pore water pressure into account in the slope stability analysis. Two hydraulic conditions are analysed:

- Steady-state condition: with totally saturated condition in Geostudio (case 1) and unsaturated in Cast3M (case 3);
- Transient condition: in Geostudio (case 2) and Cast3M (case 4), a FE calculation of the seepage through the unsaturated soils of embankment is performed using Richard's equation. Degree of saturation and hydraulic conductivity of the soil are described by empirical Van Genuchten relationships.

For the transient condition, hydraulic boundary conditions entered in the models correspond to the water level evolution in the reservoir caused by a certain flood. These water level evolutions are derived from the ones computed in the flood routing study presented in phase 3. The models take into account the worst hydraulic state, with maximal pore pressures and maximal water pool level.

In Cast3M cases, a complementary refinement is added: the mechanical calculation takes into account the rise of cohesion due to matric suction and the influence of the saturation on unit weight, in addition to pore water pressures.

Fig. 1 gives a comparison of deterministic factor of safety calculated with each model in different conditions.
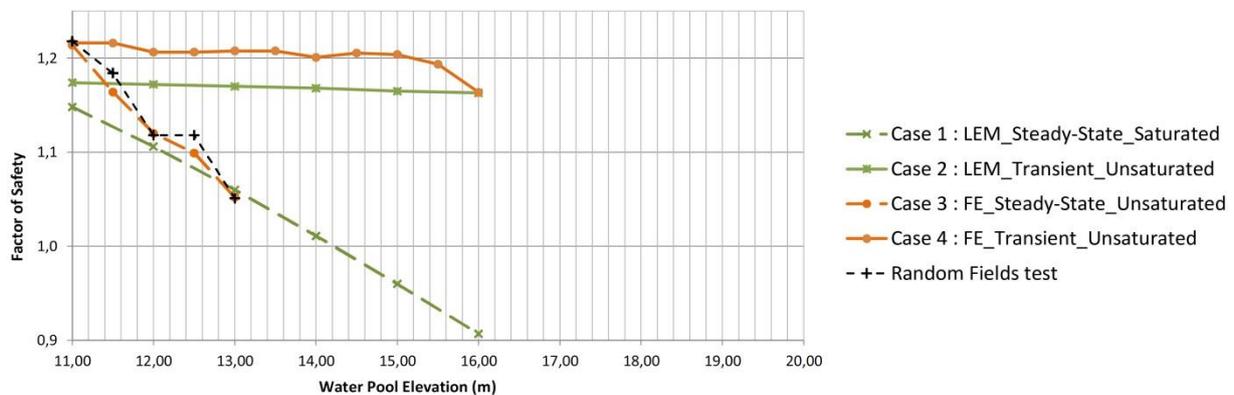
Fig. 1: Comparison of factors of safety obtained with both models

The principal difference is encountered between the steady-state and the transient conditions. Indeed, the steady-state curves represent an unrealistic condition in which the water pool level remains at the same stage during a long time. This hypothesis is obviously not relevant, especially for water level above crest elevation which will cause dam failure by overtopping before the establishment of the permanent water table in the embankment.

Taking the simplicity of the embankment's geometry into account, it could be supposed that the difference between the results of LEM and FE models could be explained by the difference of consideration of hydraulic conditions in mechanical calculations.

Probabilistic assumptions

In LEM and FE models, only the two recommended variables - cohesion and friction angle - are considered as random variables with their respective distributions for natural uncertainty: lognormal with average 10 kPa and standard deviation 3 kPa for cohesion, truncated normal with average 25° and standard deviation 2° for friction angle.

Nevertheless, the user-free code Cast3M enables more complexity and each parameter could be introduced as a random variable if necessary. This advantage of using this code is also that random fields could be introduced instead of random variables. It allows spatial variability of the material to be taken into account. A few deterministic calculations with cohesion and friction angle random fields have been made as example. The results are plotted on Fig. 1.

Epistemic uncertainty

The epistemic uncertainty results from not having enough knowledge on the analysed system because of the lack of data or assumptions made in the modelling of the structure.

In order to take this uncertainty into account in a progressive way, it is necessary to focus firstly on the mean assumptions concerning methods used for the mechanical modelling (LEM or FE) and hydraulic conditions (steady-state or transient). Indeed, they could lead to a significant difference on the final failure probability.

Once these assumptions are well defined, a sensibility analysis on hydraulic and mechanical parameters has to be done to identify which ones have the greater influence on the results.

Then, the parameters that are relevant to model more accurately on the way described in phase 5 could be chosen.

Reference Fragility Curves (Phase 2)

Sliding mode of failure

Different approaches are available to develop fragility curves. They are more specifically described in [3]. Numerical solution methods are adopted here to compute the fragility curve for slope instability. Calculations are made independently with the two models:

1. With the limit equilibrium model, the probability of failure is computed using Monte-Carlo simulation. A sample of 1,000 realizations of the two random variables is generated and the computation of the factor of safety is done. The probability of failure is approximated by the fraction of failures (FoS<1) over the total number of calculations.

2. In the case of the FE model, the Monte-Carlo simulation is time-consuming and is not suitable in our case. Indeed, the strength reduction technique, as it has been implemented, is not able yet to give a FoS in the failure domain (FoS<1). The adopted technique is based on the Response Surface Method and consists in building the limit state function from a series of FE calculations [4].
   For a series of friction angle values (from 20° to 30° by step of 2°), the value of cohesion leading to the non-convergence is researched. The limit state function is then obtained by a polynomial regression on the six (c-φ) couples which give a FoS of 1.
   The limit state functions are then built by this way for the different water pool levels in the range 11-20 m.
   Once the limit state functions are available for different load conditions, Monte-Carlo method is employed to estimate the failure probability. A sample of 10,000 realizations of the two random variables is generated and plotted in the c-φ plane with the limit state functions (cf. Fig. 2). The probability of failure is given by the ratio of the number of c-φ couples below each limit state over the total number of realizations of the sample. An estimation of probabilities of failure is then made every meter of the water pool level varying in the range 11-20 m.
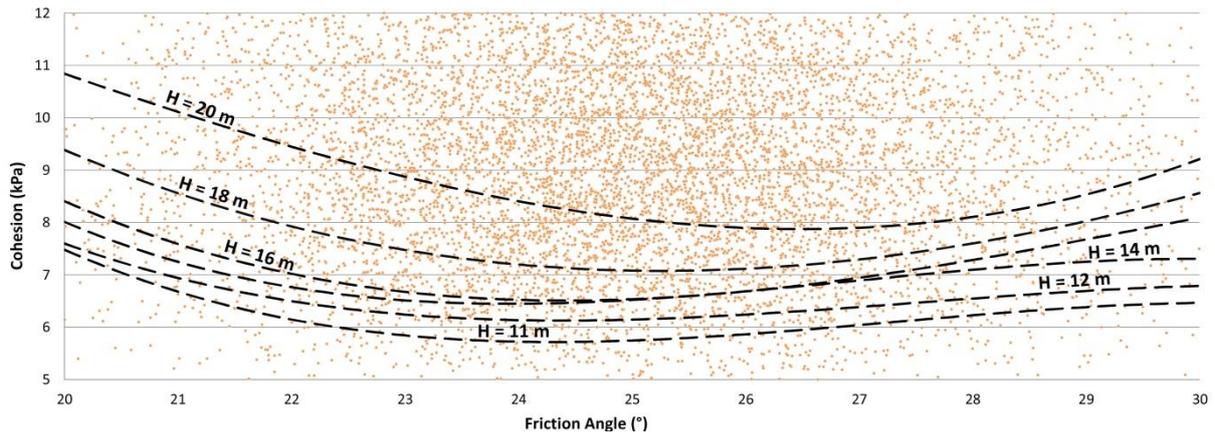
Fig. 2: Limit state functions – Case 4 (FE - Transient - Unsaturated)

Fig. 3 illustrates the results of both models for the four different cases. In steady-state condition, the fragility curves are much greater than ones in transient condition because of the unrealistic and pessimistic assumption that is made. Comparing the results of the two mechanical models in transient condition, the FE model gives higher probabilities of failure than the LEM model.
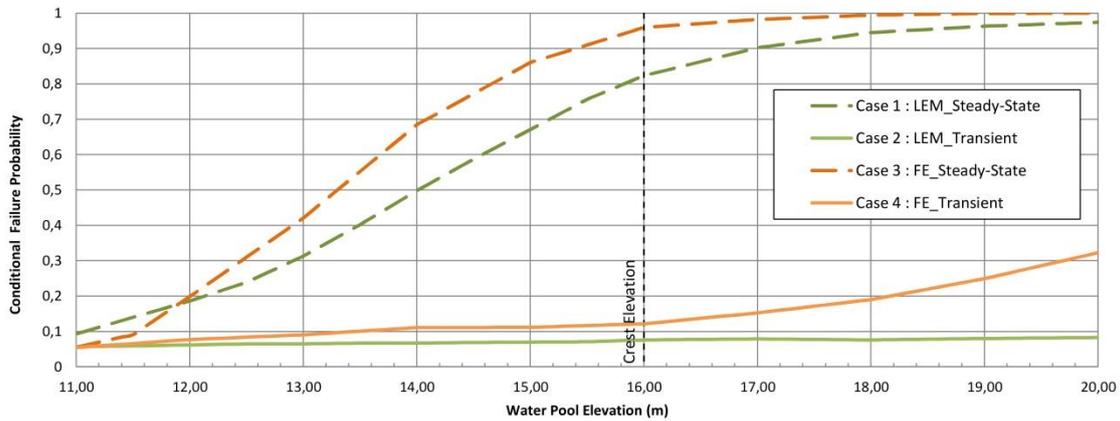
Fig. 3: Reference Fragility Curves : Sliding mode of failure

Overtopping mode of failure
The fragility curve for the overtopping mode of failure is directly obtained with a lognormal distribution with mean 17 m and standard deviation 0.2 m, as mentioned in the instructions. This curve is plotted in black on Fig. 4.

Combination of reference fragility curves
Once the reference fragility curves are available for both modes of failure, it is necessary to combine them in order to dispose of one single reference fragility curve. This one will represent the structural behaviour of the embankment. This is done here using the Common Cause Adjustment (CCA) approach which is useful when the different modes of failure affecting the system are not mutually exclusive [5]. Indeed, both modes of failures studied here – sliding and overtopping – are influenced by the maximal flood level in the dam. Their respective conditional probabilities could be adjusted using the uni-modal bounds theorem. It is described by the following inequality [5], where p_i is the conditional probability of the failure mode i and p_f is the global failure probability:

$$max_i[p_i] \ \leq \ p_f \ \leq \ 1 - \prod_i(1 - p_i) \qquad (1)$$
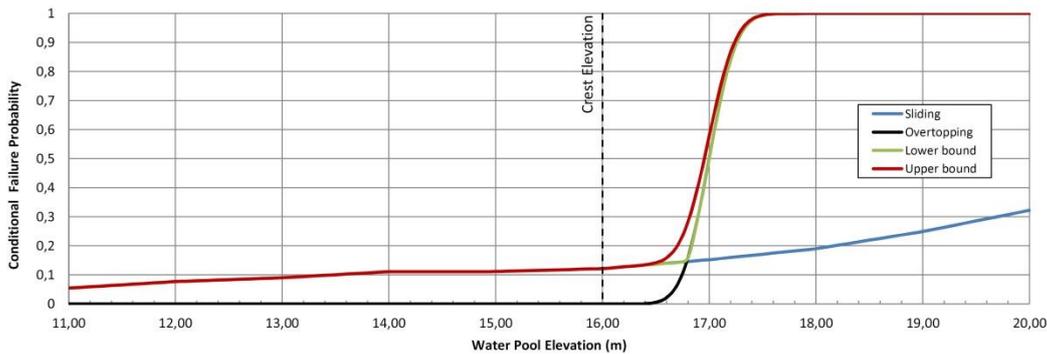
Fig. 4: Construction of the reference fragility curve – Case 4 (FE - Transient – Unsaturated)

This approach gives an interval for the global probability of failure and the adjustment could be made from the lower or the upper limit. In our case, choice has been made to make the adjustment from the higher limit (cf. Fig. 4).

Finally, Fig. 5 shows the reference fragility curves obtained by combination of the ones of each failure mode by the CCA approach for the four different cases.
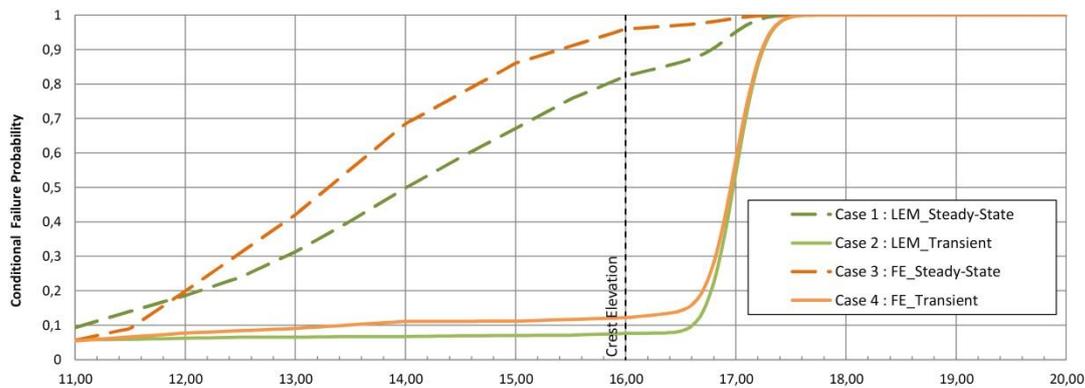
Fig. 5: Reference Fragility Curves of the embankment structural behavior

Water Pool Level Probabilities (Phase 3)

The objective of this phase is obtaining the annual exceedance probability (AEP) curve of water pool levels during floods. We proceed according to the following steps:

- Step 1: Extrapolation of the available floods hydrographs to high return periods;
- Step 2: Study of the flood routing of the dam-reservoir system for all floods;
- Step 3: Extrapolation of the maximal water levels to low return periods;
- Step 4: Construction of the AEP curve of the water pool levels during floods.

The floods hydrographs are available for return periods ranged from 10 to 10,000 years.

For the first step, the maximal discharges of given hydrographs are plotted versus the return period and an exponential law regression is fitted on the curve. The choice of an exponential law instead a linear regression is made in order to obtain higher peak discharges which give a water level up to 20 meters above the bottom of the reservoir. The hydrographs of high return period from $T=10^4$ to $T=10^8$ years are then extrapolated from the return period $T=10$ years hydrograph by multiplying by the ratio of peak discharges [6].

For the second step, the given and extrapolated hydrographs are then used to compute the hydraulic response of the system dam-reservoir.

The flood routing study is performed in an Excel spreadsheet routine considering all of the hydraulics data: the discharges curve of the spillway, the pool level-reservoir capacity curve and the previous pool level of 11 meters. The crest is considered as a spillway since the computed water pool level is above the crest elevation. For each hydrograph, two computations are made: one with and one without considering the evacuation through the bottom outlet.
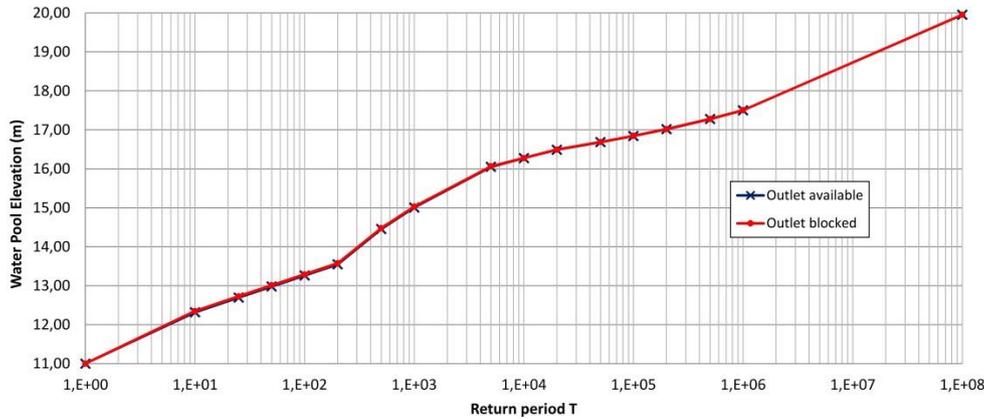
Fig. 6: Flood routing results: maximal water pool level vs. return period

The curves in Fig. 6 illustrate the results of the flood routing study for the two configurations with and without consideration of the bottom outlet. The two curves are really closed, showing that the bottom outlet has small influence on the flood water level. These curves also show that a flood of a return period of $T=10^8$ years is necessary to obtain a water level closed to 20 m.

Thirdly, a polynomial regression is done on the results of the flood routing study and give a relation between the peak discharge and the maximal water level reach during the flood. The exponential law fitted above to the maximal discharges of given hydrographs is used to obtain the peak discharges with return periods less than 10 years. Extrapolation of the maximal water levels to low return periods is done in a simplified manner using the polynomial relation to the peak discharges with return periods less than 10 years.

Finally, the generated series of water levels is sorted and annual exceedance probability is computed for each reservoir level in the range 11-20 m by step of 0.10 m. Two curves of annual exceedance probability are computed according to the two bottom outlet availability situations. These curves are weighted with coefficient of 0.85 for the situation considering the outlet and 0.15 for the other, corresponding to the bottom outlet reliability. They are then combined in one final curve shown in Fig. 7.
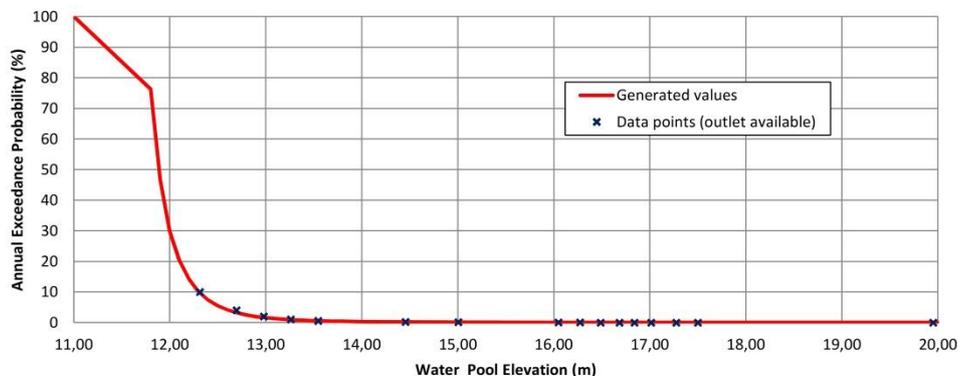
Fig. 7: Water pool levels vs. annual exceedance probability curve

Failure Probability (Phase 4)

Combination of AEP and reference fragility curves
Once the AEP curve is obtained, it is necessary to discretize it in order to combine it with the reference fragility curve and then compute the Annual Probability of Failure [7].
It has been decided to adopt a discretization with 26 intervals of variable size. These intervals are large when the curve is relatively flat (from 11 m to 11.8 and from 14 m to 20 m) and narrow when the curve is rapidly decreasing (from 11.8 m to 14 m). Fig. 8 shows a schematic plot of this discretization.
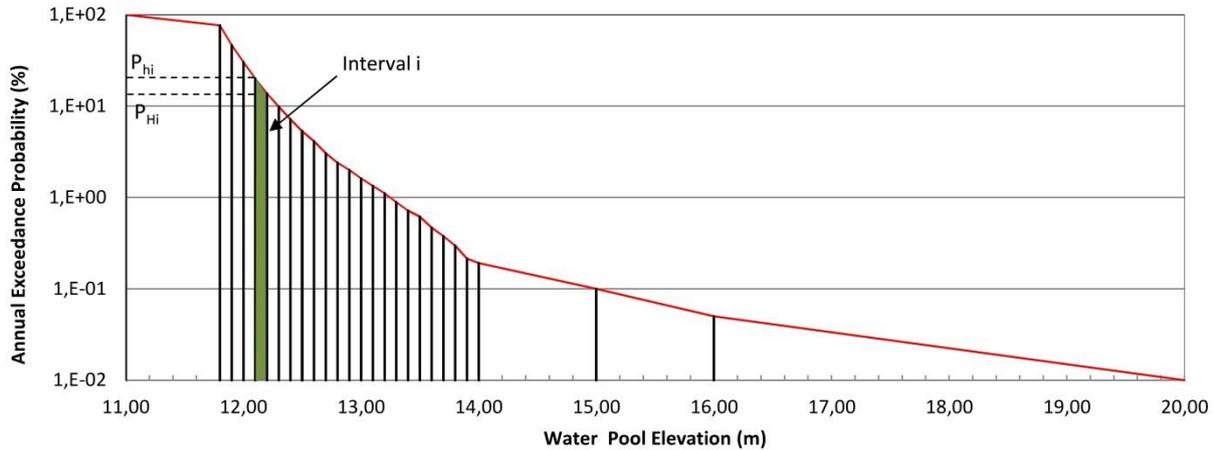
Fig. 8: Discretization of the AEP curve

Annual Probability of Failure (APF) is then computed according to the following equation:

$$APF = \sum_i^N (P_{hi} - P_{Hi}) \times P_{FC,i} \qquad (2)$$

where P_{hi} and P_{Hi} represent respectively the probability of the edges of the interval i, and $P_{FC,i}$ is the probability read in the reference fragility curve for the central water level of the interval i.
Tab. 1 gives the APF computed for each of the four cases previously defined.

Tab. 1: Annual Probability of Failure – Comparison of the different cases

Case	Case 1	Case 2	Case 3	Case 4
Annual Failure Probability	0.180	0.062	0.182	0.074

For all cases, it is striking that the probability is very high. However, we saw in Fig. 5 that the probability of failure for a constant water pool level of 11 m is already between 0.05 and 0.10. Tab. 2 shows that discretization has a small influence on the computed probabilities. Nonetheless Tab. 3 shows logically that a high number of Monte-Carlo simulations give a better accuracy of the failure probability.

Tab. 2: Influence of the AEP curve discretization

Intervals size	0.2 m	0.5 m	1.0 m	Variable
AEP – Case 3	0.196	0.188	0.161	0.182
AEP – Case 4	0.0758	0.075	0.071	0.074

Tab. 3: Influence of the numbers of MC simulations – Case 4

Numbers	100	1,000	10,000
Annual Failure Probability	0.102	0.094	0.074

Sensibility analysis

By comparing the annual failure probabilities computed for the four different cases, we can see that, as expected, the hydraulic condition assumption (steady-state or transient) have an important influence on the result. Steady-state condition leads to a much higher probability which confirms the pessimism of this assumption compared to the relative short time of the floods. However, both mechanical models (LEM and FE) give similar results and that for the steady-state condition (cases 1 and 3) and for the transient condition (cases 2 and 4).

Conclusion

The probability of failure of an embankment dam due to slope instability and overtopping has been computed using two mechanical models of different complexity: one using the Limit Equilibrium Method, and the other using Finite Element Method. Two hydraulic conditions were tested with both models to finally dispose of four cases.

These two models enable the computation of fragility curves of the sliding mode of failure representing two main parameters – cohesion and friction angle – as random variables.

On the other hand, the water pool levels probabilities have been computed according to the given flood data and the hydraulic behaviour of the dam-reservoir system.

Then, the combination of the results leads to the annual probability of failure. We focused on the comparison between the four cases. Hypotheses used in the model strongly influence the results. The steady-state conditions lead to a greater probability of failure because of the unrealistic assumptions that is behind.

LEM and FEM leads in this relatively simple case to results with no significant differences. The comparison must be done on more complex cases to highlight the benefit of FEM.

For FE model, stability calculations have been made considering random fields to represent spatial variability of embankment materials properties. This approach could be developed further in others risk assessment studies.

References

[1] Foster M., Fell R., Spannagle M. (2000). The Statistics of Embankment Dam Failures and Accidents. Canadian Geotechnical Journal n°37, pp. 1000-1024.

[2] Griffiths A., Lane P.A. (1999). Slope Stability Analysis by Finite Elements. Geotechnique n°3, pp. 387-403.

[3] Schultz M.T., Gouldby B.P., Simm J.D., Wibowo J.L. (2010). Beyond the Factor of Safety: Developing Fragility Curves to Characterize System Reliability. USACE G. a. S. Laboratory, ERDC SR-10-1.

[4] Lemaire M., in collaboration with Chateauneuf A. and Mitteau J.C. (2009). Structural Reliability, ISTE Ltd, London and J.W. & Sons Inc., New York.

[5] Hill P., Bowles D., Jordan P., Nathan R. (2003). Estimating overall risk of dam failure: practical considerations in combining failure probabilities. ANCOLD 2003 Risk Workshop

[6] Carvajal C., Peyras L., Arnaud P., Boissier D., Royet P. (2009). Assessment of hydraulic load acting on dams including filling variability and stochastic simulations, EJECE vol. 13, pp. 399-411

[7] SPANCOLD (2012). Risk Analysis Applied to Management of Dam Safety, Technical Guide on operation of Dams and Reservoirs Vol. 1.

THEME B: Probability of failure of an embankment dam due to slope instability and overtopping
Synthesis report
13th ICOLD Benchmark Workshop on Numerical Analysis of Dams

Formulators: Adrián Morales-Torres[1] and Ignacio Escuder-Bueno[1]

[1] *Universitat Politècnica de València and iPresas, Spain*

E-mail: adrian.morales@ipresas.com, iescuder@hma.upv.es

Introduction

Dam engineers can no longer ignore the techniques of performing risk assessments, which are more and more required to sanction appropriate funds for major rehabilitations.

The analyses can range from very rigorous, complex, and costly analyses to pragmatic evaluations using semi-empirical methods, all of them dealing one way or another with typically large uncertainties to make informative decisions.

Since 2011, ICOLD Committee A is contributing to address the issue from a computational perspective, but also providing enough context to understand and pay due attention to a set of decisions that are typically made in risk analyses but also in standard design techniques (frequency of events, factors of safety, breaching parameters, etc.).

The present theme followed the tradition initiated in Valencia 2011, where the aim was analyzing the *probability of failure of a concrete dam* due to sliding failure mode, and Graz 2013, where the purpose was *comparing the estimation of consequences due to dam failure*, to focus this time on the *probability of failure of embankment dams* due to slope instability and overtopping.

In this case study, inspired by a real Spanish dam but with non-real resistance and hydrological data, the main focus consists in calculating fragility curves for slope instability and overtopping failure modes and use them to calculate annualized failure probability, accounting for both *natural* and *epistemic* uncertainty.

Problem formulation

The embankment analyzed is a homogeneous earth fill dam. Its upstream slope is 23.5 degrees and its downstream slope is 28 degrees, giving a total height of 16 meters. The normal operating level in the dam is 11 meters. This geometry is shown in Fig. 1.

In recent years, this embankment had small instability problems in the downstream slope, so a quantitative risk analysis was proposed to estimate annual failure probability. Two failure modes were analyzed in this embankment: overtopping and dam instability. In both failure modes, water pool level was supposed to be the driving force of failure.
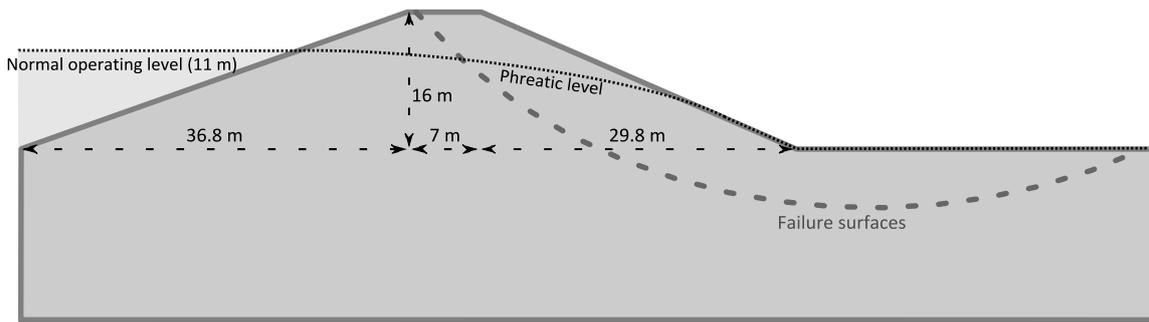
Fig. 1: Embankment Geometry.

The problem to solve was divided in five different phases:

1. **Analysis of the information for the instability failure mode:** Elaboration of a slope instability limit model for the downstream slope of the embankment and definition of the main random variables in this model. Two random variables were recommended following a Mohr-Coulomb type of failure criteria: friction angle and cohesion, although other random variables could be introduced.

2. **Calculation of reference fragility curves:** Reference fragility curve for the slope instability should be computed using the natural uncertainty distributions of the random variables defined in the previous step. Reference fragility curve for the overtopping failure mode was directly defined with a log-normal distribution. The reference fragility curves of both failure modes should be combined in order to compute a single reference fragility curve that represents the structural behavior of this embankment for different pool levels.

3. **Computation of water pool level probabilities:** The objective of this phase was calculating a relation between water pool levels and annual exceedance probability (AEP). This curve should be estimated evaluating flood routing in the reservoir for different flood events and bottom outlet availability situations, based on the floods and reservoir provided data.

4. **Computing failure probability and sensitivity analysis:** Combination of the curve computed in the previous phase with the reference fragility curve to calculate the reference failure probability. Sensitivity analysis over some of the main parameters and assumptions made in the previous phases are performed.

5. **Assessing epistemic uncertainty:** In this phase, epistemic uncertainty should be defined with a probability distribution for the mean of each random variable. These distributions were used to obtain a family of fragility curves for the instability failure mode. The family of fragility curves for the overtopping failure mode was directly defined in the formulation. Finally, the two families of fragility curves were combined to obtain a *profile of failure probability*.

Presented Contributions

Probability of Failure of an Embankment Dam Due to Slope Instability and Overtopping: First Order Second Moment Method for Assessment of Uncertainty (Andreev S.H. and Zhelyazkov A.Z.)

This solution analyzed the instability failure mode using the computer code SLOPE/W, with the limit equilibrium procedure of Morgenstern and Price and considering steady-state conditions. Properties of soil were defined of saturated and unsaturated soil. Two random variables were used: cohesion and friction angle. Monte Carlo sampling was used to calculate the conditional failure probability for instability by sampling 5000 values from the random variables for each of the prescribed pool levels, giving approximately 90% confidence in the obtained results. The obtained reference fragility curve was fitted to a Gumbel Type I distribution.

The family of fragility curves for instability was obtained modifying the reference curve following the First Order Second Moment (FOSM) method and varying the mean values of the effective friction angle and cohesion.

Next, instability and overtopping fragility curves were combined using the Uni-modal limits theorem. This curve was combined with the flood routing results to obtain a profile for the annual failure probability profile, calculated only for the case of a working bottom outlet. This profile fits precisely to a log-normal distribution with median 0.08 years^{-1}.

The sensitivity analysis of the results showed that the variation of the mean effective friction angle had the most significant effect on the median annual failure probability, followed by the use of unsaturated shear strength. Results showed large epistemic uncertainty (both from soil properties and model assumptions) for the low pool water levels.

System approach to probability of failure of an embankment dam (Westberg Wilde, M. and Vazquez Borragan, A.)

In this solution, a limit equilibrium steady-state model was created with the software Slope/W to identify slope instability. The model showed 400 failure surfaces with a critical safety factor of 1.04. Two random variables were considered in this model: cohesion and friction angle. Main epistemic uncertainties identified in this model were the assumption of saturated soils, the random variables considered, and the correlation between cohesion and friction angle.

Instability failure probability for each water level was estimated using a Monte Carlo sampling based on 2000 trials. Failure probability was estimated using the most critical failure surface in each case, although the authors point out that this approach could underestimate the failure probability, since correlation between different failure surfaces is expected to be high. Instability fragility curve was combined with the overtopping fragility curve using the two limits provided by Common Cause Adjustment techniques. Exceedance probability for each water pool level was estimated based on the flood routing data. These results were combined with the reference fragility curve to obtain failure probability. Obtained result for failure probability is 0.055 years^{-1}.

Authors remarked that input of different slope stability parameters in the same model; such as; cohesion, friction angles, unit weight, spatial variability, point loads, seismicity, slip surface limits, cross correlation c-ϕ, and piezometric lines would have a significant impact on the results. In conclusion, they point out that with the conditions analysed the slope stability was more sensitive to epistemic uncertainties than overtopping.

Probability of Failure of an Embankment Dam Due to Slope Instability and Overtopping (Mouyeaux, A., Carvajal, C., Peyras, L., Bressolette, P., Breul, P. and Bacconnet, C.)

Two mechanical models of different complexity – one using Limit Equilibrium Method (Geostudio software) and the other Finite Element Method (code Cast3M) – were developed to assess the probability of failure due to slope instability considering cohesion and friction angle as random variables. Two hydraulic conditions (steady-state and transient) were also tested for both mechanical models.

Fragility curves were obtained using a Monte Carlo method with 1000 samples for the Limit Equilibrium models and with 10000 samples for the Finite Element model. In the second case, this estimation was made after defining the response surface with this model. Results show that the assumptions made on hydraulic conditions have a great influence on the fragility curves obtained.

Fragility curves for sliding failure mode but also overtopping failure mode were then combined using the Common Cause Adjustment. In order to compute the global failure probability of the dam, the resulting fragility curve representing the structural behavior was combined with water pool level probabilities. Results obtained show that annual failure probability for all the cases is very high (from 0.18 to 0.062 years^{-1}), although there are high differences depending on the model used to analyze instability and the hydraulic conditions (steady-state or transient) considered. The authors concluded that hypotheses used in the model strongly influence the results.

Reference solution for Theme B (Morales-Torres, A. and Escuder-Bueno, I.)

This solution was presented by the problem formulators as an example of the results expected in each phase. First, instability failure mode was analyzed with a limit equilibrium model based on the Modified Bishop method. Two random variables were considered: friction angle and cohesion. Main uncertainties detected in this model were the random variables considered and the hydraulic hypothesis made.

This model was used to estimate a reference fragility curve using 10000 samples of the random variables. Reference fragility curves of overtopping and instability were combined in a single fragility curve using Common Cause Adjustment techniques, taking the average between upper and lower limits. Exceedance probability curve for water pool levels was estimated based on a flood routing analysis. These curves were introduced in a risk model made with iPresas software in order to estimate annual failure probability, obtaining a result of 0.004 years^{-1}. Results show a significant influence of the number of Monte Carlo simulations made.

Finally, a family of fragility curves for the instability failure mode was obtained repeating the previous process but modifying the distributions of the random variables as indicated in the problem formulation. The family of fragility curves for instability and overtopping failure modes were introduced in the risk model to obtain a failure probability profile.

Comparison of results

Firstly, as can be observed in the previous descriptions, very different instability approaches were considered by participants, from simple limit equilibrium models to complete finite element models. In addition, two different assumptions were compared for hydraulic conditions: steady-state or transient.

When the fragility curves obtained with these models are compared (Fig. 2), it can be observed that the participants obtained very different results, although all of them used the same random variables with the same distributions and the same geometry. These results show the high influence of the hypothesis made and the model considered in the

instability results. Results show also a significant influence of the number of Monte Carlo simulations made. In the Benchmark discussion, it was highlighted that the hydraulic hypothesis are especially significant. In this case, considering a steady-state could lead to underestimate the slope resistance capacity.

In any case, it should be remarked that when numerical models are set up, many small hypothesis are made that can influence the results. For instance, in this problem two participants with the same software, the same geometry and the same random variables obtained very different fragility curves.
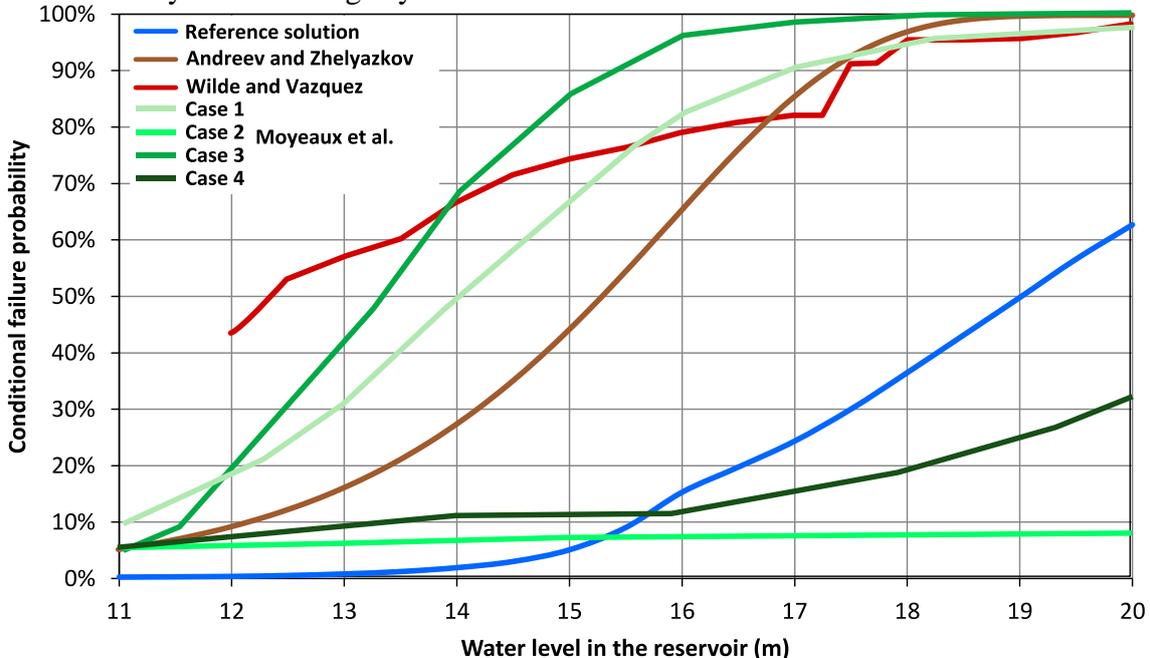
Fig. 2: Comparison of fragility curves computed by Theme B participants.

Secondly, all the participants concluded that the slope instability was clearly more significant than overtopping according to the results. In the four solutions, Common Cause Adjustment techniques were used to combine both failure modes. Using the upper or lower limit for this combination did not have a high influence on the results, since the slope instability failure mode is clearly predominant and overtopping is only activated for water pool levels with very low probability.

Thirdly, all the participants obtained very similar exceedance probability curves for water pool levels. All of them use the same floods and reservoir data and flood routing rules were very simple, so flood routing results are very similar in the four solutions.

Fourthly, the comparison of the results obtained for the annual failure probability show high differences, differing more than one order of magnitude. These differences are mainly due to the different fragility curves for instability used to compute it, which shows that the hypothesis made in the numerical models to analyze this failure mode are clearly conditioning the results.

In all the solutions, high values of annual failure probability were obtained. These high results are due to the modification of the dam resistance and hydrological data made by the problem formulators in order to increment conditional failure probabilities, reducing the number of samples and computations needed to characterize them.

Finally, only two contributions estimated the families of fragility curves and the failure probability profile to assess epistemic uncertainty, as shown in Fig. 3. There are high

differences in these two profiles, in line with the differences of the fragility curves obtained with the instability models.

In both solutions, failure probability profiles showed that small variations in the resistance parameters distributions produce important variations in the obtained fragility curves. This result remarks the importance of assessing epistemic uncertainty separately.
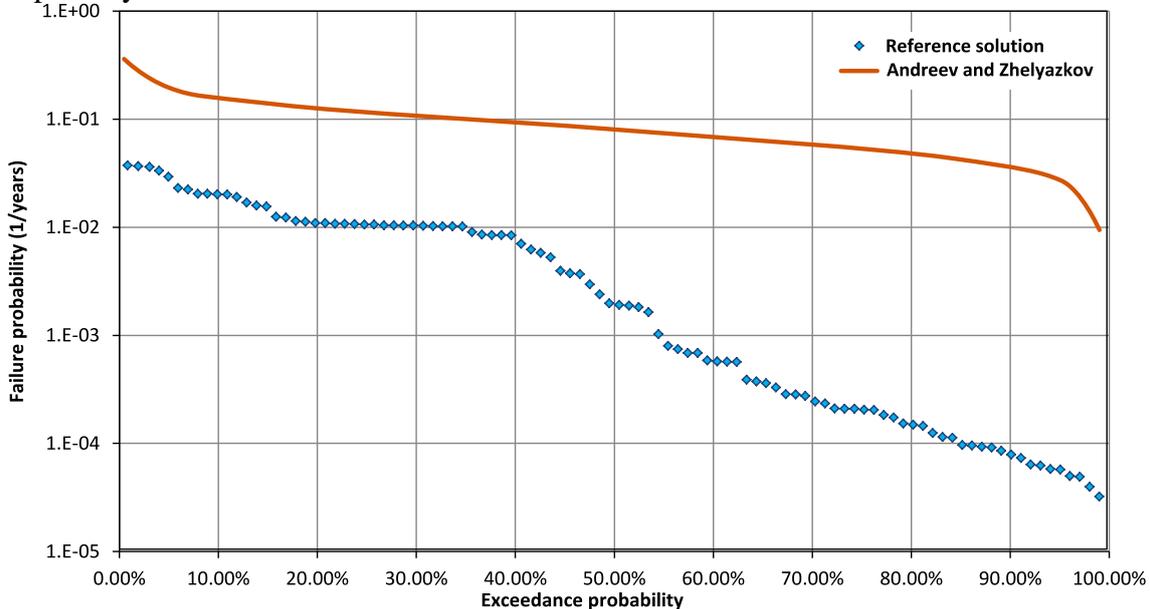
Fig. 3: Comparison of failure probability profiles computed by Theme B participants.

Conclusions

The main differences between the contributions results are due to the differences in the fragility curves introduced in the instability failure mode. The comparison made showed that very different results can be obtained depending on the hypothesis made in the models, even using the same geometry and resistance parameters. Hydraulic conditions hypothesis had an especially high influence in the results. Therefore, uncertainty is not only produced by the resistance parameters, other uncertainty sources are the slope instability model used and the hydraulic behavior of the embankment.

In this sense, risk analysis has demonstrated to be a useful tool to analyze the impact of the hypotheses made on the results. In addition, the obtained results can indicate where uncertainty reduction efforts should be focused. For this reason, in practice the distinction between natural and epistemic uncertainties is fundamental in geotechnical and dam safety governance.

Finally, the Problems Formulators would like to acknowledge and thank the Theme B participants for the very different and interesting solutions that they obtained. These solutions allowed enriching and stimulating discussions during the Benchmark.

Theme C:

DAM SAFETY

Formulation by:

Guido Mazzà[1]

1. *Ricerca sul Sistema Energetico RSE S.p.A., Milan, Italy.*
   Guido.Mazza@rse-web.it

Seismic safety analysis of dams within the context of Swiss dam safety concepts

Supervision of Dams Section, SFOE[1]

[1]*Swiss Federal Office of Energy (SFOE), Bern, Switzerland*

ABSTRACT: The origins of Swiss dam safety concepts and legislation date back to World War II. The current legal bases in Switzerland are defined in the Federal Act on Water Retaining Facilities of 1st October 2010 (WRFA) and the Water Retaining Facilities Ordinance of 17th October 2012 (WRFO). The provisions in this legislation reflect the principles of Swiss dam safety concepts, which are based on a three-pillar system of *structural safety*, *surveillance* and *emergency planning*.

Seismic safety is one of the elements of the structural safety of dams. The seismic safety assessments of Swiss dams according to the guidelines prepared under the auspice of the SFOE in the early 2000s, have been completed resulting in over 200 seismic safety reports prepared by the operators of large dams. These seismic safety assessments are currently being reviewed by the Swiss Federal Office of Energy; at present about 80 % of the review work has been completed. A wealth of information has been accumulated from these analyses for dams of different types and ages. In some cases, remedial measures have been implemented to ensure compliance with seismic safety requirements.

This paper presents the first lessons learned following the review of seismic safety assessments of dams, and places seismic safety within the context of Swiss dam safety concepts.

Contact: rocco.panduri@bfe.admin.ch

Introduction

The Swiss Federal Office of Energy (SFOE) is the federal supervisory authority responsible for the direct supervision of approximately 200 large dams in Switzerland. The main purpose of the large dams, which were mostly built in the 1950s and 1960s, is hydropower production. The largest dams are concrete structures, such as the Grande Dixence gravity dam (285 metres in height) and the arch dams of Mauvoisin (250 metres), Luzzone (225 metres) and Contra (220 metres). Two embankment dams are over 100 metres in height, namely Göscheneralp (155 metres) and Mattmark (120 metres).

Swiss legislation governing dam safety was introduced after the attack on German dams during World War II with the legislation on the protection of water-retaining structures of 1943 and the accompanying ordinance of 1957. Currently, the Federal Act on Water Retaining Facilities of 1st October 2010 (WRFA) and the Water Retaining Facilities Ordinance of 17th October 2012 (WRFO) form the legal basis for dam safety. After the coming into force of these new legal bases, the existing Swiss guidelines on dam safety of 2002 are currently being revised by the SFOE.

Requirements for seismic safety analysis of Swiss dams

Motivation and current standing

The seismic safety of large Swiss dams had been verified according to the state of knowledge at the time of design, typically assuming a horizontal peak ground acceleration of 0.1 g independent of the site and using simplified analysis approaches. The Swiss guideline on the seismic safety of dams prepared in 2003 [1] defines the technical basis for a reassessment of the original seismic analyses taking the current state of knowledge into account. In the meantime, all seismic safety assessments for dams under the direct supervision of the SFOE have been delivered for validation. At present, the SFOE has been able to verify about 80 % of these analyses.

It should be pointed out that the Swiss guidelines on dam safety are not law binding and as implied by the name, remain "guidelines" allowing or even demanding other methods and more crucially, engineering judgement based on solid experience to be applied. This judgement is also critical when making the necessary plausibility evaluation of results.

Performance criteria

The guideline on seismic safety defines three classes of dams which depend on the storage height and capacity, and thus implicitly on the potential risk for the downstream population. The class of the dam determines the return period to be taken into account for the safety evaluation earthquake (1,000, 5,000 or 10,000 years) as well as the required analysis methodology. The latter ranges from a pseudo static analysis to a response spectrum analysis up to a time history analysis.

The main requirement of SFOE in respect to the accepted performance of a dam during or following the safety evaluation earthquake (SEE) is to prevent a collapse of the dam structure, which would cause an uncontrolled release of reservoir water. Damage of the structure or permanent deformations are however acceptable, as long as the safety of the dam is not endangered and the uncontrolled release of reservoir water remains inexistent. In the case of embankment dams for example, it must be demonstrated that the overall dam stability is still guaranteed after a potential sliding and/or excessive settlements, implying in particular that a sufficient freeboard remains and that the drainage and core elements of the structure can continue to fulfil their intended purpose.

The SFOE does not require operability of the water retaining facility after a smaller earthquake than the SEE such as an operating basis earthquake; the observation of operability criteria is left at the discretion of the dam operator.

However, operability of safety related appurtenant structures (gated relief and outlet works) after the SEE is required so as to be able to empty the reservoir in order to carry out inspection and maintenance operations and to lower the level of water if there is any imminent threat to the population downstream. If the operability of these structures is not guaranteed after an earthquake, the operator has to show how and by which means the water level can be lowered or a moderate flood can be discharged.

With respect to the reservoir safety and potential impulse waves caused by sliding masses, the seismic analysis has to discuss the possibility of earthquake induced mass movements into the reservoir as well as their consequences for the safety of the dam.

Seismic hazard for analyses of dam safety

Existing seismological groundwork at the time of the preparation of the guidelines form the basis of the probability-based definition of the SEE, which is given by a set of acceleration response spectra and effective peak accelerations for various return periods. The normalized shapes of the response spectra correspond to those of Eurocode 8 [2]. They apply both for horizontal and vertical directions. The peak ground acceleration as scaling value is defined starting from maps provided in the guidelines which depend on the dam class and thus on the return period of the SEE. In effect, intensity maps are provided in the guidelines, from which the horizontal peak ground acceleration is obtained by means of an empirical intensity – acceleration relation. The maximum horizontal peak ground acceleration to be taken into account at dam sites in Switzerland amounts to about 0.45 g. The vertical peak ground acceleration is taken as two thirds of the horizontal component.

Where time-history analyses are required, namely for the highest dam classes, at least three analysis runs with different sets of stochastically independent time-histories must be performed, each set consisting of two (2D) or three (3D) components. For this purpose, "sample" normalized (artificially generated) time-histories which can be used for the safety assessment are provided by the SFOE.

Numerical Modelling requirements for different dam types
The seismic safety assessment of embankment dams is based on a decoupled two-step analysis, the first step being the evaluation of the dynamic stability of individual dam parts, whereas the second step aims to assess the potential earthquake deformations, should sliding/settlement occur. The modelling requirements for the first step depend on the dam class, ranging from simplified stability analyses with an equivalent seismic horizontal action to full dynamic finite-element calculations.

In the verification of the seismic safety of concrete and masonry dams, both a stress and a stability assessment need to be performed. In the stress analysis, usually linear elastic, the stresses resulting from the combination of static and dynamic loads are compared to the material strength. In case of overstressing, it must be demonstrated that stress redistribution is possible and that no local instability endangering the structure will occur. For the case of arch dams, this could mean the investigation of joint opening effects due to large horizontal stresses, and eventually the danger of partial block instabilities due to the change of structure behaviour in the upper dam part from arch to pure cantilever action. In the stability analysis, overturning and sliding of the whole structure are investigated. The modelling requirements for concrete and masonry dams, depending on the dam class, range from simple beam models with a pseudo-static analysis to finite element models with a time history analysis.

Swiss guidelines place a strong emphasis on the use of "as-built" information for the foundation and structure. The material parameters (soil, rock, concrete, etc.) are preferably based on the results of material tests and the numerical model calibrated in accordance with the loading conditions of the site (hydrostatic and thermal). Hence, transient analyses (thermal, seepage, etc.) may be performed over a "calibration period" of some years to determine the material parameters and external load conditions that lead to the best correlation between predicted and measured values. Special attention is also given to the extent of the finite element mesh and size of the elements so that it captures the key areas of interest in the dam and foundation. Hydrodynamic pressures may be taken into consideration as added masses applied to nodes; conditions as to when fluid compressibility becomes important are defined in the guidelines. For particular structures, seismic hazard analyses and ambient or forced vibration tests may be appropriate to define the loading conditions and dynamic material parameters.

Swiss guidelines on seismic safety, future requirements
The valid basis for the verification of the seismic safety of Swiss dams is the supporting document of 2003 [1]. A new guideline on seismic safety is in preparation and will be available by 2016. This new guideline aims to update, simplify and clarify some of the aspects of the current guideline. Being a revision after only about ten years of the original work, the main objectives and methodologies described in the new guideline will not significantly differ from those in the current guideline.

Preliminary conclusions based on the current review of submitted seismic safety evaluations

Appreciation of the work
Generally, the dam operators and their consultant engineers commissioned to perform the seismic assessments have taken their task very seriously, which is reflected in the high quality of the submitted documents. The comments of the SFOE on received seismic documents (typically a technical report with accompanying annexes) mainly consist in demands for clarifications regarding the underlying modelling assumptions or interpretations rather than the analytical methods applied per class of structure. Demands for additional analyses mainly concern the evaluation of reservoir safety (hazards due to mass/block movements or falls which

could lead to an overtopping of the reservoir in the latter case) and appurtenant structures, where these issues have not been satisfactorily addressed.

Preliminary conclusions for arch dams

The seismic evaluation of arch dams was generally carried out by means of a time history analysis or a response spectrum analysis on a 3D finite element model. A recurring issue in the modelling phase is the proper definition of boundary conditions and the modelling of the foundation whereby the former is typically restrained in the three orthogonal directions and the latter is defined as massless in order to avoid problems associated with different aspects of dam-foundation interaction. A main theme in the interpretation of the results of the time history analysis of arch dams is the capability of the structure either to withstand the tensile stresses calculated by means of a linear elastic analysis of the homogeneous structure, or to redistribute these stresses after possible joint openings or cracking. In the cases where the former behaviour could not be shown, a subsequent calculation with an adapted model was carried out to verify the latter. This mostly comprehended a second, linear elastic analysis of the modified structure with otherwise the same assumptions. The opening of joints or cracking in the model could then result in high vertical tensile stresses in the individual blocks now acting partially or temporarily as cantilevers. Finally, in the cases where these vertical stresses could lead to a substantial cracking in a horizontal block section, a third evaluation was carried out in order to assess the possibility of an instability by rocking-sliding of the detached part, taking the previously calculated seismic action at the base of the block into consideration. The mechanism of instability verified possible movement towards the upstream since the shape of single and double-curvature arch dams inhibits movement in the downstream direction.

It is also interesting to note that despite the development of numerical tools since the first publication of the guidelines, the reservoir was in general treated as incompressible and no foundation-dam interaction was considered necessary (massless foundation applied). In the case of modal analyses, the total percentage of mass and hence the number of eigenmodes respected the guidelines and damping parameters where calibrated accordingly in the case that full direct time-history evaluations were performed.

Seismic verifications invariably demonstrated that structural damage was related more to uniaxial (mainly tension) modes of behaviour. Crushing (compression) of mass concrete was not an issue of concern. In general, contraction joints constitute planes of possible opening and in the case that horizontal tensile stresses exist; the third evaluation type of rocking-sliding blocks as described above is applied. The effects of shear keys and block geometry were not explicitly taken into consideration and hence, no lateral restraint from contraction joints was considered in stability analyses.

In the vast majority of cases, the calculation following the procedure described above demonstrated the satisfactory behaviour of the structure in respect to the performance criteria previously presented.

Preliminary conclusions for gravity dams

While one of the main issues of the seismic safety evaluation of arch dams was the redistribution of tensile stresses, the calculated stresses in gravity dams turned out to be rather low, as could be expected, with the exception of locally increased stresses at the downstream surface, at the upstream toe and at inhomogeneities of the section such as inspection tunnels.

Instead, the most important issue was found to be the global safety against sliding of the considered blocks. In this respect, the assumptions made at the potential sliding surfaces (concrete-concrete, concrete-rock, rock-rock) are decisive. This comprises on one hand the shear parameters at the interface, the cohesion being the most influential parameter and on the other hand, the effects at the interface particularly related to the assumptions about uplift pressures. In the absence of measurements, the latter was taken into account in a conservative

way; in presence of measurements, a reduced uplift could be accepted, provided that the assumptions are confirmed by appropriate measurements.

Should sliding occur during one or more time steps, a subsequent Newmark analysis was carried out to assess the final earthquake-induced permanent displacements. Here, the performance criteria are such that the absolute sliding deformation of a gravity dam block is not the decisive issue; instead, differential deformations between the block and appurtenant structures (such as bottom outlet tunnels, drainage systems etc.) turned out to be the relevant issues.

Preliminary conclusions for embankment dams

Because the seismic verification was carried out assuming a considerable seismic impact, many embankment dams are supposed to suffer local slope instabilities due to the earthquake. However, the deformations within the failure zones are expected to be rather limited based on the Newmark analysis. The global stability of the dams would not be harmed by the local slope failures. The dams would remain higher than the level of the water in the reservoir.

Nevertheless, the hazard of internal erosion had to be investigated for some particular types of embankment dams. Regarding zoned-earth dams, the eventually deformed core and filter zones should still prevent the dam from internal erosion. This hazard has been found to be critical especially for high dams. For dams with impervious surfaces, the deformed lining has still to be able to prevent water from infiltrating into the embankment. Assuming a partially filled reservoir, the deformations on the upstream face are supposed to be larger, which in case of a failure mechanism outcropping below the water level may also cause conditions prone to internal erosion.

For homogenous earth dams, the hazard of internal erosion due to an earthquake is expected to be minor. Instead, the assessment of excess pore pressure while shearing becomes crucial. Some homogenous earth dams have been built in the early 20th century. Due to the lack of heavy construction machinery in those days, the embankment may be of rather loose density. These dams may also consist of organic material. Unfortunately, appropriate shear testing has hardly been performed when these dams were built. Therefore, it is a major challenge nowadays to take account for the excess pore pressure during an earthquake.

Despite these challenges regarding the seismic verification, most of the embankment dams in Switzerland were found to be able to resist the assumed seismic impact and to meet the performance criteria.

Preliminary conclusions for the reservoir

As part of the seismic verification, also the hazard due to mass movements causing impulse waves within the reservoir has been studied. Therefore, potential landslides, rock slides and rock falls were investigated. It has been checked, whether such events could lead to overtopping, harm the dam or the appurtenant structures.

Since the propagation of the impulse waves is well understood, the generation of the wave remains the major uncertainty. The initial height of the wave is mainly governed by the mass and the velocity of the sliding or falling body. If there is no current evidence of a mass movement under static conditions, it may be difficult to assess the potential mass that can fail during an earthquake. However, even more challenging is to assess the velocity of a sliding body.

With creeping landslides, the potential failing mass could be estimated by means of geotechnical monitoring. Inclinometer readings and measurements of displacements on the surface allow for an estimation of the failing mass. Nevertheless, the height of the impulse wave can hardly be accurately predicted because the velocity of the failing landslide is difficult to assess. Because creeping landslides are in dynamic equilibrium, very little additional shear strength can be mobilized. In order to be able to calculate the velocity, the shear resistance during sliding has to be known incorporating the effects of pore pressure build-up, strain rate dependency and boundaries.

Preliminary conclusions for the appurtenant structures

The operability of safety related appurtenant structures after the SEE being required, the seismic safety analyses of these structures concentrated on two main issues. Firstly, the structural integrity of the appurtenant structure following the earthquake event had to be shown; this was mainly done by means of a comparison between the static load cases and the dynamic case: the required safety factors being reduced for the case of an extreme earthquake event, it could be shown that the available static reserve is sufficient for the structures to withstand the increased loading due to dynamic forces. Secondly, it had to be shown that the expected earthquake-induced deformations during or after the earthquake event do not endanger the operability of the appurtenant structures.

While for alpine reservoirs and thus for the largest dams, the operability of the appurtenant structures rarely was a problem, ongoing verifications of weirs show that this could be an important issue for this type of dam, since the operability of the weir gates depend on the functioning of a whole chain of elements, including gear, power and control elements.

Swiss dam safety concept

In order to ensure a high level of safety, a dam needs to be designed and constructed so that it can withstand all conceivable loading and operational conditions. This results in a minimization of risk, which is sustained by a form of surveillance that permits the early identification of any anomaly relating to the behaviour and condition of the dam and/or its surroundings. Despite sound construction and adequate surveillance, a residual risk nevertheless remains. In order to deal with emergencies as effectively as possible, an emergency planning concept has also been defined. Here too surveillance plays a significant role in ensuring that any imminent uncontrolled release of reservoir water can be detected at the earliest possible stage.

While the design basis assures a minimum level of protection, which may be regarded as the enforcement of a limit on individual risk, emergency planning takes account of the societal risk, addressing the key issues of "whom to alarm" (based on dam breach analyses), "when to alarm" (as soon as an uncontrolled release of large volumes of water is detected or feared), "how to alarm" (with the aid of suitable systems) and "how to evacuate" (on the basis of evacuation maps).

The Swiss dam safety concept is based on these considerations and thus comprises three components: *structural safety, surveillance* and *maintenance, and emergency planning*.

Structural safety

Structural safety calls for sound engineering and construction practices, complying with minimum performance requirements. These also encompass extraordinary or extreme load conditions, such as earthquake safety and the safe passage of the probable maximum flood. The requirements are kept in line with the development of scientific and technological know-how.

Surveillance and maintenance

Surveillance and maintenance comprise three to four levels of activity, each of which defines specific responsibilities and actions. The content and structure of these levels for each dam are specified in surveillance regulations that have to be approved by the relevant supervisory authority.

The first level, in which the tasks are typically performed by the operator of the dam, calls for periodical visual inspections and measurements, as well as maintenance by the operator's personnel on site. This includes an annual test of the functionality of the discharge works.

At the second level, an experienced engineer is designated to carry out an initial assessment of the findings obtained from the first level, to conduct an annual inspection and to prepare an annual safety report that includes an evaluation of the condition and behaviour of the dam.

Thanks to the use of predictive behaviour models, it is possible to identify anomalies at an early stage.

The third level only applies to the largest dams. A review is carried out every five years by civil engineering and geology specialists for the purpose of determining medium-term to long-term behaviour. It addresses any specific safety issues that may arise, and assesses the condition and behaviour of the dam over a longer timeframe.

The fourth level involves the supervisory authority itself, whose specialists have to make sure that all safety requirements are complied with, carry out their own site inspections and evaluate the annual and 5-year safety reports, as well as other special reports (e.g. earthquake analyses). They also have to check the content of the technical documents in terms of plausibility, and carry out their own assessments. If necessary the owners, engineers or experts are asked to conduct additional studies.

Emergency planning

If the safety of a dam is threatened in such a way that an uncontrolled release of large volumes of water is imminent, emergency measures need to be taken both in order to prevent an uncontrolled release (as far as possible), as well as to warn, alarm and, if necessary, evacuate the population at risk before the arrival of the flood wave. Surveillance supports this process by permitting the early identification of a threat, thus providing additional time for taking the necessary measures, or ultimately for evacuating the population at risk.

Conclusions

The seismic safety evaluation of Swiss dams is embedded in the dam safety concept of Switzerland, being one of the elements of structural safety, which in turn is one of the three elements of the safety concept. This evaluation has been completed by the operators of about 200 large dams, and is currently being reviewed by the dam safety authority of the SFOE.

After the review of about 80% of all evaluations, the preliminary conclusion of SFOE with respect to the expected behaviour of dams following a large earthquake is very positive. It becomes clear that the safety requirements will be met without the need for remedial measures in all but a few cases, these exceptions being furthermore cases for which the state and behaviour had already been questioned under normal operational conditions or that have a particular structural configuration. In other words, dams that satisfy current construction and safety standards for normal operating conditions were generally also found to satisfy the requirements related to seismic actions. The lessons learned so far from large earthquake events worldwide also confirm the excellent behaviour of dams under earthquake loading.

The Swiss guidelines, currently under revision until 2016, proved to be a good basis to assess and ensure the dam safety under earthquake loading.

Acknowledgements

References and further readings

[1] Federal Office for Water and Geology FOWG (2003). Guideline, Sécurité des ouvrages d'accumulation Documentation de base pour la vérification des ouvrages d'accumulation aux séismes (French & German), Version 1.2, March 2003.

[2] Schweizerischer Ingenieur- und Architekten-Verein SIA (1987). Eurocode 8 'Auslegung von Bauwerken gegen Erdbeben', Teil 1-1 'Grundlagen - Erdbebeneinwirkungen und allgemeine Anforderungen an Bauwerke', Schweizer Norm ENV 1998-1-1, SIA Norm Ausgabe 1987 V160.811, Zürich.

[3] ICOLD Bulletin N° B155 (2013). Guidelines for use of numerical models in dam engineering, www.icold-cigb.net.

[4] Swiss Federal Office of Energy SFOE (2015). Guideline, Sécurité des ouvrages d'accumulation, Partie A : Généralités, Version 2.0, March 2015.

[5] Swiss Federal Office of Energy SFOE (2014). Guideline, Sécurité des ouvrages d'accumulation, Partie B : Risque potentiel particulier comme critère d'assujettissement, Version 2.0, June 2014.

[6] Swiss Federal Office of Energy SFOE (2015). Guideline, Sécurité des ouvrages d'accumulation, Partie E : Plan en cas d'urgence, Version 2.0, May 2015.

[7] EN 1998-1 Eurocode 8: General Rules, Seismic Actions, Rules for Buildings, December 2004.

[8] Darbre G. R. (2000). Strong-motion Records at Large Dams, 12 WCEE.

Endurance Time Analysis for the Seismic Vulnerability of Arch Dams

Meghella M.[1], Furgani L.[1]

[1]*Ricerca Sistema Energetico RSE, Via R. Rubattino 54, 20134 Milan, Italy*

ABSTRACT: This contribution summarizes the main outcomes achieved by RSE in the last two working years on the dynamic non-linear response of arch dams aimed at their seismic vulnerability assessment. On the basis of the results obtained, an alternative approach is proposed to evaluate their seismic vulnerability. The Endurance Time Analysis (ETA) introduced in 2004 is used for this purpose. The method consists in shaking the structure using a special acceleration function with increasing intensity in time able to be spectrum compatible to limit states spectra at the so called equivalent times. A relationship exists in fact between the time and the seismic intensity parameters. For each ETA function it is possible to track the nonlinear behaviour of the structure up to collapse. The method allows evaluating the time at which specific limit states are overpassed. These times, coming from a single analysis, can be then compared to the equivalent times. Compared with traditional dynamic analysis performed with Time History accelerograms, more or less artificial, this approach strongly reduces the amount of time requested for a full seismic assessment of dams giving additional information on the seismic action producing the collapse of the structure. Last but not least, the comparison between the "capacity curves" of different dams for the same ETA functions clearly allows defining the vulnerability ranking of a portfolio of arch dams against earthquakes.

E-mail: Massimo.Meghella @rse-web.it

Introduction

Since 1928 the ICOLD association worked to share experiences for the design and analysis of dams. The continuous developments in science and technology as well as the new experience collected from the past make this purpose crucial for dam safety. The recent seismic events in China (2008) and Japan (2011) gave to dam community additional feedback on the seismic response of dams. The position paper on "dams safety and earthquakes" released by the ICOLD Committee on Seismic Aspects of Dam Design (2012) offers an overview on the subject.

The first dams designed against the seismic action dated back to the 1930s. Nowadays the earthquake intensity levels and the seismic legislation are changed in a way that great part of the existing dams needs to be reassessed. These pressing duties require a sound approach to identify the most appropriate method according to the associated risk.

As in other countries, Italy is now dealing with this problem and different approaches have been adopted to fulfil the requests of the new seismic regulation of dams [8]. So far, RSE has performed several seismic reassessments relevant to a portfolio of large arch dams. The outcomes and the experience achieved up to now allow identifying the most effective way to evaluate the seismic response of arch dams.

According to that, it is possible to state that existing arch dams located in high seismicity zones require dynamic non-linear analyses in order to properly represent the behaviour of the structure. These complex and detailed analyses, which are also very time consuming, may allow to avoid expensive retrofitting measures, identified as the result of the preliminary simplified analysis (e.g. pseudo static analysis or linear analysis).

The Time History Analysis method (THA), proposed since 1986 in the ICOLD Bulletin 52, can be considered a traditional method and it is now viable thanks to the power of the new computers and the improvement of FEM codes. One of the aspects that still makes difficult its practical application is the large number of loading combinations to be analysed (as a consequence of the Limit State Design principles and the various pre-seismic states to be considered).

In this paper are presented the results of a relatively new method, named Endurance Time Analysis (ETA), introduced first in 2004 by Estekanchi et al. [2] for framed structures and applied to dams in the following years by the authors [1] and other researchers [3].

The principle of the method is to apply, instead of natural accelerograms typically used in the Time History Analysis (THA), special artificial accelerograms, named Endurance Time Acceleration Functions (ETAf), having increasing amplitude over the time. Their properties transform a conventional "dynamic non-linear analysis" in a "push-over dynamic non-linear analysis" able to provide the response of the structure at different seismic intensity levels. Considering the Limit States definitions, distinguished for the intensity level, it is possible through the ETA method to evaluate the response of the dam with just a single analysis, thereby allowing a considerable computational saving. ETAf functions can reach high levels of shaking, also beyond the usual Maximum Credible Earthquake, allowing the identification of the earthquake able to produce the dam collapse. In these terms the ETA method is one of the best candidates for the evaluation of the vulnerability of the dams. The use of the same ETAf can also improve the comparisons between different dams: the dam with the largest endurance time is actually the most resistant.

Seismic response of arch dams

Arch dams are well recognized for their capability to withstand and to transfer to foundation compressive forces. Moreover, past observations [5] confirm that among all dam type, arch dams are the most resistant against the earthquakes. This has been confirmed by a recent study investigating the response of dams for peak ground acceleration greater than 0.3g (Annual USSD Conference 2012) which shows that only one of six arch dams experienced some minor damages. Nevertheless, given the high overall risk posed by large arch dams, their seismic vulnerability must be carefully assessed.

Fig. 1 shows the failure modes and their typical evolution induced by earthquakes: opening and sliding of construction/contraction joints and damages of the concrete, corresponding to cracks.
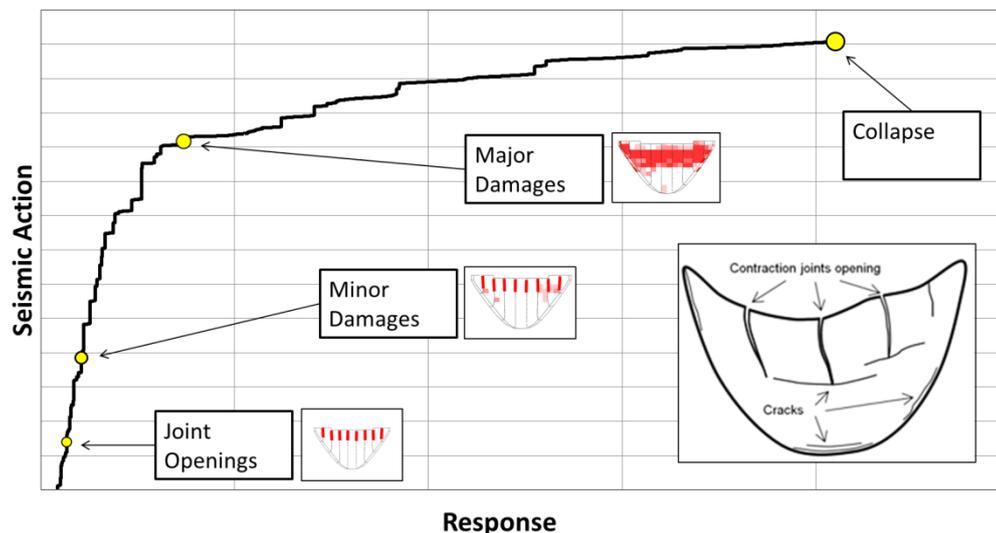

Fig. 1: Typical failures modes associated to arch dams and their evolution for increasing seismic actions

A specific aspect to be considered for arch dams is the relationship between the cyclic nature of the seismic forces and the resistant mechanism due to arch effect. If the seismic action acting in the upstream direction exceeds the hydrostatic pressure one, the arch effect can be lost

inducing a behavior that resembles an assembly of partially separated cantilevers. For this reason joint non linearity must be accounted for in the detailed analysis. If the seismic forces are high enough, tensile stresses may also overcome the concrete tensile strength, requiring an additional improvement of the numerical model, by considering material non-linearity. Because of the non-linear nature of the problem it is also important to consider different pre-seismic states to take into account the most unfavorable case. The Italian Regulation (2014) [8] requires to evaluate the seismic response of the dam both for full and empty reservoir. Both these conditions must be analyzed in combination with winter and summer temperatures, thereby resulting in four pre-seismic combinations at least.

As in most international standard [6] two main shaking intensity levels have to be considered for the assessments: one referred to the "service limit state" (SLD, "Stato Limite di Danno") and the other one correspondent to the "ultimate limit state" (SLC, "Stato Limite di Collasso") generally determined considering the Maximum Credible Earthquake (MCE) able to produce the collapse. For each limit state, the regulation provides the reference spectra, and, in case of non-linear analysis, the analyst must properly select and adapt the set of accelerograms (three components), in order to make them compatible with the reference spectra. It is worth noting that to handle with the aleatory nature of earthquakes, a minimum set of three accelerograms must be considered.

On the basis of the above considerations, the seismic non-linear analysis of arch dams represents a very challenging and time consuming task. In this light, the ETA method can be a viable alternative to THA, allowing at the same time to obtain accurate solutions while considerably reducing the computational time.

Endurance Time Analysis method (ETA)

The core of the method is the way the ETAf are defined. As depicted in Fig. 2, the acceleration grows in a way that the ETAf spectra referred to different times increase quite linearly over the time (e.g. the spectra at time t_1 is the half of that obtained at t_2).
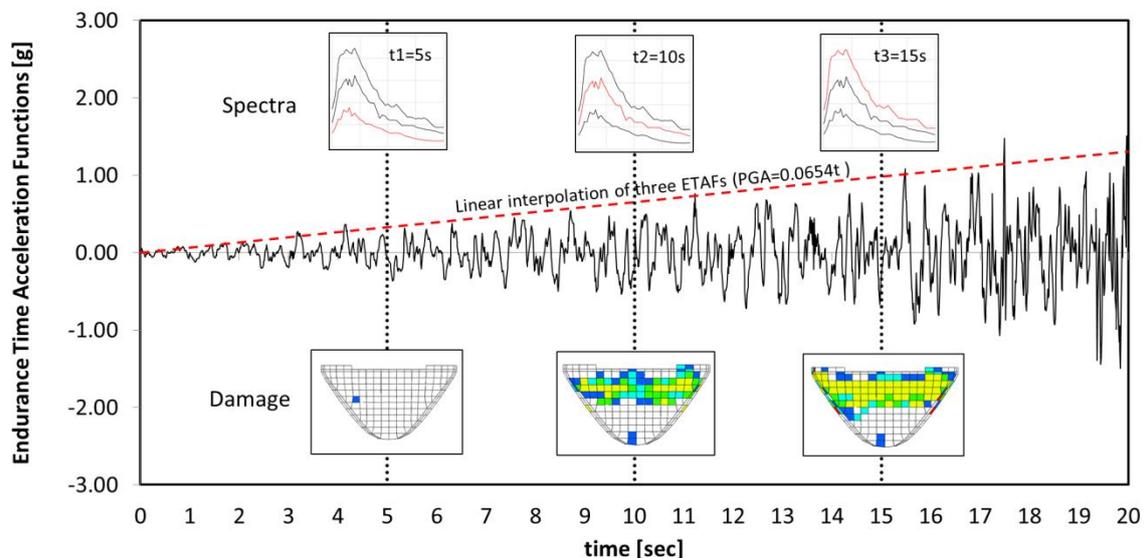

Fig. 2: Conceptual description of the ETA method

Considering this, is possible to define a relationship between time and the intensity measures as represented by the linear regression shown in the figure. When non-linear behavior of concrete or joints is considered it is possible to keep track of the non-linear effects occurring

during the transient analysis and compare them with their reference acceptance criteria, associated to a particular limit state. The method has been extensively and successfully validated by comparison with THA method ([1] and [3]).

Endurance Time Acceleration Functions (ETAf)
The main steps to generate ETAf can be summarized as follows: (1) generation of a stationary random acceleration function; (2) application of an appropriate filter to resemble real ground motions; (3) stepwise modification of ETAf in order to make the resulting response spectrum compatible with the target one; (4) modification of ETAf by a linear profile function that makes the resulting one increasing with time; (5) modification through an unconstrained optimization technique of both the acceleration and the displacement spectra to gain the compatibility [3]. At the end of the process the intensity measures of ETAf will be linearly correlated with time:

$$\text{PGA}(t) = \frac{t}{t_{trg}} PGA^{trg}, \qquad S_a(t,T) = \frac{t}{t_{trg}} S_a^{trg}(T), \qquad S_d(t,T) = \frac{t}{t_{trg}} S_d^{trg}(T) \qquad (1)$$

This property of ETAf allows to directly associate an equivalent time to a specific levels of shaking, as well as to identify the intensity of the earthquake that produces a particular non-linear effect. As previously mentioned, the new Italian dam regulation requires to consider two limit states, namely SLD and SLC, for the seismic assessment of existing dams. Their corresponding 'target times' can be evaluated in different ways [4]. In the present work the direct linear relationship between PGA and time (Fig. 2) has been used and the equivalent target times resulted in 2 sec for SLD and 8 sec for SLC corresponding to 0.13g and 0.52g respectively. As for THA, the aleatory nature of ETAf is accounted for by considering three different sets of ETAf. Each set is composed by three spatial components. The total duration of the ETAf is 20 sec, reaching a maximum PGA around 1.5g. For sake of simplicity, the results relevant to the combination with winter temperatures, full reservoir and the seismic motion acting prevalently in the upstream-downstream direction, are shown in the following.

Engineering demand parameter (EDP)
The relationship between time and intensity measures gives the opportunity to define the dam response in a different way. The measure of the response, named engineering demand parameter (EDP) [4], can be described using the envelope function reported below.

$$\Omega\big(EDP(t)\big) \equiv \max \{Abs \left(EDP(\tau) : \tau \in [0, t]\right)\} \qquad (2)$$

The expression states that the envelope Ω of a certain parameter EDP at a specific time t corresponds to the maximum absolute value reached during a range of time between the start of the simulation and the time t. By definition, this measure can only increase with time and its evolution to the collapse can effectively represent the 'seismic vulnerability card' of the dam, covering the entire range of possible site specific intensity levels, even beyond the MCE. Several types of EDP, such as, e.g., maximum displacements at the top of the vertical cantilevers, joint openings at crown level, plastic deformations, damage indexes (non-dimensional parameters ranging between 0 and 1, representing the progressive decay of the structural stiffness), etc. can be adopted [4].

Vulnerability analysis

Case Studies

The ETA method is used to evaluate and compare the responses of a portfolio of arch dams, located in areas with similar seismicity. The same ETAfs are used and the numerical models of the portfolio were built with common basic assumptions, in order to be comparable as much as possible. In particular, the fluid-structure interaction is considered by means of acoustic elements with no reflection at the boundary towards the infinite and partial absorption at the bottom of the reservoir. The massless approach is used to model the foundation. The non-linear behavior of the joint is modeled through the Coulomb friction law [10]. The non-linear behavior of the concrete is represented by the Damaged Plasticity Model (Lee and Fenves 1998) [9]. A 5% damping for the concrete is considered using the Rayleigh coefficients calibrated within a range of significant modal periods. Each seismic analysis is preceded by a three step static analysis to evaluate the effect of self-weight, hydrostatic pressure and temperatures. The dynamic analyses are performed considering the three components of the seismic actions assuming 100% in the stream direction and 30% elsewhere [1]. In the following table are listed the main dimensional features of the arch dams portfolio analyzed in the present study.

Tab. 1: Arch Dams portfolio

Dam	Height [m]	Crown Length [m]	Valley Shape	Surface [m^2]	Volume [m^3]	Lombardi Index	min/mean thickness
Case 1	59	145	"U"	6316	29000	23.2	0.39
Case 2	68	160	"U"	8485	55000	19.3	0.38
Case 3	75	119	"V"	4742	18000	16.6	0.67
Case 4	111	242	"U"	20979	290000	13.7	0.18

Because the properties of the materials are similar (concrete modulus $30 \div 40$ GPa, rock modulus $10 \div 20$ GPa), the main differences are in the geometry, that is very important as the behavior of arch dams is particularly affected by their curvatures, thicknesses and the shape of the valley. These geometric features are partly considered by the Lombardi slenderness coefficient, a sort of vulnerability index of arch dams defined considering the static loads only [7]. The Lombardi coefficient equals to $F^2 / (V \times H)$ where F, V and H are the surface, the volume and the height respectively.

Results

The following response quantities have been adopted to compare the dams in terms of deformation and damages: 1) the ratio between the top displacement of the central block and the displacement at the same location resulting from the application of the static loads only; 2) the damage developed in the dam body (reduction in concrete E modulus); 3) the max joints opening (sliding) divided by the pre-seismic ones (ranging from 0.28 to 1.3 mm). The envelopes of the maximum response quantity at each time interval (one for each of the three ETAf) are named "ETA curves" (corresponding to the previously defined EDP). In Fig. 3 the averaged ETA curves obtained for each dam are reported.

As can be seen, the ETA curves are 'increasing monotonic functions' that provide useful information on the evolution of the non-linear response of the dam. It is particularly important to identify the equivalent time corresponding to the "yielding point", from which the ETA curve abruptly increases its slope, meaning that a significant non-linear effect occurred somewhere in the dam body.
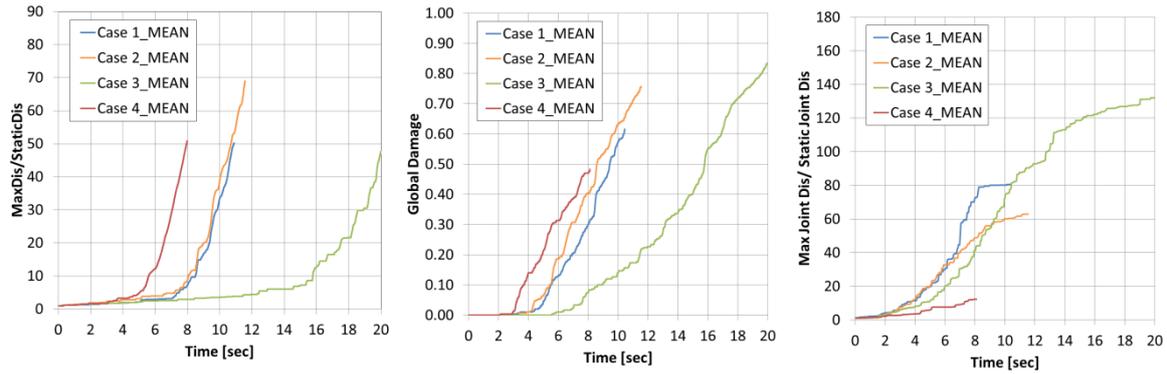
Fig. 3: Response parameters: 1) top relative displacement; 2) percentage of damaged elements and 3) joint opening (sliding)

In the first part of the analysis no concrete damage and only minor joints opening occur. After 3 seconds all dams start to experience major joint opening and concrete damages.

Some of the curves are interrupted before the completion of the analysis. This interruption is caused by the strong non-linear behavior (the software was not able to go on with the analysis with respect to the assumed convergence criteria).

The final time of the analysis, called "endurance time", could be assumed as "indicator" of the dam collapse (see Fig. 1) but, considering all approximations and uncertainties affecting the numerical analyses, this indicator is just a preliminary estimate of the collapse condition, which in the worst case may result in an overestimation of the dam capacity. Thereby for each dam case the collapse condition must be carefully identified and validated through a detailed assessment of the overall response results. For a cautious estimate of the limits exceedance and to ease the comparison, in the present study it was reasonable to assume 1% of damage (minor) as the upper bound for the SLD and 20% of damage (major) as the lower bound for the SLC (the upper bound correspond to the endurance time). Based on these definitions, the comparisons between the above conditions and the correspondent equivalent times are reported in Tab. 2. Because of the linear relationship between times and seismic intensity parameters, equivalent times can be converted in seismic intensity measures, such as the PGA.

Tab. 2: Times and PGA for "minor" and "major" damage states and for the "endurance time"

Dam	Minor Damage	Major Damage	Endurance time
Case 1	3.3 (0.22 g)	6.9 sec (0.45 g)	10.5 sec (0.69 g)
Case 2	3.4 (0.22 g)	6.3 sec (0.41 g)	11.6 sec (0.76 g)
Case 3	5.7 (0.37 g)	11.2 sec (0.73 g)	20.0 sec (1.31g)
Case 4	2.9 (0.19 g)	5.0 sec (0.33 g)	8.0 sec (0.52 g)

As can be seen the most critical dam is Case 4, the largest one with the lower "endurance time. Case 3, founded on a "V" shape valley, is the dam with the highest resistance. Its endurance time corresponds to the entire duration of ETAf, meaning the dam still has a residual capacity for higher seismic levels. Case 1 and Case 2 exhibit a very similar seismic behavior, with the latter having a slightly higher resistance. Is worth to note that for all the cases the equivalent times corresponding to the occurrence of 1% of damage are higher than 2 secs, thereby meeting the acceptance criteria for SLD. As expected, the dams with a "V" shape and the ones with higher thickness ratio are the most resistant against earthquakes.

Capacity curves

Thanks to the linear conversion between equivalent times and PGA values (Fig. 2), ETA method allows to represent the seismic vulnerability of dams through their "capacity curves", similarly to what you get from a "push over" analysis on frame structures. In this way, ETA method can be seen as a "virtual dynamic push over" test. Conceptually this curve represents the relationship between the action applied by the earthquake and the response of the structure. In this case, the parameter selected to build the capacity curve is the top displacement of the central block, u_{top}, normalized with respect to the height of the dam, H, and the Lombardi coefficient, C, ($u_{top}/(H \times C)$). Fig. 4 shows the results obtained for the entire dam portfolios.
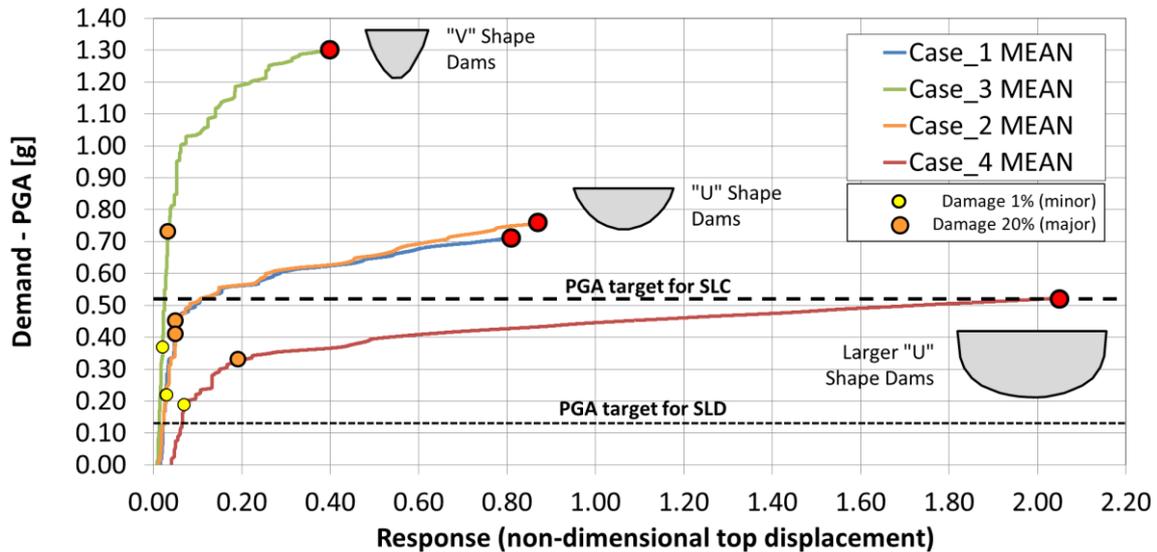
Fig. 4: Capacity curves of the selected dams portfolio

As previously stated, the capacity curves may represent synthetically the "seismic vulnerability ID" of the dam, providing the decision makers with a very powerful and practical tool to manage the seismic safety of large dams portfolios. In particular, this tool allows through the comparison of different capacity curves to identify the most vulnerable dams within the portfolio and thereby to optimize the costs for possible safety upgrading works. Also, these curves provide the capability to measure the "safety margin" of a dam with reference to certain levels of PGA. For instance, the dotted lines in Fig. 4 identify the boundary of the safe/unsafe zones referred to SLD (0.13g) and SLC (0.52g) respectively. The relevant safety margins (in terms of PGA) can be expressed as the vertical distance between the characteristic points representing the response states and the horizontal lines representing the target demand limit states.

With reference to the computational time saving, the complete seismic verifications of the entire dam portfolio with THA required to analyze an overall transient duration of 1008 sec (sum of signals duration), while ETA method required 274 sec only allowing on average a 73% saving time. Another advantage of ETA method can be represented by the possibility to develop, based on local seismicity, suitable site specific ETAfs to be used for the seismic verifications of the afferent dams, thereby removing the arbitrariness in the selection of the spectrum-compatible accelerograms (as for THA).

Conclusion

A new method, ETA, has been presented to evaluate the seismic vulnerability of arch dams. Four case studies have been analyzed to demonstrate the effectiveness of the method. The results show that ETA method can drastically decrease the computational time, while providing results as accurate as for THA. Finally, being the method able to represent the seismic vulnerability of dams through the "capacity curves", the decision makers are provided with a practical tool to synthetically represent the results of the seismic verifications and thereby to better manage the seismic safety of large dam portfolios.

References

[1] M. Meghella and L. Furgani. Application of Endurance Time Analysis Method to Non Linear Seismic Analysis of dams: Potentialities and Limitations (2014). Proc. of the 82th International ICOLD Symposium on Dams in Global Environmental Challenges, Bali (Indonesia).

[2] H.E. Estekanchi, A. Vafai and M. Sadeghazar (2004). Endurance Time Method for Seismic Analysis and Design of Structures. Scientia Iranica, Vol. 11, No. 4, 361-370, Sharif University of Technology.

[3] M.A. Hariri Ardebili and H. Mirzabozorg. Estimation of Probable Damages in Arch Dams Subjected to Strong Ground Motions using Endurance Time Acceleration Functions (2014). KSCE Journal of Civil Engineering and Architecture, Vol. 18, No. 2, 574-586.

[4] M. A. Hariri Ardebili, L. Furgani, M. Meghella and V. E. Saouma. A New Class of Seismic Damage and Performance Indices for Arch Dams via ETA Method. Engineering Structures Journal. (Under Review)

[5] ICOLD (2001). Design features of dams to resist seismic ground motion, Bulletin 120 ICOLD, Paris, France.

[6] ICOLD (2010). Selecting Seismic Parameters For Large Dams, Bulletin 148 ICOLD, Paris, France.

[7] M. Fanelli and G. Lombardi (1992). On the Lombardi slenderness coefficient for assessing the cracking potential of arch dams. In proceedings of the International Symposium on Arch Dams, Nanjing, China.

[8] Decreto Ministeriale 26 Giugno 2014. Norme Tecniche Per La Progettazione E La Costruzione Degli Sbarramenti Di Ritenuta (Dighe E Traverse). Gazzetta Ufficiale 07/07/2014 n.156. Italy.

[9] J. Lee, G. Fenves (1998): A Plastic-Damage Concrete Model For Earthquake Analysis Of Dams, Earthquake Engineering and Structural Dynamics, Vol. 27: pp. 937-956.

[10] Dassault Systèmes Simulia Corp. (1993). *Abaqus Analysis User's Manual*. Abaqus 6.11.

Dynamic evaluation of an Arch Dam-Foundation-Reservoir system considering randomly fluctuating material properties within the foundation and the dam

M. Hammami[1,2], R. Cottereau[1], E. Frossard[2]

[1]*Laboratoire MSSMat UMR 8579, CentraleSupelec, CNRS, 92290 Châtenay-Malabry, France*

[2] *Tractebel Engineering, 5 Rue du 19 Mars 1962, 92622 Gennevilliers, France*

ABSTRACT: A concrete arch dam has been analysed during seismic loading with a model based on spectral elements. We used the fine mesh provided by the formulators of the 12th ICOLD Benchmark Workshop. In this contribution, the dam and the soil are, firstly, considered as isotropic and homogeneous. Then, material parameters are modelled as random fields in order to study the structural response. Finally, an interpretation and a comparison of the results in terms of eigenfrequencies and mode-shapes is given to investigate the impact of heterogeneities within the foundation and the dam on the structural response.

E-mail: maroua.hammami@ecp.fr, regis.cottereau@ecp.fr

Introduction

The evaluation of seismic response of soils and structures constitutes an important problem in relation to the ground motion amplification. There always exist uncertainties in defining the properties of soils. This results from natural heterogeneity or the variability of the soil and limited availability of information about material properties [1]. In particular, seismic safety assessment of large arch dams is currently the subject of many international benchmark workshops [2]. The existing of heterogeneities associated with site characteristics [3] and mechanical parameters of the structure [4] may lead to a wide range of variability of the site response and could greatly affect the mechanical behaviour of the dam by inducing important local effects, such as differential displacements. Therefore, they must be properly considered in order to obtain reliable numerical simulations under strong earthquakes. Indeed, these heterogeneities in both structures and their environment call for the use of probabilistic approaches in order to provide a reliable design of the structure [5]. Thus a heterogeneous medium can be modelled as a domain with randomly fluctuating material properties.

This work aims at evaluating the influence of heterogeneities (within the foundation and the arch dam) in an arch dam response under a seismic loading. The geometrical assumptions defined on the Theme A of the 12th international benchmark workshop organised by ICOLD in 2013 [6] is used. The mass of the foundation is taken into account and a seismic source is introduced. The reservoir is considered full of water.

The results presented in this paper are the eigenfrequencies and mode shapes over a particular frequency band. A dam-reservoir is, firstly, coupled to a homogeneous soil, then to a heterogeneous foundation. Finally, we consider heterogeneity in both dam and foundation. A special attention is paid to compare the results in those different hypotheses.

Numerical modelling

The equilibrium equation is obtained by expressing that the sum of the rate of work by external forces and the rate of work by internal forces is equal to the rate of work by quantities of acceleration, that is [7]:

$$\nabla.\sigma + f = \rho \frac{\partial^2 u}{\partial t^2} \tag{1}$$

where σ is the Cauchy stress tensor, f the body forces, ρ the density and u the displacement. The isotropic linear elastic constitutive law in small strains is given by the Hooke's law:

$$\sigma(u) = \lambda \text{div}(u)\text{Id} + 2\mu\varepsilon(u) \tag{2}$$

where λ and μ denote the Lame constants, Id the identity 2nd order tensor and ε the strain tensor.

Considering Poisson's theorem, it is always possible to decompose the total displacement field u as the sum of a gradient of a scalar potential $\emptyset$ and the curl of a vectorial potential ψ :

$$u(x,t) = \nabla\emptyset(x,t) + \nabla \times \psi(x,t) \tag{3}$$

Solving the equilibrium equation in a homogeneous medium taking into account equations (2) and (3), we obtain the following equations for the potentials:

$$\frac{\partial^2\emptyset}{\partial t^2} - c_p^2.\Delta\emptyset = 0 \tag{4}$$

$$\frac{\partial^2\psi}{\partial t^2} - c_s^2.\Delta\psi = 0 \tag{5}$$

in which we consider $c_p = \sqrt{\frac{\lambda+2\mu}{\rho}}$ and $c_s = \sqrt{\frac{\mu}{\rho}}$ that denote respectively the pressure wave velocity and the shear wave velocity.

Finite element formulation

SEM is a finite element software based on a spectral formulation [8]. The displacement field u is given in each element on a base of Lagrange polynomials $f_i(x)$ at order N. Using high-order polynomials guarantee the spectral convergence. These polynomials are defined on the points of Gauss Lobatto-Legendre (GLL). Thus, $f_i(x) = 1$ on the GLL x_i. The displacement field is given by:

$$u(x,y,z) = \sum_{i,j,k} U_{i,i,k} \ \emptyset_i(x)\emptyset_j(y)\emptyset_k(z) \tag{6}$$
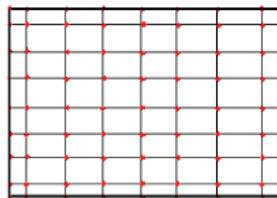
Fig. 1: Ninth order spectral 2D element

Originality of the Spectral Element Method

The estimation of all integrals in each finite element yields the equation of motion in the following matrix form:

$$M\ddot{U} + KU = F \tag{7}$$

where K is the stiffness matrix deriving from the elastic energy, M the mass matrix derived from the kinetic energy, U and $\ddot{U}$ the vectors of nodal forces. One of the originalities of the method, results from the choice of the quadrature for the numerical evaluation of the finite element formulation. Gauss points are taken astutely the same as the nodes of definition of the basic functions. Therefore, the mass matrix is diagonal.

$$M_{i,j} = \sum_k \alpha_k \; \emptyset_i(x_k)\emptyset_j(x_k) \tag{8}$$

$$\emptyset_i(x_k)\emptyset_j(x_k) = \delta_{ij} \tag{9}$$

where δ_{ij} is the Kronecker symbol.

Time integration method

We discretize the time interval of interest using a time step Δt. The semi-discrete momentum equation is then enforced in conservative form at $t_{n+\frac{1}{2}}$:

$$\frac{1}{\Delta t}M[v_{n+1} - v_n] = F^{ext}_{n+\frac{1}{2}} - F^{int}(u^h_{n+\frac{1}{2}}, v^h_{n+\frac{1}{2}}) \tag{10}$$

$$u_{n+1} = u_n + \frac{\Delta t}{2}(v_n + v_{n+1}) \tag{11}$$

$$a_{n+1} = \frac{(v_{n+1} - v_n)}{\Delta t} \tag{12}$$

where $u_{n+\frac{1}{2}} = \frac{(u_{n+1} + u_n)}{2}$ and $F^{ext}_{n+\frac{1}{2}} = \frac{(F^{ext}_{n+1} + F^{ext}_n)}{2}$. M, F^{int}, F^{ext}, u, v and a denote respectively the mass matrix, the internal forces, the external forces, the displacement, the velocity and the acceleration.

Unlike in the implicit scheme, there is no need to assemble and invert the global mass matrix. The time step Δt has to be smaller than the critical time step Δt_{cr} which in an undamped system depends on the highest frequency in the smallest element [9]:

$$\Delta t \leq \Delta t_{cr} = \frac{\Delta L}{C_L} \tag{13}$$

where ΔL is the smallest element size and C_L the velocity of the dilatational wave.

Boundary conditions: absorbing layers (PML)

Absorbing layers are finite regions "attached" at the extremities of a model. Their objective is to approximate the case of an unbounded problem by absorbing waves entering them (see Fig. 2). This type of layers is an absorbing region rather than a boundary condition per se [10]. It reduces spurious reflections at the medium boundaries using layers having specific attenuation properties.

It is for instance the case for the Perfectly Matched Layer method [11, 12, 13]. As its name indicates, a PML matches perfectly the impedance of the area of study. This means that, in theory, a wave enters a PML without reflection. Once inside it, the wave decays exponentially. A PML can therefore be used to achieve total radiation of a wave out of the area of study. In an elastic medium, modes are defined by the following equation:

$$u(x, y, z) = u_x(y)e^{i(k_x.x - \omega t)} \tag{14}$$

In the PML, this equation becomes:

$$u(x, y, z) = u_x(y)e^{i(k_x.x - \omega t)}e^{-A_x k_x \frac{x^p}{L^p}} \tag{15}$$

where L is the thickness of the layer, kx the wavenumber and Ax and p two constants.

Modal analysis of a dam coupled to a homogeneous soil

This work consists on the dynamic analysis of an arch dam under seismic loading using the SEM (Spectral Element Method) software. Details of the procedures utilized, the results of the computations and an interpretation on the results are presented in the following sections.

Mesh properties
The fine mesh provided in the theme A of the 12th ICOLD benchmark Workshop [6] was modified in order to obtain coincident meshes at fluid-concrete-rock interfaces as necessary for the proper operation of SEM (see figure 2). Mesh characteristics are listed in the Tab. 1.
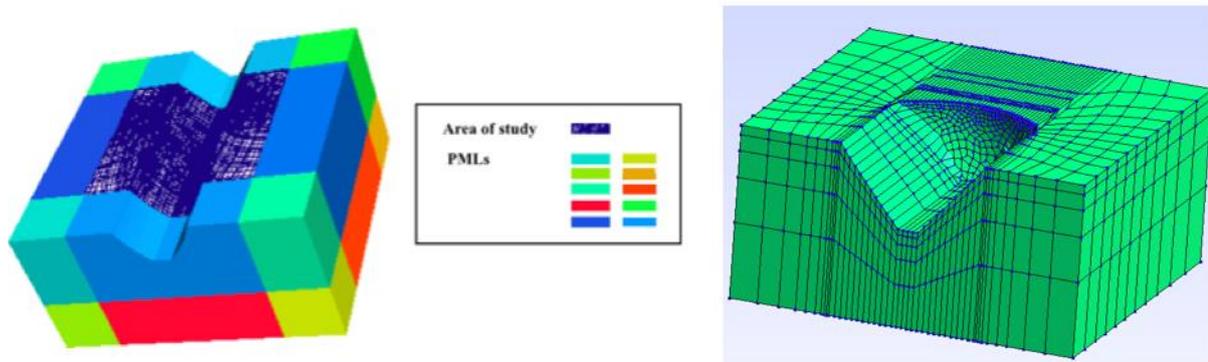
Fig. 2: (left) Area of study and its Perfectly Matched Layers, (right) Fine mesh of the dam, foundation and the reservoir

Tab. 1: Fine mesh

	number of nodes	Number of elements
Foundation	3553	2700
Dam	1320	920
Reservoir	1848	1380

Physical model
Material characteristics are listed in the Tab. 2.

Tab. 2: Material properties

	Dimensions(m)	Vp(m/s)	Vs(m/s)	ρ(kg/m^3)
Foundation	1000X1000X500	3353	2175	2200
Dam	480X80X220	3753	2195	2400
Reservoir	460	1500	-	1000

As a seismic source, we use a Ricker pulse on the corner of the foundation (see figure 3). The amplitude $x(t)$ of this seismic signal is defined by:

$$x(t) = (1 - \frac{(t - t_0)}{2\sigma^2}\, e^{-\frac{(t-t_0)^2}{2\sigma^2}}$$ (16)

The parameters t_0 and σ describe the duration of this wavelet signal. In our model, we consider a central frequency of 10 Hz and a start time equal to 0.11 s.
The power spectrum $S(\omega)$ of this wavelet has the form:

$$S(\omega) = K\omega^2 e^{-(\sigma\omega)^2}$$ (17)

where K is a constant.
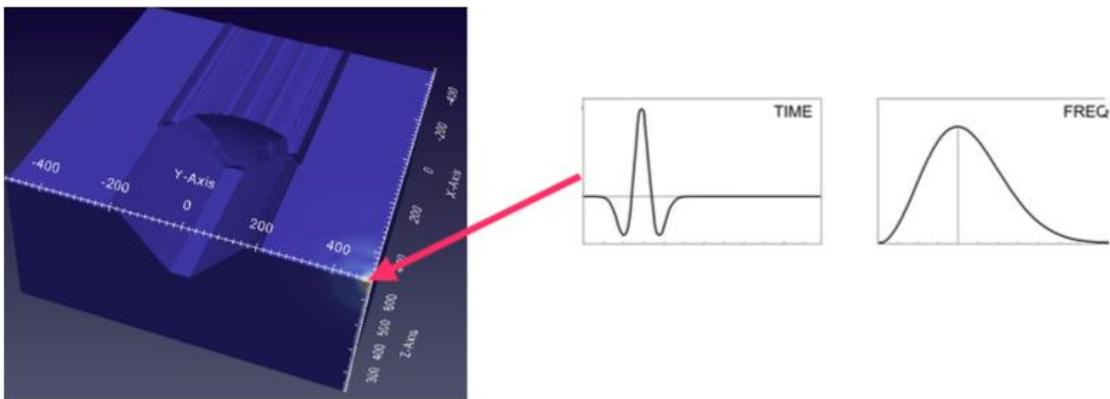
Fig. 3: Seismic source

Results
In order to analyse the behaviour of the dam under the seismic load, time responses are converted in the frequency domain by performing a Fourier Transform of the time signal. We choose seven equidistant points on the dam's crest. One of the points is considered as a reference station (see Fig. 4).
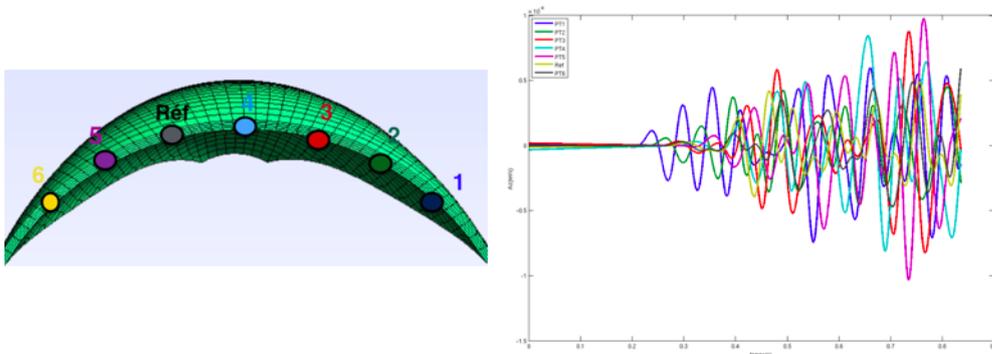
Fig. 4: Crest's stations

For the evaluation of the first modes of the structure, we use spectrum ratio between each point and the reference station [14]. Then, drawing the sum of these curves, function of frequency, it is possible to select the peaks that correspond to eigenfrequencies. In this study, cross-spectrum method is used to evaluate not only eigenfrequencies but also mode's shape. Magnitude of each cross-spectrum provides an overview of the mode's shape. Besides, phase analysis gives relative displacement between the points. Magnitude of the cumulated cross-spectrum is plotted on figure 5.
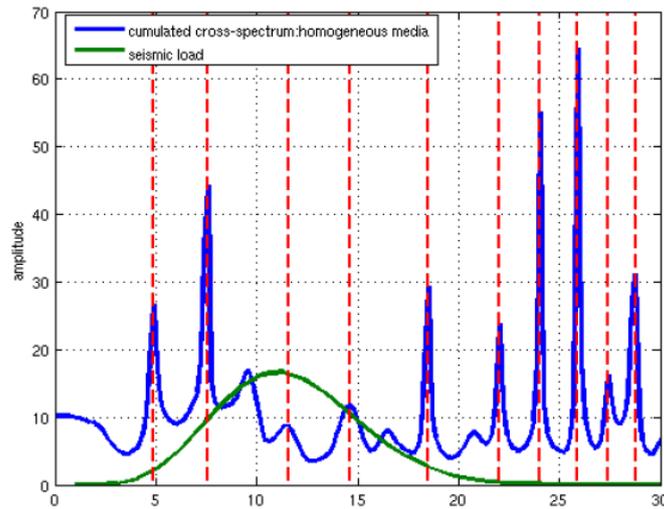
Fig. 5: Results of the homogeneous model

Looking at the magnitude curve, many peaks are highlighted at 4.88 Hz, 7.59 Hz, 9.59 Hz, 11.61 Hz, 14.63 Hz, etc. Comparing with the curve of the seismic load, we note that we do not observe modes of the lowest frequency band. That is confirmed by mode shapes plotted on figure 6.

Thus, with the chosen excitation, it is not possible to capture the fundamental mode.

With phase analysis, it is then possible to draw mode's shape at each spotted frequency. In the figure 6, we show the first and the second modes shapes of the crest (they are not the fundamental and the first harmonic mode).
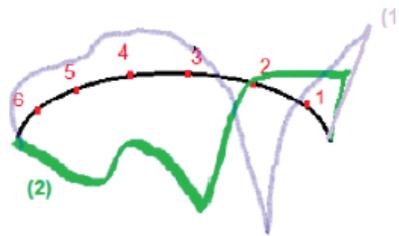
Fig. 6: 1st and 2nd modes shapes of the crest

Modal analysis considering randomly fluctuating material properties

The seismic response of a structure depends not only on its own mechanical parameters but also on its site properties. To quantify the influence of heterogeneity in the medium, probabilistic mechanical parameters can be used.

The spectral representation is a classic way to sample Gaussian random field [15]:

$$S_k(x) = \int_{k \in \omega} \hat{R}_k^{1/2} \exp(ikx) \, dW_k \quad (x \in \omega) \tag{18}$$

where S is the random field, $\hat{R}$ the Fourier transform of a correlation function R and dW the Brownian motion. In our model, S could be the density or the Lamé coefficients.

The evaluation of the response variability due to system stochasticity consists of performing the response analysis of structural systems with Gaussian correlation in their material properties.

For this reason, in our study, we consider a stochastic process with a correlation length equal to the minimum wavelength. Moreover, a Log-normal distribution is used for the material properties. We consider a standard deviation of 20 % for the log-normally distributed medium density and Lame coefficients.
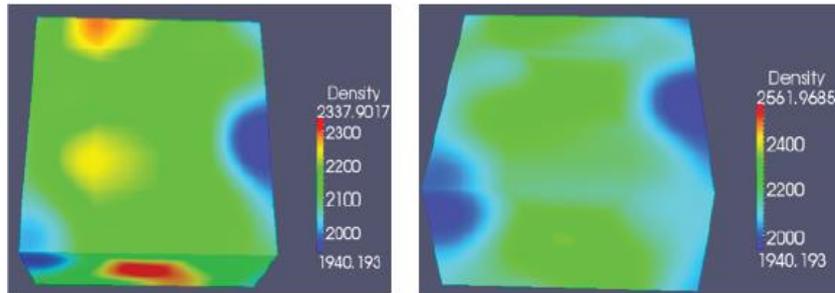
Fig. 7: Randomly fluctuating properties within (left) the foundation (right) the dam and the foundation

Results and interpretations

As for the homogeneous case, we consider the same seven equidistant points on the dam's crest. We calculate the spectrum ratio between each point and the reference station. Then, we plot the sum of these spectrum ratios, function of frequency in order to obtain the peaks that correspond to eigenfrequencies (see figure 8).
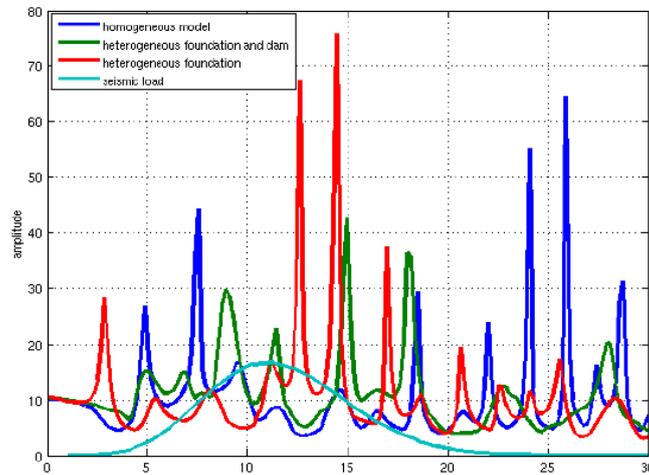
Fig. 8: Results; cumulated cross-spectrum

Looking at the red curve (heterogeneous foundation), many peaks are highlighted at 2.86Hz, 5.38 Hz, 8.07 Hz, 11.27Hz, 12.62 Hz, etc. On the green curve (heterogeneous dam and foundation), we have also peaks that correspond respectively 4.88Hz, 6.73 Hz, 8.91 Hz, 11.44 Hz, 14.97 Hz, etc. Thus, in comparison with the case in which only the foundation is heterogeneous, eigenfrequencies are higher when we consider randomly fluctuating material properties within the dam and the foundation. (The green curve is translated to the right in comparison with the red one).

The figure 9 shows the first and the second modes shapes of the dam's crest.
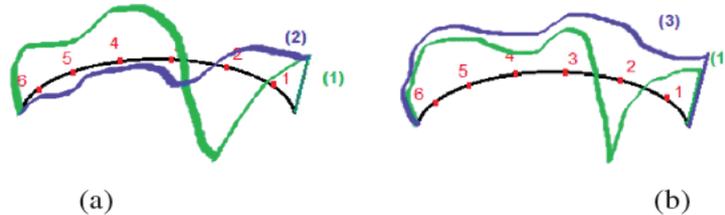
Fig. 9: 1st and 2nd modes shapes of the crest considering

(a) heterogeneous foundation (b) heterogeneous dam and foundation

(b)

In order to understand the influence of the heterogeneities on the dam-foundation-reservoir interaction, we summarize the different results obtained in the Tab. 3.

Tab. 3: Results

Model/mode	1	2	3	4	5
Homogeneous media	4.88	7.59	9.59	11.61	14.63
Heterogeneous foundation	2.86	5.38	8.07	11.27	12.62
Heterogeneous media	4.88	6.73	8.91	11.44	14.97

First of all, we should note that in comparison with 12th international benchmark workshop on numerical analysis of dams organised by ICOLD in 2013, we take into account foundation mass. Moreover, the fine mesh was modified in order to obtain coincident meshes at fluid concrete-rock interfaces as necessary for the proper operation of SEM. Indeed, our numerical model and our boundary conditions are not the same as what was used in the last benchmark. In terms of results, we remind that the first mode that we observe in the homogeneous case does not correspond to the fundamental one. Moreover, it does not appear in homogenous cases. Also, the eigenfrequencies are much higher in the case of randomly fluctuating material properties for both dam and foundation than the homogeneous media. That highlights the influence of soil and concrete heterogeneities in the structures response.

The first mode in the second model (heterogeneous foundation) does not appear in the two other models. It can be due to a localized heterogeneity in the foundation which is resulted by the log-normally distribution.

Conclusion

The results of these analyses confirmed that considering randomly fluctuating material properties within the foundation and the dam influences the site response and could change the mechanical behaviour of the dam. In this order of idea, we should precise that the numerical tests have to be pushed further. In this study, we used a correlation length l_c equal to the minimum wavelength. Although, using a lower correlation length helps us to design a large scale of heterogeneity. Also, our conclusions are based on primary results that can change if we consider for example the effect of nonlinearities in media.

References

[1] M.S. Rahman and C.H. Yeh. Variability of seismic response of soils using stochastic finite element method. Soil Dynamics and Earthquake Engineering, 18:229 – 245, 1999.

[2] Peng Lin et al. Hazard and seismic reinforcement analysis for typical large dams following the wenchuan earthquake. Engineering Geology, 3792:12 p, 2014.

[3] D. Clouteau, R. Cottereau, and G. Lombaert. Dynamics of structures coupled with elastic media-a review of numerical models and methods. Journal of Sound and Vibration, 332:2415 – 2436, 2013.

[4] C. Soize. Stochastic modeling of uncertainties in computational structural dynamicsrecent theoretical advances. Journal of Sound and Vibration, 332:2415 – 2436, 2012.

[5] R. Cottereau, D. Clouteau, and C. Soize. Probabilistic impedance of foundation: Impact of the seismic design on uncertain soils. Earthquake engineering and structural dynamics, 2008.

[6] Numerical analysis of dams, the 12th international Benchmark Workshop, ICOLD, Graz, Austria, october 2013.

[7] A. Pecker and J.F. Semblat. Waves and Vibrations in Soils. IUSS Press, 2009.

[8] D. Komatitsch, J.P. Violette, R. Vai, J.M. Castillovarrubias, and F.J. Sanchez-Sesma. The spectral element method for elastic wave equations-application to 2d and 3d seismic problems. International Journal for Numerical Methods in Engineering, 45, 1999.

[9] C. Gary and L. Qing Huo. Higher-order numerical methods for transient wave equations. The Journal of the Acoustical Society of America, 2003.

[10] F. Nataf. Absorbing boundary conditions and perfectly matched layers in wave propagation problems. Comput. Appl. Math, 14:219 – 231, 2013.

[11] P. Berenger and J.P. Violette. A perfectly matched layer for the absorption of electromagnetic waves. J. Comp. Phys, 114:185 – 200, 1994.

[12] G. Festa and J.-P. Vilotte. The newmark scheme as velocity-stress time-staggering: an efficient pml implementation for spectral element simulations of elastodynamics. Geophys. J. Int, 161(3):789 – 812, 2005.

[13] M. Brice Drozdz. Efficient finite element modelling of ultrasound waves in elastic media. PhD thesis, University of London, London, 2008.

[14] A. Robbe, A. Diallo, N. Humbert, and E. Bourdarot. Analyses of earthquakes records on concrete dams in japan. Japan Commission on Large Dams - French committee of dams and reservoirs, 2015.

[15] G. Deodatis and M. Shinozuka. Simulation of stochastic processes by spectral representation. Appl Mech Rev, 44(4), 1991.

Modelling of rock fall on the dam of Place Moulin

Frigerio A.[1] and Artaz L.[2]

[1]*1Ricerca sul Sistema Energetico RSE, Via Raffaele Rubattino 54, 20134 Milan, Italy*
[2]*C.V.A. Spa - Compagnia Valdostana delle Acque, Via Stazione 30, 11024 Chatillon, Italy*

ABSTRACT: In the past decades, on the left bank of the dam of Place Moulin landslides and collapse of rocky boulders have occurred requiring consolidation and protection works. C.V.A., owner of the structure, has thus carried out annual monitoring campaigns to assess the state of the banks of the reservoir since the early '70s. In recent surveys the structural-geologic evolution of the left slope was analysed, identifying potential events of collapse that would involve the crest and the upstream face of the dam. Each event was characterized in terms of volumes of collapse, trajectories and relative hazardous conditions.
Considering the instability phenomena that have the greatest probability of occurrence, the consequences of a rock fall with predefined dimensions and trajectories were assessed, taking into account different points of impact and analysing the damage conditions of the dam. The results of the numerical modelling have provided C.V.A. with information to plan mitigation and protection actions for the safety of the dam.

E-mail: antonella.frigerio@rse-web.it

Introduction

Several Alpine valleys, where many Italian dams are located, are characterised by hazardous instability phenomena that might give rise to the possible falling of rock blocks that require mitigations works to avoid damages to the structures.
This paper presents the case of Place Moulin dam, analysing the most hazardous instability phenomena, identified by recent geological surveys carried out on the left bank of the reservoir. The study was performed by means of a numerical modelling approach to assess the main consequences that the dam could undergo, mainly in terms of structural damage.

Instability phenomena that could involve the dam of Place Moulin

The dam of Place Moulin, located in the Municipality of Bionaz in Valpelline, in the Italian Region of Valle D'Aosta, is a concrete arch-gravity structure built between 1955 and 1965 (Fig. 1). The reservoir has a total volume of 105 Mm^3 that feeds the power station of Valpelline.

Fig. 1: downstream view of the dam of Place Moulin

The main geometric features of the dam and the reservoir are:

- Height   155,00 m
- Base thickness   41,94 m
- Crest thickness   6,44 m
- Crest length   678,00 m
- Dam volume   1,51 Mm^3
- Maximum water level   1.968 m asl

Recently, some geological surveys thoroughly investigated the instability phenomena that occurred and might still take place on the rocky slope of the orographic left bank of Place Moulin reservoir [1][2]. The outcomes of these studies allowed to characterize the structural and geomorphologic setting of the left slope but, most of all, they identified which potential kinematic mechanisms could directly threaten the dam.
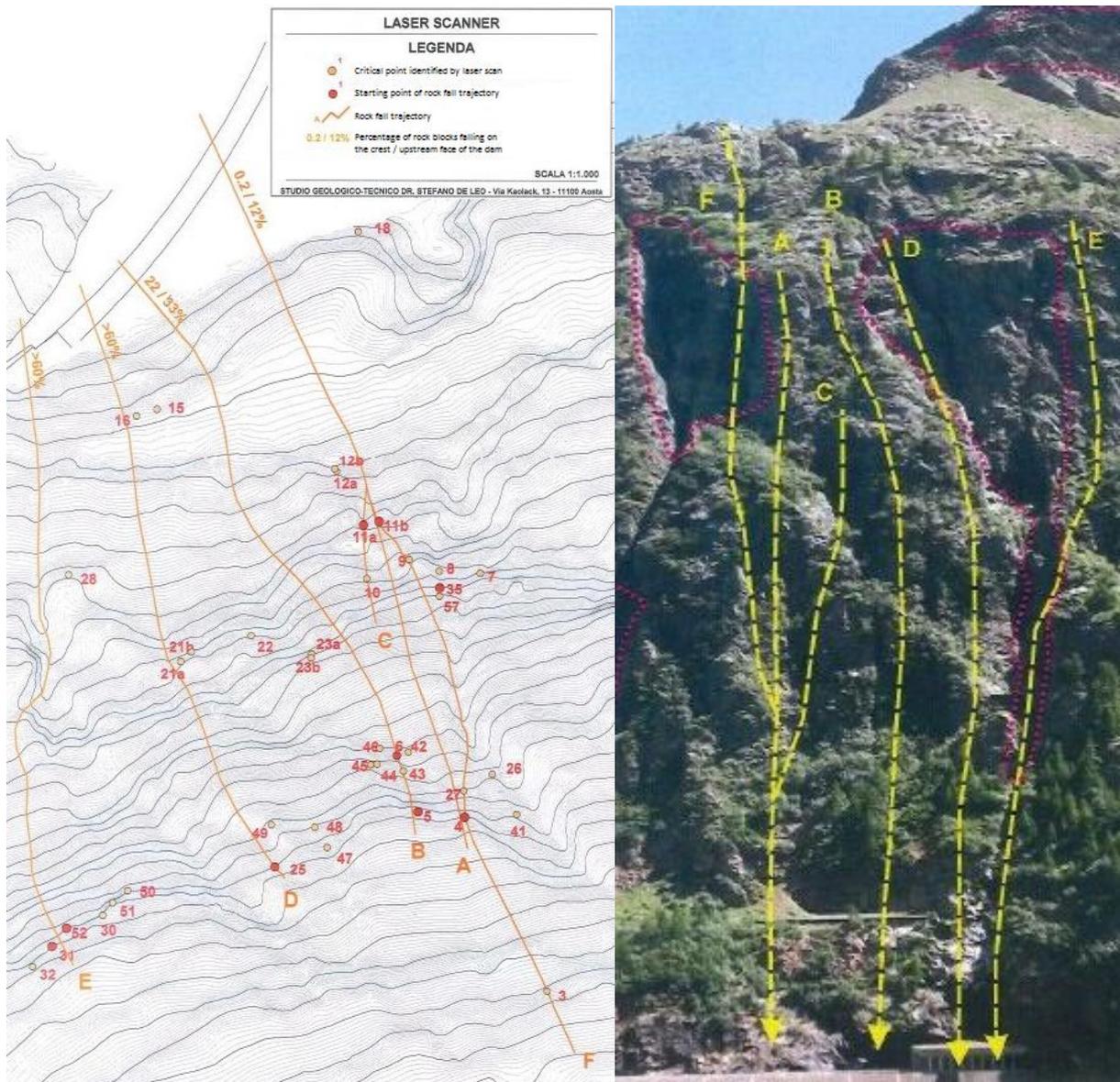

Fig. 2: layout of the rock fall trajectories on the left bank of the dam

First of all, the rocky blocks that could detach, fall off and roll along the left slope do not exceed a volume of 10 m^3 because of the strongly fractured state of the in situ rock.

The rock fall hazard simulations highlighted that the first part of the left side of the crest, 30-50 m long, has a 15÷60% probability to be threatened; the hazardous conditions progressively decrease moving towards the middle of the crest and they become nearly negligible for distance exceeding 80 m.

The trajectories and the end points of the main rock falls are mapped in Fig. 2 while the features of the most hazardous conditions for the dam are listed in F 1.

Tab. 1: features of the main rock fall trajectories

Number of the hazardous conditions	Rock fall volume [m^3]	Rock fall mass [kg]	Outcrop volume [m^3]	Maximum kinetic energy [kJ]
1	9,0	24.750	483,0	24.360
2	6,9	19.000	17,2	20.500
3	8,9	24.500	34,2	23.800
4	7,1	19.500	360,0	29.972
5	5,2	14.300	12,0	24.250

Bearing in mind these results, the hazardous condition number 4 was selected to carry out the numerical simulations of the impact of the rock boulder on the dam because this situation is characterized by the highest kinetic energy; moreover, this condition has the highest probability of occurrence.

The Finite Element model

Geometry and contact surfaces
The three dimensional Finite Element model of the dam was generated on the basis of related design drawings [3]. Considering the large size of the dam with respect to both the impact zone and the rock fall dimension, only half dam was modelled together with an extended part of the foundation (Fig. 3). This choice was endorsed by a preliminary analysis that considered the whole dam; the related results have shown that the effects of the impact are restricted to the left part of the dam, towards the abutment. For sake of simplicity, the numerical simulations has taken into account only a single rock boulder with a volume of 7,1 m^3, assuming the spherical shape as a reference one (Fig. 3, bottom-right picture).

In order to reduce the computational time of each simulation, the FE mesh was progressively refined along the following directions: starting from the main vertical section towards the left abutment, and moving from the foundation towards the crest of the dam.

The resulting model has nevertheless more than 210.000 nodes and nearly 184.000 Finite Elements, because the impact zone requires to be really well refined.

The nodes laying on the base and vertical sides of the foundation were constrained; on the main vertical section of the dam symmetric boundary conditions were assigned to take into account the stiffness of the right part, not included in the model.

The dam body was assumed monolithic, and there is also continuity between the dam and the foundation. In order to model the interaction between the rock boulder and the dam, two contact surfaces were included: the former completely covers the outer surface of the rock boulder, the latter partially covers the crest and the upstream face of the left part of the dam.
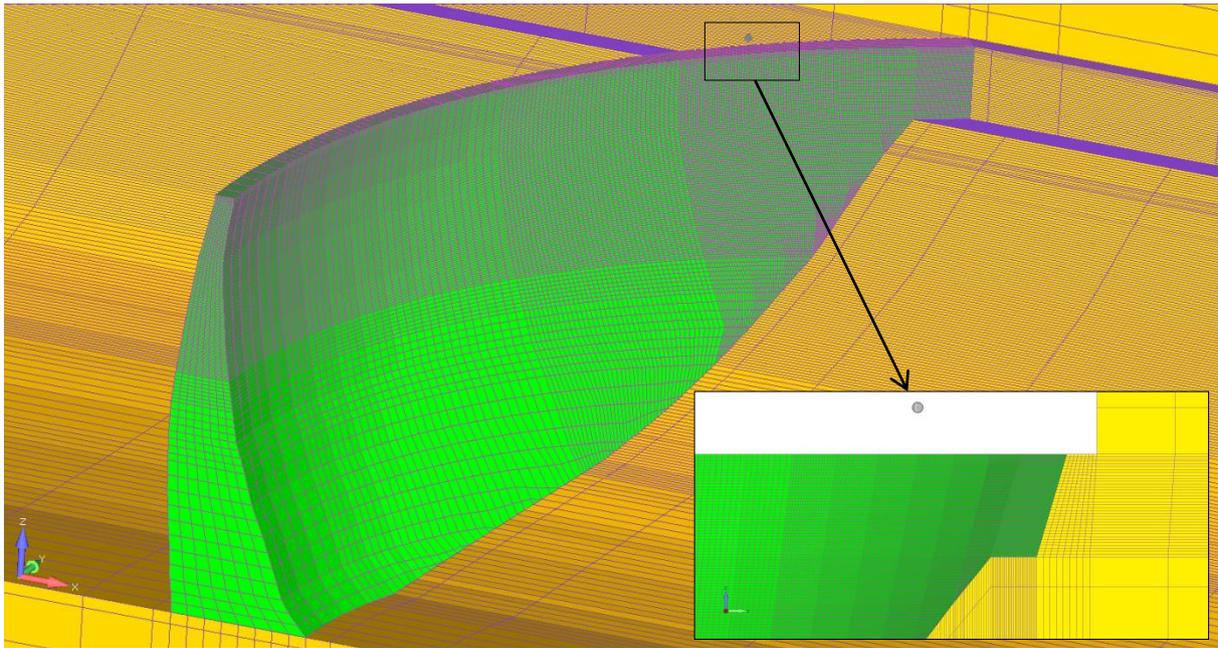
Fig. 3: Finite Element model of half dam, the foundation and the rock boulder (in the bottom-right picture a zoomed downstream view of the left part of the dam with the starting position of the rock boulder)

Impact points on the dam
The numerical simulations have taken into account the following three different impact points on the dam:

A. The upstream edge of the crest, 50 m far from the left abutment
B. The centreline of the crest, 50 m far from the left abutment
C. The upstream face, 50 m far from the left abutment and 10 m below the crest level

These positions catch the most hazardous conditions for the dam.
In Tab. 2 the impact velocity, the kinetic energy, the incidence angle from vertical, and the direction cosines of the falling trajectory are listed.

Tab. 2: features of the analysed falling trajectories

Case study	Impact velocity [m/s]	Impact kinetic energy [kJ]	Incidence angle [°]	Direction cosines		
A	52,91	27.331	50°÷55°	0,259	-0,721	-0,643
B	52,91	27.331	50°÷55°	0,259	-0,721	-0,643
C	55,51	30.083	25°÷30°	0,143	-0,397	-0,906

The incidence angle in the horizontal plane was maintained constant for all the three cases.

Constitutive models and related material parameters

In order to simulate the impact phase, non-linear constitutive models were used because the material strength is overcome both in the concrete of the dam and into the rock boulder, with the exception of the foundation being rather far from the impact zone.

The parameters of all materials are summarized in Tab. 3 while some details of the related constitutive models, adopted to simulate their mechanical behaviour, are reported in the following paragraphs.

Tab. 3: material parameters [3][4][5]

Material parameter	Foundation	Dam	Boulder
Young modulus	75.600 MPa	34.000 MPa	75.600 MPa
Poisson coefficient	0,220	0,166	0,220
Density	2.750 kg/m^3	2.450 kg/m^3	2.750 kg/m^3
Compression strength	-	424 MPa	-
Tension strength	-	32 MPa	8 MPa

Foundation

The foundation is formed by mica schist and kinzigite, thickly interspersed with amphibolite, marbles and pegmatites. These metamorphic rocks are characterized by high specific weight and hardness but they have, in general, a marked schistosity and fracturing which reduces their geomechanical properties. Anyway, the mechanical behaviour of the foundation was simulated by means of a linear elastic constitutive model, being the effect of the impact of the boulder on the dam rather localized.

Dam

The concrete behaviour of the dam was modelled by means of the Concrete Damage Plasticity Model (CDP) provided in ABAQUS [6][7][8]. The main failure mechanisms of concrete are cracking in tension and crushing in compression. The CDP model aims to capture the effects of irreversible damage associated with these failure mechanisms, taking into account:

- different yield strengths in tension and compression, with the initial yield stress in compression being a factor of 10 than the initial yield stress in tension
- softening behaviour in tension as opposed to initial hardening followed by softening in compression (Fig. 4)
- different degradation of the elastic stiffness in tension and compression, according to the following stress-strain relations under uniaxial tension and compression loading:

$$\sigma_t = (1 - d_t) E_0 \left(\varepsilon_t - \varepsilon_t^{pl} \right) \tag{1}$$

$$\sigma_c = (1 - d_c) E_0 \left(\varepsilon_c - \varepsilon_c^{pl} \right) \tag{2}$$
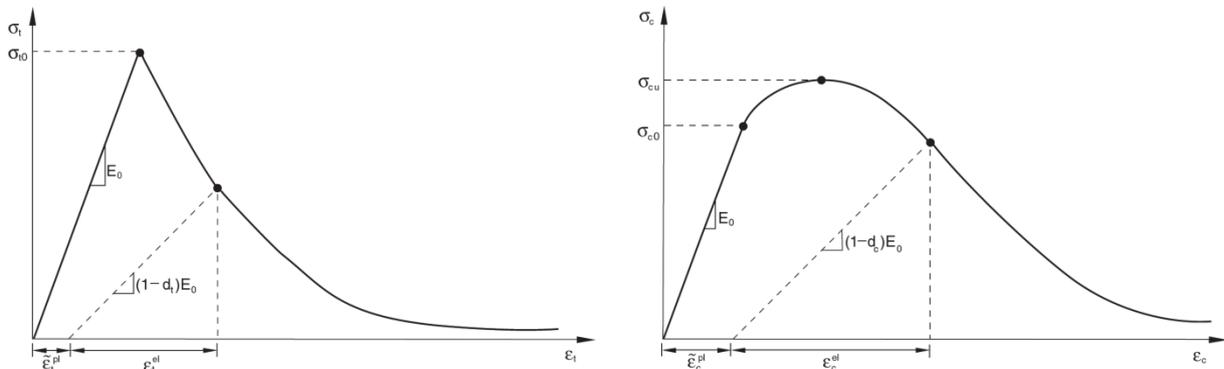

Fig. 4: response of concrete to uniaxial loading in tension (left) and compression (right)

The unloading response of concrete from any point on the strain softening branch of the stress-strain curves is weakened being the elastic stiffness degraded. This degradation is characterized by two damage variables, d_t (DAMAGET) and d_c (DAMAGEC), which are assumed to be functions of the plastic strain, ε^{pl}. The damage variables can take values from zero, representing the undamaged material, to one which denotes total loss of strength.

Boulder
The mechanical behaviour of the rocky boulder was modelled by means of the Brittle Cracking (BC) Model provided in ABAQUS [6] which is designed for applications in which the tensile cracking is the dominant failure mode. As the brittle behaviour in tension is much more relevant than the compression crushing during the impact phase of the boulder on the dam, the assumption of the BC model that the material has a linear elastic response in compression is acceptable. A crack initiation is detected by a simple Rankine criterion which states that a crack forms when the maximum principal tensile stress exceeds the tensile strength of the brittle material. Although crack detection is purely based on Mode I fracture, post cracked behaviour includes both Mode I (opening mode) and Mode II (in plane shear/sliding mode) failures (Fig. 5). During the numerical analyses, the BC model allows removal of elements based on the Rankine criterion.
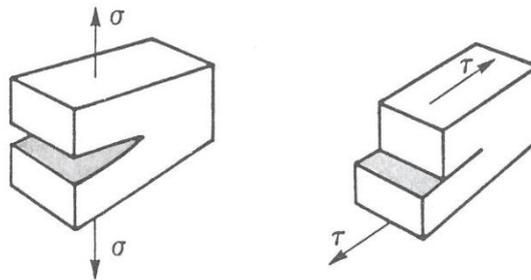
Fig. 5: Mode I – opening (left) and Mode II – in plane sliding (right) in fracture mechanics

In order to avoid mesh sensitivity into the results, the post failure stress is specified as a tabular function of displacement across the crack, u^{ck}, defining thus the energy required to open a unit area of crack in Mode I as a material parameter (Fig. 6, left).
Considering that the cracked shear modulus decreases as the crack opens, a shear retention model is adopted in which the post cracked shear modulus G_c is defined as a fraction of the uncracked shear modulus G. The shear retention factor ρ is defined as a function of the opening strain across the crack, e^{ck} (Fig. 6, right).

$$G_c = \rho\left(e_{nn}^{ck}\right) G \qquad (3)$$
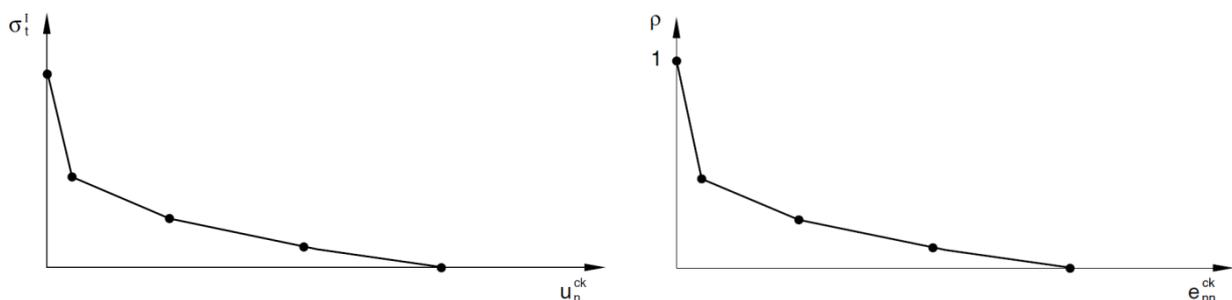
Fig. 6: post failure stress-displacement curve (left) and shear retention model (right)

Sensitivity analyses on the failure parameters of the boulder

The boulder is composed of the same metamorphic rocks of the left slope of the reservoir of the dam of Place Moulin, characterized by marked schistosity and fracturing. The choice of the strength parameters related to this type of rock is indeed important because they define how much energy the boulder could dissipate during impact breaking into several pieces. The energy dissipated by the boulder increases with its brittle behaviour, and at the same time a major shattering of the boulder corresponds to a lower damage of the dam.

Sensitivity analyses were thus carried out to assess how the compression and tension damage varies on the dam body changing the brittle behaviour of the boulder in terms of deformation at the formation of cracks and of failure deformation (Tab. 4).

Tab. 4: failure parameters of the sensitivity analyses

| Material parameter	Case 1	Case 2	Case 3
Deformation at the formation of cracks	0,0015	0,0070	0,0250
Failure deformation	0,0030	0,0090	0,0400

Making reference to the case study in which the boulder impacts against the centreline of the crest of the dam (Case B), the results in terms of the tension damage parameter value show that the damage of the concrete depends on the attained level of shattering of the boulder (Fig. 7). In the first case the boulder remains almost undamaged after the impact while in the last case it shatters almost completely. The second case is deemed to be the most realistic.
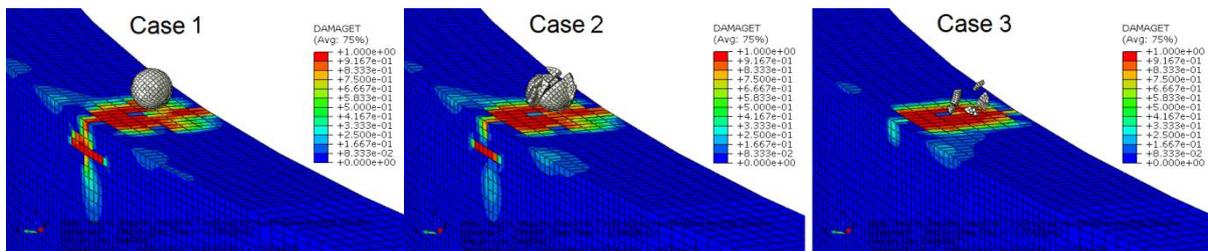
Fig. 7: contour of the DAMAGET parameter – results of the sensitivity analyses

Results of the impact analyses

In all the three case studies the impact analyses, carried out with ABAQUS/Explicit, shows that the compression damage on the concrete dam is limited to the impact area, and it is really negligible for Case C as the boulder hits almost tangentially the upstream face of the dam. The tension damage is significant in the first two cases but not in the last one (Fig. 8 and 9).
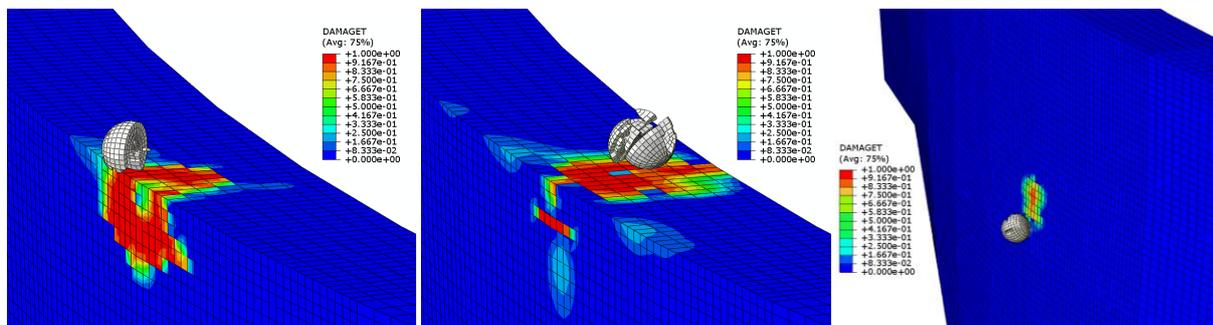
Fig. 8: contour of the DAMAGET parameter on the crown and upstream face (Case A left, Case B centre, and Case C right)
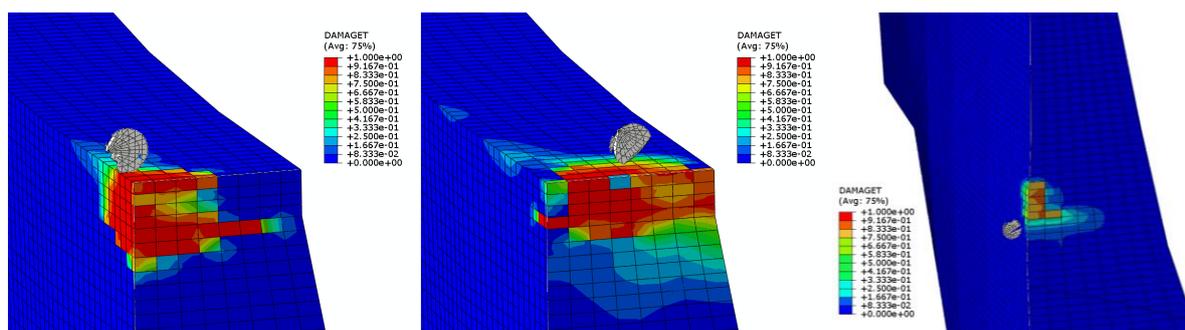
Fig. 9: contour of the DAMAGET parameter in a vertical section (Case A left, Case B centre, and Case C right)

The most damaged conditions in tension are related to Case B since the formation of cracks extends down the dam nearly 2,5 m from the crest level and propagates along the whole thickness of the structure. In Case A the tension damage extends more along the vertical direction with respect to Case B, about 4,0 m from the crest level, but it does not affect the entire dam thickness. From a numerical point of view, Case A represents the most complex analysis because the boulder impacts directly on the upstream edge of the dam that is a geometric singularity.

Conclusion

In general, the results of the impact analyses show that the rocky boulder causes damages in tension on the concrete dam of Place Moulin because of the high kinetic energy. Being the slope rather steep, in fact, the boulder attains high velocities at the end of its falling path.

The impact effects on the crest of the dam are higher than those occurring on the upstream face. Anyway, in each analysis the damaged zone in tension is quite localized because it extends maximum 4 m from the crest level and not ever it is passing along the thickness.

On the contrary, in all cases the damage in compression is rather negligible being almost localised to the impact area. A static analysis, carried out after the impact simulation, has shown that the damaged zones do not affect the whole structural behaviour of the dam in response to static loads. Therefore, the owner is planning mitigation works on the left slope to prevent rock falls that might directly involve the crest of the dam.

References

[1] De Leo S. (2014). Ispezione geologica delle sponde prospicenti la diga di Place Moulin. Studio geologico-tecnico Dr. Stefano De Leo.

[2] De Leo S. (2014). Studio geologico-strutturale del versante che costituisce la spalla sinistra della diga di Place Moulin. Studio geologico-tecnico Dr. Stefano De Leo.

[3] ENEL (1970). Le dighe di ritenuta degli impianti idroelettrici italiani. Roma, Italy.

[4] Boldrini A. (2007). Accoppiamento idromeccanico nella roccia di fondazione di dighe ad arco gravità. Esame di un caso reale. PhD Thesis in Geotechnical Engineering. University La Sapienza of Rome

[5] Ippolito I, Nicotera P., Lucini P., Civita M. and de Riso R. (1975). Geologia tecnica. Ed. ISEDI

[6] Dassault Systèmes S.A., SIMULIA. (2014). ABAQUS Theory Manual.

[7] Lubliner J. et Al. (1989). A Plastic-Damage Model for Concrete. International Journal of Solids and Structures. Vol. 25,N. 3, pp 229-326

[8] Lee J. and Fenves G. L. (1998). Plastic-Damage Model for Cyclic Loading of Concrete Structures. Journal of Engineering Mechanics. Vol. 124, N. 8, pp 892-900

Risk Analyses for Large Dams

Hinks J.L[1], Kitamura Y.[2] and Murphy A.T[1]

[1]*HR Wallingford, United Kingdom*
[2]*Electric Power Development Co. Ltd, Japan*

ABSTRACT: This paper describes the United Kingdom method for conducting risk analyses for large dams. The importance of checking results against published statistics is emphasised. Whilst the method was developed primarily for use in the United Kingdom it has been successfully used in other countries where natural hazards are greater than in UK.

The paper gives examples of how the method has been used in Japan and offers comments on the results obtained particularly with respect to risks from earthquakes and typhoons. For the rockfill dams considered it is found that indirect seismic risks (eg. From seiches and landslides) overshadow the direct risks associated with settlement and consequential overtopping. Other risks such as typhoon rainfall, internal erosion and non-operation of spillway gates are significant.

E-mail: j.hinks@hrwallingford.com

Introduction

The new UK methodology for conducting risk assessments for dams was published in 2013 and is now being used for dams in the UK. It comprises a three tier approach of which two tiers involve quantitative risk assessment. The method builds on the recommendations in ICOLD Bulletin 130[1] and on the methodologies used in Australia and the USA.

Methodology

In the UK the risk assessment for reservoirs, using the Risk Assessment for Reservoir Safety guidance[2] follows three key steps:

   Step 1. Identification of risks
   Step 2. Analysis of risks
   Step 3. Evaluation of risks

Step 1 - Identification of risks

This first step is to select the extent and level of detail or complexity for the risk assessment. This builds on the statement of purpose and on an identification of the ways in which a failure could occur. The step involves listing and describing all potential failure modes including details of the relationship between each failure mode and the types of consequences of failure it is relevant to consider to satisfy the statement of purpose.

A structured and systematic process should be followed to ensure the identification of potential failure modes is completed adequately and with the desired level of confidence. This step also includes the identification of the system loading conditions (that is, which threats) to be used in the next step – risk analysis.

Step 2 - Analysis of risks

The second step is risk estimation, which is the process of determining the response of the system to threats and the associated probability of failure. Traditional engineering analysis, reliability analysis and engineering experience and judgement are all important in estimating system response relationships.

Risk analysis also includes an estimation of the consequences for all the significant failure modes. Consequences are a function of many factors including:

- the amount of water in the reservoir
- the nature and extent of the dam failure
- the season of the year
- warning time

Dam break modelling provides the basis for the estimation of the consequences of dam failure for each failure mode, a range of exposure conditions affecting potential life loss (that is, day/night, season of year and so on).

The 'no failure' case should also be considered to allow incremental consequences to be determined. These are defined as the difference between the consequences estimated for failure and no-failure scenarios for flood-related failure modes.

Risk analysis involves both risk identification and estimation of the level of risk. It involves combining the probabilities and consequences to obtain estimates for all significant failure modes and then presenting the results in a suitable format so that they can be readily interpreted and used to support reservoir safety decision-making.

The level of detail used to assess the probability of failure and consequence vary depending on the study. The assessment of the most likely failure modes is made on the basis of expert judgement and historical data from similar dams. The consequence of dam failure can range from simple empirical methods through to breach simulation, 2D hydraulic modelling and life safety modelling.

Step 3 - Evaluation of risks
The process of examining and judging the significance of the estimated risk is termed 'risk evaluation'.

Notwithstanding the general reliability of the method (see Pilot Studies below) it has been found highly desirable to check all results against worldwide statistics such as those published by Foster, Fell and Spannagle[3] for embankment dams and Douglas, Spannagle and Fell[4] for concrete and masonry gravity dams. Approximate Annual probabilities of failure for dams over 5 years old are as given in Tab. 1 below. For fill dams the true probabilities will be higher than the figures given on the table since these are for piping only:

Tab. 1.   Average Probabilities of Failure after Foster et al.

Dam Type	Annual Probability of Failure	Return Period of Failure (Years)
Homogeneous earthfill	188 x 10-6	5,319
Concrete gravity pre 1929	93 x 10-6	10,752
Puddle core earthfill	38 x 10-6	26,315
Earthfill with filter	37 x 10-6	27,027
Clay core earth and rockfill	< 34 x 10-6	>29,412
Zoned earthfill	25 x 10-6	40,000
CFRD	< 17 x 10-6	>58,824
Concrete gravity post 1930	14 x 10-6	71,428
Concrete corewall	< 8 x 10-6	>125,000
ALL DAMS	56 x 10-6	17,857

From the above table we can conclude that the return period for failure of a modern dam will typically lie in the range 5,000 to 150,000 years. Where the calculated return period is significantly less than 5,000 or 10,000 years the question will probably be asked whether the need for some remedial works might be indicated and where the calculated return period is much higher than 150,000 years the question should be asked as to whether the calculations are credible.

Pilot Studies

Pilot Studies using the methodology have now been carried out for 12 dams in the UK with a view to assessing whether the raw results are in line with the statistical evidence.

Tab. 2. Results of Pilot Studies

Dam Name	Type	Annual Probability of Failure	Return Period (Years)
Dam A	Concrete	1.8 x 10-6	555,555
Dam B	Earthfill	7.5 x 10-6	133,333
Dam C	Concrete Core	1.0 x 10-5	100,000
Dam D	Earthfill	1.1 x 10-5	90,909
Dam E	Concrete Buttress	1.1 x 10-5	90,909
Dam F	Earthfill	3.5 x 10-5	28,571
Dam G	Earthfill	4.2 x 10-5	23,809
Dam H	Earthfill	4.2 x 10-5	23,809
Dam I	Earthfill	2.0 x 10-4	5,000
Dam J	Masonry	2.0 x 10-4	5,000
Dam K	Earthfill	5.1 x 10-4	1,960
Dam L	Earthfill	2.5 x 10-2	40

From Tab. 2 we see that 7 out of 12 dams have a calculated return period for failure in the range 10,000 to 150,000 years. The first dam in the table (Dam A) is a fairly modern concrete gravity dam for which a return period of 555,555 years is calculated. This figure seems high as

Douglas, Spannagle and Fell give a return period of only 71,428 years for a concrete gravity dam more than 5 years old during the period 1930 - 1992.

Results for the next 7 dams in the table all look reasonable. It is, however, worth mentioning Dam E, which is a buttress dam. It should easily withstand the 10,000 year earthquake but possibly not a Magnitude 6 earthquake 15 km deep beneath the dam. The probability of such an event is fortunately very low – a return period of 200,000 years was calculated for such an earthquake. This shows up in the risk assessment as does the sudden failure of one or more of the large valves in the foundation of the dam.

The last four dams in the table have worryingly low return periods for failure. Further studies would be useful but, if the calculated figures are correct, the need for some remedial works seems to be indicated. The risk calculated for Dam L is extreme.

Dam I was built at the end of the 18 th century and is 8.8 m high. It is built out of silty clay with traces of sand, gravel and organic material. The downstream slope is 2.3: 1 and the upstream slope is 1.25 : 1 and 2.6 : 1. A return period of 5,000 years seems reasonable for this dam.

Dam J is a concrete gravity dam built in 1931. It has vertical cracks, leakage and artesian pressure in pressure relief holes drilled in 2000. In the PMF the tension in the upstream face will be 0.4 MPa which would not be acceptable in a modern dam. Again a return period of 5,000 years seems reasonable for this dam.

At Dam K there was a major leakage incident in 2002 and leakage remains a significant concern. A return period of 1,960 years is not obviously wrong for this dam.

Dam L is a puddle clay filled dam with a narrow concrete core supported by rubble set in mortar. It was constructed between 1880 and 1912 and is 6 m high. In the 1980's the downstream face was protected by gabions at 1:2.5 slope which terminates in three steps at the toe. The risk assessment methodology takes no account of these gabions which may partially account for the low calculated return period.

The consequences of failure of Dam L are low. It has been estimated that a 150 year flood would overtop the dam but the probability of this causing failure would probably be about one order of magnitude less, say, 1,500 years. This may not be the right answer but it is probably more realistic than 40 years.

The tentative conclusion is that for 10 out of 12 dams in the pilot study the methodology seems to give roughly the right answer. For Dam A the calculated return period is probably too long. For Dam L the methodology is not applicable as it takes no account of the strengthening of the downstream face.

Studies in Japan
Preliminary Tier 3 studies have been carried out for two dams in Japan. Dam M is 131 m high rockfill dam with a clay core and the results of the risk analyses are reported below. Dam O is a 95 m high rockfill dam also with a clay core. The risk of failure is slightly higher than for Dam M on account of the higher leakage but is not reported here.

Internal Erosion
Internal erosion is an important failure mode although Dam M does not seem to be particularly prone. We note that although failure might be sudden (cf Teton) it is, given good monitoring, more likely to be gradual, allowing time for water level to be lowered.

Foster, Fell and Spannagle suggest an Upper Bound value of 34×10^{-6} for a central core earth and rockfill dam. In view of the fairly low leakage (less than 100 l/min) a figure of 11.3×10^{-6} is, therefore, suggested in this case.

Overtopping in a Typhoon
The perception in Japan was that typhoons are not expected to affect the catchment of Dam M and the spillway is not, therefore, designed for typhoon rainfall. Nevertheless about 2 or 3 typhoons make landfall in Japan each year.

If outflow is 42 % of inflow then we estimate that we can accept $3000/0.42 = 7142$ m3/sec inflow. If PMF inflow = 12,000 m3/sec then range of vulnerability is $151<C<250$ where C is the Creager Number in the following metric formula:

$$Q \ = \ C \ x \ 1.303 \ x \ \left(\frac{A}{2.588} \right)^{\frac{0.936}{A^{0.048}}} \ m^3 / \sec$$

(1)

For legibility A in the denominator above is raised to the power of 0.048. The numerator is 0.936.

Where C is the Creager coefficient and A is catchment Area in km^2. Q is peak reservoir inflow in m^3/sec. As will be seen C is proportional to the peak inflow flood and will vary accordingly for the PMF and for floods of various return periods.

Using an appropriate growth curve for a typhoon area we get $T_R = 20,000$ years.
So probability of getting C>151 has been taken as $1/(20,000) = 50 \times 10^{-6}$. Climatological investigations have been recommended to validate or amend this figure.

Overtopping by seismic seiche
As a first approximation we might assume an earthquake on the assumed seismogenic fault near the dam every 450 years. The Tensho earthquake of 18 January 1586 had a magnitude of about 8.0 and might have been on the nearby Fault. Howeve the fault, which is a strike slip fault, is only 67 km long. For a strike-slip fault of this length we would not expect an event with a surface wave magnitude exceeding (see Dowrick[5]) :

$M_S = 1.404 + 1.169 \text{ Log } 67000 = 7.04.$ This is equivalent to $M_W = 6.9.$ (2)

For probabilistic purposes we may assume an event of $M_W = 7.5$ on the fault every 450 years (ie assuming $6.9<M_W<8.0$).

We have two formulae for height of seiche and can assume duration of overtopping of the order of 10 minutes each cycle (cf Hebgen Dam) – The reservoir impounded by Dam M is only 8 km long as against 15 km at Hebgen.

The fault runs through the reservoir (but not under the dam) and if there is an earthquake on this fault or nearby there is a risk of a seiche which might overtop the dam. The following formula is taken from the Russian SNIP 11-7-81 dated 1991:

$$\Delta h = 0.4 + 0.76\,(I - 6)\ \text{m} \tag{3}$$

Where I is intensity on the scale of Medvedev, Sponheuer and Karnik (MSK)

It is worth noting that this formula gave a wave amplitude of 5.4 m for the Magnitude 7.4 earthquake which affected the Yuvacik Reservoir in Turkey in 1999. The actual amplitude was about 5 m. The reservoir was not full at the time.

For Dam M if we postulate intensity 10 on the MSK scale and take the amplitude of the wave as 2 x Δh then we get a wave height of 2 x Δh = 6.9 m. The above compares with total freeboard of 6 m.

Dr. Sato's formula is as follows:

$$H = \left(\frac{KT}{2\pi}\right) x \sqrt{(gh)} \tag{4}$$

For a Peak Ground Acceleration K of 0.8 g and T = 1.0 sec this gives H = 4.35 m. The predicted amplitude is, therefore, 8.7 m

For a Peak Ground Acceleration K of 0.714 g and T = 1.0 sec this gives H = 3.9 m. The predicted amplitude is, therefore, 7.8 m

Wave run-up will usually be more than wave amplitude but the large size of rip-rap at Dam M suggests a fairly modest addition.

The above should be regarded as indicative only but it does suggest that, when the reservoir is full, the dam might be vulnerable to seismic seiches.
It is probably reasonable to assume that we could get an earthquake big enough to generate an overtopping seiche every 450 years but:

- The reservoir may not be full
- The epicentre of the earthquake may be remote from the reservoir.
- The reservoir is within 2 metres of the highest level 0.46 % of the time.
- 28/67 km of the fault are within 10 km of the reservoir – ie 42 %.

So the annual probability of a dangerous seiche is about 0.46 x 0.42 x/ (450 x 100) = 4.3 x 10^{-6}

Overtopping by landslide generated wave
The main problem is to determine a probability of getting a large landslide into the reservoir. We assume here that we need an earthquake of magnitude > 7.0 to trigger the event and that

the epicentre needs to be fairly close to the reservoir. There is only, of course, a modest probability that the earthquake will trigger a landslide into the reservoir.

If we assume an earthquake of magnitude 7.5 every 450 years on the nearby fault the annual probability of getting such an event within 10 km of the reservoir will be $2222 \times 10^{-6} \times 28/67 = 928 \times 10^{-6}$. We assume the probability of this giving rise to a dangerous landslide into the reservoir will be about 1/50 so the overall probability will be $928/100 \times 10^{-6} = 9.3 \times 10^{-6}$.

The above takes no account of earthquakes on other, more distant, faults.

Settlement of Dam Crest in an Earthquake
Dams of compacted rockfill have regularly suffered settlement in earthquakes. Of the dams known to us 11 have suffered an average of 195 mm settlement. The maximum settlement was 760 mm at the 156 m high Zipingpu Dam in China in the M = 7.9 Wenchuan earthquake in 2008.

Dam M itself suffered 30 mm settlement in the M = 7 event of 1961.

With 6 m freeboard it seems that there is unlikely to be sufficient settlement to lead to overtopping. It is, however, assumed that the rockfill was properly compacted at the time of construction.

Mechanical/Electrical Failure of Spillway Gate
In work in the Dominican Republic it was assumed that the probability of failure on demand of mains supply and a diesel engine to start and run is 0.01. This figure applies for a normally reliable supply and a diesel engine tested every two weeks on load. On failure of the mains supply, the probability of failure on demand increases to 0.04, which could result in a probability of failure per annum of 0.2.

The risk of power failure at the motors can be reduced with the use of duplicate power cables. With the secondary spillway we can release an incoming flood with peak of $1000/0.42 = 2,381$ m3/sec. This is about 20% of the PMF and implies a return period of about 150 years. Overall probability of failure for this mode will be $1/150 \times 1/100 = 1/15,000 = 66 \times 10^{-6}$. However the diesel generators are well maintained and failure of the dam would not be certain so we assess annual probability of failure from this mode as 13.2×10^{-6}.

Tab. 3. Probabilities of Failure for Dam M

Failure Mode	Annual Probability of Failure
Internal Erosion	11.3×10^{-6}
Overtopping in Typhoon	50×10^{-6}
Seismic Seiche	4.3×10^{-6}
Landslide	9.3×10^{-6}
M & E Spillway Gate	13.2×10^{-6}
TOTAL	88.1×10^{-6}

Overall return period for failure is, thus, estimated at 11,350 years. The results emphasise the need to review the typhoon hydrology and to ensure that the standby generator for the spillway gate is always in full working order

Conclusions

The UK methodology was developed from work in Australia, USA and elsewhere and its predecessors have been used extensively in various countries with mixed results. Pilot studies suggest that the newest methodology is reliable if the results are checked against world statistics.

Preliminary work with large dams in Japan has given encouraging results although further work is needed on the occurrence of typhoon rainfall giving floods with Creager values exceeding 150. With further work it is hoped to firm up the figures although it may be concluded that:

- The Japanese Dams studied are very well designed and built.
- They are subject to extreme seismic conditions and also to typhoon rainfall.
- Return periods for failure are about 10,000 years which is low (on account of natural hazards).
- Further studies are needed – particularly into extreme floods.

References

[1] ICOLD Bulletin 130, Risk Assessment in Dam Safety Management, 2005.
[2] Environment Agency, 2013, Risk Assessment for Reservoir Safety. Bristol: Environment Agency
[3] Foster M, Fell R and Spannagle M, "The Statistics of Embankment Dam Failures and Accidents", Canadian Geotechnical Journal, Volume 37, pp 1000 – 1024, 2000.
[4] Douglas K, Spannagle M and Fell R, "Estimating the Probability of Failure of Concrete and Masonry Gravity Dams", University of New South Wales, 1998.
[5] Dowrick, D.J. "Earthquake Resistant Design", Second Edition, John Wiley and Sons, 1987.

Vulnerability of large dams considering hazard interactions
Conceptual application of the Generic Multi-Risk framework

Matos, J. P.[1], Mignan, A.[2] and Schleiss, A. J.[1]

[1]*Laboratory of Hydraulic Constructions(LCH), École Polytechnique Fédérale de Lausanne (EPFL), Switzerland*
[2]*Institute of Geophysics, Swiss Federal Institute of Technology Zurich (ETHZ), Switzerland*

ABSTRACT: The potential risks associated with dams are often kept in check through the adoption of demanding design criteria, frequent surveillance efforts, and the commission of maintenance and retrofitting operations. Although this approach's effectiveness is time-tested, it circumvents the probabilistic characterization of the system's response to different hazards and, to an even greater extent, to their combinations (multi-risk assessment). This background poses a challenge when the goal is to quantify the risks associated with a given infrastructure or to identify critical chains-of-events.
The Generic Multi-Risk (GenMR) framework is a probabilistic technique based on the sequential Monte Carlo method and the hazard correlation matrix concept. It presents a powerful and flexible way to characterize the often broad range of risks associated with complex systems. The present work takes advantage of the GenMR framework's capability to cope with the difficulties underpinning the assessment of the risks associated with a large dam system and describes its conceptual application. In order to simulate the system and estimate the contribution of hazard interactions to the overall risk, it accounts explicitly for the probabilistic nature of the problem, the evolution of reservoir volumes, and the state of the main system's components as they are affected by individual and/or multiple hazards.

E-mail: jose.matos@epfl.ch

Introduction

Large dams are complex, dynamical structures, with reservoirs often retaining massive volumes of water. If, on the one hand, they yield noteworthy benefits to society and the economy, on the other hand, they can entail acknowledgeable risks.

Professionals familiar to dam design, operation, surveillance, and maintenance have for long been aware of such risks. Arguably – with a reduced number of disasters set aside – they have been very successful in guaranteeing the integrity of the both the large structures and their reservoirs, ultimately protecting the potentially affected areas downstream.

Traditionally, safety design criteria for large dams have been based on deterministic approaches [1]. According to that paradigm, safety is ensured through the detailed study of reference scenarios that the dam system must withstand while guaranteeing prescribed degrees of functionality. Although historically effective in keeping dams safe, the thorough evaluation and adaptation to demanding representative scenarios does not possibly cover all the situations that may lead to failure. Also, it does not lead to a quantitative measure of the overall risk associated with the dam.

Probabilistic methodologies to safety evaluation have also been proposed e.g. [2,3]. They promote quantitative measures of risk and have the potential to provide insight into what are its predominant sources. As such, they theoretically allow for a more efficient allocation of resources in what concerns risk reduction strategies. Mostly, they can be useful when complementing traditional approaches [1].

Probabilistic risk assessments of dams have been carried out resorting to a number of different strategies. Notably, a few well-established alternatives such as event trees, fault trees, or failure modes and effects analysis can be highlighted [4]. Regardless of the chosen approach, fully depicting the risks associated with a large dam is an incredibly difficult mathematical problem and a practically impossible task. Commonly, probabilistic risk assessments focus on a limited number of triggering hazards, as the complexity of the systems tends to grow fast.

Over decades, experts have become very effective at modeling large dam systems' responses to single hazards and use them to increase security. Particularly in cases which have been designed, surveyed, and maintained according to recent recommended practices, dams can be remarkably resilient infrastructures [5]. Still, the dam industry continues the pursuit for ever-improving standards e.g. [6].

As dam design, maintenance, and surveillance evolve and address increasingly well single hazards, the main sources of risk may shift from low-probability high-intensity isolated events to low-probability combinations of lower intensity hazards or chains-of-events. Although this shift in the main sources of risk is to be expected, it can be argued that established tools, such as event trees, are of difficult application when the goal is to evaluate risks associated with low-probability combinations of hazards (e.g. earthquake followed by a series of floods leading to development of internal erosion). Furthermore, the vulnerability and losses associated to a given hazard may depend substantially on the water level in the reservoir at that time. The evolution of the reservoir levels – not easily captured, for example, in event or fault tree approaches – is therefore important to quantify overall risk. Due to these reasons, the investment in additional tools that are adapted to model large dams might be worthwhile.

The present work is part of the *Harmonized approach to stress tests for critical infrastructures against natural hazards* (STREST) project, which aims to develop standardized tools for hazard and risk assessment of low probability-high consequence events that can be systematically applied to whole classes of critical infrastructures.

Applying standardized tools to accomplish a comprehensive evaluation of risks associated with a large dam is challenging on many accounts: dams are essentially dynamic systems; they often pose risks to downstream areas where the potential losses are a function of numerous factors; and risk modeling tools must be both flexible and accurate in order to be on par with highly detailed deterministic safety assessments.

This paper aims to contribute to overcome the aforementioned challenges and explore the application of the Generic Multi-Risk (GenMR) framework [7] to large dams. In order to be applicable to large dams, an adaptation of the original GenMR is proposed and its results are analyzed and discussed for a conceptual large alpine earthfill dam. Focus is placed on the dam system itself, being losses deferred to a later study. In that light, the framework is employed as a means to preliminarily assess the relevance that the hazard interdependence might have in the system's vulnerability.

Methodology

The GenMR framework

The GenMR framework is based on a sequential Monte Carlo method and its principles are well described in [7]. It presents a powerful and flexible way to characterize the often broad range of risks associated with complex systems and is particularly well-suited to model hazard interdependencies and coincidences. In short, it conducts multiple simulations of a given system for a chosen period (usually one year), generating random events, evaluating the system's responses to them, computing damages, and assessing losses.

In order to frame the problem, events must be defined in terms of their probability of occurrence, intensity, and timing. The characterization of system elements requires the statement of vulnerability functions, recovery rates, and associated losses. Finally, event dependencies must be stated, notably in the form of an altered probability of occurrence, which constitutes a remarkably powerful approach.

As GenMR addresses low-probability events, it requires that a very high number of simulations is undertaken in order to quantify risks. For complex systems, the computation burden of a executing a full evaluation for each simulation can be overwhelming. Also, it can be wasteful

due to the fact that, in the large majority of the simulations, the low-probability events that may have an impact on the system will simply not occur.

The problem is elegantly solved by performing a two separate evaluations of the system The first focuses solely on the generation of primary hazards and is computationally cheap. The second evaluation, which requires that the full evolution of the system is performed, is only carried out for the simulations which registered at least one primary hazard. During this second evaluation – also referred to as resampling – the system is incrementally evaluated from one event to the next event. At each step, future events that are directly or indirectly dependent of those already observed are resampled. At the heart of the methodology are the matrices that define event dependencies and thus, control the process.

Description of large dams within the GenMR

The present work takes advantage of the GenMR framework's capability to cope with the difficulties underpinning the assessment of the risks associated with a large dam. It builds on a preliminary adaptation of GenMR to large dams [8].

Regarding dams as dynamic systems, there was a need to couple a reservoir routing model with GenMR. Resorting to it, the reservoir's volume and outflows are computed at each step of the resampling. As this is done, the functionality of each outflow element of the dam (such as hydropower system, bottom outlet, spillways, or crest), incoming flows (including floods), and operational orders (such as drawdown attempts) are taken into account.

All is coded in terms of events (actions or acknowledgement of an internal state) and elements (objects within the system). Events can be triggered spontaneously (if they have an associated return period), as the result of earlier events, due to specific element states (e.g. a threshold damage of the dam), or as a response to reservoir levels. A scheme of hazards, elements, system states, and interactions considered in the current application of the GenMR framework is presented in Fig. 1.

Conceptual case study

As a case-study, the adapted GenMR was applied to a conceptual large Alpine earthfill dam. The maximum supply level was assumed to be 93 Mm^3, and uncontrolled spillage starts when the reservoir holds 100 Mm^3. The crest is reached at 107 Mm^3 and average yearly inflows amount to 120 Mm^3. Over 10 000 000 simulations were conducted.

The elements, hazards, and system states considered are shown in Fig. 1. While a more detailed discussion of this conceptual system is presented in [8], some of its key features deserve being mentioned:

- Floods. Peak discharges are characterized by a Gumbel distribution conforming to the hydrology of the region (Fig. 2). As a strong correlation between flood duration and peak discharge was not evident following an initial assessment of catchments in the region, independence between both variables was assumed. The duration was modeled using a log-normal distribution (Fig. 3). The probability distribution of a flood during the year was assumed to be proportional to the expected inflows. A normalized hydrograph approach was used to shape the food (Fig. 4). Finally, it was assumed that the occurrence of rare floods increases the likelihood of smaller flood events taking place during the remainder of the year.

- Earthquakes. Have been quantified based on the Swiss dam safety regulations (OSOA, *Ordonnance sur la Sécurité des Ouvrages d'Accumulation*) [9] and maps of Medvedev-Sponheuer-Karnik (MSK) intensities of ground shaking covering the area. Damages to each element were defined qualitatively and made to comply with Swiss dam safety regulations. Fig. 5 depicts impacts on the dam and foundation (because in the case of earthfill dams the latter is only of particular relevance in specific cases such as alluvial

material, for simplicity the dam and the foundation were aggregated into a single element).
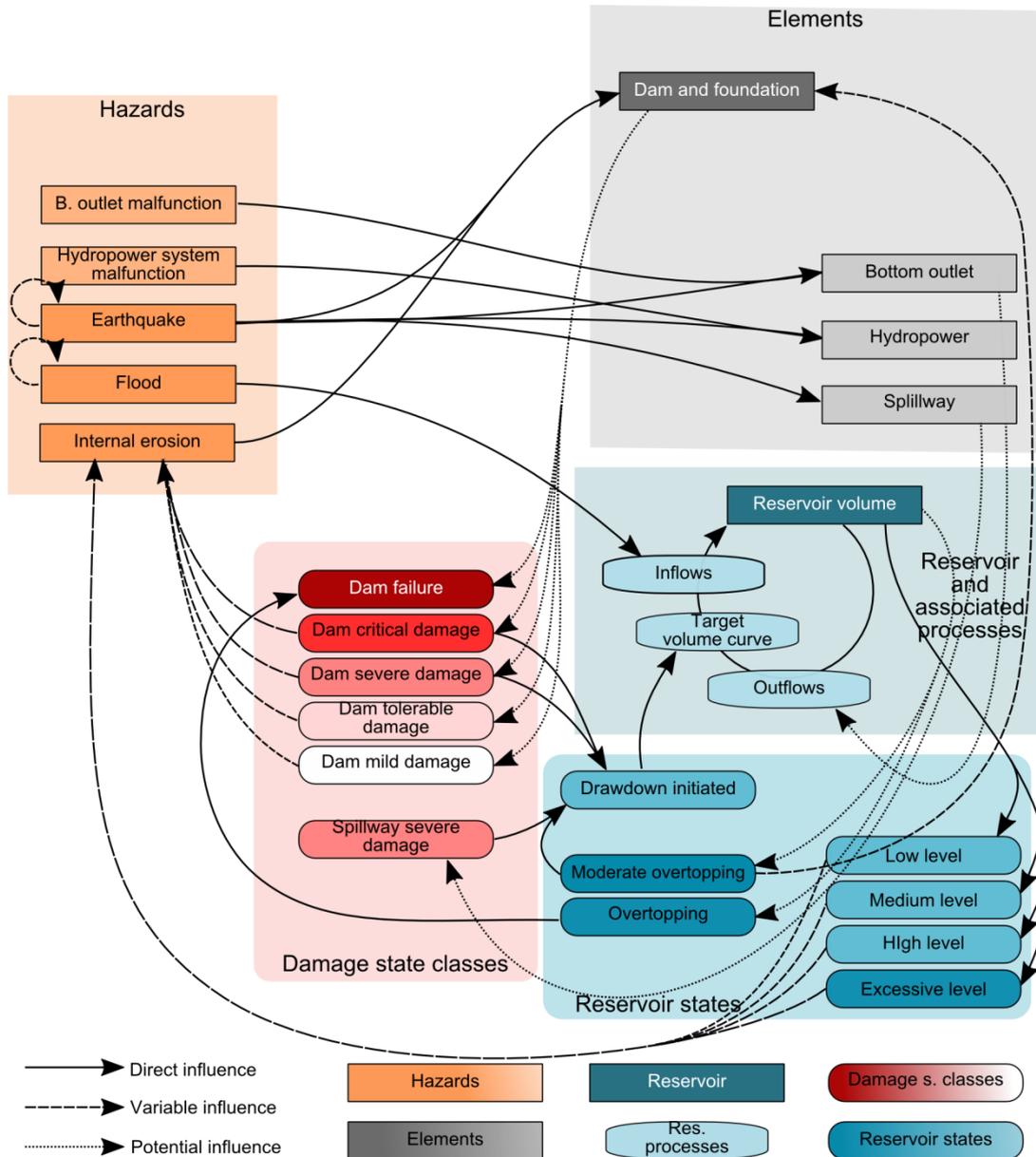
Fig. 1: Scheme of hazards, elements, system states, and interactions considered in the application of the GenMR framework to large dams. Adapted from [8].

- Internal erosion. Although approaches for the quantification of internal erosion in probabilistic risk assessments exist e.g. [10], in light of the multiple factors that affect this hazard and given the small historical record of internal erosion episodes in large dams, the damages to the dam and foundation element following internal erosion events were also defined qualitatively (see Fig. 6 depicting impacts on the dam and foundation). As indicated in Fig. 1, the return period of internal erosion events was made dependent on the damages endured by the dam and foundation and on the level of the reservoir.

- The bottom outlet and the hydropower plant system elements can also suffer damages due to random malfunctions or earthquakes.

- The functionality of outlet structures (maximum discharge) was assumed to be a linear function of their integrity and reservoir levels, but past a certain damage state they cannot be operated.
- The integrity of each element is steadily restored following damaging hazards. Recovery rates were estimated based solely on engineering judgment.
- The simulations start in March, when the reservoir is approximately at its lowest stage. This is done so that the impacts of deviations from target levels due to hazards that might occur throughout the simulated year have an impact on results.
- Hazard sampling in the GenMR framework is discrete. In the present case study primary hazards were sampled in 13 categories. These correspond to return periods from 316 to 1 260 000 years, with return periods roughly doubling at each step.
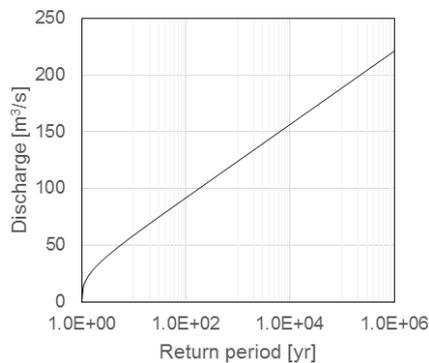

Fig. 2: Intensity vs. return period of the flood.
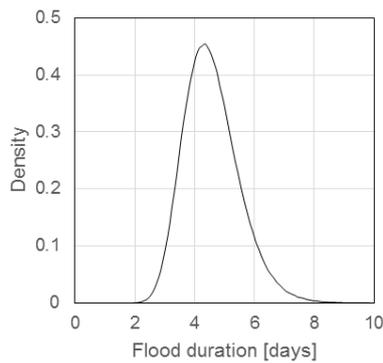
Fig. 3. Pdf of the flood duration.
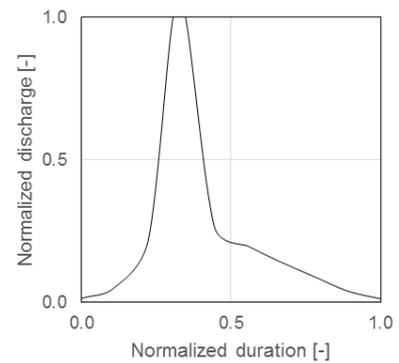
Fig. 4. Normalized hydrograph of the flood.
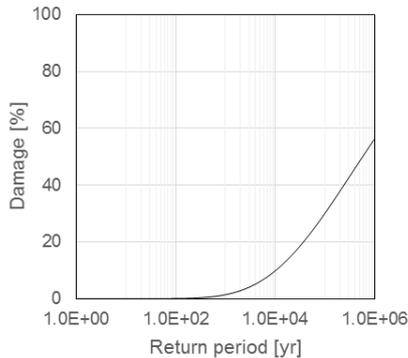
Fig. 5: Damage to the dam and foundation vs. return period of earthquake events.
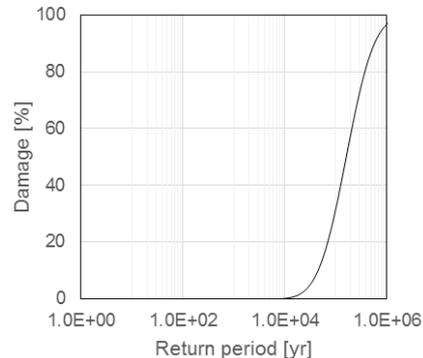
Fig. 6: Damage to the dam and foundation vs. return period of internal erosion events.

Results and discussion

Hazard sampling

The first step in the validation of the GenMR application should be to verify that hazards are being sampled as intended. For floods (whose timing changes seasonally) and internal erosion (whose occurrence is dependent on reservoir levels), this is particularly important. As can be seen in Fig. 7 floods tend to occur during the warm months, coinciding with summer storms and melting of the winter snow. Internal erosion episodes are, as intended, related to reservoir levels. The timings of earthquakes and other hazards are uniformly distributed.

Additionally, a check on the probabilities of occurrence of each hazard was made. In order to do so, assumed return periods are compared with the observed ones. Assumptions and

observations matched well, the only exception being internal erosion events. The divergence was due to the fact that resampling substantially affects the occurrence rate of internal erosion as levels rise and the dam is damaged.
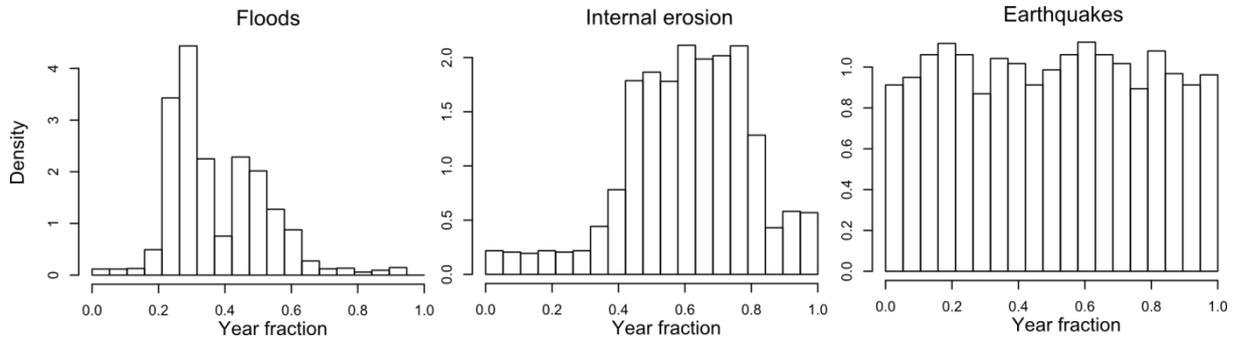
Fig. 7: Timing of flooding, internal erosion, and earthquakes from March to February of the following year.

System responses

As the overwhelming majority of the simulations are quite uninteresting, the system's response obtained during GenMR resampling is illustrated below for an artificial combination of two extreme events: a 10 000 years flood that occurs when the reservoir is full, followed by a 5 010 years earthquake (Fig. 8).
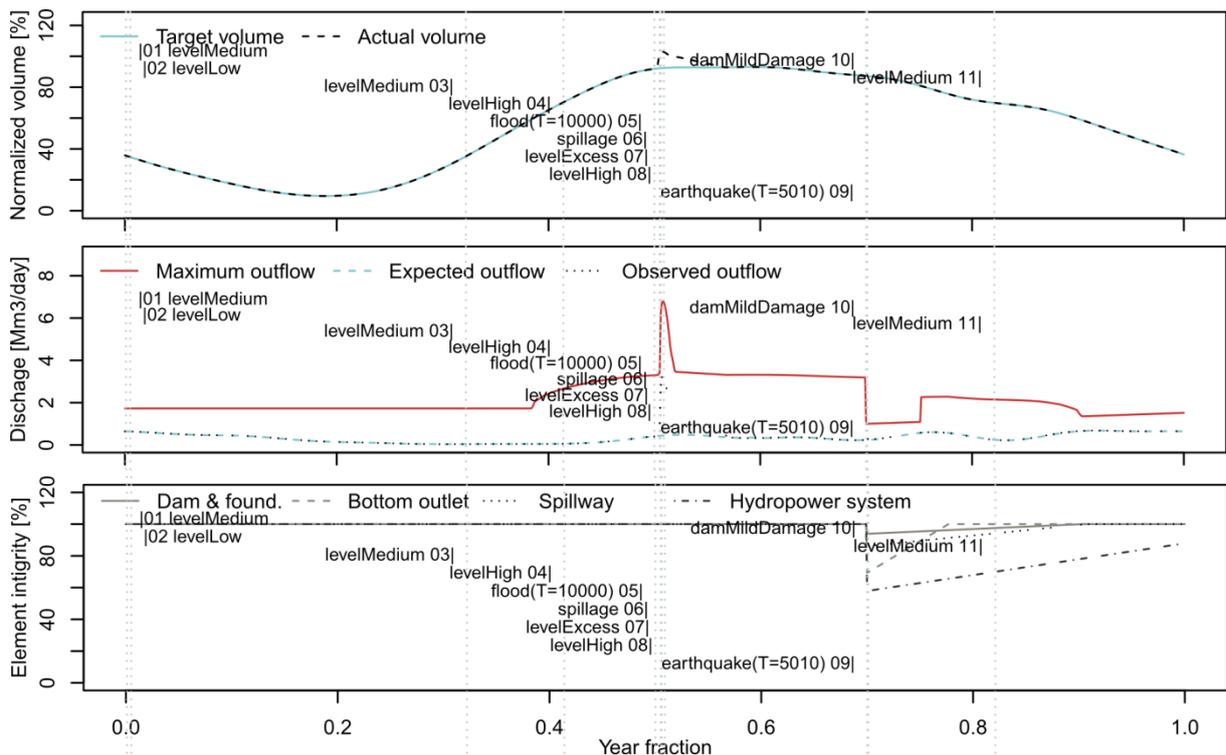
Fig. 8: Example of a system response to extreme events. Top: reservoir volumes (normalized by the initial spillage volume). Middle: outflows. Bottom: element integrities.

Even such an extreme flood, inflowing at the worst possible time, filled the reservoir only up to 103 Mm³. Also, it is worth noting that the earthquake damages all elements, but impacts on the dam and spillway are very limited. Finally, one can observe that the maximum outflow drops abruptly after the earthquake as a result of the damaged bottom outlet and hydropower

system. Notwithstanding, if the water level were to rise above the spillway, the maximum outflow would increase accordingly.

Overall, 5 000 000 simulations of this conceptual system allowed to estimate that the dam is only critically damaged with a return period of about 65 000 years and failures would have a return period close to 100 000 years (well above deterministic design criteria). Due to a large freeboard and an adequate spillway, the return period of overtopping is even higher (over 200 000 years). It is apparent that the most dangerous situations are the result of internal erosion events whose likelihood is increased by earthquakes or excessive reservoir levels.

Role of hazard interactions

The role of hazard interactions and the dynamical nature of the system were taken into account. If, on the one hand, design floods and earthquakes can occur when the reservoir is not full, which translates into a system that is less vulnerable to them that what is assumed by traditional design criteria, on the other hand hazard interactions and potentially dangerous chains-of-events are evaluated. Overall, these effects seem to balance each other quite well, with estimated failure rates reasonably close to 1×10^{-5}.

Considering hazard interactions promotes also a migration of the risk. The phenomena is well described in [7]. For the case of the analyzed conceptual large dam system, the migration is illustrated in Fig. 9, not in terms of risk, but of vulnerability of the dam structure. Each simulation would constitute a point in the plane. Most of the simulations fall in the top left corner (higher frequencies and low damages), but the most interesting part of the plane is its right edge, where damages occur. What is shown in Fig. 9 is a difference between simulations with and without interactions. Through it one may infer that hazard interactions can lead to a raise in the damages produced by low probability events. This equates to hazard interactions motivating a shift in vulnerability and, consequently, in risk.
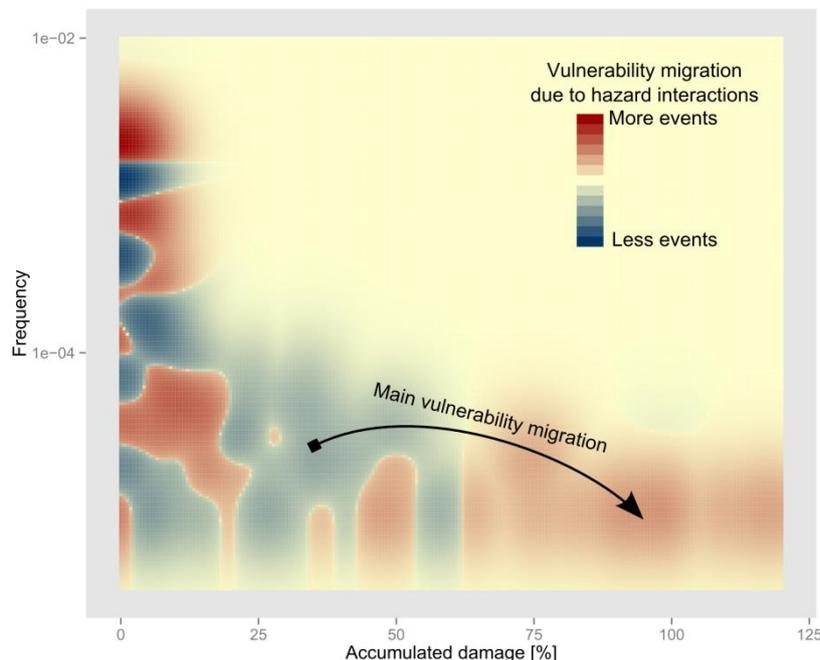

Fig. 9: Migration of vulnerability along the accumulated damage vs. frequency plane due to the consideration of hazard interactions. Adjusted scale evidences rare events.

Conclusions and future work

The present work set out to apply the GenMR framework to large dams, test the effectiveness of the adaptations to the code, and evaluate the role of hazard interactions, along with the effect of the dynamic nature in the vulnerability of the system. The presented results include a great deal of uncertainty, and any conclusions drawn from them should account for that.

Regarding the GenMR adaptation, results suggest that it can be successfully adapted to large dams, perhaps even with worthwhile advantages over established methods. Though the evaluation of a conceptual case study, it has been shown that the resampling process returns reasonable results, fully agreeing with design criteria.

Though this work it can also be inferred that hazard interactions have the potential to shift the risks associated with large dams and, therefore, deserve further study.

Future efforts will be made on three fronts. Firstly, the retrieval and derivation of more precise hazard definitions and element vulnerability functions. Secondly, by making a transition towards loss and risk assessment (though the routing of floods and the consideration of potential losses downstream). Finally, by accounting for uncertainty.

Acknowledgements

References

[1] Darbre, G.R., Dam risk Analysis, Report, Swiss Federal Office for Water Management, Bienne, 1999.

[2] Kreuzer, H., Risk analysis for existing dams: merits and limits of credibility, Int. J. Hydropower Dams. 7 (2000) 49–53.

[3] Howell, J., Anderson, L.R., Bowles, D.S., Canfield, R. V., A framework for risk analysis of earth dams, Logan, Utah, 1980.

[4] Srivastava, A., Generalized event tree algorithm and software for dam safety risk analysis, Utah State University, 2008.

[5] Lemperiere, F., Risk analysis: What sort should be applied and to which dams?, Int. J. Hydropower Dams. 6 (1999) 128–132.

[6] ICOLD, Guidelines for use of numerical models in dam engineering, International Comission on Large Dams (ICOLD Bulletin 155), Paris, 2013.

[7] Mignan, A., Wiemer, S., Giardini, D., The quantification of low-probability–high-consequences events: part I. A generic multi-risk approach, Nat. Hazards. (2014) 1–24. doi:10.1007/s11069-014-1178-4.

[8] Mignan, A., Danciu, L., Matos, J.P., Schleiss, A.J., Report on cascading events and multi-hazard probabilistic scenarios, STREST Deliverable 3.5, Zurich, 2015.

[9] Federal Office for Water and Geology, Sécurité des ouvrages d'accumulation ver. 1.1 - Ordonnance sur la sécurité des ouvrages d'accumulation (OSOA). Directives, FOWG, Biel, Switzerland, 2002.

[10] Altarejos-Garcia, L., Silva-Tulla, F., Escuder-Bueno, I., Morales-Torres, A., Practical risk assessment for embankments, dams, and slopes, in: K.-K. Phoon, J. Ching (Eds.), Risk Reliab. Geotech. Eng., CRC Press, 2014.

Analysis of concrete dam based on "Probabilistic model code for concrete dams"

Westberg Wilde M. [1,2], Johansson F. [2,3]

[1]*ÅF AB, Stockholm, Sweden*
[2]*KTH Royal Institute of Technology, Stockholm, Sweden*
[3]*SWECO Energuide, Sweden*

ABSTRACT: For design and assessment of concrete dams the standard procedure is to calculate safety factors and compare with experience-based requirements.

In a 2-year project a "Probabilistic model code for concrete dams" (PMCD) has been written. This document is built in the same way as "Probabilistic model code" by JCSS (2001) and is based on JCSS as well as Eurocode (EN 1990). As part of this project "representative" existing buttress and gravity dams were analyzed based on in order to test the methodology and to define a β-target for the dams that are considered safe according to the current guidelines.

This paper gives some background of PMCD and results of calculations for one of the analyzed gravity dams are presented. A discussion on input variables as well as output safety index and sensitivities for the dam monolith is given.

E-mail: marie.westberg.wilde@afconsult.com

Introduction

Design of essentially all infrastructures (dams, bridges, house et.c.) used to be based on safety factors. During the 1970's new design guidelines, based on partial factors, were developed and later introduced in e.g. bridge and house design in many countries. Within the European Union the Eurocodes [1] are mandatory. They are a set of harmonized technical rules developed to eliminate the disparities that hinder their free circulation within the Union and to lead to more uniform levels of safety in construction. Verification according to Eurocodes can be done by the partial factor method or by probability-based methods.

However, design and assessment of dams is not included in the Eurocodes. In most countries in the world assessments are still based on the safety factor format. One major drawbacks of such a safety format is that it does not differentiate different parameters according to uncertainty. In a probability-based design and/or assessment methodology, uncertainties in variables are input to the analysis. The advantages of a probability based design/assessment is among others that different structures with the same required safety level will have similar failure probability, regardless different loading conditions or different materials. In a partial factor method larger factors are associated with large uncertainty and in that way a more uniform safety level is achieved. For more background and information of a probability-based approach see e.g. [2], [1], [3].

In a two-year project funded by Swedish dam owners a "probabilistic model code for concrete dams" has been formulated. The two-fold aim is to formalize the possibility of performing probabilistic assessments for concrete dams and to investigate the possibility to introduce partial factors for dams. The project started in 2013 and is about to finish during 2015.

"Probabilistic model code for concrete dams" (PMCD)

In order to perform probabilistic assessments of dams in a standardized way it was believed that a model code was necessary and "PMCD" was formulated.

The PMCD describes a probability-based approach for concrete dams and follows the structure in the Probabilistic model code, issued by Joint Committee of Structural Safety in 2001 [2]. The Probabilistic model code by JCSS "is a first attempt to put together in a consistent way some of the rules, regulations, and explanations that are necessary for the design of new structures, or the assessment of existing ones from a probabilistic point of view". [2] describes basis of design, loads and resistances for structural engineering. In the same way, PMCD is a first attempt to put together in a consistent way rules, regulations and explanations necessary for design and assessment of concrete dams from a probabilistic point of view. It applies to design of new concrete dams as well as to the assessment of the structural integrity of existing dams. In the first edition it is limited to use for buttress and gravity type structures, as those are the most common for Swedish conditions. The use is primarily intended for high-consequence facilities. The present PMCD is based on the present information and assumptions are clearly described. During writing lack of important information in several areas have been identified and further research is necessary.

PMCD is built up by three parts:

PART I: BASIS OF DESIGN
Defines requirements, principles of limit state design, reliability, target reliability, verification (limit state functions), design situations and how updating of prior estimates of parameters may be done and included.

Only *ultimate limit* states are treated. The limit state functions for failure in the contact are *adjusted overturning* (where the point of rotations is moved in a way comparable to that described by Fishman [4]) and *sliding*. Adjusted overturning accounts for the possible crushing of concrete or rock mass at the downstream toe before overturning occurs. This is done by successively adjusting the point of rotation in the upstream direction as the crushing proceeds. In the calculations, the length of the crushed zone, a, is first estimated from vertical force equilibrium as the effective normal force divided by the weakest uniaxial compressive strength of the concrete or the rock mass.
Limit states for failure in the contact and concrete has also been defined.

Design situations are overall similar to those described in the deterministic guideline, however some distinctions exist. One example is that uplift reduction due to the effect of drains and grouting may only be accounted for in calculations if
- Continuous monitoring of uplift pressures is performed
- Maintenance program for the drainage system is available and an action plan on how to quickly take care of upcoming problems is present.

The reason is that in time, clogging may reduce the drain efficiency and leaching will reduce the effect of the grout curtain. In addition, even though measured pore pressure could indicate low values, a future event with clogged drains could govern the probability of failure if the return period for clogged drains is sufficiently small. Without monitoring and analysis of monitoring results there is no possibility to identify trends and thus it is not possible to know when these processes start and how they develop. For this reason, if monitoring is not present the normal design situation should be full uplift. Only for drains complemented by monitoring full drainage capacity can be included.

The target safety index is under evaluation, see section 2.

Updating of prior estimates and the possibility to incorporate test results is one of the most important possibilities in a probability-based methodology. Test results may be incorporated using a Bayesian approach.

PART II: LOAD MODELS
Includes load models, ice load, hydrostatic pressure, uplift pressure, earth pressure and soil properties. Seismic actions are not included. These are not included in the deterministic guideline, since earthquakes of significance does not appear in Sweden. It may well be discussed if seismic actions should be included in a probabilistic model code, but in the first stage it has been left out.
Ice loads is of major importance for many low dams in cold climate. High ice-loads are the result of thermal expansion of the ice sheet.

PART III: RESISTANCE MODELS
Includes general principles, self weight, shear resistance of concrete-rock interface, friction angle of rock joints, compressive and tensile strength of concrete, uniaxial compressive strength of rock mass, rock bolts and rock anchors.

The *shear resistance of the concrete-rock interface* can be divided into two separate cases; when an intact bond exists and cohesion is accounted for and when the bond is broken and no cohesion is included. Even though cohesion may exist in the interface, the uncertainties associated with this parameter are large. At this point too many questions remain related to mean value, standard deviation and extent of cohesion, and a broken bond is therefore assumed. Shear resistance of the interface with broken bond (no cohesion) is described by a base friction angle $\phi_{res,c}$ and a dilation angle , i_c. The dilation angle depends on if the rock surface is a blasted rough surface or if the dam was founded on smooth surface.

Analysis of representative cases

To determine if the dam is safe enough, a target safety index is necessary. In Eurocode [1] the target safety index is $\beta_T = 4,8$ for structures in Reliability class 2 (corresponding to annual failure probability of 10^{-6}. For reliability class 1 β_T is 5,2). Similar values may be found in e.g. [2] and others.
One way to define a target value in PMCD would be to use the same target value for dams as that in Eurocode, another is to assume that dams designed according to the present deterministic guideline are (at least on average) "safe enough". It was believed that analysis of "representative cases" is the better way forward, with a twofold purpose; to test the PMCD and to acquire enough data to define a target safety level.
The representative cases should be dams that fulfil the deterministic requirements, but are "close" to the required safety factors.
18 dam monoliths from 9 dams was chosen by the authors in cooperation with consultants and dam owners. These were considered be representative. After probabilistic analysis the resulting target safety index for sliding was found to be approximately $\beta_T = 4,6$ (although this is still under evaluation and some more changes may be required). Probabilistic analysis of one dam is shown below.

Example of analysis using PMCD

One of the dams analyzed is a 17,5 m high concrete gravity dam located in the north half of Sweden. The dam was built during 1936-1940. The total crest length of the concrete dam is 499 m.

The layout of the dam is shown below. It has a frontplate that transfer the hydrostatic pressure via beams into the dam body. It also has an additional drainage gallery further downstream in the dam body, but there are no drainage holes drilled into the rock. For that reason full uplift is considered during the base of the dam. A deterministic analysis in 1986 revealed that the dam did not fulfil the present requirements related to stability (safety factor to sliding was <1,35), and post-stressed anchors were installed (in total 125 anchors for the whole dam).
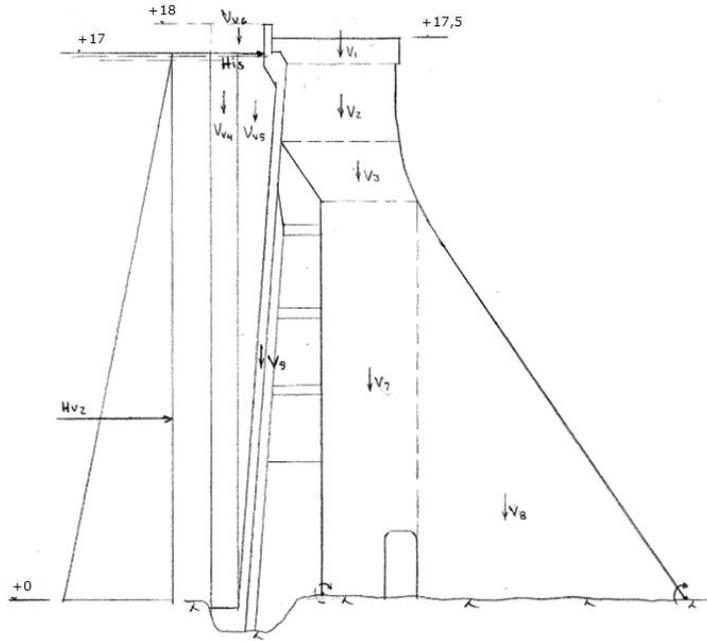
Fig. 1.Section of analyzed dam.

Limit state equation and input variables

The limit state shown below is sliding. The limit state function is defined as

$$G_{Uc} = N \cdot {}'\tan\left(\phi_{res,c} + i_c\right) - H \qquad (1)$$

Where N' is the effective normal load acting on the surface, $\phi_{res,c}$ is the residual friction angle for the macroscopic smooth but microscopic rough concrete-rock contact, i_c is the contribution from macroscopic roughness of the contact and H is the load horizontal to the failure surface.

The random variables used as input are shown in Tab. 1. These are defined in PMCD and in short the following points can be made:

- Unit weight is based on JCSS [2].
- Basic friction angle is based on Lo et al [5].
- Dilation angle depends on if the rock surface is founded on a smooth rock surface, or if the rock surface is a blasted rough surface. For a blasted rough surface it may be assumed to have mean value 15° and standard deviation of 3°. This value has to be supported by measurements of the inclination of larger asperities at the rock surface. For existing dams, this could be achieved from measurements available on construction drawings done at the time of construction. If outcrops of rock surfaces exist in spaces under or adjacent to the dam, complementary measurements could also be done there.

- For uplift pressure the linear assumption usually used for design is combined with a random variable C that accounts for variability from the linear behavior. For dams where drainage exists the variability of C is larger to account for the possibility of larger variations.
- For jacking force and losses of pre-stressing force information from JCSS [2] is applied.
- Ice load is the single most difficult variable. As described earlier ice is mostly affected by heating of the ice sheet from the sun. Very little is known about ice load and variability of ice loads. Measurements of maximum ice loads has been carried out in different parts of the world, but there are many difficulties related to analysis of those results: representativeness of measurements (are they really measuring ice loads acting on the dam structure, limited period of measurement etc), little or no information of statistical distributions and so on. For PMCD analysis was performed of measurements presented in literature and a statistical distribution was derived based on those measurements and a maximum ice load based on [6] was applied. For ice loads more analysis and further research is necessary.

Tab. 1. Variables in the probabilistic analysis.

Random Variables	Unit	Notation	Distribution	Mean Value	Standard Dev.	COV
Unit weight concrete	kN/m3	ρ_c	Normal	23,5	0,8	0,034
Basic friction angle, concrete-rock	°	$\emptyset res,c$	Normal	35	1,75	0,05
Dilation angle, concrete-rock	°	i	Lognormal	15	3	0,2
Uplift pressure	°	C	Normal	1	0,05	0,05
Jacking Force Pre-stressed Anchors	kN/m	P_0	Normal	540	40,5	0,075
Losses of Pre-stressed Force	kN/m	$\Delta P(x,t)$	Normal	54	16,2	0,30
Ice Load	kN/m	I	Lognormal	80	80	1,00
Maximum Ice Load	kN/m	$Max.I$	Normal	250	25	0,10

Results

The dam is analysed for some different load cases:
- With drains. The dam does not have drainage holes drilled into the rock at this point, but it would be possible to introduce if necessary.
- No drains. This was the case until 1986 when prestressed anchors were installed.
- No drains + prestress. This is the present situation. Observe that the prestressing force is higher than that required to fulfil sliding stability (1,49 compared to the requirement of >1,35).
- No drains + prestress "enough". This is the present case but with a prestressing force of only that required to fulfil the deterministic requirement safety factor of sliding stability of 1,35.

Probabilistic analysis was performed using software COMREL and First-Order Reliability analysis (FORM). Results are shown in table 2.

Tab. 2. Results of probabilistic analysis.

Comments	Sliding			
	Deterministic Analysis		Probabilistic Analysis	
	Safety Factor	*Requirement*	β	*pf*
Drains	1,43	>1,35	4,92	4,3E-07
No drains	1,16	>1,35	3,67	1,2E-04
No drains + prestress	1,49	>1,35	5,86	2,3E-09
No drains + prestress "enough"	1,33	>1,35	4,81	7,7E-07

As expected the case with no drains and no prestress result in much lower β than the other cases. The case with drains shows higher safety factor than the case with no drains and prestress "enough", but β values are similar. The main reason is that the variability in uplift is higher with drains, and for that reason the sensitivity values to uplift are higher for that case (approximately 0,4 compared to 0,2). The case considered most representative is the case with no drains and prestress "enough". The reason this is considered the most representative is that it is closest to the required safety factor. For this case the safety index is 4,8, which may be compared to that in Eurocode for reliability class 2. For this case sensitivity values are shown in table 3.

Tab. 3. Results of sensitivities for load case without drains and prestressed "enough"

ρ_c	Ice	Max_ice	C	Tan ϕ	tan i_c	P_0	P_{loss}	Σ
0,41	-0,45	-0,08	-0,19	0,49	0,58	0,1	0,04	1,0012

Conclusions

The probabilistic model code for concrete dams (PMCD) presents a methodology to perform systematic probabilistic analysis of concrete dams.

Preliminary results indicate that dams that are considered safe according to the present deterministic guideline have safety index of above approximately 4.6, corresponding to a nominal probability of failure of $2 \cdot 10^{-6}$. The PMCD is the first attempt to put together a methodology for concrete dams. Updating will be necessary as research is ongoing in several areas of relevance.

It is the authors belief that the PMCD will give a basis to perform systematic probabilistic analyses and become a good tool compare and communicate results to dam owners and authorities.

Acknowledgements

References

[1] EN 1990 (2001) *Eurocode – Basis of Structural Design*. CEN, Brussels.

[2] JCSS (2001) *Probabilistic model code*. Joint Committee of Structural Safety.

[3] Melchers, R.E. (1999) *Structural Reliability Analysis and Predictions*. Second Edition. John Wiley & Sons. ISBN 0-471-98771-9.

[4] Fishman (2007) Features of shear failure of brittle materials and concrete structures on rock foundations. *International Journal of Rock Mechanics and Mining Sciences*. V. 45, p. 976.

[5] Lo, K.Y.; Lukajic, B., Wang, S, Ogawa, T., Tsui, K.K. (1990), Evaluation of Parameters of Concrete Interface for Dam Safety Assessment, *Dam Safety* pp. 71-94.

[6] Carter D., Sodhi D., Stander E., Caron O., Quach T. (1998) Ice Thrust in Reservoirs. *Journal of Cold Regions*, Vol. 12, No. 4, pp. 169-183.

Multiple Failure Modes Analysis of the Dam System by Means of Line Sampling Simulation

Xueqin Zheng1[,2,3], Chongshi Gu1[,2,3], Dong Qin[1,2,3]

[1] *State Key Laboratory of Hydrology-Water Resources and Hydraulic Engineering, Hohai University, Nanjing 210098, China;*
[2] *National Engineering Research Centre of Water Resources Efficient Utilization and Engineering Safety, Hohai University, Nanjing 210098, China;*
[3] *College of Water-conservancy and Hydropower, Hohai University, Nanjing 210098, China.*

Abstract: As the number of aging dams is increasing, an efficient and feasible probabilistic method is required to analyse the uncertainties of a dam system with multiple failure modes. Due to the limitation of huge computation of Direct Simulation Monte Carlo, a new method is called for to solve the reliability problem of a dam system. This new method determines the failure domain of a complex structure by resorting to lines rather than random points. It is used to calculate the failure probability and reliability sensitivity of a gravity dam which is a large, complex structure with small probability. And the basic Monte Carlo method is also used for comparison. Results show that the new method is more efficient and feasible to analyse the reliability of a dam system with small failure probability and multiple dimensionalities.
Keywords: Dam system; Reliability; Multiple failure modes; Line sampling; Failure probability

E-mail: xueqinzheng1987@163.com

Introduction

Fuzziness and randomness are two inseparable uncertainty factors that influence dam safety. It is more objective to analyse dam reliability if these two attributes are taken into account. There are over 86,000 dams in China and they play a vital role in the national economy. Built 30 years ago, many of these dams have becoming increasingly dangerous due to improper design and mismanagement. And the number of dangerous dams currently accounts for over 40% of all the dams in China [1]. Therefore, the assessment of dam reliability and the probability of dam failure are more and more essential for people to recognize the safety of dams.

In the past years, great achievements have been gained in the analysis of dam system reliability. As we all know, "Direct Simulation Monte Carlo" technique has always been used for calculating system failure possibility. However, failures probabilities are really small when it comes to low probability events in a large complex system. Monte Carlo Simulation (MCS) is inefficient, to certain extent, as it needs a large number of samples for an accurate calculation. Another popular method called the Moment Method, which requires computational effort for high dimension problems, has also been used in the field of system reliability analysis [2], since there are multiple failure modes in large-scale structures and mutual correlations among these models, the moment method seems inapplicable to these problems, too.

Because of the shortcomings aforementioned, several novel sampling methods including Latin Hypercube Sampling (LHS) and importance sampling have been proposed. Importance sampling uses an importance sampling distribution which replaces the probability density function (PDF) in Monte Carlo simulation. It reduces the variance. But this method is more subjective because an inappropriate choice of an importance sampling distribution may lead to worse estimates. Another new sampling method is stratified sampling. This method divides

sample space into non-over-lapping stratum, and then calculates each probability of each stratum. However, it is not a practical method in real large-scale system. Although LHS is more efficient than Monte Carlo method to estimate average values and standard deviations in complex systems, it is less efficient for low probability events. To overcome this limitation, therefore, a sampling method denoted as line sampling (LS), which replaces the random *points* with *lines,* is developed to evaluate reliability in high-dimensional setting and low probability events. This technique determines the failure domain in terms of system reliability. This method has been applied widely in the area of structural reliability problems [3], [4] and it is better than basic MCS in terms of robustness and accuracy. What's more, LS can resolve the problem of multiple failures in a simple and effective way.

Therefore, LS is used to analyse the multiple failure modes of dam systems. It is the first time that LS is used in dam systems. With a series system and parallel subsystems, the dam system is a redundant structure for which the related uncertainties and multiple failure modes are accounted. The advantages of LS can be shown when compared with the method of traditional MCS and that of LHS.

The Line Sampling Method

Line sampling is a new method of simulation to calculate low failure probability. It uses random *points* instead of *lines* to determine the failure domain.

Line sampling's basic theory

Apply Nataf's transformations [5] and transform a set of non-normal correlated random variables into the set of uncorrelated normal (Gaussian) variables. It can serve as a mapping which transforms the original and the physical space into the standard normal one. Let $X = [x_1, x_2, \ldots x_n]$, $x \in R^n$ to be uncertain parameters' vectors. Transform the parameter vector x into the vector $\theta = [\theta_1, \theta_2, \ldots \theta_n]$, $\theta \in R^n$.

$$\theta = T_{x\theta}(x),$$
$$x = T_{\theta x}(\theta). \tag{1}$$

Apply Eq. (1), define the performance function on the standard normal space:

$$g^{(i)} = g_x(x^{(i)}) = g_x(T_{\theta x}(\theta^{(i)}) = g_\theta(\theta^{(i)}) \tag{2}$$

Since the function $g_\theta(\theta)$, in some cases of practical system, is unknown explicitly, it can just be calculated point-wise. For example, when we analyse a full finite element problem, the performance function $g_\theta(\theta^{(i)}) = g_x(x^{(i)})$ can be computed for each realization x^i. The number of finite element runs decides the computational cost when we evaluate the failure probability [3]. But before sampling, we should first determine *the important direction* e_α, which we call "important unit vector" or "important direction". In the standard normal space, e_α is used as pointing in the direction of "design point". And in the failure space, the most possible point is the optimal important unit vector. On the limit state space $g_\theta(\theta) = 0$, we define the "design point" as the vector point θ^* which is the nearest to the origin. [8], [9]. After that, by normalizing θ^*, α - the important unit vector will be obtained.

Take the direction of e_α as the performance function's normalized gradient. Let $g_\theta(\theta)$ as the performance function, and the gradient $\nabla g_\theta(\theta^*)$ at the vector point θ^* is then defined as

$$\nabla g_\theta(\theta^*) = \left[\frac{\partial g_\theta(\theta^*)}{\partial \theta_1} \frac{\partial g_\theta(\theta^*)}{\partial \theta_2} \cdots \frac{\partial g_\theta(\theta^*)}{\partial \theta_n} \right]^T \tag{3}$$

This is a new method to measure the relative importance of a given random variable: the larger the gradient $\nabla g_\theta(\theta^*)$'value, the larger the corresponding uncertain variable's "effect" of the performance function. By normalizing θ^*, the unit vector α can be calculated by Eq. (4)

$$e_\alpha = \nabla g_\theta(\theta^*) / \left\| \nabla g_\theta(\theta^*) \right\| \tag{4}$$

Failure probability estimation

After calculating the unit vector e_α, we apply the conditional Monte Carlo method [6] in the procedure of line sampling. The results are shown in Fig. 1. We calculate the conditional failure probabilities where x changes randomly just along the direction e_α. In Fig. 1, apply direct Monte Carlo and in the direction $\theta^\perp$, transfer the point normal into the line. The sampling density is $f(\theta)$ and the failure probability P_f is expressed in Eq. (5)

$$P_f = \int \ldots \int_F f(\theta) d(\theta) \tag{5}$$
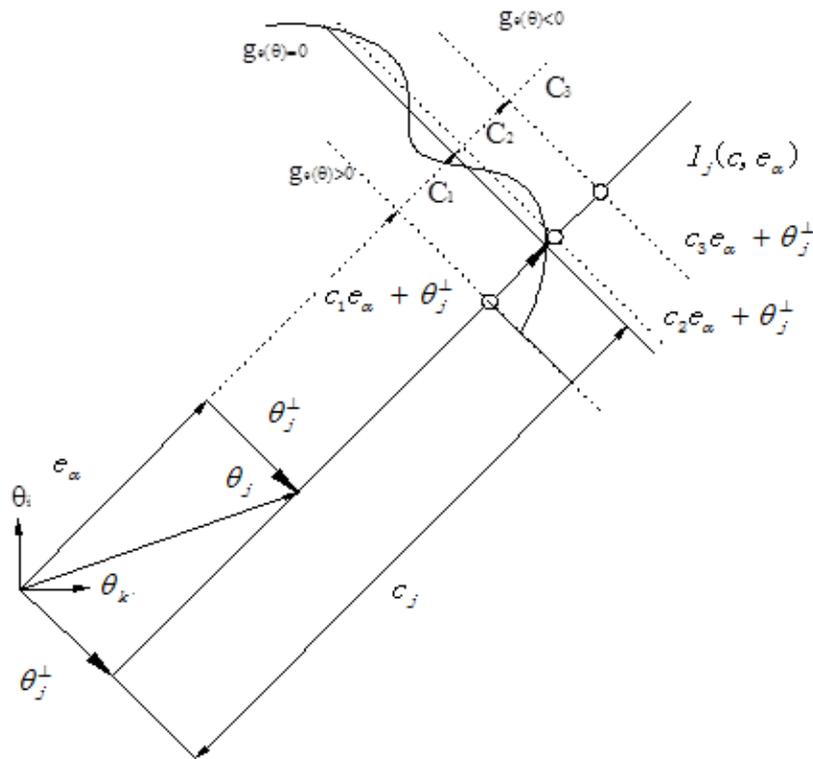
Fig. 1. single failure mode's line sampling

Then, the sampling $\tilde{\theta}$ is the total of a deterministic multiple of e_α and a generated vector $\theta^\perp$ is defined perpendicular to the direction of e_α.

$$\tilde{\theta} = ce_\alpha + \theta^\perp \tag{6}$$

And

$$\theta^\perp = \theta - \langle e_\alpha, \theta \rangle e_\alpha$$

θ is the input variables of the standard normal space with dimensions n; $\langle e_\alpha, \theta \rangle$ is the dot product of e_α and θ.

After that, apply direct Monte Carlo simulation to calculate N samples $\theta_j (j = 1,2,\ldots,N)$ and solve for each sample j which is relative one-dimensional reliability issue. Here c is only random variable. The relative failure probability can be denoted as

$$P_{fj} = \phi(-c_j) \tag{7}$$

where c_j is the junction between the limit state equation $g(x) = 0$ and the line $l_j(c, e_\alpha)$ which is shown in Fig. 1. Select three different values of c, evaluate the performance function, fit a second-order polynomial to determine the root. After that, the value c_j can be calculated.

In the next step, the estimator p_f is calculated by Eq. (8) after collecting the failure probability P_{fj},

$$P_f = \frac{1}{N} \sum_{j=1}^{N} P_{fj} \tag{8}$$

Estimation of the reliability sensitivity

Differentiating Eq. (8), μ_{x_i} and σ_{x_i} are the reliability sensitivities of P_f, which can be denoted with partial derivatives $\partial P_f / \partial \mu_{x_i}$ and $\partial P_f / \partial \sigma_{x_i}$ by Eqs. (9) and (10).

$$\frac{\partial P_f}{\partial \mu_{x_i}} = \frac{1}{N} \sum_{j=1}^{N} \frac{\partial P_{fj}}{\partial \mu_{xi}} \tag{9}$$

$$\frac{\partial P_f}{\partial \sigma_{x_i}} = \frac{1}{N} \sum_{j=1}^{N} \frac{\partial P_{fj}}{\partial \sigma_{xi}} \tag{10}$$

In line sampling, P_{fj} is correspond to the probability of $g_j(\theta) \leq 0$. c_j and reliability in β_j is equivalent to $c_j (\beta_j = c_j)$ based on the first order reliability method and the location of θ_j, $l_j(c, e_\alpha)$ in the Fig. 1

Therefore,

$$g_j(\theta) = \langle e_\alpha, (\tilde{\theta}_j - \theta) \rangle = \sum_{i=1}^{n} e_\alpha(\tilde{\theta}_{j,i} - \theta_i) = 0 \tag{11}$$

$$c_j = \frac{\mu_{g_j}}{\sigma_{g_j}} = \frac{\sum_{i=1}^{n} e_\alpha(\tilde{\theta}_{j,i} - \theta_i)}{(\sum_{i=1}^{n} e_\alpha^2 \sigma_{x_i}^2)^{1/2}} \tag{12}$$

Because:

$$\frac{\partial P_{fj}}{\partial c_j} = -\frac{1}{\sqrt{2\pi}}\exp\left(-\frac{c_j^2}{2}\right), \frac{\partial c_j}{\partial \mu_{\theta i}} = -\frac{e_\alpha}{\left(\sum_{l=1}^n e_\alpha^2 \sigma_{\theta l}^2\right)^{1/2}},$$

$$\frac{\partial c_j}{\partial \sigma_{\theta i}} = -\frac{e_\alpha^2 \sigma_{\theta i}\sum_{l=1}^n e_\alpha(\tilde{\theta}_{j,l} - \mu_{\theta l})}{\left(\sum_{l=1}^n e_\alpha^2 \sigma_{\theta l}^2\right)^{3/2}} \tag{13}$$

and the chain relationships between P_{fj}, c_j, the partial derivatives of the original normal variables x_i, $\dfrac{\partial P_{fj}}{\partial \mu_{xi}}$ and $\dfrac{\partial P_{fj}}{\partial \sigma_{xi}}$ can be expressed as follows:

$$\frac{\partial P_{fj}}{\partial \mu_{xi}} = \frac{\partial P_{fj}}{\partial c_j}\cdot\frac{\partial c_j}{\partial \mu_{\theta i}}\cdot\frac{\partial \mu_{\theta j}}{\partial \mu_{xi}}, \frac{\partial P_{fj}}{\partial \sigma_{xi}} = \frac{\partial P_{fj}}{\partial c_j}\cdot\frac{\partial c_j}{\partial \sigma_{\theta i}}\cdot\frac{\partial \sigma_{\theta j}}{\partial \sigma_{xi}} \tag{14}$$

Besides, θ_i is the linear function of x_i, therefore, we can obtain $\dfrac{\partial \mu_{fj}}{\partial \mu_{xi}}$ and $\dfrac{\partial \sigma_{fj}}{\partial \sigma_{xi}}$ by Eqs. (15)

$$\frac{\partial \mu_{\theta j}}{\partial \mu_{xi}} = \frac{1}{\sigma_{xi}}, \frac{\partial \sigma_{\theta j}}{\partial \sigma_{xi}} = \frac{1}{\sigma_{xi}} \tag{15}$$

Substituting Eqs. (15) with Eqs. (14), we can calculate the reliability sensitivities of a complex structural system:

$$\frac{\partial P_{fj}}{\partial \sigma_{xi}} = \frac{1}{N\sqrt{2\pi}}\sum_{j=1}^N \frac{\exp\left(-\dfrac{c_j^2}{2}\right)\cdot e_\alpha^2 \sigma_{\theta i}\cdot c_j}{\sigma_{xi}\left(\sum_{l=1}^n e_\alpha^2 \sigma_{\theta l}^2\right)}$$

$$\frac{\partial P_{fj}}{\partial \mu_{xi}} = \frac{1}{N\sqrt{2\pi}}\sum_{j=1}^N \frac{\exp\left(-\dfrac{c_j^2}{2}\right)\cdot e_\alpha}{\sigma_{xi}\left(\sum_{l=1}^n e_\alpha^2 \sigma_{\theta l}^2\right)^{1/2}} \tag{16}$$

Multiple failure modes analysis by the line sampling

In the reliability analysis for the structural system, we should modify some equations in Section 2 to consider the effect of the correlation among multiple failure modes when failures domains overlap among the multiple failure modes.

Take two failures modes in standard normal space [7] with two dimensions for example. Firstly, we should separate the overlapping failure zones to the failure domains where overlapping zones don't exist, as shown in Fig. 2 (a).

$$F_{[k]} = \left\{ \theta : g^{[k]} \leq 0 \right\} \text{ and } F_{[i]} = \left\{ \theta : g^{[i]} \leq 0 \right\}$$

are two correlated failure modes. The angle's bisector is formed by $e_\alpha^{[k]}$ and $e_\alpha^{[j]}$, which can be separated into two failure modes $\overline{F}_{[k]}$ and $\overline{F}_{[i]}$ where overlapping zones don't exist.

It is shown in Fig. 2 (b).
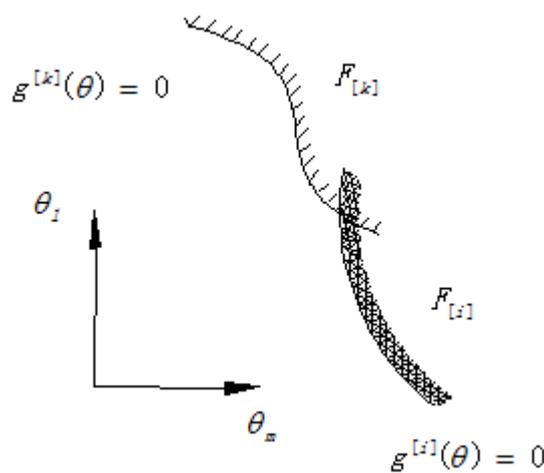
Fig. 2 (a) Overlapping regions exist in failure domains
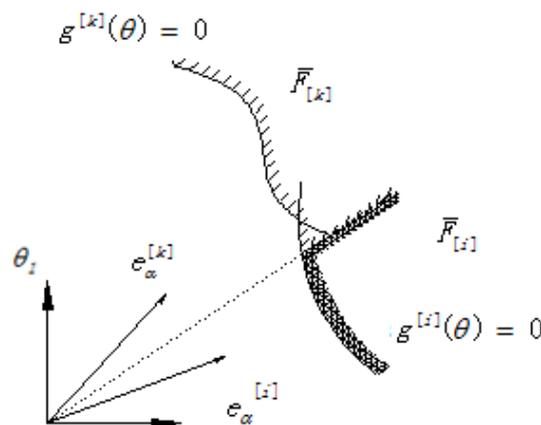
Fig. 2 (b) No overlapping regions exist in failure domains

After that, we should estimate the failure probability $\overline{P}_f^{[k]}$ on the failure region $\overline{F}_{[k]}$. Based on the line sampling method applied in the problem with one failure mode, joint probability density

function $f(\theta)$ and Monte Carlo simulation are used to calculate N samples $\theta_j(j = 1,2,\ldots, N)$. Every sample θ_j is decomposed into two parts: $c^{[k]}$ and $\theta_j^\perp$ which are mutually orthogonal. Then, we can obtain the coefficient $c_j^{[k]}$, the corresponding point $\tilde{\theta}_j^{[k]}$ which is the intersection of the line $l_j^{[k]}$ and the limit state equation.

In the next step, we should check if the points $\tilde{\theta}_j^{[k]}$ satisfy $\tilde{\theta}_j^{[k]} \in \bar{F}_{[k]}$. If all the points satisfy this limiting condition, $\bar{P}_f^{[k]}$ can be calculated with the same equation that for a single failure mode as follows:

$$\bar{P}_f^{[k]} = \frac{1}{N} \sum_{j=1}^{N} \phi(-c_j^{[k]}) \tag{17}$$

Otherwise, we should modify the coefficient $c_j^{[k]}$ into $\bar{c}_j^{[k]}$. It is showed as follows [3]

$$\bar{c}_j^{[k]} = c_j^{[k]} + sign(c_j^{[k]}) \frac{r^{[k]}(\tilde{\theta}_j^{[k]}) - r^{[i]}(\tilde{\theta}_j^{[k]})}{\sqrt{1 - \left(\left(e_\alpha^{[k]} - e_\alpha^{[i]}\right)\right)^2}} \tag{18}$$

Where, $r^{[k]}(\tilde{\theta}_j^{[k]})$ is the distance between the point of $\tilde{\theta}_j^{[k]}$ to $e_\alpha^{[k]}$ and $r^{[i]}(\tilde{\theta}_j^{[k]})$ is the distance between the point $\tilde{\theta}_j^{[k]}$ and $e_\alpha^{[i]}$, which can be shown in Fig. 3 and easy to be obtained by using the equations as follows,

$$r^{[k]}(\tilde{\theta}) = \left\| \tilde{\theta} - \left\langle e_\alpha^{[k]}, \tilde{\theta} \right\rangle e_\alpha^{[k]} \right\| \tag{19}$$

$$\tilde{\theta} \in \bar{F}_{[k]} \Leftrightarrow r^{[k]}(\tilde{\theta}) \leq r^{[i]}(\tilde{\theta}) \forall i = 1,2,\ldots, m.$$
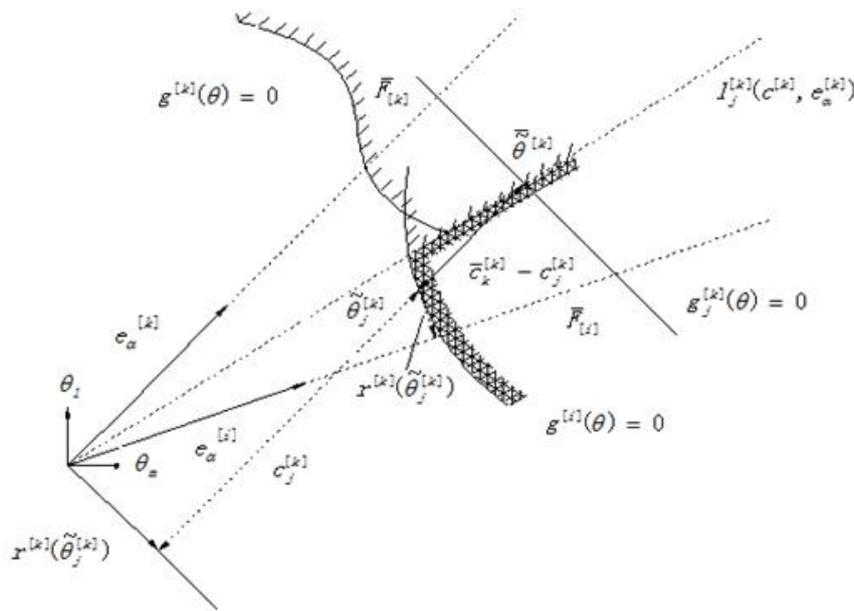
Fig. 3. Line sampling with multiple failure modes

Then, based on Eq. (17), we can obtain the probability $\overline{P}_f^{[k]}$ in the separate failure domain $\overline{F}_{[k]}$. Then the failure probability

$$P_f = \frac{1}{N} \sum_{k=1}^{m} \sum_{j=1}^{N} \phi(-\overline{c}_j^{[k]}) \qquad (20)$$

Similarly, we can calculate the reliability sensitivity for the complex system with multiple failure modes which are shown in Eqs. (19), (20)

$$\frac{\partial P_{fj}}{\partial \mu_{xi}} = \frac{1}{N\sqrt{2\pi}} \sum_{k=1}^{m} \sum_{j=1}^{N} \frac{\exp\left[-\dfrac{(c_j^{[k]})^2}{2}\right] \cdot e_{\alpha i}^{[k]}}{\sigma_{xi} \left(\sum_{l=1}^{n} e_\alpha{}^2 \sigma_{\theta l}^2\right)^{1/2}} \qquad (21)$$

$$\frac{\partial P_f}{\partial \sigma_{xi}} = \frac{1}{N\sqrt{2\pi}} \sum_{k=1}^{m} \sum_{j=1}^{N} \frac{\exp\left[-\dfrac{(\overline{c}_j^{[k]})^2}{2}\right] \cdot (e_{\alpha i}^{[k]})^2 \sigma_{\theta i} \cdot c_j^{[k]}}{\sigma_{xi} \left(\sum_{l=1}^{n} (e_{\alpha i}^{[k]})^2 \sigma_{\theta l}^2\right)} \qquad (22)$$

Application

Gravity concrete dams' failure modes
Dam failure modes are really complicated. For concrete gravity dams, the foundation problem is the dominant causes of failure, which can be summarized as the following three main failure modes: sliding failures along the base or along week plane in rock mass, tensile fractures exist in the upstream heel and compressive fractures exist in the downstream toe of a dam [10] [11]. Most of the dam system is a redundant safety system. Here, the three main failure modes are reviewed as a series system and any kind of failure mode will result in the dam structure damage.

Let us assume that the performance functions of the three main failure modes (stability against sliding along the dam foundation, tensile fractures at the upstream heel and compressive fractures at the downstream toe of the dam) are expressed as g_1, g_2 and g_3 respectively and the failure probability of the dam can be denoted as follows:

$$P_f(x) = \left(P\left\{ [g_1(x) < 0] \bigcap [g_2(x) < 0] \bigcap [g_3(x) < 0] \right\} \right) \tag{23}$$

Limit state functions of gravity concrete dams
We can see the force distribution of a typical cross section in one gravity concrete dam in Fig. 4. H_1 is the upstream water depth; H_2 is the downstream water depth; and m are the slope ratios; D_1 is the dam height; B_1 and B_2 are the widths of dam crest and dam base, respectively; γ_ω, γ_c and γ_n are unit weight of water, concrete mass and submerged unit weight of silt; φ_n is the angle of internal friction; P_1, P_2 are hydrostatic water forces upstream and downstream of the dam, respectively; P_3 is the sand pressure; W is the weight of the dam; W_2 and W_3 are the water weight upstream and downstream applied to the dam body, respectively; W_4 is the sand gravity; U is the uplift pressure acting under the interface.
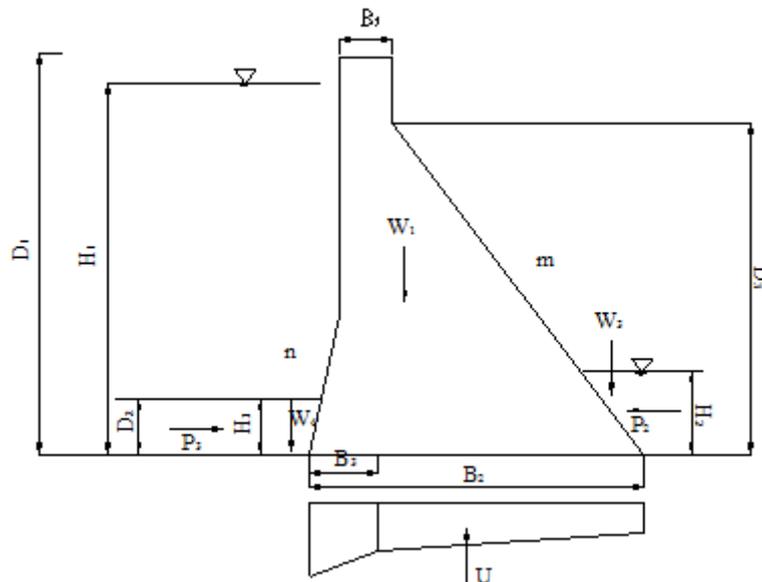

Fig. 4 One typical cross section's force distribution

Now, we will construct the limit state functions for failure of sliding, tensile fractures in the heel and compressive fractures in the toe of the dam.

For the failure mode of dam's sliding, the basic limit state function can be expressed as follows,

$$g_1 = g(H_1, H_2, H_3, \gamma_c, \gamma_n, \varphi_n, f', c', \alpha)$$
$$= f'\left(\sum W - U\right) + c'A - \sum P = 0 \tag{24}$$

where, f' and c' are the internal friction coefficient and cohesion; $\sum W$ and $\sum P$ are the total vertical and horizontal forces applied to the calculated area, respectively; U is the uplift pressure; A is the calculated sectional area.

For the strength failure of the dam, we consider the stress- strength model of the tensile stress at the upstream heel σ_s, compressive stress at the upstream heel σ_n and dam concrete tensile stress σ_1, compressive stress σ_c. Based on the equation of eccentric compression in mechanics of materials, we can get the limit state function of tensile stress-strength at the dam heel:

$$g_2 = g(\sigma_1, H_1, H_2, H_3, \gamma_c, \gamma_n, \varphi_n, \alpha) = \sigma_1 + \frac{\sum W - U}{B} + \frac{6\sum M}{B^2} = 0 \tag{25}$$

and the limit state function of compressive stress-strength at the dam toe:

$$g_2 = g(\sigma_1, H_1, H_2, H_3, \gamma_c, \gamma_n, \varphi_n, \alpha) = \sigma_c - \frac{\sum W - U}{B} - \frac{6\sum M}{B^2} = 0 \tag{26}$$

where, α is the reduction factor of uplift pressure; M is the eccentric torque on the action face; B is the width of action face.

Therefore, the safety of a gravity dam depends on the following main random variables: $H_1, H_2, \alpha, f', c', \sigma_c, \sigma_1, \gamma_c$. Due to the carbonation of concrete, the aging of curtain grouting, the erosion of environment and so on, the random variables like $\alpha, f', c', \sigma_c, \sigma_1, \gamma$ are time-varying [12].

Example analysis

The water retaining structure of a hydropower project is a concrete gravity dam, which is located in south-eastern China. The designed working life of this dam is 100 years. Here, we select one typical cross section of the gravity dam, and the geometry size is shown in Fig. 5. And the random variables and corresponding statistical characteristics are shown in Tab. 1
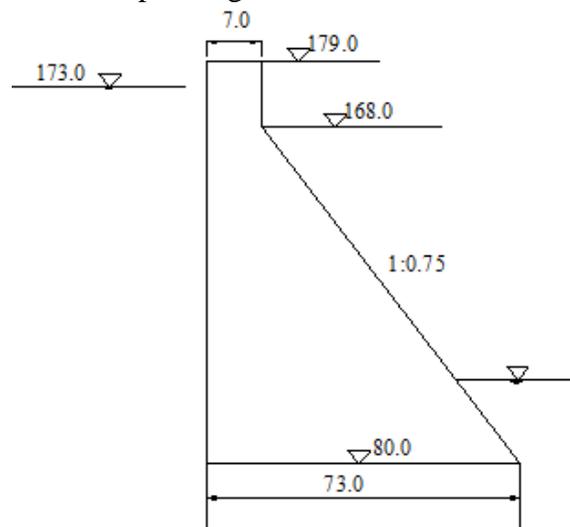

Fig. 5 The geometry size of one typical section for a gravity dam (m)

Tab. 1 The distribution parameters and the basic variables' type of a gravity dam system

Basic variable	Mean	Standard deviation	Coefficient of variation	Distribution form
H_1 (m)	93	2.79	0.03	Normal
γ_c (kN/m³)	24	0.48	0.02	Normal
α	0.3	0.045	0.15	Normal
f'	1.1	0.22	0.2	Normal
c' (10^3 N/m²)	1.1	0.33	0.3	Log-normal
σ_1 (10^3 /m²)	1.45	0.36	0.25	Log-normal
σ_c (10^3 N/m²)	15	3.75	0.25	Log-normal

Based on random variables shown in Tab. 1 and other parameters, we can obtain the limit state equations of stability against sliding, tensile stress at dam's heel and compressive stress at dam's toe [13], [14]:

$$g_1 = (3579\gamma_c - 365\alpha H_1)f'+73000c'-5H_1^2 \tag{27}$$

$$g_2 = \sigma_1 + 99.6\gamma_c - 9{,}18\alpha H_1 - 1.58H_1 - 1.88 \times 10^{-3} H_1^3 \tag{28}$$

$$g_3 = \sigma_c + \gamma_c + 0.82\alpha H_1 - 0.76H_1 - 1.88 \times 10^{-3} H_1^3 \tag{29}$$

From Eqs. (27) - (29), it is noted that the limit state equations g_1, g_2, g_3 are associated with the same impact factors. Therefore, the gravity dam's reliability problem can be regarded as the reliability problem with correlated multiple failure modes, which means overlapping failure region exist among the multiple failure zones.

In public papers published before, the values of correlation coefficient among failure modes are calculated to reflect the correlation among dam system's multiple failure modes. Here, we implement the reliability analysis among correlated multiple failure modes according to the line sampling method. It considers the overlapping failure region more directly. According to the distribution parameters and the types of random variables listed in Table1, the results of the reliability analysis in a gravity dam system can be shown in Tab. 2.

Tab. 2   Reliability analysis results of the concrete gravity dam

Random Variables x	Traditional Monte Carlo method		The line sampling method	
	Reliability sensitive $\dfrac{\partial P_f}{\partial \mu_{xi}}$	Reliability sensitivity $\dfrac{\partial P_f}{\partial \sigma_{xi}}$	Reliability sensitive $\dfrac{\partial P_f}{\partial \mu_{xi}}$	Reliability sensitive $\dfrac{\partial P_f}{\partial \sigma_{xi}}$
H_1	6.218×10^{-4}	5.293×10^{-4}	6.119×10^{-4}	5.103×10^{-4}
γ_c	-1.530×10^{-6}	2.376×10^{-5}	-1.490×10^{-6}	2.416×10^{-5}
α	3.514×10^{-6}	7.543×10^{-6}	2.501×10^{-6}	7.397×10^{-6}
$f^{'}$	-2.341×10^{-8}	3.485×10^{-8}	-2.293×10^{-8}	3.216×10^{-8}
$c^{'}$	-3.560×10^{-4}	5.297×10^{-4}	-3.435×10^{-4}	5.199×10^{-4}
σ_l	-4.673×10^{-6}	4.531×10^{-6}	-4.541×10^{-6}	4.461×10^{-6}
σ_c	-7.493×10^{-5}	5.206×10^{-5}	-8.417×10^{-5}	4.621×10^{-5}
Failure probability	1.372×10^{-5}		1.475×10^{-5}	
Sampling size	10^8		3500	

From Tab. 2, it can be seen that the results of failure probability and the sensitivity analysis calculated by the line sampling method are in accordance with the results generated by the Monte Carlo method. The results obtained by Monte Carlo are regarded as the exact results. And it is obvious that the proposed new method is better than the basic method with regard to computational efficiency. More importantly, it is direct to calculate the reliability sensitivity with small computation effort. For the analysis of the concrete gravity dam risk shown in Tab. 2, we can see that the failure probability is 1.372×10^{-5}. This is lower than the tolerable failure probability 1.0×10^{-4} in China [15], which is referred to UDSR in China for the dams of safety Grades 1-2. Therefore, this gravity dam is relatively safe for the time being.

Meanwhile, according to the results of $\dfrac{\partial P_f}{\partial \mu_{xi}}$ and $\dfrac{\partial P_f}{\partial \sigma_{xi}}$, it is found that for the dam system,

the failure is strongly sensitive to the factor of the upstream water depth H_1 and cohesion of

the interface c'. Therefore, this is a new idea for determining the failure in a complex dam

system.

$$\frac{\partial P_f}{\partial \mu_{xi}} \text{ and } \frac{\partial P_f}{\partial \sigma_{xi}}$$

Conclusions

The assessment of multiple failure modes of gravity dams is performed by using the line sampling method. Due to computational efforts of the traditional method applied to analyse the reliability in a dam system, line sampling method of multiple failure modes is employed to calculate a gravity dam's failure probability and reliability sensitivity, thus directly solving the relevancy problem among multiple failure modes. The proposed method is easily manageable when a large sum of relative variables with uncertainties is involved. In comparison with the results based on the basic Monte Carlo method, we can see that the proposed method is more efficient in analysing the reliability problem of a dam system with small failure probability and multiple dimensionalities. In the dam system, this method is proposed and used for the first time.

It should also be noted that the random variables like $\alpha, f', c', \sigma_c, \sigma_1, \gamma$ are time-varying due to the carbonation of concrete, the aging of curtain grouting, and the erosion of environment and so on, as previously mentioned. However, we didn't take the problem of time-varying into account. Therefore, in future study, it is more important to consider the time-variation characteristics of the important unit vector e_α and uncertain parameters of a dam system.

Acknowledgments

References

[1] Wu ZR, Li J, Gu CS, Su HZ. Review on hidden trouble detection and health diagnosis of hydraulic concrete structures. Science in China Series E: Technological ciences.2007.50(1): P34-50

[2] Kiureghian AD,Ke JB. The stochastic finite element method in structural reliability. Probabilistic Engineering Mechanics.1988.3(2): P83–91.

[3] Krishnamurthy S, Mathur AP. On the estimation of reliability of a software system using reliabilities of its components. Soft Reliability Engineering. 1997.P146-155.

[4] Raykov T.Estimation of congeneric scale reliability using covariance structure analysis with nonlinear constraints. British Journal of Mathematical and Statistical Psychology. 2001.54(2): P315-323.

[5] Huang B, Du X.A robust design method using variable transformation and Gauss–Hermiteintegration. International Journal for Numerical Methods in Engineering 2006.66: P1841–58.

[6] John MB, Mark BG. Conditional Monte Carlo: a simulation technique for stochastic network analysis. Management Science.1971.18(3):P207-217

[7] Bourinet JM, Deheeger F,Lermaire M. Estimation of small failure probabilities in high dimensions by subset simulation. Structural Safety. 2011.33(6): P343-353.

[8]   Au SK, Beck JL. First excursion probabilities for linear systems by very efficient importance sampling. Probabilistic Engineering Mechanics. 2001; 16:193–207

[9]   Masanobu S. Basic analysis of structural safety. Journal of Structural Engineering. 1983.109(3): P721-740.

[10]   Ibrahim RA, Liu PL. Structural Dynamics with Parameter Uncertainties. Probabilistic Engineering Mechanics.2008.40(3):309-328.

[11]   Hermanns RL.Niedermann S,Ochs SL,Kubik PW.Rock avalanching into a landslide-dammed lake causing multiple dam failure in Las Conchas valley (NW Argentina) — evidence from surface exposure dating and stratigraphic analyses.Landslides.2004.1(2):P113-122.

[12]   Dong JJ,Tung YH,Liao JJ,Pan YW.Logistic regression model for predicting the failure probability of a landslide dam. Engineering Geology.2011.117(1-2): P52-61.

[13]   Schueller GI. A critical appraisal of methods to determine failure probabilities. Structural Safety.1987.4(4): P293-309.

[14]   Rackwitz R, Flessler B.A critical appraisal of methods to determine failure probabilities. Computers&Structures.1978.9(5): P489-494

[15]   Kuo JT, Yen BC, Hsu YC，Lin HF. Risk analysis for dam overtopping—Feitsui reservoir as a case study. Journal of Hydraulic Engineering. 2007.133(8): P955-963.

Influence of measuring intervals on goodness of fit of dam behaviour analysis models

Bühlmann M.[1], Vetsch D. F.[1] and Boes R. M.[1]

[1]*Laboratory of Hydraulics, Hydrology and Glaciology (VAW), ETH Zurich, Hönggerbergring 26
CH-8093 Zürich, Switzerland*

ABSTRACT: Concrete dams are exposed to long-term processes such as alkali aggregate reaction or concrete ageing that may lead to damages with serious consequences. Thus the structure must be monitored. A common procedure for that is the observation-prediction comparison of a measured behaviour indicator and its predicted value. Therefore, the displacement of the dam and environmental conditions are recorded at certain intervals. For the dam behaviour analysis, multiple linear regression models are used, where environmental conditions are related to the displacement. Since the measurement values change slowly in time, correlated errors are expected in the analysis. The significance of considered environmental factors can be determined with a hypothesis test that is based on the mean value and the standard error of the estimated coefficients. If correlated errors exist, the coefficient estimates are valid, but the standard errors will be too small. Thus insignificant factors may be included in the model. The objective of this work is to show how to estimate correlated errors and how they affect the results. For this, a case study of the Schlegeis dam, where daily measurement data are available, is carried out. Two methods for the calculation of appropriate *p*-values are presented.

E-mail: buehlmann@vaw.baug.ethz.ch

Introduction

Long term processes such as alkali aggregate reaction, concrete ageing, valley and foundation deformation, and changes in seepage flow may lead to damages or even to the failure of concrete dams. To have enough time for the development, design and implementation of rehabilitation works it is important to recognise an abnormal behaviour of the structure at an early stage.

The analysis of the behaviour can be carried out by an observation-prediction comparison of a measured behaviour indicator M, the radial displacement at crest level for instance, to its predicted value P (Fig. 1). The predicted value P is calculated by a model based on environmental conditions that affect the behaviour of the structure. In the case of radial displacement at the crest level, these are mainly the water level h, the concrete temperature T_{ci} and the age t of the structure. One part of the available data is used for calibration, another for validation and the remaining data can be used to check for abnormal behaviour. For this, the difference D between M and P is estimated and analysed.

Generally, there are two different modelling approaches. On the one hand, deterministic models link the influences and the behaviour by physical laws. For that purpose usually finite element models are set up. On the other hand, statistical models relate the influences and the behaviour by statistical procedures. Commonly, multiple linear regression models with a least square approach for approximation are used. Statistical models are set up by choosing a model equation that should represent the physical behaviour of the structure. There are different types of model equations; an overview is given in [1].

In statistical models, measurement time-series of the behaviour indicator and the influences are used. The data is inherently correlated and hence correlated errors are expected in the regression model. This correlation depends on the ratio of the variation of the measured quantity to the measurement interval. If the measurement interval is short and the variation is small, as expected for the displacement of concrete dams, the errors are highly correlated. In Switzerland there are no rules on how measurement intervals shall be selected. The objective of this work is to show how the correlation of the errors can be estimated, how it affects the results and how it can be accounted for.
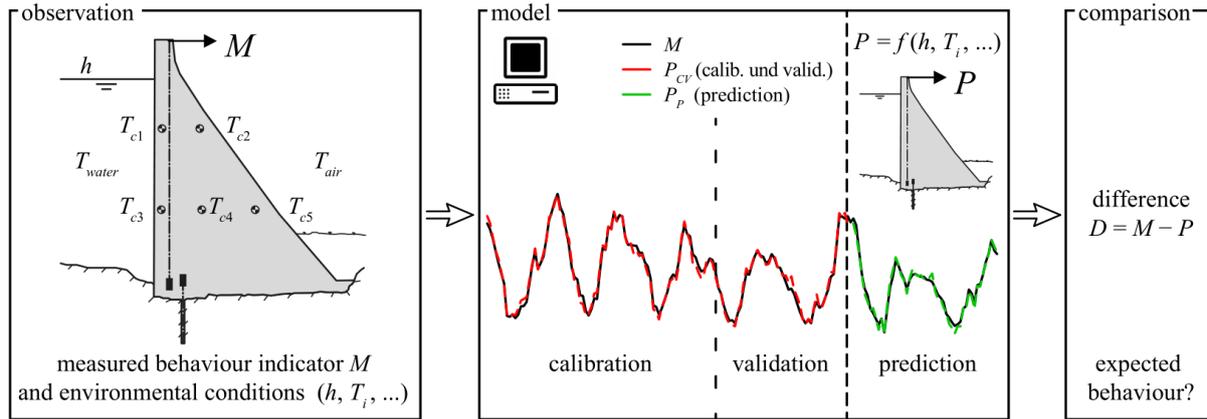
Fig. 1: Scheme of the observation-prediction comparison

Data assessment

The behaviour indicators and the environmental influences are measured at certain intervals. The horizontal displacement is usually measured with a direct or an inverted pendulum. The advantage of the pendulum is that the displacement can be measured directly. The water level is determined by pressure measurements at the lower part of the reservoir. Typically, the temperatures of water, air and concrete dam body are measured. The recording of measurement values is carried out either manually or electronically. In Fig. 2 the time series of the water level measurement of the Schlegeis arch dam in Austria is shown as an example. The recordings follow a seasonal trend due to the operation mode of the storage power plant fed by the Schlegeis reservoir.
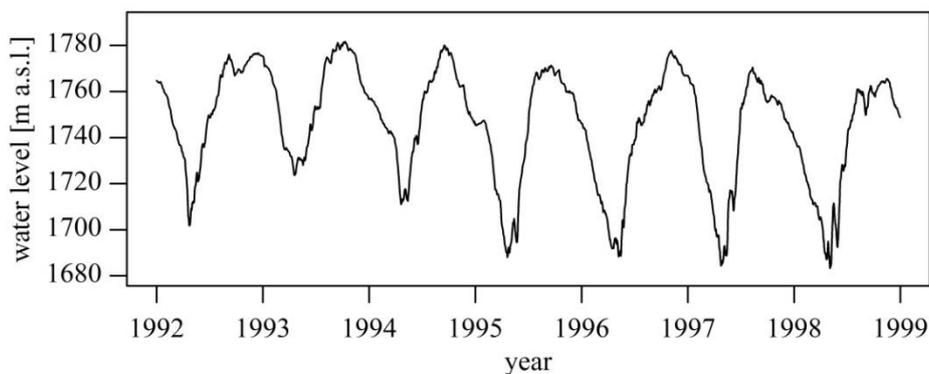
Fig. 2: Time series of the water level measurements of the Schlegeis dam

Linear regression

Linear regression analysis is used to analyse and model a linear relation between measured regressor variables and a response variable. If only one regressor variable is present, it is called simple linear regression, otherwise multiple linear regression (MLR). Generally, the relation between a response variable $\mathbf{y}$ that is related to k regressor variables $\mathbf{x_i}$ can be formulated as

$$\mathbf{y} = \beta_0 + \beta_1 \mathbf{x_1} + \beta_2 \mathbf{x_2} + ... + \beta_k \mathbf{x_k} + \varepsilon. \tag{1}$$

The regression coefficients β_i are linear, but the response $\mathbf{y}$ must not be a linear function of the regressor variables $\mathbf{x_i}$. Thus the response can be a curved surface for example [2]. The error term ε, often called residuals, is the difference between the observed values and the modelled

values. The coefficients β_i are commonly determined by the least square approach, i.e. the coefficients β_i are determined so that the sum of the squared residuals is minimised. Besides the estimated values for the coefficients β_i their standard error $\sigma(\beta_i)$ is determined. The standard error gives information about the accuracy of the estimate for the coefficient. A hypothesis test to check if a certain coefficient is zero ($H_0 : \beta_i = 0$) can be done. For every coefficient the t-test statistics is calculated by $t = \beta_i / \sigma(\beta_i)$ [4]. The t-value is a measure for the number of standard deviations that β_i is away from zero [4]. On the basis of the t-value, the p-value is calculated [3] by using integral tables of distribution functions. A small p-value indicates that a relation between the influence and the behaviour indicator due to chance is unlikely [4].

Consider a normally distributed coefficient β_i with mean value of 0.5 and standard error of 0.1 (Fig. 3a). This results in a p-value of 0 and a relation between the influence and the response is highly significant. In contrary, consider a coefficient β_i with mean value of 0.5 and standard error of 0.4 (Fig. 3b). A relation between the influence and the response due to chance is likely since the p-value is 0.18. Thus, this influence could be omitted in the model.
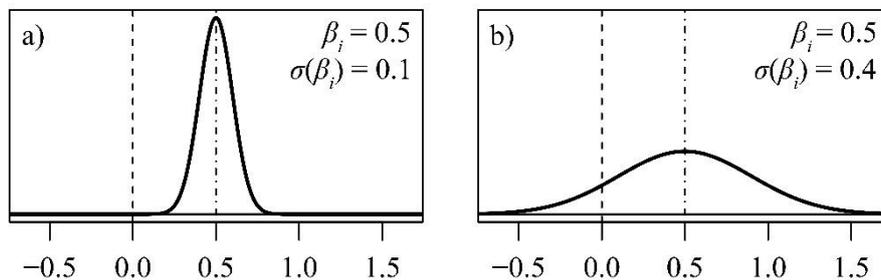

Fig. 3: Example cases with a) $\beta_i = 0.5$ and $\sigma(\beta_i) = 0.1$; b) $\beta_i = 0.5$ and $\sigma(\beta_i) = 0.4$

On the role of autocorrelation

One of the general assumptions for a least square estimate is that the residuals are uncorrelated. When using time-series data in regression models, this assumption will likely be violated and the errors are autocorrelated. Autocorrelation means that the errors are correlated by themselves at different times [2].

For example, consider two identical datasets. Instead of n observations, there are $2n$ observations available. The values of the regression coefficients will be exactly the same for both datasets by doing MLR analysis but the standard errors will be smaller by $\sqrt{2}$ since more observations are available [4]. It will even become worse, if the dataset is copied several times. If measurements of time series are recorded at short intervals in relation to the variation of the value of the behaviour indicator, almost the same quantities are measured multiple times. As in the example described above, this will result in smaller standard errors and smaller p-values of the regression coefficients compared to uncorrelated data. As a consequence, statistically insignificant regressors may are included in the model. Thus, it is important to check for autocorrelation of residuals and to eliminate this phenomenon if the standard errors of the coefficients and the p-values are of interest.

Another reason for autocorrelation is the absence of one or more important influence variables in the model [2]. This leads to systematic deviations and wrong estimates of the other regression coefficients.

Detection

Autocorrelation can be detected visually by plotting the autocorrelation function (ACF) and the partial autocorrelation function (PACF), see for example Fig. 6. If the decay of the ACF is exponential and there is a cut-off in the PACF at a certain lag, the errors are correlated [5]. This

can be seen well in Fig. 6(a) and (b). In Fig. 6(e) and (f) the ACF and PACF plot indicate no significant correlation of the errors.

Treatment

A first and simple approach is to thin out the dataset if correlated errors are present. This will reduce the correlation of the residuals and if the time lags are large enough, the residuals will be uncorrelated. But keep in mind that some data and information get lost.

Another approach is the so-called block-bootstrap method. It can be used to calculate the regression coefficients and its standard errors. When applying the block-bootstrap, the data is divided into blocks of size l [6]. Afterwards, new data sets are created by sampling these blocks. A block can be used more than once, thus some of the original data might not be present in the new dataset. This procedure is usually repeated 200 to 1'000 times [2]. Ordinary least square (OLS) regression is performed to all of these datasets. Every regression will lead to slightly different regression coefficients. On the basis of these different coefficients a mean value and a standard error can be calculated. Since the sampled data sets depend on the block length, it should be selected with care.

Case study Schlegeis arch dam

The analysis in this case study is carried out for the Schlegeis arch dam, whose data is available from the 6th international benchmark workshop on numerical analysis of dams [7]. The Schlegeis dam is located in the Zillertal Alps in Austria and was built between 1967 and 1971. The dam has a height of 131 m with a crest length of 725 m. Daily measurement data of the radial pendulum displacement at crest level, 6 concrete temperature measurements on two different levels and the air temperature are available from 1992 – 1998 (Fig. 4). The data from 1992 – 1996 is used for calibration and the data from 1997 – 1998 for validation.
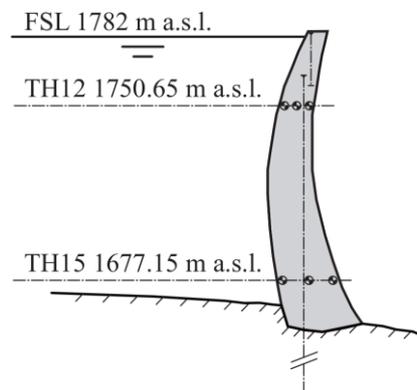
Fig. 4: Cross section of the Schlegeis arch dam (adapted from [8])

In this study, a HTT (Hydrostatic, Temperature, Time) model equation is used for the MLR (Equation (2)). The influence of the water level is considered by a fourth order Chebyshev-polynomial. In addition, a time-delayed reversible deformation h_v (viscous elastic deformation of the structure) that is influenced by the water level is taken into account [9]. Including the delayed part leads to a more accurate model with less autocorrelation of the residuals. The temperatures are pre-processed by a thermal analysis with the software TADAM [10] to get an instantaneous temperature field on both levels H12 and H15. The mean temperature T_m and the gradient temperatures T_g are calculated using the approach described in [11]. Since the two mean and gradient temperatures are correlated (multicollinearity), only the first principal components of the temperature data are considered in the model. The drift is considered as a linear function of time t.

$$P(h,T,t) = \beta_0 + \beta_1 h + \beta_2 h^2 + \beta_3 h^3 + \beta_4 h^4 + \beta_5 h_v + \beta_6 T_{m,\mathrm{I}} + \beta_7 T_{g,\mathrm{I}} + \beta_8 t \qquad (2)$$

Daily measurement data

For calibration of the model, a least-square fit is carried out for equation (2) based on daily measurement data. Due to the consideration of a time-delayed water level displacement by 308 days, the calibration period starts in autumn 1992. The resulting MLR model has an adjusted coefficient of determination $R^2_{adj} = 0.991$ and mean squared residuals $MS_{Res} = 1.50 \text{ mm}^2$. For the validation period $R^2_{pred} = 0.982$ and $MS_{Res,pred} = 1.75 \text{ mm}^2$. The ACF and the PACF indicate highly correlated residuals (Fig. 5), thus the standard errors and the p-values might be too low compared to uncorrelated data.
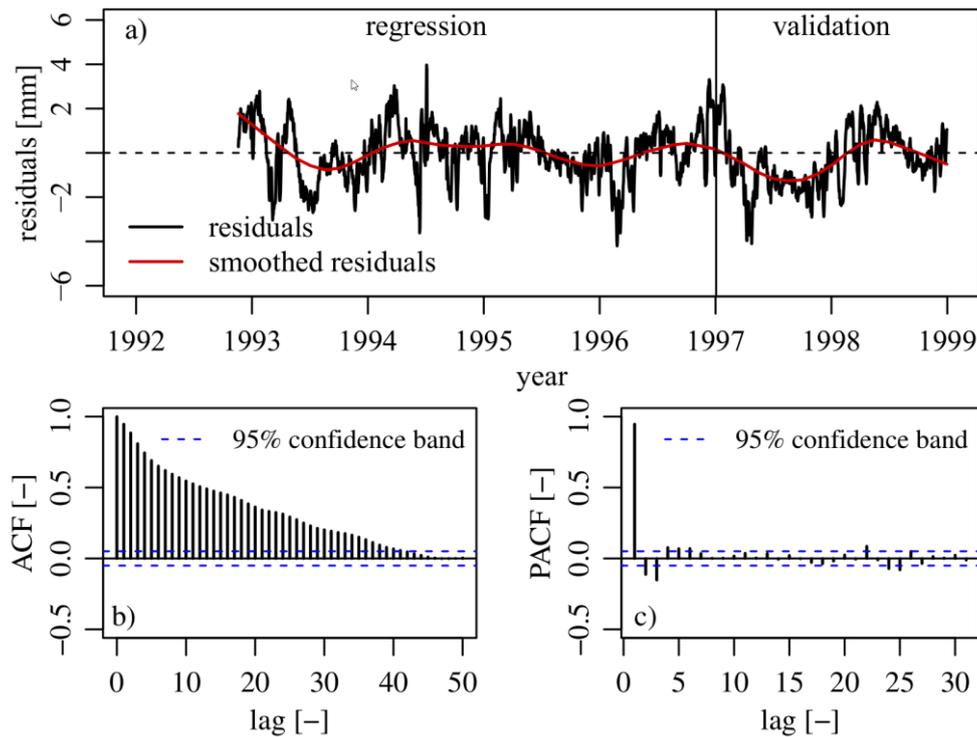
Fig. 5: Regression based on daily measurement data: a) residuals, b) ACF and c) PACF

Thinned out data

In order to reduce autocorrelation, the dataset with daily measurement data is thinned out considering intervals of 7, 14 and 28 days. For the datasets with 28 day intervals, two different start dates are chosen. The new data sets can be seen as data sets with larger measurement intervals.

The values of the regression coefficients β_i and the corresponding p-values are displayed in Tab. 1. The coefficient of determination R^2_{adj} and the mean square residuals MS_{Res} for the calibration and the validation period are summarised in Tab. 2. The results show that the autocorrelation gets weaker with increasing measurement interval. In the case of the 7 and 14 day intervals, a first order autocorrelation of the residuals is recognisable (Fig. 6a – d). There is no significant autocorrelation for 28 day intervals (Fig. 6e and f). The regression coefficients β_i do not differ much for the different time-intervals but their p-values do (Tab. 1). All coefficents are significant for the 7 and 14 day time-interval. On the contrary, for the 28 day interval the coefficients of the water level influence fourth order h_4 and the drift t are insignificant. The statistical values only slightly differ for the calibration period but they

are worse for the validation period. Comparing the two different models with 28 day intervals, their coefficients and statistical values are different, especially for the validation period.
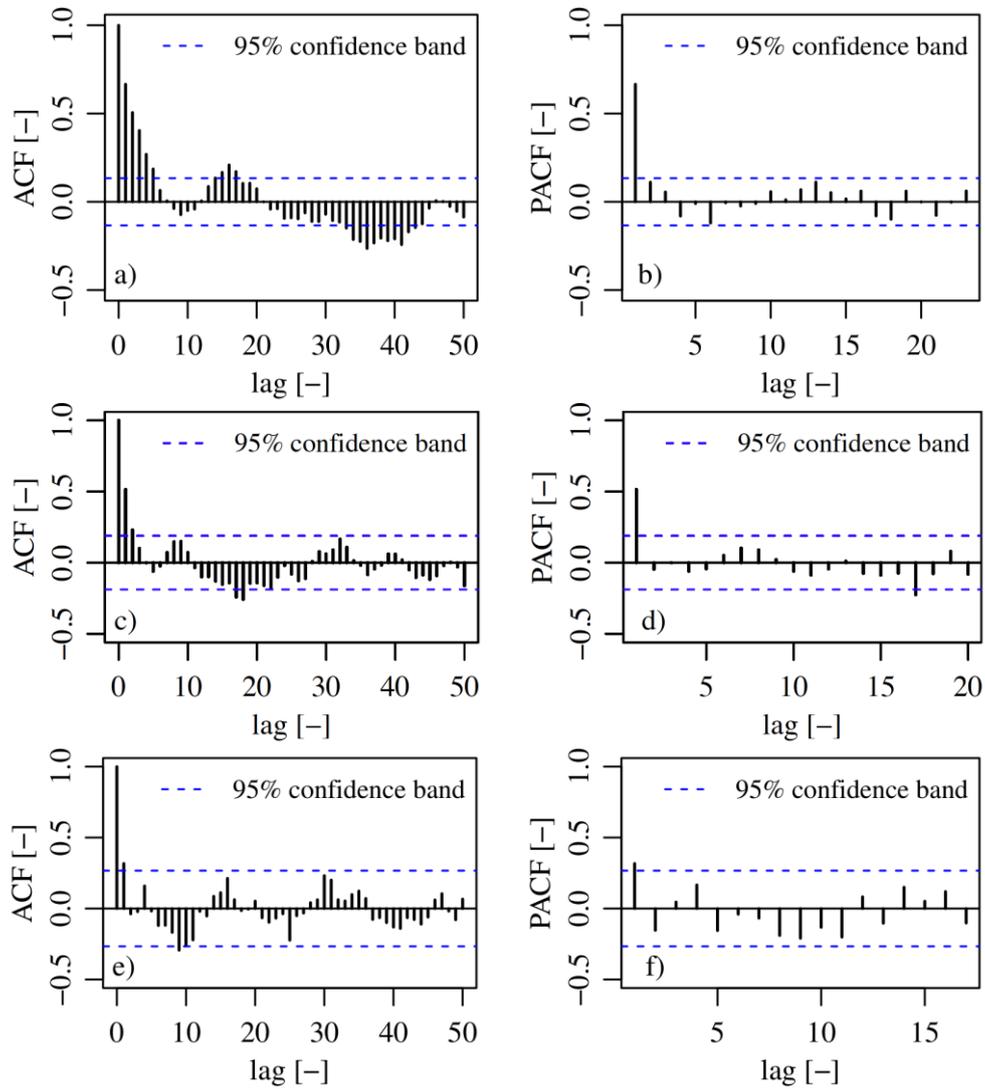

Fig. 6: ACF and PACF for thinned out data sets: a) and b) 7 days; c) and d) 14 days; e) and f) 28 days

Block bootstrap

The block bootstrap (BBS) was sampled with a block size of 40 days corresponding to the period where correlation of the daily measurement data was detected (Fig. 5). The data were sampled for 1000 times. On the basis of 1000 MLR calculations using different datasets based on the same data, the mean value of the regression coefficients β_i and the corresponding p-values were calculated (

Tab. 1). The statistical values are presented in Tab. 2. The influences of the water level of fourth order h_4 and of the drift t are insignificant. The model adequacy is very good with $R^2_{pred} = 0.981$ and $MS_{Res,pred} = 1.86 \text{ mm}^2$.

Tab. 1: Values of regression coefficients and p-values (*** $p<0.001$; ** $p<0.01$; * $p<0.05$; . $p<0.1$) resulting from the MLR regression for the different models

			1d	7d	14d	28d (I)	28d (II)	BBS
β_0	Intercept	value	61.43	61.40	61.31	60.20	60.25	61.30
		p	***	***	***	***	***	***
β_1	h_1	value	24.08	23.72	23.30	22.81	21.36	23.94
		p	***	***	***	***	***	***
β_2	h_2	value	7.21	7.08	6.87	6.60	5.81	7.08
		p	***	***	***	***	***	***
β_3	h_3	value	1.37	1.30	1.28	1.29	0.96	1.42
		p	***	**	***	***	**	***
β_4	h_4	value	0.46	0.49	0.48	0.52	0.37	0.44
		p	***	***	*	.		.
β_5	h_v	value	0.29	0.29	0.32	0.32	0.33	0.30
		p	***	***	***	***	***	***
β_6	$T_{m,I}$	value	-3.92	-3.95	-3.94	-4.06	-3.87	-3.89
		p	***	***	***	***	***	***
B_7	$T_{g,I}$	value	-0.48	-0.50	-0.46	-0.43	-0.51	-0.45
		p	***	***	***	***	***	***
β_8	t	value	0.32	0.32	0.37	0.29	0.46	0.35
		p	***	**	*		.	

Tab. 2: Statistical values resulting from the different models

		1d	7d	14d	28d (I)	28d (II)	BBS
calibration	R^2_{adj}	0.991	0.991	0.991	0.991	0.988	0.991
	MS_{Res}	1.50	1.46	1.61	1.56	1.94	1.52
validation	R^2_{pred}	0.982	0.982	0.979	0.984	0.971	0.981
	$MS_{Res,pred}$	1.75	1.90	2.13	1.73	2.95	1.86

Summary and conclusions

Measurement data used for dam monitoring are recorded in the form of time series with a certain interval. These data can be used in combination with statistical models for dam behaviour analysis, whereas a model equation containing the significant influences has to be defined. The significance of the chosen influences can be evaluated on basis of the *p*-values. When autocorrelation of the residuals occurs, the mean values of the regression coefficients are still unbiased and valid but their standard errors are underestimated [2]. Since the *p*-values are calculated based on the ratio between the regression coefficients and the standard errors, they are small if the residuals are correlated. Hence, insignificant influences may be included in the model. In addition, the residuals are inherently correlated since the data is time-dependent.

The influence of autocorrelation on *p*-values is presented by the case study of the Schlegeis arch dam. Since daily measurement data are available, the residuals are highly correlated. Thus the *p*-values of all considered influences are low and all of the influences are significant for a model with daily measurement data.

To improve the model, two approaches for the calculation of appropriate *p*-values have been applied. Firstly, the measurement data was thinned out considering intervals of 7, 14 and 28 days. The results show that autocorrelation decreases and the *p*-values increase with larger measurement interval. With an interval of 28 days no autocorrelation is present. In this case, the fourth order influence of the water level h_4 and the drift t are insignificant. Thus, they can be excluded from the model. However, the two different 28 days' datasets indicate significantly different statistical values concerning the goodness of fit (see Tab. 2: Statistical values resulting from the different models). Secondly, the block bootstrap approach was applied, where all of the daily measurement data is used but sampled in blocks of a given length. This procedure was repeated 1000 times and each of the datasets was used for MLR. The 1000 different regression coefficients β_i were used to calculate mean values and standard errors and finally the *p*-values. The standard errors and the *p*-values are similar to the values of the 28-days data but the regression coefficients are similar to the full model with daily measurement data. Since the bootstrap model is based on more data, it is more accurate and more robust for prediction. The difficulty lies in the choice of the block length. For this case study, the block length was selected as long as the period where correlation of the daily measurement data has been detected. It is not clear if the boot strap approach just worked well for the present case and the method has to be tested with data from other dams.

The results summarised in Tab. 2 show that the more data is available, the better the coefficient of determination R^2_{pred} and the mean squared error $MS_{Res,pred}$. In the case of the Schlegeis arch dam, weekly or bi-weekly measurement data would lead to an accurate model, the use of monthly measurement data is not suggested.

Acknowledgements

References

[1]   Swiss Committee on Dams (2003). Methods of analysis for the prediction and the verification of dam behaviour, Wasser Energie Luft, Vol. 95(3/4), pp. 73-109.

[2]   D. C. Montgomery, E. A. Peck and G. G. Vining (2012). Introduction to linear regression analysis, Fifth edition, John Wiley and Sons, Hoboken, New Jersey, USA.

[3]   D. C. Montgomery, E. and G. C. Runger (2011). Applied Statistics and Probability for Engineers, Fifth edition, John Wiley and Sons, Hoboken, New Jersey, USA.

[4]   James, G., Witten, D., Hastie, T. & Tibshirani, R. (2013). An Introduction to statistical learning. Springer, New York, USA.

[5]   J. D. Cryer and K.-S. Chan (2008).Time series analysis – with applications in R. Springer, New York.

[6]   S. Gonçalves and H. White (2005). Bootstrap standard error estimates for linear regression, Journal of the America Statistical Association, Vol. 100(471), pp. 970-979.

[7]   G. Zenz and P. Obernhuber (2001). ICOLD benchmark workshops on dam safety, The International Journal on Hydropower & Dams, Vol 8(2), pp. 75-78.

[8]   B. Weber (2002). Vorhersage des Verhaltens von Talsperrenmit Hilfe des Soll-Ist-Vergleichs - Statistischer Teil, BWG, Bern, Switzerland.

[9]   F. Perner and P. Obernhuber (2010). Analysis of arch dam deformations, Frontiers of Architecture and Civil Engineering in China, Vol. 4(1), pp. 102-108.

[10]   M. Leclerc and P. Léger (2004). TADAM – Thermal analysis of concrete dams (http://www.polymtl.ca/structures/doc/TADAM.zip), École Polytechnique de Montréal, Canada.

[11]   P. Léger and M. Leclerc (2007). Hydrostatic, temperature, time-displacement model for concrete dams, Journal of Engineering Mechanics (ASCE), Vol 133(3), pp. 267-277.

Redundancy like Safety: the cross analysis of the monitoring data of Ridracoli dam

Manciola P.[1], Gambi A.[2], Cortezzi F.[2], Buffi G.[1]

[1]*Institute of Civil and Environmental Engineering of Perugia, Via G. Duranti, Perugia, Italy*

[2] *Romagna Acque Società delle Fonti, Forlì, Italy*

ABSTRACT: Monitoring is the essential tool for controlling the status of dam safety and the management of water resources governed by them. The registration of an anomalous trend of a greatness, acquired by a single instrument, is index of its own malfunction and not of a possible degenerative process, which would be warned and monitored typically by one or more groups of instruments. This paper proposes an analysis procedure of typical measurements in a concrete dam. Deformations, stresses, displacements, temperatures, hydrostatic levels, uplift pressures and moreover greatness are implemented in a single data base to be correlate at the occurrence of the same condition and to compare them with expected results. Object of study was the Ridracoli dam characterized by a control system strongly redundant in relation to the numerosity of instruments, of multiple capacity of anomalies detection and of modality of acquisition. An example of redundancy: the trend of a tensiometric capsule, in relation with hydrostatic level, apparently at odds with theoretical behavior of the structure, is explained by the cross analysis with temperature. The possibility to validate the functionality of instruments, and then of the structure, from different point of view, goes towards a redundancy of safety.

E-mail: giulia.buffi@unipg.it

Introduction

The measures, acquired by the monitoring system of a dam, in order to fully describe the state of conservation of the structure and of the sides and, in this way, to ensure the safety of the system, must necessarily be correlated between them. In fact the variability of some measures may be justified by the analysis of variations of "cause" quantities [1], such as the hydrostatic level and the temperature. Furthermore, an asynchronous trend of the same measure in different regions of the structure can depend on the operating rule of the same. An increase of specific values that are not directly attributable to the cause greatness can instead serve as a wake-up call for the identification of ongoing processes that could affect the operation of the dam or even safety. Hence the need for a capacity of interpretation and intercorrelation that extends to all instrumental apparatus [2].

Ridracoli dam

The structure

The Ridracoli dam is an arch-gravity dam in simple concrete (height 101 m and crest length 432 m) that closes a very wide U-shaped valley in the Tuscan-Romagna Apennines in Italy [1,3]. The water supply is the reservoir primary use for 48 communities in the Ravenna, Forli-Cesena and Rimini Provinces, and from 1989 also the San Marino Republic [4,5]. The dam was completed in 1982 and it was filled completely for the first time in 1986[1]. The body dam is a double curvature structure, symmetric respect to the key section, it rests on a "pulvino", a foundation saddle [6], which extends along the entire perimeter of the excavation [7]. The body dam is made up of 27 ashlars, with an independent static operation in order to avoid the deformations of the structure as a result of increase of hydrostatic level or of temperature variation or of other actions and to avoid fissuring of the structure. The connection of the ashlars

is been realized by the insertion of neoprene elements that are disposed around all the outer perimeter of the cross section and of the tunnels that cross longitudinally the dam and the foundation. They have the dual function of preventing infiltration of the water and spillage of the cement grout, used for the suture of the joint, injected radially and in subsequent times from tunnels during the construction phase.

The monitoring system
The control of the behaviour of the structure, of the foundation rock, of the reservoir banks and of the downstream rocky slopes is achieved through a complex monitoring system activated since the phase of construction [8]. Most of the instruments and of the measuring points are located in five radial sections of the structure: the key section, the two external laterals and the two intermediate laterals [6,7,8], as shown in the Fig. 1.

    A.   Downstream view
    B.   Strain-gauge disposition
    C.   Piezometer disposition
    1.   Grouting and drainage galleries
    2.   Direct pendulum
    3.   Inverse pendulum
    4.   Strain-gauge
    5.   Piezometer
    6.   Teledilatometer
    7.   Concrete thermometer
    8.   Stress-gauge capsule
   9.   Grout curtain
    10. Joint number
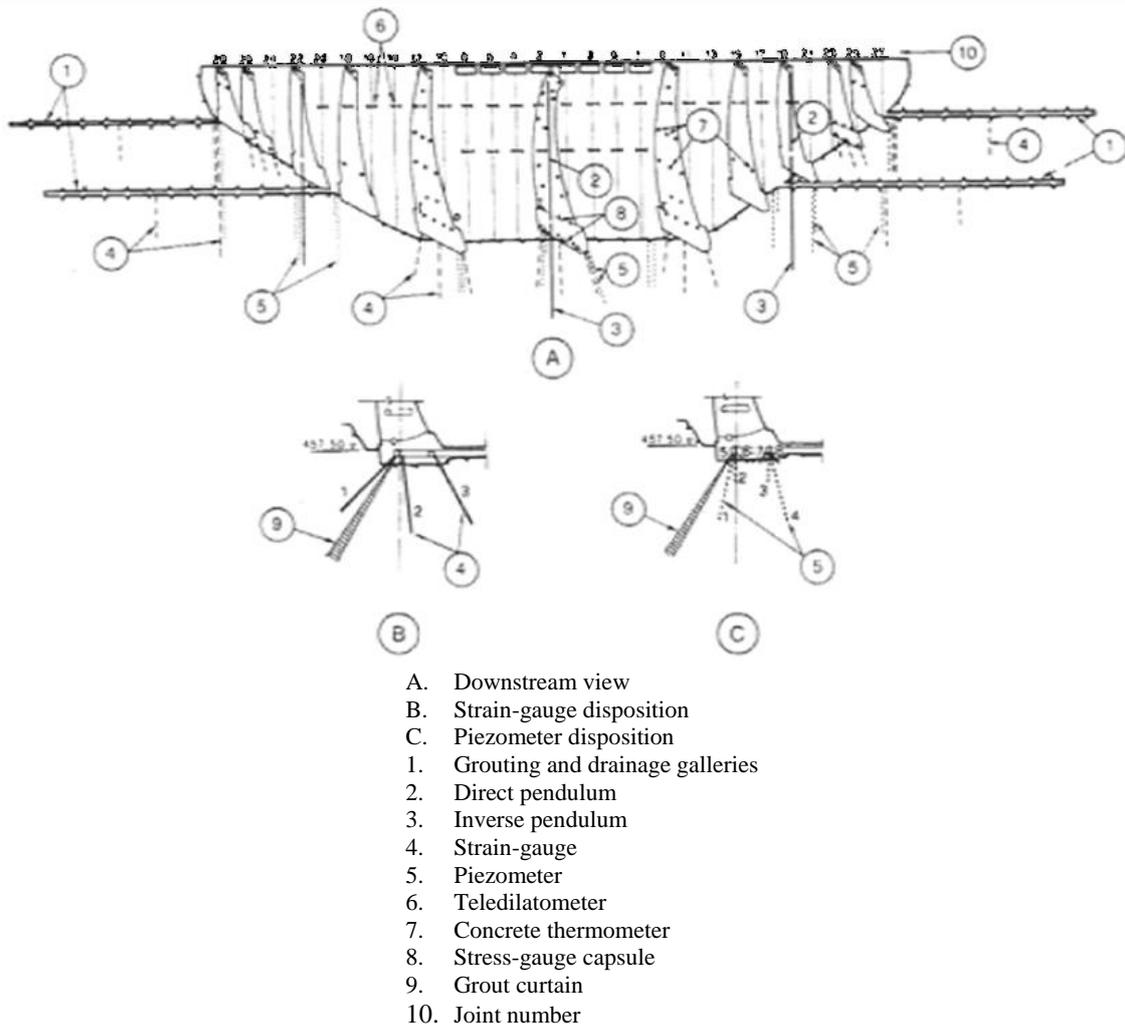
Fig. 1: Dam Main Instrumentation[6]

The cause and effect quantity, analysed in the present work, are reported below.
- Hydrostatic Level

The primary tool that makes the reading is the dynamometric balance. It detects, records and transmits the hydrostatic level with great accuracy and extended measuring range [9]. It is based on the first class lever principle and it includes the installation with hydrostatic pressure outlet and level meter placed at the minimum level to be measured [9] at an height of 483 m.a.s.l.. The instrument allows the reading of the level at the place of installation and in the monitoring

room in the warden house. The validation of the measurement is also realized through the read of staff gauges placed in the right rock side.

- Temperature

The temperature measurement is performed by electrical thermometers and also with stringed vibrating instruments designed for other measures such as strain gauges [8]. The temperature of the structure concrete, of the air and of the water is detected. The thermometers that detect the external temperature are placed in key section 1-2 and in the two lateral sections 10-12 and 9-11, respectively in the right and left side.

- Horizontal displacement

The horizontal displacements of the structure are monitored using various instruments: direct and inverted pendulums, collimations and geodetic measurements. The system called plumb line (or pendulum) allows the determination of the two planimetric components of the relative displacements of various points of a structure located along the same vertical. The direct pendulum is a steel wire whose upper end is anchored to a point of the structure as high as possible, while the lower is linked a heavy body to ensure the straightness and verticality, followed by a body immersed in a viscous liquid (damper) to avoid any oscillatory motions [9]. The direct pendulum measures the motion of the dam body with respect to the dam foundation. The height of the structure does not allow the use of a single instrument; therefore, more pendulums are used with measuring points intermediate. The motion of the foundation compared to the rock foundation is detected by the pendulum reverse, in this case the lower end of the wire is anchored in the rock, while the upper is fixed to a float submerged in a container containing viscous liquid able to dampen the motion [9]. The pendulums are present in the main section 1-2, in the two lateral sections 20-22 (right) and 19-21(left) and in the rock of the lateral sides. The direct pendulum PD/1-2/AY and the inverted pendulum PR/1-2/1Y, placed in the main section, as shown in the Fig. 2, which register the upstream-downstream motion of the structure, are taken into account in this work.
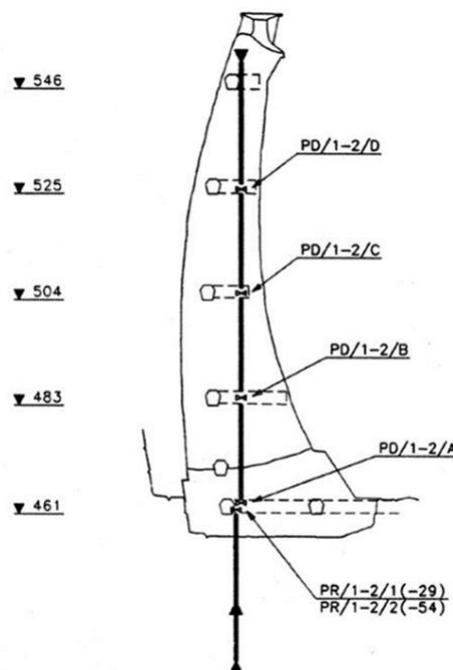

Fig. 2 : Pendulums in the key section

- Stress

The evaluation of the stress state within the concrete structure is achieved by means of the electroacoustic tensiometric capsules. Embedded in the concrete of the dam body and of the

foundation, they measure directly the state of tension present in the structure (Kg / cm^2) [9]. These tools are based on the measurement of deformation according to the load of two plates, connected to each other along the circular contour, the measurement is detected by a vibrating string stretched between the plates themselves [9]. Capsules are placed in the key section 1-2 and in the lateral 24-26 and 23-25 respectively at the right and at the left. They are placed in the transverse direction to the contact between the foundation and the bedrock and, at a higher level, between the foundation and dam body, as shown in the Fig. 3. The capsules in the main section C/1-2/4 and C/1-2/6, respectively in the vicinity of the upstream and downstream face, and in the lateral sections C/24-26/6 and C/23-25/6, both adjacent to the downstream face, are taken into account in this paper.
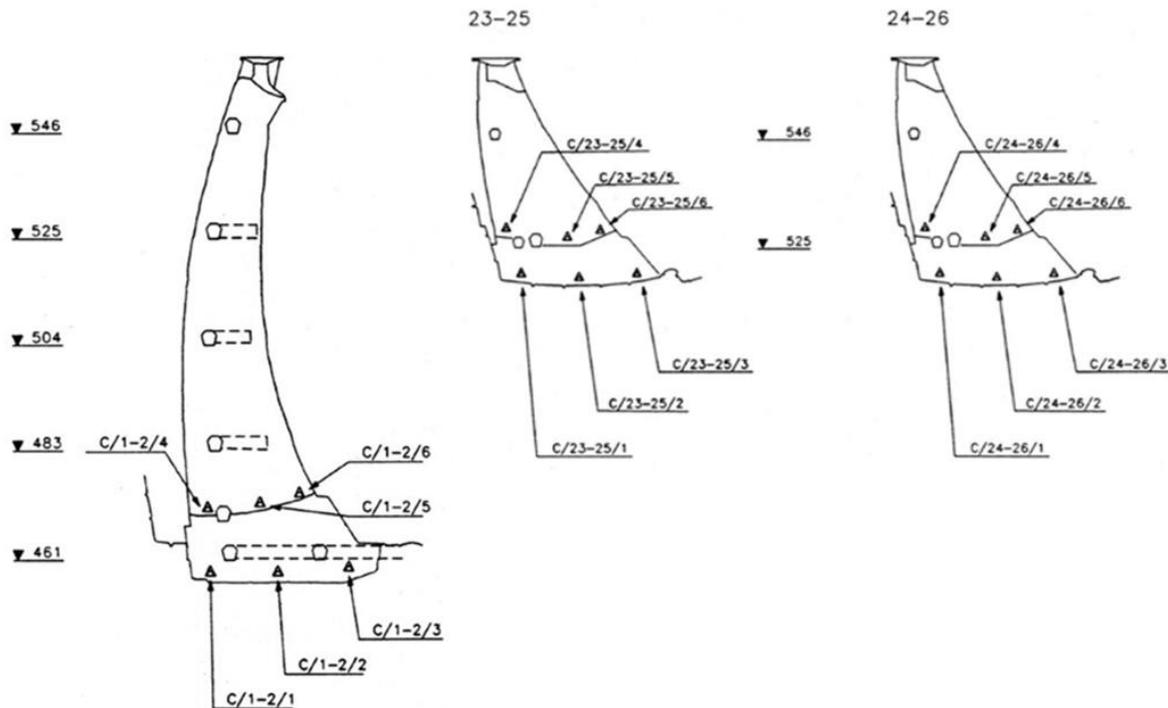

Fig. 3 : Tensiometric capsules in the key section and in the two lateral

The control system

In the monitoring room, located in the warden house of Ridracoli dam, through to the use of about 4 km of electric cables, the centralized reading of about 284 instruments from a total of 985, many of which have been installed to assess the construction phase and first filling of the dam, is realized [6]. The concept of security as analysis redundancy is also observed in the system of dual control, on-line and off-line, present in the Ridracoli dam.

The on-line control
The individual measuring instruments and manual measurements are linked to the panels placed in the tunnels of the dam. Data acquisition takes place, with different temporal frequencies, using automatic remote selection of the panels. The automated data are archived using a computerized system called INDACO, active since 1992 and connected in line with the institute CESI - ISMES of Bergamo. This system allows the creation of greatnesses trend diagrams and the storage of the measures. Moreover, the system allows the real time comparison of the effective behaviour of the structure with the one provided by a theoretical model contained in MISTRAL, a decision support system, which analyses and filters the data from 42 automatic tools deemed significant for the identification of the state of the structure [1,10].

The off-line control
The data of the automatic monitoring system are stored along with those acquired manually in a database called MIDAS that allows the analysis and the subsequent interpretation of greatnesses. The effective behaviour is validated, dually to the on-line control, through a finite element model that can predict the behaviour of the structure as a result of cause greatnesses changes [1].
The two control systems verify independently that the effective behaviour of the structure is consistent with that predicted by models, but, at the same time, they are complementary. In fact, the off-line control provides to the periodic determination of the parameters employed in on-line one [1].

The monitoring data

The organization and the correlation of the greatnesses of the monitoring system are realized through the creation of an interactive data base. Interest data ranges were extracted from this, and thereafter correlated using the Pearson correlation index.

Ridracoli dam Database
Most of the data included in the database covers a period of time from the end of the structure construction phase, around 1982, to 02/02/2015. The structure, on which the program is based, is founded on building of tables organized in fields(columns) and records(rows) and on subsequent establishment of relations between them. The correct functioning of the database can be validated by the construction of "Queries" that are real questions of the archive. The imposition of more selection criteria simultaneously allows to obtain a range of data like the result of the intersection of more circumstances. The use of Query is useful in order to have available in the same database in addition at the data of the monitoring system, also the characteristics of individual instruments that realize the acquisition.

Recall of descriptive statistic
Some necessary definitions to the discussion of the criteria adopted to determine the eventual correlation between two variables are reported below. From the covariance and the standard deviations of two random variables X and Y, it is possible to define a further characteristic constant that explains a possible linear relationship between them, the correlation index of Pearson [11]. It is given by the ratio between the covariance of the two variables and the product of their standard deviations,

$$\rho_{XY} = \frac{\sigma_{XY}}{\sigma_X \cdot \sigma_Y} [11].$$ (1)

The characteristic constant always assumes values between -1 and +1,

$$-1 \leq \rho_{XY} \leq +1 [11].$$ (2)

The extreme values are assumed only if a variable is a linear function of the other, namely respectively inversely or directly proportional with probability equal to 1[11]. The correlation index assumes the value 0 if the two variables are independent, and therefore a variation of one does not influence the other and vice versa, and are called uncorrelated [11].

Correlation hydrostatic level – temperature – displacement – stress
The operating principle of the arch-gravity dams is composite. This typology is adopted when there are good, but not exceptional, characteristics of the sides and therefore the hydrostatic thrust is partly absorbed by them and partly discharged on the foundation. The load at which the structure is subject, in fact, is divided on the sides, through the "arch" principle, and on the foundation, by the "cantilever" function. The latter will be analysed in this paper. Taking into

account the part placed between the sections 1 and 2, namely placed in the main section, as shown in the Fig. 1, it can be assumed wedged to the base, free at the top and independent from adjacent segments. The study focuses on annual cyclical behaviour of the structure. Therefore, in the Fig. 4, are reported only the trends recorded in the year 30/06/2013 - 30/06/2014 of: hydrostatic level, displacements upstream - downstream detected by the pendulum direct PD/1-2/AY and inverted PR/1-2/1Y placed in the key section and stress at the contact between the dam body and foundation recorded from the tensiometric capsules C/1-2/4 and C/1-2/6 placed in the same section. The cantilever behaviour of the structure parts, in particular the one of the main section, is analysed. The analysis of the Pearson correlation coefficient, reported in Tab. 1, explains how, at an increase of the hydrostatic load, the displacements of the dam body compared to the foundation and of the foundation respect to the bedrock, measured respectively by PD/1-2/AY and PR/1-2/1Y, are related directly with it. Although, as it is obvious, the motion of the pulvino is much reduced compared to that of the dam body. Therefore, the hydrostatic level increase involves a "rotation" of the element towards the valley, as shows also the trend of the deformed of the main cantilever during the phase of progressive filling of the dam, shown in the Fig. 5, which determines a discharge of the tensiometric capsule of upstream C/1-2/4. In fact the capsule measures a stress that is inversely correlated with the cause greatness. An overload of the downstream tool C/1-2/6 should be awaited but the measure recorded appears instead uncorrelated with the hydrostatic load being $\rho \approx 0$. The absence of relation is only partially explained by the cantilever behaviour of an arch-gravity dam. In fact, an important component is the arc behaviour. Moreover, the recorded tension by the capsule C/1-2/6 is characterized by a strong positive correlation with the outside air temperature, with a value of ρ close to unity. The instrument is in fact close to the surface of the downstream face and it is therefore affected by the external temperature and by the solar radiation. Tensiometric capsules that are placed at the same contact between the dam body and the foundation, in the lateral sections 24-26 and 23-25, respectively at right and at left respect to the key section, have the same influence by the outside temperature. In Tab. 2 are in fact visible the correlation indices of Pearson close to unity.

Conclusions

The monitoring system of the Ridracoli dam, in relation to number of instruments, of acquisition mode and of control systems, is characterized by a strong redundancy. The on-line and off-line control systems allow independently the comparison of the effective behaviour of the structure with that expected by a theoretical model in view of an interpretation redundancy. The validation of the correct operation of the individual elements that realize the monitoring system is necessary. The registration of an anomalous trend of a greatness in fact, acquired by a single instrument, is index of its own malfunction or of a dependence on various factors and not of a possible degenerative process. The cross analysis that characterized the tensiometric capsule in the main section near the downstream face C/1-2/6 showed that the lack of correlation with the cause greatness, the hydrostatic level, can be explained by the strong dependence by the second cause greatness, the outside temperature, as well as by the dual arc-gravity behaviour. The result was confirmed by the same dependence by the external temperature of the tensiometric capsules placed in the lateral sections near the downstream face C/24-26/6 and C/23-25/6. The instrumental multiplicity has allowed the explanation of a phenomenon otherwise not rebuttable. Although it is not index of an abnormal behaviour, which would be typically warned and monitored instead by one or more groups of instruments. Hence the need of an interpretive capacity that must be extended to all instrumental apparatus. The possibility of acquiring the measures also manually increases the safety level of the monitoring system especially in the case of an eventual out of service of the ordinary automatic system. In every extraordinary situation, such as that of a seismic event, the real-time monitoring of the system is thus assured

in order to ensure the surveillance of the structure and the safety of the population downstream. The functionality validation of instruments, of storage and data interpretation systems, and then of entire structure, from different angles of analysis, goes in the direction of a redundancy of safety.
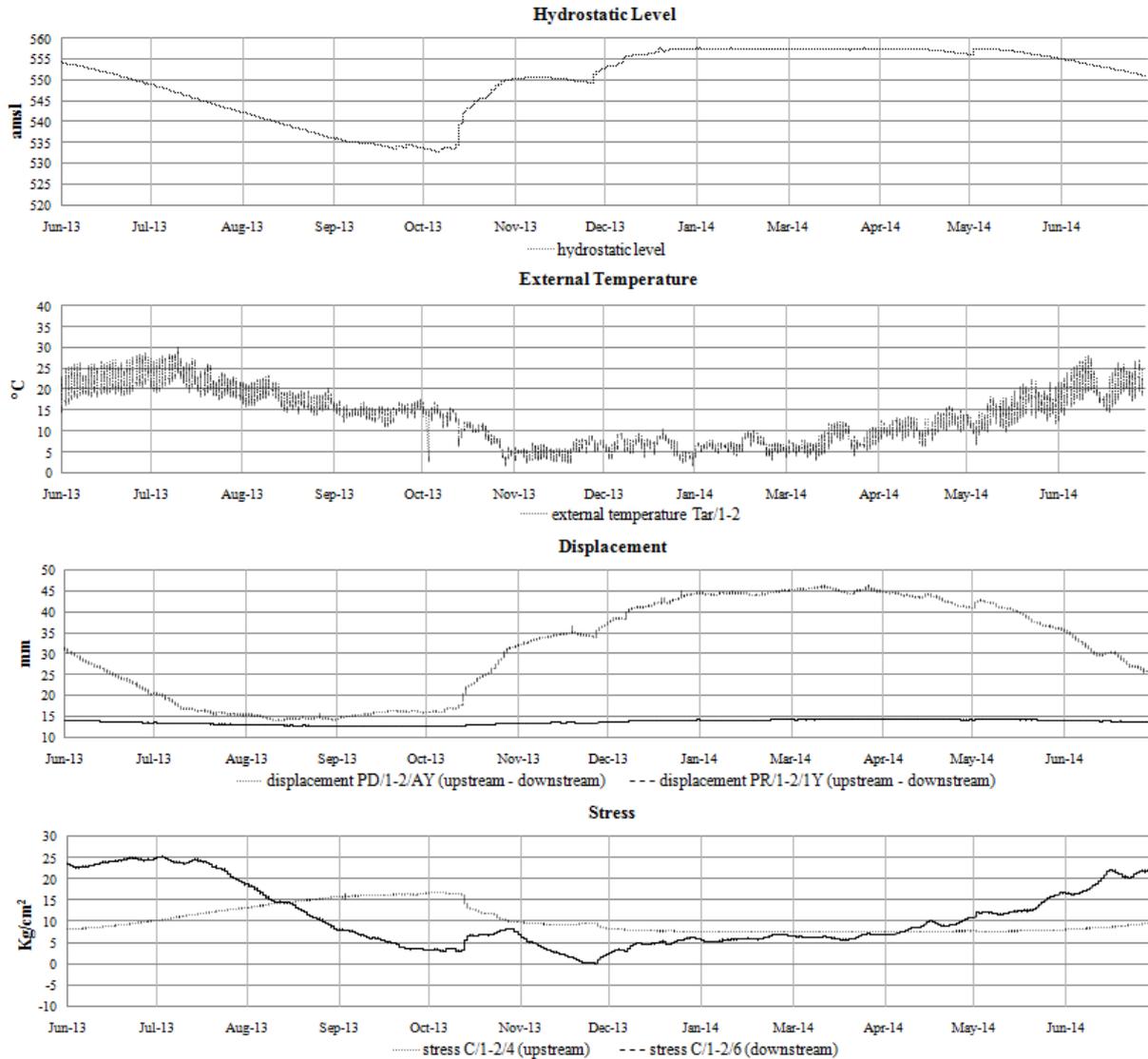

Fig. 4: Hydrostatic Level, External Temperature, Displacement and Stress

Tab. 1: Pearson Correlation Coefficient ρ

	Hydrostatic level	External temperature TAr/1-2
PD/1-2/AY	0,91	-0,64
PR/1-2/1Y	0,98	-0,32
C/1-2/4 (upstream)	-0,94	0,22
C/1-2/6 (downstream)	-0,14	0,89

Tab. 2: Pearson Correlation Coefficient ρ

	External temperature TAr/9-11
C/23-25/6 (downstream)	0,94
	External temperature TAr/10-12
C/24-26/6 (downstream)	0,82
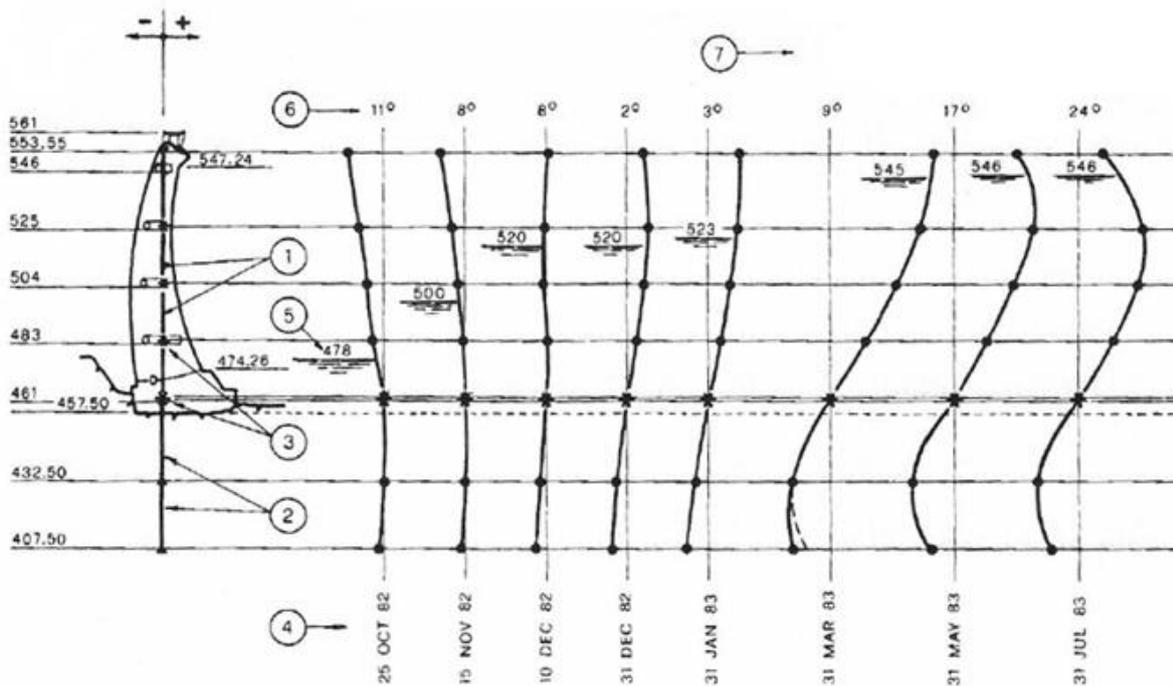
1. Direct pendulum
2. Inverted pendulum
3. Recording stations
4. Date
5. Reservoir water level
6. Air mean temperature
7. Scale of radial displacements

Fig. 5: Central Cantilever Deformation [6]

References

[1] Lancini S., Masera A., Piccinelli F. G., Farina F.(2000).Ridracoli dam – A decision support system for managing dam surveillance. 20th Congress ICOLD, Beijing, China, Vol. 3, Q.78 – R.30, pp. 443-453.

[2] Buffi G.(2014). Master degree thesis. University of Perugia.

[3] Marini P. P., Baldoni P., Farina F., Cortezzi F., Masera A.(2004).Ridracoli Dam: surveillance and safety evaluation reported on internet page. Long-term benefits and performance of Dams, Henry Hewlett, pp.247-255.

[4] Romagna Acque Società delle Fonti Spa. Progetto di Gestione.

[5] Romagna Acque Società delle Fonti Spa(2013). Bilancio di sostenibilità 2013.

[6] Piccinelli F., Bavestrello F., Gallico A.(1985).Ridracoli dam: test and data acquisition. 15th ICOLD Congress, Lausanne, Switzerland, Vol.1, Q.56 – R.73, pp.1415-1438.

[7] Consorzio Acque per le Province di Forlì e Cesena (1991). L'acquedotto della Romagna.

[8] Consorzio Acque Forlì Ravenna, Alpina Spa(1985). La diga di Ridracoli.

[9] Pizzi F.. Strumenti e sistemi per controllo dighe e grandi strutture, Officine Galileo-Ditta Pizzi.

[10] Lazzari M., Salvaneschi P.(1994).Improved Monitoring and surveillance through integration of artificial intelligence and information management system. 10th IEEE Conference on Artificial Intelligence for Applications, San Antonio, Texas.

[11] Cicchitelli G.(2003). Probabilità e Statistica. Second Edition, Maggioli Editore.

Safety Incidences in large Rockfill Dams Stability and Behaviour, Resulting from Scale Effects in Rockfill Shear Strength.

Frossard E[1]., Nieto-Gamboa C.[1]

[1]TRACTEBEL Engineering-COYNE et BELLIER, 5 Rue du 19 Mars 1962, 92622 Gennevilliers, France

ABSTRACT: A wide set of investigations developed in France in the last ten years on mechanical behaviour of rockfill dams, are summarized. A material scale effect has been evidenced inside of the shear strength of these granular materials, related to size of rock pieces, due to the physical laws of Fracture Mechanics ruling grain breakage.

This scale effect on shear strength is ruled by a simple analytical "Scale Effect Rule", operating on the shear strength envelope, explicitly proven by micro-mechanics, and validated on a wide set of independent experimental results.

A first incidence of this "Scale Effect Rule" is a new rational method to assess shear strength of coarse rockfill, from measured properties on scaled down gravel material made of same mineral, mobilizing reasonable laboratory testing means.

A second set are direct explicit incidences on the stability of rockfill slopes and corresponding safety factors, leading to dam engineering design applications.

A third set are the incidences on the strain characteristics (stress-strain curves and rigidity modulus) of these scale effects, supported by experimental and monitoring data, with other dam engineering applications.

Last, detailed numerical models incorporating these scale effects inside of constitutive relations, have shown that past incidents occurred recently at commissioning various large CFRD, are explained in large part by excessive deformations related to these scale effects.

E-mail: Etienne.frossard@gdfsuez.com

Introduction

Large rockfill dams construction has developed widely in the past decades, either as central earth core dams, with projects over 300m high in construction or under design, or as concrete faced rockfill dams (CFRD). For these last ones, significant incidents at commissioning, occurred during the last decade in China, Brazil, and Lesotho [1], have outlined the limits of empirical extrapolations from existing more modest prototypes, which ruled their design approaches, particularly for the CFRDs. These incidents have also prompted to come back to more rational design approaches, like in any large civil engineering structure, including detailed modelling of the structure behaviour, based on constitutive laws representative of the construction materials involved, whose parameters are calibrated on relevant testing performed on these construction materials. However, this approach presents here a major experimental challenge: how to perform representative mechanical testing on materials including so large pieces? In effect, commonly used large rockfills display a D_{Max} up to 600mm, for which a cylindrical "representative specimen" should, according to usual rules, measure 3,60 m in diameter (*6 x D_{Max}*) by about 8,50 m in height (*2,4 x diameter*), and weight about 190 tons (*86 m³*)!

The present paper summarizes a large set of investigations developed in France in the last ten years on mechanical behaviour of rockfill, and rockfill dams, which not only provides rational answer to the above essential question, but also developed new results and applications to rockfill dam engineering, based on a size effects in mechanical behaviour due to grain breakage according to Fracture Mechanics, and its consequences on shear strength.

Scale Effects in Mechanical Behaviour due to Grain Breakage

Basic Representation of Grain Breakage

Basic representation of elementary grain breakage when internal forces evolve in granular media, may be summarized as follows – Fig.1a) and b) -:

- as contact forces increase, failure threshold is exceeded inside of some grains, where sudden propagation of pre-existing micro-cracks inside of grain material triggers failure, according to Fracture Mechanics, in Mode I or indirect tensile failure (similar to "Brazilian test");
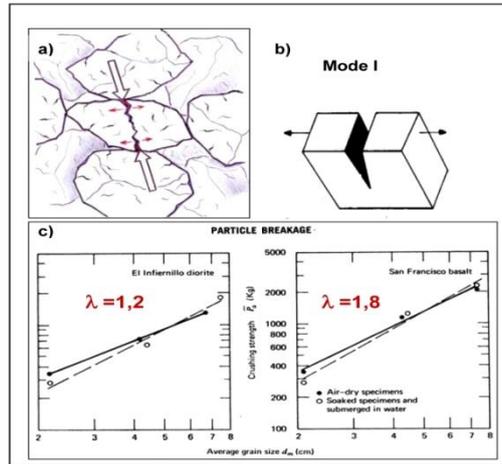

Fig. 1: a, b) Typical particle failure - c) Crushing strength typical results (Marsal)

- for a given mineral original stock, the statistical distribution of these flaws and of the resulting grain crushing strength, are ruled by a Weibull distribution, describing the probability of survival *Ps* within a population of grains of volume *V*, exposed to significant crushing stress σ;

$$P_s(V) = \exp\left[-\frac{V}{V_0}\left(\frac{\sigma}{\sigma_0}\right)^m\right]$$

(1)

now, representing "failure" as a given threshold of the probability of survival *Ps*, as grain volume V is proportional to the cube of its diameter *d*, this makes that the average crushing failure stress in the grains is a power function of their average diameter;

- a direct correspondence may be drawn with classical results of R. Marsal (1972, [3]) on direct grain crushing tests, showing that average force required for crushing gravels or rock pieces F_{cr}, Fig. 1c), is a power function of average particle diameter $\bar{d}$;

$$\bar{F}_{cr} = \eta.\bar{d}^{\lambda}$$

(2)

The comparison of both approaches lays a simple mean to fit a Weibull distribution parameter *m* for a given rockfill material, from a set of crushing tests on grains, gravels, rock pieces, etc., in function of their diameters:

$$\lambda = 2 - \frac{3}{m} \quad \text{or} \quad m = \frac{3}{2-\lambda}$$

(3)

In the wide range of materials investigated by Marsal, the exponent λ ranged between 1,2 and 1,8, with a *central value* about $\lambda=1,5$. This corresponds to a Weibull parameter *m* between 4 and 15, with a *central value* for this Weibull parameter about *m*=6.

Scale Effects in Macroscopic Shear Strength

Compilations of experimental results on shear strength of granular fills and rockfills, such as Leps compilation (1970, [4]) and others, have displayed a wide dispersion of results, and significant curvature of the shear strength envelope: the "internal friction" measured in triaxial compression tests, reduces significantly when confining stress is increased. This effect has been attributed to grain breakage, by comparing material gradations before / after shear tests: as grain breakage reduces the dilatancy of granular material during shear, the mobilized internal friction decreases, and when confining stress is increased, the grain breakage intensifies, which increases the incidence on shear strength.

An exceptional experimental work was reported by Marachi et al. (1969, [5]), including large size triaxial tests. Sets of triaxial tests were performed on three groups of materials coming from three mineral homogeneous stocks, whose gradations had been tuned to be geometrically similar, and compacted to the same density within each group. On the three groups of materials investigated by Marachi et al., Fig. 2 (solid lines), the diagram shows a clear size effect: the shear strength weakens when gradation becomes coarser.
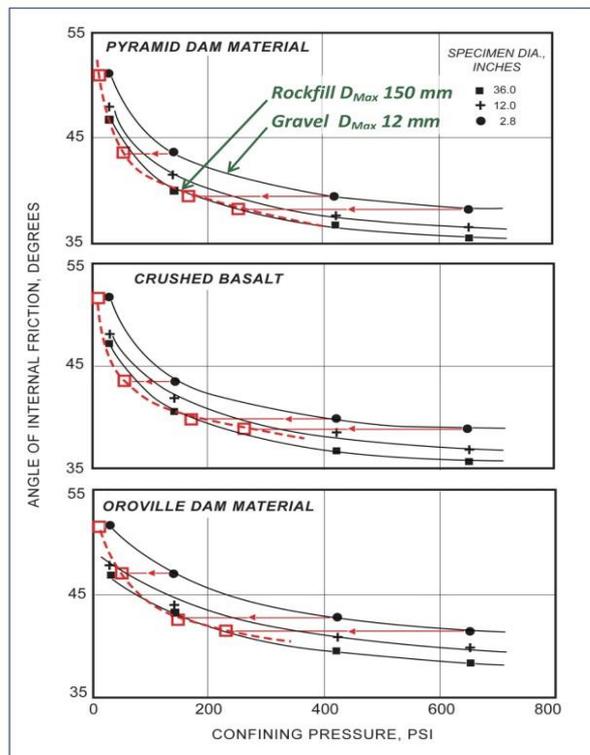

Fig. 2: Shear strength in sets of similar materials (from Marachi)

These groups of materials had been prepared in a way securing the conditions of geometrical similarity (in each group, similar gradations and same initial compacity). For this kind of situation of physical similarity, it has been shown through micromechanics (Frossard et al, 2012, [6]), that provided the grain breakage features are effectively represented as outlined above, then the shear strength envelopes of 2 materials shall correspond in a similarity of ratio (D1/D2)-3/m, where D1 and D2, are characteristics diameters of the 2 granular materials (for example the DMax).

Such transformed strength envelopes are drawn (red dotted lines) on the diagrams Fig. 2, extrapolating the data from tests on material DMax=12mm, in order to get a prediction of the envelope for material with DMax=150mm. The correspondence with the real experimental data is very satisfactory, and suggests that from shear testing performed on gravel sized material (here 12 mm max), with same initial compacity and geometrically similar gradations, it is

possible to determine the shear strength of rockfill made of quite coarser elements (here 150 mm max) from same mineral stock.

The method validity has been cross checked on other compilations and other granular materials (Frossard et al, 2012, [6]): it states a true size effect, of general impact, checked also by other investigators, under true three-dimensional stress-paths (Xiao et al.,2014, [7])

The Scale Effects Rule on Shear Strength Envelope

The similarity correspondence outlined above may be expressed in a true "Scale Effect Rule" operating on shear strength envelopes:

- considering two granular media constituted by the same homogeneous mineral material, compacted to same initial density, with geometrically similar gradations G_0 and G_1, characterized by a "characteristic diameter "D_0 $_{and}$ D_1 (for instance D_{Max}), our two granular media do correspond in a geometrical similarity with ratio D_1/D_0;

- if the shear strength envelope measured on granular medium G_0 is given by

$$\tau_{G0} = f(\sigma_n, D_{Max})$$
(4)

- Then the shear strength envelope for the granular medium G1, will be given by:

$$\tau_{G1} = \left(\frac{D_1}{D_0}\right)^{\frac{-3}{m}} \cdot f\left\{\sigma_n \cdot \left(\frac{D_1}{D_0}\right)^{\frac{3}{m}}, D_0\right\}$$
(5)

In the particular situation of a power law, or De Mello Criterion, the above Size Effect Rule leads to:

$$\begin{cases} \tau_{G0}(\sigma_n) = A_{G0} \cdot \sigma_n^b \quad \text{with } b < 1 \\ \Rightarrow \tau_{G1}(\sigma_n) = \left(\frac{D_1}{D_0}\right)^{\frac{-3(1-b)}{m}} \cdot \tau_{G0}(\sigma_n) = A_{G0} \cdot \left(\frac{D_1}{D_0}\right)^{\frac{-3(1-b)}{m}} \cdot \sigma_n^b \end{cases}$$
(6)

For this particular situation of a power law, the Scale Effect incidence occurs to be concentrated on the sole constant A (not in exponent b). Basically, this scale effect resulting from grain breakage is not specifically linked to any given formulation of shear strength, so its incidences may be drawn also for other formulations, such as Hoek & Brown Criterion [8].

The set of test compilations interpreted by this approach, have led also to assess a "central trend shear strength envelope" for rockfills with maximum stone diameter 150mm, with a parabolic formulation:

$$\begin{cases} \tau \approx 3,5 \cdot \sigma_n^{0,80} \\ \text{with } \tau \text{ and } \sigma_n \text{ in } kPa, \text{and for } D_{Max} \text{ 150mm} \end{cases}$$
(7)

A Rational Method for Evaluation of Coarse Rockfill Shear Strength Envelope

Furthermore, these results allow also the implementation of a rational method to evaluate the shear strength envelope of a given large size rockfill, on the basis of tests performed on gravel sized granular fill similar to the rockfill, produced from the same mineral stock, with reduced geometrically similar gradation, and compacted to same density [2]. This rational method brings a practical answer to the essential questions outlined above in the introduction: in good conditions, it allows the evaluation of shear strength envelope of rockfills up to D_{Max} 600mm, from triaxial testing on gravel sized fill not exceeding D_{Max} 40mm.

Scale Effects in the Behaviour of Large Rockfill Dams

The Question of Stability Assessment

In recent large rockfill dams, economic pressure has oriented design and construction trends towards using coarser gradations for the materials, in order to minimize quarrying costs, and towards using steeper slopes, in order to minimize the required materials volumes (*or at least to extrapolate slopes of mid-sized embankments to very large sized ones*). Because of above detailed testing limitations, the stability of such large works is mostly estimated through extrapolations with typical values for shear strength of materials, without real measurements.

So the incidence on stability of such trends –*coarser gradations, steeper slopes, higher embankments* -, deserves to be analysed.

The Fig. 3 summarizes these combined effects: starting from the Safety Factor of a mid-sized rockfill slope, built with height H_0, average rockfill gradation $G(D_0)$ and slope β_0, can we express the Safety Factor for a higher rockfill slope, built with height H, coarser gradation $G(D)$, and steeper slope β ?
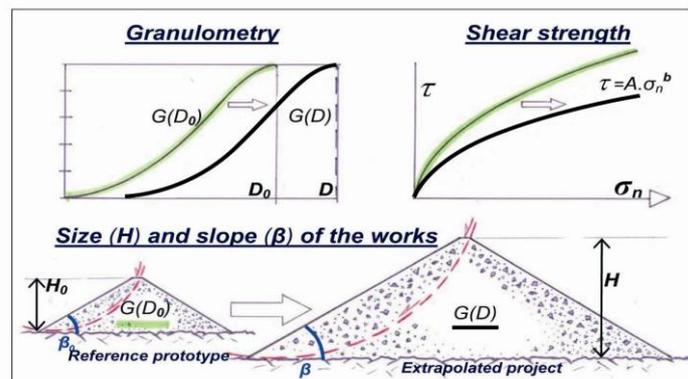

Fig. 3: The question of scale effects in stability assessment

Provided that considered materials have geometrically similar gradations, same mineral stock origin, and are compacted to the same density, the previously analysed Scale Effects brings part of the answer as regards material shear strength, key of slope stability matters. Associated with our results on Scale Effects, results published by Charles & Soares (1984) [12] on the stability of rockfill slopes against circular shear failures, analysed by Bishop method of slices, together with a power-law shear strength relation, bring other part of the answer to the above question of stability assessment (Frossard,2009, [2]).

Explicit Scale Effects in Safety Factors (Slope static Stability against Shear Failure)

Charles & Soares have shown that mathematical structure of static equilibrium equations of the problem, leads to write the Safety Factor (ratio between the available shear strength, versus the shear forces exerted in equilibrium conditions, along the most unfavourable potential slip line) in the following explicit form:

$$F_S = \frac{A.\varGamma^{(b,\beta)}}{(\gamma.H)^{(1-b)}}$$

(8)

This lays in separate factors height H, coefficient A of the power-law representing shear strength (Eq. (7)), and an adimensional stability coefficient $\varGamma$, depending on slope β and on exponent b of the shear strength relation. Numerical computations of this adimensional stability coefficient

Γ by Charles & Soares, reveal it is practically linear in function of slope $cotg\beta$, at least for usual range of slopes, between 1.2h/1v and 2h/1v. It follows that:

- the Safety Factor, for a projected slope in relation to a reference prototype, will be given by the relation

$$\frac{F_S}{F_{S_0}} = \left(\frac{H}{H_0}\right)^{(b-1)} \times \frac{A}{A_0} \times \frac{\Gamma_{(b,\beta)}}{\Gamma_{(b_0,\beta_0)}}$$

(9)

- the first factor gives directly the scale effect due to embankment height H_0;
- our Scale Effect Relation (Eq. (6)) on shear strength, allows to express the second factor explicitly in function of the gradations of constitutive materials;
- the quasi-linearity of the a-dimensional stability coefficient Γ in function of the slope $cot\beta$, allows to express the third factor in function of slope, through a linearization of Charles & Soares diagram of Γ.

The question of the Safety Factor for extrapolated project with higher embankment, coarser gradation, and steeper slope, compared with the reference prototype, may be answered now:

$$\frac{F_S(H,D,\beta)}{F_{S_0}(H_0,D_0,\beta_0)} \approx \left(\frac{H}{H_0}\right)^{(b-1)} \cdot \left(\frac{D}{D_0}\right)^{\frac{3(b-1)}{m}} \cdot \left(\frac{c+d.cot\beta}{c+d.cot\beta_0}\right)$$

(10)

As an example, considering a 250m high rockfill slope, with rockfill D_{Max}= 110cm, and slope 1.3h / 1v, extrapolated from a reference mid-sized prototype 125m high, with rockfill D_{Max}=45cm of same mineral origin and same compacity, and a slope of 1.4h/1v, together with our typical values for shear strength b=0,80, and m=6, and deduced from Fig. 4 diagram c=0,61 and d=1,25; the above relation (12) lays:

$$\frac{F_S(200m, D_{100cm}, 1.3h/1v)}{F_{S_0}(100m, D_{40cm}, 1.4h/1v)} \approx \frac{1}{1,37}$$

(11)

We note that the safety margin in the extrapolated project, results heavily reduced as compared with the reference prototype.

Compensation of Scale Effects on static Stability

Used in a reverse way, above relations for Safety Factors may be also used to determine constraints to be satisfied on gradations and slopes in projected works, in order to keep the Safety Factor at a given level, for example Fs=1,50, Fig. 4.
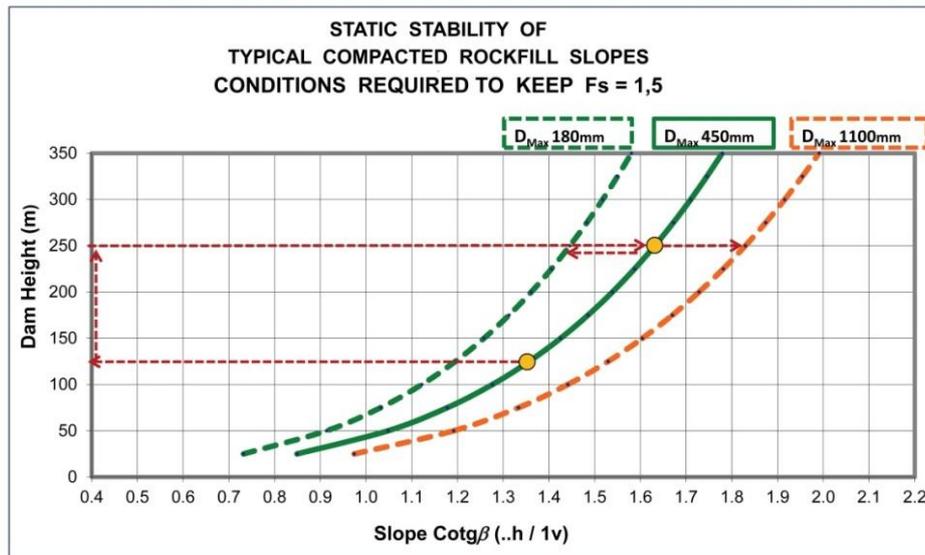
Fig. 4: Compensation of mixed Scale Effects related to dam height, slope, and rockfill size.

On this Fig. 4, designed from above typical values, and Scale Effect Relation (Eq. (6), (9), (10), unit weight γ 22kN/m3) starting from our reference prototype 125m high with 1,35h/1v slope and 450 mm rockfill satisfying the condition Fs=1,50, the extrapolation to a 250m high project results in:

- the 1,3h / 1v slope would be definitely too steep, unless to reduce strongly the maximum size of rockfill;
- should 450mm rockfill be kept for extrapolated 250m project, the slope should be flattened to about 1,63h / 1v, to comply with the same Safety Factor Fs=1,50;
- should coarser rockfill be preferred, for instance a 1100mm maximum size, then the slope should be flattened even more, to about 1,83h/1v, to keep this Safety Factor at Fs=1,50.

Incidences on deformation features
Beyond the incidences on shear strength and stability, grain breakage and resulting scale effects do play an important role in deformation features of rockfill, and rockfill dams. Indeed, grain breakage ease the deformation under given stresses, which result globally in weaker "rigidity modulus". Thus, assuming that grain breakage does play a key role in deformation behaviour of granular materials, then to get a same strain state in two granular media under physical similarity as considered above (section 2.3), it will be required to exert stress states satisfying the condition of a same global breakage rate. This condition, which applies on stress tensors, is identical to the one originating the scale effects displayed above:

$$\underline{\sigma}_1 = \underline{\sigma}_0 \cdot \left(\frac{D_1}{D_0} \right)^{-3/m} \tag{12}$$

This has been validated (Nieto, 2011, [11]) by analysis of stress-strain experimental curves of materials satisfying the above conditions of similarity (back analysis of results of Marachi et al. 1969). Fig. 5 displays the case of the material used for construction of Pyramid Dam:

- the dotted red line represents the estimation calculated by this method, for the coarser material (D_{Max} = 6in., 150mm approx.), on the basis of experimental data for "reduced material" (D_{Max} = 0,47in., 12mm approx.) dashed blue line;

- this estimation is to be compared with experimental data for coarser material, represented by the solid blue lines.
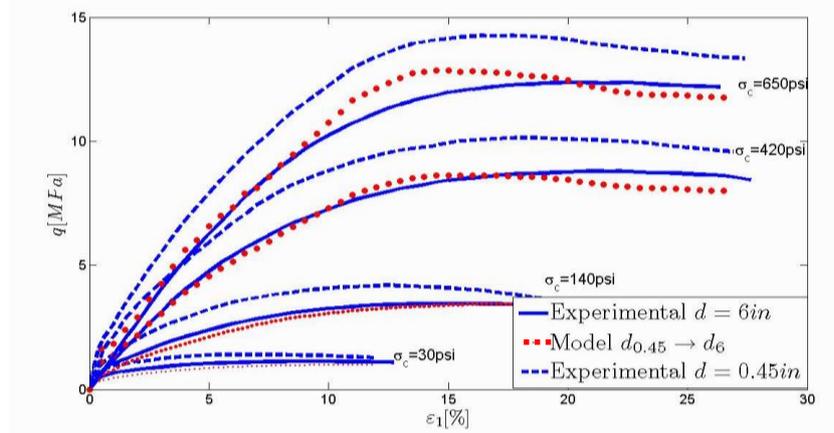

Fig.5: Scale effects on stress-strain curves (material from Pyramid Dam)

Thus, in complement to above section 2.3, this method allows to estimate also stress-strain curves of rockfill up to $D_{Max} = 600$ mm, from triaxial tests on gravel not exceeding $D_{Max}=40$ mm. This condition applies also to the apparent rigidity modulus of both granular media:

$$E_1 = E_0 \cdot \left(D_1 \big/ D_0 \right)^{-3/m} \tag{13}$$

This relation on apparent rigidity modulus has been validated by various results of measurements performed on constructed embankments and dams [2]. It has been shown also that it participates to explain the sensitivity of large CFRD dams to the risks of failure of the concrete facing by excessive strains within the underlying rockfill (Frossard,2012, [8]).
Last, these scale effects have been incorporated in a new constitutive model, applied to detailed modelling and refined analysis of the pathology occurred in commissioning large CFRD type dams (Yuguang, 2012, [12]). The results found, particularly on a new detailed model of Mohale dam behaviour, do confirm that these scale effects have without doubt played a significant role in the observed strains, and their consequences (Yuguang et al, 2014, [13])

Conclusions

The bulk of the above results, on which more precisions and details will be found in the selected bibliographic references, do improve significantly our knowledge of behaviour of rockfill and rockfill dams. In author's opinion, this would deserve more extended experimentations, in order to widen the data base, provide wider support to the trends already found, and make clear the limits of the method.

References

[1]   CBDB-ICOLD (2007) Symposium on CFRDs Honouring Barry Cooke- Florianopolis, Brazil,

[2]   Frossard E. (2009)   On the structural safety of large rockfill Dams-Proceedings XXIII° ICOLD, Q.91-R39, Brasilia, May 2009

[3]   Marsal R. (1972) Mechanical Properties of Rockfill – In Embankment Dam Engineering –Casagrande Volume, 109-200 - Wiley, New York -

[4]   Leps T. M. (1970) Review of The Shearing Strength of Rockfill, J. Of Soil Mech. & Found. Div. ASCE, Vol 96 – N° SM 4, 1159-1170

[5]   Marachi N.D., Chan C.K., Bolton Seed H., Duncan J.M. (1969) Strength and Deformation of Rockfill - Report N° Te-69-5 Dept. Of Civil Engng./Geotechn. Engng.-Univ. Of California-Berkeley.140p.

[6]   Frossard E., Hu W., Dano C., Hicher P.Y. (2012) Rockfill shear strength evaluation: a rational method based on size effects -Géotechnique Vol. 62, n°5, 415-427

[7]   Xiao Y.,Liu H., Chen Y., Zhang W. (2014) Particle size effects in granular soils under true triaxial conditions- Géotechnique, Vol. 64, N°8, 667-672

[8]   Frossard E. (2012) Granular Materials in Civil Engineering: Recent Advances in the Physics of their mechanical Behaviour, Applications to Engineering- in Multiscale Geomechanics–, Dir. P.Y Hicher, ISTE-Wiley, Chap.3 p.35-81, ISBN 978-1-84821-246-6 -

[9]   Charles J.A., Soares M.M. (1984) Stability of compacted rockfill slopes- Géotechnique, Vol. 34, N°1, 61-70 –

[10]   Maranha Das Neves E. (1994) Advances in Rockfill structures- Kluwer Publ (Nedl.)-

[11]   Nieto C. (2011) Mechanical behaviour of Rockfill – Applications to Rockfill Dams – PhD Thesis- Ecole Centrale Paris

[12]   Yuguang C. (2012) Modélisation du comportement mécanique des grands CFRD- Identification des caractéristiques des enrochements et comportement du masque d'étanchéité amont- PhD Thesis – Ecole Centrale Lyon -

[13]   Yuguang C., Fry J.J., Laigle F., Vincens E. Froiio F. (2014) Assessment of face slabs cracks in high CFRD using L&K Enroch model. Hydropower & Dams, Issue 1, 63-68

Numerical analysis of concrete faced rockfill dams using gradient plasticity

Dakoulas, P., Stavrotheodorou, E. and Giannakopoulos, A.E.

Department of Civil Engineering, University of Thessaly, Volos 38334, Greece

ABSTRACT: The behaviour of concrete face rockfill dams is investigated numerically using Lade's constitutive model, which allows a realistic simulation of the stress-strain and volumetric-shear strain behaviour of rockfill in a wide range of confining stresses. The model is implemented in ABAQUS employing the Runge-Kutta-Dromand-Prince integration scheme. An enhancement based on gradient plasticity is proposed for preventing numerical difficulties on specific elements subjected to high shearing. The study examines the performance of two 200m-high CFRDs built in a narrow canyon, the first made of excellent quality rockfill and the second of average quality rockfill. The analysis simulates the staged construction, impoundment and anticipated creep and dynamic settlements. Similar analyses are repeated for dam heights of 100m and 300m, and the results are compared with field measurements. The study shows the effect of rockfill stiffness and dam height on the compressive stresses in the slab and relates the location of such high compression to the location of observed concrete slab failures in specific dams. It is concluded that the use of excellent quality rockfill at small void ratios (0.2) results to small construction settlements and relatively small deflections and compressive stresses in the slab even in the case of extra tall (300 m) dams.

E-mail: dakoulas@uth.gr

Introduction

Designed to prevent water leakage into the interior of the dam, the concrete face slab is the most critical element in the performance and safety of concrete face rockfill dams (CFRDs). Naturally, its behaviour depends significantly on the deformational response of the underlying gravel and rockfill materials. Recent incidents of crack development in the concrete face slab observed in high CFRDs, such as the 202m-high Campos Novos Dam (Brazil), the 186m-high Barra Grande Dam (Brazil) and the 145m-high Mohale Dam (Lesotho), are attributed to excessive deformation of the rockfill material. For example, Campos Novos Dam that was built from basalt rockfill having a low average modulus of 50-60 MPa [11], experienced failure of the central vertical joint due to compression along the vertical joints during impoundment, as shown in Fig. Due to compression in the longitudinal direction of the panels, several panels experienced shifting and superposition by 0.12 to 0.15 m at about 30% to 40% of the dam height over a length of 300 m (Fig. 1). As a result, there was rupture of the water stops and significant leakage of about 1500 lt/s. For dams in earthquake regions, seismic transient stresses and additional stresses due to accumulated dynamic settlements may increase further the compression along the walls of the vertical joints causing shear failure spalling [3,4], as in the case of the 156m-high Zipingpu Dam (China) during the May 12, 2008 Wenchuan earthquake [7,13].

Undoubtedly, proper modelling of the deformational characteristics of the underlying rockfill materials under generalized loading conditions is essential to successful face-slab performance predictions. During the past decades, the analysis of CFRDs has been based on simplified constitutive models for the rockfill material, such as the widely used hyperbolic Duncan and Chang model [5,6]. The main advantage of the latter model is the considerable accumulated experience regarding the required parameters for various types of rockfill materials, for which laboratory testing is difficult [6]. However, this is a simple model based on nonlinear elasticity, which is incapable of representing some important aspects of soil behaviour such as the dilation and softening during shear.
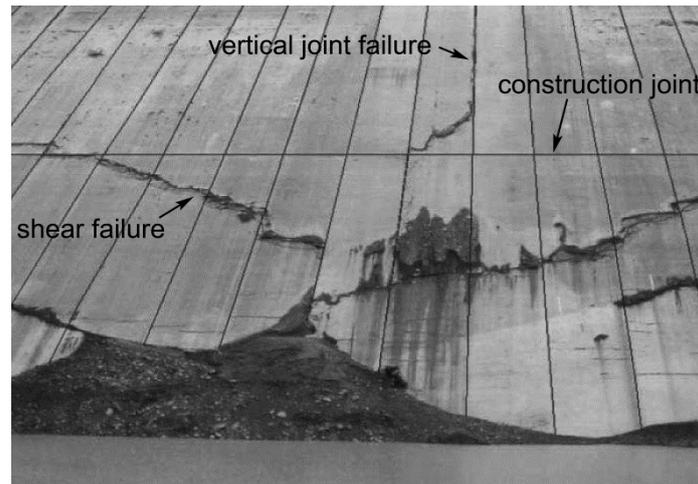
Fig. 1: Concrete face slab failure due to compression at Campos Novos Dam

This study uses Lade's elasto-plastic model for the rockfill materials subjected to a wide range of confining stresses. In addition, it employs an optional gradient plasticity tool for improving numerical stability in regions of intense material softening behaviour.

Numerical model

Lade's model for rockfill
Lade's elasto-plastic isotropic hardening model with a single yield surface has been developed based on extensive sets of data from experiments on frictional materials including sand, clay, concrete and rock [8]. The model adopts a single yield surface, which is shaped as an asymmetric tear-drop, with the pointed axis at the axes origin in the stress space. The value of the plastic work derived from both shear and volumetric strains is the hardening parameter that is used to define the yield surface characteristics. The model adopts a non-associated flow rule based on a potential function that is shaped as a cigar with an asymmetric cross-section. Although the model is primarily aimed at frictional materials, a cohesion term may be easily accommodated by an appropriate shift of the axis of origin in the principal stress space. A detailed description of its incremental form is given by Lade and Jakobsen [8]. The 3D principal stress space formulation of Lade's model is implemented here as a user-defined material in the finite-element program ABAQUS [1]. Due to better accuracy and lower computational cost, the present study adopts the Runge-Kutta-Dormand-Prince scheme for Lade's constitutive model implementation in the three-dimensional principal stress space.

Gradient plasticity
Strain localization in granular materials is associated with plastic strain concentration in narrow shear bands and rupture. For the analysis of earth and rockfill dams, such plastic strain concentrations may develop near the abutments and along sharply inclined interfaces of material zones of different stiffness. Here, a simple gradient theory by Bassani [2] is adopted merely for the purpose of preventing numerical difficulties at critical locations. This methodology allows a local increase of hardening in finite elements experiencing very intense plastic strain gradient, as described below. Based on the gradient of the equivalent deviatoric plastic strain e_q^p within a finite element, a coefficient c_1 is computed from the expression

$$c_1 = \left[1 + l^2 \left(\frac{g_r}{\gamma_0} \right)^2 \right]^{1/2} \tag{1}$$

where l = intrinsic length scale, which may be the average or maximum particle diameter; γ_0 =reference strain, representing the range of the essentially elastic region of the material; and g_r =the norm of the gradient of e_q^p. The coefficient c_1 is used to modify the hardening behaviour of the material in two different ways:

(a) The plastic modulus H is modified as follows

$$H^* = \begin{cases} Hc_1 & \textit{for hardening} \\ H/c_1 & \textit{for softening} \end{cases} \tag{2}$$

thereby increasing the hardening modulus or decreasing the softening modulus at elements with high values of g_r.

(b) In the case that some small artificial cohesion a is used for numerical stability, the effective cohesion is modified as $a^* = ac_1$. This artificial cohesion, which takes relatively small values (e.g. $a = 5$ kPa) compared to the rockfill shear strength, may be helpful for numerical stability during the simulation of the staged construction of the embankment slopes. Note that for uniform distribution of the equivalent deviatoric plastic strain, $c_1 = 1$. This simple gradient plasticity scheme has been proven to be effective in preventing numerical problems associated with local element straining associated with abrupt change in material stiffness near the abutments or interfaces.

Gravel behaviour

Two actual rockfill materials with quite different stiffness characteristics are considered:

(a) Rockfill A: an excellent quality rockfill based on data from the shell of Oroville Dam [10]. Its particles are well rounded to rounded, well graded, having very high strength and isotropic behaviour. This material was selected due to its high strength and very low compressibility, resulting to the excellent observed performance of Oroville Dam.

(b) Rockfill B: a medium quality rockfill based on data from the shell of Pyramid Dam [10]. The rockfill particles are relatively angular, poorly graded, weak and anisotropic with respect to their strength. This material was selected to represent a rockfill of medium to relatively high compressibility.

The derivation of Lade's model parameters for each of the two materials was based on published results from isotropic compression and four triaxial compression tests at confining stresses equal to 207, 965, 2896 and 4413 kPa, on specimens with maximum particle diameter equal to 0.15m and specimen diameter equal to 0.914m. The derived Lade's model parameters are given in Tables 1 and 2 (corresponding to zone 3B) for each of the two rockfill materials, respectively. Due to lack of space, Fig. 2 presents representative comparison of the experimental data (circles) and model predictions (solid curves) on the stress-strain behaviour and volumetric strains from triaxial compression tests of rockfill A at only two of the four confining stresses, namely at 207 kPa and 2896 kPa. Similarly, Fig. 3 plots the experimental data and the model predictions for rockfill B at 207 kPa and 2896 kPa. The results in Figs. 2 to 3 show that the model can capture in a realistic way the stress-strain behaviour and the volumetric strain at various levels of confining stress for both rockfill materials.
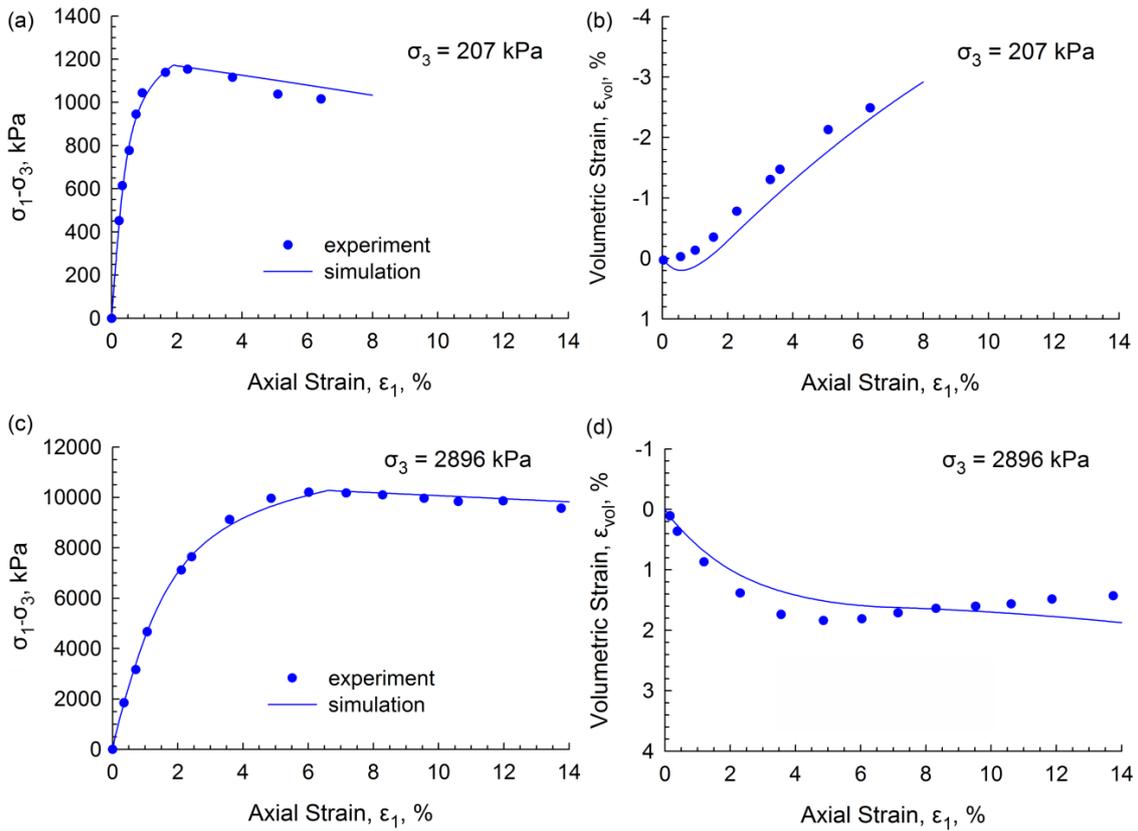
Fig. 2: Rockfill A: Experiments and numerical predictions from triaxial compression tests at confining stress of 207 kPa and 2896 kPa
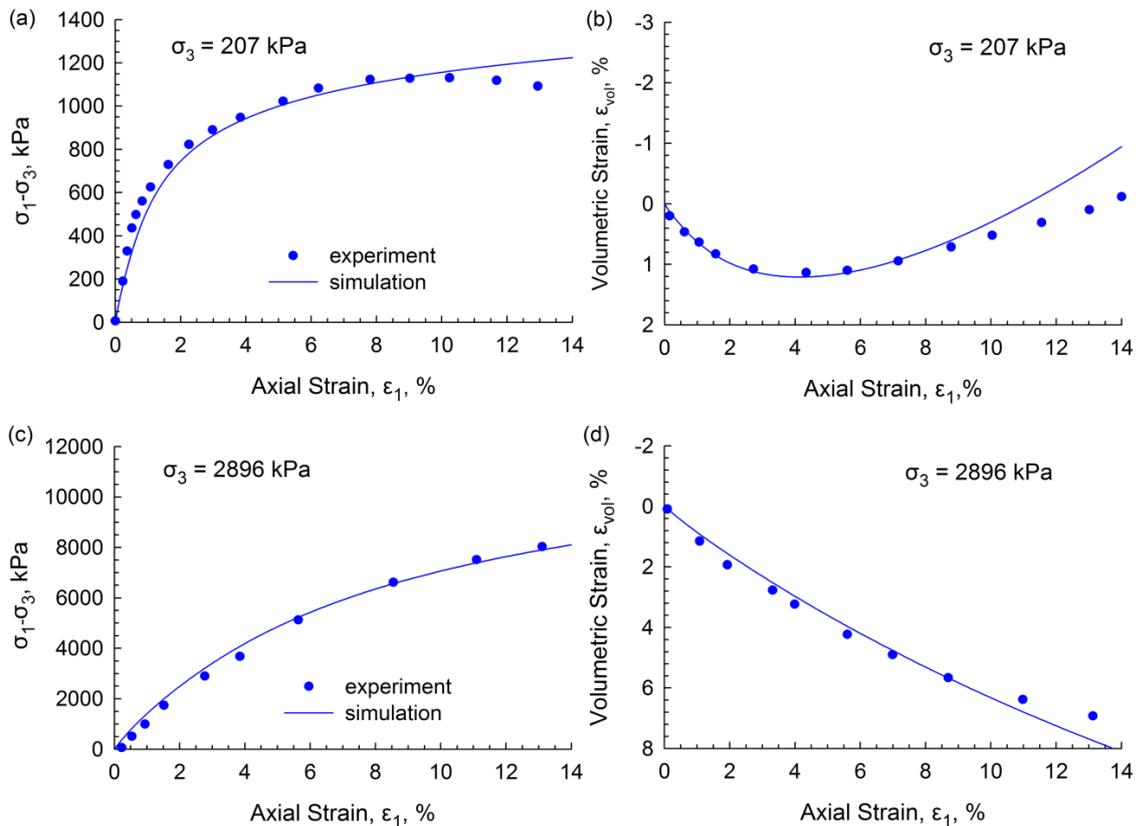

Fig. 3: Rockfill B: Experiments and numerical predictions from triaxial compression tests at confining stress of 207 kPa and 2896 kPa

Concrete behaviour
The damage plasticity constitutive model for concrete by Lee et al. [9] is used for modelling the behaviour of the slab panels. The model takes into account the effects of strain softening, distinguishing between the damage variables for tension and compression. Moreover, it incorporates a degradation mechanism that represents the effects of damage on the elastic stiffness and its recovery of after crack closure. Fiber-reinforced concrete is used for the face slab by mixing plain concrete of compressive strength 37 MPa and fiber corresponding to a reinforcing index 2.5%. Based on Nataraja et al. [11], the fiber-reinforced concrete is estimated to have compressive strength of 42.4 MPa and tensile strength of 3.7 MPa.

Dam geometry
Fig. 4a illustrates the cross-section and the material zones of the dam, which has a height of 200 m and is built in a narrow canyon of trapezoidal shape with aspect ratio equal to L/H=2. The main material zones considered for the numerical analysis are the upstream rockfill zone 3B, the downstream rockfill zone 3C and the transition gravel zone 2B beneath the slab. The material properties for each zone are given in Tables 1 and 2, corresponding to the rockfill materials A and B, respectively. The upstream slab consists of 28 independent concrete panels. The slab panels have a width of 15 m and a variable thickness given by $t = 0.30 + 0.003h$, where h is the height of the overlying water. Fig. 4b illustrates the numerical discretization of the half of the dam geometry considering its symmetry with regard to mid-section.
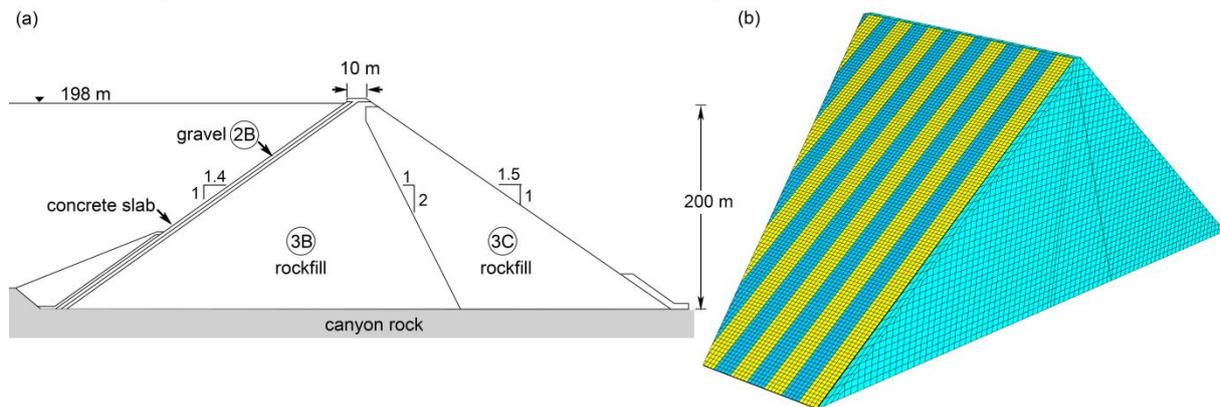

Fig. 4: (a) Cross-section and material zones (b) Numerical model of the 200m-high dam

Tab. 1. Model parameters for dam built with rockfill type A

Zone	ρ Kg/m^3	m	η_1	M	λ	v	ψ_2	μ	C	p	b	h	α
3B	2435	0.3	167.3	1340	0.19	0.24	-3.06	2.7	4.2 10^{-5}	1.7	0.2	0.85	0.6
2B	2435	0.3	167.3	2010	0.19	0.24	-3.06	2.7	4.2 10^{-5}	1.7	0.2	0.85	0.6
3C	2435	0.3	167.3	1005	0.19	0.24	-3.06	2.7	4.2 10^{-5}	1.7	0.2	0.85	0.6

Tab. 2. Model parameters for dam built with rockfill type B

Zone	ρ Kg/m^3	m	η_1	M	λ	v	ψ_2	μ	C	p	b	h	α
3B	2150	0.239	163.0	700	0.12	0.24	-3.06	3.0	1.2 10^{-4}	1.8	0.1	0.70	0.8
2B	2150	0.239	163.0	1050	0.12	0.24	-3.06	3.0	1.2 10^{-4}	1.8	0.1	0.70	0.8
3C	2150	0.239	163.0	525	0.12	0.24	-3.06	3.0	1.2 10^{-4}	1.8	0.1	0.70	0.8

Analysis and results

Figs. 5a and 5b plot the distribution of settlements at the end of construction for the two dams made of rockfill A and B, with maximum settlements equal to 0.60m and 1.99m, respectively. The behaviour of the dam made of rockfill A (Oroville material) appears to be excellent, with a maximum settlement to height ratio $S_c/H = 0.30\%$. This is comparable to the settlement ratio of the actual 244m-high (earth-core rockfill) Oroville dam (California) that was $S_c/H = 0.31\%$. On the other hand, the behaviour of the Pyramid rockfill dam is rather average with a settlement to height ratio $S_c/H \approx 1\%$. Fig. 6 shows the effect of dam height and rockfill stiffness on the maximum construction settlement, based on the numerical predictions of three dams having heights equal to 100m, 200m and 300m, considering both rockfill A (blue circles) and rockfill B (blue triangles). The shaded area represents the range of variation between the two different qualities of rockfill. Also shown in Fig. 6 are available measurements of construction settlements from existing CFRDs with void ratios e between 0.18-0.25 (circles) and between 0.25-0.31 (triangles). Moreover, the construction settlements of Campos Novos, Barra Grande and Mohale dams, which experienced failure in the concrete slab during first impoundment, are shown in the figure. All reported measurements in Fig. 6 correspond only to dams in narrow canyons with a shape factor $0.9 < A_s/H^2 < 4$.
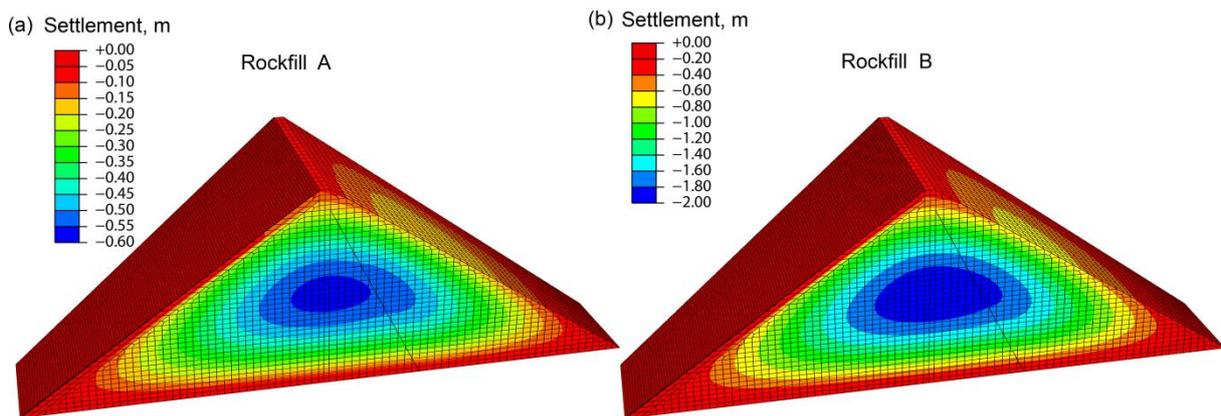

Fig. 5: Construction settlements for the dam made of (a) rockfill A and (b) rockfill B.
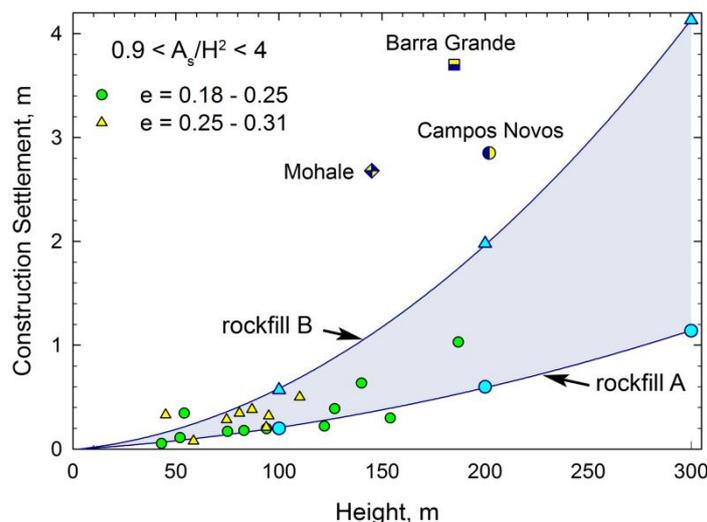

Fig. 6: Computed and measured construction settlements of rockfill compacted at different void ratios versus dam height (for dams in narrow canyons).
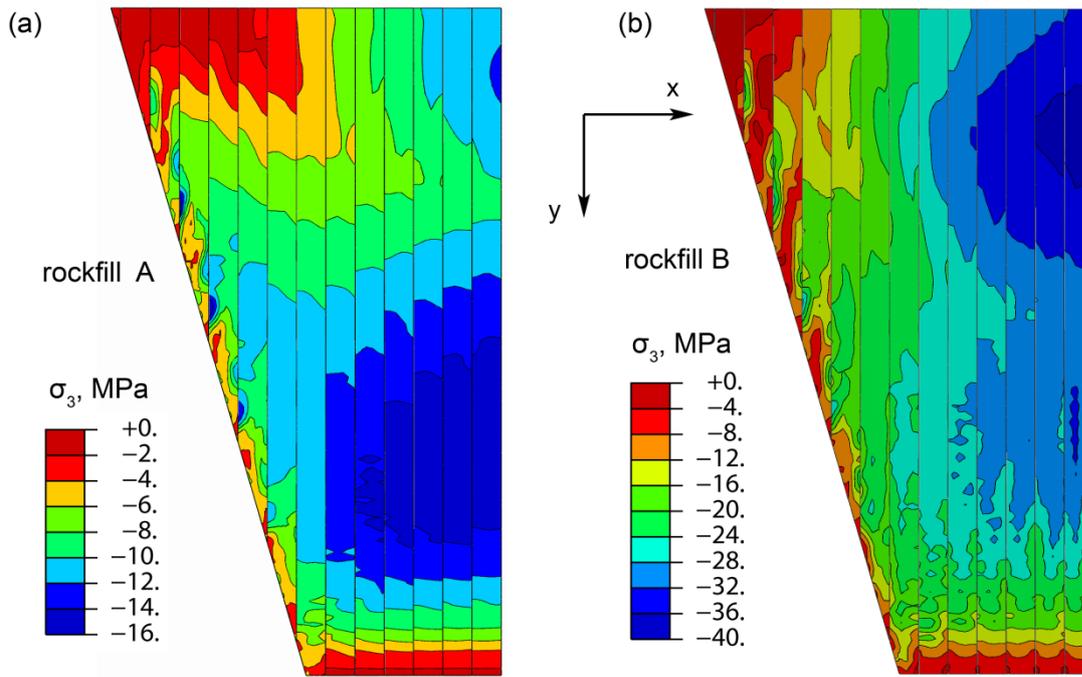
Fig. 7: (a) Cross-section and material zones (b) Numerical model of the 200m-high dam
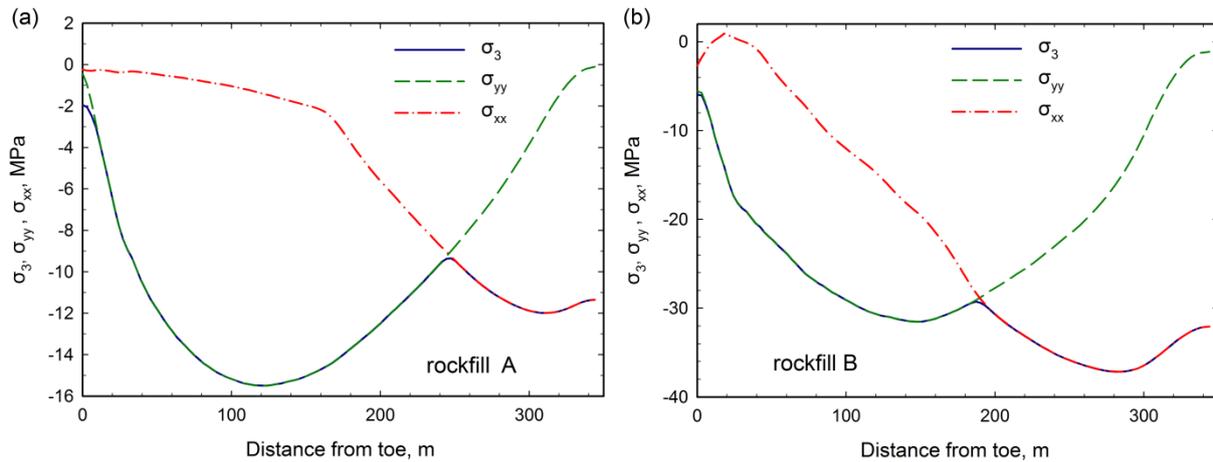

Fig. 8: (a) Cross-section and material zones (b) Numerical model of the 200m-high dam

It is evident from Fig. 6 that dams compacted to lower void ratios tend to yield settlements that are closer to the results of rockfill A, whereas dams compacted to higher void ratios yield settlements that are closer to those of rockfill B. It is also shown that the construction settlements of Campos Novos, Barra Grande and Mohale dams are much higher than the range of the measured and numerically predicted settlements.

The maximum post-impoundment settlement, consisting of creep and possible dynamic settlements, is assumed here to be equal to 50% of the maximum construction settlement. Fig. 7 plots the distribution of maximum compressive stresses in the slab due to post-impoundment settlements. Moreover, Fig. 8 plots the distribution of the minor principal stress σ_3, and stresses σ_{yy} and σ_{xx} (see directions x, y in Fig. 7) along the length of concrete panel at mid-section. The results show the maximum compression due to impoundment occurs due to stresses σ_{yy} in the longitudinal panel direction, at about 40% of the dam height. By contrast, the maximum compression due to post-impoundment settlement is caused by increase in σ_{xx} at the upper part

of the slab. Based on results from all analyses, for extra tall dams this increase of σ_{xx} is more critical than the maximum compression given by σ_{yy}.

Conclusions

1. The use of Lade's constitutive model for modelling the behaviour of rockfill allows a very realistic simulation of the experimental results in terms of the stress-strain behaviour and volumetric strains in a very wide range of confining stresses.
2. The use of excellent quality rockfill at small void ratios (0.2) results to small construction settlements and relatively small deflections and compressive stresses in the slab even in the case of extra tall (300 m) dams.
3. The design of CFRDs of average-quality, compressible rockfill at heights equal or larger than 200m is not recommended, unless special provisions are undertaken.

Acknowledgements

References

[1] ABAQUS (2014). Users' Manual, Simulia, Providence, RI, USA.
[2] Bassani JL. (2001). Incompatibility and a simple gradient theory of plasticity, Journal of Mechanics and Physics of Solids, 49:1983-1996.
[3] Dakoulas P. (2012) Nonlinear seismic response of tall concrete faced rockfill dams in narrow canyons, Soil Dynamics and Earthquake Engineering, 34:11-24.
[4] Dakoulas P. (2012). Longitudinal vibrations of tall concrete faced rockfill dams in narrow canyons, Soil Dynamics and Earthquake Engineering, 41:44-58.
[5] Duncan JM, Chang CY. (1970). Nonlinear analysis of stress and strain in soils, J. of Soil Mech. and Found. Engineering, ASCE; 96(5):1629-1653.
[6] Duncan JM, Byrne P. Wong K, Mabry P. (1980). Strength, stress-strain and bulk modulus parameters for finite element analyses of stresses and movements in soil masses, Report UCB/GT/80-01, Univ. of California, Berkeley, Ca, USA.
[7] Guan Z. (2009). Investigation of the 5.12 Wenchuan Earthquake damages to Zipingpu Water Control Project and an assessment of its safety state, Science in China, Series E, Technological Sciences, 52(4):820-834.
[8] Lade PV, Jakobsen KP. (2002). Incrementalization of a single hardening constitutive model for frictional materials, Num. and Anal. Methods in Geomechanics, 26:549-659.
[9] Lee J, Fenves GL. (1998). A plastic-damage concrete model for earthquake analysis of dams, Journal of Earthq. Eng. & Struct. Dynamics, 27: 937-596.
[10] Marachi ND, Chan CK, Seed HB. (1972). Evaluation of Properties of Rockfill Materials, J. of Soil Mech. and Found. Div., ASCE, 98:95-114.
[11] Nataraja MC, Dhang N, Gupta AP. (1999). Stress-strain curves for steel-fiber reinforced concrete under compression, Cement & Concrete Composites, 21:383-390.
[12] Sobrinho JA, Xavier LV, Albertoni C, Correa C, Fernandes R. (2007). Performance and concrete repair at Campos Novos, Hydropower Dams, 2.
[13] Wieland, M. (2009). Concrete faced rockfill dams in highly seismic regions, 1st Intern. Symposium on Rockfill Dams, Chengdu, China, October 18-21.

Stability of concrete dams - Some basic requirements

Amberg F.

Lombardi Engineering Ltd., Via R. Simen 19, P.O.Box 1535, CH-6648 Minusio, Switzerland

ABSTRACT: The safety of dams is based on proper design and construction, while the monitoring allows to subsequently verify if the behaviour is regular or if unforeseen phenomena need to be re-evaluated. The paper exposes some basic issues related to the safety of concrete dams.

The stability of gravity dams depends primarily on the slenderness of the structure and on the condition of the lateral blocks when taking the effect of the valley slope inclination into account. This last aspect is somehow neglected by the classical design approach, but in certain conditions it might present a potential failure mode.

The stability of arch dams depends on the other hand on the arch effect under compression and on the integrity of the structure near the foundation due to the role of the shear forces on crack stability.

Finally, a relevant challenge is the assessment of the foundation. The rock quality by itself defined involving usual rock mechanical approaches does not present a reliable parameter. Actually, it is the discontinuities that play a determinant role and which therefore have to be taken duly into account.

The paper concludes with some considerations on monitoring and the long term behavior of dams focusing in particular on possible impacts of concrete swelling on the structural safety.

E-mail: francesco.amberg@lombardi.ch

Introduction

The present paper aims to give an overview of relevant aspects related with the safety of concrete dams and of some current topics linked to their monitoring and long term behavior.

First, the structural robustness of concrete dams is considered by addressing the main aspects that finally allow to guarantee their stability. Specific issues for gravity dams, for arch dams as well as for the foundation are individually presented, emphasizing the potential damage mechanisms that have to be faced with appropriate analysis approaches. To design an economic dam that behaves without problems, there are further aspects that have to be considered, as for example the control of thermal cracking. But these minimum requirements are mandatory and should be verified with higher priority. Unfortunately, this is in practice not always the case and several codes do also surpass some of the aspects here presented.

The realization of a solid structure is fundamental, the prerequisite for safety, but the situation might also change during the service life. The monitoring and the maintenance are therefore equally important to the solid nature of the structure. The concrete expansion is one typical occurrence that might change the state and the safety of a dam.

Stability of gravity dams

When the stability of a gravity dam is verified without taking the tensile strength into account, it is possible to identify the threshold when the concrete weight by itself becomes insufficient, so that the dam stability cannot anymore rely exclusively on the gravity force.

Fig. 1 shows how the stability against overturning and against sliding changes as a function of the inclination of the downstream dam face. The upstream dam face is vertical, the unit weight of concrete varies between 23.5 and 24.5 kN/m^3 and the shear strength is provided only by friction, assumed to be at its residual angle of 48° according to [1].
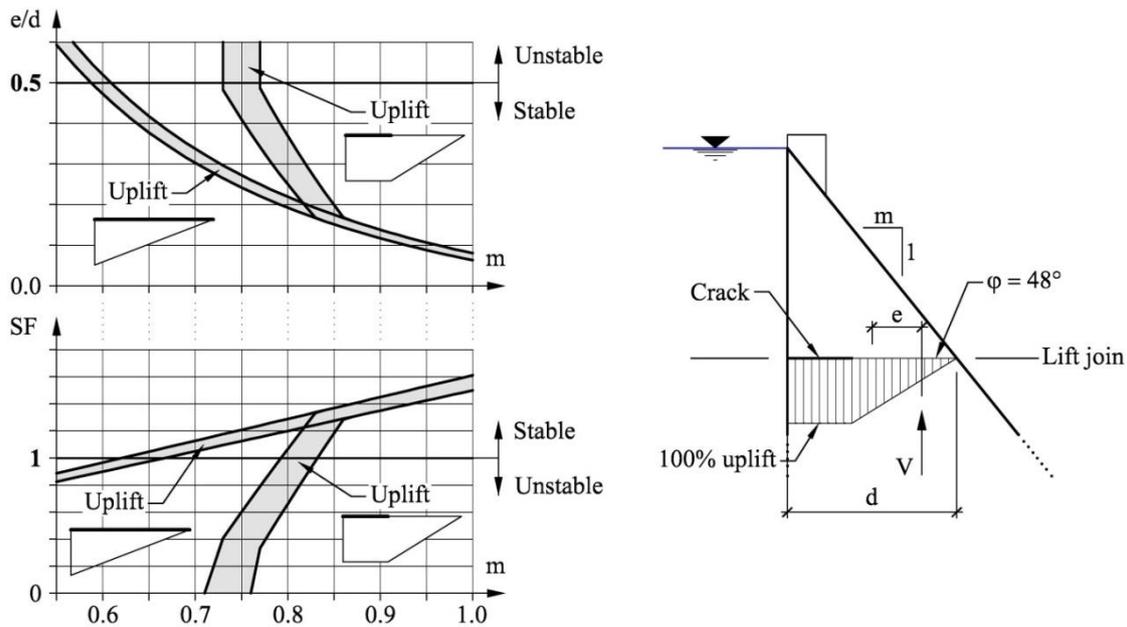
Fig. 1: Stability of gravity dams: overtopping (upper graph) and sliding (lower graph).

Two assumptions are made for the uplift pressure in case of crack initiation at the upstream face. Following the first, more conservative assumption, the pressure within the crack corresponds to the full water pressure, which then decreases linearly through the remaining section. In the second hypothesis the uplift pressure simply varies linearly from 100% at the upstream to 0% at the downstream face. The first distribution is expected in case of a dam partially cracked in its upstream part, while the second one corresponds to the case of constant permeability, i.e. if a dam is completely cracked at a certain elevation. The second assumption is rather unlikely and also not particularly conservative since the permeability probably progressively reduces towards downstream direction with the increase of the vertical compression. However, the crack opening might be quite complex as it is the case of dams affected by concrete expansion [2].

According to Fig. 1 a gravity dam is stabilized exclusively by its own weight if the downstream dam face is inclined less than 0,80 to 0,84 (values for m in Fig. 1). The sliding becomes the determining criterion due to the conservative value for the residual shear strength assumed on the horizontal lift joints. In case of a higher shear strength or inclined lift joints, the overturning might become critical if the dam thickness is less than 73 to 77% of the height. These basic stability criteria might actually allow to significantly simplify the required gravity dam analyses.

It is interesting to observe that some gravity dams, in particular those of limited height, show thicknesses of 60% of the height or even less. The stability of these dams depends actually on the tensile strength. The well know case history of Bouzey gravity dam in France, that collapsed in 1895, was quite slender and according to Fig. 1 not stable. One should always consider the possible loss of the tensile strength, as it occurs in case of cracking during an earthquake or due to concrete expansion.

At the interface between concrete and rock, on the other hand, dominate unfavourable conditions that are too often overlooked. The stability of the lateral blocks is in fact influenced by the valley slope. Here the vertical dead load force, which gives a stabilizing effect by friction, decomposes into a normal and a shear component to the inclined interface (N and T in Fig. 2), causing a twofold reducing effect on stability: the normal stabilizing force reduces while the

shear component increases compared to the situation on an horizontal shear plane. Furthermore the uplift force increases as the foundation surface increases (see Fig. 2).
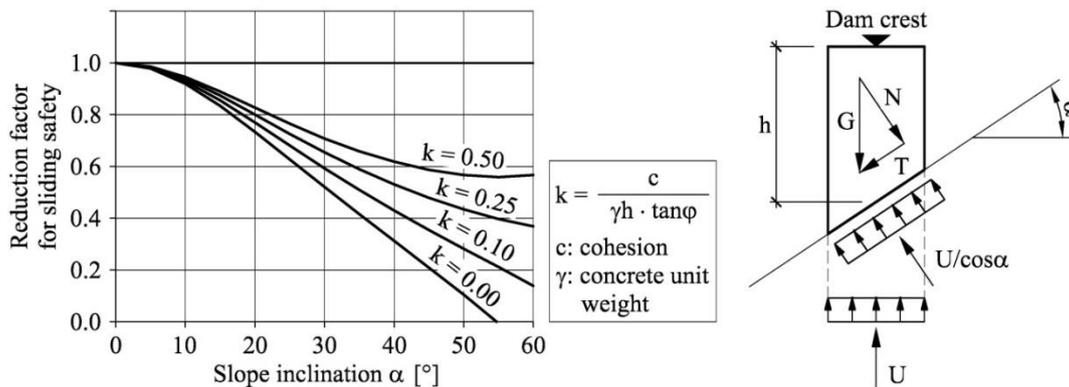

Fig. 2: Impact of the slope inclination towards the river on the sliding safety factor of an independent block (inclination of downstream face 0.8:1, uplift reduced at 80%).

The equilibrium of a single block resting on the slope is easily defined, but the consequent conclusion might most probably give an insufficient sliding stability. The possible interaction between the lateral blocs of a dam needs therefore to be taken into account. A possible analysis approach was proposed by Lombardi [3], but the actual equilibrium is quite uncertain. The lateral component T can be supported for one part by the adjacent block, and transferred towards the central part of the dam, and another part is directly taken by shear strength at the foundation. However, this latter will in turn reduce the available strength against sliding in downstream direction.

The amount of the lateral shear force transferred to the foundation is not simply defined a priory, but it depends on the process of construction, the eventual grouting of the vertical contraction joints, the thermal state (the thermal expansion in summer pushes the lateral blocks towards the river and reduces the mentioned shear strength), the loading condition as well as the relative rigidity between dam and foundation.

Independent from the most probable equilibrium in normal operating conditions, one can also assume that at limit of stability, when the dam is sensitive to downstream movement, the full strength tends to turn in upstream direction, i.e. in opposite direction to the movement. This is certainly acceptable, but in this case one has to take the cohesion conservatively into account, since it likely reduces with failure. The uplift pressure needs also to be re-evaluated at sliding limit.

Considering these aspects, it becomes clear that it is quite difficult to advise how to perform this type of analysis properly, and it should be kept in mind that the results are variable in function of the hypothesis considered. Concluding, it can be stated that the stability of a gravity dam is not as straight forward as it may appear and that its assessment requires a sound engineering judgment and not only the fulfilment of pre-defines rules.

Stability of arch dams

The stability and the safety within the body of an arch dam depends basically on the following two major elements:

- The strength margins on the compression of the arches;
- The integrity of the concrete sections near the foundation (crack stability with respect to the shear forces).

The first point needs simply to be verified by common structural analyses and is generally not so critical. Preliminary assessments can also be made according to the Lombardi's slenderness coefficient [4], [5].

Due to the clamping effect, an arch dam may be subjected to crack near the foundation. The effect of this cracking is not so relevant for the dam stability, unless the shear force is high compared to the normal force. Bending cracks develop nearly perpendicular to the mean axis of the vault so that the effect is somehow comparable with the pulvino considered in certain design practices. Obviously, the presence of a crack along the foundation is perceptually not comparable to the presence of a well-designed peripheral joint, even if both elements might have structural similarities.

In case of a full reservoir, a section parallel to the foundation surface is certainly in compression; an eventual bending crack can therefore only develop up to a limited depth before it reaches a stable equilibrium. This situation can change in case of relevant shear forces. To properly assess the stability of a crack, it is necessary to analyse the stress state within the dam body. It is known that the shear stresses in a concrete section progressively change with increasing cracking from the original parabolic distribution to a nearly triangular one [5]. As shown in Fig. 3, this causes practically a pure shear stress state in front of the crack apex. Adopting for example the failure criterion of Griffith [6], the failure is likely to occur in tension, developing a crack inclined at 45°.
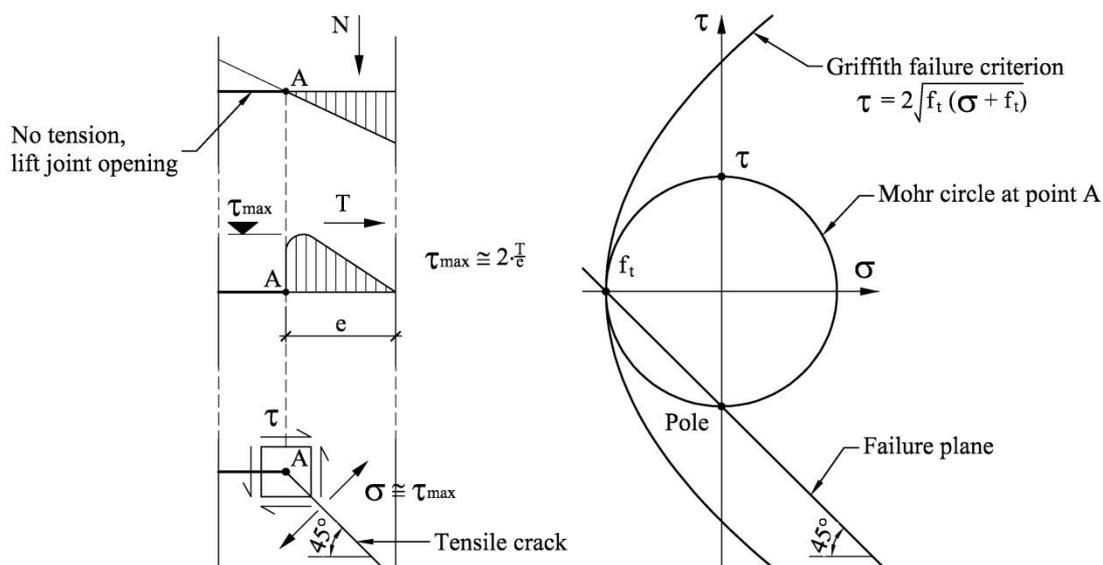

Fig. 3: Deflection of a horizontal crack due to shear force T.

In a very preliminary way, if the shear force T exceeds the value of $f_t \cdot e/2$ the crack becomes unstable. A more detailed FE-analysis of the stress around the crack apex is in any case recommended to better assess the stability of the crack. In case the horizontal crack occurs at the upstream dam face, one should also take into account the effect of the water pressure acting within the crack. This concept of crack stability or instability according to Lombardi [5] is exposed in Fig. 4.

Fig. 4: Stable and instable cracks.

In practice it is not so evident to assess this particular aspect, since the stresses at the foundation typically show singularities and since the mesh adopted for the whole dam mode is too rough for the detailed analysis of the stress near a crack apex. However, the effect of the shear stresses on the crack stability is of primary importance for the assessment of the safety of an arch dam. A tensile stress in a region and direction not affected by shear forces is in fact irrelevant for the dam safety. A tensile stress in a region with relevant shear forces, on the other hand, should be allowed with prudence by considering larges safety margins.

The allowable tensile stress should in fact be defined not only as a function of the type of load combination, but also as function of the consequences of an eventual crack.

Foundation stability

Foundation failure is the principal occurrence of concrete dam collapse. Tigra (India, collapsed in 1917), Vaughn Creek (USA, 1926), St. Francis (USA, 1928), Zerbino (Italy, 1935), Malpasset (France, 1959) and Camarà (Brasil, 2004) are some relevant examples. The assessment of the rock mass strength is very challenging due to the complexity of their nature. The orientation of discontinuities and their characteristics may strongly affect the bearing capacity of the foundation. A rock mass with horizontal bedding, very high RQD values and generally rough discontinuities surfaces can be characterized as good according to the RMR classification, but due to the potential presence of a single, horizontal and very smooth discontinuity, it is in fact considered as not suitable for a gravity dam of about 200 m height. If such a smooth discontinuity is located around 5 m below the excavation limit, it might easily represent a potential sliding surface for this very high dam. The discontinuities play therefore a major role for the stability of the foundation.

The analysis method proposed by Londe [7] is well known. It aims to determine the equilibrium condition of a wedge delimited by an upstream face, where the hydrostatic water pressure applies, and two discontinuities oriented towards the downstream direction. The wedge is loaded by its dead weight, the already mentioned hydrostatic pressure, the thrust forces from the dam as well as the uplift pressure on both sliding discontinuities.

Even if this method is reliable in certain conditions, it may overestimate the strength of the rock mass in others. Fig. 5 shows how in case of various discontinuities a wedge would be supported by others wedges that are likewise potentially unstable. With the aim to account also for this

357

situation, an alternative method is proposed involving the analysis of a rock slice, of unit thickness, nearly perpendicular to the concrete to rock interface and which is delimited by the same planes as the single wedge considered by Londe. This slice is independent of the adjacent slices since the stability conditions are quite similar.
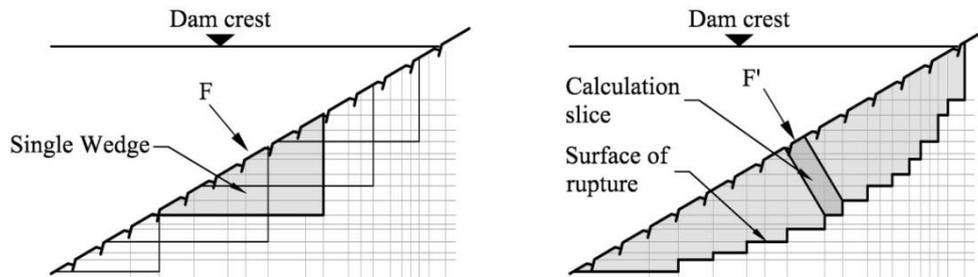

Fig. 5: Transition from a single wedge stability analysis to an analysis of independent planes nearly perpendicular to the foundation limit.

The resistance applies only on the sliding planes at the base of the analysed slice. One might consider this alternative as a generalization of the Londe method where the interaction from a wedge to the others is fully avoided by the analysis of independent slices.

This kind of analysis allows to study various hypotheses, such as the opening of the upstream tension crack, the presence of a grout curtain or a drainage system.

Long term behaviour and monitoring

Within the framework of monitoring, interpretative models are widely used to analyse the dam behaviour, in particular the displacements. There exist basically two types of models: deterministic and statistic. Actually, both approaches are not fully comparable. The establishment of a deterministic model requires the review and assessment of some basic aspects of the dam, that are otherwise only treated in the design stage. Statistic models, on the other hand, are a purely mathematical exercise having in fact nothing to do with the actual structure. The deterministic approach promotes the engineering knowledge and is on a long term probably more reasonable in the context of dam safety.

Dams might be sensitive to temperature changes. The physically correct analysis of this aspect is not trivial and represents the main challenge in the establishment of deterministic models [8]. For statistic models, on the other hand, the thermal part does never appear as a problem, but this is actually not the case. Within statistical models the presence of various thermometers with a similar behaviour is not handled satisfactory and the obtained influence coefficients are fully arbitrary. Also the eventual elimination of thermometers is in fact arbitrary. As long as the engineer properly qualifies the situation and considers the statistical model just as a tool that might help to verify if the present dam behaviour is consistent with the past, the statistical approach is acceptable. However, giving a physical meaning to the results, as for example when deciding on the placement of new thermometers, referring exclusively to the statistic model, is not reasonable.

The fact that a dam behaves regularly at beginning of its service life, does not imply that it will continue to do so, remaining safe also in the future. An increasing number of concrete dams worldwide shows permanent displacements that might be correlated with the chemical expansion of concrete (AAR o ISA). The effect starts to be visible only several years after construction, i.e. 20 years, and the drift might be quite slow so that up to now for various cases

it was sufficient to monitor just the behaviour. Worldwide, the situation appears to be still in the initial stage and rehabilitations have been performed only in single cases.

Concrete expansion in dams is generally not uniform within the structure, but it varies mainly as a function of temperature and stress state [2]. This characteristic clearly complicates the assessment of the actual consequences due to expansion. The problem is schematically presented in Fig. 6.
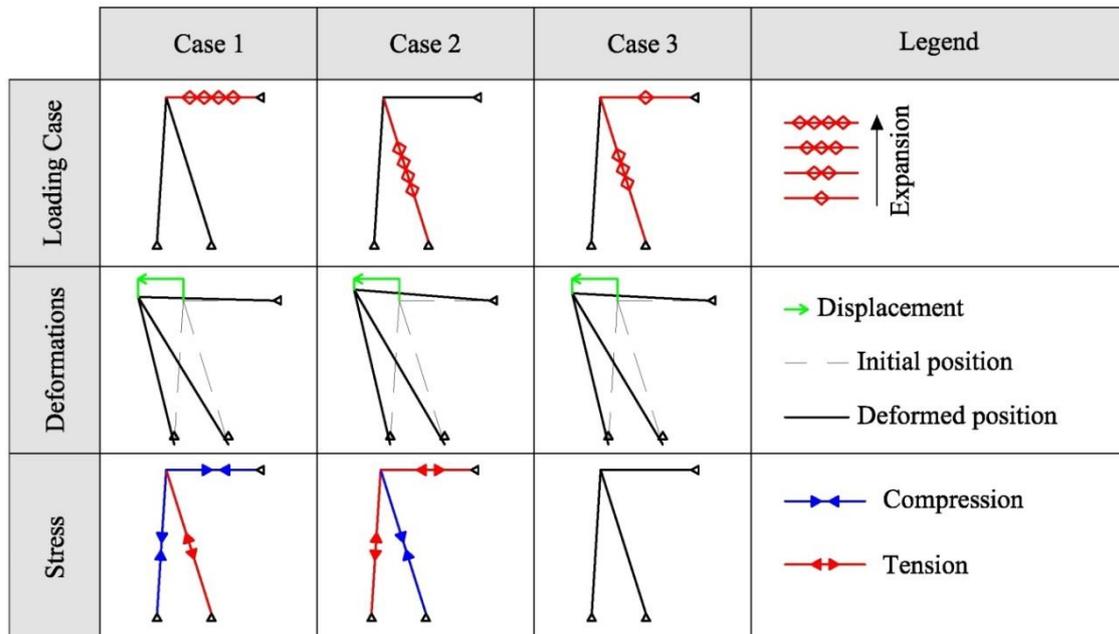

Fig. 6: Variation of static equilibrium due to internal expansion.

A structure formed by 3 beams is considered for 3 different load cases, which produce practically the same displacement of the common node towards the left.

For Case 1, an expansion only for the horizontal beam is considered. Since its free expansion is partially hindered by the stiffness of both sub-vertical beams, a compressive stress might occur within the horizontal beam. Since the two other beams are pushed towards the left hand side, a tensile stress is obtained for the right beam and a compressive for the left one.

For Case 2, expansion occurs only within the right sub-vertical beam. The elongation of said beam is somehow hindered by the left sub-vertical beam, and due to their interaction a rotation and deformation towards the left hand side occurs. The horizontal beam reacts on this deformation. Finally, both the horizontal and the left sub-vertical beams are in traction, while the right sub-vertical beam is in compression.

Case 1 and 2 might show the same macroscopic deformations, but the internal stresses are completely different. One might also imagine a combination of these two loading cases, where finally no stresses are induced within the structure. This situation is represented by Case 3.

This example is strongly simplified, but allows to highlight the difficulties encountered by assessing the effective state of stress within a dam affected by expanding concrete. In an arch or an arch gravity dam, the horizontal beam corresponds to the arch effect, while both sub-vertical beams stand for the cantilever effects.

In order to optimize the maintenance of dams and to identify the most appropriate countermeasure, the assessment of the actual behaviour together with the effective state of the structure is of primary importance.

The correct estimation of the internal stress state might be of a certain relevance for the safety assessment of a dam. In case of an arch-gravity dam, the compressive stresses induced by the

expansion in the arches, according to the distribution of expansion adopted, might vary from 0 to 3-4 MPa [2]. In this latter case the horizontal trust force transferred to the shoulder of the wide valley might be high enough to cause a sliding of the lateral concrete blocks, especially in combination with the water pressure of the reservoir. For the other hypothesis the effects of the concrete swelling are practically irrelevant for the dam safety.

Conclusions

Tensile stresses are not irrelevant for concrete dams, since they might indicate the transition from a fully regular behaviour to a situation characterized by defects, such as cracks. But it should be noted that they are not directly related to the safety of this type of structure. Others criteria have to be taken into account.

1. Stability within gravity dams:
   - The static stability, verified with appropriate methods, should depend only on the weight of the structure. The tensile strength might disappear in case of cracking for any reason.
   - The stability of the lateral blocks, influenced by the lateral slope inclination.
2. Stability within arch dams:
   - The strength of the arches compared to the compressive stresses.
   - The effect of the shear force for the integrity of the structure near the foundation.
3. The foundation stability, avoiding the risk of superposition of potential unstable wedges.

The safety has to be also periodically verified and maintained during the service life. A reliable monitoring and its correct interpretation is the required prerequisite. Numerous cases of concrete expansion show how threats are effectively present. The assessment of this expansion is particularly difficult since displacements and stresses, and therefore the safety, cannot be directly correlated.

References

[1] Ruggeri G. et al. (2004). Sliding safety of Existing gravity dams. Report of the European Working Group of ICOLD.
[2] Amberg F. (2012). A. review of expanding concrete cases and consequences on dam performance. Hydro 2012 Conference, Bilbao.
[3] Lombardi G. (2007). 3D Analysis of Gravity Dams. Hydropower and Dams, Issue One, 2007.
[4] Kaech A., Lombardi G. (1953). Einige Betrachtungen über Bogenstaumauern. Schweiz. Bauzeitung, Nr. 38, Zürich.
[5] Lombardi G. (1998). Querkraftbedingte Schäden in Bogensperren. Wasser, Energie, Luft, Heft 5/6.
[6] Griffith A.A. (1921). The Phenomenon of Flow and Rupture in Solids. Phil Trans. Royal Society, London, Vol. A221.
[7] Londe P. (1973). Analysis of the stability of rock slopes. Q. Jl Engng Geol., Vol. 6, pp. 93-127
[8] Amberg F. (2009). Interpretative models for concrete dam displacements. 23rd International Congress on Large Dams, Brasilia

Partial demolition of Beauregard dam to guarantee its life extension
The role of numerical modelling in the choice of the design solution

Frigerio A.[1], Mazzà G.[1], Artaz L.[2], Canella G.[2], Martinotti G.[2], Marcello C.[3], Meda P.[3]

[1]*Ricerca sul Sistema Energetico RSE, Via R. Rubattino 54, 20134 Milan, Italy*
[2]*C.V.A. Spa - Compagnia Valdostana delle Acque, Via Stazione 30, 11024 Chatillon, Italy*
[3]*Ing. C. Marcello S.R.L., Via Visconti di Modrone 18, 20122 Milan, Italy*

ABSTRACT: The paper describes the case-history of the Beauregard dam (Italy), a concrete arch-gravity structure 132m high built between 1951 and 1958 on the Dora di Valgrisenche River. The design reservoir volume was about 70Mm^3.

The geological and geotechnical investigations carried out since the dam construction and deepened in the last decades have underlined that a Deep-Seated Gravitational Slope Deformation (DSGSD) is located on the left slope. Since the first fillings of the reservoir, the interaction between the DSGSD and the dam was recognized to have relevant implications on the dam structural safety. For that reason, the Italian Dam Authorities in 1969 prescribed a limitation of the reservoir level with a corresponding reduction of its volume to 6.8Mm^3, about 1/10 of the initial design volume.

The investigations, which include a detailed analysis and thorough interpretation of the monitoring data over a time span of more than 50 years, have allowed to gain insights into the understanding of the DSGSD behaviour and its interaction with the dam.

The interpretation of the effects of the slide movements against the dam, the forecast of the future possible trends and the choice of the design solution to guarantee the long-term safety operation of the dam - consisting in the demolition of the upper part of the structure in order to drastically avoid the foreseen occurrence of large deformations and displacements in the dam body associated to the DSGSD movement - have been performed making resort to complex numerical modelling activities that are widely described in the paper.

E-mail: antonella.frigerio@rse-web.it

Introduction

The Beauregard dam, located in the Aosta Valley, Italy (Fig. 1) was completed in 1958. Operated by the Italian Electric Energy Company (ENEL) up to July 2001, the entire scheme was then acquired by CVA (Compagnia Valdostana delle Acque).
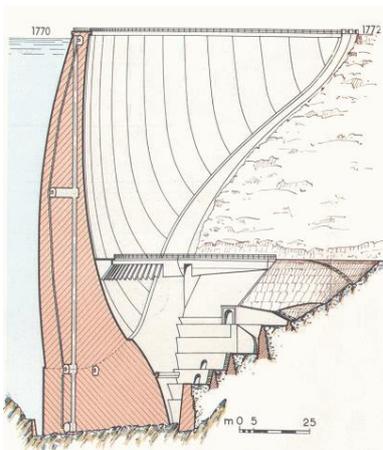

Fig. 1: Beauregard dam - cross section and aerial view

The 132m high arch-gravity dam, provided with a *pulvino*, had a crest length of 408m, a thickness of 45.6m at the base and of 5m at the crest level. The maximum operating design level was foreseen at 1770m a.s.l. and the total reservoir design volume was about70 Mm³. The fillings of the reservoir were undertaken in stages between 1958 and 1968.

Since the dam construction, the monitoring system installed on the left slope abutment showed the presence of a clear relationship between the reservoir level and the rate of movement of the Deep Seated Gravitational Slope Deformation (DSGSD) located on the left slope (Figures 2 and 3).
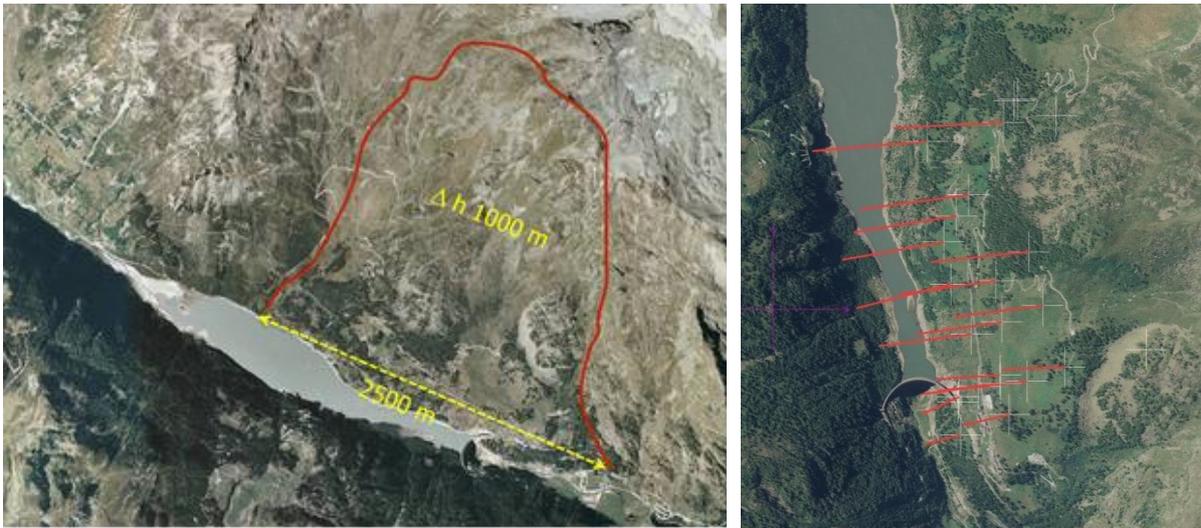
Fig. 2: Aerial view of the Beauregard DSGSD (left) and displacement vectors measured by surface targets from 1968 to 2014 (right)
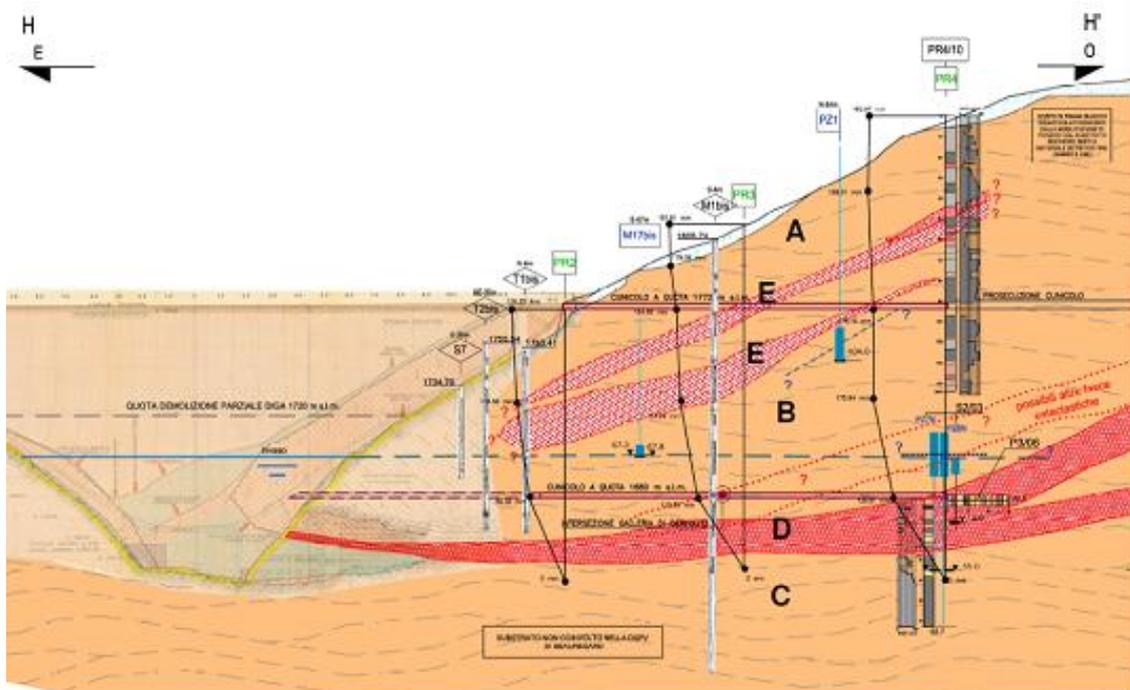
Fig. 3: Horizontal displacement distribution along the plumb-lines installed in the lower portion of the slope close to the dam

Coherently with the left bank movement, the dam was observed to deflect upstream, due to the trust of the slope against the vault, having as a consequence the appearance of cracks on the downstream face (Fig. 4). As a consequence, in 1969 the operational reservoir level was lowered down from 1770m a.s.l. to 1710m a.s.l., corresponding to a reservoir volume of 6.8Mm^3, as enforced by the Italian Dam Authorities.

Fig. 4: The dam was observed to deflect upstream with cracks (depicted in red) appearing on the downstream face and openings of some upstream vertical joints
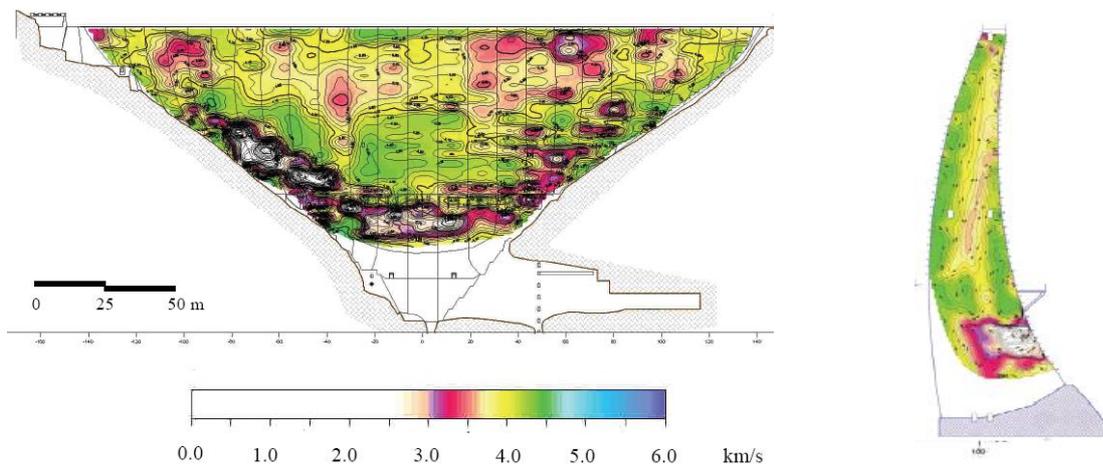
Fig. 5: P-wave velocity tomogram: (left) downstream face; (right) main cross section

The continuous monitoring of the DSGSD and of the dam, started by ENEL and continued by CVA, has allowed to operate the hydroelectric power scheme under closely controlled conditions. However, the interaction between the DSGSD and the dam has been recognized to have relevant effects on the long-term dam behaviour as the cracking pattern was continuously progressing in time. Fig. 5 shows the results of an on-site investigation carried out with a tomographic system that put into evidence the areas of the dam where cracking phenomena are particularly important [1].

Keeping into account the possible long-term implications for the civil protection of the downstream valley as well as the energy production, the Owner decided to start a deep study, making also reference to the support offered by numerical modelling, with the aim to find the most suitable and long-term solution of the problem.

The contribution of numerical modelling to identify the rehabilitation solution

Synthetically, the main aims of the numerical model were:

- The interpretation of the dam behaviour experienced since its first fillings
- The calibration of the mechanical parameters of the dam-rock system in terms of comparison between the observed dam behaviour and model results
- The forecast of the future dam behaviour at short-middle-term resorting to the calibrated model
- The support to the designer to assess possible technical solutions to guarantee the long term operation of the dam.

A three-dimensional finite element model of the concrete arch dam including a proper portion of the surrounding rock mass foundation was generated in order to carry out numerical analyses (Fig. 6). In the rock mass foundation, the active portion of the DSGSD has been taken into account as well as the shear surface, modelled in terms of an interface whose behaviour is described by a frictional law. The nodes where the DSGSD movements were imposed are outlined with red spots in Fig. 6.
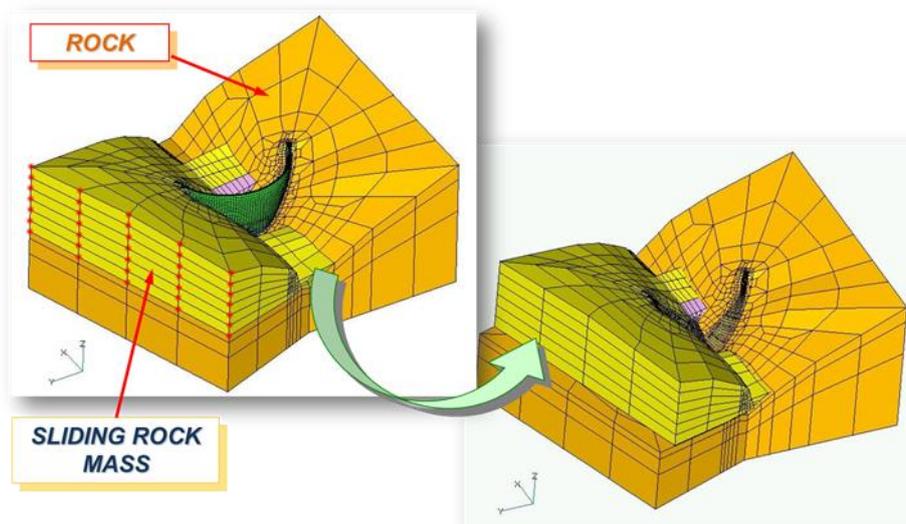
Fig. 6: Finite Element mesh of the dam and the surrounding rock mass

A linear elastic isotropic constitutive law was assumed for the rock mass foundation whose mechanical parameters were defined on the basis of the results provided by the more recent geotechnical investigations.

The Concrete Damaged Plasticity constitutive law [2] was adopted to describe the concrete behaviour (Fig. 7).

The model assumes that the uniaxial tensile and compressive responses of concrete are characterized by damaged plasticity. Under uniaxial tension the stress-strain response is linear-elastic until the failure value is attained; beyond this value a strain softening relationship follows.

In compression the softening behaviour occurs after an initial stress hardening. On the basis of the results of the indirect tensile tests, two different sets of material parameters were assigned to the concrete of the dam body and the *pulvino*.
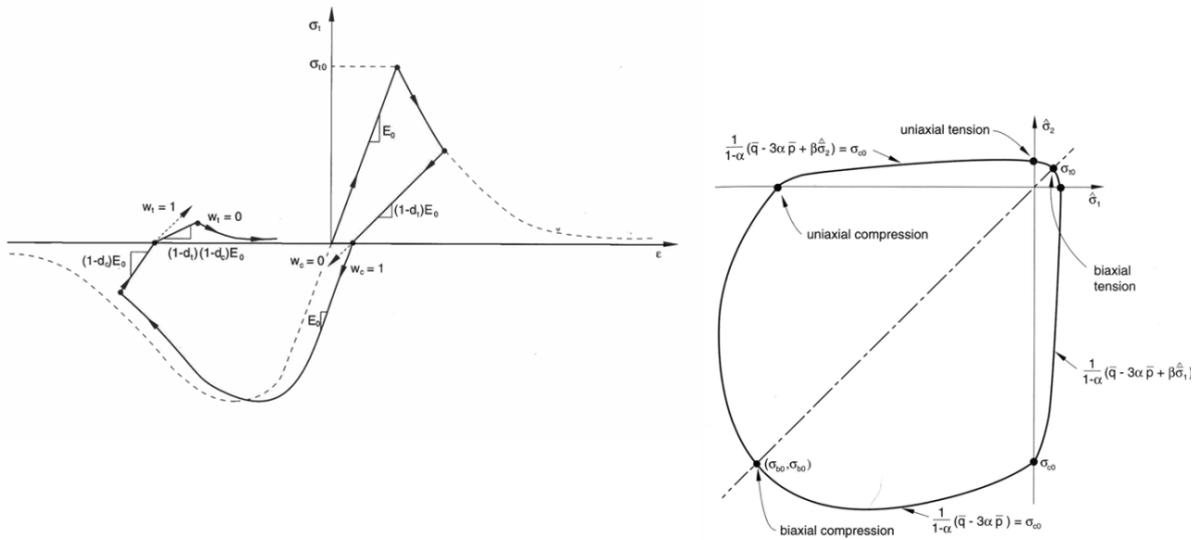
Fig. 7: The Concrete Damage Plasticity constitutive law [2] has been assumed for concrete and pulvino of the dam

Several preliminary analyses were carried out to identify the numerical model (calibration phase) in order to reproduce the real dam behaviour dealing with the interaction between the structure and the slope sliding.

The movement of the left slope abutment was imposed by appropriate displacement boundary conditions applied at the nodes marked in red (as explained above, Fig. 6) and the hydrostatic load was firstly considered taking into account the variation relevant to the first fillings; afterwards, a constant reservoir level at 1710m a.s.l. was assumed, according to the present operational conditions.

The identification process was mainly based on:

- The measured displacements along the dam crest
- The monitoring points of two plumb lines, located inside the dam body in the main cross section and in the fourth block towards the left abutment, respectively
- The computed damage pattern of the structure to be compared with the tomographic investigations.
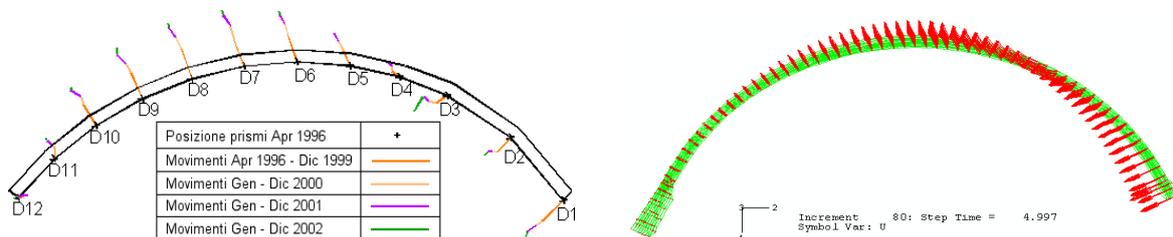
Fig. 8. Deformation of the dam crest: (left) based on monitoring; (right) based on computations

As shown in Figures 8 and Fig. 9 (the latter to be compared with Fig. 5), the identified numerical model exhibits a good agreement with the deformation of the dam crest as well as the damage localization.

The identified numerical model was afterwards used to forecast the future behaviour of the structure considering a continuous increase of the landslide movement according to the trend foreseen on the basis of the past behaviour.
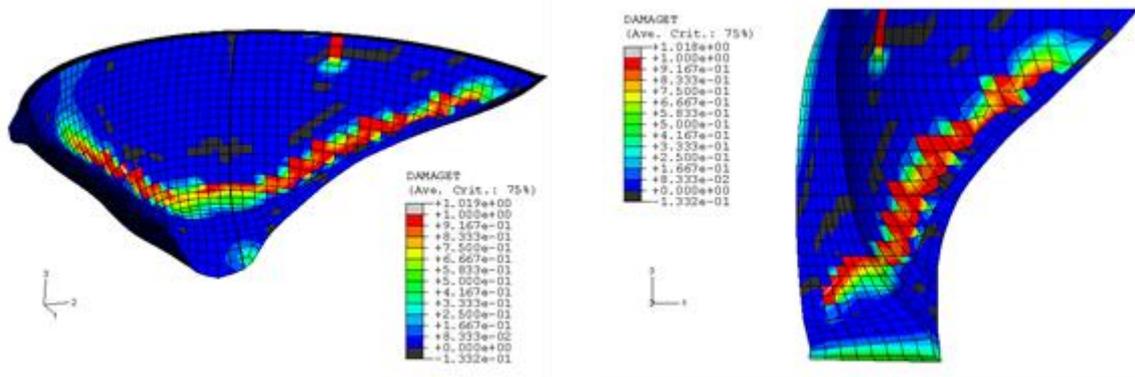

Fig. 9. Localization of damage computed with the 3D numerical model: (left) on the downstream face of the dam; (right) on the main cross section

The main purpose of the analyses was to assess if the dam might undergo to local or global instability phenomena such as snap-back.

The curve nr. 1 in Fig. 10 allows to exclude snap-back instability for the overall structure because beyond the peak value the reaction force on the main cross section of the dam decreases gradually as the landslide movement increases.

Although the measured displacement towards the upstream direction of the middle point of the dam crest (about 0.21 m) is close to the peak value of the reaction force curve, it has to be bear in mind that the structure is subjected to an imposed deformation rate due to the DSGSD movement. Hence the structure should be able to follow the softening branch of the reaction force curve avoiding a sudden failure when the peak value would have been attained.
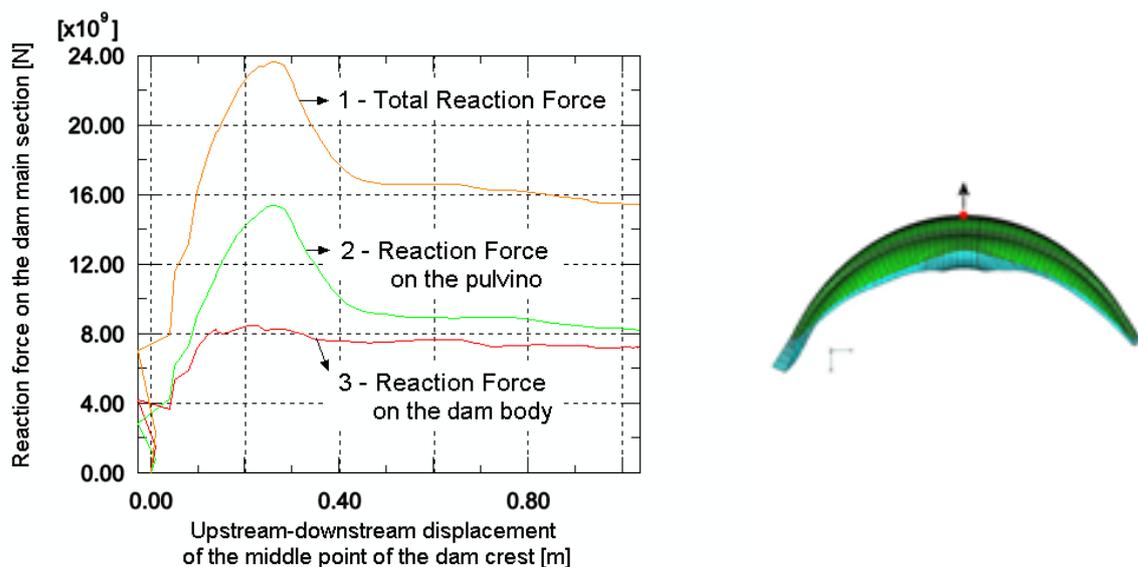
Fig. 10. Reaction force on the main cross section of the dam vs the upstream-downstream displacement of the middle point of the crest dam

However, even if according to the results of the numerical model a sudden failure was highly improbable, in the medium-long term rather large deformations on the dam body had to be

expected. On the other hand, the possibility to stabilize the DSGSD, given its dimensions and the geotechnical characteristics, was considered as unfeasible.

Hence, it was decided to find a long-term solution capable to guarantee the safety of the population and the operation of the power plant.

The rehabilitation of Beauregard dam

Different possible long-term solutions were considered by the designer who was in charge of the rehabilitation project. Numerical modelling was widely adopted in order to analyse the different solutions which main aim was the reduction of the trust effect of the rock sliding against the dam. The partial demolition of the upper part of the structure was the one finally chosen for the rehabilitation design. The demolition of the upper part of the dam lowered the crest elevation from 1772m to 1720m a.s.l. [3][4].

The operating methodology that has been selected as more suitable for the demolition of about 160,000 m^3 has been a controlled blasting: the explosives have been installed in a dense mesh of perforations located and directed according to a specific study, which ensures the control of blasting and the orientation of the fall trajectory of the material produced by the explosion. It was considered that blasting was better than using breakers installed on excavators, due to the reduced continuous noise.
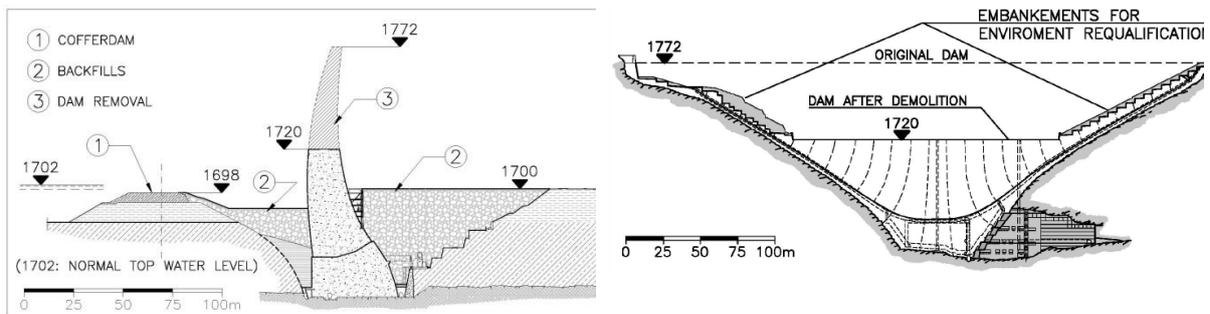

Fig. 11. Cross section and downstream view of the dam: final configuration after the demolition

The demolition started in the Spring of 2013 and ended in Summer 2014. The demolished material has been used to fill the two volumes located at the upstream and downstream dam toes (Fig. 11). Figures 12 shows some phases of the dam demolition. The final situation can be seen in the picture of Fig. 13, where it is shown the dam seen from downstream. The new elevation of the crest has been verified against water waves possibly caused by landslides falling from both sides of the valley into the reservoir.

Additional works have been carried out in the frame of the rehabilitation interventions, among which the improvement of the hydraulic scheme with the construction of a gated spillway which discharges the waters in an existing tunnel. Moreover, a water drainage and a water channelling system was built to gather the waterfalls that flew in the detachment cliff of the DSGSD. These interventions have partially reduced the speed of the DSGSD [5].

Conclusions

The case history of Beauregard dam is an emblematic case that has posed to the dam engineers in charge of operation and safety assessment very critical choices, considering that the construction of new dams, and structures in general, represents their main mission.

Fig. 12. Different sequences of the dam demolition

Fig. 13. The present dam seen from downstream

In the Beauregard dam case it has been deemed necessary to proceed, as sometimes happen for the human life, with a sort of a limb amputation in order the save the dam life.

The decision has been difficult to take and it has been necessary to investigate very deeply and for long time on all possible aspects affecting the system, deciding which could have been the most reasonable solution from the engineering point of view.

The choice has been taken considering the different facets of the problem: safety (basically), energy production, environment protection.

References

[1] Barla G. et Al. (2006). The Beauregard dam (Italy) and the deep-seated gravitational deformation on the left slope. Hydropower 2006, Kunming, China, October 2006.

[2] Fenves, G. and Lee, J. (1998) Plastic-Damage Model for Cyclic Loading of Concrete Structures. Journal of Engineering Mechanics.

[3] Marcello C.; Meda P. (2013). The rehabilitation design of the Beauregard Dam. Proc. 9th ICOLD European Club Symposium, Venice.

[4] Frigerio A., Mazzà G. (2013). The rehabilitation of Beauregard Dam: the contribution of the numerical modeling. Proc. 12th Benchmark-Workshop on Computational Aspects on Dam Analysis and Design, Graz.

[5] Artaz L. et Al. (2015). Partial demolition of Beauregard Dam by blasting to guarantee its life extension. Proc. 25th ICOLD Congress, Stavanger.

Janneh dam Project
Non-linear numerical simulation of an arch-gravity dam

A. Yziquel[1], F. Andrian.[1] and P. Agresti[1]

[1]ARTELIA Eau & Environnement. 6, rue de Lorraine, 38130 Echirolles, France

ABSTRACT: The Janneh RCC dam is currently under construction in Lebanon. The impounded reservoir will supply water, irrigate agricultural areas and generate hydropower.

The project site is located in high-seismicity region. The Peak Ground Accelerations are 0.37g and 0.51g respectively for OBE and SEE.

Under such seismic loads, the initially designed straight gravity dam would have required very gentle up-and-downstream batters. In order to avoid a costly structure, the geometry of the dam has been curved and now benefits from arch effect.

The resulting arch-gravity dam behaves differently from both straight gravity and arch dams. For thick dams, arch effect generates openings at the dam/foundation interface. Such behaviour is allowed but the design of the dam must accommodate the mentioned displacement.

A new non-linear calculation methodology has been developed in order to ensure the structural safety of the dam and to assist the design of its components under static and dynamic conditions.

E-mail: alain.yziquel@arteliagroup.com

Project context

The Janneh dam is a 162-meter high Roller Compacted Concrete arch-gravity dam under construction in the Nahr Ibrahim Valley of Lebanon. The multi-purpose project will provide water for Northern Beirut, irrigate agricultural areas and generate hydropower.

ARTELIA is the lead firm for the supervision of works and has provided technical assistance for the design of the dam.

The project site is located 40km North-East of Beirut, 15km West of Yammouneh fault and lies within the range of the Mount Lebanon Thrust (figure 1).
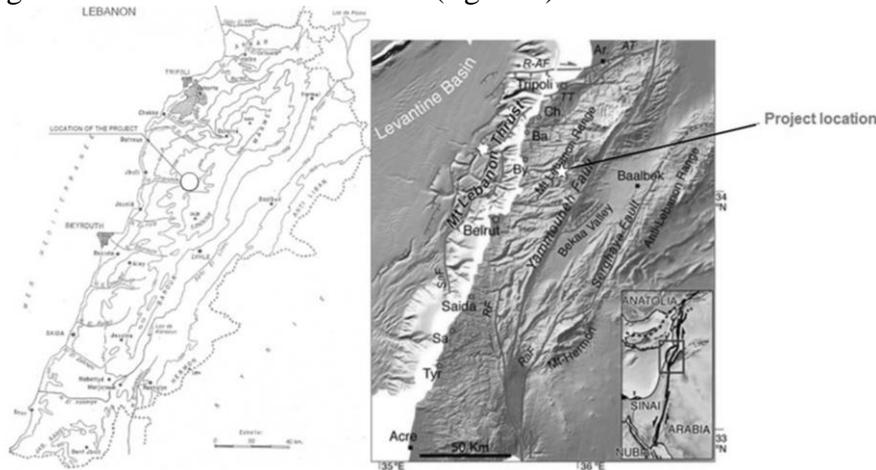

Fig. 1: Janneh dam location (Lebanon map on the left and tectonic map on the right)

The Peak Ground Acceleration (PGA) of the Maximum Credible Earthquake (MCE) assessed at the project site is 0.51 g. A progressive modelling, in accordance with the French practice [1], was carried out based on the initially designed straight gravity dam alternative. Rigid-block, response spectra as well as non-linear time history analyses were subsequently performed. The post-seismic displacement calculated at the dam/foundation interface is about 15cm. Such displacement may severely damage the dam base and the neighbouring bedrock. The induced

leakage may saturate the drainage system and significantly increase the pore pressure distribution. The stability of the dam under post-seismic conditions is not satisfactory. Therefore, the dam geometry requires to be reviewed accordingly.

A straight gravity dam complying with international seismic regulations would have been costly. Consequently, the dam geometry has been curved in order to benefit from arch effect (figure 2). Such a configuration is allowed since the bedrock is made of sound dolomitic limestone and Jurassic dolomite. However, the riverbed is covered by a 60m deep alluvium layer to be excavated. This alternative allows for a saving of 20% of concrete volume.
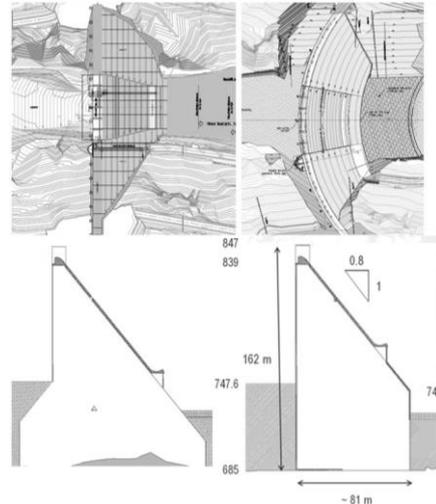
Fig. 2: Straight gravity (on the left) and arch-gravity (on the right) alternatives with the corresponding central sections

The arch effect combined with converging excavation geometry will prevent from any overall sliding toward downstream. However, the mechanical behaviour of an arch-gravity dam differs significantly from that of both straight gravity and arch gravity dams. For an arch-gravity dam, opening occurs at the upstream toe of the dam. Therefore, the grout curtain and the drainage system must be designed conveniently, in any case on the opened regions.

In order to assess the overall safety of the dam, a new nonlinear numerical simulation has been developed for the purpose of the project and is detailed hereafter.

Configuration at detailed design stage

The dimensions of the dam at detailed design stage (figure 2) are as follows:
- 162m high above the bedrock and 315m long at the crest;
- 0.8H/1V downstream batter with a vertically truncated toe;
- 81m maximum base width; and
- 240m upstream face radius.

The ongoing excavations and geotechnical investigations show that the bedrock is at higher elevation than expected. The maximum height of the dam may be consequently reduced.

The bedrock is provided with a specific converging geometry (figure 3). Down to El. 742, the resultant of water pressure is perpendicular to the downstream abutment faces. This is due to arch effect. Down to the base, the dam is blocked against sliding should an earthquake occur.
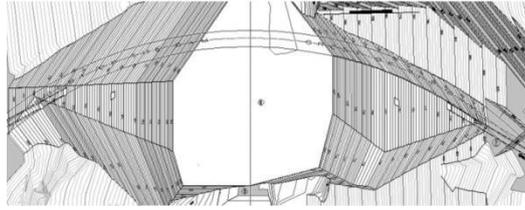
Fig. 3: Converging excavation

Approaches of calculations and numerical model

Modelling targets

Beyond the safety evaluation of the dam, the calculations intend to provide its components with a more refined design. Consequently, the corresponding numerical model aims to reach the following targets:

- Assess the overall stability of the dam and its stress state;
- Simulate opening and possibly sliding at dam/foundation interface;
- Take into account more realistically the effect of pore pressures and uplifts, especially at interface regions where opening occurs;
- Carry out dynamic calculations under non-linear conditions.

FLAC3D numerical model

FLAC3D, developed by Itasca, was chosen for its better ability to model non-linearity compared to standard implicit finite element codes, especially under dynamic conditions.

The used numerical model (figure 4) includes bedrock extending 1.5 times the height of the dam on lateral and vertical directions.

FLAC3D enables the use of radiative boundary conditions. This feature avoids an overestimation of accelerations and stresses by a factor up to 3 as already mentioned by Chopra [2]. Several studies under progress or already carried out (by ARTELIA) [1] confirm the risk of overdesign due to the use of a simplified massless foundation model.

The model comprises 270,000 nodes. The alluvium materials as well as the replacement backfills are modeled to account for the radiation of the seismic waves to the far field.
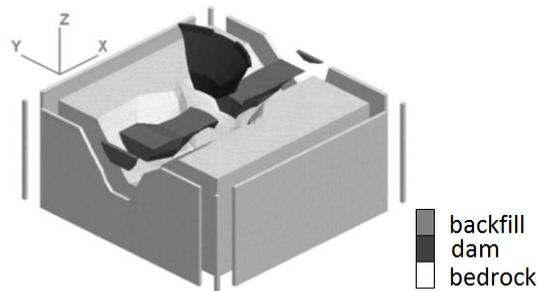

Fig. 4: Exploded view of the model with the side radiative boundary conditions

Constitutive laws

Discrete element method is used at the dam/foundation interface. This allows for a better simulation of the contact where a Coulomb friction model without tensile strength is used.

The dam and the foundation follow an isotropic linear elastic constitutive law whereas Mohr Coulomb law is used for backfill and alluvium materials.

The used material properties are given in the following table.

Tab. 1: Material properties for the numerical model

Material	Unit weight (kN/m³)	Static Young's modulus (GPa)	Dynamic Young's modulus (GPa)	Poisson's ratio	Friction angle (°)
RCC	24	25	31.25	0.2	-
Bedrock	28	20	25	0.25	-
Dam/Foundation interface	-	-	-	-	45
Backfill	18	0.1	0.1	0.25	38

The presented RCC properties are those of the detailed design stage. They are to be reviewed according to values obtained from in-situ tests and trial mixes.

For the time being, the model takes into account the construction of independent blocks. At the end of the construction, the dam is considered monolithic. Construction provisions will be adopted in order to achieve this state or to reach an acceptable behaviour of the dam (joint grouting and shear keys). The design of these features is currently on progress and assisted by a thermo-mechanical analysis.

Pore pressures and criterion for opening permeability

The pore pressures are among the variables of the model. Uplifts, here the resultant of the pore pressures, are more finely taken into account compared to simplified external forces.

External forces are only applied at opened contact regions.

An opening is considered nearly watertight if its width is lower than 0.2mm. For higher widths, water pressure and pore pressure incrementally propagate in the contact and neighbouring elements. The full reservoir pressure is then applied at the permeable regions. Between 0.2mm and the downstream face, the pressure linearly decreases down to downstream water pressure. Such approach may be slightly more pessimistic than the Poiseuille's cubic law but does not require any prior calibration (Fig. 5).
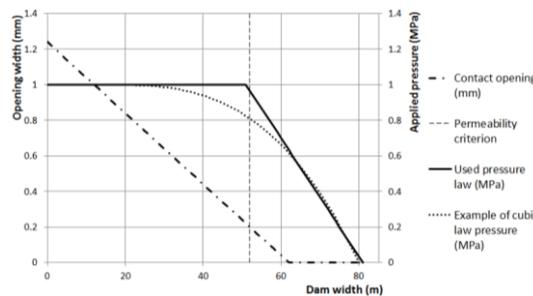

Fig. 5: Example of pressure distribution at opened contact

Static analysis

Arch effect and criterion for stability

The impoundment of the reservoir generates arch effect within the upper 70-80m of the dam. The maximum crest displacement toward downstream is about 1.5cm for the normal water level and the maximum arch stress is 1.1MPa (Fig. 6).
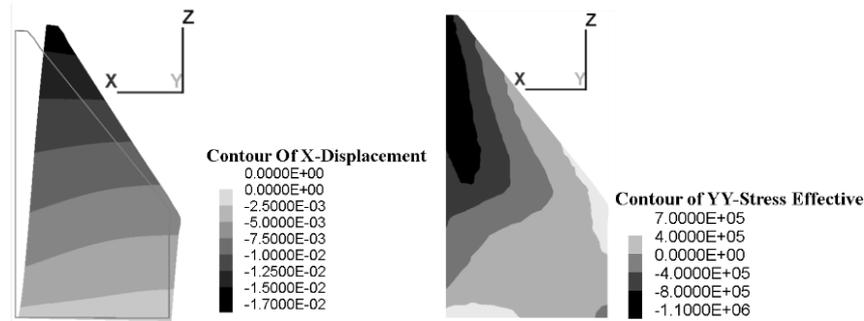
Fig. 6: Exaggerated downstream displacement (m) and effective arch stress (Pa) at the central section (negative compression)

The global sliding safety factor of gravity dams is usually assessed by means of the ratio of the normal to the tangential resultants at the base of individual blocks. Due to the tridimensional behaviour of Janneh dam, such method is not relevant. More specifically, the truncated-toe central blocks will not match the sliding criterion.

Here, a local safety factor method is adopted. The shear friction factor (equation 1) is calculated at each element of the dam/foundation interface.

$$SF = \frac{\sigma'_N \times \tan(\phi)}{\tau} \tag{1}$$

Where σ'_N is the effective normal stress of the interface element, ϕ is the friction angle and τ is the tangential stress.

Assuming that a safety factor of 1.5 is satisfactory, the dam withstands sliding by means of its selfweight for the central blocks and by arch effect for the bank blocks (Fig. 7). The safety factor reaches a value of 3 at the base of the central blocks and 5 at the bank higher abutments for normal water level. For high water level (NWL+6.5m), the stability of the central blocks slightly decays: the upstream toe lifts. This is in opposition to that of the bank block which enhances. The dam clearly behaves in a composite arch-and-gravity way.
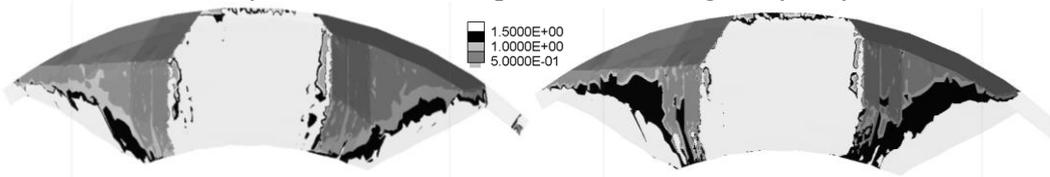

Fig. 7: Local sliding safety factor at normal water level (left) and high water level (right)

Moving back the grout curtain and drainage galleries
Arch effect offloads the central blocks and overloads the banks blocks at normal water level. Therefore, opening occurs at the upstream toe of the latter. The maximum opening width is 5mm at high water level.

For straight gravity dams, the grout curtain and the drainage galleries are generally placed as close to the upstream face as possible in order to improve their efficiency. Here, these components are moved back in order to avoid the saturation of the drainage system. As an opening is considered nearly watertight if its width is lower than 0.2mm, this is the adopted limit to place the dam components (Fig. 8). 0.2mm opening iso-value for high water level is used as to prevent from the possibility of high leakage discharge through the galleries under static conditions.
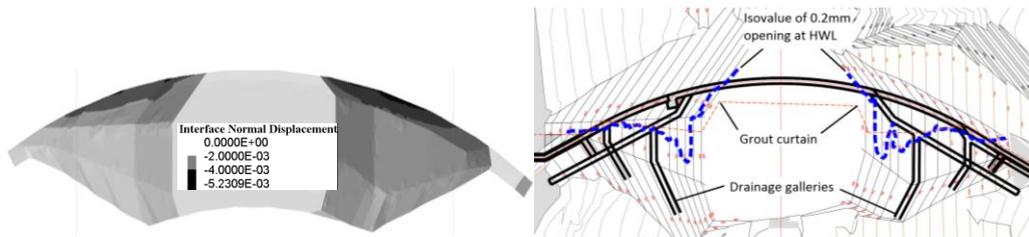
Fig. 8: Contact opening (m) at HWL and location of drainage galleries and grout curtain

Seismic analysis

The dam layout was curved in order to withstand the expected high seismic loads. Arch effect combined with converging excavation exclude the risk of collapse or downstream overall sliding during strong earthquakes. Therefore, only the calculations corresponding to OBE are detailed in the following. The dam and its appurtenant structures shall remain functional when such an earthquake occurs. However, some minor but easily repairable damages are tolerated [3]. For economic reasons, the return period of OBE for the Janneh dam is within the higher range: 945 years. The corresponding PGA is 0.37g. Several existing signals were adjusted to fit the site spectrum. The one leading to the maximum post-seismic displacement for 2D calculations is shown here (Fig. 9).
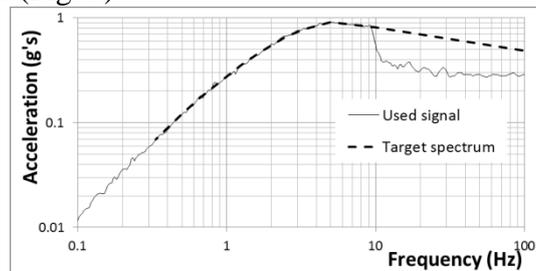

Fig. 9: Site and used signal spectra

The used signal shows a significant offset from the site spectrum down to 10Hz. However, the calculations show that the response of the system is negligible for such frequencies, despite the mesh size able to solve up to 20Hz [4].

The explicit calculations do not allow for a prior determination of the eigenmodes of the system. They are assessed by means of Fourier transform of acceleration histories at several locations. Moreover, due to the non-linearity of the system, the overall response cannot be obtained by means of the superimposition of independent load cases. Therefore, the initial state of the seismic calculations is the impoundment at normal water level.

For seismic calculations, water pressures at opened regions are considered steady. The fluid-structure interaction is approached by means of Westergaard generalized added masses.

The material damping is based on hysteretic formulation, i.e. damping is proportional to distortion. Here, the maximum damping value is 7% in the dam.

Dam body accelerations

At the crest of the central block, the peak acceleration is 14.5m/s². The maximum crest acceleration, 18m/s², is measured on a bank block. This is likely the effect of a 5-6Hz complex mode, falling within the spectrum plateau, whereas the fundamental mode is at 2.7Hz (Fig. 10). The amplification of the PGA is then about 5 and the amplitude of the crest displacement is about 10-11cm.
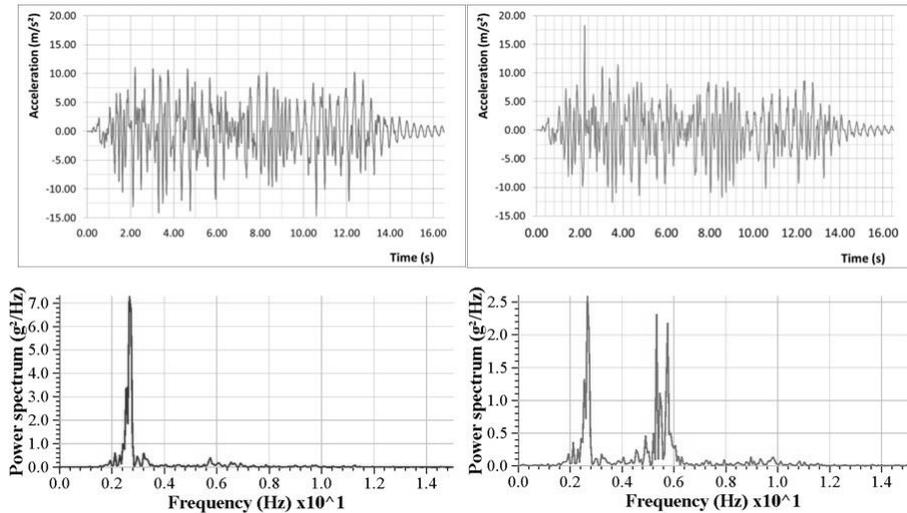
Fig. 10: Crest acceleration histories and corresponding power spectra (central block on the left, bank block on the right)

A thorough analysis of accelerations allows for the definition of level-based design accelerations for the appurtenant structures. For example, an acceleration of 4m/s² is considered for the low-level outlet and 14.5m/s² for the spillway bridge.

Moreover, a seismic belt will be constructed in the vicinity of the dam crest [5] in order to mitigate the effect of complex modes, thereby preventing adjacent blocks offset. A similar provision has been adopted for Katse dam (Lesotho) for example.

Stress analysis

Due to its thickness, the seismic behaviour of the dam is not critical with regard to compressive stresses. The highest tensile stresses are noticed when the crest tilts the furthest toward upstream. Arch stresses are not meaningful as they are due to the monolithic model whereas the cantilever ones are of concern. The analysis is carried out for a bank block where the maximum acceleration is measured (Fig. 11).
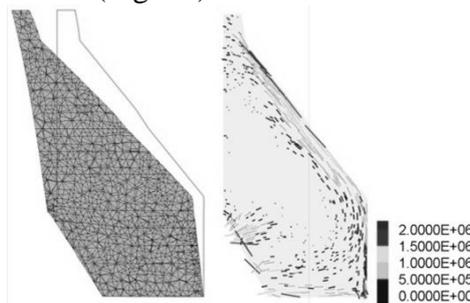

Fig. 11: Exaggerated deformation and tensor of tensile stress (MPa) at the most critical time on a bank block

The highest stresses are mostly located on the upper part of the downstream face. Their direction is parallel to the face. The maximum value is less than 2MPa whereas the RCC dynamic strength is about 1.5MPa. Minor cracking is expected due to the short time when concrete is overstressed. On the downstream face, cracks are not in contact with the reservoir and consequently do not affect the post-seismic behaviour of the dam. Therefore, they can be tolerated.

Post-seismic displacements

The use of interface elements allows for a refined analysis of the post-seismic displacements. The normal stress at the upstream toe of the dam decreases when the crest moves toward downstream. This relaxes the shear stress due to the water pressure and leads to incremental plastic relative displacements of the toe toward downstream.

The final displacement pattern at the interface confirms that there is no overall sliding (Fig. 12). On the other side, a toe rearrangement occurs, here localized at the interface but may actually be spread around the dam/concrete interface.
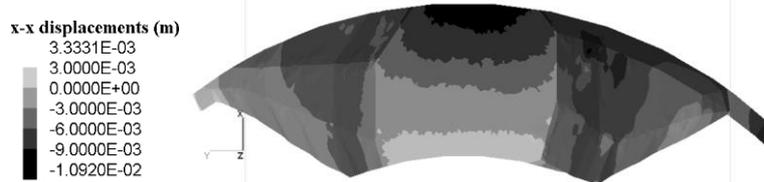

Fig. 12: Post-seismic displacement at the dam/foundation interface

Due to dilatancy, such rearrangement may increase the discharge through the drainage galleries. Such behaviour has already been noticed on several large dams subject to earthquakes [6]. Here, Louis's [7] formulas are used to assess the water discharge through the dilatancy-induced opening. Then, the capacity of the drainage holes is checked. For example, a discharge of 13l/s is expected for a 7° dilatancy with the maximum post-seismic displacement of 7mm in the vicinity of the lowest drainage gallery.

Conclusion

The Janneh dam has been curved in order to withstand the expected high seismic loads. This leads to more than 20% saving on the concrete volume. However, due to the proved arch effect, the behaviour of the dam requires a specific design of its components compared to that of straight gravity ones.

The newly developed non-linear method proposed in this paper was used in order to become more confident in the design of the dam. The location of its components has benefitted from a refined design and the safety of the overall structure is verified under both static and dynamic conditions. The main feature of this method is the specific placement of the drainage gallery and the grout curtain, here optimized by means of a less restraining but still realistic permeability criterion.

The non-linear seismic analysis allows for the assessment of post-seismic displacements. Evaluated with a simplified approach here, the calculations show that a dam may exhibit plastic behaviour without any overall sliding. This may be related to the increase of leakage noticed on some large dams after having experienced an earthquake. If an OBE earthquake triggers such a behaviour on the Janneh dam, the capacity of the designed drainage holes will likely be able to carry the corresponding discharge.

In France, the forthcoming guidelines for the verification of stability of existing arch dams will comprise most of the described method. In an international context, it may be used on several projects where arch-gravity RCC dams become more and more economically and financially interesting.

Acknowledgements

References

[1] Andrian. F. (2014). French state-of-the art seismic analysis of concrete gravity dams – 2D progressive modeling: from pseudo-static to non-linear time history analysis. Symposium on earthquake analysis of dams, CFBR, Challes-les-Eaux, France.

[2] Chopra A.K. (2008). Earthquake analysis of arch dams: factors to be considered, The 14th World Conference on Earthquake Engineering.

[3] Selecting seismic parameters for large dams. Bulletin 72, 2010 Revision, ICOLD.

[4] Kuhlmeyer R.L., Lysmer J. (1973). Finite Element Method Accuracy for Wave Propagation Problems. Journal of Soil Mechanics, Div. ASCE, 99(SM5).

[5] Yziquel A., Andrian. F., Lemoine I. (2015). Static and seismic design of Janneh dam. International Water Power & Dam Construction, February 2015, pp. 40-43.

[6] Observed performance of dams during earthquakes, Volume III, February 2014, USSD.

[7] De Marsily G. (2004), Cours d'Hydrogéologie, Université de Paris VI.

High Arch Dam Reservoir Basin Deformation & Its Effect

Erfeng Zhao[1,2], Chongshi Gu[1,2]

[1]*State Key Laboratory of Hydrology-Water Resources and Hydraulic Engineering, Hohai University, 210098 Nanjing, China*
[2]*National Engineering Research Center of Water Resources Efficient Utilization and Engineering Safety, Hohai University, 210098 Nanjing, China*

ABSTRACT: It is found that the reservoir basin shows a warping deformation with settlement in front of the dam and a little uplift behind the dam, according to monitoring data of high arch dam reservoir basin deformation. Therefore, in order to study the deformation of high arch dam reservoir basin and its effect on dam service behavior, corresponding affect factors were studied firstly. Furthermore, Xiaowan wide range numerical model is built, including reservoir area, rock base and dam. The research results reveal the general law of reservoir basin deformation. Moreover, it is proposed that the deformation caused by reservoir basin should be taken into consideration when evaluating dam operating behavior.

E-mail: zhaoerfeng@hhu.edu.cn

0 Introduction

In western China, a plenty of high dams with large storage are under or planned to be built at present. Concrete dams occupy a certain percentage of these projects. Xiaowan arch dam is 294.5m and its reservoir storage is 15 billion m^3. Jinping 1st stage hydropower station is 305m and its reservoir storage is 7.765 billion m^3. Baihetan arch dam is 289m and its total reservoir storage is 20.62 billion m^3. The technical difficulty of these projects is quite high, so requirements to engineers have been high to ensure the engineering safety and scientific design. The engineering experience suggests that the maximum radial replacement of arch dam is always one of the most significant indexes to evaluate arch dam operating behavior. However, the effect of reservoir basin is always ignored in the general analysis on high arch dam operating behavior. In the early 1980s, some engineers have noticed such problems caused by high arch dam reservoir basin deformation and some exploratory researches have been carried out as well. With the development of hydropower station design and construction, great attention has been attracted on these problems. Hence, it is necessary to conduct researches on key scientific and technical problems of high arch dam reservoir basin deformation.

Introduction

Problem proposed

It has been noticed that numerical calculation results of arch dam deformation are very different from monitoring data in practical projects. The monitoring data in storage stage demonstrates that dam would show upstream deformation under the effect of water, temperature, reservoir basin deformation and specified dam structures. Longyangxia hydropower station and Xiaowan hydropower station are taken into analysis as follows.

Fig. 1: Longyangxia Hydropower station   Fig. 2: Xiaowan Hydropower station

Case 1: Longyangxia Hydropower Station

Longyangxia hydropower station was built in 1980s. It is 178m, the crest elevation is 2610m and the total reservoir storage is 24.7 billion m^3. In the storage stage, numerical calculation results of crown cantilever are larger than monitoring data. In 2600m elevation, monitoring value of plumb line is 16.28mm when the water level is 2575m. Calculation results are in good coincidence with monitoring value when considering with the reservoir basin deformation component. The calculation results are consist of three parts, they are water component (22.99mm), temperature component (2.97mm), reservoir basin deformation component (-10.00mm). The calculation value is 15.97mm and the ratio of monitoring value and calculation value is 1.02.

Case 2: Xiaowan Hydropower Station

Xiaowan arch dam is 294.5m, the normal water level is 1240m and the total reservoir storage is 15 billion m^3. During the storage stage, the arch dam radius deformation shows that great difference exists among calculation results and monitoring values, shown in Fig. 3.
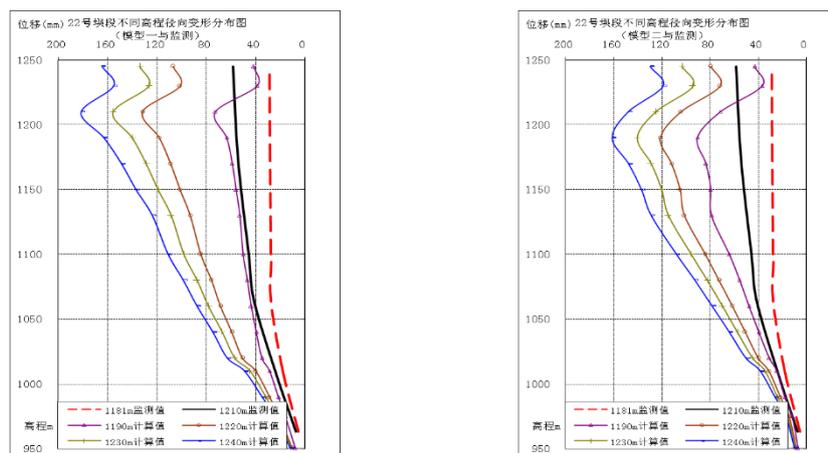

Fig. 3: The radius deformation of FEM and monitoring value of 22# dam

In view of Fig. 3, monitoring values is smaller than calculation values. Even though the different starting point of monitoring data and calculation value is one of the reasons resulted in such difference, it is not the whole reason since the monitoring data in water level 1210m can match

the data in 1190m. According to the pervious researches on Longyangxia hydropower station, the reservoir basin deformation has a certain effect on dam deformation when dam is high and the reservoir is large enough.

Influence factors of high arch dam reservoir basin deformation

The influence factors of high arch dam reservoir basin deformation contain water body size, geological condition, reservoir basin type and its influence area. Since the geological condition is too complex, the reservoir basin type and its simulation range, water pressure are mainly studied in the paper.

(1) Reservoir basin type: the effect of different reservoir basin type, such as linear type river channel (Fig. 4a), branch-off type river channel (Fig. 4b) and sudden-enlargement type river channel (Fig. 4c).

(2) Reservoir basin influence range: the impact of width, depth and length of reservoir basin on reservoir basin deformation, as well as the impact of different extended length towards downstream.

(3) water pressure: the influence of water pressure on the reservoir basin deformation under different water levels with certain terrain conditions, reservoir basin type, geological condition and reservoir basin influence area.
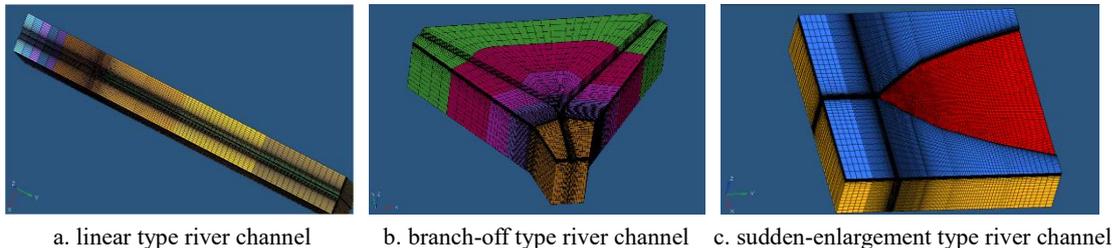
a. linear type river channel   b. branch-off type river channel   c. sudden-enlargement type river channel

Fig. 4: Reservoir basin type of high arch dams with large storage

Fig. 5 shows calculation results of the settlement of above three reservoir basins. It is obvious that the settlement reaches the maximum in the middle of the river channel, and the value declines gradually along two sides and with the depth increase. Meanwhile, the settlement is relatively small in the downstream. The maximum settlement of linear type, branch-off type and sudden-enlargement type river channel appears at the middle of the channel, bifurcation part and the center of water gravity respectively. With the increase of the upstream range of reservoir basin (5km→30km), the deformation distribution on longitudinal profile vertical to river channel tends to convergence. The deformation of reservoir basin tends to convergence as well with the increases of bedrock depth (3km→10km). The downstream range has less impact on the reservoir basin deformation. At the same time, the settlement of reservoir basin increases with the rise of upstream water level.

| a. linear type river tunnel | b. branch-off type river tunnel | c. sudden-enlargement type river tunnel |
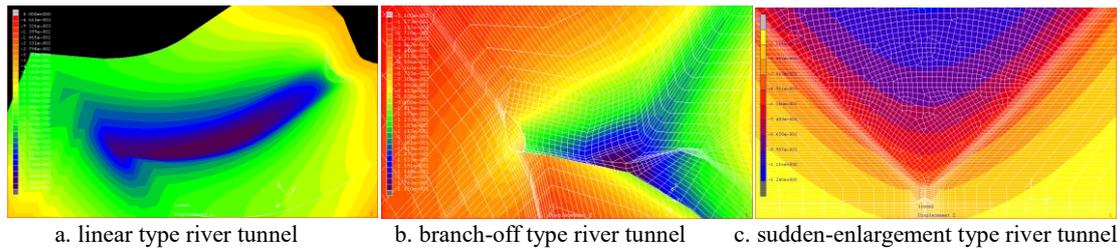
Fig. 5: Calculated settlement of three reservoir basin type

In terms of those influence factors, such as reservoir type, bedrock depth, the extended length of upstream and downstream and different water levels, the improved entropy method can be applied to build weight calculating model. Weights of above factors are 0.37, 0.17, 0.11, 0.55 and 0.30 respectively. Apparently, the sudden-enlargement type river channel has the largest effect on the reservoir basin deformation since the water is the heaviest. When the river channel width is certain, the upstream deformation and settlement would increase with the water rise. The bedrock depth also has a certain impact on the deformation. However, when the model is deep enough, the influence tends to convergence. The weight of the upstream and downstream length is small comparatively.

In this paper, Xiaowan reservoir basin model will be built based on monitoring data to explore the impact of reservoir basin deformation on dam work behavior.

Analysis of Xiaowan reservoir basin deformation and effects

Xiaowan arch dam locates in the middle reaches of Lancang River which is at the junction of Nanjian County in Dali Prefecture and Fengqing County in Lincang City, east of Yunnan Province. It is a branch-off type reservoir (at the junction of Lancang River and Heihui River).

Monitoring deformation rules of Xiaowan reservoir basin

The benchmark network for deformation monitoring of Xiaowan reservoir basin is shown in Fig. 6. The monitoring scope ranges from 1km upstream to 4km downstream, with a total observation line of 33km.

The whole deformation monitoring network of reservoir basin has 33 benchmarks of which 15 dots are arranged upstream and 18 dots are arranged downstream. According to the measured benchmark results, Xiaowan reservoir basin shows warping deformation, with settlement upstream and a little uplift downstream. Monitoring settlement ranges from -1.6mm to 35mm, where the maximum is 1km upstream from dam site while the minimum is 4km downstream. As shown in Fig. 7, the reservoir basin in dam area has a slight rotation toward the upstream.
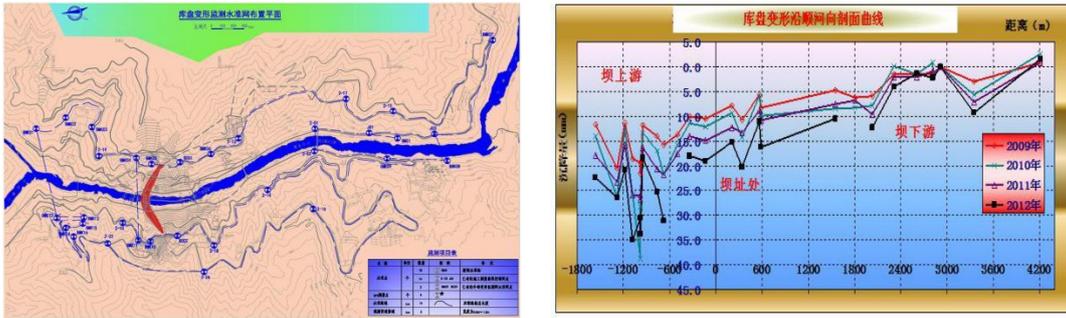
Fig. 6: Benchmark network & settlement distribution of Xiaowan reservoir basin

Numerical analysis and deformation modulus inversion

FEM model of Xiaowan reservoir basin has been shown in Fig. 7. Combining the research results of modeling scope for branch-off type river channel, it includes generalized geological layers of near dam and reservoir area and main geological structure such as fault zone F1、F2 and fault F7. The FEM model boundary of Xiaowan reservoir basin is 44km upstream, 21km downstream, 40km along the left bank, 50km along the right bank and 10km in depth. The model has 934740 elements and 958636 nodes in all.
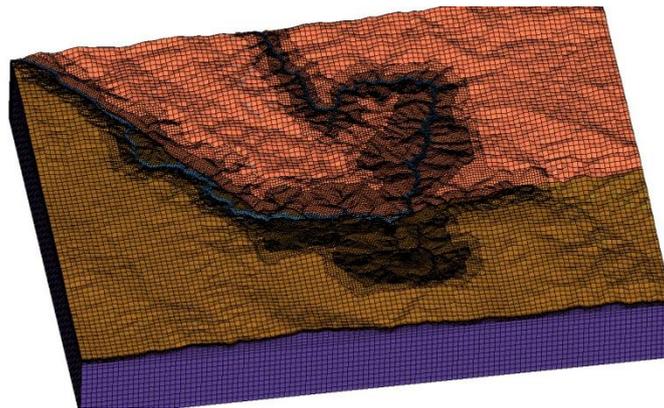

Fig. 7: Numerical analysis model of Xiaowan reservoir basin

Based on monitoring data of benchmarks around dam site in Xiaowan reservoir area, the optimizing objective function for inversion is conducted by the average square error of monitoring and calculated displacement of benchmark as follows.

$$S = \frac{1}{K} \sum_{j=1}^{K} \sqrt{\frac{1}{N} \sum_{i=1}^{N} (\delta_{ic} - \delta_{im})^2}$$

(1)

Where δ_{ic} are the calculated value of nodes at benchmark points in the reservoir model, δ_{im} are the monitoring value of benchmark points in the reservoir, N is the number of benchmarks,

K is the number of repeated measurements. When the value of S reaches minimum, corresponding parameters of the FEM model represents the true material parameters of Xiaowan reservoir basin.

When deformation modulus inversion of reservoir basin is taken, various combinations of material parameters should be set to calculate deformation of benchmark. Each group of material parameters is determined as follows:

$$E = (1-\lambda)E_l + \lambda E_u \qquad (2)$$

Where E_u and E_l are the upper and lower limits of proposed parameter interval, λ is distribution coefficient. When λ is set to be 0, 0.5 and 1, parameters denote the lower limits, middle values and upper limits of proposed interval respectively.

Combining with monitoring data of benchmark in Xiaowan reservoir basin, parameters of each rock layers in Xiaowan reservoir basin are inverted by applying the optimizing method. As shown in Fig. 8, the objective function reaches its minimum when the distribution coefficient λ is 0.576. Therefore, the relationship of deformation modulus of upstream foundation rock in Xiaowan reservoir basin with depth can be described as follows:

$$E = 6.3535 * lnh + 25.41 \qquad (3)$$

Where E represents the deformation modulus of foundation rock in reservoir basin, h represents the foundation depth in reservoir basin. The deformation modulus of surface weathered rock in Xiaowan reservoir basin is 1.9GPa.
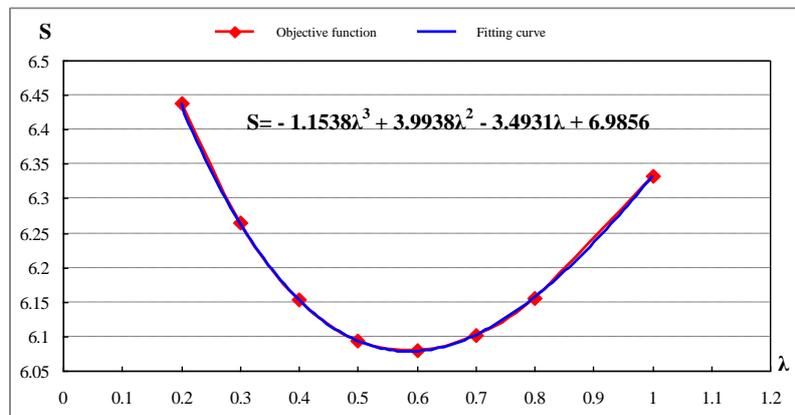

Fig.8: Relationship curve between λ and S

Elastic modulus inversion of Xiaowan arch dam

Based on the deformation analysis of reservoir basin, FEM model of Xiaowan near dam area is established, shown in Fig. 9. Elastic modulus of Xiaowan dam is inverted to study the influence of reservoir deformation on Xiaowan high arch dam [4]. In order to simulate the complicated geological conditions in Xiaowan near dam area accurately, the near dam FEM model includes 779914 elements and 821914 nodes totally, where 530173 elements belong to the dam body.
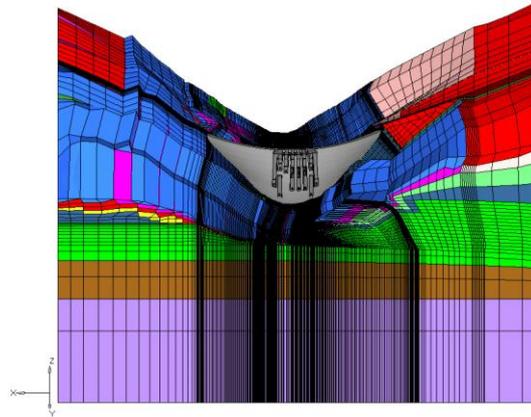
Fig. 9: 3-D FEM model of Xiaowan near dam area

According to the time and space analysis of Xiaowan arch dam horizontal displacement monitoring data, main affect factors of dam deformation are pressure, temperature and aging components. Namely, the displacement consists of water pressure component, temperature component and time-dependent component.

$$\delta = a_0 + \sum_{i=1}^{4}\left[a_{1i}(H_u^i - H_{u0}^i)\right] + \sum_{i=1}^{2}\left[b_{1i}\left(\sin\frac{2\pi it}{365} - \sin\frac{2\pi it_0}{365}\right) + \right.$$
$$\left. b_{2i}\left(\cos\frac{2\pi it}{365} - \cos\frac{2\pi it_0}{365}\right)\right] + d_1(\theta - \theta_0) + d_2(\ln\theta - \ln\theta_0) \tag{4}$$

Therefore, the water pressure component, temperature component and time-dependent component can be gradually separated, shown in Fig. 10.
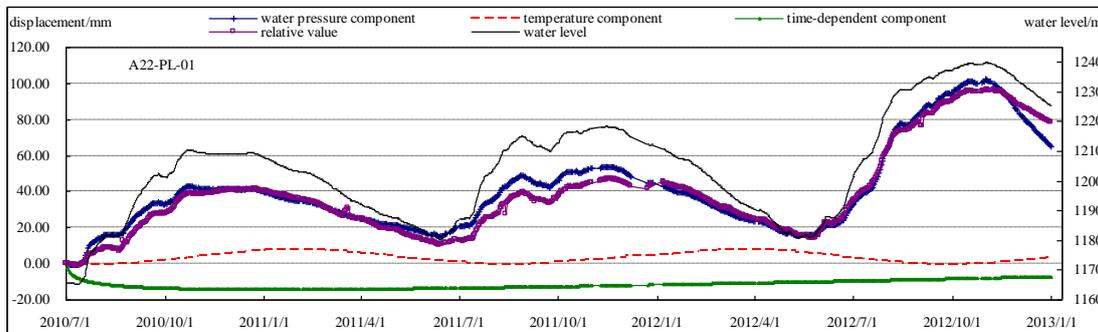

Fig. 10： The component separation of Xiaowan riverbed dam block crest deformation

It can be seen from Fig. 10, among all components of Xiaowan dam radial displacement, water pressure component occupies the largest proportion, and dam downstream displacement arises along with the rising water level. Meanwhile, temperature change also have some influences on dam radial displacement, namely, increasing temperature causes the upstream deformation and decreasing temperature causes the downstream deformation. And the higher elevation, the greater the temperature component is. Moreover, dam has a certain time-dependent component which indicates that dam deformation has the trend towards downstream.

Considering the impact of Xiaowan reservoir basin deformation, dam deformation under water pressure is calculated. On the basis, dam elastic modulus is inverted with the previously separated water pressure component. Inversion results are shown in Tab. 1. Concrete elastic modulus of Xiaowan dam A, B, and C district are 27.96GPa, 27.18GPa, 26.19GPa respectively.

Tab. 1 The concrete elastic modulus inversion results of Xiaowan dam

material	μ	E_0	f'	c'	E afeter inversion
A District	0.18	25.89	1.4	1.6	27.96
B District	0.18	25.17	1.4	1.6	27.18
C District	0.18	24.25	1.4	1.6	26.19

During the 4th storage stage of Xiaowan dam in 2012, concrete dam comprehensive elastic modulus is inversed using monitoring data of dam plumb line (9#, 15#, 19#, 22#, 25#, 29# and 35# dam block) and the result is 33.05GPa (without considering the reservoir basin deformation). Compared with results in Tab. 1, the comprehensive elastic modulus is certainly reduced after considering the effect of reservoir basin deformation. Therefore, for those high dam projects, due to the settlement and small angle inclination towards upstream caused by reservoir water pressure on the reservoir basin, the deformation has a certain impact on dam operating behavior. Hence, reservoir basin deformation is suggested to be considered in dam and rock mechanical parameters back analysis to get more reliable parameters.

Effects of reservoir basin deformation

Xiaowan arch dam horizontal displacement under reservoir basin deformation (1240m water level) is shown in Fig. 11. Considering the reservoir basin deformation, Xiaowan dam has a toppling deformation towards upstream and the deformation is relatively larger in the riverbed dam block. Preliminary calculation results demonstrate that the upstream displacement of 22# dam crest is 18.46mm, the displacement towards upstream of dam foundation inverted plumb point at 963m is 13.26mm, the upstream displacement of bedrock inverted plumb base is 12.01mm. Therefore, relative to the base point, the upstream displacement of 22# dam crest is 6.45mm. However, the current study only considers the reservoir basin deformation, the influence of reservoir basin deformation on dam stress and overall stability could be analyzed in future.
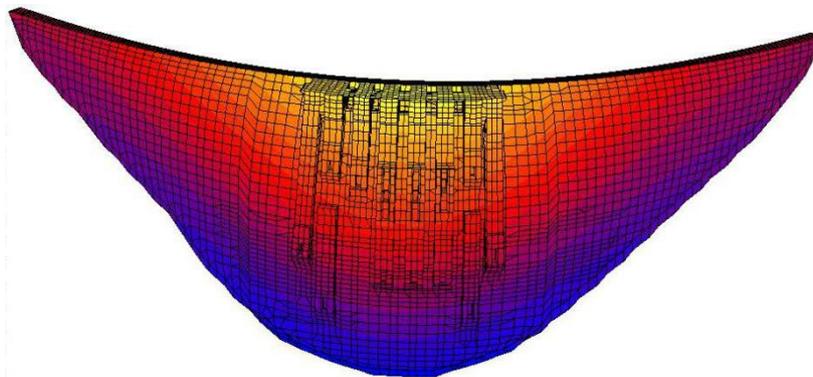

Fig. 11: Xiaowan Dam horizontal displacement distribution

Conclusion

In this paper, combined with Xiaowan dam, a preliminary study of high arch dam reservoir basin deformation and its effect on dam operating behavior were carried out. The conclusions are as follows.

(1) The reservoir basin deformation of high dam projects and its influence on the dams have attracted more and more attention from hydropower engineers, and more future studies need to be done.

 (2) Influence factors of reservoir basin deformation have been explored, such as reservoir basin types, reservoir basin range and water pressure. And weighting model has been established based on the improved entropy method to calculate the impact weight of each factor. Influence laws of each factor on the numerical analysis of high arch dam reservoir basin deformation have been revealed.

 (3) Xiaowan reservoir basin deformation modulus and dam concrete elastic modulus have been inversed using monitoring data of reservoir basin settlement and dam horizontal displacement. And the inversion values of comprehensive elastic modulus has a certain reduce when considering reservoir basin deformation effect.

 (4) Research results can be used to analyze the "doubtful deformation points" exist in those running hydropower projects. At the same time, for high dam with large reservoir, due to the settlement and deformation caused by reservoir water pressure on the reservoir basin, it is recommended that reservoir basin deformation should be taken into account when analyzing and evaluating dam operating behavior.

 (5) Arch dam is a statically indeterminate structure. The effect of reservoir basin deformation is not only a simple problem of the whole rigid body deformation of dam and its foundation. Reservoir basin deformation is influenced by reservoir type, geological conditions, reservoir water pressure, etc. The problem is extremely complex. At home and abroad, there are a certain amount of super high arch dams with capacity of more than 10 billion m^3. The research of corresponding problems should be carried out to study the criterion of the existence of reservoir deformation further. Meanwhile, general laws of high arch dam reservoir basin deformation should be summarized and refined considering geological conditions, water pressure and different reservoir types.

Acknowledgements

References

[1] PAN Jiazheng，HE Jing. Large dams in China - a fifty-year review[M]. Beijing：China Water Power Press，2000.

[2] LI Zan，CHEN Fei，ZHENG Jianbo，et al. Study on key problems of super high arch dam[M]. Beijing：China Electric Power Press，2004

[3] LIU Yunfang. Geostress and engineering construction[M]. Wuhan：Hubei Science and Technology Press，2000.

[4] GU Chongshi, WU Zhongru. Safety monitoring of dams and dam foundations － theories & methods and their application [M]. Nanjing：Hohai University Press，2006.

Dam Break Analysis under Uncertainty
Introducing *BASEbreach*

Peter S.J.[1], Siviglia A.[1] and Boes R.M.[1]

[1] *Laboratory of Hydraulics, Hydrology and Glaciology, ETH Zurich, Hönggerbergring 26, CH-8093 Zürich*

ABSTRACT: Due to their high hazard in case of failure, earthen embankment and rock fill dams have to be designed, constructed, operated and monitored with utmost care and attention. History and today's experience indicate that some do fail, however. Society, i.e. political decision makers, insurance companies, and residents downstream of dams, ask for quantitative flood risk assessment. To perform the flood wave propagation from the failing dam downstream to the inundated area, a realistic dam breach hydrograph prediction is needed. Despite a multitude of sophisticated dam break modeling techniques, the lack of data useful for model calibration is pervasive. In addition, the highly non-linear and hardly measurable dam breach processes cause large uncertainties in hydrograph predictions that are neither understood nor entirely quantified yet. Deterministic dam breach models cannot account for these uncertainties and result in unreliable hydrograph predictions. Thus we propose a novel dam breach parameter model, embedded in a probabilistic framework, as new backbone of the next generation dam break models. Given the sparse available data of real-case dam break events, inverse modeling was applied to calibrate the stochastic parameter model. An application example is shown to illustrate the advantages of our probabilistic approach.

E-mail: peter@vaw.baug.ethz.ch

Introduction

In order to analyse the problem related to the failure of a dam, three steps have to be considered: Dam break modelling, flood wave calculation, and impact assessment. For a sound assessment of the downstream risk of a failing dam we need to quantify the hydraulic variables in the floodplain accordingly. Since (1) topographical data are digitally available at high resolution and (2) due to advances in the numerical solution of the shallow water equations, the most sensitive parameter of a flood wave calculation remains the inflow boundary condition. This hydrograph is commonly represented by the breach outflow hydrograph calculated by some dam break model.

Focusing on embankment dams, many dam break models (also called them dam breach models) exist, varying in their complexity and parametrization: from simple regression based formulae predicting the peak breach outflow [1] or breach formation parameters [2], through parameter models that describe the gradual dam failure in simplified but physically based manner [3], to more detailed models describing the processes in one-, two- or even three-dimensions in space [4]. An ASCE Task Committee on Dam/Levee Breaching recently published a comprehensive summary on existing dam breach modelling approaches [5].

In the case of dam break risk assessment, predictions of outflow hydrographs or at least peak outflows are needed. These predictions must be reliable. Since the assessment of risk does not only involve the impact but as well the probability of an event, a dam breach model should be able to answer questions as

- How do we define a worst case scenario?
- What is the most realistic or most likely scenario?
- How do the scenarios look like for which we should implement certain countermeasures?

None of the above questions can be answered by applying deterministic dam breach models. The uncertainties in dam breach modelling are large, both in the mathematical description of the physical processes during a dam break event and in their parametrization. Because these uncertainties are ignored during model calibration of deterministic models, their implications

on the predicted dam break hydrograph are not obvious. Hence there are large differences between dam breach predictions, depending on the deterministic model that was chosen. This is clearly demonstrated by the results of the ICOLD numerical benchmark of dam breach modelling [6] (see Fig. 1). The discrepancy between the different models cast doubt on the validity of deterministic dam breach models if predictions of a dam break hydrograph are needed. Generally speaking, the uncertainty in peak discharge predictions is around 0.5 to 1.0 orders of magnitude [5].

It is the aim of this article to contribute to answer the questions above. A newly developed dam breach model called *BASEbreach* is designed as a probabilistic model framework where dam breach scenarios and their hydrographs are connected to probabilities. Each scenario represents a deterministic evaluation of a simplified parameter model set up. The uncertainties originate from the input parameters (epistemic) on the one hand and from the natural variability of the dam break phenomenon (aleatory) on the other hand.
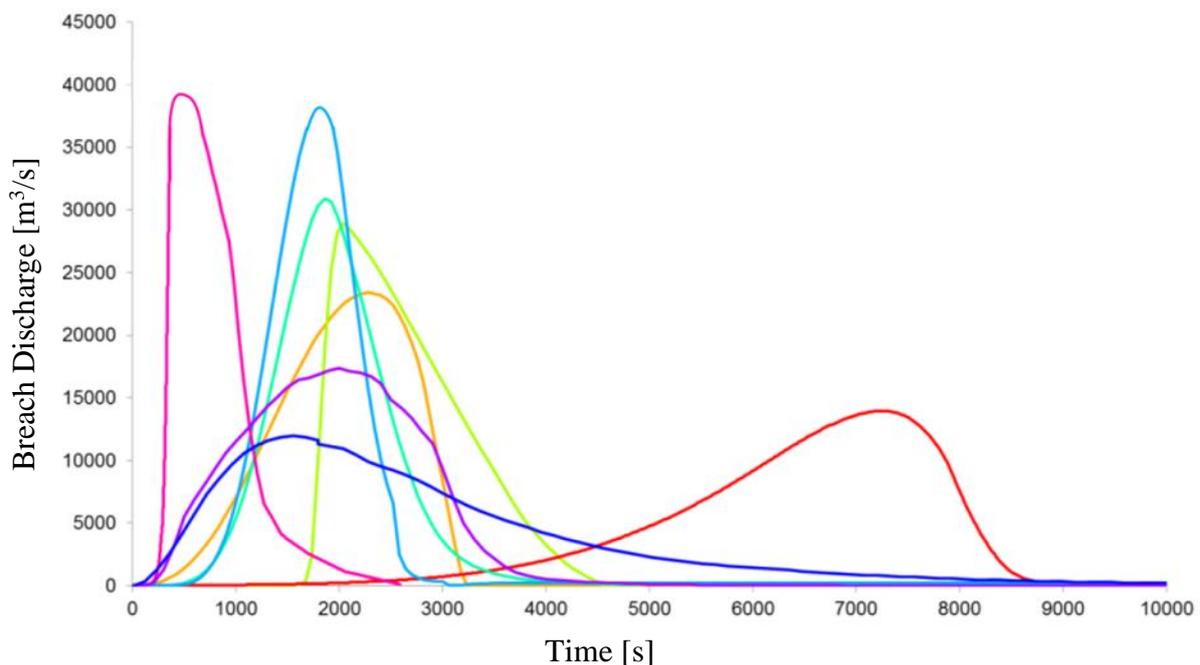

Fig. 1: Results from a dam break model benchmark [6]: Dam break hydrograph predictions of different modelling experts applying different dam breach models. The data about the hypothetical dam was perfectly known by all modellers.

Methods

Formulation of the dam breach model

The aim of *BASEbreach* is to model the breach development of homogeneous embankment dams. To cope with the need of a probabilistic framework where millions of model runs are required, *BASEbreach* is implemented as a physically-based but simplified model. The physical processes that are included in the model are described by integral values, i.e.

- gradual erosion of dam material,
- development of a breach,
- increasing discharge through that breach,
- decreasing water level in the reservoir behind the dam.

All variables and processes are defined for one critical cross section within the breach (see Fig. 2). In physically based but simplified dam breach models many a-priori assumptions have to be made, especially to describe the breach shape and its development. In *BASEbreach* the number of a-priori assumptions and the involved parameters is kept as small as possible in order to simplify the quantification of the parameter uncertainties:

- The erosion of dam material induced by overtopping is regarded as the main process. The head-cut erosion process is not considered because non-cohesive material is focused on. In case of a dam failure initiated by other mechanisms, such as internal erosion (piping), embankment slope instability, or structural failure, the breach enlargement is assumed to be predominated by the process of overtopping as well [7, 3]. This assumption brings an additional benefit since the prediction of proneness of a dam to specific failure causes is hardly to achieve. In addition, other processes than overtopping are difficult to parametrize and introduce additional uncertainties instead of making the model more reliable.

- Breach development goes from vertical erosion to lateral widening (see Fig. 3).

- The reservoir basin is characterized by a power law function relating the reservoir volume V_r to the water level Z

$$V_r \propto Z^\alpha, \tag{1}$$

  where α represents a parameter to describe the basin geometry.

- In analogy to a broad crested weir, critical flow conditions occur close to the top of the breach (critical cross section, see Fig. 2).

- The breach shape is represented by any geometry between a triangular and a rectangular cross section. Simultaneously the breach side wall angle at the top of the breach β is kept constant and represents a material property (see Fig. 3). The initial breach width is defined in such a way that the initial breach discharge is not dependent on the choice of the breach top angle.

- To quantify the sediment transport in the critical cross section q_s a power formulation is used, whereat critical shear stress for the onset of transport is neglected

$$q_s = f_e \cdot v^A \cdot r_h{}^B. \tag{2}$$

  Many classic empirical transport formulae can be simplified and rewritten in this form, with v being the flow velocity and r_h the hydraulic radius. The exponents A and B vary strongly among the empirical formulae, mainly dependent on the application purpose, e.g. Meyer-Peter & Müller [8] formula for bedload transport in alpine rivers where $A = 1.5$ and $B = -0.5$. Any constant factors that are needed to quantify q_s (properties of dam material, friction laws, empirical transport formulas) are collected in one single coefficient f_e. This scaling coefficient is used to control the global erosion velocity of the breach and therefore can be used for calibration purposes.

- The progressive failure is then described by two partial differential equations, one balancing the erosion of the dam material, i.e.

$$\frac{\partial Y}{\partial t} = Q_s \left(\frac{\partial V_b}{\partial Y} \right)^{-1}, \tag{3}$$

  and the other balancing the reservoir outflow through the breach

$$\frac{\partial Z}{\partial t} = Q_b \left(\frac{\partial V_r}{\partial Z} \right)^{-1}. \tag{4}$$

Y and Z are the breach level and reservoir level, Q_s and Q_b the sediment and water discharge in the breach, and V_b and V_r are the breach volume and the reservoir volume, respectively (see Fig. 2). The computation of the sediment and water discharge is based on classical engineering formulae. The reservoir and breach volume change rates are calculated by simple geometrical relations.
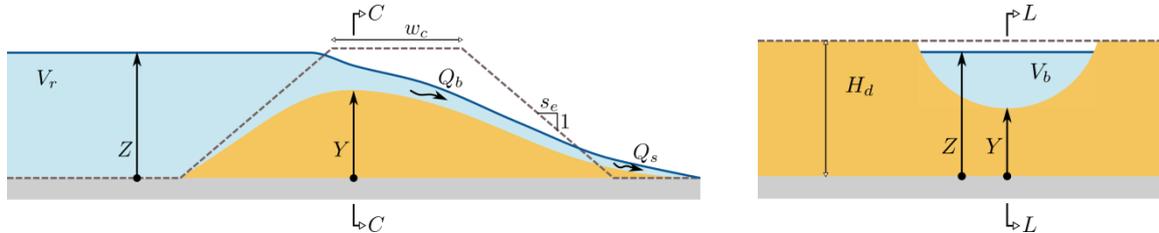
Section L-L with parameters: crest width (w_c) and embankment slope (s_e); and variables: reservoir (Z) and breach (Y) level, reservoir volume (V_r), breach discharge (Q_b) and sediment discharge (Q_s).

Section C-C with parameter: dam height (H_d); and variables: reservoir (Z) and breach (Y) level, breach volume (V_b).

Fig. 2: Longitudinal (left) and transverse (right) section of the dam-reservoir system and the main parameters and variables of *BASEbreach*.
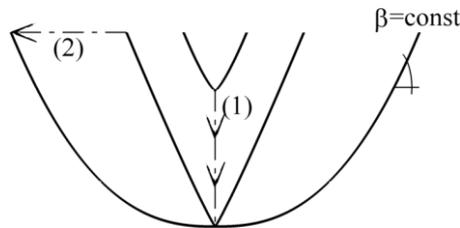

Fig. 3: Development of breach shape through (1) vertical erosion and (2) lateral widening, with breach shape as polynomial function and breach top angle β kept constant.

Calibration of the probabilistic dam breach model

For the model calibration a dataset with historical dam break failures is available, containing at least information about the breach height, the released water volume, and the estimated peak outflow [9]. Other dam breach models have used similar data [10, 3] (see Tab. 1).

In *BASEbreach* different parameter categories and their uncertainties are considered:

- Parameters that are assumed to be known quite accurately (reservoir volume, dam height, initial reservoir level, crest width, embankment slope)
- Parameters that are not known exactly but empirical knowledge is available. In the calibration procedure the following empirics were used (from large dam break data sets [11]):
  - crest width w_c (where no data is available):
    lognormal distribution with parameters 1.55 and 0.51 (see equation (5)),
  - embankment slope s_e (where no data is available):
    normal distribution with mean of 2.16 and standard deviation of 0.66,
  - breach side angle β: uniform distribution bounded by 50 and 85,
  - reservoir shape α: uniform distribution bounded by 1 and 4.

- Parameters that are not known and need to be calibrated, i.e. parameters of the transport formula:
  - exponents of flow velocity A and hydraulic radius B,
  - scaling coefficient f_e, that is assumed to follow a lognormal distribution described by the uncertain hyper-parameters λ and ζ, i.e.

$$P_{[f_e=x]} = \frac{1}{x\zeta\sqrt{2\pi}} \cdot e^{\frac{-(\ln x - \lambda)^2}{2\zeta^2}}. \tag{5}$$

The task of calibrating a stochastic model is similar to calibrating a deterministic model: "How to select the calibration parameter(s) in order to produce the best results compared to the reference dataset?" When calibrating *BASEbreach* we have to find a location in the four dimensional parameter space (λ, ζ, A, B) that reproduces the reference data best, i.e. the estimated peak discharges of the historical data (see Tab. 1).

This is done by applying the method of Markov Chain Monte Carlo (MCMC) incorporated in a Bayesian framework in order to update prior knowledge about the calibration parameters. The main goal of MCMC is to sample the probability distribution functions of the calibration parameters. Here a Metropolis-Hastings sample algorithm was used [12, 13].

Tab. 1: Data set of historical dam break events used for calibration of *BASEbreach*: Mode P indicates a failure caused by piping whereas O indicates an overtopping triggered event, V_W is the total water volume that was released during the event and H_W the according drop in reservoir level, H_b is the final breach height, s_e and w_c are the embankment slope and the crest width of the dam, Y_0 is the assumed initial breach level relative to H_W, and Q_p is the estimated peak discharge.

ID	Dam	Mode	V_W [hm3]	H_W [m]	H_b [m]	s_e [-]	w_c [m]	Y_0 [-]	Q_p [m3/s]
1	Apisapha	P	22.2	28.0	31.1	2.5	4.88	0.8	6850
2	Baldwin Hills	P	0.910	12.2	21.3	1.9	19.2	0.4	1130
3	Butler	O	2.38	7.16	7.16	-	-	0.8	810
4	Fred Burr	P	0.750	10.2	10.4	-	-	0.8	654
5	French Landing	P	3.87	8.53	14.2	2.25	2.4	0.8	929
6	Frenchman Creek	P	16.0	10.8	12.5	2.5	6.1	0.8	1420
7	Hatchtown	P	14.8	16.8	18.3	2.25	6.1	0.8	3080
8	Ireland no. 5	P	0.160	3.81	5.18	3.0	2.4	0.8	110
9	Johnstown	O	18.9	24.4	24.4	1.75	3.05	0.8	8500
10	Lawn Lake	P	0.798	6.71	7.62	1.55	2.4	0.8	510
11	Lily Lake	P	0.093	3.35	3.66	-	-	0.8	71
12	Little Deer Creek	P	1.36	22.9	27.1	3.05	6.1	0.4	1330
13	Lower Latham	P	7.08	5.79	7.0	3.02	4.6	0.8	340
14	Prospect	P	3.54	1.68	4.42	2.0	4.3	0.8	116
15	Quail Creek	P	30.8	16.7	21.3	-	-	0.8	3110

Results

Calibration Procedure

After 10'000 accepted Markov Chain steps the four dimensional probability distribution function converged and the most probable values are found to be: $A = 6.5$ and $B = -2.3$ (see Equation 2), and $\lambda = -10$ and $\zeta = 0.7$ (see Equation 5). Fig. 4 shows the resulting peak discharge distributions for the 15 historical events in Tab. 1 when applying the parameters found through calibration.

The width of the resulting peak discharge distributions is mainly dependent on the width of the scaling coefficient f_e, described by ζ which was determined through the calibration. This uncertainty comprises the natural variability of the dam breach process and model uncertainties that are not captured by input parameters. Therefore, we expect most peak discharge values to match quite well (reference data around the mode), and we expect some data points to stay rather in the tail region of the peak discharge distributions. This is exactly the case for dam ID 2 and 13. Since these "outliers" are an implicit part of the calibration procedure itself we do not have to find reasons for observing them.

The values obtained for the erosion law exponents A and B can be interpreted from a physical point of view. Known values for A range from 1 to 5 dependent on the application, ascending from bed load transport over suspension load to total load formulae. The higher this exponent, the more material is transported with high flow velocities but having almost no transport for low flow velocities. The exact transport mechanism in the breach of a failing dam is not known, but it is likely to have even more extreme material transport than in case of total load due to high turbulence in the breach. Therefore, a value greater than 5 is still possible from a physical perspective. The exponent of the hydraulic radius B represents a geometrical influence. The smaller the hydraulic radius, the larger is the wetted area compared to the flow area, meaning a narrow breach. Narrow and deep cross sections add additional turbulence to the flow and probably lead to higher transport rates. Hence we expect a negative exponent B to capture this effect. From literature we know sediment transport formulae for rivers and streams ($B \sim -0.5$) or the sediment transport formula by Smart & Jäggi [14] which is applicable to steep and narrow mountain creeks ($B = -1.6$). In Case of a dam breach the value of $B = -2.3$ denotes an even higher geometrical effect than mountainous environment, which is physically reasonable as well.
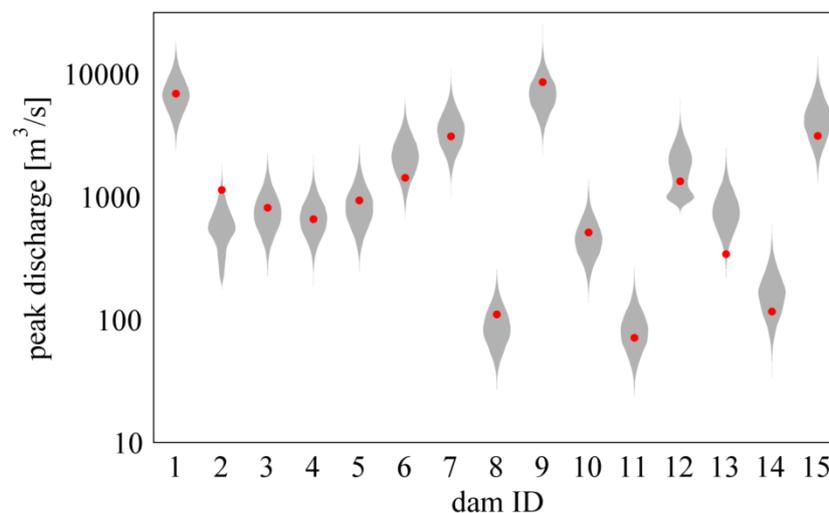

Fig. 4: Results of the calibration of *BASEbreach*: probability distribution functions of modelled peak discharge (grey violins) compared to the reference data of the 15 historical dam break events (red dots).

Application Example

In order to illustrate the advantages of a probabilistic modelling approach, peak discharge predictions are made by (1) a standard breach formulation[1] (SB) [15], (2) a regression based empirical formulation, including the uncertainty originating from the regression analysis (FR) [10], and (3) the probabilistic model *BASEbreach* (BB). We consider two hypothetical but realistic dam-reservoir systems, both with a reservoir storage volume of 20'000 m^3 but having different dam heights: 2 m and 6 m respectively. In Fig. 5 the peak discharge predictions for these two cases applying the three dam breach models SB, FR, and BB are shown. Since SB assumes a breach size that is independent of the reservoir size, the peak discharge prediction is very low for small height-volume ratios H_d/V_r (see Fig. 5a), and vice versa (see Fig. 5b). FR takes the reservoir size into account. Therefore, the peak discharge predictions are more reliable for extreme values of H_d/V_r. In addition, if we include the regression errors as uncertainty in the prediction, we get a feeling of possible peak outflow ranges. The peak discharge predictions by (BB) show similar results, but the range of possible peak outflows is mostly larger than with (FR). In simplified physical models as *BASEbreach* other parameters than dam height and reservoir size are considered. Hence we can gather more information about the dam under investigation. By knowing the crest width and the embankment slope, analysing digital elevation maps to estimate the basin shape and assuming a dam material that can be represented by a breach side top angle, the parameter uncertainties can be reduced. Accordingly, the uncertainties in the peak discharge predictions get smaller as well, what can be of great importance when quantifying the impact of the dam failure.
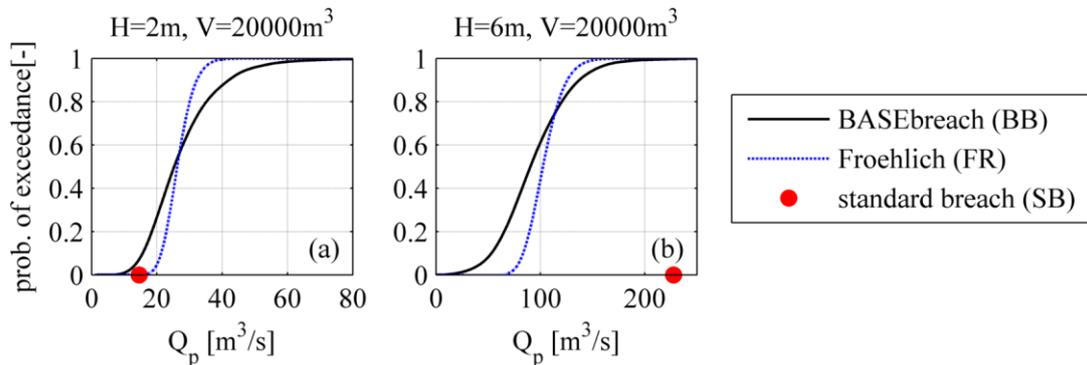

Fig. 5: Cumulative distribution functions of the peak discharge predictions for two hypothetical dam-reservoir systems using different simplified dam breach models.

Conclusions and Outlook

The parametrization and calibration of the probabilistic dam breach model *BASEbreach* was presented. The advantage of its application is the reliable peak discharge predictions including their probabilities of exceedance. Not only information about the peak discharge is available but the full probabilistic hydrograph. It is possible to update the predictions with expert knowledge or additionally gathered data.

The implications of probabilistic hydrograph properties on the flood wave calculation still have to be investigated. Nevertheless, the subsequent risk assessment has to be reformulated as well. This yields for new methodologies, and appropriate guidelines are needed, as has been claimed for ten years [16].

---

[1] Analytical solution of an instantaneously failing dam with fixed breach size

Acknowledgements

References

[1] Wahl T.L. (2004). Uncertainty of Predictions of Embankment Dam Breach Parameters. Journal of Hydraulic Engineering, Vol. 130, pp. 389-397.

[2] Froehlich D.C. (2008). Embankment Dam Breach Parameters and Their Uncertainties. Journal of Hydraulic Engineering, Vol. 134, pp. 1708-1721.

[3] Macchione F. (2008). Model for Predicting due to Earthen Dam Breaching I: Formulation and Evaluation. Journal of Hydraulic Engineering, Vol. 134, pp. 1688-1696.

[4] Volz C. (2013). Numerical Simulation of Embankment Breaching Due to Overtopping. Swiss Federal Institute of Technology, Zurich, Dissertation ETH No. 21371.

[5] Wu W., ASCE/EWRI Task Committee on Dam/Levee Breaching (2011). Earthen Embankment Breaching. Journal of Hydraulic Engineering, Vol. 137, pp. 1549-1564.

[6] Zenz G., Goldgruber M. (2013). 12th International benchmark workshop on numerical analysis of dams, Austrian National Committee on Large Dams.

[7] Singh V.P. (1996). Dam Breach Modeling Technology, Kluwer Academic Publishers.

[8] Meyer-Peter E., Müller R. (1948). Formulas for Bed-Load Transport. 2nd Meeting IAHR, Stockholm, Sweden, IAHR.

[9] Wahl T.L. (1998). Prediction of Embankment Dam breach Parameters - A Literature Review and Needs Assessment. Dam Safety Research Report No. DSO-98-004. U.S. Department of the Interior, Bureau of Reclamation.

[10] Froehlich D.C. (1995). Peak Outflow from Breached Embankment Dam. Journal of Water Resources Planning and Management, Vol. 121, pp. 90-97.

[11] Eicher A. (2014). Bayesian Multilevel Model Calibration of a Simplified Dam Breach Model. Swiss Federal Institute of Technology, Zurich, Master Thesis.

[12] Sudret B. (2007). Uncertainty propagation and sensitivity analysis in mechanical models - Contributions to structural reliability and stochastic methods. Université Blaise Pascal - Clermont II.

[13] Wu F.-C., Chen C.C. (2009). Bayesian Updating of Parameters for a Sediment Entrainment Model via Markov Chain Monte Carlo. Journal of Hydraulic Engineering, Vol. 135, pp. 22-37.

[14] Smart G.M., Jaeggi M.N.R. (1983). Sediment Transport on Steep Slopes. Mitteilungen der Versuchsanstalt für Wasserbau, Hydrologie und Glaziologie (VAW). Swiss Federal Institute of Technology, Zurich.

[15] Bundesamt für Energie (BFE), Sektion Aufsicht Talsperren (2014). Richtlinie über die Sicherheit der Stauanlagen – Teil B: Besonderes Gefährdungspotenzial als Unterstellungskriterium. Bern.

[16] Pappenberger F., Beven K.J. (2006). Ignorance is bliss: Or seven reasons not to use uncertainty analysis. Water Resources Research, Vol. 42, pp. W05302.

13th Benchmark Workshop on the Numerical Analysis of Dams
SYNTHESIS OF THEME C – Open Theme

Guido Mazzà[1]

[1]*Ricerca sul Sistema Energetico RSE S.p.A., Milan, Italy*

Foreword

During the long benchmark activities of the ICOLD Technical Committee on Computational Aspects of Dam Analysis and Design, the technical organization was based on the proposal of one/two Themes related to concrete dams and one/two Themes related to embankment dams.

However, more recently a session on "Open Themes" have also been introduced in the organization with three main aims:

- to gather ideas and suggestions useful for the next BWs;
- to have an overview about the progress of numerical modeling;
- to enlarge the participation to the workshops.

The Open Themes proposed for acceptance to the 13th Benchmark Workshop have been primarily linked to the basic Themes A and B.

This means that the participants were basically asked to send their own contributions on the following key topics:

- Seismic analysis, tightly linked to Theme A;
- Risk analysis, tightly linked to Theme B.

Moreover, two other topics have been considered, coherently with the mission of the Committee:

- Safety assessment of dams and appurtenant works;
- Numerical modelling.

Participation to the 13th BW - Theme C

The participation to the Theme C has been particularly large compared with the recent past BW: eighteen papers have been presented. For the sake of homogeneity, the papers have been subdivided in four sessions as shown in the table below:

Sessions	Theme C Topics	Number of contributions
1	Seismic/Dynamic Analysis	4
2	Risk Assessment/Probabilistic Analysis	4
2	Data Assessment & Management	2
3 & 4	Safety Assessment	8
Total		**18**

Some general remarks and comments are given here below related to the papers presented in the different sessions.

SESSION 1 - Seismic/Dynamic Analysis
The paper presented by R. Panduri "*Seismic safety analysis of dams within the context of Swiss dam safety concepts*" has given a wide overview of the Swiss Federal Office of Energy (SFOE) activity on the seismic reassessment of Swiss dams.

An innovative approach on the seismic reassessment of concrete dams has been presented by M. Meghella and L. Furgani in the paper "*Endurance Time Analysis for the Seismic Vulnerability of Arch Dams*". The approach needs to be more widely verified, however it shows a great potential to reduce the computation effort when seismic reassessments have to be performed.

A very particular case history related to the modelling of rock fall impacting directly on a large concrete dam has been presented by A. Frigerio and L. Artaz in the paper "*Modelling of rock fall on the dam of Place Moulin*". This case history could be also considered as a possible theme for a next BW.

SESSION 2 - Risk Assessment/Probabilistic Analysis
Three of the four papers related to risk analysis have been presented orally. The quality of the papers is excellent. The socio-cultural aspects remain more open than the technical questions about the difficulties of these methodologies to take roots in regions different to the Anglo-Saxon world, and in Europe in particular, where deterministic/semi-probabilistic approaches basically remain the most widely used approaches.

Lausanne is going to be the third Benchmark Workshop in which a Risk Analysis Theme has been addressed, and it closes a cycle: Failure risk of concrete dams (Valencia 2011), analysis of the consequences (Graz 2013) and failure risk of embankment dams (Lausanne 2015). The ICOLD Technical Committee has taken the decision to write a synthesis paper on the lessons learnt from the previous three events and by the contributions received for Theme C.

SESSIONS 3 & 4 - Safety Assessment
Some of the papers presented in the Sessions 3 & 4 could be profitably used as possible themes for the 14th Benchmark Workshop.

In particular, the papers "*Numerical analysis of concrete faced rockfill dams using gradient plasticity*" presented by P. Dakoulas et Al., "*Janneh dam Project. Non-linear numerical simulation of an arch-gravity dam*" presented by A. Yziquel et Al., and "*Partial demolition of Beauregard dam to guarantee its life extension. The role of numerical modelling in the choice of the design solution*" presented by A. Frigerio et Al. could represent good examples to this

aim. Of course, a suitable simplification of the true case histories should also be considered in order to make more affordable the themes proposed.

Moreover, the paper "*Safety Incidences in large Rockfill Dams Stability and Behavior, resulting from Scale Effects in Rockfill Shear Strength*" (Frossard et al.) could be a good basis for a parametric numerical investigation.

Conclusive remarks

Next year, May 2016 in Johannesburg, during the ICOLD Annual Meeting, the Committee has to examine several aspects, amongst which the organization of the 14th BW shall be addressed. In addition to the selection of the host, date and venue of the 14th Benchmark Workshop 2017, the set of Themes A, B and C shall be decided. With reference to the latter Theme, several hints can be taken from the papers presented during the Lausanne event.

Special care will be devoted to the possibility to propose a Theme on the behavior of appurtenant structures (spillways? outlets? gates?) vs. seismic loadings. Unfortunately, no cases on these structures have been presented even if they deserve special attention for the role these works play in the safety of the whole schemes.

A particularly import aspect that is worthwhile mentioning is relevant to the initiative of the Committee for the capitalization of the very large amount of results gathered during the Benchmark Workshops held so far. The results (now available in the ICOLD website) will be organized in a database so that it will be possible through key words to facilitate the search of information. The database should be ready for Johannesburg Annual Meeting (May 2016) or the Antalya European Club of ICOLD Symposium (October 2016).

Schweizerisches Talsperrenkomitee
Comite suisse des barrages
Comitate svizzero delle dighe
Swiss Committee on Dams